Oxidative Medicine and Cellular Longevity

Oxidative Stress in Disease and Aging: Mechanisms and Therapies 2018

Lead Guest Editor: Claudio Cabello-Verrugio
Guest Editors: Cristian Vilos, Raquel Rodrigues-Díez, and Lisbell Estrada

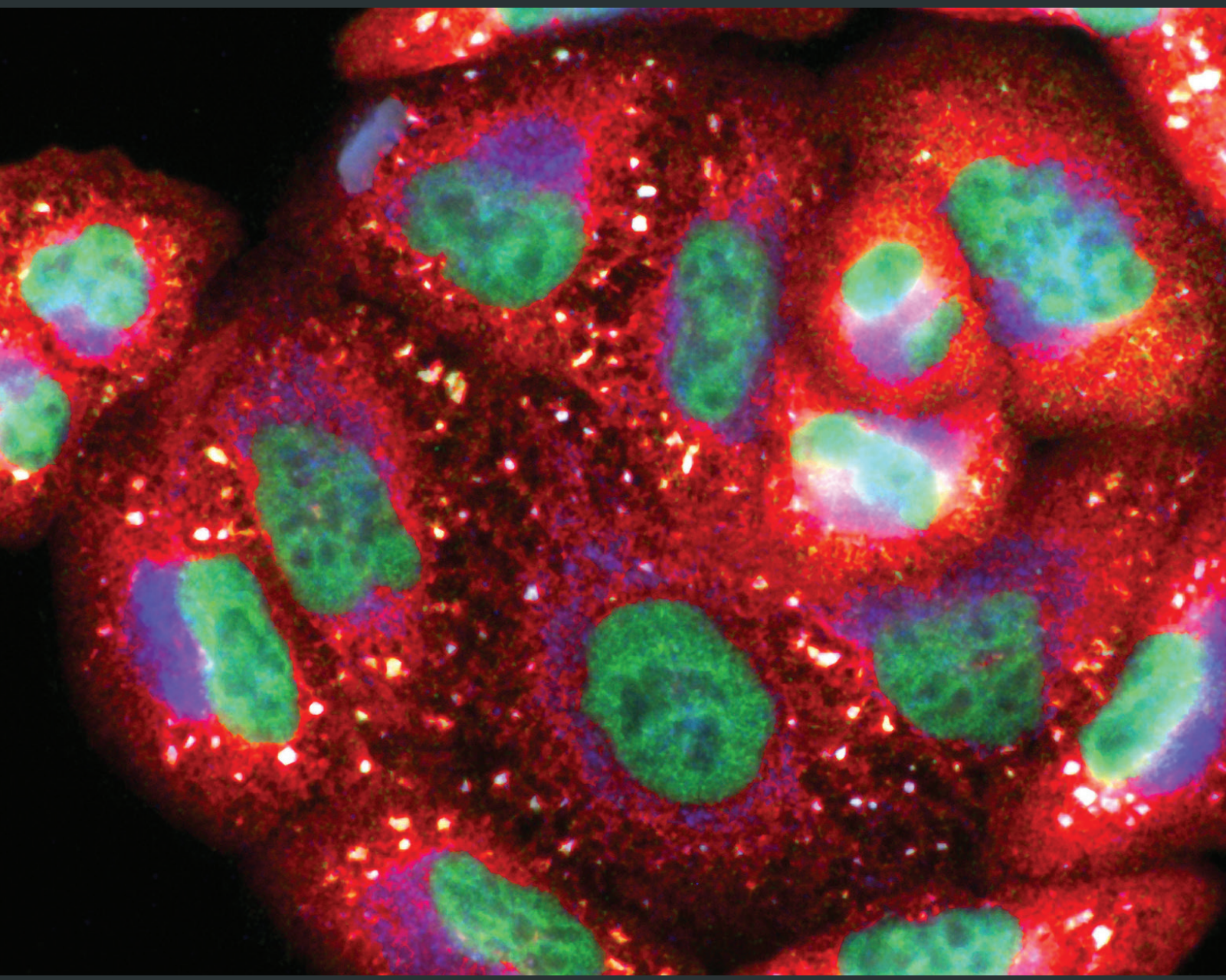

Oxidative Stress in Disease and Aging: Mechanisms and Therapies 2018

Oxidative Medicine and Cellular Longevity

Oxidative Stress in Disease and Aging: Mechanisms and Therapies 2018

Lead Guest Editor: Claudio Cabello-Verrugio
Guest Editors: Cristian Vilos, Raquel Rodrigues-Díez, and Lisbell Estrada

Editorial Board

Contents

Hindawi
Oxidative Medicine and Cellular Longevity
Volume 2018, Article ID 2835189, 2 pages
https://doi.org/10.1155/2018/2835189

Editorial

Oxidative Stress in Disease and Aging: Mechanisms and Therapies 2018

Claudio Cabello-Verrugio,[1] **Cristian Vilos**,[1] **Raquel Rodrigues-Diez**,[2] **and Lisbell Estrada**[3]

[1]*Universidad Andres Bello, Santiago, Chile*
[2]*Universidad Autónoma de Madrid, Spain*
[3]*Universidad Bernardo O'Higgins, Santiago, Chile*

Correspondence should be addressed to Claudio Cabello-Verrugio; claudio.cabello@unab.cl

Received 29 July 2018; Accepted 29 July 2018; Published 23 September 2018

Among the key factors influencing human health are the chronic diseases and aging, which have been increasing in the last decades. These pathological states are produced by several and diverse causes, and a common factor involved in most of them is oxidative stress. Cellular oxidative stress is defined as an imbalance between oxidative status, mainly by the formation of reactive oxygen species (ROS), and antioxidant defense mechanisms. Due to the broad and profound biological effects of ROS, in the last years, numerous experimental and clinical studies have focused their attention on the participation of oxidative stress as a key regulator in chronic pathological status and aging. Regarding this relationship, the aim of many ongoing studies is to elucidate the underlying mechanisms and role of oxidative stress in disease onset and development. In particular, there is an emphasis on finding new therapeutic strategies for chronic diseases and aging by decreasing oxidative stress.

This version of the annual special issue of "Oxidative Stress in Disease and Aging: Mechanisms and Therapies 2018" presents novel and relevant research regarding the mechanisms by which oxidative stress induces damage in the contexts of diseases and aging. Focus is given to the use of novel antioxidant strategies. The manuscripts within this special issue are all equally recommended by the editors, but the following contain especially interesting points worth comment.

G. Rowicka et al. evaluated the intensity of oxidative processes and the efficiency of antioxidant defense in children with celiac disease. The results do not shown differences; however, they demonstrated that the strict adherence to a gluten-free diet by children with celiac disease seems to be important for maintaining oxidative-antioxidant balance.

J. Ábrigo et al. shown a review of the mechanisms involved in the development of cachexia and their close relation and fine regulation of oxidative stress. The wide vision of the process and how oxidative stress is a key factor that can be targeted to treat the muscular dysfunction secondary to chronic diseases and aging are clearly presented in this review.

W. B. Jang et al. developed a novel antioxidant molecule, a novel antioxidant defined as MHY-1684, and studied its effect on the therapeutical effect of resident cardiac progenitor cells (CPCs) in diabetic cardiomyopathy. The authors demonstrated that the treatment with MHY-1684 may affect the activation and inhibition of mitochondrial dynamics-related signaling and mitochondrial function in response to ROS stress. In addition, the data allow concluding that the novel compound MHY-1684 acts as an ROS scavenger and might provide an effective therapeutic strategy for CPC-based cell therapy against diabetic cardiomyopathy.

C. He et al. investigated the effect of the antioxidant edaravone on the cardiac dysfunction during sepsis. The study showed that in a rat model of septic myocardial dysfunction, edaravone suppressed oxidative stress and protected the heart against septic myocardial injury and dysfunction through the induction of the HIF-1α/HO-1 pathway.

All of these highlighted studies, as well as the other manuscripts contained in this special issue, advance improvements on pathological statuses by using diverse antioxidant strategies. We firmly believe that these findings will be of relevance to research concerning OS, chronic diseases, and aging.

Conflicts of Interest

The authors declare that they have no conflicts of interest.

Acknowledgments

The editors thank all of the authors who submitted their research to this special issue. The editors also thank each reviewer for their valuable contributions. The lead guest editor thanks all of the collaborating guest editors for their critical and exhaustive reviews and support, which were critical for the successful publication of this special issue.

Claudio Cabello-Verrugio
Cristian Vilos
Raquel Rodrigues-Diez
Lisbell Estrada

Hindawi
Oxidative Medicine and Cellular Longevity
Volume 2018, Article ID 1393641, 10 pages
https://doi.org/10.1155/2018/1393641

Research Article

Epigallocatechin Gallate Attenuates Bladder Dysfunction via Suppression of Oxidative Stress in a Rat Model of Partial Bladder Outlet Obstruction

Meng Gu,[1] **Chong Liu**,[1] **Xiang Wan**,[1] **Tianye Yang**,[2] **Yanbo Chen**,[1] **Juan Zhou**,[1] **Qi Chen**,[1] **and Zhong Wang**[1]

[1]*Department of Urology, Shanghai Ninth People's Hospital Affiliated to Shanghai Jiao Tong University School of Medicine, Shanghai 200011, China*
[2]*Department of Emergency, Shanghai Ninth People's Hospital Affiliated to Shanghai Jiao Tong University School of Medicine, Shanghai 200011, China*

Correspondence should be addressed to Qi Chen; qiqi_chenqi@163.com and Zhong Wang; zhongwang2000@sina.com

Received 19 December 2017; Revised 29 April 2018; Accepted 14 May 2018; Published 22 July 2018

Academic Editor: Claudio Cabello-Verrugio

Purpose. To investigate the protective effect of epigallocatechin gallate (EGCG), a green tea extract, and its underlying mechanism on bladder dysfunction in a rat model of bladder outlet obstruction (BOO). *Materials and Methods*. Sprague-Dawley rats of BOO were surgically induced and followed by treatment with EGCG (5 mg/kg/day) or saline (control) via intraperitoneal injection. Cystometry was performed on four weeks postoperatively in conscious rats. H&E, Masson trichrome, and TUNEL staining were performed to observe tissue alterations. Oxidative stress markers were measured, and protein expression of Nrf2-ARE pathway was examined by immunohistochemistry and Western blotting. *Results*. Our data showed that EGCG could increase the peak voiding pressure and bladder compliance and prolong micturition interval of BOO rats compared with control and finally reduce the frequency of urinary. EGCG could ameliorate the increase of collagen fibers and ROS induced by obstruction and increase the activity of SOD, GSH-Px, and CAT. The level of cell apoptosis was decreased in BOO rats treated with EGCG compared with control, and caspase-3 expression was reduced as well. Moreover, EGCG could activate the Nrf2 expression with elevation of its target antioxidant proteins. *Conclusions*. EGCG alleviates BOO-induced bladder dysfunction via suppression of oxidative stress and activation of the protein expression of Nrf2-ARE pathway.

1. Introduction

Benign prostatic hyperplasia (BPH) characterized by gradually nonmalignant enlargement of prostate gland [1, 2] is a very common chronic disease in elderly men. As people age, most BPH patient will induce bladder outlet obstruction (BOO) with high bladder pressure and low flow [3]. BOO is a common disorder of the urinary tract that could affect quality of life and is a very rarely life-threatening disease but can induce significant structural and functional changes of the bladder, which in turn brings lower urinary tract symptoms (LUTS) including urinary frequency, urgency, nocturia, and urge incontinence [4]. BOO caused by BPH has become increasingly prevalent with age and been considered as the major public health problem that seriously affects the quality of life of patients and their partners.

As showed in previous studies, oxidative stress is considered to be one of the mechanisms that triggers reactions chain involved in the development and progression of BPH and leads to injured function of the bladder [5]. Oxidative stress occurs in the cellular environment when there is an imbalance between the production of reactive oxygen species (ROS) and the ability of biological systems to repair oxidative damage or neutralize the effects of reactive intermediates including peroxides and free radicals. Production of high levels of ROS causes a significant decrease in antioxidant defense mechanisms leading to protein, lipid, and DNA damage and subsequent disruption of cellular functions and

cell death but at lower levels induce subtle changes in intracellular signaling pathways. An increase in ROS may contribute to alter bladder function in aging [6]. Superoxide dismutase (SOD) is one of the cell's chief defenses against activated oxygen free radicals. Presenting in the peroxisomes of nearly all aerobic cells, catalase (CAT) act in association with SOD protects cells against free radical damage [7, 8]. SOD and CAT activities are associated with the shift from compensated to decompensated function of the bladder [7]. As a transcription factor, nuclear erythroid-related factor 2 (Nrf2) could promote expression of antioxidative genes through the antioxidant response element (ARE) to regulate cellular antioxidative responses and redox status [9]. It has been established in the literature that activation of the Nrf2-ARE pathway may ameliorate bladder dysfunction caused by bladder outlet obstruction [10].

As a major component of green tea, epigallocatechin-3-gallate (EGCG) has been studied for its antioxidative and anti-inflammatory properties. Reports revealed that pretreatment with EGCG could induce Nrf2 activation in cells as demonstrated by increasing expression and nuclear translocation of Nrf2 [11, 12]. Mechanical stretch and hypoxia have been reported to contribute to the functional and structural changes in the bladder after BOO, and previous studies have indicated that the activation of Nrf2 pathway by EGCG shows effective protection in various diseases. However, whether EGCG could protect bladder tissue by activating the Nrf2 pathway in the BOO model has not been well defined. Based on our previous study [10] that demonstrated the decrease of oxidative stress and activation of the Nrf2-ARE pathway may ameliorate bladder dysfunction induced by BOO, we explored the ability of EGCG to ameliorate bladder dysfunction by inhibiting oxidative stress via the regulation of the Nrf2-ARE pathway in a rat model of BOO in the present study.

2. Materials and Methods

2.1. BOO Model and Drug Treatment. BOO model of SD was established in adult male Sprague-Dawley rats (SD) weighing 240 to 260 g (Animal Center of the Shanghai Ninth People's Hospital of Shanghai Jiao Tong University School of Medicine, Shanghai, China) according to our previous method [10]. All animals were housed by two per cage in a room under controlled temperature, humidity, and 12-hour light/12-hour dark cycles with free access to food and water. The rats were allowed to acclimatize for at least five days before the experiment. All experimental procedures were approved by the Ethics Committee of Shanghai Jiao Tong University School of Medicine. The SD rats were randomly divided into three groups: the sham-operated group, the BOO group, and the BOO treated with EGCG (purity > 98%, Biotech Co. Ltd, China) group, and 8 rats were included in each group. BOO surgical operation was applied according to the method described previously in detail [13]. Briefly, the rats were anesthetized and then abdominal midline incision (about 1.0 cm) was made to expose the bladder and proximal urethra. The proximal urethra was loosely tied with the needle using 3–0 silk thread after a 19-G needle was placed around it after which the needle was removed and incision was closed. Sham operations were performed in an identical manner without tying the silk thread.

From the first day after operation, rats of the BOO + EGCG group received daily intraperitoneally injections of EGCG (5 mg/kg). EGCG was dissolved in PBS, and rats of the sham group and BOO group were given the same volume of PBS.

2.2. Cystometry Preparation and Cystometric Analysis. The cystometry preparation and cystometric analysis were performed four weeks after operation. A catheter was placed in the bladder of rats of all groups three days before cystometric analysis. As described in previous study, flaring the end of the polyethylene tubing 50 (PE-50) to become a balloon serves as an anchor to maintain the tube within the bladder [7, 11]. A 1 cm incision was made on the dorsum between the scapulas in anesthetized rats followed by developing a plane between the skin and the underlying muscle to create a tunnel around the ventral abdomen. Cystometry preparation was carried out as followed that rats were anesthetized and a 1 cm incision was made on the dorsum between the scapulas. Then, we developed a plane between the skin and the underlying muscle to create a tunnel around the ventral abdomen. After an abdominal midline incision was made to expose the bladder, we grasped the smooth end of the PE-50 tubing with the clamp and pull it back through the dorsum incision. Following the bulbed end was placed in the bladder dome and the purse string suture around the tubing was pulled tight, the dorsal and abdominal incisions were closed for cystometric analysis.

For cystometry, the conscious rats were placed in a metabolic cage, and the indwelling tubing was attached to a two-way valve that was connected to a pressure transducer as well as an infusion pump. Saline was infused into the bladder at a rate of 12 ml/h at room temperature in all groups. The cystometric parameters of maximal pressure, bladder capacity, and others were measured. The rats were euthanized after the experiment, and the bladder tissue was collected for further study.

2.3. Histological Examination and Immunohistochemical Staining. 5 μm sections were made after bladders being fixed in 4% paraformaldehyde and embedded in paraffin. Hematoxylin and eosin (H&E) staining was performed to observe general morphology of the bladders, and Masson trichrome staining was used to evaluate the level of tissue fibrosis. Immunohistochemical staining was also conducted as previously described in our study. Briefly, the sections were subjected with 10 mM sodium citrate buffer (pH 6.0) to heat for antigen retrieval. The primary antibodies of anti-Nrf2 (Abcam, Cambridge, UK), HO-1 (Abcam, Cambridge, UK), PCNA (CST, Danvers, MA, USA), secondary antibodies of goat-anti-rabbit IgG-HRP (DAKO, Denmark), goat-anti-mouse IgG-HRP (DAKO, Denmark), and DAB detection kit (DAKO, Denmark) were used according to the manufacturer's instructions. Histological analysis was performed by a pathologist in a blinded manner.

Table 1: Outcomes of cystometric parameters in conscious rats.

	Sham	BOO	BOO + EGCG
Peak voiding pressure	23.54 ± 2.13	42.4 ± 1.44*	55.16 ± 2.6*#
Capacity (ml)	1.15 ± 0.31	3.33 ± 0.38*	4.12 ± 0.49*
Compliance (μl/cm H_2O)	24.37 ± 3.12	13.17 ± 3.26*	21.36 ± 2.75#
Micturition interval (min)	3.67 ± 0.64	2.07 ± 0.47*	3.03 ± 1.41*#

*Significantly different versus the sham group ($P < 0.05$). #Significantly different versus the BOO group ($P < 0.05$).

2.4. Apoptosis Assay by TUNEL. The apoptosis level in the bladder smooth muscle was measured by the one-step TUNEL apoptosis assay kit (KeyGen Biotech, Nanjing, China) according to the manufacturer's instructions. In brief, the sections were regularly hydrated and immersed in 1% Triton X-100 followed by being incubated with proteinase K solution for 30 minutes. And the sections were reacted with TdT solution for 1 hour and then streptavidin-TRITC solution for 30 minutes in a humidified and dark chamber, respectively. Finally, DAB detection kit was used to stain the sections to observe and analyze apoptotic cells by a pathologist in a blinded manner.

2.5. MDA, GSH-Px, Total SOD (tSOD), ROS, and CAT Determination. According to our previous study [10], we choose some marker routine laboratory indexes of oxidative stress as malondialdehyde (MDA), glutathione peroxidase (GSH-Px), total superoxide dismutase (tSOD), and catalase activity (CAT) were conducted. The content of MDA, GSH-Px, total tSOD, and CAT in the bladder tissues was measured according to the manufacturer's protocols of the assay kit of MDA, tSOD, GSH-Px, and CAT (Nanjing Jiancheng Bioengineering Institute, Nanjing, China). Briefly, the maximum absorbance was at 532 nm based on thiobarbituric acid (TAB) method to detect MDA level, the tSOD activity was measured based on the combination of xanthine and xanthine oxidase and the absorbance was read at 550 nm, and the GSH-Px activity assay was performed using the enzyme-catalyzed reaction product (reduced glutathione) and the absorbance was recorded at 412 nm. To measure the CAT activity, hydrogen peroxide reacted with ammonium molybdate, and the absorbance at 405 nm was then detected. Considering accumulation of reactive oxygen species (ROS) occurs and leads to functional alterations and pathological conditions such as a bladder dysfunction developed with age [6, 14, 15]; ROS was also detected in our study. According to the procedure of the ROS assay kit (Sigma-Aldrich, MO, USA), DCFDA was used as fluorescent probe following by washing using assay buffer. Immediately after the excitation at a wavelength of 485 nm, the absorbance is read at 535 nm.

2.6. Western Blotting. Total protein was extracted from frozen bladder tissues selected randomly from each group ($n = 3$) by trypan blue in RIPA buffer containing protease inhibitors. Muscle lysates were centrifuged at 10000 ×g/min at 4°C for 10 min, and the supernatant was collected and used as total protein extracts. The nuclear protein was extracted according to the manufacturer's instructions of nuclear protein extraction kit (Beyotime Institute of Biotechnology, Shanghai, China). Following the steps outlined below, bladder tissues were cut in pieces and homogenized in cytoplasm protein extraction reagent containing protease inhibitors, the lysates were centrifuged (10000 ×g/min) at 4°C for 5 min, and then the precipitation was collected and mixed with nucleoprotein extraction reagent for 30 min on ice; after the lysates were centrifuged (10000 ×g/min) at 4°C for 10 min, the supernatant was collected and used as nuclear protein extracts. Protein concentrations were measured using BCA protein assay kit (Thermo Scientific, MA, USA). The samples were run on 10% SDS-polyacrylamide gels (20 μg/lane), and then, proteins were transferred to PVDF membranes by electroblotting (200 mA). PVDF membranes were incubated in 5% BSA for 2 hours at room temperature, followed by three 5 minutes washing in TBST. The PVDF membranes were then incubated overnight at 4°C with anti-Nrf2 (1 : 1000), HO-1 (1 : 1000), NQO1 (1 : 1000), Caspase-3 (CST, Danvers, MA, USA) (1 : 1000), GAPDH (CST, Danvers, MA, USA) (1 : 2000), and Lamin-B (CST, Danvers, MA, USA) (1 : 2000) antibodies. GAPDH and Lamin-B were used as internal normalizer. Then, the membranes were washed for 10 min three times in TBST and incubated with IgG-HRP antibody (1 : 2000) for 2 hours and finally examined by chemiluminescence.

2.7. Statistical Analysis. The values were presented as mean ± SD. SPSS 17.0 was used to evaluate the difference. Differences between groups were analyzed using one-way ANOVA with $P < 0.05$ considered significant.

3. Results

3.1. EGCG Ameliorated Voiding Dysfunction Induced by BOO. The cystometry results in each group are showed in Table 1 which were obtained according to the urodynamic curve (Figure 1). The voiding pressure was significantly increased in obstructed rats compared with sham rats. The peak voiding pressure in obstructed rats with EGCG treatment is higher than obstructed rats at the 4-week time point. Bladder capacity was significantly higher in BOO rats compared with sham rats. Rats in the BOO + EGCG group showed the highest bladder capacity among all groups. Bladder compliance decreased significantly at the 4-week time point after BOO. EGCG may rescue the compliance deterioration through increasing bladder capacity. It was found that the interval of micturition was shorter in BOO

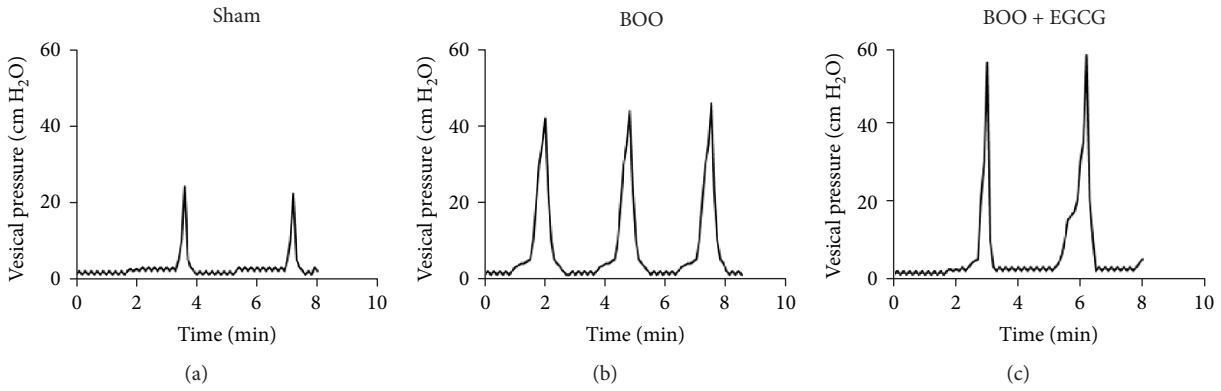

Figure 1: Effect of EGCG on urodynamic changes in conscious rats.

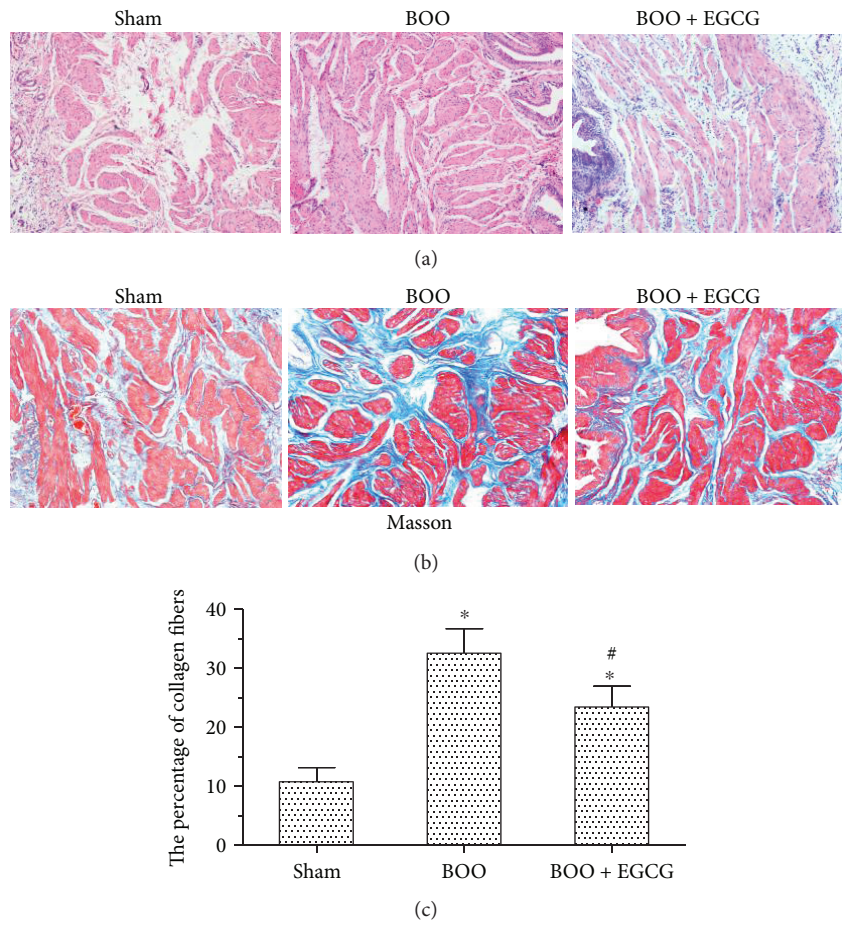

Figure 2: Effect of EGCG on bladder histological changes in BOO rats. Original magnification ×100. H&E (a) and Masson trichrome (b) staining in the sham, BOO, and BOO + EGCG bladders and (c) the percentage of collagen fibers in muscular layer in the sham, BOO, and BOO + EGCG bladders; $^{*}P < 0.05$, $n = 6$ versus the sham group; $^{\#}P < 0.05$, $n = 6$ versus the BOO group.

rats than in sham rats, and the micturition interval in BOO + EGCG rats was significantly increased compared to BOO rats.

3.2. Effect of EGCG in Bladder Detrusor of BOO Rats on Histological Changes. As showed in Figure 2(a), EGCG had some protective effect on BOO bladder based on H&E staining. BOO caused obvious histological changes, such as the structural damage of detrusor smooth muscle while treatment with EGCG significantly alleviated these histological changes in the bladders of BOO rats. The area ratio of collagen fibers was 10.77 ± 2.39, 32.53 ± 4.15, and 23.41 ± 3.53 in the sham group, BOO group, and BOO + EGCG group, respectively (Figure 2(c)). EGCG suppressed collagen fibers

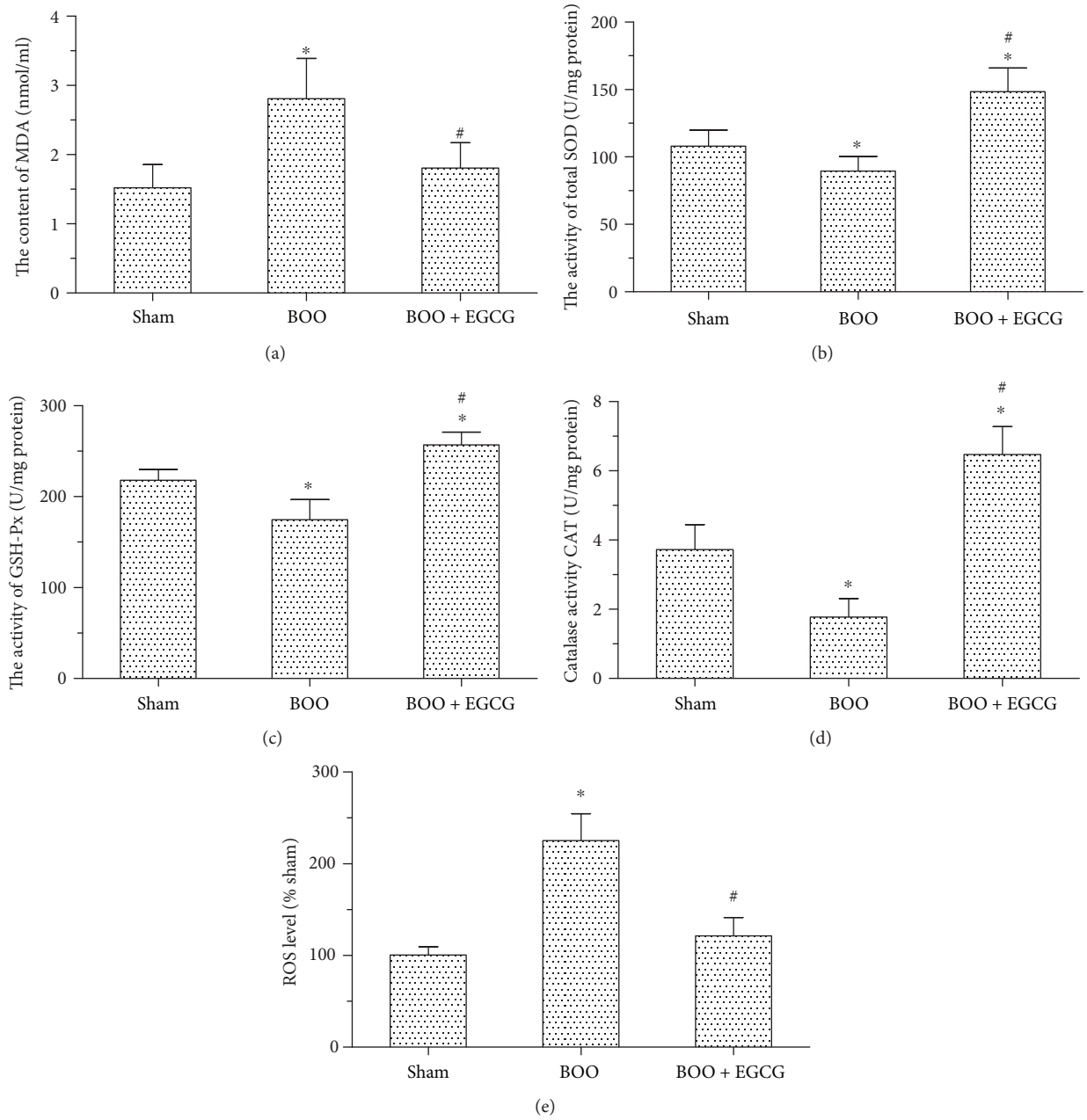

Figure 3: Effect of EGCG on oxidative stress in the bladder of BOO rats. (a) MDA level in the bladder of the three groups, $^{*}P < 0.05$ versus the sham group, $n = 6$; $^{\#}P < 0.05$ versus the BOO group, $n = 6$. (b) The activity of total SOD in the bladder of the three groups, $^{*}P < 0.05$ versus the sham group, $n = 6$; $^{\#}P < 0.05$ versus the BOO group, $n = 6$. (c) The activity of GSH-Px in the bladder of the three groups, $^{*}P < 0.05$ versus the sham group, $n = 6$; $^{\#}P < 0.05$ versus the BOO group, $n = 6$. (d) The activity of CAT in the bladder of the three groups, $^{*}P < 0.05$ versus the sham group, $n = 6$; $^{\#}P < 0.05$ versus the BOO group, $n = 6$. (e) The relative activity of ROS in the bladder of the three groups, $^{*}P < 0.05$ versus the sham group, $n = 6$; $^{\#}P < 0.05$ versus the BOO group, $n = 6$.

in the BOO + EGCG group as compared with that in the BOO group (Figure 2(b)).

3.3. EGCG Attenuated Oxidative Stress in the Bladder of BOO Rats. To evaluate the level of oxidative stress, we measured the content of MDA, SOD, GSH-Px, CAT activity, and ROS. As showed in Figure 3(a), the content of MDA in the bladder was significantly increased in BOO rats compared with sham rats (2.81 ± 0.58 versus 1.52 ± 0.33). Compared with BOO rats, EGCG treatments significantly inhibited MDA level increase induced by BOO (1.81 ± 0.37 versus 2.81 ± 0.58). The activities of tSOD and GSH-Px had some content of decrease in BOO rats compared with sham rats (89.65 ± 10.70 versus 108.06 ± 11.88; 174.71 ± 11.68 versus 218.18 ± 12.44), respectively. However, EGCG treatment could significantly increase the tSOD and GSH-Px activities in BOO rats (Figures 3(b) and 3(c)). As compared with sham rats, CAT activity significantly decreased in the BOO group

($P < 0.05$), which was upregulated by EGCG, even compared with the sham group (Figure 3(d)). In contrast to CAT, ROS was increased in the BOO group as compared with the sham group, and EGCG decreased it significantly ($P < 0.05$) (Figure 3(e)).

3.4. EGCG Inhibited Cell Apoptosis and Prompted Proliferation in the Bladder of BOO Rats. TUNEL staining was performed to explore the effect of EGCG on the cell apoptosis of the bladder in BOO rats. The number of apoptotic cells in the bladder of BOO rats was markedly increased compared with sham rats ($p < 0.01$), whereas EGCG treatment significantly decreased the number of apoptotic cells in the bladder of BOO rats ($p < 0.05$) (Figures 4(a) and 4(b)). Western blotting showed that the caspase-3 expression was significantly increased in the bladder of BOO rats; however, the expression of caspase-3 was decreased in BOO + EGCG rats (Figure 4(c)) which was in accordance with the result of TUNEL staining. Moreover, the expression of PCNA measured by the immunohistochemical staining showed that EGCG caused significantly increase on cell proliferation in the BOO + EGCG group compared with the BOO group (Figure 4(d)).

3.5. EGCG Affected Protein Expression of the Nrf2-ARE Pathway. Considering that Nrf2 is a vital mediator in regulating cellular antioxidative response, we explored the effect of EGCG on Nrf2 and its downstream target proteins in our study. The expression of Nrf2 measured by immunohistochemical staining was significantly higher in the muscular layers of the bladder in the BOO + EGCG group compared with the BOO group (Figure 5(a)). The expression of Nrf2 in the cell (t-Nrf2) and nucleus (n-Nrf2) was also measured by Western blotting. It is shown in Figures 5(b) and 5(c) that Nrf2 expression (t-Nrf2 and n-Nrf2) was significantly increased in the bladder of the BOO + EGCG group compared with the BOO group, and the t-Nrf2 was increased in the bladder of the BOO group compared with the sham group. It was worth noting that our results demonstrated the expression of Nrf2 was mainly located in the nucleus of the bladder cells while the expression of Nrf2 in the nucleus showed no significant difference between the BOO group and the sham group. We then detected the expression of Nrf2's downstream target proteins as HO-1 and NOQ1 to investigate its antioxidative function. Our data indicated that the expression of HO-1 was increased in the BOO + EGCG group compared with the BOO group, which was consistent with the result of n-Nrf2 expression (Figures 5(d) and 5(e)). The level of NQO1 in the BOO group was higher than that in the sham group, but lower than that in the BOO + EGCG group (Figure 5(f)).

4. Discussion

As investigated in animal models, chronic bladder ischemia might produce oxidative leading to denervation of the bladder and the expression of tissue-damaging molecules in the bladder wall, which could be responsible for the development of bladder hyperactivity progressing to bladder underactivity [16, 17]. It is also suggested that oxidative stress plays a critical role in bladder outlet obstruction-mediated bladder dysfunction [16, 17]. BOO-induced bladder remodeling in a rat model is similar to that in patients with BPH who suffered from bladder outlet obstruction. It was showed in our previous study that rats of BOO model were useful models to explore structural and functional alterations in the bladder [10]. Therefore, exploring good ways to reduce oxidative stress of bladder caused by BOO has been considerably attractive.

EGCG is a major catechin in green tea with functions of antioxidant, antiproliferative, anti-inflammatory, and attenuating metabolic syndrome, without adverse effects [18, 19]. Hsieh et al. reported that EGCG can attenuate the prostate enlargement in BPH rats accompanied with metabolic syndrome induced by high-fat diet combined with testosterone injection [10]. For human, according to reports in the literature, ten days' repeated administration of oral doses of EGCG of up to 800 mg per day was found to be safe and very well tolerated. The content of EGCG in green tea is about 10%. No obvious side effects occur in the amount of 20 cups of green tea per day [20]. In the present study, we investigated the effect of EGCG on BOO-induced bladder dysfunction in vivo and the daily intraperitoneal injection dose (5 mg/kg EGCG) was used which was similar to the dose that has been proved effective in other's study [10, 21].

We performed urodynamic studies in conscious rats of BOO to accurately reflect the real situation. The cystometric parameters such as bladder capacity, maximal pressure, compliance, and micturition interval were measured; we found that the micturition interval, capacity, and compliance were significantly increased, and the peak voiding pressure had some extent of increase by treatment with EGCG in BOO rats. The histological staining showed that bladder smooth muscle bundles were severely damaged and collagen deposition was increased in BOO rats. This increase of collagen deposition was suppressed by EGCG treatment for 4 weeks in BOO model rats. Our results indicated that there is an inverse relationship between bladder compliance and collagen fibers, and EGCG could protect bladder from BOO-induced dysfunction and morphological damage.

In order to investigate antioxidant activity of EGCG in the bladder of BOO rats, we measured MDA level of bladder tissue in the three groups. MDA level is used as an indicator of lipid peroxidation, as lipids in the cell membrane are destroyed to generate MDA in an amount proportional to the degree of tissue destruction. Our results showed that BOO significantly increased the level of MDA in the bladder. It was also showed in our results that the increase in the level of MDA was significantly reduced in BOO rats treated with EGCG which corresponds with other antioxidants [9]. We found that the activities of some redox status markers, such as GSH-Px and total SOD, were significantly decreased in the BOO group compared with the sham group which is similar to the forecast result and other literature [10], and EGCG significantly enhanced the activities of these markers in BOO rats. Our data also showed that EGCG could upregulate CAT activity and downregulate ROS induced by BOO

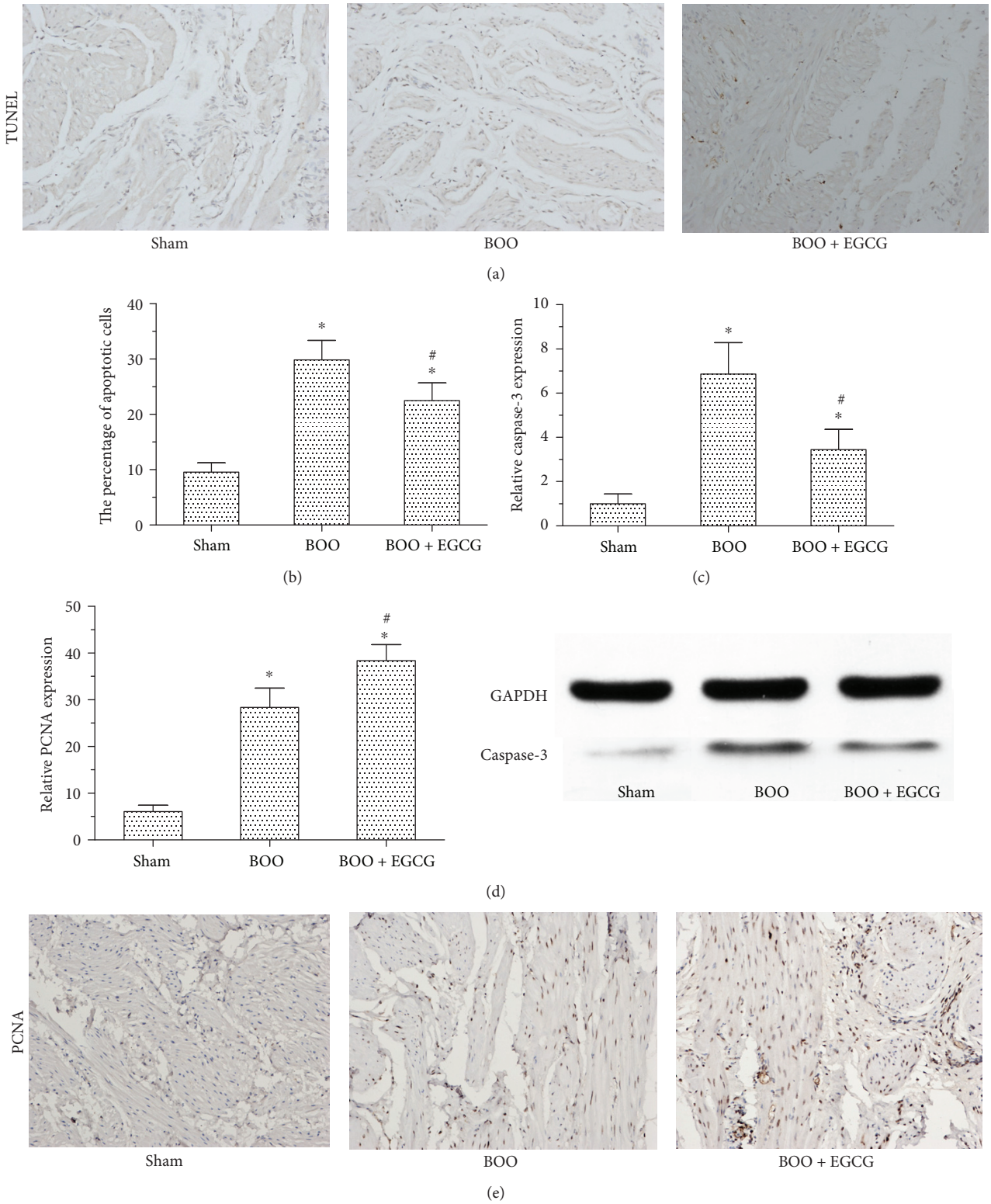

Figure 4: Effect of EGCG on cell apoptosis and proliferation in BOO rats. (a) TUNEL staining showed the cell apoptosis level of the bladder in all the three groups. (b) The statistical results of TUNEL staining in the three groups. $^{*}P < 0.01$, $n = 6$ versus the sham group; $^{\#}P < 0.01$, $n = 6$ versus the BOO group. (c) The protein expression of caspase-3 in the bladder of the three groups. (d-e) The statistical results of PCNA in the bladder of the three groups using immunohistochemical staining to show cell proliferation. $^{*}P < 0.05$ versus the sham group; $^{\#}P < 0.05$ versus the BOO group. Original magnification ×200 for TUNEL and immunohistochemical staining.

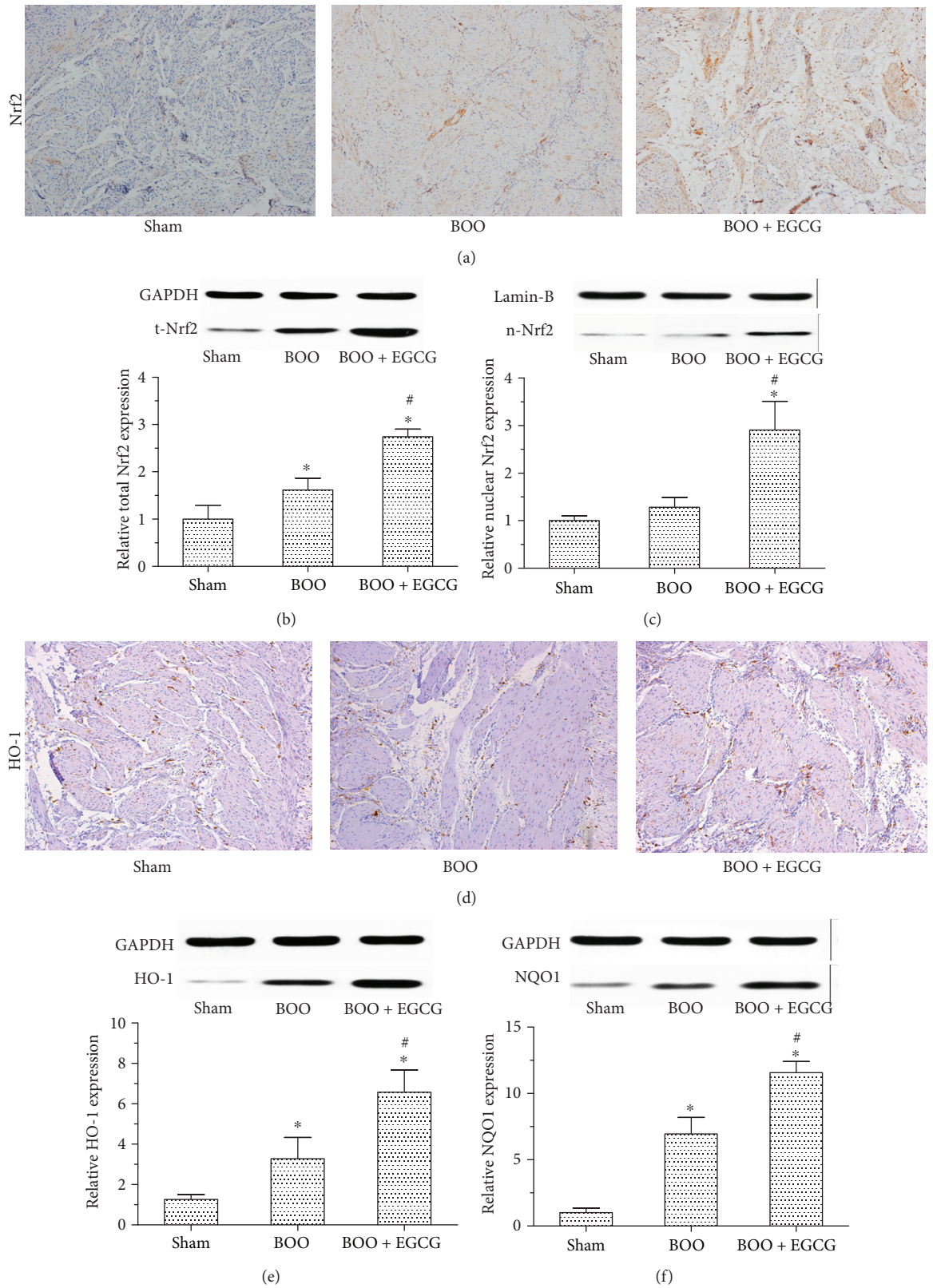

Figure 5: Effect of EGCG on protein expression of the Nrf2-ARE pathway. (a) The immunohistochemical staining of Nrf2. Protein expression of total Nrf2 (t-Nrf2) and nuclear Nrf2 (n-Nrf2) in the bladder of the three groups measured by Western blotting is shown in (b) and (c). The protein expression of HO-1 measured by immunohistochemical staining and Western blotting in the bladder of the three groups is shown in (d) and (e). (e) The protein expression of NQO1 in the bladder of the three groups. $^{*}P < 0.05$ versus the sham group; $^{\#}P < 0.05$ versus the BOO group.

compared with the sham group. It was worth noting that increase of CAT activity in bladder tissue of BOO rats after 4 weeks was similar to our previous study [22], while not all match the other report that CAT activity increased after 2–4 weeks of obstruction, but it decreased markedly in the rabbit bladder with decompensation 8 weeks after partial bladder outlet obstruction (PBOO) [7], which need us to further explore. All the results may indicate that EGCG could alleviate oxidative stress by increasing the activities of antioxidative enzymes in BOO rats.

It is well known that cell apoptosis plays a vital role in leading to bladder dysfunction in BOO model. In our study, TUNEL staining results manifested that a significant reduction of the number of apoptotic cells was found in the treatment of EGCG in BOO rats; it is also found that the expression of caspase-3 in the bladder was decreased in BOO rats when treated with EGCG. These results suggested that EGCG as an antioxidant might protect bladder against BOO-induced apoptosis via decreasing the expression of caspase-3. Meanwhile, the effect of EGCG on cell proliferation by PCNA staining was also measured. Results showed that the cell proliferation level was significantly higher in the bladder of BOO rats with EGCG treatment.

EGCG reported recently can exert a protective effect on rats with obstructive nephropathy by activating the Nrf2 signaling pathway. The H_2O_2-exposed hMSCs showed cellular senescence with significantly increased protein levels of acetyl-p53 and acetyl-p21 in comparison with the control hMSCs which was prevented by pretreatment with EGCG [21, 23]. By contrast, in Nrf2-knockdown hMSCs, EGCG lost its antioxidant effect, exhibiting high levels of acetyl-p53 and acetyl-p21 following EGCG pretreatment and H_2O_2 exposure. This indicates that Nrf2 may be involved in the antisenescent effect of EGCG in hMSCs [10]. Taken together, these findings suggested the important role of EGCG in preventing oxidative stress-induced cellular senescence and apoptosis through Nrf2 activation. Antioxidants could ameliorate bladder dysfunction in BOO rats according to our previous study [10]; the effect of EGCG on ameliorating bladder dysfunction in BOO model and changing the Nrf2-ARE signaling pathway was investigated in present study. By immunohistochemical staining and Western blotting, we found that the expression of Nrf2 protein in the bladder of BOO rats with EGCG treatment was significantly increased compared to BOO rats. In addition, the level of Nrf2 in the nucleus was markedly increased in the BOO rats when treated with EGCG. The result indicated that EGCG could promote the transportation of Nrf2 into nucleus and the transcription of its target antioxidant genes. We next measured the expression level of HO-1 and NQO1, the downstream genes of Nrf2-ARE pathway by Western blotting. The levels of HO-1 and NQO1 increased significantly in BOO rats after EGCG treatment. Above all, our study suggested that EGCG could promote Nrf2's translocation into the nucleus and the expression of its target antioxidant genes, which ameliorated the oxidative stress in BOO rats.

In conclusion, our study suggested that EGCG has significant protective effects against oxidative stress and could ameliorate bladder dysfunction which may be activation of the Nrf2-ARE pathway and suppressing cellular apoptosis in the bladder of BOO rats.

Abbreviations

ARE: Antioxidant response element
BOO: Bladder outlet obstruction
BPH: Benign prostatic hyperplasia
GSH-Px: Glutathione peroxidase
CAT: Catalase activity
H&E: Hematoxylin and eosin
HO-1: Heme oxygenase-1
LUTS: Lower urinary tract symptoms
MDA: Malondialdehyde
NQO1: NAD(P)H : quinone oxidoreductase 1
Nrf2: Nuclear erythroid-related factor 2
PE-50: Polyethylene tubing 50
ROS: Reactive oxygen species
EGCG: Epigallocatechin-3-gallate
SOD: Superoxide dismutase
TUNEL: TdT-mediated dUTP nick end labeling.

Conflicts of Interest

The authors declare that they have no competing interests.

Authors' Contributions

Meng Gu and Chong Liu contributed equally to this study.

Acknowledgments

This research was supported by the Program of Shanghai City Committee of Science and Technology (15DZ1941502 and 15DZ1941503), Shanghai Pudong New Area Health and Family Planning Project (no. PW2013D-3), Key Disciplines Group Construction Project of Pudong Health Bureau of Shanghai (PWZxq2014-11), and Program for Outstanding Medical Academic Leader and Speciality Construction Project of Pudong Health and Family Planning Commission of Shanghai (no. PWZz2013-16).

References

[1] J. L. H. Ruud Bosch, W. C. J. Hop, W. J. Kirkels, and F. H. Schröder, "Natural history of benign prostatic hyperplasia: appropriate case definition and estimation of its prevalence in the community," *Urology*, vol. 46, no. 3, Supplement 1, pp. 34–40, 1995.

[2] J. M. Fitzpatrick, "The natural history of benign prostatic hyperplasia," *BJU International*, vol. 97, no. s2, pp. 3–6, 2006.

[3] S. Madersbacher, G. Alivizatos, J. Nordling, C. R. Sanz, M. Emberton, and J. J. M. C. H. de la Rosette, "EAU 2004 guidelines on assessment, therapy and follow-up of men with lower urinary tract symptoms suggestive of benign prostatic obstruction (BPH guidelines)," *European Urology*, vol. 46, no. 5, pp. 547–554, 2004.

[4] M. Oelke, R. Kirschner-Hermanns, N. Thiruchelvam, and J. Heesakkers, "Can we identify men who will have complications from benign prostatic obstruction (BPO)? ICI-RS

2011," *Neurourology and Urodynamics*, vol. 31, no. 3, pp. 322–326, 2012.

[5] P. L. Minciullo, A. Inferrera, M. Navarra, G. Calapai, C. Magno, and S. Gangemi, "Oxidative stress in benign prostatic hyperplasia: a systematic review," *Urologia Internationalis*, vol. 94, no. 3, pp. 249–254, 2015.

[6] L. Nocchi, D. M. Daly, C. Chapple, and D. Grundy, "Induction of oxidative stress causes functional alterations in mouse urothelium via a TRPM8-mediated mechanism: implications for aging," *Aging Cell*, vol. 13, no. 3, pp. 540–550, 2014.

[7] A. Guven, C. Kalorin, B. Onal et al., "Novel biomarkers of bladder decompensation after partial bladder obstruction," *Neurourology and Urodynamics*, vol. 26, no. 7, pp. 1036–1042, 2007.

[8] I. N. Zelko, T. J. Mariani, and R. J. Folz, "Superoxide dismutase multigene family: a comparison of the CuZn-SOD (SOD1), Mn-SOD (SOD2), and EC-SOD (SOD3) gene structures, evolution, and expression," *Free Radical Biology & Medicine*, vol. 33, no. 3, pp. 337–349, 2002.

[9] B. Zhang, B. Wang, S. Cao, and Y. Wang, "Epigallocatechin-3-gallate (EGCG) attenuates traumatic brain injury by inhibition of edema formation and oxidative stress," *The Korean Journal of Physiology & Pharmacology*, vol. 19, no. 6, pp. 491–497, 2015.

[10] J. T. Hsieh, K. L. Kuo, S. H. Liu et al., "Epigallocatechin gallate attenuates partial bladder outlet obstruction-induced bladder injury via suppression of endoplasmic reticulum stress-related apoptosis—in vivo study," *Urology*, vol. 91, pp. 242.e1–242.e9, 2016.

[11] R. Kanlaya, S. Khamchun, C. Kapincharanon, and V. Thongboonkerd, "Protective effect of epigallocatechin-3-gallate (EGCG) via Nrf 2 pathway against oxalate-induced epithelial mesenchymal transition (EMT) of renal tubular cells," *Scientific Reports*, vol. 6, no. 1, article 30233, 2016.

[12] J. Oliva, F. Bardag-Gorce, B. Tillman, and S. W. French, "Protective effect of quercetin, EGCG, catechin and betaine against oxidative stress induced by ethanol in vitro," *Experimental and Molecular Pathology*, vol. 90, no. 3, pp. 295–299, 2011.

[13] S. Matsumoto, M. Watanabe, K. Hashizume et al., "Effects of chronic treatment with cilostazol, a phosphodiesterase 3 inhibitor, on female rat bladder in a partial bladder outlet obstruction model," *Urology*, vol. 83, no. 3, pp. 675.e7–675.e11, 2014.

[14] P. J. Gomez-Pinilla, M. J. Pozo, and P. J. Camello, "Aging impairs neurogenic contraction in guinea pig urinary bladder: role of oxidative stress and melatonin," *American Journal of Physiology-Regulatory, Integrative and Comparative Physiology*, vol. 293, no. 2, pp. R793–R803, 2007.

[15] K. C. Kregel and H. J. Zhang, "An integrated view of oxidative stress in aging: basic mechanisms, functional effects, and pathological considerations," *American Journal of Physiology-Regulatory, Integrative and Comparative Physiology*, vol. 292, no. 1, pp. R18–R36, 2007.

[16] M. Nomiya, K. E. Andersson, and O. Yamaguchi, "Chronic bladder ischemia and oxidative stress: new pharmacotherapeutic targets for lower urinary tract symptoms," *International Journal of Urology*, vol. 22, no. 1, pp. 40–46, 2015.

[17] J. Camões, A. Coelho, D. Castro-Diaz, and F. Cruz, "Lower urinary tract symptoms and aging: the impact of chronic bladder ischemia on overactive bladder syndrome," *Urologia Internationalis*, vol. 95, no. 4, pp. 373–379, 2015.

[18] R. A. Isbrucker, J. A. Edwards, E. Wolz, A. Davidovich, and J. Bausch, "Safety studies on epigallocatechin gallate (EGCG) preparations. Part 2: dermal, acute and short-term toxicity studies," *Food and Chemical Toxicology*, vol. 44, no. 5, pp. 636–650, 2006.

[19] P. Tay, C. Tan, F. Abas, H. Yim, and C. Ho, "Assessment of extraction parameters on antioxidant capacity, polyphenol content, epigallocatechin gallate (EGCG), epicatechin gallate (ECG) and iriflophenone 3-C-β-glucoside of agarwood *(Aquilaria crassna)* young leaves," *Molecules*, vol. 19, no. 8, pp. 12304–12319, 2014.

[20] U. Ullmann, J. Haller, J. D. Decourt, J. Girault, V. Spitzer, and P. Weber, "Plasma-kinetic characteristics of purified and isolated green tea catechin epigallocatechin gallate (EGCG) after 10 days repeated dosing in healthy volunteers," *International Journal for Vitamin and Nutrition Research*, vol. 74, no. 4, pp. 269–278, 2004.

[21] P. Zhou, J. F. Yu, C. G. Zhao, F. X. Sui, X. Teng, and Y. B. Wu, "Therapeutic potential of EGCG on acute renal damage in a rat model of obstructive nephropathy," *Molecular Medicine Reports*, vol. 7, no. 4, pp. 1096–1102, 2013.

[22] C. Liu, H. Xu, S. Fu et al., "Sulforaphane ameliorates bladder dysfunction through activation of the Nrf2-ARE pathway in a rat model of partial bladder outlet obstruction," *Oxidative Medicine and Cellular Longevity*, vol. 2016, Article ID 7598294, 12 pages, 2016.

[23] H. S. Zhang, T. C. Wu, W. W. Sang, and Z. Ruan, "EGCG inhibits Tat-induced LTR transactivation: role of Nrf2, AKT, AMPK signaling pathway," *Life Sciences*, vol. 90, no. 19-20, pp. 747–754, 2012.

Hindawi
Oxidative Medicine and Cellular Longevity
Volume 2018, Article ID 4321714, 27 pages
https://doi.org/10.1155/2018/4321714

Review Article

Cellular Stresses and Stress Responses in the Pathogenesis of Insulin Resistance

Arnold N. Onyango

Department of Food Science and Technology, Jomo Kenyatta University of Agriculture and Technology, P.O. Box 62000, Nairobi 00200, Kenya

Correspondence should be addressed to Arnold N. Onyango; arnold.onyango@jkuat.ac.ke

Received 1 January 2018; Accepted 18 February 2018; Published 9 July 2018

Academic Editor: Claudio Cabello-Verrugio

Insulin resistance (IR), a key component of the metabolic syndrome, precedes the development of diabetes, cardiovascular disease, and Alzheimer's disease. Its etiological pathways are not well defined, although many contributory mechanisms have been established. This article summarizes such mechanisms into the hypothesis that factors like nutrient overload, physical inactivity, hypoxia, psychological stress, and environmental pollutants induce a network of cellular stresses, stress responses, and stress response dysregulations that jointly inhibit insulin signaling in insulin target cells including endothelial cells, hepatocytes, myocytes, hypothalamic neurons, and adipocytes. The insulin resistance-inducing cellular stresses include oxidative, nitrosative, carbonyl/electrophilic, genotoxic, and endoplasmic reticulum stresses; the stress responses include the ubiquitin-proteasome pathway, the DNA damage response, the unfolded protein response, apoptosis, inflammasome activation, and pyroptosis, while the dysregulated responses include the heat shock response, autophagy, and nuclear factor erythroid-2-related factor 2 signaling. Insulin target cells also produce metabolites that exacerbate cellular stress generation both locally and systemically, partly through recruitment and activation of myeloid cells which sustain a state of chronic inflammation. Thus, insulin resistance may be prevented or attenuated by multiple approaches targeting the different cellular stresses and stress responses.

1. Introduction

The hormone insulin plays an important role in maintaining physiological levels of blood glucose, through various effects on insulin target cells. In endothelial cells, it promotes the release of nitric oxide and endothelin, which, respectively, promote vasodilation and vasoconstriction, and the combined vasodilatory and vasoconstrictive effects improve the distribution of blood glucose to target organs such as skeletal muscles [1]. It promotes glycogen synthesis in hepatocytes, skeletal myocytes, and adipocytes [2, 3], downregulates the expression of gluconeogenetic enzymes in hepatocytes, and promotes glucose uptake through the GLUT 4 receptor in skeletal myocytes and adipocytes [2, 3]. In specific types of hypothalamic neurons, it inhibits the expression of orexigenic neuropeptides such as neuropeptide Y (NYP) or agouti-related peptide (AgRP) and thereby contributes to decreased food intake [4–8]. Insulin also inhibits food intake by promoting expression of anorexigenic neuropeptides such as proopiomelanocorticotropin (POMC) and cocaine- and amphetamine-regulated transcript (CaRT) in the arcuate nucleus, which together promote the activity of α-melanocyte-stimulating hormone in neurons in the paraventricular nucleus (4–8). Besides inhibiting AgRP synthesis, insulin-induced hyperpolarization of the AgRP-expressing arcuate neurons reduces the firing rate of these neurons and results in the generation and transmission of signals from the motor nucleus of the vagus nerve to the liver, resulting in increased hepatic interleukin 6 (IL-6) production, IL-6-mediated activation of signal transducer and activator of transcription 3 (STAT-3), and STAT-3-mediated decrease in the expression of gluconeogenic genes such as glucose-6-phosphatase and phosphoenol pyruvate carboxykinase (PEPCK) [9–12].

Insulin resistance refers to a condition in which insulin-responsive cells undergo a less than normal response to insulin, such as a reduced activation of endothelial nitric oxide synthase in endothelial cells [13]. It involves disruption of specific events in the insulin signaling pathways. Insulin

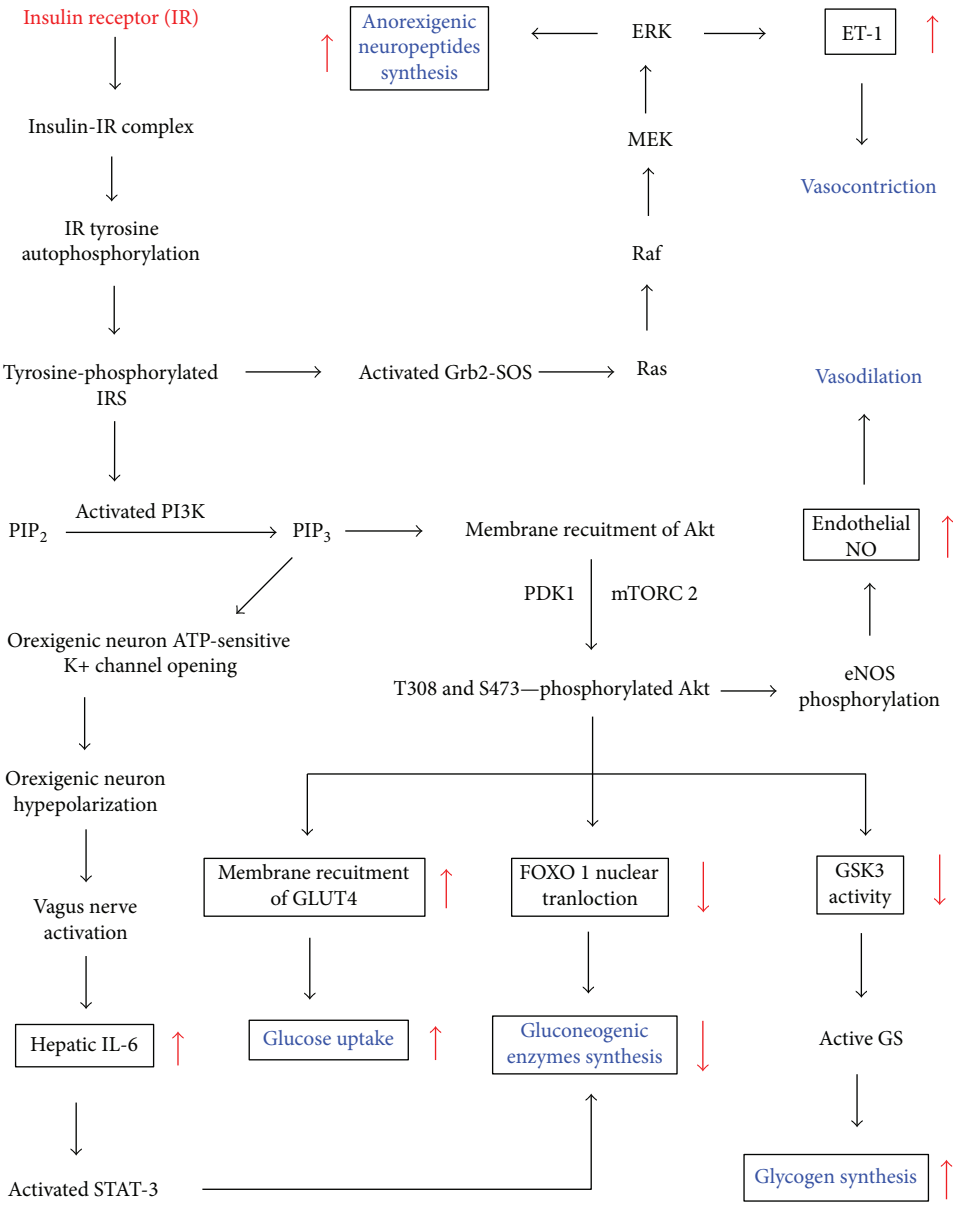

Figure 1: Insulin signaling pathways via the insulin receptor (IR) and insulin receptor substrates (IRS) [1–4, 9–12]. ERK: extracellular signal-regulated kinase; eNOS: endothelial nitric oxide synthase; FOXO: forkhead box O transcription factor; GLUT 4: glucose transporter 4; Grb2-SOS: growth factor receptor-bound 2- (Grb2-) son of sevenless (Sos) protein complex; GS: glycogen synthase; GSK3: glycogen synthase kinase 3; IL-6: interleukin 6; MEK: MAPK (mitogen-activated protein kinase)/ERK kinase; mTORC 2: mammalian target of rapamycin 2; NO: nitric oxide; PDK 1: 3-phosphoinositide-dependent kinase-1; PIP_2: phosphatidyl inositol 4,5-biphosphate; PIP_3: phosphatidyl inositol 3,4,5-triphosphate; STAT-3: signal transducer and activator of transcription 3.

signaling begins with insulin binding to the insulin receptor (IR), a receptor tyrosine kinase, which then undergoes autophosphorylation of various intracellular tyrosine residues, resulting in the recruitment and tyrosine phosphorylation of adaptor proteins including insulin receptor substrates (IRS) such as IRS1 and IRS2 (Figure 1).

Signaling downstream of IRS occurs by several pathways (Figure 1). One such pathway sequentially involves activation of phosphatidyl inositol 3-kinase (PI3K); conversion of phosphatidyl inositol 4,5-biphosphate (PIP2) to phosphatidyl inositol 3,4,5-triphosphate (PIP_3); recruitment of Akt (protein kinase B (PKB)) to the plasma membrane; phosphorylation of Akt by 3-phosphoinositide-dependent kinase-1 (PDK 1) and mammalian target of rapamycin complex 2 (mTORC 2); and Akt-mediated phosphorylation of a number of downstream protein substrates that induce effects such as activation of glycogen synthase (GS) in adipocytes, skeletal myocytes, and hepatocytes, translocation of glucose transporter 4 (GLUT 4) to the plasma membrane of adipocytes and skeletal myocytes, phosphorylation of the forkhead transcription factor (FOXO 1) to inhibit expression of gluconeogenic enzymes in hepatocytes, or activation of endothelial nitric oxide synthase in endothelial cells [1–3, 13] (Figure 1). Akt also activates mTORC 1 which not only is

involved in feedback inhibition of IRS but also inhibits synthesis of orexigenic neuropeptides by hypothalamic neurons (not shown) [14].

In another pathway which involves orexigenic (AgRP-producing) hypothalamic neurons, PI3K promotes opening of ATP-sensitive K+ channels, resulting in sequential hyperpolarization of these neurons, transmission of signals from the vagus nerve to the liver, increased hepatic IL-6 synthesis, activation of STAT-3, and decreased expression of gluconeogenic enzymes (Figure 1) [9–12]. On the other hand, insulin-mediated upregulation of the production of anorexigenic neuropeptides by hypothalamic neurons proceeds through IRS-mediated activation of the growth factor receptor-bound 2- (Grb2-) son of sevenless (Sos) protein complex (Grb2-Sos) and downstream activation of the Ras-Raf-MEK-ERK pathway [4]. In endothelial cells, ERK promotes the synthesis of endothelin-1 [1].

Because insulin resistance contributes to the development of noncommunicable diseases such as diabetes, cardiovascular disease, fatty liver disease, Alzheimer's disease, and impaired lung function [12, 13, 15–18], much effort has been directed toward understanding the mechanisms of its pathogenesis through studies involving cell cultures, animal models, and clinical studies. Cell cultures of hepatocytes, adipocytes, skeletal muscle cells, endothelial cells, or neurons incubated with palmitate or high sugar concentrations develop insulin resistance [19–26]. Some of the cellular events and mechanisms that have been shown to be involved in the development of insulin resistance in these cells both in vitro and in vivo include (i) toll-like receptor 4 (TLR4) and associated inhibitor of kappa B kinase- (IKK-) nuclear factor kappa B (NF-κB) signaling [27–31]; (ii) advanced glycation end products (AGEs) or uric acid-induced receptor for AGE (RAGE) signaling via NF-κB [30, 32–34]; (iii) oxidized low-density lipoprotein- (oxLDL-) mediated RAGE or Lox-1 signaling and the resultant activation of NF-κB and formation of peroxynitrite [30, 35, 36]; (iv) upregulation of NADPH oxidase (Nox) expression and activity [20, 21, 30, 37–39]; (v) increased mitochondrial reactive oxygen species (ROS) generation [30, 40]; (vi) upregulation of inducible nitric oxide synthase (INOS) [30, 41–43]; (vii) increased diacylglycerol synthesis [30, 44]; (viii) increased ceramide synthesis [30, 45, 46]; (ix) activation of protein kinase C (PKC) isoforms [30, 37, 47]; (x) activation of mitogen-activated protein kinases (MAPKs) such as c-Jun N-terminal kinase (JNK), p38 MAPK, and extracellular signal-regulated kinase (ERK) [20, 28, 30]; (xi) endoplasmic reticulum stress and the unfolded protein response [30, 43, 48–50]; (xii) dysregulation of the heat shock response [51–53]; (xiii) autophagy dysregulation [54]; (xiv) apoptosis [55]; (xv) p53 activation [56]; and (xvi) inflammasome activation [57, 58]. Thus, insulin resistance is regarded as a complex disorder that defies a single etiological pathway [59].

This review summarizes the above mechanisms into a unifying hypothesis that the pathogenesis of insulin resistance involves generation of oxidative stress, nitrosative stress, carbonyl stress, endoplasmic reticulum stress, and genotoxic stress through interconnected pathways; induction of various responses to these stresses, such as the unfolded protein response (UPR), the ubiquitin proteasome pathway (UPP), DNA damage response (DDR), the NRLP3 inflammasome, and apoptosis; and the dysregulation of stress responses such as autophagy, heat shock response, and nuclear factor erythroid-2-related factor 2 (Nrf2) signaling in insulin target cells (as exemplified in Figure 2). Each of the stresses, stress responses, and stress response dysregulations contributes to insulin resistance in multiple ways.

2. Pathways to Cellular Stresses in Insulin Target Cells

2.1. Pathways to Oxidative and Nitrosative Stresses in Response to Overnutrition, Physical Inactivity, Hypoxia, Psychological Stress, or Environmental Pollutants. As illustrated in Figure 2, cell surface receptors such as the TLR4, RAGE, Lox-1, and angiotensin receptor type 1 (AT_1) are involved in signaling pathways that generate oxidative stress and nitrosative stress.

A high-fat or high-fructose diet promotes the growth of gram-negative bacteria in the colon, resulting in endotoxemia and the release of enteric lipopolysaccharide (LPS) into blood plasma [60, 61]. LPS is a direct ligand for TLR4 and induces TLR4-dependent oxidative stress and inhibition of insulin signaling in both peripheral insulin target cells and hypothalamic neurons [28, 30, 62, 63]. TLR4 signaling via MyD88 and IRAK 4 leads to the activation of IKK [28, 30, 64]. One of the most important targets of IKK activation is NF-κB, which, for example, was found to be essential for palmitate-induced insulin resistance in C2C12 skeletal muscle cells [65]. NF-κB induces expression of protein tyrosine phosphatase B (PTPB), a negative regulator of the insulin receptor [66] and proinflammatory genes such as tumor necrosis factor-α (TNF-α), interleukin 1β (IL-1β), and interleukin 6 (IL-6) [67]. It also upregulates the expression of Nox and iNOS, which produce superoxide anions (O_2^-) and nitric oxide (NO), respectively [28–30, 68, 69]. Superoxide anions are rapidly converted to hydrogen peroxide (H_2O_2) by superoxide dismutase (SOD) [70]. Superoxide anions also rapidly react with NO to form peroxynitrite ($OONO^-$) [70], which reacts with hydrogen peroxide (H_2O_2) to form singlet oxygen ($^1O_2$) [30, 71], which in turn reacts with biomolecules such as lipids and proteins to form organic hydroperoxides (ROOH) [30]. Excessive production of reactive oxygen species (ROS) such as superoxide anions, hydrogen peroxide, organic hydroperoxides, and singlet oxygen results in oxidative stress when the ROS outweigh the cellular antioxidant capacity [72]. Likewise, excessive formation of peroxynitrite results in nitrosative stress. NF-κB-dependent induction of iNOS and Nox may further contribute to mitochondrial oxidative and nitrosative stresses. This is because, even when H_2O_2 and NO are generated extramitochondrially, they readily enter the mitochondria and induce electron leakage from the electron transport chain (ETC), thus promoting the generation of mitochondrial superoxide anions, H_2O_2, peroxynitrite, singlet oxygen, and lipid hydroperoxides [30, 70].

The nonenzymatic reaction of sugars with proteins (Maillard reaction) leads to the formation of hydrogen

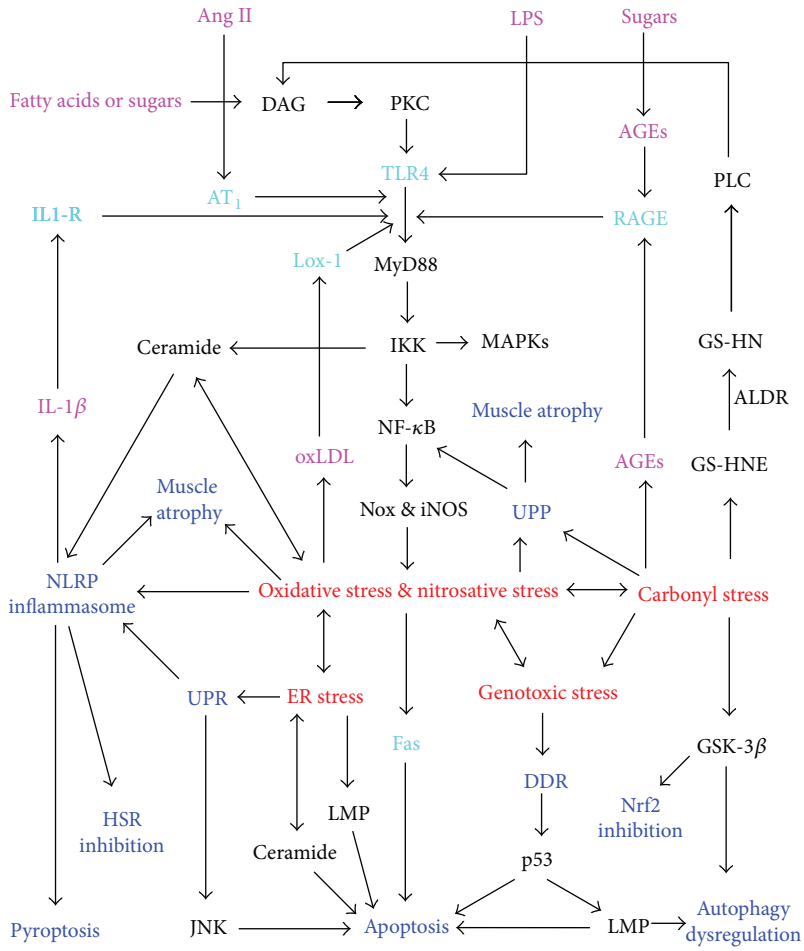

Figure 2: Pathways to interconnected cellular stresses, stress responses, and stress response dysregulations that contribute to insulin resistance in insulin target cells exposed to excess nutrients (sugars or fatty acids such as palmitate), angiotensin II (Ang II), or bacterial lipopolysaccharide (LPS). ALDR: aldose reductase; AGE: advanced glycation end product; AT_1: angiotensin receptor type 1; DAG: diacylglycerol; DDR: DNA damage response; GS-HNE: glutathione-HNE adduct; GS-HN: glutathionyl-1,4-dihydroxynonene; GSK: glycogen synthase kinase; HSR: heat shock response; IL-1β: interleukin 1β; IL1-R: interleukin 1 receptor; iNOS: inducible nitric oxide synthase; IKK: inhibitor of kappa B kinase; LMP: lysosomal membrane permeabilization; MAPK: mitogen-activated protein kinase; NF-κB: nuclear factor kappa B; Nox: NADPH oxidase; PKC: protein kinase C; PLC: phospholipase C; TLR4: toll-like receptor 4; UPP: ubiquitin-proteosome pathway; UPR: unfolded protein response. The stresses, stress responses, and signaling pathways generating them contribute to insulin resistance by multiple mechanisms as described in the text. Insulin resistance may occur because of the combined effects of different components of the system, and these components may promote IR to different extents in different cell types.

peroxide, singlet oxygen, and advanced glycation end products (AGEs) such as glyoxal lysine and methylglyoxal lysine [73, 74]. AGEs accumulate in plasma and tissues of animals and humans on diets rich in fructose or preformed AGEs [75]. AGEs signal via the RAGE receptor to induce activation of NF-κB via some components of the TLR4 pathway and thus produce similar effects as LPS, including the induction of oxidative and nitrosative stresses (Figure 2) [30, 32, 76].

Oversupply of fatty acids to insulin target cells occurs because of excessive dietary intake, obesity, or muscle inactivity-associated decrease in beta oxidation of fatty acids [59, 77, 78]. Palmitate and laurate can induce the activation of IKK, NF-κB, and oxidative stress independently of LPS [79–84]. This at least partly involves increased synthesis of diacylglycerol (DAG), a cofactor of protein kinase C (PKC) isoforms which activate Nox isoforms and NF-κB [30, 59, 80, 82–85]. Similarly, exposure of endothelial cells to high glucose levels results in DAG formation and subsequent activation of PKC and Nox [80]. The activation of Nox and NF-κB by PKC isoforms may involve PKC-induced TLR4 signaling as shown in Figure 2 [30, 64, 81]. However, DAG-PKC-induced insulin resistance without TLR4 activation has also been reported [84].

Palmitate is a substrate of serine palmitoyl transferase (SPT) in the first step of the de novo biosynthesis of the sphingolipid ceramide, an inhibitor of insulin signaling by multiple mechanisms including activation of protein phosphatase 2A (PP2A) and PKC-ζ, which promote dephosphorylation of Akt or serine phosphorylation of IRS, respectively [45, 81, 86, 87]. Long-term ceramide action also promotes serine phosphorylation of IRS via sequential activation of the double-stranded RNA-activated protein kinase (PKR)

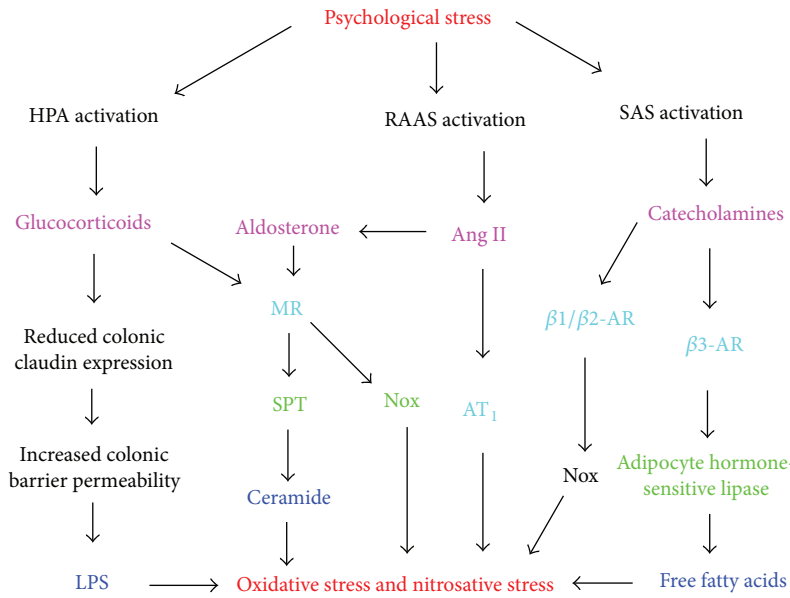

Figure 3: Psychological stress-dependent pathways to oxidative and nitrosative stresses. Psychological stress activates the renin-angiotensin-aldosterone system (RAAS), the hypothalamic-pituitary-adrenal axis (HPA), and the sympathetic adrenomedullary system (SAS), leading to increased availability of angiotensin II (Ang II), aldosterone, glucocorticoids, catecholamines, and free fatty acids which induce oxidative and nitrosative stresses in insulin target cells [109, 117–120, 127, 128]. Glucocorticoids and aldosterone promote de novo ceramide synthesis in endothelial cells and may thereby contribute to plasma ceramides [111, 121–123]. Glucocorticoids also increase colon epithelial barrier permeability and thus increase circulating LPS [124–126]. Angiotensin II, glucocorticoids, aldosterone, and catecholamines upregulate Nox activity in various insulin target cells [105, 110, 130, 132].

and JNK [88]. Palmitate-induced TLR4-IKK signaling promotes ceramide biosynthesis by upregulating the synthesis of SPT and ceramide synthases (Figure 2) [81, 86]. Ceramide is an important contributor to oxidative stress. It induces mitochondrial superoxide anion and H_2O_2 generation by blocking the electron transport system at complex III [89]. Mitochondrial superoxide anions generated in this manner induce opening of the mitochondrial permeability transition pore, allowing mitochondrial ROS to move into the cytoplasm [90]. Some mechanisms by which ceramide induces insulin resistance, such as apoptosis induction, JNK activation, and mitochondrial fission, depend on such ceramide-induced oxidative stress [91–95]. ROS and NO promote mitochondrial fission, which in turn promotes ROS formation through cytochrome c oxidase [96, 97].

In a recent clinical trial, a high-saturated-fat diet increased the serum concentrations of angiotensin-converting enzyme (ACE) independently of weight gain [98]. In the classical renin-angiotensin system (RAS), ACE converts angiotensin I to the active angiotensin II which signals via angiotensin receptors 1 and 2 (AT_1 and AT_2) [99] and TLR4 to induce NF-κB activation, mitochondrial fission, and insulin resistance in skeletal muscle cells, vascular smooth muscle cells, and endothelial cells [31, 99–104]. Angiotensin II signaling upregulates xanthine oxidase protein expression and activity in a Nox-dependent manner in endothelial cells [105]. Furthermore, it activates 12-lipoxygenase, whose product, 12-hydroxyeicosatetraenoic acid (12-HETE), induces NF-κB in endothelial cells and aldosterone in adrenal glomerulosa cells [106, 107]. Aldosterone levels increase in humans during obesity, and this hormone correlates with insulin resistance independently of the body mass index [108, 109]. Aldosterone increases superoxide production in endothelial cells though mineralocorticoid receptor- (MR-) mediated activation of Nox and Rac 1 [110]. It also promotes MR-induced de novo ceramide synthesis in these cells [111]. This adrenal hormone readily enters the brain, such that its levels in the brain are directly proportional to its plasma levels in rats [112]. It activates the hypothalamic renin-angiotensin system and associated oxidative stress in hypothalamic neurons [112, 113].

Psychological stress (PS) is another major inducer of oxidative stress and insulin resistance [114–116]. This is partly through increased production of aldosterone [109], angiotensin II [117], and glucocorticoids such as corticosterone and cortisol (Figure 3) [118–120]. Glucocorticoids upregulate the expression of SPT and ceramide synthases and thus contribute to ceramide-mediated oxidative stress and insulin resistance [121, 122]. They have a higher affinity for the mineralocorticoid receptor than for the glucocorticoid receptor, and their binding to the former increases Nox expression in adipocytes [123]. PS also contributes to LPS-induced oxidative stress and insulin resistance by promoting colonic barrier permeability and the translocation of bacteria and LPS from the intestinal lumen to the blood [124]. Chronic peripheral administration of corticotropin-releasing factor was demonstrated to cause such colonic barrier dysfunction in rats [125]. This involves glucocorticoid-mediated downregulation of the intestinal epithelial tight junction protein, claudin 1 [126].

Chronic activation of the sympathetic nervous system and the associated increase in catecholamines such as epinephrine and norepinephrine are another hallmark of PS

[127]. These catecholamines contribute to insulin resistance in the heart by activating β-adrenergic receptors (β-AR) [128]. Activation of β-AR induces oxidative stress in cardiomyocytes, adipocytes, and endothelial cells, at least partly by β2-AR-mediated upregulation of Nox [128–132]. The β3-AR activates hormone-sensitive lipase in adipocytes and thus promotes accumulation of free fatty acids and the associated increase in ceramide synthesis and MAPK activation [133]. AR stimulation inhibits adiponectin gene expression in adipocytes via protein kinase A [134], and this should further promote ceramide accumulation and ceramide-dependent oxidative stress because adiponectin increases ceramidase activity [135].

Mountain climbing or obstructive sleep apnea (OSA) induces insulin resistance, and this is associated with hypoxia-induced oxidative and nitrosative stresses [136, 137]. OSA worsens during periods of rapid weight gain [138]. Chronic asthma also induces intermittent hypoxia [139], and an association between asthma and insulin resistance was demonstrated in children and adolescents [18, 140, 141]. Many mechanisms have been reported to be involved in hypoxia-induced oxidative and nitrosative stresses. During the switch from normoxia to hypoxia, a burst of superoxide formation occurs at mitochondrial complex 1 due to deactivation of this complex in cells such as endothelial cells and neurons [142]. Hypoxia also increases superoxide formation at mitochondrial complex III [143]. In human umbilical endothelial cells, hypoxia was found to induce expression of the human circadian locomotor output cycle protein kaput (hCLOCK), which promoted the production of ROS, which in turn promoted Rhoa and NF-κB signaling [144]. Hypoxia upregulates 12/15-lipoxygenase, whose metabolites, namely, 13-hydroperoxyoctadecadienoc acid (13-HPODE), 12-hydroxyeicosatetraenoic acid (12-HETE), and 15-hydroxy-eicosatetraenoic acid (15-HETE), activate NF-κB, iNOS, and mitochondrial oxidative stress in endothelial cells, cardiomyocytes, smooth muscle cells, neurons, and adipocytes [145–151]. Since 13-HPODE, 12-HETE, and 15-HETE activate PKC isoforms [149, 152, 153], the 12/15-lipoxygenase-dependent, hypoxia-induced oxidative and nitrosative stresses may follow the pathway outlined in Figure 4.

As indicated in this figure, 15-S-HETE also activates xanthine oxidase (XO) in endothelial cells [154]. Such increase in XO activity occurs during hypoxia [155] and leads to increased uric acid (UA) formation in lowlanders at high altitude [156]. Uric acid is a promoter of oxidative stress via the RAGE receptor in endothelial cells [34]. During intermittent hypoxia, XO-derived ROS activate Nox2 [157]. In addition, hypoxia increases catecholamine production [158] and, like psychological stress, has been reported to induce mucosal barrier failure and endotoxemia in rats and primates [159, 160]. However, a recent study in humans found that hypoxia increased gut inflammation but not gut permeability [161].

Long-term exposure to traffic-related air pollution was found to be positively associated with insulin resistance in children [162]. Particulate matter, ozone, nitrogen oxides, and transition metals are among the potent oxidants in polluted air that induce endogenous ROS formation and

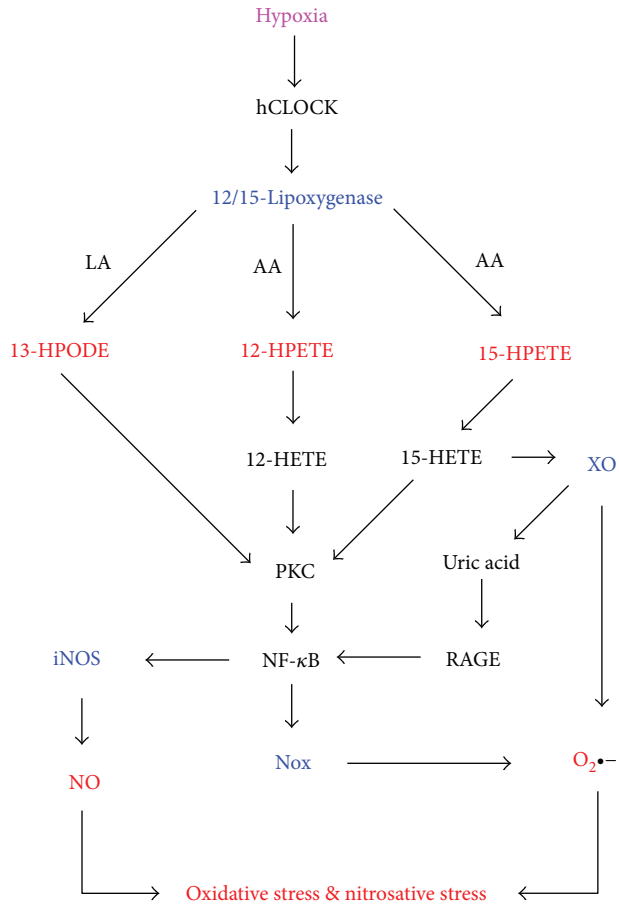

Figure 4: Pathways for the hypoxia-induced generation of oxidative and nitrosative stresses through the human circadian locomotor output cycle protein kaput- (hCLOCK-) mediated 12/15-lipoxygenase activation [143–150]. 12/15-Lipoxygenase catalyses the production of ROS in the form of 13-hydroperoxy-octadecadienoic acid (13-HPODE) from linoleic acid (LA) or 12-hydroperoxy-eicosatetraenoic acid (12-HPETE) and 15-hydroperoxy-eicosatetraenoic acid (15-HPETE) from arachidonic acid (AA). 13-HPODE, 12-HPETE, and 15-HPETE are reduced to the corresponding hydroxy derivatives 13-HODE, 12-HETE, and 15-HETE, respectively. 13-HPODE, 12-HETE, and 15-HETE activate PKC isoforms [148, 151, 152], which promote activation of NF-κB, NADPH oxidase (Nox) isoforms, and inducible nitric oxide synthase (iNOS) [30, 144–150]. iNOS and Nox produce nitric oxide (NO) and superoxide anions ($O_2^{\bullet-}$), respectively, which undergo enzymatic and nonenzymatic reactions that lead to the formation of other ROS such as hydrogen peroxide and singlet oxygen, as well as the RNS, peroxynitrite [30]. 15-HETE activates xanthine oxidase (XO) [154], which catalyses the formation of both superoxide anions and uric acid, and the latter signals via the receptor for advanced glycation end products (RAGE) to activate NF-κB [34].

oxidative stress [163]. Cadmium, a heavy metal pollutant from industrial plants, which makes its way into the food chain and induces oxidative stress was recently found to be positively associated with insulin resistance [164].

2.2. Oxidative Stress Produces Carbonyl Stress and Vice Versa. Decomposition of lipid hydroperoxides produces

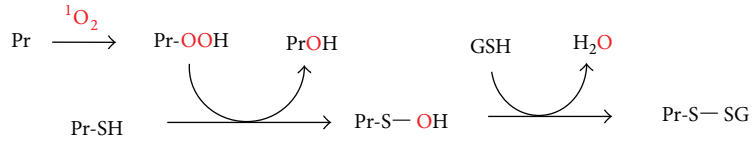

Figure 5: Mechanism of singlet oxygen-mediated protein glutathionylation. Reaction of $^1O_2$ with a protein (Pr) on residues such as tryptophan and histidine generates a protein hydroperoxide (Pr-OOH). Reaction of Pr-OOH with cysteine residues in other proteins (Pr-SH) converts the latter to sulfenic acids (Pr-SOH) [189], which readily react with glutathione (GSH) to form glutathionylated proteins (Pr-S-SG) [190, 191].

reactive carbonyl compounds including acrolein, glyoxal, methylglyoxal, malondialdehyde, 4-hydroperoxy-2-nonenal, 4-hydroxy-2-nonenal (HNE), 4-oxo-2-nonenal, 2,4-decadienal, and 9-oxo-nonanic acid [165]. Elevated formation of such products constitutes carbonyl stress. Thus, oxidative stress, through increased production of lipid hydroperoxides, promotes carbonyl stress. As mentioned in the previous section, methylglyoxal- and glyoxal-derived AGEs promote oxidative stress via the RAGE receptor. Likewise, 4-HNE, one of the predominant lipid-derived aldehydes formed in insulin-responsive cells during high-fat or high-glucose diets, promotes the formation of reactive oxygen and nitrogen species [166]. Cholesterol secosterol aldehydes, which are produced via the reaction of cholesterol with singlet oxygen or ozone [30, 167], increase oxidative stress by inactivating catalase and thus promoting the accumulation of hydrogen peroxide and lipid hydroperoxides [168].

2.3. Oxidative and Carbonyl Stresses Promote Endoplasmic Reticulum Stress and Vice Versa. Noncytoplasmic and nonmembrane proteins synthesized at the rough endoplasmic reticulum (ER) undergo translocation into the ER lumen, where calcium-dependent molecular chaperones assist their folding into the correct tertiary structures [169]. The ER calcium transporter, sarco- (endo-) plasmic reticulum Ca^{2+} ATPase (SERCA), pumps calcium ions into this organelle and thereby promotes the activity of the molecular chaperones [170, 171]. The reversible S-glutathionylation of SERCA thiols by NO and peroxynitrite increases SERCA activity, but the irreversible sulfonation of these thiols by ROS such as hydrogen peroxide and singlet oxygen causes its inactivation [30, 170–172]. The ensuing accumulation of unfolded or misfolded proteins in the ER constitutes ER stress [173]. Carbonylation by aldehydes such as acrolein, methylglyoxal, glyoxal, and HNE also reduces SERCA activity [174, 175]. ER stress leads to enhanced Nox 4 activity in the ER, resulting in increased hydrogen peroxide formation and oxidative stress [176]. Such increased ER oxidative stress promotes calcium efflux from the ER and calcium influx into the mitochondria, which induces mitochondrial ROS production and oxidative stress [30, 176]. Thus, there is a vicious cycle between ER stress and oxidative stress [30, 177].

2.4. Oxidative, Carbonyl, and Nitrosative Stresses Generate Genotoxic Stress. Oxidative stress, carbonyl stress, and nitrosative stress contribute to genotoxic stress by availing genotoxic reactive oxygen, carbonyl, and nitrogen species that modify DNA. ROS react with the nitrogenous bases in DNA to induce a variety of base modifications. One of the most common of such modifications is the conversion of guanine to 8-oxo-7,8-dihydroguanine (8-oxoG), whose levels in urine have been suggested to be a marker of whole-body oxidative stress [178, 179]. 8-oxoG is most readily formed by singlet oxygen, although the hydroxyl radical also contributes to its formation [180, 181]. Mitochondrial DNA is exposed to singlet oxygen generated through mechanisms such as the reaction of peroxynitrite with hydrogen peroxide or cytochrome c-mediated conversion of cardiolipin hydroperoxide to triplet carbonyls in the mitochondria [30]. DNA-damaging hydroxyl radicals may be generated by the Fenton reaction between DNA-bound Fe2+ and hydrogen peroxide [182]. 8-oxoG undergoes further oxidative modifications, as well as crosslinking with lysine to generate protein-DNA adducts [183]. The reaction of singlet oxygen or hydroxyl radicals with deoxyribose in DNA generates single-strand breaks, but double-strand breaks can be generated when the single-strand breaks occur in close proximity [178, 184]. Peroxynitrite induces single-strand breaks in DNA through deoxyribose oxidation or via the formation of 8-nitroguanine [185]. Reactive carbonyl compounds derived from the decomposition of lipid hydroperoxides react with DNA bases to form exocyclic propano- and etheno-DNA adducts, as recently reviewed [186]. The glycoxidation of histone proteins by glyoxal and methylglyoxal promotes the oxidative generation of DNA strand breaks [187]. The formation of hydrogen peroxide and singlet oxygen during protein glycoxidation [74] may explain this phenomenon. Genotoxic stress in turn promotes oxidative stress (Section 3.4).

3. Mechanisms of the Inhibition of Insulin Signaling by Cellular Stresses

3.1. Oxidative Stress. The oxidative modifications of biomolecules including lipids, nucleic acids, and proteins contribute to insulin resistance. Some common types of oxidative protein modifications include hydroperoxidation, glutathionylation, and sulfonation. As shown in Figure 5, proteins (Pr) react with singlet oxygen to form protein hydroperoxides (Pr-OOH). The latter is relatively long lived and inactivates enzymes even when singlet oxygen is no longer in the system [188, 189]. Pr-OOHs react with thiol (-SH) groups in other proteins to form hydroxy proteins (Pr-OH) and protein sulfenic acids (Pr-S-OH), and the latter readily reacts with glutathione (GSH) to form glutathionylated proteins (Pr-S-SG) [190–192]. Hydrogen peroxide also induces protein glutathionylation, analogously to protein hydroperoxides, but

the latter is more reactive [189]. Sulfenic acids (Pr-SOH) react further with H_2O_2 to form sulfinic acids (Pr-SO_2H), which react with H_2O_2 to form sulfonic acids (Pr-SO_3H) [190]. The reaction of superoxide radicals with thiols may also lead to the conversion of the latter to sulfonates via persulphenyl derivatives [193]. Ozone or ozone-like oxidants have been suggested to be formed in biological systems [74, 167]. Ozone largely converts thiolate ions to sulfonates [194] and was postulated to be an important contributor to the conversion of methionine sulfoxide to methionine sulfonate [195].

At low levels, ROS including H_2O_2 and singlet oxygen stimulate insulin signaling by the PI3K-Akt pathway through inhibition of protein tyrosine phosphatase 1B (PTP1B) which dephosphorylates the insulin receptor [196, 197]. On the other hand, a high concentration of H_2O_2 was found to induce insulin resistance in hepatocytes, and systemic removal of hydrogen peroxide improved insulin resistance in obese mice [196, 198]. ROS activate stress-sensitive kinases which reduce insulin signaling [199], and it was proposed that at high H_2O_2 concentrations, JNK activation outweighs PTP1B inactivation [196].

Activation of JNK and p38 by ROS occurs through the modification of their regulatory proteins. For example, MAPK phosphatase 1 deactivates JNK and p38 MAPK by dephosphorylation, but glutathionylation targets this phosphatase for proteosomal degradation [199].

Protein-protein interaction between glutathione S-transferase P (GSTP) and JNK keeps the latter in an inactive state, but oxidative modification of the former breaks this interaction and activates JNK [200, 201]. Another protein whose oxidative modification promotes insulin resistance is thioredoxin which, in the native state, binds to and inactivates apoptotic signaling kinase 1 (ASK1), an upstream activator of both JNK and p38 pathways [202, 203]. While the release of thioredoxin from ASK would also allow the former to act as a thiol-reducing antioxidant, oxidative stress promotes the p38 MAPK- and FOXO-dependent expression of thioredoxin-interacting protein (TXNIP) [204] and transfer of the latter from the nucleus to the cytoplasm and mitochondria, where it binds to thioredoxin 1 and thioredoxin 2, respectively, and this aggravates oxidative stress [204, 205]. Increased oxidative stress also favors the activatory binding of TXNIP to the NLRP3 inflammasome [205], a key contributor to insulin resistance as described in Section 4.5.

Several studies have reported that the inhibition of glycolysis in muscle cells induces insulin resistance [206–208], for example, through a compensatory increase in lipid uptake [208]. Protein peroxides generated by singlet oxygen inhibit the glycolytic enzyme glyceraldehyde-3-phosphate dehydrogenase (GPD) [209]. Besides reduced glycolysis, GPD inhibition enhances the conversion of dihydroxyacetone phosphate to methylglyoxal [210], which is one of the major reactive carbonyls contributing to insulin resistance (Section 3.3).

Reactive oxygen species such as H_2O_2 promote Ser637 dephosphorylation of the GTPase, dynamin-related protein 1 (Drp1), resulting in translocation of the latter to the mitochondria, where its polymerization into a ring-like structure induces mitochondrial fission [211], an important contributor to insulin resistance and oxidative stress [94, 95].

Perhaps one of the greatest contributions of oxidative stress to insulin resistance is that it generates metabolites that create positive feedback loops for potentiation of TLR4, RAGE, and other signaling pathways associated with activation of NF-κB and insulin signal-inhibiting serine kinases such as PKC, IKK, JNK, and p38 MAPK. For example, oxidative stress leads to the oxidation of low-density lipoproteins (LDL), and oxidized LDL (oxLDL) signals via Lox-1, RAGE, and Fas receptors to activate NF-κB and MAPKs as recently reviewed [30], and the plasma concentration of oxLDL is an independent risk factor for insulin resistance [212].

p38 MAPK promotes the expression of aldose reductase (ALDR) [213], which is subsequently activated by oxidative modification [214], and makes a major contribution to insulin resistance [215]. ALDR reduces HNE-glutathione adduct (GS-HNE) to glutathionyl-1,4-dihydroxynonene (GS-HN), which activates phospholipase C, leading to DAG formation and the activation of PKC, MAPKs, and NF-κB (Figure 2) [166, 216]. DAG oxidation also contributes to PKC-dependent signaling, since DAG hydroperoxide is a more potent activator of PKC than unoxidized DAG [217]. In the presence of excess glucose, ALDR catalyses the first reaction of the polyol pathway, which leads to the production of both DAG and AGES, thus contributing to signaling via both TLR4 and RAGE [218]. The role of ALDR in potentiating LPS-TLR4 signaling via PKC is evidenced by findings that its inhibition alleviates endotoxin-induced inflammatory diseases [216, 219, 220].

Mammalian xanthine dehydrogenase (XDH) is reversibly converted to xanthine oxidase (XO) by oxidative modification of specific cysteine residues [221]. As already mentioned, lipoxygenase-mediated 15-HETE formation during hypoxia activates XO. Fructose metabolism in hepatocytes is associated with increased XO-mediated conversion of AMP to uric acid [85, 222–224], which promotes insulin resistance through RAGE, TLR4, NF-κB, Nox, mitochondrial oxidative stress, ER stress, and skeletal muscle atrophy [30, 34, 223–227].

Oxidative stress promotes ceramide synthesis even independently of SPT and ceramide synthases. Singlet oxygen converts sphingomyelin to ceramide, even in protein-free liposomes [228]. In glioma cells, superoxide promotes ceramide formation through activation of neutral sphingomyelinase [229]. Sphingomyelinase inhibition reduces intramyocellular ceramide and protects muscle cells from insulin resistance [230, 231].

H_2O_2 downregulates the expression of carnitine palmitoyl transferase 1 (CPT1), acyl COA oxidase (ACOX), and peroxisome proliferator-activated receptor-alpha (PPAR-α) in hepatocytes [232] and PPAR-γ in endothelial cells [233]. CPT1 and ACOX are involved in fatty acid oxidation and reduction of DAG and ceramide levels [232, 234, 235]. PPAR-α reduces oxidative stress by upregulating superoxide dismutase and catalase expression and inhibiting NF-κB activity [232, 236, 237]. PPAR-γ inhibits NF-κB and upregulates the expression of adiponectin, an adipokine that improves insulin sensitivity [238–240].

3.2. Nitrosative Stress. The importance of nitrosative stress in insulin resistance is evidenced by reports that inhibition of iNOS or peroxynitrite in various cell types prevents insulin resistance [41–43]. Peroxynitrite decomposes into radicals that cause inhibitory tyrosine nitration of proteins in the insulin signaling pathway [70]. The reaction of peroxynitrite with proteins generates thyl radicals and sulfenates, leading to protein glutathionylation [192]. Nitrosoglutathione causes glutathionylation and inhibition of GADPH [241]. Peroxynitrite contributes to palmitate-induced DNA damage and inflammasome activation [23, 242]. It also induces ceramide formation in endothelial cells [243]. Nevertheless, the effects of peroxynitrite are mediated to some extent by ROS since peroxynitrite-derived radicals can initiate free radical lipid peroxidation [244], and the reaction of peroxynitrite with hydrogen peroxide generates singlet oxygen [30, 71]. Thus, iNOS and NO donor-induced IRS-1 degradation in skeletal muscle cells was accentuated by concomitant oxidative stress [245].

3.3. Carbonyl/Electrophilic Stress. Reactive carbonyl species contribute to insulin resistance in various ways. Methylglyoxal, HNE, and cholesterol secosterol aldehydes participate in the generation of oxidative stress and associated NF-κB and MAPK activation (Sections 2.1, 2.2, and 3.1). In addition, methylglyoxal adducts insulin and inhibits the latter's proper interaction with the insulin receptor [246]. Protein-HNE adducts correlate with intramyocellular lipid content and the severity of insulin resistance in humans [247]. HNE forms Michael adducts with His196 and Cys311 of Akt2 and thus inhibits downstream phosphorylation of Akt substrates such as glycogen synthase kinase 3β (GSK3β) and MDM2, resulting in the activation of the former and inhibition of the latter [247]. GSK3β inhibits glycogen synthase and IRS and thus prevents both glycogen synthesis and glucose transport [248–250]. It also promotes hepatic gluconeogenesis by an unknown mechanism [251] and contributes to the dysregulation of the Nrf2 antioxidant response [252]. MDM2 is a negative regulator of the p53 protein, which promotes insulin resistance as discussed in Section 3.4.

Human adipocytes and white adipose tissue express the full enzymatic machinery required for the synthesis and metabolism of asymmetric NGNGdimethylarginine (ADMA) which uncouples NOS and thus promotes ROS formation, increases TLR4 expression, decreases IRS-1 and GLUT-4 expression, and inhibits IRS-1 tyrosine phosphorylation and GLUT-4 translocation [253–256]. Plasma levels of ADMA increase during oxidative stress, mainly due to decreased expression and activity of the ADMA-degrading enzyme, dimethylarginine dimethylaminohydrolase (DDAH) [255–259]. HNE downregulates DDAH-1 expression through an miR-21-dependent mechanism [259].

3.4. Genotoxic Stress. Increased oxidative DNA damage determined as serum 8-hydroxy-2-deoxy-guanosine (8-OHdG) was found in lean normoglycemic offspring of type 2 diabetics, who are more predisposed to insulin resistance [260]. Similarly, serum level of 8-OHdG was found to be increased in prediabetes [261]. Mice deficient in 8-oxoguanine DNA glycosylase (the enzyme that performs base excision repair of DNA by cleaving 8-oxoG and other modified bases) were found to be prone to insulin resistance upon high-fat feeding [262]. Mitochondrial DNA damage promotes palmitate-induced insulin resistance mainly by increasing mitochondrial oxidative stress, ER stress, JNK activation, and apoptosis, since overexpression of DNA glycosylase/apurinic/apyrimidinic lyase (hOGG1) in the mitochondria of skeletal muscle cells abrogated these effects [263, 264]. Interestingly, prevention of mitochondrial DNA damage in cardiomyocytes exposed to angiotensin II prevented mitochondrial superoxide production in these cells [265]. In the latter study, mtDNA damage was found to cause impairments in mitochondrial protein expression, cellular respiration, and complex 1 activity prior to enhanced mitochondrial superoxide production. In addition, oxidized mitochondrial DNA released into the cytoplasm during apoptotic signaling activates the NLRP3 inflammasome [266].

3.5. Endoplasmic Reticulum Stress. Endoplasmic reticulum stress contributes to insulin resistance by promoting oxidative stress, especially mitochondrial oxidative stress and the resultant carbonyl and genotoxic stresses (Section 2.3) and ceramide synthesis [46], as well as by triggering the unfolded protein response [267], inflammasome activation [268], and apoptosis (Section 4.4).

4. Inhibition of Insulin Signaling by Cellular Stress Responses

4.1. The Ubiquitin-Proteosome Pathway. The ubiquitin-proteosome pathway (UPP) is the major cytosolic mechanism for the selective degradation of damaged proteins, such as oxidatively modified proteins, whereby the damaged proteins are conjugated to multiple ubiquitin molecules and then degraded by the 26S proteasome [269]. This system is upregulated by mild and moderate oxidative stress and is required for cells to cope with oxidative stress [269]. On the other hand, UPP-mediated degradation of the NF-κB inhibitor, iKB, causes activation of NF-κB [270]. NF-κB promotes oxidative stress and induces expression of proinflammatory cytokines including TNF-α and IL-6 which, via the JAK-STAT pathway, upregulate expression of suppressors of cytokine signaling (SOCS) proteins such as SOCS1 and SOCS3 [271–273]. Association of the SOCS proteins with IRS targets the latter for degradation by the ubiquitin-proteosome pathway in multiple cell types [271–273]. Accordingly, palmitate-induced insulin resistance in L6 myotubes was found to be dependent on constitutive phosphorylation of STAT 3 and the associated increase in protein expression of SOCS 3 [274], and the ubiquitination and proteosomal degradation of IRS-1 and Akt was demonstrated to contribute to palmitate or NO donor-induced insulin resistance in HepG2 cells and skeletal muscle cells, respectively [245, 275]. Moreover, increased SOCS1/SOCS3 expression during uveitis induces insulin resistance in neuroretina [276], and SOCS3 overexpression is responsible for the induction of insulin resistance in mice infected with hepatitis C virus [277].

Several factors contribute to increased UPP during the pathogenesis of insulin resistance. For example, the 15-lipoxygenase product, 15-HETE, induces the expression of key enzymes of the UPP pathway [150]. Inhibition of the adipose tissue ERK1/2 pathway during a high-fat diet was reported to enhance the UPP-mediated degradation of adiponectin [278], although contradictory results that ERK activity increases in hypertrophic adipocytes have also been obtained [279]. Increased HNE activity during a high-fat diet enhances the ubiquitin-proteosome-mediated degradation of adiponectin [280]. This is detrimental since adiponectin improves insulin sensitivity by (i) upregulating ceramidase activity to decrease ceramide levels [135]; (ii) increasing the levels of tetrahydrobiopterin (BH4), which lowers hepatocyte gluconeogenesis by activating AMP-activated kinase (AMPK) in an eNOS-dependent process [281]; and (iii) upregulating the silent information regulator 1 (SIRT1), a nicotinamide adenine dinucleotide-dependent histone deacetylase [282].

SIRT1 plays a role in the reduction of oxidative stress through increased expression of superoxide dismutase and catalase subsequently to FOXO4 deacetylation [283]. It also activates AMP-activated kinase (AMPK), which promotes insulin sensitivity by inhibiting PKC isoforms and the associated NF-κB activation, oxidative stress, ER stress, and apoptosis [284–291]. AMPK also induces mitochondrial biogenesis, which limits endothelial cell dysfunction, for example, in response to angiotensin II signaling [292]. Phosphorylation of SIRT1 by JNK1 primes SIRT1 for ubiquitination and degradation, and persistent JNK1 activation in obesity causes severe hepatic SIRT1 degradation [293]. SIRT1 reduction is detrimental to insulin signaling in various tissues including liver, skeletal muscle, and adipose tissues [294–296]. AMPK1 is also diminished in insulin-resistant individuals, and pharmacological agents that activate it, such as metformin, improve insulin signaling [290].

Increased mitochondrial DNA methylation in NADH dehydrogenase 6 (ND6) and displacement loop (D-loop) regions significantly correlates with insulin resistance, and SIRT1 deregulation was suggested to be involved in such epigenetic changes [297]. Since AMPK-mediated phosphorylation results in inhibition of DNA methyl transferase 1 (DNMT1) [298], UPP-mediated SIRT1 downregulation may induce such epigenetic changes through AMPK inhibition. Inflammasome activation might also contribute to this process by promoting DNMT1 expression (see Section 4.5). On the other hand, one study recently found that oxidative stress downregulated DNMT1 isoform 3, the isoform that is responsible for mitochondrial DNA methylation [299]. Further studies are necessary to resolve this apparent contradiction.

The UPP may especially be relevant in skeletal muscle insulin resistance by contributing to skeletal muscle atrophy, which occurs in two steps, namely, (i) the release of myofilaments from the sarcomere by cysteine proteases such as calpain and caspases and (ii) UPP-mediated degradation of the myofilament fragments [300, 301]. Calpain activation may in turn rely on the release of calcium from the ER during ER stress. Calpain activation in the skeletal muscle results in inhibited Akt activity, which in turn results in the activation of Foxo transcription factors that activate expression of components of the ubiquitin-proteosome system involved in muscle protein degradation [301]. Muscle atrophy per se has been associated with insulin resistance due to a decline in muscle oxidative capacity [302]. Exposure of C2C12 myotubes to 25 μM H_2O_2 induced calpain-dependent atrophy without cell death [300]. Exposure of C2 myotubes to peroxynitrite induced degradation of the myosin heavy chain muscle through activation of p38 MAPK and upregulation of the muscle-specific E3 ubiquitin ligases atrogin-1 and MuRF1 [303]. Increased expression of the transforming growth factor-β (TGF-β) and myostatin, via NF-κB, induces proteosomal degradation of cellular proteins [304, 305], and muscle myostatin mRNA correlates with HOMA2-IR in nondiabetic individuals [306].

While mild or moderate oxidative stress upregulates the ubiquitin-proteosome pathway, severe or sustained oxidative stress inactivates this system, especially the 26S proteasome [269, 307]. This also contributes to insulin resistance since proteosomal dysfunction, characterized by increased levels of carbonylated and ubiquitinated proteins, aggravates oxidative stress and ER stress [308].

4.2. The Unfolded Protein Response. ER stress triggers a transcriptional and translational response referred to as the unfolded protein response (UPR), aimed at reducing the translation of global proteins, enhancing the degradation of unfolded proteins, and increasing the transcription of genes that enhance the protein folding capacity of the ER [267]. The double-stranded RNA-dependent protein kinase-(PKR-) like ER kinase (PERK), the inositol requiring kinase 1 (IRE 1), and activating transcription factor 6 (ATF 6) are ER transmembrane proteins that are key components of three different UPR signaling pathways [267]. Details of the signaling events that occur after activation of PERK, IRE1, and ATF 6 have been described elsewhere [267, 309].

All three UPR pathways promote NF-κB activity and oxidative stress [310, 311]. Besides, IRE-1 stimulates ASK-1 and thus activates JNK and p38 MAPK [312]. PERK promotes insulin resistance by (i) activating JNK and p38 MAPK [49, 313]; (ii) phosphorylating FOXO on S298, a site which is not phosphorylated by Akt and whose phosphorylation counteracts the effects of Akt [49]; (iii) downregulating expression of the serine protease prostatin (PRSS8), which regulatorily degrades TLR4 [314]; (iv) inducing the pseudokinase tribble 3 (TRB3), which is increased in the liver of obese mice and humans and contributes to hepatic insulin resistance [49, 315]. TRB3 binds to Akt and prevents insulin-mediated Akt phosphorylation [49, 173, 315].

Low-grade hypothalamic inflammation induced by TNF-α was found to reduce oxygen consumption and the expression of thermogenic proteins in adipose tissue and skeletal muscles, and this was associated with insulin resistance in a rat model [316]. PERK, to a lesser extent, ATF, and IRE upregulate the C/EBP homologous protein (CHOP) [317], which downregulates cAMP-induced upregulation of uncoupling protein 1 in adipocytes and thus prevents adaptive thermogenesis [318].

4.3. The DNA Damage Response. The DNA damage response is a complex mechanism to detect DNA damage, including strand breaks or base modifications, promote their repair, and in case of excessive damage to activate cell death pathways [319]. Sensing of double-strand breaks by the Mre11-Rad50-Nbs1 (MRN) complex leads to the activation of ataxia telangiectasia mutated (ATM) and subsequent activation of DNA damage checkpoints [319]. ATM activates NF-κB following DNA damage [320]. Checkpoints induce changes in telomeric chromatin, recruit DNA repair proteins to sites of DNA damage, and induce cell death by apoptosis [321]. One of the checkpoints, Chk2, promotes transcription of genes involved in DNA repair and phosphorylates tumor suppressor p53, thereby reversing inhibition of the latter by MDM2 [319]. Chk2 also phosphorylates MDM4 and thereby reduces p53 degradation [319]. Such activation of the p53 pathway is upregulated in adipose, endothelial, hepatic, and skeletal muscle tissues of obese rodents and humans [322–326]. Although this protein exhibits antioxidant activity at low levels of oxidative stress, it becomes prooxidant at higher oxidative stress levels, through activation of NF-κB [327] and promotion of ceramide synthesis by upregulating ceramide synthases [328]. p53 promotes cellular senescence in adipose tissue, and this is associated with increased production of proinflammatory cytokines, which promote adipose tissue infiltration by neutrophils and macrophages, and systemic insulin resistance [322–326]. Many other metabolic effects of p53 are opposed to insulin signaling, as has been exhaustively reviewed [322, 327], including but not limited to JNK activation; apoptosis; repressed expression of the insulin receptor and glucose transporters 1, 3, and 4; enhanced transcription of phosphatase and tensin homologue (PTEN) which reduces phosphorylation of P13K and Akt; Akt degradation; glycolysis inhibition; and downregulated expression of peroxisome proliferator-activated receptor-γ coactivator-1α (PGC-1α) in the skeletal muscle, leading to the reduction in mitochondrial biogenesis and energy consumption. Reduced mitochondrial biogenesis leads to a lower capacity for fatty acid metabolism in skeletal muscle cells and accumulation of intramyocellular lipids including DAG which is a major contributor to skeletal muscle insulin resistance [329, 330].

4.4. Apoptosis. Apoptosis is a type of programmed cell death in response to cellular damage or other physiological cues, characterized by controlled autodigestion of the cell by caspases [331, 332]. It is regarded as extrinsic when it involves death receptors such as CD95 (Fas) or intrinsic if it occurs independently of such receptors, and both forms of apoptosis were found to be involved in insulin resistance in a mouse model [55]. Caspase-8 and caspase-9, respectively, act as initiator caspases for extrinsic and intrinsic apoptosis, and each initiator caspase starts off a cascade for the activation of executer caspases, which degrade key cellular proteins [333].

Oxidative stress promotes Fas ligand expression in various cell types and thus promotes extrinsic apoptosis [334]. Activation of the Fas receptor by metabolites such as IL-1β, oxLDL, singlet oxygen, HNE, or JNK leads to its intracellular recruitment of the adaptor protein FADD to form a death-inducing complex (DISC) which activates initiator caspase-8, while the autocatalytic activation of procaspase-9, the initiator of intrinsic apoptosis, requires the assembly of a multiprotein complex, the apoptosome, which comprises seven copies of heterodimers between apoptotic protease-activating factor 1 (Apaf-1) and cytochrome c [331–335]. Thus, the release of the latter from the mitochondrial membrane into the cytoplasm is a key event in intrinsic apoptosis.

During unresolved ER stress, ER calcium efflux promotes lysosomal membrane permeabilization (LMP) and the release of lysosomal cathepsins, which promote mitochondrial outer membrane permeabilization (MOMP) and the release of cytochrome c from the mitochondrial intermembrane space [331, 332]. Localization of p53 protein on the lysosomal membrane upon sustained DNA damage also contributes to LMP [336]. Activated JNK contributes to apoptosis in various ways including (i) inducing the expression of proapoptotic genes through transactivation of c-jun or p53, (ii) phosphorylating the BH3-only family of Bcl2 proteins which antagonize the antiapoptotic activity of Bcl2 or Bcl Xl, and (iii) activating Bim, a BH3-domain-only protein which activates Bax, which in turn promotes MOMP and cytochrome c release [337].

In humans, the progression of nonalcoholic fatty liver disease is associated with increasing apoptosis and insulin resistance in the muscle, liver, and adipose tissue [338]. The link between hepatocyte apoptosis and insulin resistance was demonstrated in a mouse model [56]. Adipocytes of obese mice were found to display a proapoptotic phenotype, and genetic inactivation of the key proapoptotic protein Bid protected against adipose tissue macrophage infiltration and systemic insulin resistance [55]. Prevention of apoptosis prevents palmitate-induced insulin resistance in hypothalamic neurons [339]. Palmitate induces apoptosis and insulin resistance in skeletal muscle myotubes, and cell-permeable effector caspase inhibitors reverse the insulin resistance, indicating that cellular remodeling associated with apoptotic signaling induces insulin resistance [340]. In these cells, caspases inhibit glycolysis, in particular the glycolysis-limiting enzymes phosphofructokinase and pyruvate kinase [340, 341]. In adipocytes, the proapoptotic caspase-3 and caspase-6, which participate in both intrinsic and extrinsic apoptosis, cleave peroxisome proliferator-activated receptor-γ (PPAR-γ), which results in the nuclear export and cytoplasmic degradation of this transcription factor [342]. Inactivation of PPAR-γ in adipocytes leads to downregulation of some genes that are important for insulin sensitivity not only in adipose tissue but also in other tissues such as those of the skeletal muscle. For example, PPAR-γ inactivation results in decreased expression of GLUT 4 and decreased secretion of adiponectin [343, 344]. Extensive apoptosis of adipocytes, hepatocytes, and skeletal muscle cells is also expected to contribute to systemic hyperglycemia and hyperglycemia-induced stresses that lead to insulin resistance.

4.5. NRLP3 Inflammasome Activation. Interleukin-1β (IL-1β) is an inflammatory cytokine which activates both myeloid and nonmyeloid cells to produce other inflammatory

cytokines and chemokines [345, 346]. Processing of the inactive pro-IL-1β into the active IL-1β requires the formation and activation of a cytoplasmic multiprotein complex called the inflammasome [58, 345]. One of the most intensively studied inflammasomes is the NLRP3 inflammasome which is expressed by myeloid cells and some nonmyeloid cells such as adipocytes, hepatocytes, endothelial cells, skeletal muscle cells, and aortic smooth muscle cells [345, 347–350]. Components of the NLRP3 inflammasome include the NLRP3 sensor, ASC adaptor, and caspase-1 [345]. Signaling pathways through NF-κB, p38, and ERK1 are involved in the expression of both NLRP3 and pro-IL-1β [345, 351–353]. Assembly of the NLRP3 components into the active inflammasome complex occurs in response to "danger signals" including increased intracellular ceramide; RAGE- or IREα-dependent increased expression of thioredoxin-binding protein (TXNIP); oxidation of thioredoxin and its dissociation from TXNIP, allowing the latter to bind to the inflammasome; release of lysosomal cathepsin B as a result of LMP; IRE1-α- and PERK-dependent activation of CHOP; and release of oxidized mitochondrial DNA as a result of MOMP [58, 204, 205, 265, 267, 353–359].

IL-1β is a ligand for the IL-1 receptor which, like TLR4, signals via MyD88, IL-1 receptor-activated kinases (IRAK1 to 4), IKK, and NF-κB (Figure 2) [57, 58, 360] and should thus potentiate the whole model for insulin resistance in insulin target cells (Figure 2). It downregulates IRS-1 expression and reduces tyrosine phosphorylation of IRS-1 in adipocytes [58, 361]. Preadipocytes release IL-1β, which both controls adipocyte differentiation and promotes adipocyte insulin resistance even in the absence of macrophages [58]. IL-1β also induces epigenetic changes that promote insulin resistance. For example, it stimulates the expression of DNA methyl transferase 1, which hypermethylates the adiponectin promoter and thereby suppresses the expression of this proinsulin signaling adipokine [362].

While inflammasome assembly, caspase-1 activation, and IL-1β processing occur and promote insulin resistance in hepatocytes and mature adipocytes, secretion of IL-1β by these cells is controversial [58, 268, 363]. Nevertheless, caspase-1 induces the highly inflammatory pyroptotic death of these cells, and this could contribute to the recruitment and activation of inflammatory myeloid cells such as macrophages that secrete IL-1β [268, 363]. In the skeletal muscle, activation of the inflammasome contributes to muscle atrophy through activation of atrogenic genes such as MuRF1 and atrogin 1 [350].

NLRP inflammasome activation in endothelial cells leads to increased IL-1β in serum and C-reactive protein (CRP) production by endothelial cells [349]. IL-1β stimulates endothelial cell production of chemokines such as monocyte chemoattractant protein-1 (MCP-1) and vascular cell adhesion molecule-1 (VCAM-1) which promote leukocyte-endothelium interactions [349, 364], and this may contribute to the transient migration of neutrophils into adipose tissue that occurs at an early stage of high-fat feeding [365]. This process may be further facilitated by the chemotactic effects of H_2O_2 and IL-8 produced by adipocytes [30, 366]. Once in adipose tissue, neutrophils may produce large quantities of chemokines and cytokines including IL-1β and IL8, resulting in the recruitment of other immune system cells such as macrophages which sustain chronic inflammation [367, 368].

5. Inhibition of Insulin Signaling through the Dysregulation of Cellular Stress Responses

5.1. Dysregulation of the Heat Shock Response. The heat shock response, which relies on heat shock proteins such as HSP70, is important for physiological resolution of inflammation [369]. Cellular HSP70, HSP72, and HSP25 protect against insulin resistance in humans by mechanisms involving prevention of JNK phosphorylation and apoptosis [51–53]. Obese, insulin-resistant individuals have reduced expression of HSP72 [51]. In adipocytes, downregulation of HSP expression follows sustained NLRP3 inflammasome activation and the associated caspase-1-mediated cleavage of HuR, an mRNA-binding protein that enhances the expression of SIRT1 [369]. This results in reduced SIRT1-dependent upregulation of the transcription and activity of heat shock factor 1 (HSF1), the transcription factor of heat shock proteins [369].

5.2. Autophagy Dysregulation. (Macro)autophagy is a homoeostatic process for the bulk degradation of cytoplasmic components including damaged organelles, misfolded proteins, and oxidized lipids, whereby such components are enclosed into double-membraned vesicles called autophagosomes that subsequently fuse with lysosomes [54, 370–372]. Autophagy-related proteins (Atg) are involved in autophagosome formation, and these are functionally categorized into several units, namely, the Atg1/ULK complex (mammals express Ulk 1/2), the class III phosphatidyl inositol 3-kinase (PI3K) complex, the Atg2-Atg18/WIPI complex, the Atg12 conjugation system, the Atg8/LC3 conjugation system, and Atg9 vesicles [373].

Low levels of ROS induce autophagy [373–375], but higher ROS levels inhibit this response [376]. Obesity, which is associated with oxidative stress, is characterized by inhibited autophagy [377], even in adipose tissue that has elevated expression of autophagy genes [378]. Autophagy inhibition occurs partly due to (i) degradation of autophagy proteins by cell death proteases including calpain 1 and caspases such as caspase-3, caspase-6, and caspase-8 [379], (ii) LMP and the release of cathepsins [379, 380], (iii) SIRT downregulation [381, 382], (vi) inhibition of PPAR-α [383], and (vii) increased expression of GSK3β [384].

Severe hepatic downregulation of the autophagy gene Atg7 was found to occur in genetic and dietary models of obesity, and this caused insulin resistance through enhanced ER stress [54]. Paradoxically, muscle- or liver-specific knockout of the Atg7 gene protected mice from obesity and insulin resistance by upregulating the expression of fibroblast growth factor (FGF21) [385]. FGF21 improves insulin sensitivity by inhibiting mTORC 1 [385, 386], activating NRf2 antioxidant signaling, suppressing the NF-κB pathway, enhancing adiponectin production, and promoting thermogenesis [387–391]. The apparently contradictory effects of obesity-associated downregulation of Atg7 and genetic knockout of Atg7 on

hepatocyte insulin resistance [54, 385] may be better understood by considering that Atg7 knockout prevents obesity [385]. In obesity, but not in the lean state, there is resistance to FGF21, because of downregulation of its receptor machinery, including β-klotho protein levels [392–394]. Although klotho is critical for FGF21 function [395], it was recently reported that factors beyond β-klotho downregulation are important contributors to adipose tissue FGF21 resistance [396].

5.3. Dysregulation of the Nrf2 Antioxidant Response. The nuclear factor erythroid-2-related factor-2 (Nrf2) is the master regulator of antioxidant responses, attenuating both oxidative and electrophilic stresses [397, 398]. Under basal conditions, Nrf2 localizes on the cytoskeleton, where its activity is limited through interaction with Kelch-like ECH-associated protein 1 (Keap1), which targets it for ubiquitination and proteosomal degradation [399]. Modification of cysteine residues in Keap1 by ROS, RNS, or RCCs frees Nrf2 to translocate to the nucleus and induce transcription of antioxidant genes having the antioxidant response element in the promoter region [397, 400]. Nevertheless, Nrf2 levels were found to be lower in prediabetic and diabetic patients than in healthy subjects [401], and short-term treatment of high-fat diet-fed mice with curcumin was found to improve insulin sensitivity through attenuating Nrf2 signaling defect [402].

Suppression of Nrf2 activity may be partly due to the direct interaction of p53 with ARE-containing promoters [403]. ERK activation was reported to induce Nrf2 suppression and insulin resistance in cardiomyocytes exposed to hydrogen peroxide [404], but an opposite effect of ERK activation was reported in HepG2 cells exposed to methylglyoxal [405]. In neuronal cells exposed to H_2O_2, GSK3β activation was shown to be responsible for the cytoplasmic accumulation of Nrf2 [251]. This may involve H_2O_2-mediated activatory phosphorylation of tyrosine 216 of GSK3β, and the latter phosphorylates the tyrosine kinase Fyn, which then translocates to the nucleus, and phosphorylates tyrosine 568 of Nrf2, leading to Nrf2 export from the nucleus [406].

Nrf2 antioxidant response is also downregulated by cortisol [407], whose production is increased during psychological stress [117]. Obesity is associated with higher adipose tissue expression of 11β-hydroxysteroid dehydrogenase type 1 (11βHSD1), an enzyme that converts cortisone to active cortisol [408, 409]. Cortisol is a ligand for the mineralocorticoid receptor, whose expression increases in obesity [122].

Notably, Nrf2 is Janus-faced, and its overexpression was found to worsen insulin resistance in mice [410]. Nrf2-knockout mice on a long-term high-fat diet had increased FGF21 expression and better insulin sensitivity than wild-type mice on the same diet, and overexpression of Nrf2 in ST-2 cells was found to decrease insulin sensitivity associated with decreased FGF21 mRNA levels and activity [411]. Nrf2 overexpression may occur during autophagy blockade, which is associated with an increase in the cellular levels of p62 [412, 413]. p62 normally participates in autophagosome formation and undergoes lysosomal degradation with the contents of the autophagosome [412, 413]. However, during autophagy blockade, it sequesters Keap1 into autophagosomes, leading to stabilization and overactivation of Nrf2 by the so called noncanonical pathway [412]. Thus, for beneficial effects, the level of Nrf2 activation needs tight regulation.

6. Conclusion

There is substantial literature in support of the hypothesis that insulin resistance develops from a coordinated interplay between various cellular stresses and stress responses that develop upon the exposure of insulin-responsive cells to hypoxia, excess sugars or certain types of fatty acids, environmental pollutants, or hormones released during psychological stress and obesity. This knowledge will help in the design of better strategies for the prevention and management of insulin resistance.

Conflicts of Interest

The author declares that there are no conflicts of interests regarding the publication of this paper.

References

[1] C. M. Kolka and R. N. Bergman, "The endothelium in diabetes: its role in insulin access and diabetic complications," *Reviews in Endocrine and Metabolic Disorders*, vol. 14, no. 1, pp. 13–19, 2013.

[2] K. Siddle, "Signalling by insulin and IGF receptors: supporting acts and new players," *Journal of Molecular Endocrinology*, vol. 47, no. 1, pp. R1–R10, 2011.

[3] G. Dimitriadis, P. Mitrou, V. Lambadiari, E. Maratou, and S. A. Raptis, "Insulin effects in muscle and adipose tissue," *Diabetes Research and Clinical Practice*, vol. 93, Supplement 1, pp. S52–S59, 2011.

[4] L. J. Fick and D. D. Belsham, "Nutrient sensing and insulin signaling in neuropeptide-expressing immortalized, hypothalamic neurons: a cellular model of insulin resistance," *Cell Cycle*, vol. 9, no. 16, pp. 3186–3193, 2010.

[5] L. Plum, B. F. Belgardt, and J. C. Bruning, "Central insulin action in energy and glucose homeostasis," *Journal of Clinical Investigation*, vol. 116, no. 7, pp. 1761–1766, 2006.

[6] A. Kleinridders, H. A. Ferris, W. Cai, and C. R. Kahn, "Insulin action in brain regulates systemic metabolism and brain function," *Diabetes*, vol. 63, no. 7, pp. 2232–2243, 2014.

[7] K. A. Posey, D. J. Clegg, R. L. Printz et al., "Hypothalamic proinflammatory lipid accumulation, inflammation, and insulin resistance in rats fed a high-fat diet," *American Journal of Physiology-Endocrinology and Metabolism*, vol. 296, no. 5, pp. E1003–E1012, 2009.

[8] D. J. Clegg, K. Gotoh, C. Kemp et al., "Consumption of a high-fat diet induces central insulin resistance independent of adiposity," *Physiology & Behavior*, vol. 103, no. 1, pp. 10–16, 2011.

[9] A. C. Könner, R. Janoschek, L. Plum et al., "Insulin action in AgRP-expressing neurons is required for suppression of hepatic glucose production," *Cell Metabolism*, vol. 5, no. 6, pp. 438–449, 2007.

[10] S. Obici, B. B. Zhang, G. Karkanias, and L. Rossetti, "Hypothalamic insulin signaling is required for inhibition of glucose

production," *Nature Medicine*, vol. 8, no. 12, pp. 1376–1382, 2002.

[11] A. Pocai, T. K. T. Lam, R. Gutierrez-Juarez et al., "Hypothalamic K_{ATP} channels control hepatic glucose production," *Nature*, vol. 434, no. 7036, pp. 1026–1031, 2005.

[12] E. Blázquez, E. Velázquez, V. Hurtado-Carneiro, and J. M. Ruiz-Albusac, "Insulin in the brain: its pathophysiological implications for states related with central insulin resistance, type 2 diabetes and Alzheimer's disease," *Frontiers in Endocrinology*, vol. 5, p. 161, 2014.

[13] M. H. Shanik, Y. Xu, J. Skrha, R. Dankner, Y. Zick, and J. Roth, "Insulin resistance and hyperinsulinemia: is hyperinsulinemia the cart or the horse?," *Diabetes Care*, vol. 31, Supplement 2, pp. S262–S268, 2008.

[14] K. R. Watterson, D. Bestow, J. Gallagher et al., "Anorexigenic and orexigenic hormone modulation of mammalian target of rapamycin complex 1 activity and the regulation of hypothalamic agouti-related protein mRNA expression," *Neurosignals*, vol. 21, no. 1-2, pp. 28–41, 2013.

[15] M. Milanski, A. P. Arruda, A. Coope et al., "Inhibition of hypothalamic inflammation reverses diet-induced insulin resistance in the liver," *Diabetes*, vol. 61, no. 6, pp. 1455–1462, 2012.

[16] C.-L. Lin and C.-N. Huang, "The neuroprotective effects of the anti-diabetic drug linagliptin against Aß-induced neurotoxicity," *Neural Regeneration Research*, vol. 11, no. 2, pp. 236-237, 2016.

[17] S. M. de la Monte, "Insulin resistance and neurodegeneration: progress towards the development of new therapeutics for Alzheimer's disease," *Drugs*, vol. 77, no. 1, pp. 47–65, 2017.

[18] E. Forno, Y.-Y. Han, R. H. Muzumdar, and J. C. Celedón, "Insulin resistance, metabolic syndrome, and lung function in US adolescents with and without asthma," *Journal of Allergy and Clinical Immunology*, vol. 136, no. 2, pp. 304–311.e8, 2015.

[19] Q. Wang, X. L. Cheng, D. Y. Zhang et al., "Tectorigenin attenuates palmitate-induced endothelial insulin resistance via targeting ROS-associated inflammation and IRS-1 pathway," *PLoS One*, vol. 8, no. 6, article e66417, 2013.

[20] D. Gao, S. Nong, X. Huang et al., "The effects of palmitate on hepatic insulin resistance are mediated by NADPH oxidase 3-derived reactive oxygen species through JNK and $p38^{MAPK}$ pathways," *Journal of Biological Chemistry*, vol. 285, no. 39, pp. 29965–29973, 2010.

[21] A. S. P. de Figueiredo, A. B. Salmon, F. Bruno et al., "Nox2 mediates skeletal muscle insulin resistance induced by a high fat diet," *Journal of Biological Chemistry*, vol. 290, no. 21, pp. 13427–13439, 2015.

[22] L. Yuzefovych, G. Wilson, and L. Rachek, "Different effects of oleate vs. palmitate on mitochondrial function, apoptosis, and insulin signaling in L6 skeletal muscle cells: role of oxidative stress," *American Journal of Physiology-Endocrinology and Metabolism*, vol. 299, no. 6, pp. E1096–E1105, 2010.

[23] L. I. Rachek, S. I. Musiyenko, S. P. LeDoux, and G. L. Wilson, "Palmitate induced mitochondrial deoxyribonucleic acid damage and apoptosis in l6 rat skeletal muscle cells," *Endocrinology*, vol. 148, no. 1, pp. 293–299, 2007.

[24] F. Renström, J. Burén, M. Svensson, and J. W. Eriksson, "Insulin resistance induced by high glucose and high insulin precedes insulin receptor substrate 1 protein depletion in human adipocytes," *Metabolism*, vol. 56, no. 2, pp. 190–198, 2007.

[25] N. Jaiswal, C. K. Maurya, J. Pandey, A. K. Rai, and A. K. Tamrakar, "Fructose-induced ROS generation impairs glucose utilization in L6 skeletal muscle cells," *Free Radical Research*, vol. 49, no. 9, pp. 1055–1068, 2015.

[26] B. Kwon and H. W. Querfurth, "Opposite effects of saturated and unsaturated free fatty acids on intracellular signaling and metabolism in neuronal cells," *Inflammation and Cell Signaling*, vol. 1, no. 2, 2014.

[27] J. C. Moraes, A. Coope, J. Morari et al., "High-fat diet induces apoptosis of hypothalamic neurons," *PLoS One*, vol. 4, no. 4, article e5045, 2009.

[28] J. J. Kim and D. D. Sears, "TLR4 and insulin resistance," *Gastroenterology Research and Practice*, vol. 2010, Article ID 212563, 11 pages, 2010.

[29] L. A. Velloso, F. Folli, and M. J. Saad, "TLR4 at the crossroads of nutrients, gut microbiota, and metabolic inflammation," *Endocrine Reviews*, vol. 36, no. 3, pp. 245–271, 2015.

[30] A. N. Onyango, "The contribution of singlet oxygen to insulin resistance," *Oxidative Medicine and Cellular Longevity*, vol. 2017, Article ID 8765972, 14 pages, 2017.

[31] T. Nakashima, S. Umemoto, K. Yoshimura et al., "TLR4 is a critical regulator of angiotensin II-induced vascular remodeling: the roles of extracellular SOD and NADPH oxidase," *Hypertension Research*, vol. 38, no. 10, pp. 649–655, 2015.

[32] M. Sakaguchi, H. Murata, K. Yamamoto et al., "TIRAP, an adaptor protein for TLR2/4, transduces a signal from RAGE phosphorylated upon ligand binding," *PLoS One*, vol. 6, no. 8, article e23132, 2011.

[33] K. H. J. Gaens, G. H. Goossens, P. M. Niessen et al., "N^{ε}-(carboxymethyl)lysine-receptor for advanced glycation end product axis is a key modulator of obesity-induced dysregulation of adipokine expression and insulin resistance," *Arteriosclerosis, Thrombosis, and Vascular Biology*, vol. 34, no. 6, pp. 1199–1208, 2014.

[34] W. Cai, X.-M. Duan, Y. Liu et al., "Uric acid induces endothelial dysfunction by activating the HMGB1/RAGE signaling pathway," *BioMed Research International*, vol. 2017, Article ID 4391920, 11 pages, 2017.

[35] B. Scazzocchio, R. Varì, M. D'Archivio et al., "Oxidized LDL impair adipocyte response to insulin by activating serine/threonine kinases," *Journal of Lipid Research*, vol. 50, no. 5, pp. 832–845, 2009.

[36] N. Clavreul, M. M. Bachschmid, X. Hou et al., "S-Glutathiolation of p21ras by peroxynitrite mediates endothelial insulin resistance caused by oxidized low-density lipoprotein," *Arteriosclerosis, Thrombosis, and Vascular Biology*, vol. 26, no. 11, pp. 2454–2461, 2006.

[37] S. Pereira, E. Park, Y. Mori et al., "FFA-induced hepatic insulin resistance in vivo is mediated by PKCδ, NADPH oxidase, and oxidative stress," *American Journal of Physiology-Endocrinology and Metabolism*, vol. 307, no. 1, pp. E34–E46, 2014.

[38] P. Sukumar, H. Viswambharan, H. Imrie et al., "Nox2 NADPH oxidase has a critical role in insulin resistance–related endothelial cell dysfunction," *Diabetes*, vol. 62, no. 6, pp. 2130–2134, 2013.

[39] L. J. den Hartigh, M. Omer, L. Goodspeed et al., "Adipocyte-specific deficiency of NADPH oxidase 4 delays the onset of insulin resistance and attenuates adipose tissue inflammation

in obesity," *Arteriosclerosis, Thrombosis, and Vascular Biology*, vol. 37, no. 3, pp. 466–475, 2017.

[40] E. J. Anderson, M. E. Lustig, K. E. Boyle et al., "Mitochondrial H_2O_2 emission and cellular redox state link excess fat intake to insulin resistance in both rodents and humans," *The Journal of Clinical Investigation*, vol. 119, no. 3, pp. 573–581, 2009.

[41] H.-N. Cha, S. E. Song, Y.-W. Kim, J.-Y. Kim, K.-C. Won, and S.-Y. Park, "Lack of inducible nitric oxide synthase prevents lipid-induced skeletal muscle insulin resistance without attenuating cytokine level," *Journal of Pharmacological Sciences*, vol. 117, no. 2, pp. 77–86, 2011.

[42] A. Charbonneau and A. Marette, "Inducible nitric oxide synthase induction underlies lipid-induced hepatic insulin resistance in mice: potential role of tyrosine nitration of insulin signaling proteins," *Diabetes*, vol. 59, no. 4, pp. 861–871, 2010.

[43] T. M. Zanotto, P. G. F. Quaresma, D. Guadagnini et al., "Blocking iNOS and endoplasmic reticulum stress synergistically improves insulin resistance in mice," *Molecular Metabolism*, vol. 6, no. 2, pp. 206–218, 2017.

[44] D. M. Erion and G. I. Shulman, "Diacylglycerol-mediated insulin resistance," *Nature Medicine*, vol. 16, no. 4, pp. 400–402, 2010.

[45] M. Campana, L. Bellini, C. Rouch et al., "Inhibition of central de novo ceramide synthesis restores insulin signaling in hypothalamus and enhances β-cell function of obese Zucker rats," *Molecular Metabolism*, vol. 8, pp. 23–36, 2018.

[46] J. A. Chavez and S. A. Summers, "A ceramide-centric view of insulin resistance," *Cell Metabolism*, vol. 15, no. 5, pp. 585–594, 2012.

[47] S. Turban and E. Hajduch, "Protein kinase C isoforms: mediators of reactive lipid metabolites in the development of insulin resistance," *FEBS Letters*, vol. 585, no. 2, pp. 269–274, 2011.

[48] E. Panzhinskiy, J. Ren, and S. Nair, "Protein tyrosine phosphatase 1B and insulin resistance: role of endoplasmic reticulum stress/reactive oxygen species/nuclear factor kappa B axis," *PLoS One*, vol. 8, no. 10, article e77228, 2013.

[49] W. Zhang, V. Hietakangas, S. Wee, S. C. Lim, J. Gunaratne, and S. M. Cohen, "ER stress potentiates insulin resistance through PERK-mediated FOXO phosphorylation," *Genes & Development*, vol. 27, no. 4, pp. 441–449, 2013.

[50] B. Diaz, L. Fuentes-Mera, A. Tovar et al., "Saturated lipids decrease mitofusin 2 leading to endoplasmic reticulum stress activation and insulin resistance in hypothalamic cells," *Brain Research*, vol. 1627, pp. 80–89, 2015.

[51] J. Chung, A. K. Nguyen, D. C. Henstridge et al., "HSP72 protects against obesity-induced insulin resistance," *Proceedings of the National Academy of Sciences of the United States of America*, vol. 105, no. 5, pp. 1739–1744, 2008.

[52] P. C. Geiger and A. A. Gupte, "Heat shock proteins are important mediators of skeletal muscle insulin sensitivity," *Exercise and Sport Sciences Reviews*, vol. 39, no. 1, pp. 34–42, 2011.

[53] L. Chichester, A. T. Wylie, S. Craft, and K. Kavanagh, "Muscle heat shock protein 70 predicts insulin resistance with aging," *The Journals of Gerontology Series A: Biological Sciences and Medical Sciences*, vol. 70, no. 2, pp. 155–162, 2015.

[54] L. Yang, P. Li, S. Fu, E. S. Calay, and G. S. Hotamisligil, "Defective hepatic autophagy in obesity promotes ER stress and causes insulin resistance," *Cell Metabolism*, vol. 11, no. 6, pp. 467–478, 2010.

[55] N. Alkhouri, A. Gornicka, M. P. Berk et al., "Adipocyte apoptosis, a link between obesity, insulin resistance, and hepatic steatosis," *Journal of Biological Chemistry*, vol. 285, no. 5, pp. 3428–3438, 2010.

[56] Z. Derdak, C. H. Lang, K. A. Villegas et al., "Activation of p53 enhances apoptosis and insulin resistance in a rat model of alcoholic liver disease," *Journal of Hepatology*, vol. 54, no. 1, pp. 164–172, 2011.

[57] O. Nov, A. Kohl, E. C. Lewis et al., "Interleukin-1β may mediate insulin resistance in liver-derived cells in response to adipocyte inflammation," *Endocrinology*, vol. 151, no. 9, pp. 4247–4256, 2010.

[58] R. Stienstra, C. J. Tack, T.-D. Kanneganti, L. A. B. Joosten, and M. G. Netea, "The inflammasome puts obesity in the danger zone," *Cell Metabolism*, vol. 15, no. 1, pp. 10–18, 2012.

[59] V. T. Samuel and G. I. Shulman, "Mechanisms for insulin resistance: common threads and missing links," *Cell*, vol. 148, no. 5, pp. 852–871, 2012.

[60] S. Pendyala, J. M. Walker, and P. R. Holt, "A high-fat diet is associated with endotoxemia that originates from the gut," *Gastroenterology*, vol. 142, no. 5, pp. 1100-1101.e2, 2012.

[61] B. di Luccia, R. Crescenzo, A. Mazzoli et al., "Rescue of fructose-induced metabolic syndrome by antibiotics or faecal transplantation in a rat model of obesity," *PLoS One*, vol. 10, no. 8, article e0134893, 2015.

[62] L. Jia, C. R. Vianna, M. Fukuda et al., "Hepatocyte Toll-like receptor 4 regulates obesity-induced inflammation and insulin resistance," *Nature Communications*, vol. 5, p. 3778, 2014.

[63] R. Rorato, B. d. C. Borges, E. T. Uchoa, J. Antunes-Rodrigues, C. F. Elias, and L. L. K. Elias, "LPS-induced low-grade inflammation increases hypothalamic JNK expression and causes central insulin resistance irrespective of body weight changes," *International Journal of Molecular Sciences*, vol. 18, no. 12, p. 1431, 2017.

[64] D. J. Loegering and M. R. Lennartz, "Protein kinase C and toll-like receptor signaling," *Enzyme Research*, vol. 2011, Article ID 537821, 7 pages, 2011.

[65] J. Zhang, W. Wu, D. Li, Y. Guo, and H. Ding, "Overactivation of NF-κB impairs insulin sensitivity and mediates palmitate-induced insulin resistance in C2C12 skeletal muscle cells," *Endocrine*, vol. 37, no. 1, pp. 157–166, 2010.

[66] I.-C. Yu, H.-Y. Lin, N.-C. Liu et al., "Neuronal androgen receptor regulates insulin sensitivity via suppression of hypothalamic NF-κB–mediated PTP1B expression," *Diabetes*, vol. 62, no. 2, pp. 411–423, 2013.

[67] L. Chen, R. Chen, H. Wang, and F. Liang, "Mechanisms linking inflammation to insulin resistance," *International Journal of Endocrinology*, vol. 2015, Article ID 508409, 9 pages, 2015.

[68] T. Kawasaki and T. Kawai, "Toll-like receptor signaling pathways," *Frontiers in Immunology*, vol. 5, p. 461, 2014.

[69] M. J. Morgan and Z. Liu, "Crosstalk of reactive oxygen species and NF-κB signaling," *Cell Research*, vol. 21, no. 1, pp. 103–115, 2011.

[70] R. Radi, "Protein tyrosine nitration: biochemical mechanisms and structural basis of functional effects," *Accounts of Chemical Research*, vol. 46, no. 2, pp. 550–559, 2013.

[71] P. di Mascio, E. J. H. Bechara, M. H. G. Medeiros, K. Briviba, and H. Sies, "Singlet molecular oxygen production in the reaction of peroxynitrite with hydrogen peroxide," *FEBS Letters*, vol. 355, no. 3, pp. 287–289, 1994.

[72] J. Lugrin, N. Rosenblatt-Velin, R. Parapanov, and L. Liaudet, "The role of oxidative stress during inflammatory processes," *Biological Chemistry*, vol. 395, no. 2, pp. 203–230, 2014.

[73] A. Elgawish, M. Glomb, M. Friedlander, and V. M. Monnier, "Involvement of hydrogen peroxide in collagen cross-linking by high glucose in vitro and in vivo," *Journal of Biological Chemistry*, vol. 271, no. 22, pp. 12964–12971, 1996.

[74] A. N. Onyango, "Endogenous generation of singlet oxygen and ozone in human and animal tissues: mechanisms, biological significance, and influence of dietary components," *Oxidative Medicine and Cellular Longevity*, vol. 2016, Article ID 2398573, 22 pages, 2016.

[75] M. Aragno and R. Mastrocola, "Dietary sugars and endogenous formation of advanced glycation endproducts: emerging mechanisms of disease," *Nutrients*, vol. 9, no. 12, p. 385, 2017.

[76] C. O. Silva, O. A. da Silva, G. P. Duarte, B. Descomps, and S. La, "Apocynin decreases AGEs-induced stimulation of NF-κB protein expression in vascular smooth muscle cells from GK rats," *Pharmaceutical Biology*, vol. 53, no. 4, pp. 488–493, 2015.

[77] J. W. Eriksson, "Metabolic stress in insulin's target cells leads to ROS accumulation – a hypothetical common pathway causing insulin resistance," *FEBS Letters*, vol. 581, no. 19, pp. 3734–3742, 2007.

[78] E. Salaun, L. Lefeuvre-Orfila, T. Cavey et al., "Myriocin prevents muscle ceramide accumulation but not muscle fiber atrophy during short-term mechanical unloading," *Journal of Applied Physiology*, vol. 120, no. 2, pp. 178–187, 2016.

[79] C. Y. Han, A. Y. Kargi, M. Omer et al., "Differential effect of saturated and unsaturated free fatty acids on the generation of monocyte adhesion and chemotactic factors by adipocytes: dissociation of adipocyte hypertrophy from inflammation," *Diabetes*, vol. 59, no. 2, pp. 386–396, 2010.

[80] T. Inoguchi, P. Li, F. Umeda et al., "High glucose level and free fatty acid stimulate reactive oxygen species production through protein kinase C–dependent activation of NAD(P)H oxidase in cultured vascular cells," *Diabetes*, vol. 49, no. 11, pp. 1939–1945, 2000.

[81] W. L. Holland, B. T. Bikman, L.-P. Wang et al., "Lipid-induced insulin resistance mediated by the proinflammatory receptor TLR4 requires saturated fatty acid–induced ceramide biosynthesis in mice," *The Journal of Clinical Investigation*, vol. 121, no. 5, pp. 1858–1870, 2011.

[82] P. Barma, S. Bhattacharya, A. Bhattacharya et al., "Lipid induced overexpression of NF-κB in skeletal muscle cells is linked to insulin resistance," *Biochimica et Biophysica Acta (BBA) - Molecular Basis of Disease*, vol. 1792, no. 3, pp. 190–200, 2009.

[83] L. C. Joseph, E. Barca, P. Subramanyam et al., "Inhibition of NAPDH oxidase 2 (NOX2) prevents oxidative stress and mitochondrial abnormalities caused by saturated fat in cardiomyocytes," *PLoS One*, vol. 11, no. 1, article e0145750, 2016.

[84] T. Galbo, R. J. Perry, M. J. Jurczak et al., "Saturated and unsaturated fat induce hepatic insulin resistance independently of TLR-4 signaling and ceramide synthesis in vivo," *Proceedings of the National Academy of Sciences of the United States of America*, vol. 110, no. 31, pp. 12780–12785, 2013.

[85] D. Cosentino-Gomes, N. Rocco-Machado, and J. R. Meyer-Fernandes, "Cell signaling through protein kinase C oxidation and activation," *International Journal of Molecular Sciences*, vol. 13, no. 12, pp. 10697–10721, 2012.

[86] M. Maceyka and S. Spiegel, "Sphingolipid metabolites in inflammatory disease," *Nature*, vol. 510, no. 7503, pp. 58–67, 2014.

[87] D. J. Powell, S. Turban, A. Gray, E. Hajduch, and H. S. Hundal, "Intracellular ceramide synthesis and protein kinase Cζ activation play an essential role in palmitate-induced insulin resistance in rat L6 skeletal muscle cells," *Biochemical Journal*, vol. 382, no. 2, pp. 619–629, 2004.

[88] R. Hage Hassan, A. C. Pacheco de Sousa, R. Mahfouz et al., "Sustained action of ceramide on the insulin signaling pathway in muscle cells: implication of the double-stranded RNA-activated protein kinase," *Journal of Biological Chemistry*, vol. 291, no. 6, pp. 3019–3029, 2016.

[89] C. García-Ruiz, A. Colell, M. Marí, A. Morales, and J. C. Fernández-Checa, "Direct effect of ceramide on the mitochondrial electron transport chain leads to generation of reactive oxygen species," *Journal of Biological Chemistry*, vol. 272, no. 17, pp. 11369–11377, 1997.

[90] E. P. Taddeo, R. C. Laker, D. S. Breen et al., "Opening of the mitochondrial permeability transition pore links mitochondrial dysfunction to insulin resistance in skeletal muscle," *Molecular Metabolism*, vol. 3, no. 2, pp. 124–134, 2014.

[91] T. Matsunaga, S. Kotamraju, S. V. Kalivendi, A. Dhanasekaran, J. Joseph, and B. Kalyanaraman, "Ceramide-induced intracellular oxidant formation, iron signaling, and apoptosis in endothelial cells: protective role of endogenous nitric oxide," *Journal of Biological Chemistry*, vol. 279, no. 27, pp. 28614–28624, 2004.

[92] J. D. Symons and E. D. Abel, "Lipotoxicity contributes to endothelial dysfunction: a focus on the contribution from ceramide," *Reviews in Endocrine and Metabolic Disorders*, vol. 14, no. 1, pp. 59–68, 2013.

[93] S. P. Didion and F. M. Faraci, "Ceramide-induced impairment of endothelial function is prevented by CuZn superoxide dismutase overexpression," *Arteriosclerosis, Thrombosis, and Vascular Biology*, vol. 25, pp. 90–95, 2004.

[94] M. E. Smith, T. S. Tippetts, E. S. Brassfield et al., "Mitochondrial fission mediates ceramide-induced metabolic disruption in skeletal muscle," *Biochemical Journal*, vol. 456, no. 3, pp. 427–439, 2013.

[95] H. F. Jheng, P. J. Tsai, S. M. Guo et al., "Mitochondrial fission contributes to mitochondrial dysfunction and insulin resistance in skeletal muscle," *Molecular and Cellular Biology*, vol. 32, no. 2, pp. 309–319, 2012.

[96] H. Yuan, A. A. Gerencser, G. Liot et al., "Mitochondrial fission is an upstream and required event for bax foci formation in response to nitric oxide in cortical neurons," *Cell Death & Differentiation*, vol. 14, no. 3, pp. 462–471, 2007.

[97] G. Zhao, K. Cao, C. Xu et al., "Crosstalk between mitochondrial fission and oxidative stress in paraquat-induced apoptosis in mouse alveolar type II cells," *International Journal of Biological Sciences*, vol. 13, no. 7, pp. 888–900, 2017.

[98] R. Schüler, M. A. Osterhoff, T. Frahnow et al., "High-saturated-fat diet increases circulating angiotensin-converting enzyme, which is enhanced by the rs4343 polymorphism defining persons at risk of nutrient-dependent increases of blood pressure," *Journal of the American Heart Association*, vol. 6, no. 1, article e004465, 2017.

[99] C. Cabello-Verrugio, M. G. Morales, J. C. Rivera, D. Cabrera, and F. Simon, "Renin-angiotensin system: an old player with novel functions in skeletal muscle," *Medicinal Research Reviews*, vol. 35, no. 3, pp. 437–463, 2015.

[100] M. Ruiz-Ortega, O. Lorenzo, M. Ruperez, S. Konig, B. Wittig, and J. Egido, "Angiotensin II activates nuclear transcription factor κB through AT_1 and AT_2 in vascular smooth muscle cells: molecular mechanisms," *Circulation Research*, vol. 86, no. 12, pp. 1266–1272, 2000.

[101] Y. Ji, J. Liu, Z. Wang, and N. Liu, "Angiotensin II induces inflammatory response partly via toll-like receptor 4-dependent signaling pathway in vascular smooth muscle cells," *Cellular Physiology and Biochemistry*, vol. 23, no. 4-6, pp. 265–276, 2009.

[102] M.-S. Zhou, C. Liu, R. Tian, A. Nishiyama, and L. Raij, "Skeletal muscle insulin resistance in salt-sensitive hypertension: role of angiotensin II activation of NFκB," *Cardiovascular Diabetology*, vol. 14, no. 1, p. 45, 2015.

[103] M. Mitsuishi, K. Miyashita, A. Muraki, and H. Itoh, "Angiotensin II reduces mitochondrial content in skeletal muscle and affects glycemic control," *Diabetes*, vol. 58, no. 3, pp. 710–717, 2009.

[104] Y. Chen, J.-R. Lin, and P.-J. Gao, "Mitochondrial division inhibitor Mdivi-1 ameliorates angiotensin II-induced endothelial dysfunction," *Acta Physiologica Sinica*, vol. 68, no. 5, pp. 669–676, 2016.

[105] U. Landmesser, S. Spiekermann, C. Preuss et al., "Angiotensin II induces endothelial xanthine oxidase activation: role for endothelial dysfunction in patients with coronary disease," *Arteriosclerosis, Thrombosis, and Vascular Biology*, vol. 27, no. 4, pp. 943–948, 2007.

[106] C. Vonach, K. Viola, B. Giessrigl et al., "NF-κB mediates the 12(S)-HETE-induced endothelial to mesenchymal transition of lymphendothelial cells during the intravasation of breast carcinoma cells," *British Journal of Cancer*, vol. 105, no. 2, pp. 263–271, 2011.

[107] J. L. Nadler, R. Natarajan, and N. Stern, "Specific action of the lipoxygenase pathway in mediating angiotensin II-induced aldosterone synthesis in isolated adrenal glomerulosa cells," *The Journal of Clinical Investigation*, vol. 80, no. 6, pp. 1763–1769, 1987.

[108] T. Bruder-Nascimento, M. A. B. da Silva, and R. C. Tostes, "The involvement of aldosterone on vascular insulin resistance: implications in obesity and type 2 diabetes," *Diabetology & Metabolic Syndrome*, vol. 6, no. 1, p. 90, 2014.

[109] L. D. Kubzansky and G. K. Adler, "Aldosterone: a forgotten mediator of the relationship between psychological stress and heart disease," *Neuroscience & Biobehavioral Reviews*, vol. 34, no. 1, pp. 80–86, 2010.

[110] F. Iwashima, T. Yoshimoto, I. Minami, M. Sakurada, Y. Hirono, and Y. Hirata, "Aldosterone induces superoxide generation via Rac1 activation in endothelial cells," *Endocrinology*, vol. 149, no. 3, pp. 1009–1014, 2008.

[111] Y. Zhang, Y. Pan, Z. Bian et al., "Ceramide production mediates aldosterone-induced human umbilical vein endothelial cell (HUVEC) damages," *PLoS One*, vol. 11, no. 1, article e0146944, 2016.

[112] Z.-H. Zhang, Y. Yu, Y.-M. Kang, S.-G. Wei, and R. B. Felder, "Aldosterone acts centrally to increase brain renin-angiotensin system activity and oxidative stress in normal rats," *American Journal of Physiology-Heart and Circulatory Physiology*, vol. 294, no. 2, pp. H1067–H1074, 2008.

[113] B. S. Huang, H. Zheng, J. Tan, K. P. Patel, and F. H. H. Leenen, "Regulation of hypothalamic renin-angiotensin system and oxidative stress by aldosterone," *Experimental Physiology*, vol. 96, no. 10, pp. 1028–1038, 2011.

[114] L. Wang, G. Muxin, H. Nishida, C. Shirakawa, S. Sato, and T. Konishi, "Psychological stress-induced oxidative stress as a model of sub-healthy condition and the effect of TCM," *Evidence-Based Complementary and Alternative Medicine*, vol. 4, no. 2, 202 pages, 2007.

[115] L. Li, X. Li, W. Zhou, and J. L. Messina, "Acute psychological stress results in the rapid development of insulin resistance," *Journal of Endocrinology*, vol. 217, no. 2, pp. 175–184, 2013.

[116] K. Aschbacher, A. O'Donovan, O. M. Wolkowitz, F. S. Dhabhar, Y. Su, and E. Epel, "Good stress, bad stress and oxidative stress: insights from anticipatory cortisol reactivity," *Psychoneuroendocrinology*, vol. 38, no. 9, pp. 1698–1708, 2013.

[117] M. Hayashi, K. Takeshita, Y. Uchida et al., "Angiotensin II receptor blocker ameliorates stress-induced adipose tissue inflammation and insulin resistance," *PLoS One*, vol. 9, no. 12, article e116163, 2014.

[118] K. M. M. Hasan, M. S. Rahman, K. M. T. Arif, and M. E. Sobhani, "Psychological stress and aging: role of glucocorticoids (GCs)," *Age*, vol. 34, no. 6, pp. 1421–1433, 2012.

[119] A. Zafir and N. Banu, "Modulation of in vivo oxidative status by exogenous corticosterone and restraint stress in rats," *Stress*, vol. 12, no. 2, pp. 167–177, 2009.

[120] A. Joergensen, K. Broedbaek, A. Weimann et al., "Association between urinary excretion of cortisol and markers of oxidatively damaged DNA and RNA in humans," *PLoS One*, vol. 6, no. 6, article e20795, 2011.

[121] W. L. Holland, J. T. Brozinick, L.-P. Wang et al., "Inhibition of ceramide synthesis ameliorates glucocorticoid-, saturated-fat-, and obesity-induced insulin resistance," *Cell Metabolism*, vol. 5, no. 3, pp. 167–179, 2007.

[122] T.-C. Chen, D. I. Benjamin, T. Kuo et al., "The glucocorticoid-Angptl4-ceramide axis induces insulin resistance through PP2A and PKCζ," *Science Signaling*, vol. 10, no. 489, article eaai7905, 2017.

[123] A. Hirata, N. Maeda, H. Nakatsuji et al., "Contribution of glucocorticoid–mineralocorticoid receptor pathway on the obesity-related adipocyte dysfunction," *Biochemical and Biophysical Research Communications*, vol. 419, no. 2, pp. 182–187, 2012.

[124] K. de Punder and L. Pruimboom, "Stress induces endotoxemia and low-grade inflammation by increasing barrier permeability," *Frontiers in Immunology*, vol. 6, p. 223, 2015.

[125] A. A. Teitelbaum, M. G. Gareau, J. Jury, P. C. Yang, and M. H. Perdue, "Chronic peripheral administration of corticotropin-releasing factor causes colonic barrier dysfunction similar to psychological stress," *American Journal of Physiology-Gastrointestinal and Liver Physiology*, vol. 295, no. 3, pp. G452–G459, 2008.

[126] G. Zheng, G. Victor Fon, W. Meixner et al., "Chronic stress and intestinal barrier dysfunction: glucocorticoid receptor and transcription repressor HES1 regulate tight junction protein claudin-1 promoter," *Scientific Reports*, vol. 7, no. 1, p. 4502, 2017.

[127] S. Ranabir and K. Reetu, "Stress and hormones," *Indian Journal of Endocrinology and Metabolism*, vol. 15, no. 1, pp. 18–22, 2011.

[128] S. Mangmool, T. Denkaew, W. Parichatikanond, and H. Kurose, "β-Adrenergic receptor and insulin resistance in the heart," *Biomolecules & Therapeutics*, vol. 25, no. 1, pp. 44–56, 2017.

[129] Y.-C. Fu, S.-C. Yin, C.-S. Chi, B. Hwang, and S.-L. Hsu, "Norepinephrine induces apoptosis in neonatal rat endothelial cells via a ROS-dependent JNK activation pathway," *Apoptosis*, vol. 11, no. 11, pp. 2053–2063, 2006.

[130] T. Theccanat, J. L. Philip, A. M. Razzaque et al., "Regulation of cellular oxidative stress and apoptosis by G protein-coupled receptor kinase-2; the role of NADPH oxidase 4," *Cellular Signalling*, vol. 28, no. 3, pp. 190–203, 2016.

[131] D. C. Andersson, J. Fauconnier, T. Yamada et al., "Mitochondrial production of reactive oxygen species contributes to the β-adrenergic stimulation of mouse cardiomycytes," *The Journal of Physiology*, vol. 589, no. 7, pp. 1791–1801, 2011.

[132] Q. Xu, A. Dalic, L. Fang et al., "Myocardial oxidative stress contributes to transgenic β_2-adrenoceptor activation-induced cardiomyopathy and heart failure," *British Journal of Pharmacology*, vol. 162, no. 5, pp. 1012–1028, 2011.

[133] E. P. Mottillo, X. J. Shen, and J. G. Granneman, "β3-adrenergic receptor induction of adipocyte inflammation requires lipolytic activation of stress kinases p38 and JNK," *Biochimica et Biophysica Acta (BBA) - Molecular and Cell Biology of Lipids*, vol. 1801, no. 9, pp. 1048–1055, 2010.

[134] M. Fasshauer, J. Klein, S. Neumann, M. Eszlinger, and R. Paschke, "Adiponectin gene expression is inhibited by β-adrenergic stimulation via protein kinase A in 3T3-L1 adipocytes," *FEBS Letters*, vol. 507, no. 2, pp. 142–146, 2001.

[135] W. L. Holland, J. Y. Xia, J. A. Johnson et al., "Inducible overexpression of adiponectin receptors highlight the roles of adiponectin-induced ceramidase signaling in lipid and glucose homeostasis," *Molecular Metabolism*, vol. 6, no. 3, pp. 267–275, 2017.

[136] M. Siervo, H. L. Riley, B. O. Fernandez et al., "Effects of prolonged exposure to hypobaric hypoxia on oxidative stress, inflammation and gluco-insular regulation: the not-so-sweet price for good regulation," *PLoS One*, vol. 9, no. 4, article e94915, 2014.

[137] L. Lavie, "Oxidative stress—a unifying paradigm in obstructive sleep apnea and comorbidities," *Progress in Cardiovascular Diseases*, vol. 51, no. 4, pp. 303–312, 2009.

[138] G. S. Hamilton and S. A. Joosten, "Obstructive sleep apnoea and obesity," *Australian Family Physician*, vol. 46, no. 7, pp. 460–463, 2017.

[139] R.-B. Guo, P. L. Sun, A. P. Zhao et al., "Chronic asthma results in cognitive dysfunction in immature mice," *Experimental Neurology*, vol. 247, pp. 209–217, 2013.

[140] M. Arshi, J. Cardinal, R. J. Hill, P. S. W. Davies, and C. Wainwright, "Asthma and insulin resistance in children," *Respirology*, vol. 15, no. 5, pp. 779–784, 2010.

[141] L. Cottrell, W. A. Neal, C. Ice, M. K. Perez, and G. Piedimonte, "Metabolic abnormalities in children with asthma," *American Journal of Respiratory and Critical Care Medicine*, vol. 183, no. 4, pp. 441–448, 2011.

[142] P. Hernansanz-Agustín, E. Ramos, E. Navarro et al., "Mitochondrial complex I deactivation is related to superoxide production in acute hypoxia," *Redox Biology*, vol. 12, pp. 1040–1051, 2017.

[143] N. S. Chandel, D. S. McClintock, C. E. Feliciano et al., "Reactive oxygen species generated at mitochondrial complex III stabilize hypoxia-inducible factor-1α during hypoxia," *Journal of Biological Chemistry*, vol. 275, no. 33, pp. 25130–25138, 2000.

[144] X. Tang, D. Guo, C. Lin et al., "hCLOCK causes Rho-kinase-mediated endothelial dysfunction and NF-κB-mediated inflammatory responses," *Oxidative Medicine and Cellular Longevity*, vol. 2015, Article ID 671839, 9 pages, 2015.

[145] L. Song, H. Yang, H. X. Wang et al., "Inhibition of 12/15 lipoxygenase by baicalein reduces myocardial ischemia/reperfusion injury via modulation of multiple signaling pathways," *Apoptosis*, vol. 19, no. 4, pp. 567–580, 2014.

[146] R. Choudhary, U. Malairaman, and A. Katyal, "Inhibition of 12/15 LOX ameliorates cognitive and cholinergic dysfunction in mouse model of hypobaric hypoxia via. attenuation of oxidative/nitrosative stress," *Neuroscience*, vol. 359, pp. 308–324, 2017.

[147] S. Pallast, K. Arai, X. Wang, E. H. Lo, and K. van Leyen, "12/15-Lipoxygenase targets neuronal mitochondria under oxidative stress," *Journal of Neurochemistry*, vol. 111, no. 3, pp. 882–889, 2009.

[148] D. D. Sears, P. D. Miles, J. Chapman et al., "12/15-Lipoxygenase is required for the early onset of high fat diet-induced adipose tissue inflammation and insulin resistance in mice," *PLoS One*, vol. 4, no. 9, article e7250, 2009.

[149] R. Natarajan, M. A. Reddy, K. U. Malik, S. Fatima, and B. V. Khan, "Signaling mechanisms of nuclear factor-κB-mediated activation of inflammatory genes by 13-hydroperoxyoctadecadienoic acid in cultured vascular smooth muscle cells," *Arteriosclerosis, Thrombosis, and Vascular Biology*, vol. 21, no. 9, pp. 1408–1413, 2001.

[150] A. S. Whitehouse, J. Khal, and M. J. Tisdale, "Induction of protein catabolism in myotubes by 15(S)-hydroxyeicosatetraenoic acid through increased expression of the ubiquitin–proteasome pathway," *British Journal of Cancer*, vol. 89, no. 4, pp. 737–745, 2003.

[151] J. Li, J. Rao, Y. Liu et al., "15-Lipoxygenase promotes chronic hypoxia–induced pulmonary artery inflammation via positive interaction with nuclear factor-κB," *Arteriosclerosis, Thrombosis, and Vascular Biology*, vol. 33, no. 5, pp. 971–979, 2013.

[152] L. Guo, X. Tang, X. Chu et al., "Role of protein kinase C in 15-HETE-induced hypoxic pulmonary vasoconstriction," *Prostaglandins, Leukotrienes and Essential Fatty Acids*, vol. 80, no. 2-3, pp. 115–123, 2009.

[153] D. G. Tang, C. A. Diglio, and K. V. Honn, "12(S)-HETE-induced microvascular endothelial cell retraction results from PKC-dependent rearrangement of cytoskeletal elements and $\alpha V\beta 3$ integrins," *Prostaglandins*, vol. 45, no. 3, pp. 249–267, 1993.

[154] R. Chattopadhyay, A. Tinnikov, E. Dyukova et al., "12/15-Lipoxygenase-dependent ROS production is required for diet-induced endothelial barrier dysfunction," *Journal of Lipid Research*, vol. 56, no. 3, pp. 562–577, 2015.

[155] L. S. Terada, D. M. Guidot, J. A. Leff et al., "Hypoxia injures endothelial cells by increasing endogenous xanthine oxidase activity," *Proceedings of the National Academy of Sciences of the United States of America*, vol. 89, no. 8, pp. 3362–3366, 1992.

[156] S. Sinha, S. N. Singh, and U. S. Ray, "Total antioxidant status at high altitude in lowlanders and native highlanders: role of uric acid," *High Altitude Medicine & Biology*, vol. 10, no. 3, pp. 269–274, 2009.

[157] J. Nanduri, D. R. Vaddi, S. A. Khan et al., "HIF-1α activation by intermittent hypoxia requires NADPH oxidase stimulation by xanthine oxidase," *PLoS One*, vol. 10, no. 3, article e0119762, 2015.

[158] G. K. Kumar, V. Rai, S. D. Sharma et al., "Chronic intermittent hypoxia induces hypoxia-evoked catecholamine efflux in adult rat adrenal medulla via oxidative stress," *Journal of Physiology*, vol. 575, no. 1, pp. 229–239, 2006.

[159] F. Zhang, W. Wu, Z. Deng et al., "High altitude increases the expression of hypoxia-inducible factor 1α and inducible nitric oxide synthase with intest-inal mucosal barrier failure in rats," *Interantional Journal of Clinical and Experimental Pathology*, vol. 8, pp. 5189–5195, 2015.

[160] S. L. Gaffin, J. Brock-Utne, A. Zanotti, and M. T. Wells, "Hypoxia-induced endotoxemia in primates: role of reticuloendothelial system function and anti-lipopolysaccharide plasma," *Aviation, Space, and Environmental Medicine*, vol. 57, pp. 1044–1049, 1986.

[161] R. Šket, N. Treichel, T. Debevec et al., "Hypoxia and inactivity related physiological changes (constipation, inflammation) are not reflected at the level of gut metabolites and butyrate producing microbial community: the PlanHab study," *Frontiers in Physiology*, vol. 8, p. 250, 2017.

[162] E. Thiering, J. Cyrys, J. Kratzsch et al., "Long-term exposure to traffic-related air pollution and insulin resistance in children: results from the GINIplus and LISAplus birth cohorts," *Diabetologia*, vol. 56, no. 8, pp. 1696–1704, 2013.

[163] M. Lodovici and E. Bigagli, "Oxidative stress and air pollution exposure," *Journal of Toxicology*, vol. 2011, Article ID 487074, 9 pages, 2011.

[164] G. Pizzino, N. Irrera, A. Bitto et al., "Cadmium-induced oxidative stress impairs glycemic control in adolescents," *Oxidative Medicine and Cellular Longevity*, vol. 2017, Article ID 6341671, 6 pages, 2017.

[165] A. N. Onyango, "Small reactive carbonyl compounds as tissue lipid oxidation products; and the mechanisms of their formation thereby," *Chemistry and Physics of Lipids*, vol. 165, no. 7, pp. 777–786, 2012.

[166] K. V. Ramana, A. Bhatnagar, S. Srivastava et al., "Mitogenic responses of vascular smooth muscle cells to lipid peroxidation-derived aldehyde 4-hydroxy-*trans*-2-nonenal (HNE): role of aldose reductase-catalyzed reduction of the HNE-glutathione conjugates in regulating cell growth," *Journal of Biological Chemistry*, vol. 281, no. 26, pp. 17652–17660, 2006.

[167] P. Wentworth Jr., J. Nieva, C. Takeuchi et al., "Evidence for ozone formation in human atherosclerotic arteries," *Science*, vol. 302, no. 5647, pp. 1053–1056, 2003.

[168] L. Laynes, A. C. Raghavamenon, O. D'Auvergne, V. Achuthan, and R. M. Uppu, "MAPK signaling in H9c2 cardiomyoblasts exposed to cholesterol secoaldehyde – role of hydrogen peroxide," *Biochemical and Biophysical Research Communications*, vol. 404, no. 1, pp. 90–95, 2011.

[169] I. Braakman and D. N. Hebert, "Protein folding in the endoplasmic reticulum," *Cold Spring Harbor Perspectives in Biology*, vol. 5, no. 5, article a013201, 2013.

[170] T. Adachi, R. M. Weisbrod, D. R. Pimentel et al., "S-Glutathiolation by peroxynitrite activates SERCA during arterial relaxation by nitric oxide," *Nature Medicine*, vol. 10, no. 11, pp. 1200–1207, 2004.

[171] A. Pastore and F. Piemonte, "Protein glutathionylation in cardiovascular diseases," *International Journal of Molecular Sciences*, vol. 14, no. 12, pp. 20845–20876, 2013.

[172] F. Qin, D. A. Siwik, S. Lancel et al., "Hydrogen peroxide–mediated SERCA cysteine 674 oxidation contributes to impaired cardiac myocyte relaxation in senescent mouse heart," *Journal of the American Heart Association*, vol. 2, no. 4, article e000184, 2013.

[173] U. Ozcan, Q. Cao, E. Yilmaz et al., "Endoplasmic reticulum stress links obesity, insulin action, and type 2 diabetes," *Science*, vol. 306, no. 5695, pp. 457–461, 2004.

[174] P. Haberzettl, E. Vladykovskaya, S. Srivastava, and A. Bhatnagar, "Role of endoplasmic reticulum stress in acrolein-induced endothelial activation," *Toxicology and Applied Pharmacology*, vol. 234, no. 1, pp. 14–24, 2009.

[175] C. H. Shao, H. L. Capek, K. P. Patel et al., "Carbonylation contributes to SERCA2a activity loss and diastolic dysfunction in a rat model of type 1 diabetes," *Diabetes*, vol. 60, no. 3, pp. 947–959, 2011.

[176] H. Zeeshan, G. Lee, H.-R. Kim, and H.-J. Chae, "Endoplasmic reticulum stress and associated ROS," *International Journal of Molecular Sciences*, vol. 17, no. 12, p. 327, 2016.

[177] R. Chaube and G. H. Werstuck, "Mitochondrial ROS versus ER ROS: which comes first in myocardial calcium dysregulation?," *Frontiers in Cardiovascular Medicine*, vol. 3, p. 36, 2016.

[178] A. N. Osipov, N. M. Smetanina, M. V. Pustovalova, E. Arkhangelskaya, and D. Klokov, "The formation of DNA single-strand breaks and alkali-labile sites in human blood lymphocytes exposed to 365-nm UVA radiation," *Free Radical Biology & Medicine*, vol. 73, pp. 34–40, 2014.

[179] A. Valavanidis, T. Vlachogianni, and C. Fiotakis, "8-hydroxy-2′-deoxyguanosine (8-OHdG): a critical biomarker of oxidative stress and carcinogenesis," *Journal of Environmental Science and Health, Part C*, vol. 27, no. 2, pp. 120–139, 2009.

[180] J. Cadet and J. R. Wagner, "DNA base damage by reactive oxygen species, oxidizing agents, and UV radiation," *Cold Spring Harbor Perspectives in Biology*, vol. 5, article a012559, 2013.

[181] S. Frelon, T. Douki, A. Favier, and J. Cadet, "Hydroxyl radical is not the main reactive species involved in the degradation of DNA bases by copper in the presence of hydrogen peroxide," *Chemical Research in Toxicology*, vol. 16, no. 2, pp. 191–197, 2003.

[182] E. S. Henle, Z. Han, N. Tang, P. Rai, Y. Luo, and S. Linn, "Sequence-specific DNA cleavage by Fe^{2+}-mediated Fenton reactions has possible biological implications," *Journal of Biological Chemistry*, vol. 274, no. 2, pp. 962–971, 1999.

[183] B. Thapa, B. H. Munk, C. J. Burrows, and H. B. Schlegel, "Computational study of oxidation of guanine by singlet oxygen ($^1\Delta_g$) and formation of guanine:lysine cross-links," *Chemistry - A European Journal*, vol. 23, no. 24, pp. 5804–5813, 2017.

[184] L. Woodbine, H. Brunton, A. A. Goodarzi, A. Shibata, and P. A. Jeggo, "Endogenously induced DNA double strand breaks arise in heterochromatic DNA regions and require ataxia telangiectasia mutated and Artemis for their repair," *Nucleic Acids Research*, vol. 39, no. 16, pp. 6986–6997, 2011.

[185] B. ul Islam, S. Habib, P. Ahmad, S. Allarakha, Moinuddin, and A. Ali, "Pathophysiological role of peroxynitrite induced DNA damage in human diseases: a special focus on poly(ADP-ribose) polymerase (PARP)," *Indian Journal of Clinical Biochemistry*, vol. 30, no. 4, pp. 368–385, 2015.

[186] F. Gentile, A. Arcaro, S. Pizzimenti et al., "DNA damage by lipid peroxidation products: implications in cancer, inflammation and autoimmunity," *AIMS Genetics*, vol. 4, no. 2, pp. 103–137, 2017.

[187] M. J. Roberts, G. T. Wondrak, D. C. Laurean, M. K. Jacobson, and E. L. Jacobson, "DNA damage by carbonyl stress in human skin cells," *Mutation Research/Fundamental and Molecular Mechanisms of Mutagenesis*, vol. 522, no. 1-2, pp. 45–56, 2003.

[188] M. Gracanin and M. J. Davies, "Inhibition of protein tyrosine phosphatases by amino acid, peptide, and protein hydroperoxides: potential modulation of cell signaling by protein oxidation products," *Free Radical Biology & Medicine*, vol. 42, no. 10, pp. 1543–1551, 2007.

[189] A. S. Rahmanto, P. E. Morgan, C. L. Hawkins, and M. J. Davies, "Cellular effects of photogenerated oxidants and long-lived, reactive, hydroperoxide photoproducts," *Free Radical Biology & Medicine*, vol. 49, no. 10, pp. 1505–1515, 2010.

[190] V. Gupta and K. S. Carroll, "Sulfenic acid chemistry, detection and cellular lifetime," *Biochimica et Biophysica Acta (BBA) - General Subjects*, vol. 1840, no. 2, pp. 847–875, 2014.

[191] I. Dalle-Donne, R. Rossi, D. Giustarini, R. Colombo, and A. Milzani, "S-Glutathionylation in protein redox regulation," *Free Radical Biology & Medicine*, vol. 43, no. 6, pp. 883–898, 2007.

[192] C. L. Grek, J. Zhang, Y. Manevich, D. M. Townsend, and K. D. Tew, "Causes and consequences of cysteine S-glutathionylation," *The Journal of Biological Chemistry*, vol. 288, no. 37, pp. 26497–26504, 2013.

[193] H. Wefers and H. Sies, "Oxidation of glutathione by the superoxide radical to the disulfide and the sulfonate yielding singlet oxygen," *European Journal of Biochemistry*, vol. 137, no. 1-2, pp. 29–36, 1983.

[194] S. Enami, M. R. Hoffmann, and A. J. Colussi, "Ozone oxidizes glutathione to a sulfonic acid," *Chemical Research in Toxicology*, vol. 22, no. 1, pp. 35–40, 2009.

[195] A. N. Onyango, "Alternatives to the 'water oxidation pathway' of biological ozone formation," *Journal of Chemical Biology*, vol. 9, no. 1, pp. 1–8, 2016.

[196] S. Iwakami, H. Misu, T. Takeda et al., "Concentration-dependent dual effects of hydrogen peroxide on insulin signal transduction in H4IIEC hepatocytes," *PLoS One*, vol. 6, no. 11, article e27401, 2011.

[197] S. Zhuang and I. E. Kochevar, "Singlet oxygen–induced activation of Akt/protein kinase B is independent of growth factor receptors," *Photochemistry and Photobiology*, vol. 78, no. 4, pp. 361–371, 2003.

[198] M. Ikemura, M. Nishikawa, K. Hyoudou, Y. Kobayashi, F. Yamashita, and M. Hashida, "Improvement of insulin resistance by removal of systemic hydrogen peroxide by PEGylated catalase in obese mice," *Molecular Pharmaceutics*, vol. 7, no. 6, pp. 2069–2076, 2010.

[199] Y. Son, Y.-K. Cheong, N.-H. Kim, H.-T. Chung, D. G. Kang, and H.-O. Pae, "Mitogen-activated protein kinases and reactive oxygen species: how can ROS activate MAPK pathways?," *Journal of Signal Transduction*, vol. 2011, Article ID 792639, 6 pages, 2011.

[200] M. Castro-Caldas, A. N. Carvalho, E. Rodrigues, C. Henderson, C. R. Wolf, and M. J. Gama, "Glutathione *S*-transferase pi mediates MPTP-induced c-Jun N-terminal kinase activation in the nigrostriatal pathway," *Molecular Neurobiology*, vol. 45, no. 3, pp. 466–477, 2012.

[201] K. D. Tew, Y. Manevich, C. Grek, Y. Xiong, J. Uys, and D. M. Townsend, "The role of glutathione *S*-transferase P in signaling pathways and S-glutathionylation in cancer," *Free Radical Biology & Medicine*, vol. 51, no. 2, pp. 299–313, 2011.

[202] L.-O. Klotz, K.-D. Kröncke, and H. Sies, "Singlet oxygen-induced signaling effects in mammalian cells," *Photochemical & Photobiological Sciences*, vol. 2, no. 2, pp. 88–94, 2003.

[203] J. Matsukawa, A. Matsuzawa, K. Takeda, and H. Ichijo, "The ASK1-MAP kinase cascades in mammalian stress response," *Journal of Biochemistry*, vol. 136, no. 3, pp. 261–265, 2004.

[204] X. Li, Y. Rong, M. Zhang et al., "Up-regulation of thioredoxin interacting protein (Txnip) by p38 MAPK and FOXO1 contributes to the impaired thioredoxin activity and increased ROS in glucose-treated endothelial cells," *Biochemical and Biophysical Research Communications*, vol. 381, no. 4, pp. 660–665, 2009.

[205] T. Lane, B. Flam, R. Lockey, and N. Kolliputi, "TXNIP shuttling: missing link between oxidative stress and inflammasome activation," *Frontiers in Physiology*, vol. 4, no. 50, 2013.

[206] C. S. Choi, Y.-B. Kim, F. N. Lee, J. M. Zabolotny, B. B. Kahn, and J. H. Youn, "Lactate induces insulin resistance in skeletal muscle by suppressing glycolysis and impairing insulin signaling," *American Journal of Physiology-Endocrinology and Metabolism*, vol. 283, no. 2, pp. E233–E240, 2002.

[207] M. Kleinert, L. Sylow, D. J. Fazakerley et al., "Acute mTOR inhibition induces insulin resistance and alters substrate utilization in vivo," *Molecular Metabolism*, vol. 3, no. 6, pp. 630–641, 2014.

[208] L. C. Chao, K. Wroblewski, Z. Zhang et al., "Insulin resistance and altered systemic glucose metabolism in mice lacking nur77," *Diabetes*, vol. 58, no. 12, pp. 2788–2796, 2009.

[209] P. E. Morgan, R. T. Dean, and M. J. Davies, "Inhibition of glyceraldehyde-3-phosphate dehydrogenase by peptide and protein peroxides generated by singlet oxygen attack," *European Journal of Biochemistry*, vol. 269, no. 7, pp. 1916–1925, 2002.

[210] P. J. Beisswenger, S. K. Howell, K. Smith, and B. S. Szwergold, "Glyceraldehyde-3-phosphate dehydrogenase activity as an independent modifier of methylglyoxal levels in diabetes," *Biochimica et Biophysica Acta (BBA) - Molecular Basis of Disease*, vol. 1637, no. 1, pp. 98–106, 2003.

[211] S. Iqbal and D. A. Hood, "Oxidative stress-induced mitochondrial fragmentation and movement in skeletal muscle myoblasts," *American Journal of Physiology-Cell Physiology*, vol. 306, no. 12, pp. C1176–C1183, 2014.

[212] K. Park, M. Gross, D.-H. Lee et al., "Oxidative stress and insulin resistance: the coronary artery risk development in young adults study," *Diabetes Care*, vol. 32, no. 7, pp. 1302–1307, 2009.

[213] Z. Huang, Q. Hong, X. Zhang et al., "Aldose reductase mediates endothelial cell dysfunction induced by high uric acid concentrations," *Cell Communication and Signaling*, vol. 15, no. 1, p. 3, 2017.

[214] K. V. Ramana, B. Friedrich, R. Tammali, M. B. West, A. Bhatnagar, and S. K. Srivastava, "Requirement of aldose reductase for the hyperglycemic activation of protein kinase C and formation of diacylglycerol in vascular smooth muscle cells," *Diabetes*, vol. 54, no. 3, pp. 818–829, 2005.

[215] M. A. Lanaspa, T. Ishimoto, N. Li et al., "Endogenous fructose production and metabolism in the liver contributes to the development of metabolic syndrome," *Nature Communications*, vol. 4, p. 2434, 2013.

[216] K.-W. Zeng, J. Li, X. Dong et al., "Anti-neuroinflammatory efficacy of the aldose reductase inhibitor FMHM via phospholipase C/protein kinase C-dependent NF-κB and MAPK pathways," *Toxicology and Applied Pharmacology*, vol. 273, no. 1, pp. 159–171, 2013.

[217] K. Toriumi, Y. Horikoshi, R. Yoshiyuki Osamura, Y. Yamamoto, N. Nakamura, and S. Takekoshi, "Carbon tetrachloride-induced hepatic injury through formation of oxidized diacylglycerol and activation of the PKC/NF-κB pathway," *Laboratory Investigation*, vol. 93, no. 2, pp. 218–229, 2013.

[218] S. K. Srivastava, U. C. S. Yadav, A. B. M. Reddy et al., "Aldose reductase inhibition suppresses oxidative stress-induced inflammatory disorders," *Chemico-Biological Interactions*, vol. 191, no. 1-3, pp. 330–338, 2011.

[219] S. Pandey, S. K. Srivastava, and K. V. Ramana, "A potential therapeutic role for aldose reductase inhibitors in the treatment of endotoxin-related inflammatory diseases," *Expert Opinion on Investigational Drugs*, vol. 21, no. 3, pp. 329–339, 2012.

[220] X.-M. Song, Q. Yu, X. Dong et al., "Aldose reductase inhibitors attenuate β-amyloid-induced TNF-α production in microlgia via ROS-PKC-mediated NF-κB and MAPK pathways," *International Immunopharmacology*, vol. 50, pp. 30–37, 2017.

[221] T. Nishino, K. Okamoto, B. T. Eger, E. F. Pai, and T. Nishino, "Mammalian xanthine oxidoreductase – mechanism of transition from xanthine dehydrogenase to xanthine oxidase," *FEBS Journal*, vol. 275, no. 13, pp. 3278–3289, 2008.

[222] M. F. Abdelmalek, M. Lazo, A. Horska et al., "Higher dietary fructose is associated with impaired hepatic adenosine triphosphate homeostasis in obese individuals with type 2 diabetes," *Hepatology*, vol. 56, no. 3, pp. 952–960, 2012.

[223] M. A. Lanaspa, L. G. Sanchez-Lozada, Y. J. Choi et al., "Uric acid induces hepatic steatosis by generation of mitochondrial oxidative stress: potential role in fructose-dependent and -independent fatty liver," *Journal of Biological Chemistry*, vol. 287, no. 48, pp. 40732–40744, 2012.

[224] R. Spiga, M. A. Marini, E. Mancuso et al., "Uric acid is associated with inflammatory biomarkers and induces inflammation via activating the NF-κB signaling pathway in HepG2 cells," *Arteriosclerosis, Thrombosis, and Vascular Biology*, vol. 37, no. 6, pp. 1241–1249, 2017.

[225] Y. J. Choi, H. S. Shin, H. S. Choi et al., "Uric acid induces fat accumulation via generation of endoplasmic reticulum stress and SREBP-1c activation in hepatocytes," *Laboratory Investigation*, vol. 94, no. 10, pp. 1114–1125, 2014.

[226] M. Kanbay, T. Jensen, Y. Solak et al., "Uric acid in metabolic syndrome: from an innocent bystander to a central player," *European Journal of Internal Medicine*, vol. 29, pp. 3–8, 2016.

[227] F. Derbre, B. Ferrando, M. C. Gomez-Cabrera et al., "Inhibition of xanthine oxidase by allopurinol prevents skeletal muscle atrophy: role of p38 MAPkinase and E3 ubiquitin ligases," *PLoS One*, vol. 7, no. 10, article e46668, 2012.

[228] S. Grether-Beck, G. Bonizzi, H. Schmitt-Brenden et al., "Non-enzymatic triggering of the ceramide signalling cascade by solar UVA radiation," *The EMBO Journal*, vol. 19, no. 21, pp. 5793–5800, 2000.

[229] M. Sawada, S. Nakashima, T. Kiyono et al., "p53 regulates ceramide formation by neutral sphingomyelinase through reactive oxygen species in human glioma cells," *Oncogene*, vol. 20, no. 11, pp. 1368–1378, 2001.

[230] J. R. Ussher, T. R. Koves, V. J. J. Cadete et al., "Inhibition of de novo ceramide synthesis reverses diet-induced insulin resistance and enhances whole-body oxygen consumption," *Diabetes*, vol. 59, no. 10, pp. 2453–2464, 2010.

[231] M. Verma, A. Yateesh, K. Neelima et al., "Inhibition of neutral sphingomyelinases in skeletal muscle attenuates fatty-acid induced defects in metabolism and stress," *SpringerPlus*, vol. 3, no. 1, p. 255, 2014.

[232] J.-L. Li, Q.-Y. Wang, H.-Y. Luan, Z.-C. Kang, and C.-B. Wang, "Effects of L-carnitine against oxidative stress in human hepatocytes: involvement of peroxisome proliferator-activated receptor alpha," *Journal of Biomedical Science*, vol. 19, no. 1, p. 32, 2012.

[233] C. Blanquicett, B.-Y. Kang, J. D. Ritzenthaler, D. P. Jones, and C. M. Hart, "Oxidative stress modulates PPARγ in vascular endothelial cells," *Free Radical Biology & Medicine*, vol. 48, no. 12, pp. 1618–1625, 2010.

[234] M. B. Paumen, Y. Ishida, M. Muramatsu, M. Yamamoto, and T. Honjo, "Inhibition of carnitine palmitoyltransferase I augments sphingolipid synthesis and palmitate-induced apoptosis," *Journal of Biological Chemistry*, vol. 272, no. 6, pp. 3324–3329, 1997.

[235] S. M. H. Chan, R.-Q. Sun, X.-Y. Zeng et al., "Activation of PPARα ameliorates hepatic insulin resistance and steatosis in high fructose–fed mice despite increased endoplasmic reticulum stress," *Diabetes*, vol. 62, no. 6, pp. 2095–2105, 2013.

[236] N. Zhang, E. S. H. Chu, J. Zhang et al., "Peroxisome proliferator activated receptor alpha inhibits hepatocarcinogenesis through mediating NF-κB signaling pathway," *Oncotarget*, vol. 5, no. 18, pp. 8330–8340, 2014.

[237] M. Pawlak, P. Lefebvre, and B. Staels, "Molecular mechanism of PPARα action and its impact on lipid metabolism, inflammation and fibrosis in non-alcoholic fatty liver disease," *Journal of Hepatology*, vol. 62, no. 3, pp. 720–733, 2015.

[238] X. Liu, Z. Yu, X. Huang et al., "Peroxisome proliferator-activated receptor γ (PPARγ) mediates the protective effect of quercetin against myocardial ischemia-reperfusion injury via suppressing the NF-κB pathway," *American Journal of Translational Research*, vol. 8, no. 12, pp. 5169–5186, 2016.

[239] Y. Zhang, R.-X. Zhan, J.-Q. Chen et al., "Pharmacological activation of PPAR gamma ameliorates vascular endothelial insulin resistance via a non-canonical PPAR gamma-dependent nuclear factor-kappa B trans-repression pathway," *European Journal of Pharmacology*, vol. 754, pp. 41–51, 2015.

[240] M. Bouskila, U. B. Pajvani, and P. E. Scherer, "Adiponectin: a relevant player in PPARγ-agonist-mediated improvements in hepatic insulin sensitivity?," *International Journal of Obesity*, vol. 29, no. S1, pp. S17–S23, 2005.

[241] S. Mohr, H. Hallak, A. de Boitte, E. G. Lapetina, and B. Brüne, "Nitric oxide-induced *S*-glutathionylation and inactivation of glyceraldehyde-3-phosphate dehydrogenase," *Journal of Biological Chemistry*, vol. 274, no. 14, pp. 9427–9430, 1999.

[242] I. Bellezza, S. Grottelli, E. Costanzi et al., "Peroxynitrite activates the NLRP3 inflammasome cascade in SOD1(G93A) mouse model of amyotrophic lateral sclerosis," *Molecular Neurobiology*, 2017.

[243] A. Pautz, R. Franzen, S. Dorsch et al., "Cross-talk between nitric oxide and superoxide determines ceramide formation and apoptosis in glomerular cells," *Kidney International*, vol. 61, no. 3, pp. 790–796, 2002.

[244] M. Morita, Y. Naito, T. Yoshikawa, and E. Niki, "Plasma lipid oxidation induced by peroxynitrite, hypochlorite, lipoxygenase and peroxyl radicals and its inhibition by antioxidants as assessed by diphenyl-1-pyrenylphosphine," *Redox Biology*, vol. 8, pp. 127–135, 2016.

[245] H. Sugita, M. Fujimoto, T. Yasukawa et al., "Inducible nitric-oxide synthase and NO donor induce insulin receptor substrate-1 degradation in skeletal muscle cells," *Journal of Biological Chemistry*, vol. 280, no. 14, pp. 14203–14211, 2005.

[246] C. Nigro, G. A. Raciti, A. Leone et al., "Methylglyoxal impairs endothelial insulin sensitivity both in vitro and in vivo," *Diabetologia*, vol. 57, no. 7, pp. 1485–1494, 2014.

[247] K. H. Ingram, H. Hill, D. R. Moellering et al., "Skeletal muscle lipid peroxidation and insulin resistance in humans," *The Journal of Clinical Endocrinology & Metabolism*, vol. 97, no. 7, pp. E1182–E1186, 2012.

[248] C. T. Shearn, K. S. Fritz, P. Reigan, and D. R. Petersen, "Modification of Akt2 by 4-hydroxynonenal inhibits insulin-dependent Akt signaling in HepG2 cells," *Biochemistry*, vol. 50, no. 19, pp. 3984–3996, 2011.

[249] S. J. Orena, A. J. Torchia, and R. S. Garofalo, "Inhibition of glycogen-synthase kinase 3 stimulates glycogen synthase and glucose transport by distinct mechanisms in 3T3-L1 adipocytes," *Journal of Biological Chemistry*, vol. 275, no. 21, pp. 15765–15772, 2000.

[250] K. MacAulay and J. R. Woodgett, "Targeting glycogen synthase kinase-3 (GSK-3) in the treatment of type 2 diabetes," *Expert Opinion on Therapeutic Targets*, vol. 12, no. 10, pp. 1265–1274, 2008.

[251] C. Sutherland, "What are the *bona fide* GSK3 substrates?," *International Journal of Alzheimer's Disease*, vol. 2011, Article ID 505607, 23 pages, 2011.

[252] A. I. Rojo, M. R. . Sagarra, and A. Cuadrado, "GSK-3β down-regulates the transcription factor Nrf2 after oxidant damage: relevance to exposure of neuronal cells to oxidative stress," *Journal of Neurochemistry*, vol. 105, no. 1, pp. 192–202, 2008.

[253] B. Spoto, R. M. Parlongo, G. Parlongo, E. Sgro', and C. Zoccali, "The enzymatic machinery for ADMA synthesis and degradation is fully expressed in human adipocytes," *Journal of Nephrology*, vol. 20, no. 5, pp. 554–559, 2007.

[254] H. Iwasaki, "Activities of asymmetric dimethylarginine-related enzymes in white adipose tissue are associated with circulating lipid biomarkers," *Diabetology & Metabolic Syndrome*, vol. 4, no. 1, p. 17, 2012.

[255] Z.-C. Yang, K. S. Wang, Y. Wu et al., "Asymmetric dimethylarginine impairs glucose utilization via ROS/TLR4 pathway in adipocytes: an effect prevented by vitamin E," *Cellular Physiology and Biochemistry*, vol. 24, no. 1-2, pp. 115–124, 2009.

[256] J. Zheng, K. Wang, P. Jin et al., "The association of adipose-derived dimethylarginine dimethylaminohydrolase-2 with insulin sensitivity in experimental type 2 diabetes mellitus," *Acta Biochimica et Biophysica Sinica*, vol. 45, no. 8, pp. 641–648, 2013.

[257] M. Trocha, A. Merwid-Lad, A. Szuba, T. Sozanski, J. Magdalan, and A. Szelag, "Asymmetric dimethylarginine synthesis and degradation under physiological and pathological conditions," *Advanced Clinical and Experimental Medicine*, vol. 19, pp. 233–243, 2010.

[258] P. Chen, K. Xia, Z. Zhao, X. Deng, and T. Yang, "Atorvastatin modulates the DDAH1/ADMA system in high-fat diet-induced insulin-resistant rats with endothelial dysfunction," *Vascular Medicine*, vol. 17, no. 6, pp. 416–423, 2012.

[259] L. Chen, J.-P. Zhou, D.-B. Kuang, J. Tang, Y.-J. Li, and X.-P. Chen, "4-HNE increases intracellular ADMA levels in cultured HUVECs: evidence for miR-21-dependent mechanisms," *PLoS One*, vol. 8, no. 5, article e64148, 2013.

[260] A. Zengi, G. Ercan, O. Caglayan et al., "Increased oxidative DNA damage in lean normoglycemic offspring of type 2 diabetic patients," *Experimental and Clinical Endocrinology & Diabetes*, vol. 119, no. 8, pp. 467–471, 2011.

[261] H. A. Al-Aubaidy and H. F. Jelinek, "8-Hydroxy-2-deoxyguanosine identifies oxidative DNA damage in a rural prediabetes cohort," *Redox Report*, vol. 15, no. 4, pp. 155–160, 2010.

[262] H. Sampath, V. Vartanian, M. R. Rollins, K. Sakumi, Y. Nakabeppu, and R. S. Lloyd, "8-Oxoguanine DNA glycosylase (OGG1) deficiency increases susceptibility to obesity and metabolic dysfunction," *PLoS One*, vol. 7, no. 12, article e51697, 2012.

[263] L. V. Yuzefovych, V. A. Solodushko, G. L. Wilson, and L. I. Rachek, "Protection from palmitate-induced mitochondrial DNA damage prevents from mitochondrial oxidative stress, mitochondrial dysfunction, apoptosis, and impaired insulin signaling in rat L6 skeletal muscle cells," *Endocrinology*, vol. 153, no. 1, pp. 92–100, 2012.

[264] L. V. Yuzefovych, S. P. LeDoux, G. L. Wilson, and L. I. Rachek, "Mitochondrial DNA damage via augmented oxidative stress regulates endoplasmic reticulum stress and autophagy: crosstalk, links and signaling," *PLoS One*, vol. 8, no. 12, article e83349, 2013.

[265] C. Ricci, V. Pastukh, J. Leonard et al., "Mitochondrial DNA damage triggers mitochondrial-superoxide generation and apoptosis," *American Journal of Physiology-Cell Physiology*, vol. 294, no. 2, pp. C413–C422, 2008.

[266] K. Shimada, T. R. Crother, J. Karlin et al., "Oxidized mitochondrial DNA activates the NLRP3 inflammasome during apoptosis," *Immunity*, vol. 36, no. 3, pp. 401–414, 2012.

[267] I. Kim, W. Xu, and J. C. Reed, "Cell death and endoplasmic reticulum stress: disease relevance and therapeutic opportunities," *Nature Reviews Drug Discovery*, vol. 7, no. 12, pp. 1013–1030, 2008.

[268] C. Lebeaupin, E. Proics, C. H. D. de Bieville et al., "ER stress induces NLRP3 inflammasome activation and hepatocyte death," *Cell Death & Disease*, vol. 6, no. 9, article e1879, 2015.

[269] F. Shang and A. Taylor, "Ubiquitin–proteasome pathway and cellular responses to oxidative stress," *Free Radical Biology & Medicine*, vol. 51, no. 1, pp. 5–16, 2011.

[270] Z. J. Chen, "Ubiquitin signalling in the NF-κB pathway," *Nature Cell Biology*, vol. 7, no. 8, pp. 758–765, 2005.

[271] B. Emanuelli, P. Peraldi, C. Filloux et al., "SOCS-3 inhibits insulin signaling and is up-regulated in response to tumor necrosis factor-α in the adipose tissue of obese mice," *Journal of Biological Chemistry*, vol. 276, no. 51, pp. 47944–47949, 2001.

[272] L. Rui, M. Yuan, D. Frantz, S. Shoelson, and M. F. White, "SOCS-1 and SOCS-3 block insulin signaling by ubiquitin-mediated degradation of IRS1 and IRS2," *Journal of Biological Chemistry*, vol. 277, no. 44, pp. 42394–42398, 2002.

[273] J. J. Senn, P. J. Klover, I. A. Nowak et al., "Suppressor of cytokine signaling-3 (SOCS-3), a potential mediator of interleukin-6-dependent insulin resistance in hepatocytes," *Journal of Biological Chemistry*, vol. 278, no. 16, pp. 13740–13746, 2003.

[274] F. Mashili, A. V. Chibalin, A. Krook, and J. R. Zierath, "Constitutive STAT3 phosphorylation contributes to skeletal muscle insulin resistance in type 2 diabetes," *Diabetes*, vol. 62, no. 2, pp. 457–465, 2013.

[275] M. Ishii, A. Maeda, S. Tani, and M. Akagawa, "Palmitate induces insulin resistance in human HepG2 hepatocytes by enhancing ubiquitination and proteasomal degradation of key insulin signaling molecules," *Archives of Biochemistry and Biophysics*, vol. 566, pp. 26–35, 2015.

[276] X. Liu, M. G. Mameza, Y. S. Lee et al., "Suppressors of cytokine-signaling proteins induce insulin resistance in the retina and promote survival of retinal cells," *Diabetes*, vol. 57, no. 6, pp. 1651–1658, 2008.

[277] H. Lerat, M. R. Imache, J. Polyte et al., "Hepatitis C virus induces a prediabetic state by directly impairing hepatic glucose metabolism in mice," *Journal of Biological Chemistry*, vol. 292, no. 31, pp. 12860–12873, 2017.

[278] D. Gu, Z. Wang, X. Dou et al., "Inhibition of ERK1/2 pathway suppresses adiponectin secretion via accelerating protein degradation by ubiquitin–proteasome system: relevance to obesity-related adiponectin decline," *Metabolism*, vol. 62, no. 8, pp. 1137–1148, 2013.

[279] K.-I. Ozaki, M. Awazu, M. Tamiya et al., "Targeting the ERK signaling pathway as a potential treatment for insulin resistance and type 2 diabetes," *American Journal of Physiology-Endocrinology and Metabolism*, vol. 310, no. 8, pp. E643–E651, 2016.

[280] Z. Wang, X. Dou, D. Gu et al., "4-Hydroxynonenal differentially regulates adiponectin gene expression and secretion via activating PPARγ and accelerating ubiquitin–proteasome degradation," *Molecular and Cellular Endocrinology*, vol. 349, no. 2, pp. 222–231, 2012.

[281] A. Abudukadier, Y. Fujita, A. Obara et al., "Tetrahydrobiopterin has a glucose-lowering effect by suppressing hepatic gluconeogenesis in an endothelial nitric oxide synthase–dependent manner in diabetic mice," *Diabetes*, vol. 62, no. 9, pp. 3033–3043, 2013.

[282] Z. Shen, X. Liang, C. Q. Rogers, D. Rideout, and M. You, "Involvement of adiponectin-SIRT1-AMPK signaling in the protective action of rosiglitazone against alcoholic fatty liver in mice," *American Journal of Physiology-Gastrointestinal and Liver Physiology*, vol. 298, no. 3, pp. G364–G374, 2010.

[283] Y. Cheng, H. Takeuchi, Y. Sonobe et al., "Sirtuin 1 attenuates oxidative stress via upregulation of superoxide dismutase 2 and catalase in astrocytes," *Journal of Neuroimmunology*, vol. 269, no. 1-2, pp. 38–43, 2014.

[284] G. Ceolotto, A. Gallo, I. Papparella et al., "Rosiglitazone reduces glucose-induced oxidative stress mediated by NAD(P)H oxidase via AMPK-dependent mechanism," *Arteriosclerosis, Thrombosis, and Vascular Biology*, vol. 27, no. 12, pp. 2627–2633, 2007.

[285] M. Balteau, A. van Steenbergen, A. D. Timmermans et al., "AMPK activation by glucagon-like peptide-1 prevents NADPH oxidase activation induced by hyperglycemia in adult cardiomyocytes," *American Journal of Physiology-Heart and Circulatory Physiology*, vol. 307, no. 8, pp. H1120–H1133, 2014.

[286] J. M. Cacicedo, N. Yagihashi, J. F. Keaney Jr, N. B. Ruderman, and Y. Ido, "AMPK inhibits fatty acid-induced increases in NF-κB transactivation in cultured human umbilical vein endothelial cells," *Biochemical and Biophysical Research Communications*, vol. 324, no. 4, pp. 1204–1209, 2004.

[287] A. Salminen, J. M. T. Hyttinen, and K. Kaarniranta, "AMP-activated protein kinase inhibits NF-κB signaling and inflammation: impact on healthspan and lifespan," *Journal of Molecular Medicine*, vol. 89, no. 7, pp. 667–676, 2011.

[288] W. M. Yang and W. Lee, "CTRP5 ameliorates palmitate-induced apoptosis and insulin resistance through activation of AMPK and fatty acid oxidation," *Biochemical and Biophysical Research Communications*, vol. 452, no. 3, pp. 715–721, 2014.

[289] K.-L. Tsai, L.-H. Chen, S.-H. Chiou et al., "Coenzyme Q10 suppresses oxLDL-induced endothelial oxidative injuries by the modulation of LOX-1-mediated ROS generation via the AMPK/PKC/NADPH oxidase signaling pathway," *Molecular Nutrition & Food Research*, vol. 55, no. S2, pp. S227–S240, 2011.

[290] N. B. Ruderman, D. Carling, M. Prentki, and J. M. Cacicedo, "AMPK, insulin resistance, and the metabolic syndrome," *Journal of Clinical Investigation*, vol. 123, no. 7, pp. 2764–2772, 2013.

[291] W. S. Cheang, X. Y. Tian, W. T. Wong et al., "Metformin protects endothelial function in diet-induced obese mice by inhibition of endoplasmic reticulum stress through 5′ adenosine monophosphate–activated protein kinase–peroxisome proliferator–activated receptor δ pathway," *Arteriosclerosis, Thrombosis, and Vascular Biology*, vol. 34, no. 4, pp. 830–836, 2014.

[292] C. Li, M. M. Reif, S. M. Craige, S. Kant, and J. F. Keaney Jr, "Endothelial AMPK activation induces mitochondrial biogenesis and stress adaptation via eNOS-dependent mTORC1 signaling," *Nitric Oxide*, vol. 55-56, pp. 45–53, 2016.

[293] Z. Gao, J. Zhang, I. Kheterpal, N. Kennedy, R. J. Davis, and J. Ye, "Sirtuin 1 (SIRT1) protein degradation in response to persistent c-Jun N-terminal kinase 1 (JNK1) activation contributes to hepatic steatosis in obesity," *Journal of Biological Chemistry*, vol. 286, no. 25, pp. 22227–22234, 2011.

[294] Y. Cao, X. Jiang, H. Ma, Y. Wang, P. Xue, and Y. Liu, "SIRT1 and insulin resistance," *Journal of Diabetes and Its Complications*, vol. 30, no. 1, pp. 178–183, 2016.

[295] A. Salminen, K. Kaarniranta, and A. Kauppinen, "Crosstalk between oxidative stress and SIRT1: impact on the aging process," *International Journal of Molecular Sciences*, vol. 14, no. 2, pp. 3834–3859, 2013.

[296] H.-H. Zhang, X.-J. Ma, L.-N. Wu et al., "SIRT1 attenuates high glucose-induced insulin resistance via reducing mitochondrial dysfunction in skeletal muscle cells," *Experimental Biology and Medicine*, vol. 240, no. 5, pp. 557–565, 2015.

[297] L. D. Zheng, L. E. Linarelli, J. Brooke et al., "Mitochondrial epigenetic changes link to increased diabetes risk and early-stage prediabetes indicator," *Oxidative Medicine and Cellular Longevity*, vol. 2016, Article ID 5290638, 10 pages, 2016.

[298] T. L. Marin, B. Gongol, F. Zhang et al., "AMPK promotes mitochondrial biogenesis and function by phosphorylating the epigenetic factors DNMT1, RBBP7, and HAT1," *Science Signaling*, vol. 10, no. 464, article eaaf7478, 2017.

[299] S. K. Saini, K. C. Mangalhara, G. Prakasam, and R. N. K. Bamezai, "DNA methyltransferase1 (DNMT1) isoform3 methylates mitochondrial genome and modulates its biology," *Scientific Reports*, vol. 7, no. 1, p. 1525, 2017.

[300] J. M. McClung, A. R. Judge, E. E. Talbert, and S. K. Powers, "Calpain-1 is required for hydrogen peroxide-induced myotube atrophy," *American Journal of Physiology-Cell Physiology*, vol. 296, no. 2, pp. C363–C371, 2009.

[301] I. J. Smith, S. H. Lecker, and P.-O. Hasselgren, "Calpain activity and muscle wasting in sepsis," *American Journal of Physiology-Endocrinology and Metabolism*, vol. 295, no. 4, pp. E762–E771, 2008.

[302] M. L. Dirks, B. T. Wall, B. van de Valk et al., "One week of bed rest leads to substantial muscle atrophy and induces whole-body insulin resistance in the absence of skeletal muscle lipid accumulation," *Diabetes*, vol. 65, no. 10, pp. 2862–2875, 2016.

[303] O. Rom, S. Kaisari, A. Z. Reznick, and D. Aizenbud, "Peroxynitrite induces degradation of myosin heavy chain via p38 MAPK and muscle-specific E3 ubiquitin ligases in C2 skeletal myotubes," *Advances in Experimental Medicine and Biology*, vol. 832, pp. 1–8, 2014.

[304] G. Carnac, B. Vernus, and A. Bonnieu, "Myostatin in the pathophysiology of skeletal muscle," *Current Genomics*, vol. 8, no. 7, pp. 415–422, 2007.

[305] S. Sriram, S. Subramanian, D. Sathiakumar et al., "Modulation of reactive oxygen species in skeletal muscle by myostatin is mediated through NF-κB," *Aging Cell*, vol. 10, no. 6, pp. 931–948, 2011.

[306] C. Brandt, A. R. Nielsen, C. P. Fischer, J. Hansen, B. K. Pedersen, and P. Plomgaard, "Plasma and muscle myostatin in relation to type 2 diabetes," *PLoS One*, vol. 7, no. 5, article e37236, 2012.

[307] B. Catalgol, I. Ziaja, N. Breusing et al., "The proteasome is an integral part of solar ultraviolet a radiation-induced gene expression," *Journal of Biological Chemistry*, vol. 284, no. 44, pp. 30076–30086, 2009.

[308] A. Díaz-Ruiz, R. Guzmán-Ruiz, N. R. Moreno et al., "Proteasome dysfunction associated to oxidative stress and proteotoxicity in adipocytes compromises insulin sensitivity in human obesity," *Antioxidants & Redox Signaling*, vol. 23, no. 7, pp. 597–612, 2015.

[309] Y. Mei, M. D. Thompson, R. A. Cohen, and X. Y. Tong, "Endoplasmic reticulum stress and related pathological processes," *Journal of Pharmacological & Biomedical Analysis*, vol. 1, no. 2, 2013.

[310] A. B. Tam, E. L. Mercado, A. Hoffmann, and M. Niwa, "ER stress activates NF-κB by integrating functions of basal IKK activity, IRE1 and PERK," *PLoS One*, vol. 7, no. 10, article e45078, 2012.

[311] J. A. Willy, S. K. Young, J. L. Stevens, H. C. Masuoka, and R. C. Wek, "CHOP links endoplasmic reticulum stress to NF-κB activation in the pathogenesis of nonalcoholic steatohepatitis," *Molecular Biology of the Cell*, vol. 26, no. 12, pp. 2190–2204, 2015.

[312] R. Sano and J. C. Reed, "ER stress-induced cell death mechanisms," *Biochimica et Biophysica Acta (BBA) - Molecular Cell Research*, vol. 1833, no. 12, pp. 3460–3470, 2013.

[313] S. S. Cao, K. L. Luo, and L. Shi, "Endoplasmic reticulum stress interacts with inflammation in human diseases," *Journal of Cellular Physiology*, vol. 231, no. 2, pp. 288–294, 2016.

[314] K. Uchimura, M. Hayata, T. Mizumoto et al., "The serine protease prostasin regulates hepatic insulin sensitivity by modulating TLR4 signalling," *Nature Communications*, vol. 5, p. 3428, 2014.

[315] K. Du, S. Herzig, R. N. Kulkarni, and M. Montminy, "TRB3: a *tribbles* homolog that inhibits Akt/PKB activation by insulin in liver," *Science*, vol. 300, no. 5625, pp. 1574–1577, 2003.

[316] A. P. Arruda, M. Milanski, A. Coope et al., "Low-grade hypothalamic inflammation leads to defective thermogenesis, insulin resistance, and impaired insulin secretion," *Endocrinology*, vol. 152, no. 4, pp. 1314–1326, 2011.

[317] Y. Li, Y. Guo, J. Tang, J. Jiang, and Z. Chen, "New insights into the roles of CHOP-induced apoptosis in ER stress," *Acta Biochimica et Biophysica Sinica*, vol. 46, no. 8, pp. 629–640, 2014.

[318] M. Okla, W. Wang, I. Kang, A. Pashaj, T. Carr, and S. Chung, "Activation of Toll-like receptor 4 (TLR4) attenuates adaptive thermogenesis via endoplasmic reticulum stress," *Journal of Biological Chemistry*, vol. 290, no. 44, pp. 26476–26490, 2015.

[319] S. Nowsheen and E. S. Yang, "The intersection between DNA damage response and cell death pathways," *Experimental Oncology*, vol. 34, no. 3, pp. 243–254, 2013.

[320] B. Piret, S. Schoonbroodt, and J. Piette, "The ATM protein is required for sustained activation of NF-κB following DNA damage," *Oncogene*, vol. 18, no. 13, pp. 2261–2271, 1999.

[321] B. B. S. Zhou and S. J. Elledge, "The DNA damage response: putting checkpoints in perspective," *Nature*, vol. 408, no. 6811, pp. 433–439, 2000.

[322] J. Strycharz, J. Drzewoski, J. Szemraj, and A. Sliwinska, "Is p53 involved in tissue-specific insulin resistance formation?," *Oxidative Medicine and Cellular Longevity*, vol. 2017, Article ID 9270549, 23 pages, 2017.

[323] I. Shimizu, Y. Yoshida, M. Suda, and T. Minamino, "DNA damage response and metabolic disease," *Cell Metabolism*, vol. 20, no. 6, pp. 967–977, 2014.

[324] T. Minamino, M. Orimo, I. Shimizu et al., "A crucial role for adipose tissue p53 in the regulation of insulin resistance," *Nature Medicine*, vol. 15, no. 9, pp. 1082–1087, 2009.

[325] I. Shimizu, Y. Yoshida, T. Katsuno et al., "p53-induced adipose tissue inflammation is critically involved in the development of insulin resistance in heart failure," *Cell Metabolism*, vol. 15, no. 1, pp. 51–64, 2012.

[326] B. Vergoni, P. J. Cornejo, J. Gilleron et al., "DNA damage and the activation of the p53 pathway mediate alterations in metabolic and secretory functions of adipocytes," *Diabetes*, vol. 65, no. 10, pp. 3062–3074, 2016.

[327] V. Picco and G. Pagès, "Linking JNK activity to the DNA damage response," *Genes & Cancer*, vol. 4, no. 9-10, pp. 360–368, 2013.

[328] L. A. Heffernan-Stroud and L. M. Obeid, "p53 and regulation of bioactive sphingolipids," *Advances in Enzyme Regulation*, vol. 51, no. 1, pp. 219–228, 2011.

[329] K. F. Petersen, S. Dufour, D. Befroy, R. Garcia, and G. I. Shulman, "Impaired mitochondrial activity in the insulin-resistant offspring of patients with type 2 diabetes," *New England Journal of Medicine*, vol. 350, no. 7, pp. 664–671, 2004.

[330] J. Szendroedi, T. Yoshimura, E. Phielix et al., "Role of diacylglycerol activation of PKCθ in lipid-induced muscle insulin resistance in humans," *Proceedings of the National Academy of Sciences of the United States of America*, vol. 111, no. 26, pp. 9597–9602, 2014.

[331] J. M. Matés, J. A. Segura, F. J. Alonso, and J. Márquez, "Oxidative stress in apoptosis and cancer: an update," *Archives of Toxicology*, vol. 86, no. 11, pp. 1649–1665, 2012.

[332] M. Zhou, Y. Li, Q. Hu et al., "Atomic structure of the apoptosome: mechanism of cytochrome c- and dATP-mediated activation of Apaf-1," *Genes & Development*, vol. 29, no. 22, pp. 2349–2361, 2015.

[333] S. P. Cullen and S. J. Martin, "Caspase activation pathways: some recent progress," *Cell Death & Differentiation*, vol. 16, no. 7, pp. 935–938, 2009.

[334] M. Suzuki, K. Aoshiba, and A. Nagai, "Oxidative stress increases Fas ligand expression in endothelial cells," *Journal of Inflammation*, vol. 3, no. 1, p. 11, 2006.

[335] A. Sommerfeld, R. Reinehr, and D. Häussinger, "Free fatty acids shift insulin-induced hepatocyte proliferation towards CD95-dependent apoptosis," *Journal of Biological Chemistry*, vol. 290, no. 7, pp. 4398–4409, 2015.

[336] A.-C. Johansson, H. Appelqvist, C. Nilsson, K. Kågedal, K. Roberg, and K. Öllinger, "Regulation of apoptosis-associated lysosomal membrane permeabilization," *Apoptosis*, vol. 15, no. 5, pp. 527–540, 2010.

[337] H. Malhi, S. F. Bronk, N. W. Werneburg, and G. J. Gores, "Free fatty acids induce JNK-dependent hepatocyte lipoapoptosis," *Journal of Biological Chemistry*, vol. 281, no. 17, pp. 12093–12101, 2006.

[338] D. M. S. Ferreira, R. E. Castro, M. V. Machado et al., "Apoptosis and insulin resistance in liver and peripheral tissues of morbidly obese patients is associated with different stages of non-alcoholic fatty liver disease," *Diabetologia*, vol. 54, no. 7, pp. 1788–1798, 2011.

[339] C. M. Mayer and D. D. Belsham, "Palmitate attenuates insulin signaling and induces endoplasmic reticulum stress and apoptosis in hypothalamic neurons: rescue of resistance and apoptosis through adenosine $5'$ monophosphate-activated protein kinase activation," *Endocrinology*, vol. 151, no. 2, pp. 576–585, 2010.

[340] S. M. Turpin, G. I. Lancaster, I. Darby, M. A. Febbraio, and M. J. Watt, "Apoptosis in skeletal muscle myotubes is induced by ceramides and is positively related to insulin resistance," *American Journal of Physiology-Endocrinology and Metabolism*, vol. 291, no. 6, pp. E1341–E1350, 2006.

[341] L. A. Pradelli, E. Villa, B. Zunino, S. Marchetti, and J.-E. Ricci, "Glucose metabolism is inhibited by caspases upon the induction of apoptosis," *Cell Death & Disease*, vol. 5, no. 9, article e1406, 2014.

[342] A. Guilherme, G. J. Tesz, K. V. P. Guntur, and M. P. Czech, "Tumor necrosis factor-α induces caspase-mediated cleavage of peroxisome proliferator-activated receptor γ in adipocytes," *Journal of Biological Chemistry*, vol. 284, no. 25, pp. 17082–17091, 2009.

[343] M. Keuper, I. Wernstedt Asterholm, P. E. Scherer et al., "TRAIL (TNF-related apoptosis-inducing ligand) regulates adipocyte metabolism by caspase-mediated cleavage of PPARgamma," *Cell Death & Disease*, vol. 4, no. 1, article e474, 2013.

[344] S. El Akoum, "PPAR gamma at the crossroads of health and disease: a masterchef in metabolic homeostasis," *Endocrinology & Metabolic Syndrome*, vol. 3, no. 1, p. 126, 2014.

[345] J. Tőzsér and S. Benkő, "Natural compounds as regulators of NLRP3 inflammasome-mediated IL-1β production," *Mediators of Inflammation*, vol. 2016, Article ID 5460302, 16 pages, 2016.

[346] G. Meng, F. Zhang, I. Fuss, A. Kitani, and W. Strober, "A mutation in the *Nlrp3* gene causing inflammasome hyperactivation potentiates Th17 cell-dominant immune responses," *Immunity*, vol. 30, no. 6, pp. 860–874, 2009.

[347] P. Libby, J. M. Ordovas, K. R. Auger, A. H. Robbins, L. K. Birinyi, and C. A. Dinarello, "Endotoxin and tumor necrosis factor induce interleukin-1 gene expression in adult human vascular endothelial cells," *The American Journal of Pathology*, vol. 124, no. 2, pp. 179–185, 1986.

[348] T. N. Tangi, A. A. Elmabsout, T. Bengtsson, A. Sirsjö, and K. Fransén, "Role of NLRP3 and CARD8 in the regulation of TNF-α induced IL-1β release in vascular smooth muscle cells," *International Journal of Molecular Medicine*, vol. 30, no. 3, pp. 697–702, 2012.

[349] Y. Li, P. Wang, X. Yang et al., "SIRT1 inhibits inflammatory response partly through regulation of NLRP3 inflammasome in vascular endothelial cells," *Molecular Immunology*, vol. 77, pp. 148–156, 2016.

[350] N. Huang, M. Kny, F. Riediger et al., "Deletion of *Nlrp3* protects from inflammation-induced skeletal muscle atrophy," *Intensive Care Medicine Experimental*, vol. 5, no. 1, p. 3, 2017.

[351] F. G. Bauernfeind, G. Horvath, A. Stutz et al., "Cutting edge: NF-κB activating pattern recognition and cytokine receptors license NLRP3 inflammasome activation by regulating NLRP3 expression," *Journal of Immunology*, vol. 183, no. 2, pp. 787–791, 2009.

[352] M. G. Ghonime, O. R. Shamaa, S. Das et al., "Inflammasome priming by lipopolysaccharide is dependent upon ERK signaling and proteasome function," *Journal of Immunology*, vol. 192, no. 8, pp. 3881–3888, 2014.

[353] Q. He, H. You, X.-M. Li, T.-H. Liu, P. Wang, and B.-E. Wang, "HMGB1 promotes the synthesis of pro-IL-1β and pro-IL-18 by activation of p38 MAPK and NF-κB through receptors for advanced glycation end-products in macrophages," *Asian Pacific Journal of Cancer Prevention*, vol. 13, no. 4, pp. 1365–1370, 2012.

[354] B. Vandanmagsar, Y.-H. Youm, A. Ravussin et al., "The NLRP3 inflammasome instigates obesity-induced inflammation and insulin resistance," *Nature Medicine*, vol. 17, no. 2, pp. 179–188, 2011.

[355] H. Scheiblich, A. Schlütter, D. T. Golenbock, E. Latz, P. Martinez-Martinez, and M. T. Heneka, "Activation of the NLRP3 inflammasome in microglia: the role of ceramide," *Journal of Neurochemistry*, vol. 143, no. 5, pp. 534–550, 2017.

[356] O. Gross, C. J. Thomas, G. Guarda, and J. Tschopp, "The inflammasome: an integrated view," *Immunological Reviews*, vol. 243, no. 1, pp. 136–151, 2011.

[357] R. Zhou, A. S. Yazdi, P. Menu, and J. Tschopp, "A role for mitochondria in NLRP3 inflammasome activation," *Nature*, vol. 469, no. 7329, pp. 221–225, 2011.

[358] A. G. Lerner, J. P. Upton, P. V. K. Praveen et al., "IRE1α induces thioredoxin-interacting protein to activate the NLRP3 inflammasome and promote programmed cell death under irremediable ER stress," *Cell Metabolism*, vol. 16, no. 2, pp. 250–264, 2012.

[359] M. R. de Zoete, N. W. Palm, S. Zhu, and R. A. Flavell, "Inflammasomes," *Cold Spring Harbor Perspectives in Biology*, vol. 6, no. 12, 2014.

[360] C. Li, J. Zienkiewicz, and J. Hawiger, "Interactive sites in the MyD88 toll/interleukin (IL) 1 receptor domain responsible for coupling to the IL1β signaling pathway," *Journal of Biological Chemistry*, vol. 280, no. 28, pp. 26152–26159, 2005.

[361] J. Jager, T. Grémeaux, M. Cormont, Y. Le Marchand-Brustel, and J. F. Tanti, "Interleukin-1β-induced insulin resistance in adipocytes through down-regulation of insulin receptor substrate-1 expression," *Endocrinology*, vol. 148, no. 1, pp. 241–251, 2007.

[362] A. Y. Kim, Y. J. Park, X. Pan et al., "Obesity-induced DNA hypermethylation of the adiponectin gene mediates insulin resistance," *Nature Communications*, vol. 6, no. 1, p. 7585, 2015.

[363] A. Wree, A. Eguchi, M. D. McGeough et al., "NLRP3 inflammasome activation results in hepatocyte pyroptosis, liver inflammation, and fibrosis in mice," *Hepatology*, vol. 59, no. 3, pp. 898–910, 2014.

[364] H. Xiao, M. Lu, T. Y. Lin et al., "Sterol regulatory element binding p1rotein 2 activation of NLRP3 inflammasome in endothelium mediates hemodynamic-induced atherosclerosis susceptibility," *Circulation*, vol. 128, no. 6, pp. 632–642, 2013.

[365] V. Elgazar-Carmon, A. Rudich, N. Hadad, and R. Levy, "Neutrophils transiently infiltrate intra-abdominal fat early in the course of high-fat feeding," *Journal of Lipid Research*, vol. 49, no. 9, pp. 1894–1903, 2008.

[366] K. Makki, P. Froguel, and I. Wolowczuk, "Adipose tissue in obesity-related inflammation and insulin resistance: cells, cytokines, and chemokines," *ISRN Inflammation*, vol. 2013, Article ID 139239, 12 pages, 2013.

[367] A. Mantovani, M. A. Cassatella, C. Costantini, and S. Jaillon, "Neutrophils in the activation and regulation of innate and adaptive immunity," *Nature Reviews Immunology*, vol. 11, no. 8, pp. 519–531, 2011.

[368] M. Mraz and M. Haluzik, "The role of adipose tissue immune cells in obesity and low-grade inflammation," *The Journal of Endocrinology*, vol. 222, no. 3, pp. R113–R127, 2014.

[369] P. Newsholme and P. I. H. de Bittencourt Jr., "The fat cell senescence hypothesis: a mechanism responsible for abrogating the resolution of inflammation in chronic disease," *Current Opinion in Clinical Nutrition and Metabolic Care*, vol. 17, no. 4, pp. 295–305, 2014.

[370] P. Codogno and A. J. Meijer, "Autophagy: a potential link between obesity and insulin resistance," *Cell Metabolism*, vol. 11, no. 6, pp. 449–451, 2010.

[371] G. S. Hotamisligil, "Endoplasmic reticulum stress and the inflammatory basis of metabolic disease," *Cell*, vol. 140, no. 6, pp. 900–917, 2010.

[372] Y. Zhao, C.-F. Zhang, H. Rossiter et al., "Autophagy is induced by UVA and promotes removal of oxidized phospholipids and protein aggregates in epidermal keratinocytes," *Journal of Investigative Dermatology*, vol. 133, no. 6, pp. 1629–1637, 2013.

[373] S. T. Shibutani and T. Yoshimori, "A current perspective of autophagosome biogenesis," *Cell Research*, vol. 24, no. 1, pp. 58–68, 2014.

[374] M. Rahman, M. Mofarrahi, A. S. Kristof, B. Nkengfac, S. Harel, and S. N. A. Hussain, "Reactive oxygen species regulation of autophagy in skeletal muscles," *Antioxidants & Redox Signaling*, vol. 20, no. 3, pp. 443–459, 2014.

[375] A. Sasnauskiene, J. Kadziauskas, N. Vezelyte, V. Jonusiene, and V. Kirveliene, "Damage targeted to the mitochondrial interior induces autophagy, cell cycle arrest and, only at high doses, apoptosis," *Autophagy*, vol. 5, no. 5, pp. 743-744, 2009.

[376] C. Luo, Y. Li, H. Wang et al., "Mitochondrial accumulation under oxidative stress is due to defects in autophagy," *Journal of Cellular Biochemistry*, vol. 114, no. 1, pp. 212–219, 2013.

[377] M. Portovedo, L. M. Ignacio-Souza, B. Bombassaro et al., "Saturated fatty acids modulate autophagy's proteins in the hypothalamus," *PLoS One*, vol. 10, no. 3, article e0119850, 2015.

[378] H. Soussi, K. Clément, and I. Dugail, "Adipose tissue autophagy status in obesity: expression and flux—two faces of the picture," *Autophagy*, vol. 12, no. 3, pp. 588-589, 2016.

[379] J. M. Norman, G. M. Cohen, and E. T. W. Bampton, "The in vitro cleavage of the hAtg proteins by cell death proteases," *Autophagy*, vol. 6, no. 8, pp. 1042–1056, 2010.

[380] N. Rodríguez-Muela, A. M. Hernández-Pinto, A. Serrano-Puebla et al., "Lysosomal membrane permeabilization and autophagy blockade contribute to photoreceptor cell death in a mouse model of retinitis pigmentosa," *Cell Death & Differentiation*, vol. 22, no. 3, pp. 476–487, 2015.

[381] M. S. Goligorsky, "SIRTing out the link between autophagy and ageing," *Nephrology Dialysis Transplantation*, vol. 25, no. 8, pp. 2434–2436, 2010.

[382] J.-H. Cho, G.-Y. Kim, C.-J. Pan et al., "Downregulation of SIRT1 signaling underlies hepatic autophagy impairment in glycogen storage disease type Ia," *PLoS Genetics*, vol. 13, no. 5, article e1006819, 2017.

[383] M. Jiao, F. Ren, L. Zhou et al., "Peroxisome proliferator-activated receptor α activation attenuates the inflammatory response to protect the liver from acute failure by promoting the autophagy pathway," *Cell Death & Disease*, vol. 5, no. 8, article e1397, 2014.

[384] F. Ren, L. Zhang, X. Zhang et al., "Inhibition of glycogen synthase kinase 3β promotes autophagy to protect mice from acute liver failure mediated by peroxisome proliferator-activated receptor α," *Cell Death & Disease*, vol. 7, no. 3, article e2151, 2016.

[385] K. H. Kim, Y. T. Jeong, H. Oh et al., "Autophagy deficiency leads to protection from obesity and insulin resistance by inducing Fgf21 as a mitokine," *Nature Medicine*, vol. 19, no. 1, pp. 83–92, 2013.

[386] Q. Gong, Z. Hu, F. Zhang et al., "Fibroblast growth factor 21 improves hepatic insulin sensitivity by inhibiting mammalian target of rapamycin complex 1 in mice," *Hepatology*, vol. 64, no. 2, pp. 425–438, 2016.

[387] Y. Yu, J. He, S. Li et al., "Fibroblast growth factor 21 (FGF21) inhibits macrophage-mediated inflammation by activating Nrf2 and suppressing the NF-κB signaling pathway," *International Immunopharmacology*, vol. 38, pp. 144–152, 2016.

[388] Z. Lin, H. Tian, K. S. L. Lam et al., "Adiponectin mediates the metabolic effects of FGF21 on glucose homeostasis and

insulin sensitivity in mice," *Cell Metabolism*, vol. 17, no. 5, pp. 779–789, 2013.

[389] W. L. Holland, A. C. Adams, J. T. Brozinick et al., "An FGF21-adiponectin-ceramide axis controls energy expenditure and insulin action in mice," *Cell Metabolism*, vol. 17, no. 5, pp. 790–797, 2013.

[390] P. Xu, Y. Zhang, W. Wang et al., "Long-term administration of fibroblast growth factor 21 prevents chemically-induced hepatocarcinogenesis in mice," *Digestive Diseases and Sciences*, vol. 60, no. 10, pp. 3032–3043, 2015.

[391] J. Zhang and Y. Li, "Fibroblast growth factor 21 analogs for treating metabolic disorders," *Frontiers in Endocrinology*, vol. 6, p. 168, 2015.

[392] F. M. Fisher, P. C. Chui, P. J. Antonellis et al., "Obesity is a fibroblast growth factor 21 (FGF21)-resistant state," *Diabetes*, vol. 59, no. 11, pp. 2781–2789, 2010.

[393] J. Y. Jeon, S.-E. Choi, E. S. Ha et al., "Association between insulin resistance and impairment of FGF21 signal transduction in skeletal muscles," *Endocrine*, vol. 53, no. 1, pp. 97–106, 2016.

[394] J. M. Gallego-Escuredo, J. Gomez-Ambrosi, V. Catalan et al., "Opposite alterations in FGF21 and FGF19 levels and disturbed expression of the receptor machinery for endocrine FGFs in obese patients," *International Journal of Obesity*, vol. 39, no. 1, pp. 121–129, 2015.

[395] A. C. Adams, C. C. Cheng, T. Coskun, and A. Kharitonenkov, "FGF21 requires βklotho to act in vivo," *PLoS One*, vol. 7, no. 11, article e49977, 2012.

[396] K. R. Markan, M. C. Naber, S. M. Small, L. Peltekian, R. L. Kessler, and M. J. Potthoff, "FGF21 resistance is not mediated by downregulation of beta-klotho expression in white adipose tissue," *Molecular Metabolism*, vol. 6, no. 6, pp. 602–610, 2017.

[397] S. Kim, H.-G. Lee, S.-A. Park et al., "Keap1 cysteine 288 as a potential target for diallyl trisulfide-induced Nrf2 activation," *PLoS One*, vol. 9, no. 1, article e85984, 2014.

[398] J. A. David, W. J. Rifkin, P. S. Rabbani, and D. J. Ceradini, "The Nrf2/Keap1/ARE pathway and oxidative stress as a therapeutic target in type II diabetes mellitus," *Journal of Diabetes Research*, vol. 2017, Article ID 4826724, 15 pages, 2017.

[399] B. Chen, Y. Lu, Y. Chen, and J. Cheng, "The role of Nrf2 in oxidative stress-induced endothelial injuries," *Journal of Endocrinology*, vol. 225, no. 3, pp. R83–R99, 2015.

[400] S. Fourquet, R. Guerois, D. Biard, and M. B. Toledano, "Activation of NRF2 by nitrosative agents and H_2O_2 involves KEAP1 disulfide formation," *Journal of Biological Chemistry*, vol. 285, no. 11, pp. 8463–8471, 2010.

[401] A. Jiménez-Osorio, A. Picazo, S. González-Reyes, D. Barrera-Oviedo, M. Rodríguez-Arellano, and J. Pedraza-Chaverri, "Nrf2 and redox status in prediabetic and diabetic patients," *International Journal of Molecular Sciences*, vol. 15, no. 12, pp. 20290–20305, 2014.

[402] H.-J. He, G.-Y. Wang, Y. Gao, W.-H. Ling, Z.-W. Yu, and T.-R. Jin, "Curcumin attenuates Nrf2 signaling defect, oxidative stress in muscle and glucose intolerance in high fat diet-fed mice," *World Journal of Diabetes*, vol. 3, no. 5, pp. 94–104, 2012.

[403] R. Faraonio, P. Vergara, D. di Marzo et al., "p53 suppresses the Nrf2-dependent transcription of antioxidant response genes," *Journal of Biological Chemistry*, vol. 281, no. 52, pp. 39776–39784, 2006.

[404] Y. Tan, T. Ichikawa, J. Li et al., "Diabetic downregulation of Nrf2 activity via ERK contributes to oxidative stress–induced insulin resistance in cardiac cells in vitro and in vivo," *Diabetes*, vol. 60, no. 2, pp. 625–633, 2011.

[405] A.-S. Cheng, Y.-H. Cheng, C.-H. Chiou, and T.-L. Chang, "Resveratrol upregulates Nrf2 expression to attenuate methylglyoxal-induced insulin resistance in Hep G2 cells," *Journal of Agricultural and Food Chemistry*, vol. 60, no. 36, pp. 9180–9187, 2012.

[406] A. K. Jain and A. K. Jaiswal, "GSK-3β acts upstream of Fyn kinase in regulation of nuclear export and degradation of NF-E2 related factor 2," *Journal of Biological Chemistry*, vol. 282, no. 22, pp. 16502–16510, 2007.

[407] D. V. Kratschmar, D. Calabrese, J. Walsh et al., "Suppression of the Nrf2-dependent antioxidant response by glucocorticoids and 11β-HSD1-mediated glucocorticoid activation in hepatic cells," *PLoS One*, vol. 7, no. 5, article e36774, 2012.

[408] M. Matsuda and I. Shimomura, "Roles of oxidative stress, adiponectin, and nuclear hormone receptors in obesity-associated insulin resistance and cardiovascular risk," *Hormone Molecular Biology and Clinical Investigation*, vol. 19, no. 2, pp. 75–88, 2014.

[409] D. J. Wake, E. Rask, D. E. W. Livingstone, S. Söderberg, T. Olsson, and B. R. Walker, "Local and systemic impact of transcriptional up-regulation of 11β-hydroxysteroid dehydrogenase type 1 in adipose tissue in human obesity," *The Journal of Clinical Endocrinology & Metabolism*, vol. 88, no. 8, pp. 3983–3988, 2003.

[410] J. Xu, S. R. Kulkarni, A. C. Donepudi, V. R. More, and A. L. Slitt, "Enhanced Nrf2 activity worsens insulin resistance, impairs lipid accumulation in adipose tissue, and increases hepatic steatosis in leptin-deficient mice," *Diabetes*, vol. 61, no. 12, pp. 3208–3218, 2012.

[411] D. V. Chartoumpekis, P. G. Ziros, A. I. Psyrogiannis et al., "Nrf2 represses FGF21 during long-term high-fat diet–induced obesity in mice," *Diabetes*, vol. 60, no. 10, pp. 2465–2473, 2011.

[412] A. Lau, X. J. Wang, F. Zhao et al., "A noncanonical mechanism of Nrf2 activation by autophagy deficiency: direct interaction between Keap1 and p62," *Molecular and Cellular Biology*, vol. 30, no. 13, pp. 3275–3285, 2010.

[413] A. Lau, Y. Zheng, S. Tao et al., "Arsenic inhibits autophagic flux, activating the Nrf2-Keap1 pathway in a p62-dependent manner," *Molecular and Cellular Biology*, vol. 33, no. 12, pp. 2436–2446, 2013.

Hindawi
Oxidative Medicine and Cellular Longevity
Volume 2018, Article ID 2025914, 19 pages
https://doi.org/10.1155/2018/2025914

Research Article

The Isoquinoline Alkaloid Dauricine Targets Multiple Molecular Pathways to Ameliorate Alzheimer-Like Pathological Changes *In Vitro*

Pan Liu,[1] **Xiao Chen**,[2] **Haizhe Zhou**,[3] **Liqun Wang**,[1] **Zaijun Zhang**,[4] **Xiaohu Ren**,[2] **Feiqi Zhu**,[5] **Yi Guo**,[6] **Xinfeng Huang**,[2] **Jianjun Liu**,[2] **Peter S. Spencer**,[7] **and Xifei Yang**[2]

[1]*College of Pharmaceutical Engineering & Life Science, Changzhou University, Changzhou 213164, China*
[2]*Key Laboratory of Modern Toxicology of Shenzhen, Shenzhen Center for Disease Control and Prevention, Shenzhen 518055, China*
[3]*Department of Encephalopathy, Shaanxi University of Chinese Medicine, Xianyang, Shanxi 712000, China*
[4]*Institute of New Drug Research and Guangzhou Key Laboratory of Innovative Chemical Drug Research in Cardio-cerebrovascular Diseases, Jinan University College of Pharmacy, Guangzhou 510632, China*
[5]*Cognitive Impairment Ward of Neurology Department, The 3rd Affiliated Hospital of Shenzhen University, Shenzhen 518055, China*
[6]*Department of Neurology, Second Clinical College, Jinan University, Shenzhen 518020, China*
[7]*Department of Neurology, School of Medicine, Oregon Institute of Occupational Health Sciences, Oregon Health & Science University, Portland, OR 97239, USA*

Correspondence should be addressed to Liqun Wang; wlq@cczu.edu.cn and Xifei Yang; xifeiyang@gmail.com

Received 5 November 2017; Revised 2 March 2018; Accepted 22 April 2018; Published 2 July 2018

Academic Editor: Lisbell Estrada

Alzheimer's disease (AD), the most common neurodegenerative disease, has no effective treatment. Dauricine (DAU), a benzyl tetrahydroisoquinoline alkaloid isolated from the root of *Menispermum dauricum* DC, reportedly has neuroprotective effects in cerebral ischemia. Here, we investigated the effects of DAU on N2a cells stably transfected with Swedish mutant amyloid precursor protein (N2a/APP), an AD-like cell model. ELISA and Western blot analysis revealed that DAU inhibited APP processing and reduced Aβ accumulation. In addition, DAU ameliorated tau hyperphosphorylation via PP2A, p35/25, and CDK5 pathways in N2a/APP cells. The amelioration of tau hyperphosphorylation by DAU was also validated in HEK293/Tau cells, another cell line with tau hyperphosphorylation. Proteomic analysis revealed 85 differentially expressed proteins in the lysates between the wild-type N2a cells (N2a/WT) and the N2a/APP cells in the presence or absence of DAU; these were classified into 6 main categories according to their functions: endoplasmic reticulum (ER) stress-associated proteins, oxidative stress-associated proteins, cytoskeleton proteins, molecular chaperones, mitochondrial respiration and metabolism-related proteins, and signaling proteins. Taken together, we demonstrated that DAU treatment reduces AD-like pathology, thereby suggesting that DAU has potential therapeutic utility in AD.

1. Introduction

Alzheimer's disease (AD), a progressive and irreversible neurodegenerative disorder, contributes to individual morbidity and mortality and burdens the social healthcare system [1, 2]. AD has complex neuropathological features, but neurofibrillary tangles consisting of abnormal phosphorylated tau and neuritic amyloid β (Aβ) plaques are hallmarks of the disease. The approved medications for AD show consistent but modest clinical effects [3, 4]; on the contrary, hundreds of trials with candidate AD drugs have been terminated because they were clinically ineffective. A medication that can prevent, delay, or reverse the disease has yet to be discovered.

Bisbenzylisoquinolines form a class of natural products with a therapeutic potential for neurodegeneration [5]. Dauricine (DAU) is a bisbenzylisoquinoline alkaloid derivative (Figure 1(a)) extracted from the rootstock of *Menispermum*

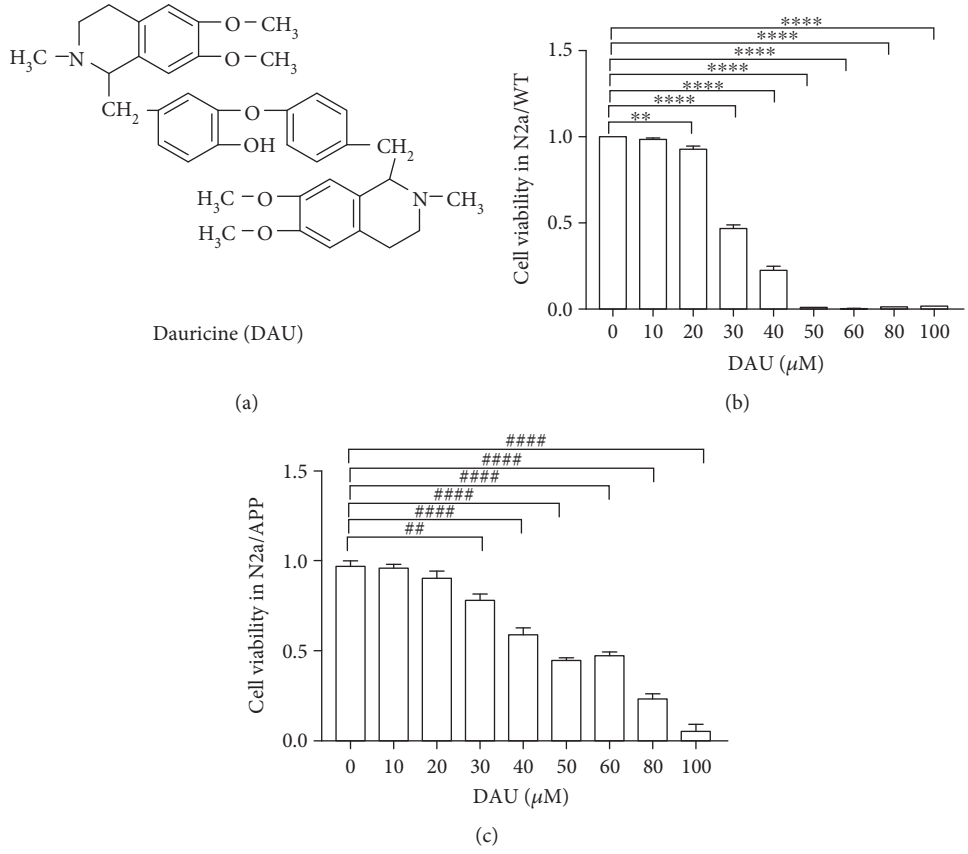

Figure 1: DAU has low cytotoxicity to N2a/WT and N2a/APP cells. (a) Chemical structure of DAU. (b) Cell viability of N2a/WT with respect to DAU treatment. (c) Cell viability of N2a/APP with DAU treatment. $N = 3$. $^{**}P < 0.01$ and $^{****}P < 0.0001$ compared with N2a/WT cells treated with vehicle. $^{\#\#}P < 0.01$, $^{\#\#\#\#}P < 0.0001$ compared with vehicle-treated N2a/APP cells.

dauricum DC, a traditional medicine listed in the Chinese Pharmacopoeia. The neuroprotective effects of DAU have been widely reported. DAU inhibited apoptosis of a transient focal cerebral ischemia model in part via a mitochondrial pathway [6]. DAU protected cortical neurons from ischemia by inhibiting entry of extracellular Ca^{2+} and intracellular release of Ca^{2+} from endoplasmic reticulum [6]. DAU reduced neurological deficits, diminished DNA fragmentation, increased Bcl-2 expression, and reduced Bax expression in ischemic cerebral infarcts via modulation of Bcl-2 family proteins [6]. DAU attenuated tau hyperphosphorylation by promoting the release of bradykinin, which raised intracellular neuronal calcium [7]. Another bisbenzylisoquinoline alkaloid, tetrandrine, has been reported to attenuate spatial memory impairment and hippocampal inflammation by inhibiting NF-κB activation in a rat model of AD induced by $A\beta_{1-42}$ [5]. However, the therapeutic potential of DAU has yet to be evaluated in a transgenic model of AD.

Given that bisbenzylisoquinolines are potential AD drug candidates, we examined the neuroprotective effects of DAU in a murine neuroblastoma cell line (N2a) stably transfected with the human Swedish mutant form of amyloid protein precursor (APP) [8]. By employing this well-studied cell model [9], which overexpresses APP and hyperphosphorylates tau, we found that DAU not only attenuated the level of tau hyperphosphorylation but also reduced Aβ plaque formation. Accompanying these changes, DAU altered the unfolded protein response, mitochondrial function, and clearance of reactive oxygen species.

2. Methods and Material

2.1. Reagents. DAU (stated purity $\geq$ 98%) was purchased from Shanghai Aladdin Biochemical Technology Co. Ltd. (CAS: 524-17-4, D115683, Shanghai, China). The purity of the DAU was confirmed by HPLC. The stock solution of DAU (10 mM) was prepared in DMSO (Thermo Fisher Scientific, Waltham, MA, USA) and was used directly. The antibodies used in this study are listed in Table 1.

2.2. Cells and Cell Culture. Wild-type murine neuroblastoma Neuro2a cells (N2a/WT) were purchased from the Cell Bank of China (CODE: IFO50495, Shanghai, China). N2a cells stably transfected with human APP Swedish mutant (N2a/APP) and Human Embryonic Kidney 293 cells stably transfected with tau protein (HEK293/Tau) were gifts from Professor Jian-zhi Wang (Tongji Medical School, Wuhan, China) [8–10]. The cells were cultured in the following medium with 5% CO_2 and at 37°C: Minimum Essential Medium Eagle (MEM) (Grand Island, NY, USA) with 10% fetal bovine serum (FBS, Grand Island, NY, USA) for N2a/WT cells; Dulbecco's modified Eagle's medium (DMEM, Grand Island,

Table 1: The primary antibodies used in this study.

Antibody	Cat.	RRID	Type	Dilution	Source
t-APP	ab32136	AB_2289606	Rabbit	1 : 3000	Abcam
p-APP	#6986	BDSC_6986	Rabbit	1 : 1000	Cell Signaling
sAPPα	11088	Unknown	Mouse	1 : 50	Immuno-Biological
sAPPβ	10321	Unknown	Mouse	1 : 50	Immuno-Biological
BACE1	#5606	AB_1903900	Rabbit	1 : 1000	Cell Signaling
PS1	#5643	AB_10706356	Rabbit	1 : 1000	Cell Signaling
pS396	ab109390	AB_10860822	Rabbit	1 : 20000	Abcam
pS404	sc-12952	RRID:AB_656753	Goat	1 : 3000	Santa Cruz
pT231	355200	AB_2533210	Mouse	1 : 1000	Thermo Fisher
pS262	44750G	AB_2533743	Rabbit	1 : 1000	Thermo Fisher
Tau 1	MAB3420	AB_94855	Mouse	1 : 200000	Millipore
Tau 5	ab80579	AB_1603723	Mouse	1 : 3000	Abcam
p-GSK3α/β	#9331	AB_329830	Rabbit	1 : 1000	Cell Signaling
GSK3α/β	#5676	AB_10547140	Rabbit	1 : 1000	Cell Signaling
p-PP2A (Y307)	AF3989	AB_2169636	Rabbit	1 : 1000	R&D Systems
PP2A	#2259	AB_10695752	Rabbit	1 : 1000	Cell Signaling
p35/25	#2680	AB_1078214	Rabbit	1 : 1000	Cell Signaling
CDK5	ab40773	AB_726779	Rabbit	1 : 3000	Abcam
GRP78	sc-376768	Unknown	Mouse	1 : 1000	Santa Cruz
GRP75	sc-133137	AB_2120468	Mouse	1 : 1000	Santa Cruz
PDIA1	ab2792	AB_303304	Mouse	1 : 1000	Abcam
HMGB1	ab79823	AB_1603373	Rabbit	1 : 50000	Abcam
14-3-3-z	ab155037	Unknown	Rabbit	1 : 3000	Abcam
PRDX4	ab16943	AB_443567	Rabbit	1 : 1000	Abcam
8-OHdG	ab10802	AB_297482	Goat	1 : 400	Abcam
p-PERK	#3179	AB_2095853	Rabbit	1 : 1000	Cell Signaling
p-eIF2α	#3597	RRID:AB_390740	Rabbit	1 : 1000	Cell Signaling
eIF2α	#5324	AB_10692650	Rabbit	1 : 1000	Cell Signaling
ATF-4	#11815	AB_2616025	Mouse	1 : 1000	Cell Signaling
CHOP	#2895	AB_2089254	Rabbit	1 : 1000	Cell Signaling
β-Actin	sc-47778	AB_626632	Mouse	1 : 3000	Santa Cruz
α-Tubulin	sc-73242	AB_1130901	Mouse	1 : 3000	Santa Cruz

NY, USA) with 10% FBS for HEK293/Tau cells; and a medium containing 42% DMEM and 50% Opti-MEM, complemented by 8% FBS for N2a/APP cells. Geneticin (0.2 g/L) (Grand Island, NY, USA) was dissolved in a medium to select transfected N2a/APP and HEK293/Tau cells.

2.3. Cell Viability Assay. After subculture, the N2a/APP cell suspension was placed on a 96-well tissue culture plate. Each well of the plate contained 10^4 cells in 100 μL cell culture medium. After 16 h in 5% CO_2 at 37°C, the medium was removed and replaced with 200 μL cell culture medium with DAU or vehicle (0.5% DMSO) (Thermo Fisher Scientific, Waltham, MA, USA). After another 24 h in 5% CO_2 at 37°C, the medium was decanted and replaced by 100 μL cell culture medium with 10 μL cell counting kit-8 solution (Dojindo Laboratories, Kumamoto, Japan) and incubated for 1 h. The plate was read by a plate reader (TECAN Group Ltd., San Jose, CA, USA) at 450 nm. Cell viability was calculated as the absorbance of the well with cell and cell culture medium minus the well with cell culture medium only. The relative cell viability was the viability of the treated cell normalized by the viability of the control (vehicle).

2.4. ELISA of $A\beta_{1-40}$ and $A\beta_{1-42}$. The ELISA kits for $A\beta_{1-40}$ and $A\beta_{1-42}$ (R&D Systems, Minneapolis, MN, USA) were used according to the manufacturer's protocol. N2a/WT and N2a/APP cells were treated with DAU or vehicle in 25 cm^2 culture flasks for 24 h (Grand Island, NY, USA). Cells and culture medium were collected separately. The cells were lysed in 200 μL IP buffer (Beyotime, Beijing, China) with protease and phosphatase inhibitor cocktail (Thermo Fisher Scientific, Rockford, IL, USA) on ice for 20 min and centrifuged at 18,000 at 4°C for 20 min. The resultant supernatant was diluted 40 times before assay, and the cell culture medium was used directly. A standard curve of $A\beta_{1-40}$ or $A\beta_{1-42}$ was built, and the $A\beta_{1-40}$ or $A\beta_{1-42}$ in the samples

was calculated and normalized by total protein content determined with a Pierce™ BCA protein assay kit (Thermo Fisher Scientific, Rockford, IL, USA).

2.5. Western Blot Analysis. After 24 h treatment with DAU or vehicle, cells were collected and lysed in 200 μL of IP buffer with protease and phosphatase inhibitor cocktail on ice for 20 min and centrifuged at 14,000 g at 4°C for 20 min. Supernatants were used for protein content determination and SDS-PAGE separation. The total protein content of each sample was determined with the Pierce BCA protein assay kit. Before loading onto the SDS-PAGE gel, samples were mixed with Pierce Lane Marker Reducing Sample Buffer (Thermo Fisher Scientific, Rockford, IL, USA) and denatured (boiled for 10 min). SDS-PAGE (10–12%) gels were used to separate target proteins and then transferred to polyvinylidene fluoride (PVDF) membranes (Merck Millipore Ltd., Merck KGaA, Darmstadt, GER). Membranes were blocked with nonfat milk powder dissolved in TBS-Tween 20 buffer for 2 h and then incubated with primary antibody (dilutions of the antibodies are listed in Table 1) at 4°C overnight. The membranes were washed and incubated with anti-mouse, anti-rabbit, or anti-goat IgG conjugated to horseradish peroxidase (HRPs) (1 : 3000) at room temperature (RT) for 1 h before development. Enhanced chemiluminescent solution (Thermo Fisher Scientific, Rockford, IL, USA) was applied for development. The densitometry of the blots was quantified by ImageQuant 1D software (GE. Healthcare, Pittsburgh, PA, USA).

2.6. Comparative Proteomics

2.6.1. Protein Preparation and Labeling. After 24 h treatment with DAU or vehicle, cells were collected and lysed in 500 μL DIGE-specific lysis buffer (7 M urea, 2 M thiourea, 30 mM Tris–HCl, 4% CHAPS, pH 8.5) on ice for 30 min. Ultrasonication (Fisher 550 Sonic Dismembrator, Pittsburgh, PA, USA) was applied to assist cell lysation. Samples were centrifuged at 20,000 g for 60 min. For each sample, 200 μL of lysis buffer was added to the supernatant, and then the mixture was ultrafiltered in a centrifugal filter (Merck Millipore Ltd., Billerica, MA, USA) to remove salts. The protein solution was collected, and protein concentrations quantified were with a 2-D Quant kit (GE Healthcare, Chicago, IL, USA) according to the manufacturer's guidelines.

Fifteen protein samples were used for the proteomics study and for each treatment group, and three biological repeats were performed for each group. Each protein sample was diluted with lysis buffer to a final concentration of 5 μg/μL. The protein solution (5 μL) was labeled with Cy3 (GE Healthcare, 25-8008-61) or Cy5 dye (GE Healthcare, 25-8008-62) in the dark for 30 min. Cy2 stained the internal standard that was pooled from 15 protein study samples. The reaction of protein labeling was quenched by adding 1 μL of 10 mM lysine (Sigma-Aldrich, L5626), and three samples labeled with Cy2, Cy3, and Cy5 were mixed as a group. The mixture was then resolved in rehydration buffer (7 M urea, 2 M thiourea, 2% CHAPS, 2.8% DTT, 0.5% IPG buffer (pH 3–11 NL) and 0.002% bromophenol blue) to a final volume of 450 μL prior to transfer onto immobilized pH gradient strips.

2.6.2. 2-Dimensional Electrophoresis. The strips were first rehydrated and then isoelectric-focused (IEF) in Ettan IPGphor Isoelectric Focusing (IEF) System (GE Healthcare). After IEF, strips were allowed to stand at RT for 10 min. The focused strips were immediately equilibrated in a 15 mL reducing equilibration buffer of 6 M urea, 30% (v/v) glycerol, 2% (w/v) SDS, 75 mM Tris-HCl buffer (pH 8.8), and 1% (w/v) DTT (Sigma-Aldrich, St. Louis, MO, USA) for 15 min at RT on a shaking table and subsequently reequilibrated in the same buffer containing 6 M urea, 75 mM Tris–HCl buffer (pH 8.8), 30% (v/v) glycerol, 2% (w/v) SDS, and 4.5% (w/v) IAA (Sigma-Aldrich) afterwards. The equilibrated strips were loaded on the top of 12.5% SDS-PAGE gels and covered with 0.5% (w/v) ultralow melting point agarose sealing solution (25 mM Tris, 192 mM glycine, 0.1% SDS, 0.5% (w/v) agarose, 0.02% bromophenol blue). Protein separation in the second dimension employed an Ettan DALTsix Electrophoresis System (GE Healthcare) with the running buffer (25 mM Tris, 192 mM lycine, 0.1% SDS, pH 8.3) at 12°C by the following steps: 1 W/gel for 1 h, subsequently 11 W/gel for 5 h in the dark. Afterward, gels were immediately scanned in a Typhoon TRIO Variable Mode Imager (GE Healthcare) after a prescan at 1000 micrometer resolution to determine the optimum PMT voltage for each channel. Image acquisition was done with a resolution of 100 micrometers. To achieve variation in the signal across gels, the PMT was set to ensure the maximum pixel intensity of all gel images remained within a range of 40,000–60,000 pixels.

2.6.3. Image Analysis. Following the manufacturer's instruction, DIGE gels were analyzed with the DeCyder software package (version 6.5 GE Healthcare, Milwaukee, USA). Each gel image was imported into the software and then individually processed with the differential in-gel analysis (DIA) and the biological analysis (BVA) modules to analyze protein spots. The volume of each protein spot in the Cy3 or Cy5 channels was normalized against the volume of the same Cy2 spot. The normalized volume of each spot was compared across the gels among the replicate groups. Differentially expressed protein spots ($P < 0.05$) were shortlisted for identification.

2.6.4. In-Gel Tryptic Digestion. Replicate preparative gels of 1000 μg of N2a/WT and N2a/APP cell proteins were prepared as for DIGE but without protein labeling. The gel was immersed overnight in dye (Coomassie blue solution containing 0.12% Coomassie brilliant blue G-250, 20% ethanol, 10% phosphoric acid, and 10% ammonium sulfate). Differential protein spots of interest identified by Decyder software analysis were manually excised from the stained gel. Gel pieces were destained and digested overnight at 37°C with 0.01 μg/μL trypsin (Promega Corp., WI, USA) as described by Robinson et al. [11]. The tryptic peptides were used for analysis by matrix-assisted laser desorption/ionization time-of-flight tandem mass spectrometry (MALDI-TOF-MS/MS)

(SCIEX TOF/TOF™ 5800 System, AB SCIEX, Framingham, MA, USA).

2.6.5. Mass Spectrometry and Database Searching. MALDI mass measurements were carried out with a Bruker Ultraflex III MALDI-TOF/TOF mass spectrometer (Bruker, Billerica, MASS, USA). For each protein sample, a total of 0.8 μL peptide extract was used for MALDI-TOF-MS/MS analysis, and the peptide extract was cocrystallized with 0.8 μL and 10 mg/mL α-cyano-4-hydroxycinnamic acid (CHCA) in 0.1% TFA, 50% acetonitrile (ACN) directly on the target, and dried at RT. The spectra were externally calibrated. MASCOT (Matrix Science, UK) was used for database searching against the SwissProt databases for murine cells proteins. The search was performed in the *Mus musculus* database and conducted with a tolerance on a mass measurement of 100 ppm in the MS mode and 0.5 Da in the MS/MS mode. Up to two missed cleavages per peptide were allowed. A fixed carbamidomethyl modification was taken into account. Protein MW and PI information were also considered to evaluate the protein identification based on the location of the excised protein spot from the 2-D gel.

2.6.6. Immunocytochemistry. Cells were planted on a coverslip within a well of a 6-well plate. After the cells attached to the slip, they were treated with DAU or vehicle for 24 h. Cells on the coverslip were fixed in 4% polyaldehyde for 10 min at RT, permeabilized in 0.3% Triton X-100 in PBS for 30 min, and blocked with 5% BSA in PBST. After blocking, the coverslip was incubated with anti-8-OHdG (1 : 400) at 4°C overnight. After washing, the coverslip was incubated with anti-goat IgG conjugated to HRPs (1 : 200) (Santa Cruz Biotechnology, Santa Cruz, CA, USA) in the dark for 1 h. The cells on the coverslip were then stained with DAPI (4′,6-diamidino-2-phenylindole) for 5 min and developed with Fluo-Antifading Medium (Beyotime, Beijing, China). Cells were examined by laser confocal microscopy.

2.6.7. Bioinformatics Analysis and Statistics. Functional annotation of differentially expressed proteins was performed with the Database for Annotation, Visualization and Integrated Discovery Resource (DAVID, https://david.ncifcrf.gov). Gene ontology (GO) terms for biological processes (BP), molecular functions (MF), and charts and cellular components (CC) were obtained with default statistical parameters.

Results were expressed as the mean ± SEM. One-way ANOVA was used to determine the statistical significance of differences among groups and following post hoc assessment by the Student-Newman-Keuls Method (GraphPad Prism 7.0, http://www.graphpad.com/). A P value less than 0.05 was considered statistically significant.

3. Results

3.1. DAU Has Low Cytotoxicity to N2a/WT and N2a/APP Cells. DAU is a bisbenzylisoquinoline alkaloid derivate (Figure 1(a)) extracted from the rootstock of *Menispermum dauricum* DC, a traditional medicine listed in the Chinese Pharmacopoeia. We investigated the cytotoxicity of DAU on both N2a/WT and N2a/APP cells using a 24 h cell-based assay. CCK-8, a water-soluble tetrazolium salt that is converted to a water-soluble formazan dye by living cell mitochondria, was exploited to examine cell viability. No significant inhibition of cell viability was observed in N2a/WT cells treated with less than 20 μM DAU compared with vehicle-treated cells (Figure 1(b)). We did not observe obvious reductions of cell viability when the N2a/APP cells were treated with 10 μM or 20 μM DAU (Figure 1(c)). We therefore concluded that no significant cytotoxicity was induced by 24 h treatment of DAU even at the concentration of 20 μM, the maximum concentration of DAU used in the following study.

3.2. DAU Inhibited APP Processing and Aβ Accumulation in N2a/APP Cells. We then investigated the effect of DAU on Aβ generation with ELISA. The level of Aβ_{1-42} toxic fragments was significantly higher in N2a/APP cell lysates (2538 pg/mL versus 646.5 pg/mL, $P = 0.0029$) compared to N2a/WT cell lysates, and the Aβ_{1-42} level in N2a/APP cells treated with 20 μM DAU was nearly three times lower (909.6 pg/mL versus 2538 pg/mL, $P = 0.0085$) (Figure 2(a)). The mean level of Aβ_{1-42} in N2a/APP cell culture medium was also higher than that of N2a/WT cells (89.21 pg/mL versus 48.71 pg/mL, $P = 0.0996$) (Figure 2(b)). On the contrary, there was no significant difference in the level of nontoxic amyloid Aβ_{1-40} in either the cell lysate (278.5 pg/mL versus 270.8 pg/mL, $P = 0.9894$) (Figure 2(c)) or cell culture medium (18.26 pg/mL versus 13.58 pg/mL, $P = 0.1975$) in N2a/WT or N2a/APP cells (Figure 2(d)). The ratio of Aβ_{1-42}/Aβ_{1-40} in the lysates of N2a/APP cells was 3 times higher than that of N2a/WT cells (9.05 versus 2.41, $P = 0.0026$), and a comparable reduction was observed in the ratio of Aβ_{1-42}/Aβ_{1-40} in N2a/APP cells treated with 20 μM DAU lysates compared with the lysates from cells treated with vehicle (3.54 versus 9.05, $P = 0.0099$) (Figure 2(e)). A diagram of the ratio of Aβ_{1-42}/Aβ_{1-40} (Figure 2(f)) shows a similar trend, but there was no difference between the groups.

The effect of DAU on APP processing was investigated further by Western blot analysis. N2a/APP cells had a significantly higher level of phosphorylated (amyloid precursor protein) APP and presenilin 1 (PS1) than N2a/WT cells (Figures 2(g) and 2(h)). The mean levels of β-secretase (BACE1) and insoluble β-secretase-cleaved amyloid precursor protein (sAPPβ) were also higher in N2a/APP cells compared to N2a/WT cells. DAU-treated N2a/APP cells significantly decreased the expression of total APP, phosphorylated APP, and BACE1. DAU-treated N2a/APP cells also showed reduced mean levels of sAPPβ and PS1, while the mean level of α-secretase-cleaved amyloid precursor protein (sAPPα) was higher. DAU-induced changes in APP processing appeared to correlate with changes in Aβ levels assayed by ELISA.

3.3. DAU Attenuated Tau Pathology via PP2A and p35/25 in Both N2a/APP Cells and HEK293/Tau Cells. We next used Western blot analysis to investigate the effect of DAU on the tau pathology of N2a/APP cells. Vehicle-treated N2a/APP cells had significantly increased tau phosphorylation at serine 396 than N2a/WT cells (Figures 3(a) and 3(b)).

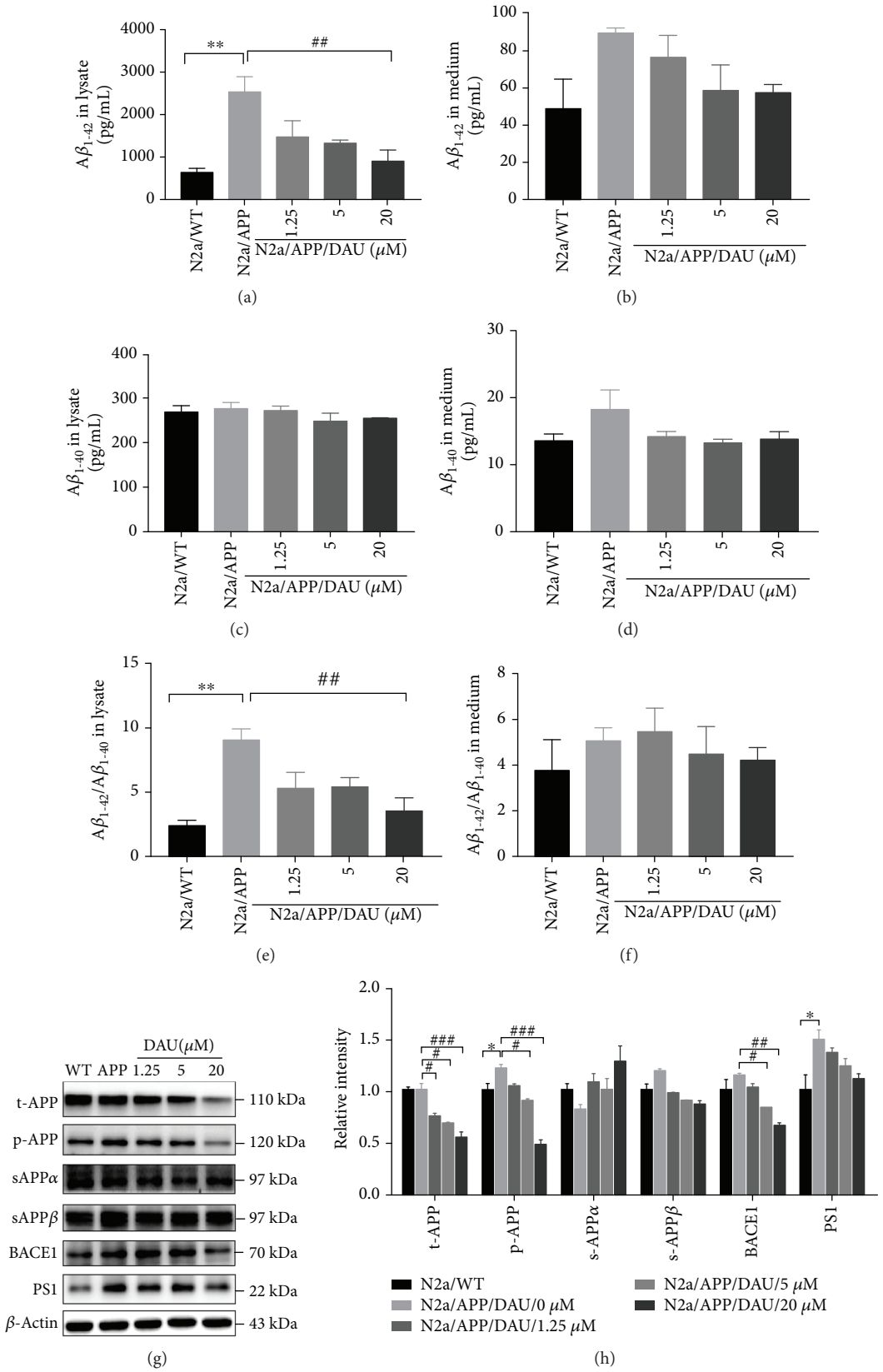

FIGURE 2: DAU inhibited APP processing and Aβ accumulation. Levels of $A\beta_{1-42}$ (a, b), $A\beta_{1-40}$ (c, d), and $A\beta_{1-42}/A\beta_{1-40}$ (e, f) of cell lysates (a, c, e) and cell culture media (b, d, f) as a function of DAU concentration were determined by ELISA. Levels of t-APP, p-APP, s-APPα, s-APPβ, BACE1, and PS1 were determined by Western blot analysis (g, h). β-Actin was used as a loading control. $N = 3$. Data show the mean ± SEM. $^{*}P < 0.05$ and $^{**}P < 0.01$ compared to N2a/WT cells. $^{\#}P < 0.05$, $^{\#\#}P < 0.01$, and $^{\#\#\#}P < 0.001$ compared to untreated N2a/APP cells.

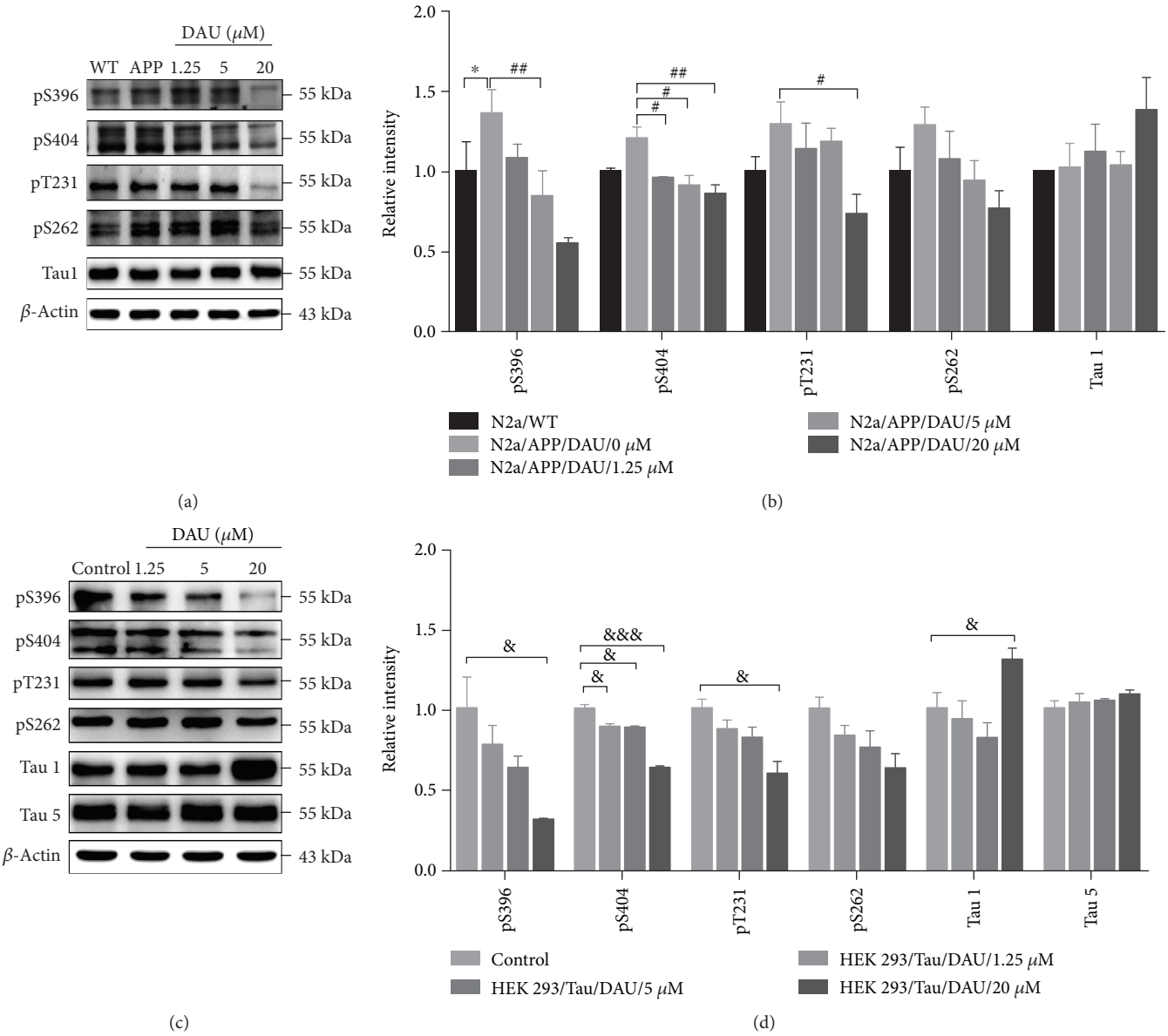

Figure 3: DAU attenuated tau phosphorylation in both N2a/APP cells and HEK293/Tau cells. Levels of phosphorylated tau and total tau in N2a/WT and N2a/APP cells (a, b) and in HEK293/Tau cells (c, d) as determined by Western blot analysis. β-Actin was used as a loading control. $N = 3$. Data show the mean ± SEM. $^{*}P < 0.05$ compared to N2a/WT cells, $^{\#}P < 0.05$ and $^{\#\#}P < 0.01$ compared to untreated N2a/APP cells, and $^{\&}P < 0.05$ and $^{\&\&\&}P < 0.001$ compared to untreated HEK293/Tau cells.

The mean levels of phosphorylated tau at serine 404, serine 262, and threonine 231 sites were higher in N2a/APP cells compared to N2a/WT cells, while the mean level of dephosphorylated tau (Tau-1) was lower in N2a/APP cells compared to tau phosphorylation at serine 396, serine 404, and threonine 231 sites. The levels of phosphorylated tau at serine 404, serine 396, and threonine 231 were significantly reduced in DAU-treated N2a/APP cells compared with the vehicle-treated N2a/APP cells. The mean levels of phosphorylated tau at serine 262 were reduced in DAU-treated N2a/APP cells compared with the vehicle-treated N2a/APP cells, while mean levels of Tau-1 were increased in DAU-treated N2a/APP cells versus vehicle-treated N2a/APP cells. To verify the results from N2a/WT and N2a/APP cells, we examined the effects of DAU treatment on the phosphorylation of tau on HEK293/Tau cells that overexpresses tau. As shown in Figures 3(c) and 3(d), we observed similar reductions of tau phosphorylation (serine 396, serine 404, and threonine 231) and similar enhancement of the level of Tau-1. DAU did not alter the expression of total tau protein.

While phosphorylation of tau can arise from the action of many catalyzing kinases and phosphatases [12], we investigated DAU-induced changes in those pathways shown to be key to tau phosphorylation, namely, glycogen synthase kinase-3β (GSK-3β), protein phosphatase2A (PP2A), and the p35/25 pathways. DAU treatment lowered the mean phosphorylation levels of glycogen synthase kinase-3α

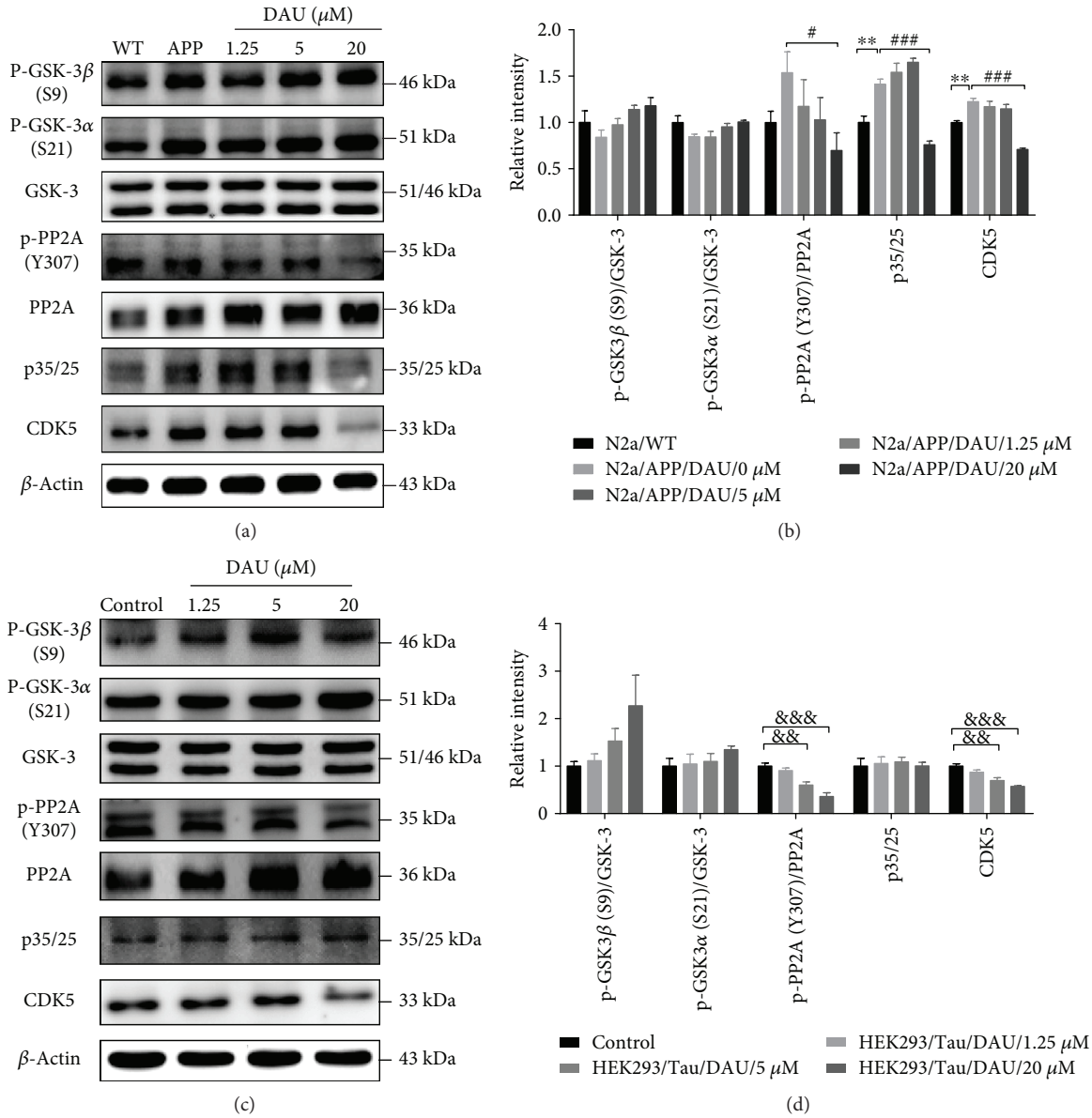

Figure 4: DAU ameliorated tau pathology via PP2A and p35/25 in both N2a/APP cells and HEK293/Tau cells. Phosphorylation of GSK3 and PP2A and levels of p35/25 and CDK5 in N2a/APP cells (a, b) and HEK293/Tau cells (c, d) as determined by Western blot analysis. β-Actin was used as a loading control. $N = 3$. Data show the mean ± SEM. $^{**}P < 0.01$ compared to N2a/WT cells, $^{\#}P < 0.05$ and $^{\#\#\#}P < 0.001$ compared to untreated N2a/APP cells, and $^{\&\&}P < 0.01$ and $^{\&\&\&}P < 0.001$ compared to untreated HEK293/Tau cells.

(GSK-3α) and GSK-3β in N2a/APP cells more than in N2a/WT cells (Figures 4(a) & 4(b)). The mean phosphorylation state of PP2A and the levels of p35/25 and cyclin-dependent kinase 5 (CDK5) were enhanced in N2a/APP cells compared with N2a/WT cells. DAU treatment enhanced the mean levels of both GSK-3α and β in N2a/APP cells compared with vehicle-treated N2a/APP cells. More importantly, 20 μM DAU significantly decreased the phosphorylation of PP2A and levels of p35/25 and CDK5 in N2a/APP cells compared with vehicle-treated N2a/APP cells. As a supplemental validation, the phosphorylation of PP2A and levels of p35/25 and CDK5 in HEK293/Tau cells were similarly modulated by DAU treatment. Thus, DAU may ameliorate tau pathology via PP2A, p35/25, and CDK5, rather than GSK-3β.

3.4. DAU Modified Proteins That Involve Oxidative Stress, Mitochondrial Function, and ER Stress of N2a/APP Cells. To explore molecular species affected by DAU treatment, we performed a comparative proteomic analysis using 2D-DIGE separation and MS identification. A total of 85 proteins in 2D-DIGE gels was significantly different in any four comparison pairs (N2a/APP versus N2a/WT, 1.25 μM DAU versus N2a/APP, 5 μM DAU versus N2a/APP, or 20 μM DAU versus N2a/APP) (shown in Figure 5). Six protein categories were impacted by DAU treatment: endoplasmic reticulum (ER) stress-associated proteins, oxidative stress-associated proteins, cytoskeleton-associated proteins, molecular chaperones, mitochondrial respiration, and metabolism signaling proteins. In addition, we found some common

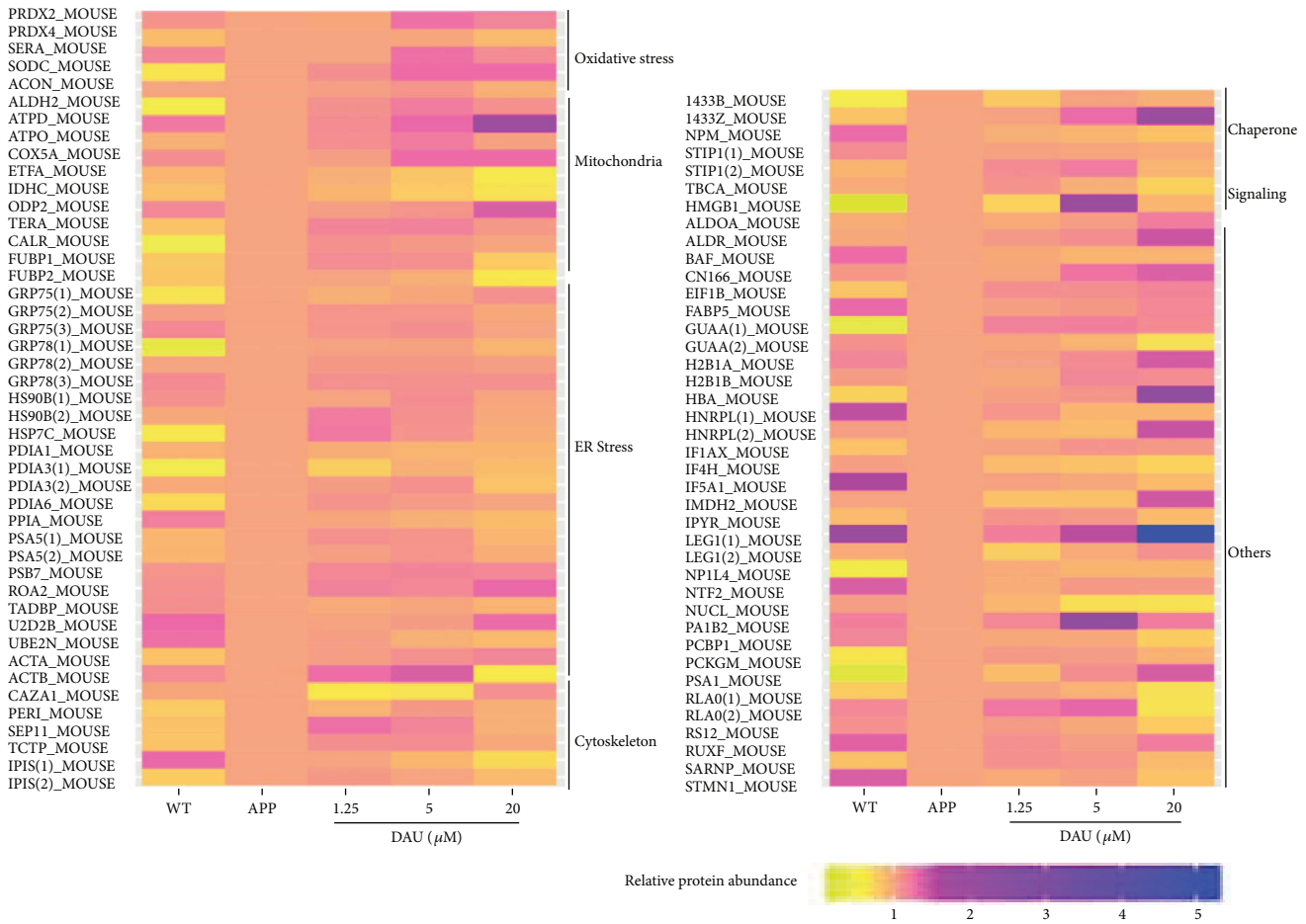

Figure 5: DAU caused differential expression of proteins in N2a/APP cells. DAU caused differential expression of 49 proteins including oxidative stress-associated proteins, endoplasmic reticulum (ER) stress-associated proteins, metabolism-associated proteins, cytoskeleton-associated proteins, molecular chaperones-associated proteins, signaling-associated proteins, and others. Protein expression was significantly altered in any four comparison pairs (N2a/APP versus N2a/WT, 1.25 μM DAU versus N2a/APP, 5 μM DAU versus N2a/APP, or 20 μM DAU versus N2a/APP).

proteins that were differentially expressed among the four comparison groups (Figure S1A and Tables S1–4). These differential proteins included signaling protein high-mobility group protein B1 (HMGB1) a mediator of neurite degeneration through the identification of the pathological signaling pathway in AD [13]; molecular chaperones (heat shock cognate 71 kDa protein (HSP7C)), a molecular chaperone and a member of the heat shock protein family that plays an integral role in the stress response [14]; translationally controlled tumor protein (TCTP), which has critical roles in the defense against oxidative and thermal stresses [15] (shown in Table S1); endoplasmic reticulum (ER) stress-associated protein (protein disulfide-isomerase A6 (PDIA6)), a protein related to ER stress that plays a critical role in most biological processes [16]; oxidative stress-associated protein (D-3-phosphoglycerate dehydrogenase (SERA)), a protein involved in the metabolism and development of the central nervous system [17]; cytoskeleton-associated protein (peripherin (PERI)), a type III intermediate filament (IF) protein that plays a contributory role in motor neuron disease [18, 19]; molecular chaperone (stress-induced-phosphoprotein 1 (STIP1)), a cochaperone intermediating Hsp70/Hsp90 exchange of client proteins and involved in prion protein-mediated neuronal signaling [20] (shown in Table S2); and cytoskeleton-associated protein (TPIS) (shown in Table S3). We found that two proteins, namely, isocitrate dehydrogenase [NADP] cytoplasmic (IDHC), which plays important roles in energy and biosynthesis metabolisms [21], and eukaryotic translation initiation factor 1b (EIF1B), an antiapoptotic protein that protects cells uniquely from Fas-induced apoptosis [22], were commonly changed in various concentrations of DAU-treated N2a/APP cells compared with the vehicle-treated N2a/APP cells (shown in Figure S1B and Table S8). In addition, some common proteins were differentially expressed among the three DAU-treated groups (shown in Figure S1B and Tables S5–6); these included ER stress-associated protein (Far upstream element-binding protein 1 (FUBP1)), a multifunctional DNA- and RNA-binding protein [23]; mitochondrial respiration and metabolism (IDHC) (cytochrome oxidase subunit 5A, mitochondrial (COX5A)), an electron transport chain- (ETC-) related protein (shown in Table S5); ER stress-associated proteins (78 kDa glucose-regulated protein (GRP78), stress-70 protein, and mitochondrial protein (GRP75)); molecular chaperones (heat shock

protein HSP 90-beta (HSP90B)), essential molecular chaperone involved in signal transduction, cell cycle control, stress management, and folding, degradation, and transport of proteins [24]; nucleophosmin (NMP), which has a key role activating autophagy induced by nucleolar disruption [25], mitochondrial respiration, and metabolism (IDHC) (shown in Table S6); ER stress-associated protein (protein disulfide-isomerase A3 (PDIA3)), which is mainly involved in the regulation of ER stress (ERS) and protects neurons from ERS-induced apoptosis [26]; and mitochondrial respiration and metabolism (IDHC) (shown in Table S7).

The differentially expressed proteins in DAU-treated N2a/APP cells versus vehicle-treated N2a/APP cells were analyzed and characterized using DAVID. In the vehicle-treated N2a/APP cells, DAVID-defined biological functions for the major clusters of differentially expressed proteins were "protein folding," "positive regulation of catalytic activity," and "cell redox homeostasis" (Figure 6(a)), and DAVID-defined protein functions included "poly(A) RNA binding," "ATP binding," and "enzyme binding" (Figure 6(b)). DAVID identified DAU-affected cellular compartments as "smooth ER," "cell-cell adherent junction," and "ER lumen" (Figure 6(c)). In contrast, DAVID results from the DAU-treated N2a/APP cells were different: the major clusters of differentially expressed proteins were "response to ER stress," "ATP metabolic process," and "protein folding," when categorized according to biological processes of proteins (Figure 6(d)); "poly(A) RNA binding," "RNA binding," and "unfolded protein binding," when categorized according to the molecular function of proteins (Figure 6(e)); and "extracellular exosome," "melanosome," and "mitochondria," when categorized according to cellular component of the proteins (Figure 6(f)).

To supplement and verify the results of proteomic profiling, we used Western blot analysis to investigate the expression of peroxiredoxin-4 (PRDX4, a member of peroxiredoxin family that regulates redox status of ER) (Figure 7(b), Figure S5A, B, and C); disulfide-isomerase (PDIA1, a member of the PDI family that regulates redox status of ER) (Figure 7(c), Figure S4A, B, and C); GRP75, a mitochondrial chaperone that regulates the mitochondria-associated ER membrane (Figure 7(d), Figure S3A, B, and C); 78 kDa glucose-regulated protein (GRP78, a chaperone binds to ER stress sensor) (Figure 7(e), Figure S2A, B, C, and D); HMGB1 (Figure 8(a), Figure S6A, B, and C), a mediator of neurite degeneration through the identification of the pathological signaling pathway in AD; and 14-3-3 protein zeta/delta (14-3-3-z, a chaperone that involves mitochondrial respiration) (Figure 8(b), Figure S7A, B, and C). The mean level of PRDX4 in N2a/APP cells was significantly higher than that in N2a/WT cells, and the mean level of PRDX4 was reduced in DAU-treated N2a/APP cells. The mean level of PDIA1 in N2a/APP cells was markedly higher than that in N2a/WT cells and reduced in DAU-treated N2a/APP cells. Similar trends were observed for GRP75, GRP78, and HMGB1. The opposite trend was observed for 14-3-3-z.

3.5. DAU Reduced Oxidative Stress and ER Stress of N2a/APP Cells. Given the modulation of oxidative stress and ER stress-related proteins by DAU, we investigated the effects of DAU on reactive oxygen species (ROS) and the unfolded protein response (UPR). Shown in Figure 7(a), the staining of 8-oxo-2′-deoxyguanosine (8-OHdG), an indicator of reactive oxygen species (ROS), was significantly higher in N2a/APP cells than in N2a/WT cells. N2a/APP cells treated with DAU at all three concentrations showed significant reductions in 8-OHdG staining compared with that in vehicle-treated N2a/APP cells. We also investigated the protein expressions of most implicated UPR markers, such as GRP75 (Figure 7(d)), GRP78 (Figure 7(e)), phosphorylated pancreatic ER eIF2α kinase (p-PERK) (Figure 7(f)), phosphorylated eukaryotic initiation factor-2 alpha (p-eIF2-α), eukaryotic translation initiation factor 2 subunits (eIF2α) (Figure 7(g)), activating transcription factor-4 (ATF-4) (Figure 7(h)), and transcriptional factor C/EBP homologous protein (CHOP) (Figure 7(i)). The phosphorylation of PERK and eIF2α was significantly higher in N2a/APP cells compared with N2a/WT cells, and these phosphorylated proteins were markedly reduced in DAU-treated N2a/APP cells compared with vehicle-treated N2a/APP cells. In addition, the mean levels of GRP75, GRP78, ATF-4, and CHOP were higher in N2a/APP cells compared with N2a/WT cells, and the mean levels of these proteins were reduced in DAU-treated N2a/APP cells compared with vehicle-treated N2a/APP cells.

4. Discussion

Dysregulation of neuronal calcium homeostasis plays a crucial role in the progression of AD and therefore is a potential therapeutic target for the treatment of this disease [27]. DAU has been reported to inhibit cellular influx of extracellular Ca^{2+} and restrict the endoplasmic release of Ca^{2+} in various models [28, 29]. Disturbed calcium signaling could lead to ER stress and activate the UPR [30]. Experiments showing DAU's ability to modulate calcium homeostasis have been performed to support the claim that DAU promotes neuronal cell survival [6] and corrects Ca^{2+}-mediated arrhythmia in muscle cells [31]. In the present study, DAU suppressed APP processing and Aβ production in a cell model of AD. DAU attenuated tau pathology in N2a/APP cells via the PP2A and p35/25 pathways; this is consistent with a previous report of the effects of DAU on bradykinin-treated N2a cells, which showed that DAU prevents bradykinin-induced alteration of calcium homeostasis and tau hyperphosphorylation in N2a cells [7]. DAU also significantly altered the expression of 85 proteins relevant to oxidative stress, mitochondrial function and metabolism, UPR, and the cytoskeleton.

4.1. Oxidative Stress. Oxidative stress-related proteins represent one class of proteins altered by DAU treatment. Oxidative stress is a consequence of calcium influx mediated by *N*-methyl-D-aspartate receptors in AD pathology [32, 33]. Our proteomic profiling showed that some oxidative stress-related proteins were perturbed in N2a/APP cells versus N2a/WT cells. Although protein perturbation does not necessarily link with functional loss of protein, we found that DAU-treated N2a/APP cells retained the

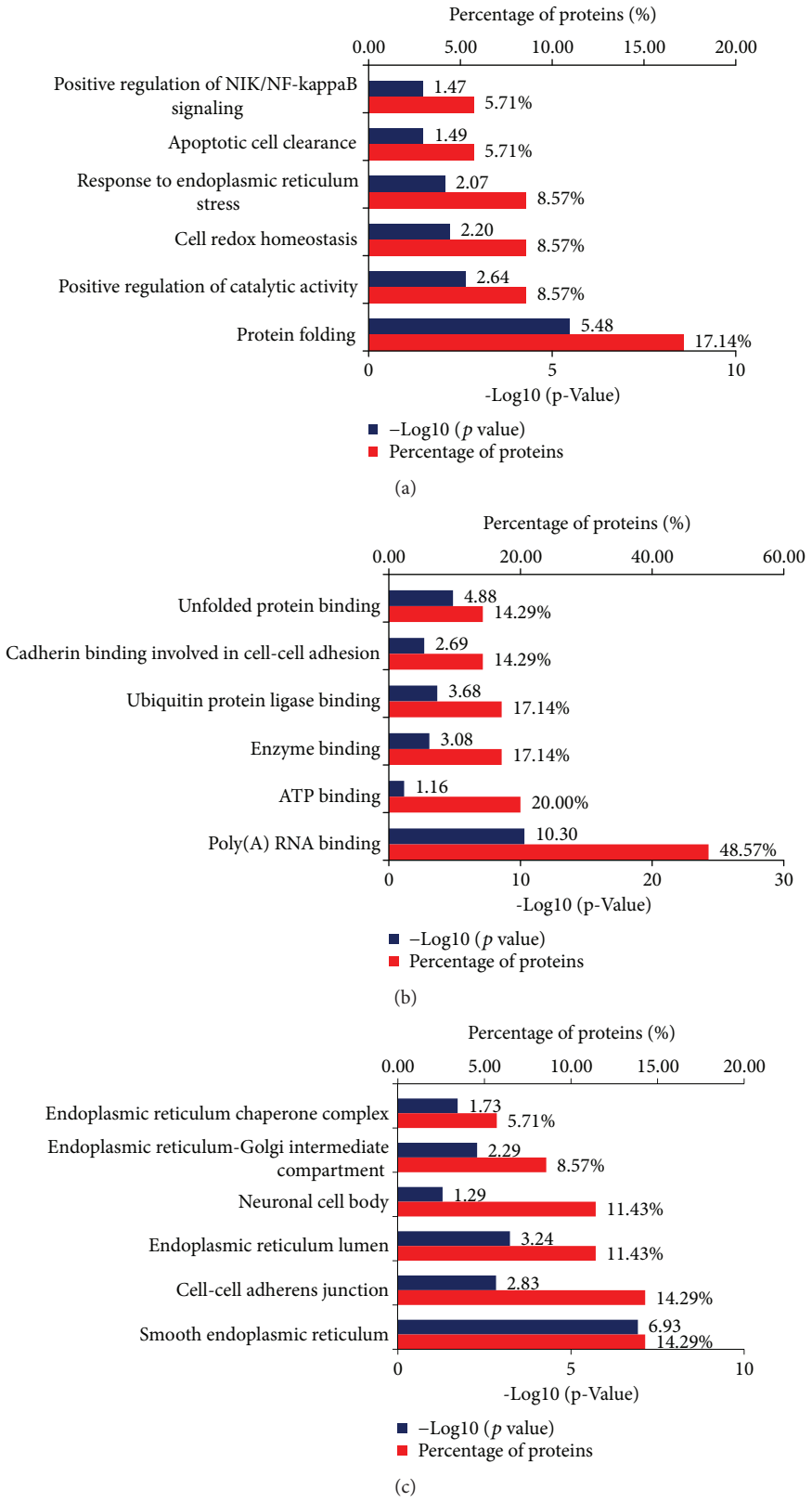

Figure 6: Continued.

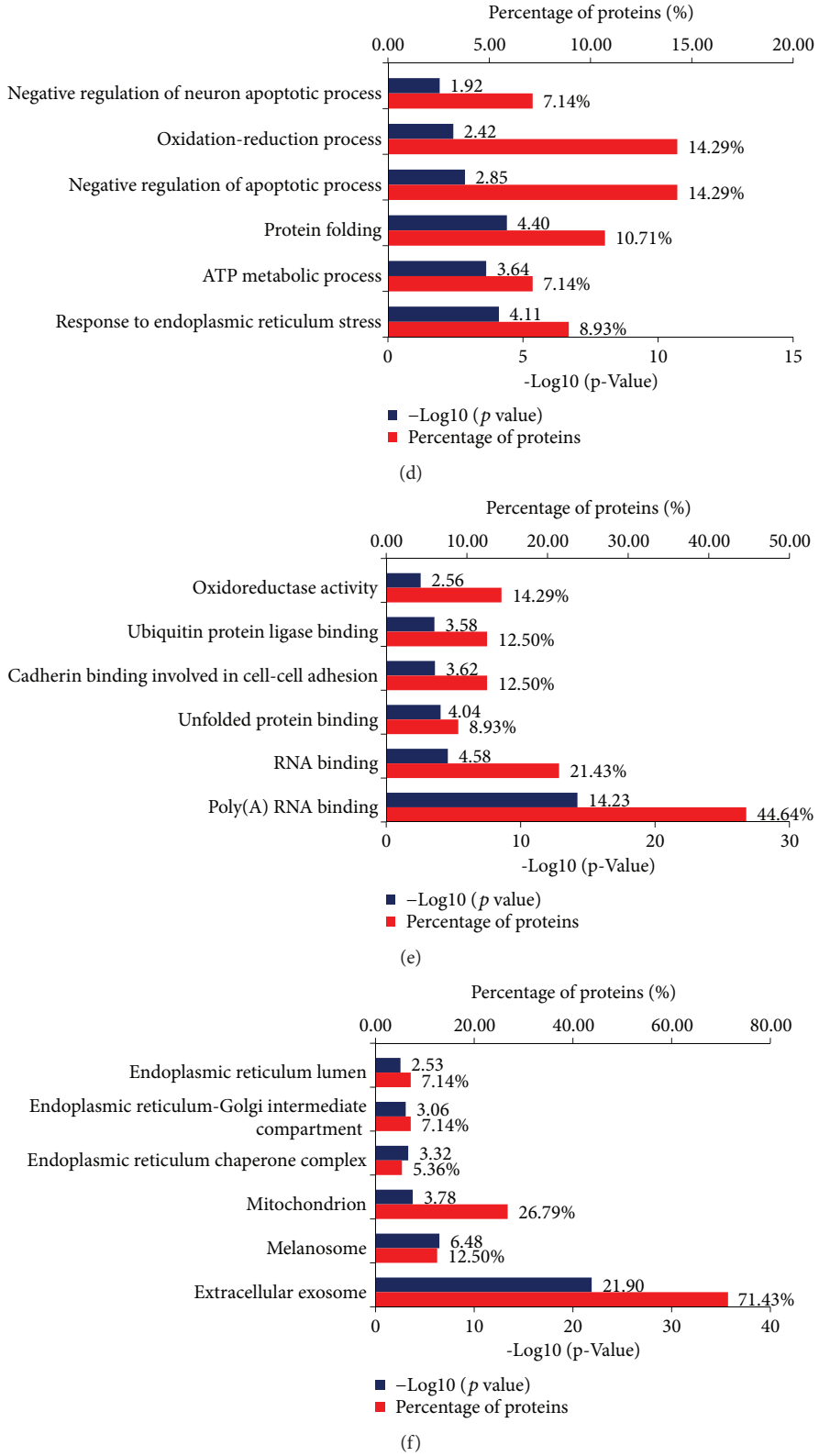

Figure 6: DAVID Gene Ontology enrichment analysis for the dysregulated proteins in N2a/APP cells and DAU-treated N2a/APP cells. (a) Enrichment analysis for the differential proteins by biological process, (b) enrichment analysis for the differential proteins by molecular function, and (c) the cellular component enrichment in Gene Ontology terms of the differentially expressed proteins in N2a/APP cells (when compared with N2a/WT cells). (d) The biological processes, (e) the molecular function, and (f) the cellular component enrichment of the differentially expressed proteins in DAU-treated N2a/APP cells (when compared with untreated N2a/APP cells).

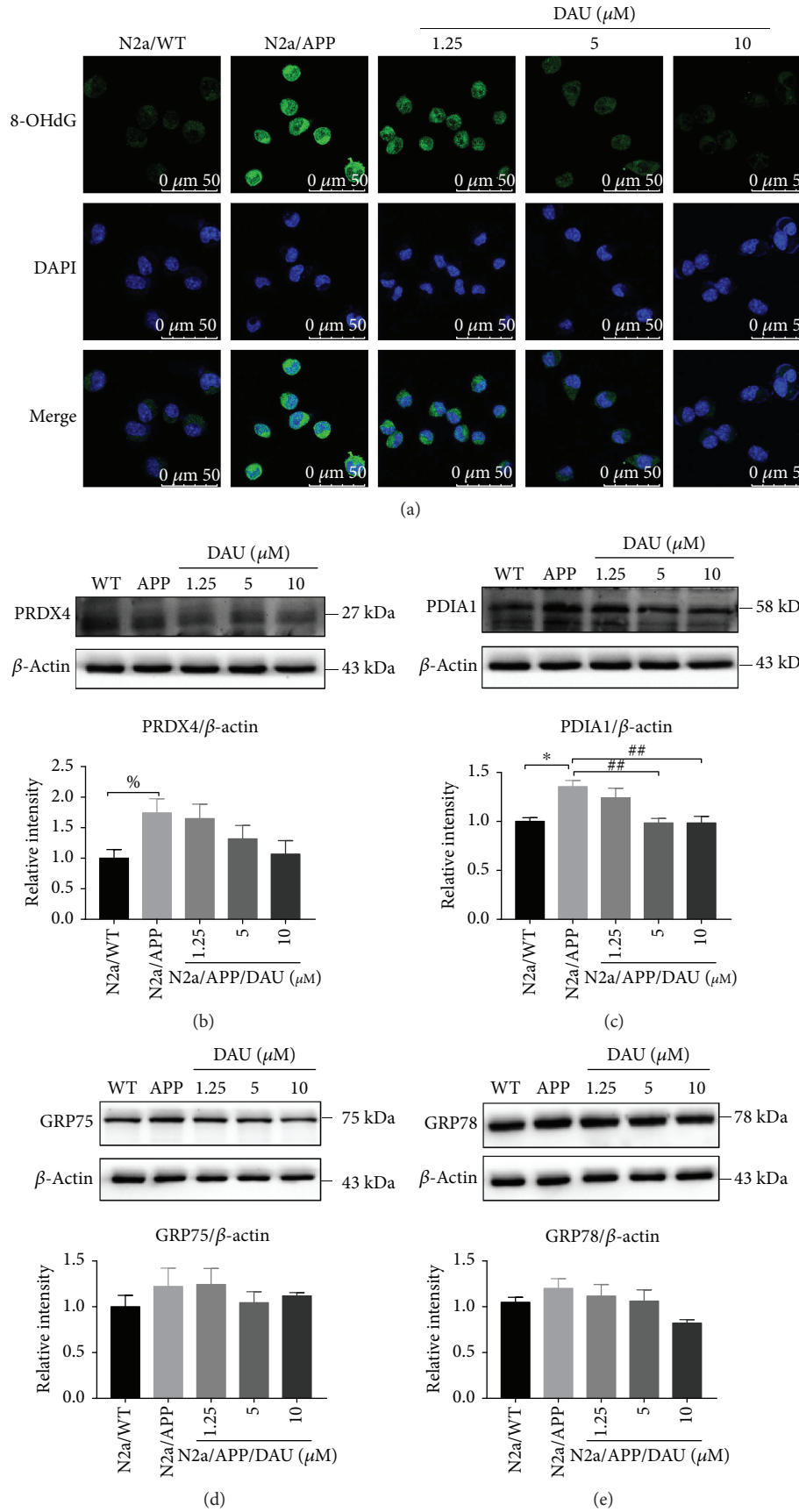

Figure 7: Continued.

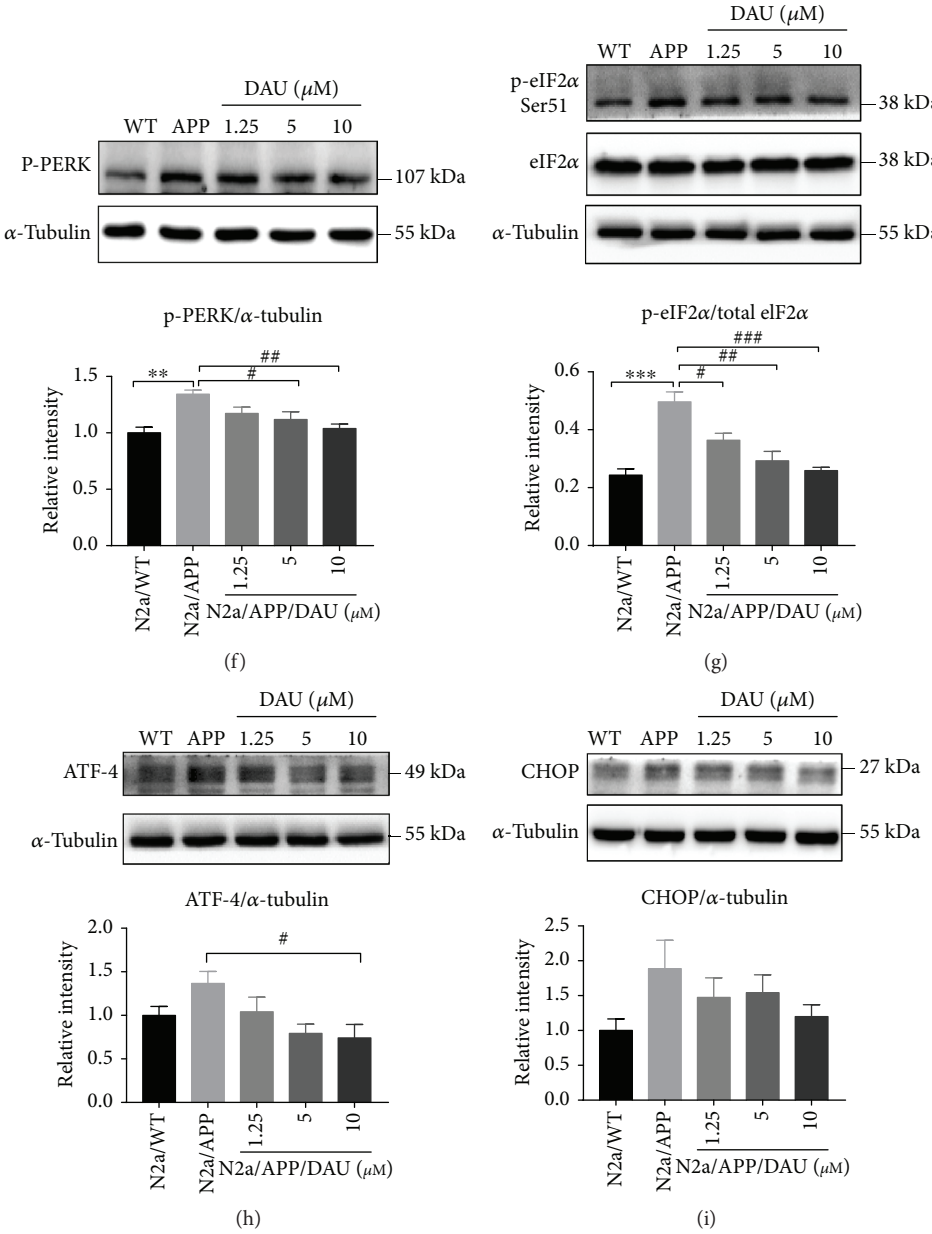

Figure 7: DAU reduced oxidative stress and ER stress of N2a/APP cells. (a) 8-OHdG (in green) immunostaining of N2a/WT and N2a/APP cells. DAPI (in blue) stained the cell nuclei. Proteins PRDX4 (b), PDIA1 (c), GRP75 (d), GRP78 (e), p-PERK (f), p-eIF2α, eIF2α (g), ATF-4 (h), and CHOP (i) in N2a/WT and N2a/APP cells were determined by Western blot analyses. β-Actin was used as a loading control for PRDX4, GRP78, GRP75, and PDIA1. α-Tubulin was used as a loading control for ATF-4, CHOP, and p-PERK. Total eIF2α was used as a loading control for p-eIF2α. $N = 3$. Data show the mean ± SEM. $^{\%}P = 0.0052$, $^{*}P < 0.05$, $^{**}P < 0.01$, and $^{***}P < 0.001$ compared to N2a/WT cells. $^{\#}P < 0.05$, $^{\#\#}P < 0.01$, and $^{\#\#\#}P < 0.001$ compared to untreated N2a/APP.

expression of peroxiredoxin-2 (PRDX2), PRDX4, and SERA seen in N2a/WT cells (Figure 5). In addition, we observed the level of 8-OHdG was suppressed in the three groups of DAU-treated cells, and the level of 8-OHdG in 5 μM DAU-treated cells was the same as that in N2a/WT cells (shown in Figure 7(a)). This implies that DAU suppressed oxidative stress, which is consistent with previous reports of the antioxidative activities of DAU [34]. The antioxidative effects of DAU could also result from its inhibition of Ca^{2+} influx [7].

4.2. Mitochondrial Proteins. Mitochondrial dysfunction is closely linked with oxidative stress in pathological aging and AD [35], and mitochondrial proteins formed another cluster of proteins modified by DAU treatment. In this study, we observed suppression of ATP synthase subunit delta, mitochondrial (ATPD), COX5A, and dihydrolipoyllysine-residue acetyltransferase component of p (ODP2) and enhancement of aldehyde dehydrogenase, mitochondrial (ALDH2), ATP synthase subunit O, mitochondrial (ATPO), electron transfer flavoprotein subunit alpha, mitochondrial

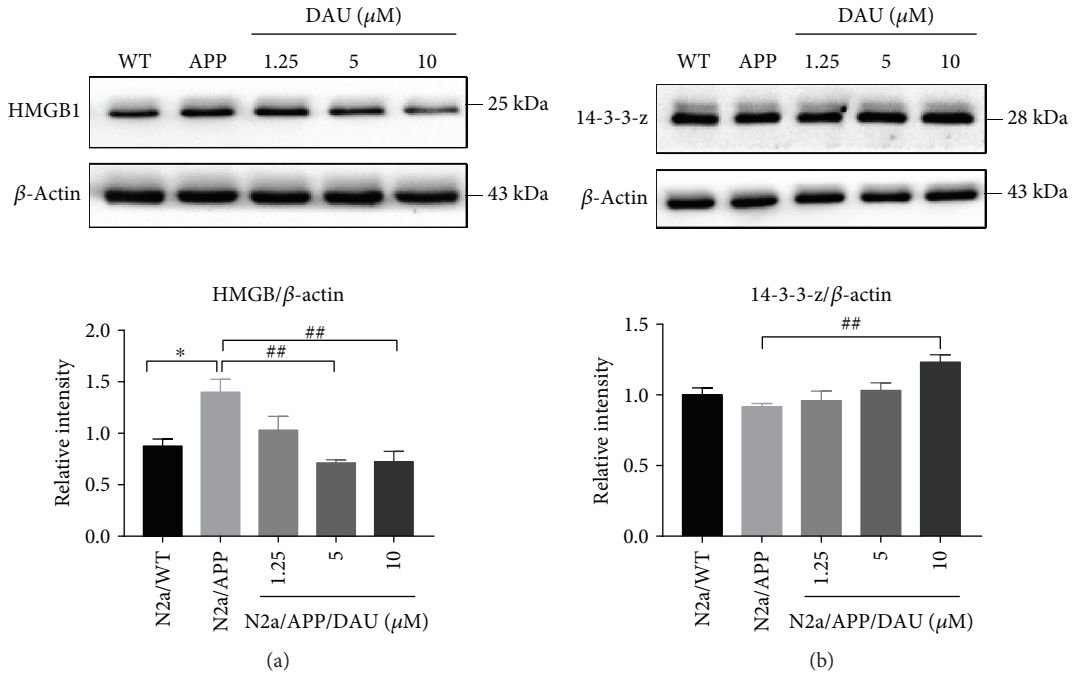

Figure 8: DAU altered the expression of HMGB1 and 14-3-3-z. HMGB1 (a) and 14-3-3-z (b). $N = 3$. Data show the mean ± SEM. $^{*}P < 0.05$ compared to N2a/WT cells and $^{\#\#}P < 0.01$ compared with untreated N2a/APP cells.

(ETFA), IDHC, and transitional endoplasmic reticulum ATPase (TERA) in N2a/APP cells, while protein expression of ACON, ATPD, COX5A, ETFA, IDHC, and ODP2 was retained in DAU-treated cells. This observation may correlate with the report that DAU enhanced the activity of mitochondrial ATPase in a mouse model of cerebral ischemia [36]; however, more functional assays, such as levels of ATP and activities of mitochondrial ATPase, should be included in a future study to validate this correlation. The effect of DAU on mitochondrial function may be related to the modulation of calcium homeostasis by this isoquinoline alkaloid.

4.3. Unfolded Protein Response. The unfolded protein response (UPR), an ER stress response to a disturbance in protein folding, is implicated in neurodegenerative diseases [37], including the possibility that accumulation of tau initiates the UPR [37]. UPR-related proteins formed the largest category of proteins modulated by DAU treatment. In the proteomics study, we found that calreticulin (CALR) and Ca^{2+}/calmodulin-dependent protein phosphatase had a higher expression in DAU-treated N2a/APP cells versus vehicle-treated N2a/APP cells, suggesting calcium hemostasis was modulated by DAU. In the functional study, we found ER stress markers (Figure 7) were enhanced in N2a/APP cells and suppressed in DAU-treated cells. Calcium homeostasis is also crucial for the function of both ER and mitochondria for the following reasons: (1) Ca^{2+} is predominantly stored in the ER and influx of Ca^{2+} from ER to the mitochondria can be triggered by ER stress [38], and (2) calcium depletion in ER is thought to initiate chronic Ca^{2+} overload in the mitochondria and Bcl-2 dependent apoptosis [39] that DAU suppresses ER stress could be linked to DAU modulation of calcium homeostasis.

Although we categorized the DAU-modulated proteins into oxidative stress, ER stress, and mitochondrial dysfunction, intensive studies reveal these processes are closely related. The oxidative environment in the ER is maintained by the formation of disulfide bonds and the concentration of glutathione, both of which are regulated by the PDI and peroxiredoxin families [40, 41]. Imbalance of redox status or oxidative stress results in ER stress and activates the UPR [30]. During UPR, three classes of ER stress sensors (namely, ATF6, PERK, and IRE1), as well as sensor-bound chaperones (i.e., GRP78), are activated [42–44]. UPR also induces ER stress response genes [44] and proapoptotic transcription factors like CHOP [43]. In the case of AD, the accumulation of Aβ and hyperphosphorylation of tau increase the production of ROS, which results in progressive mitochondrial damage and ER stress via a disturbance of Ca^{2+} homeostasis [45, 46]. Although we did not monitor the Ca^{2+} flow in N2a/APP cells, we investigated the levels of most of the aforementioned proteins, the results of which implied that Ca^{2+} homeostasis may be disturbed in N2a/APP cells. More detailed studies are required to illuminate the mechanisms by which DAU ameliorates mitochondrial dysfunction, ER stress, and oxidative stress by modulating calcium homeostasis. DAU treatment also modified proteins in other categories, including cytoskeleton, molecular chaperone, and signaling proteins. Further investigations on the functions of these proteins might illuminate the novel pharmacological actions of DAU.

4.4. Toxicity. The potential toxicity of DAU needs to be addressed. Some toxicological studies of DAU have claimed the isoquinoline alkaloid is biotransformed to a quinone methide intermediate by CYP3A family proteins, and

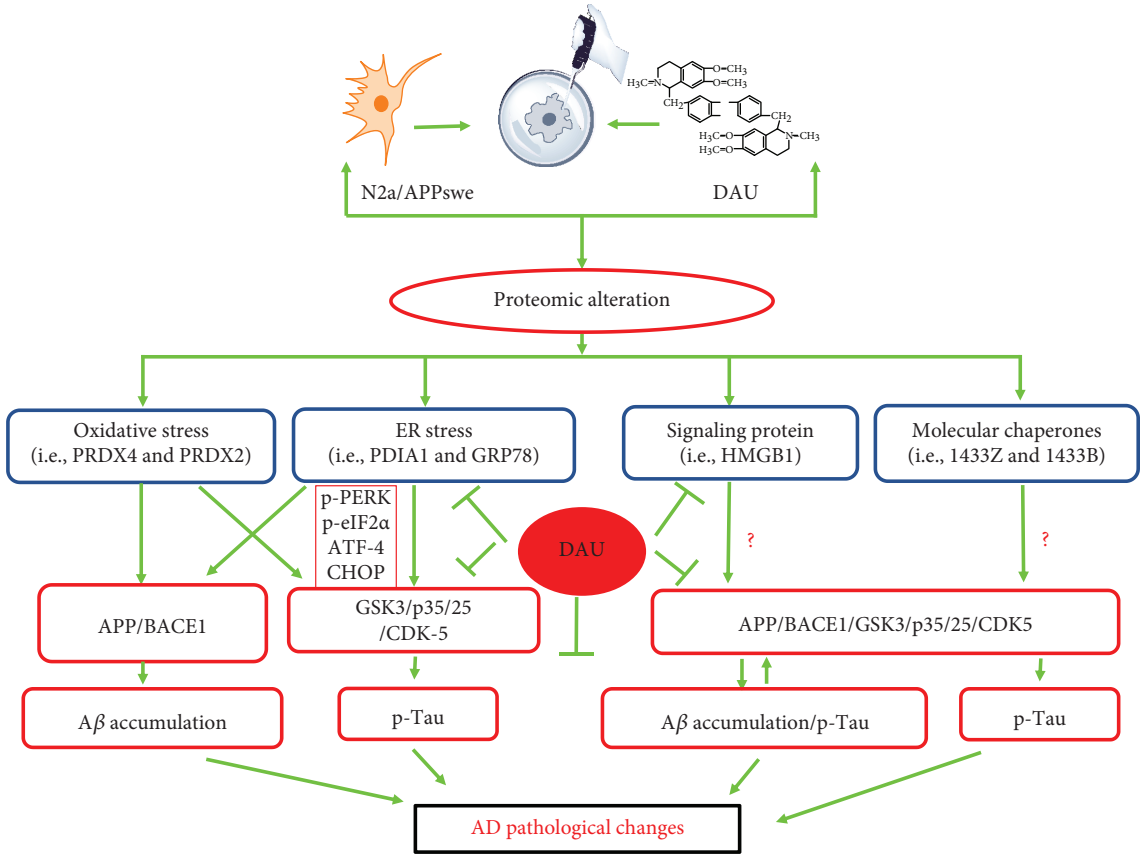

Figure 9: The mode of action of DAU. DAU treatment suppressed AD-related changes, notably Aβ accumulation and tau phosphorylation via APP processing and the CDK5, PP2A, and p35/25 pathways, which may be attributed to the modification of proteins related to functions of oxidative stress, ER stress, molecular chaperones, and signaling protein.

accumulation of the intermediate could then deplete glutathione (GSH) and induce cell apoptosis [47, 48]. Besides, some of the 1,2,3,4-tetrahydroisoquinolines are claimed to be moderate inhibitors of complex I activity and mitochondrial respiration [49]. However, N2a/APP cells could tolerate more than 20 μM DAU without significant loss of cell viability (Figure 1(c)), and N2a/APP cells seem to tolerate higher concentrations of DAU than N2a/WT cells (we observed significant viability loss in N2a/WT cells treated with >10 μM of DAU) (Figure 1(b)). Further investigation into the expression of CYP family proteins in N2a/APP cells is necessary to understand the apparent DAU tolerance of N2a/APP cells. More important, however, is that DAU was protective when N2a/APP cells were treated with concentrations as low as 1.25 μM and, at this concentration, the toxic potential of DAU might be marginal. In a future preclinical study of DAU, dosage should be chosen cautiously to avoid adverse events, including changes in GSH and mitochondrial complex 1 status.

In conclusion, we found DAU treatment attenuated hyperphosphorylation of tau and production of Aβ in N2a/APP cells. DAU also reduced molecular deficits in N2a/APP cells, such as those relating to oxidative stress, ER stress, signaling proteins, and molecular chaperones (summarized in Figure 9). Although N2a/APP cells tolerated higher concentrations of DAU, we recommend focus on the lowest effective concentrations and doses of DAU to avoid adverse events in cell culture and animal studies, respectively.

Abbreviations

AD:	Alzheimer's disease
DAU:	Dauricine
2D-DIGE:	Two-dimensional fluorescence difference gel electrophoresis
APP:	Amyloid precursor protein
sAPPβ:	β-Secretase-cleaved amyloid precursor protein
sAPPα:	α-Secretase-cleaved amyloid precursor protein
BACE1:	β-Site APP cleaving enzyme 1
GSK-3α:	Glycogen synthase kinase-3α
GSK-3β:	Glycogen synthase kinase-3β
CDK5:	Cyclin-dependent kinase 5
N2a/WT:	Wild-type murine neuroblastoma
N2a/APP:	Murine neuroblastoma N2a cells stably transfected with Swedish mutant of amyloid precursor protein
PP2A:	Protein phosphatase2A
HEK293/Tau:	Human embryonic kidney 293 cells stably transfected with tau protein
ER stress:	Endoplasmic reticulum stress

$A\beta_{1-42}$: Amyloid-β 1–42
$A\beta_{1-40}$: Amyloid-β 1–40
GO: Gene ontology
BP: Biological processes
MF: Molecular functions
CC: Cellular components
PS1: Presenilin 1
HMGB1: High-mobility group protein B1
HSP7C: Heat shock cognate 71 kDa protein
TCTP: Translationally controlled tumor protein
PDIA6: Protein disulfide-isomerase A6
SERA: D-3-Phosphoglycerate dehydrogenase
PERI: Peripherin
STIP1: Stress-induced phosphoprotein 1
IDHC: Isocitrate dehydrogenase [NADP] cytoplasmic
EIF1B: Eukaryotic translation initiation factor 1b
FUBP1: Far upstream element-binding protein 1
COX5A: Cytochrome c oxidase subunit 5A, mitochondrial
GRP78: 78 kDa glucose-regulated protein
GRP75: Stress-70 protein, mitochondrial protein
HSP90B: Heat shock protein HSP90-beta
NMP: Nucleophosmin
PDIA3: Protein disulfide-isomerase A3
PRDX4: Peroxiredoxin-4
PDIA1: Disulfide-isomerase
14-3-3-z: 14-3-3 protein zeta/delta
ROS: Reactive oxygen species
UPR: Unfolded protein response
8-OHdG: 8-Oxo-2′-deoxyguanosine
ATF-4: Activating transcription factor-4
CHOP: Transcriptional factor C/EBP homologous protein
p-eIF2α: Phosphorylated eukaryotic initiation factor-2 alpha
p-PERK: Pancreatic ER eIF2α kinase
UPR: Unfolded protein response
PRDX2: Peroxiredoxin-2
ATPD: ATP synthase subunit delta, mitochondrial
ODP2: Dihydrolipoyllysine-residue acetyltransferase component of p
ALDH2: Aldehyde dehydrogenase, mitochondrial
ATPO: ATP synthase subunit O, mitochondrial
ETFA: Electron transfer flavoprotein subunit alpha, mitochondrial
TERA: Transitional endoplasmic reticulum ATPase.

Conflicts of Interest

The authors declare that they have no conflict of interest to disclose.

Authors' Contributions

Pan Liu, Xiao Chen, and Haizhe Zhou contributed equally to this work.

Acknowledgments

This work was supported by National Natural Science Foundation of China (81673134, 81401570), Guangdong Provincial Natural Science Foundation (2014A030313715, 2016A030313051), Guangdong Provincial Scheme of Science and Technology (to Xifei Yang), Shenzhen Special Fund Project on Strategic Emerging Industry Development (JCYJ20160428143433768, JCYJ20150529164656093, JCYJ20150529153646078, JCYJ20160422143433757, and JCYJ20150529112551484), and Sanming Project of Medicine in Shenzhen (SZSM201611090).

Supplementary Materials

Figure S1: common proteins differentially expressed among the different comparison groups. Figure S2–S7: MALDI-TOF-MS map of GRP78 (Figure S2), GRP75 (Figure S3), PDIA1 (Figure S4), PRDX4 (Figure S5), HMGB1 (Figure S6), and 14-3-3-z (Figure S7). Table S1–S8: list of common proteins differentially expressed among the different comparison groups. *(Supplementary Materials)*

References

[1] C. Oboudiyat, H. Glazer, A. Seifan, C. Greer, and R. Isaacson, "Alzheimer's disease," *Seminars in Neurology*, vol. 33, no. 4, pp. 313–329, 2013.

[2] C. Ballard, S. Gauthier, A. Corbett, C. Brayne, D. Aarsland, and E. Jones, "Alzheimer's disease," *The Lancet*, vol. 377, no. 9770, pp. 1019–1031, 2011.

[3] L. S. Schneider, F. Mangialasche, N. Andreasen et al., "Clinical trials and late-stage drug development for Alzheimer's disease: an appraisal from 1984 to 2014," *Journal of Internal Medicine*, vol. 275, no. 3, pp. 251–283, 2014.

[4] E. J. M. Bierman, H. C. Comijs, C. Jonker, and A. T. F. Beekman, "Symptoms of anxiety and depression in the course of cognitive decline," *Dementia and Geriatric Cognitive Disorders*, vol. 24, no. 3, pp. 213–219, 2007.

[5] F.-Q. He, B.-Y. Qiu, X.-H. Zhang et al., "Tetrandrine attenuates spatial memory impairment and hippocampal neuroinflammation via inhibiting NF-κB activation in a rat model of Alzheimer's disease induced by amyloid-β(1–42)," *Brain Research*, vol. 1384, pp. 89–96, 2011.

[6] Y. H. Li and P. L. Gong, "Neuroprotective effect of dauricine in cortical neuron culture exposed to hypoxia and hypoglycemia: involvement of correcting perturbed calcium homeostasis," *Canadian Journal of Physiology and Pharmacology*, vol. 85, no. 6, pp. 621–627, 2007.

[7] L. Wang, X. Wang, H. Li, D. Wang, X. Zhou, and J. Wang, "Dauricine prevents bradykinin–induced alteration of calcium homeostasis and tau hyperphosphorylation in N2a cells," *Sheng Wu Hua Xue Yu Sheng Wu Wu Li Jin Zhan*, vol. 32, no. 7, pp. 612–617, 2005.

[8] Y. P. Wang, Z. F. Wang, Y. C. Zhang, Q. Tian, and J. Z. Wang, "Effect of amyloid peptides on serum withdrawal-induced cell differentiation and cell viability," *Cell Research*, vol. 14, no. 6, pp. 467–472, 2004.

[9] G. Thinakaran, D. B. Teplow, R. Siman, B. Greenberg, and S. S. Sisodia, "Metabolism of the "Swedish" amyloid precursor protein variant in neuro2a (N2a) cells. Evidence that cleavage

at the "beta-secretase" site occurs in the golgi apparatus," *Journal of Biological Chemistry*, vol. 271, no. 16, pp. 9390–9397, 1996.

[10] Y. Feng, Y. Xia, G. Yu et al., "Cleavage of GSK-3β by calpain counteracts the inhibitory effect of Ser9 phosphorylation on GSK-3β activity induced by H_2O_2," *Journal of Neurochemistry*, vol. 126, no. 2, pp. 234–242, 2013.

[11] R. A. S. Robinson, G. Joshi, Q. Huang et al., "Proteomic analysis of brain proteins in APP/PS-1 human double mutant knock-in mice with increasing amyloid β-peptide deposition: Insights into the effects of in vivo treatment with *N*-acetylcysteine as a potential therapeutic intervention in mild cognitive impairment and Alzheimer's disease," *Proteomics*, vol. 11, no. 21, pp. 4243–4256, 2011.

[12] P. Rudrabhatla, "Regulation of neuronal cytoskeletal protein phosphorylation in neurodegenerative diseases," *Journal of Alzheimer's Disease*, vol. 41, no. 3, pp. 671–684, 2014.

[13] K. Fujita, K. Motoki, K. Tagawa et al., "HMGB1, a pathogenic molecule that induces neurite degeneration via TLR4-MARCKS, is a potential therapeutic target for Alzheimer's disease," *Scientific Reports*, vol. 6, no. 1, p. 31895, 2016.

[14] K. R. Urquhart, Y. Zhao, J. A. Baker et al., "A novel heat shock protein alpha 8 (*Hspa8*) molecular network mediating responses to stress- and ethanol-related behaviors," *Neurogenetics*, vol. 17, no. 2, pp. 91–105, 2016.

[15] C. Ren, T. Chen, X. Jiang, Y. Wang, and C. Hu, "The first characterization of gene structure and biological function for echinoderm translationally controlled tumor protein (TCTP)," *Fish & Shellfish Immunology*, vol. 41, no. 2, pp. 137–146, 2014.

[16] H. Gao, B. Sun, H. Fu et al., "PDIA6 promotes the proliferation of HeLa cells through activating the Wnt/β-catenin signaling pathway," *Oncotarget*, vol. 7, no. 33, pp. 53289–53298, 2016.

[17] L. W. J. Klomp, T. J. de Koning, H. E. M. Malingré et al., "Molecular characterization of 3-phosphoglycerate dehydrogenase deficiency—a neurometabolic disorder associated with reduced L-serine biosynthesis," *American Journal of Human Genetics*, vol. 67, no. 6, pp. 1389–1399, 2000.

[18] J. M. Beaulieu, M. D. Nguyen, and J. P. Julien, "Late onset of motor neurons in mice overexpressing wild-type peripherin," *The Journal of Cell Biology*, vol. 147, no. 3, pp. 531–544, 1999.

[19] L. Hjørnevik, A. Frøyset, T. Grønset, K. Rungruangsak-Torrissen, and K. Fladmark, "Algal toxin azaspiracid-1 induces early neuronal differentiation and alters peripherin isoform stoichiometry," *Marine Drugs*, vol. 13, no. 12, pp. 7390–7402, 2015.

[20] F. H. Beraldo, A. Thomas, B. Kolisnyk et al., "Hyperactivity and attention deficits in mice with decreased levels of stress-inducible phosphoprotein 1 (STIP1)," *Disease Models & Mechanisms*, vol. 8, no. 11, pp. 1457–1466, 2015.

[21] M. M. Jin, P. Wang, X. Li et al., "Biochemical characterization of $NADP^+$-dependent isocitrate dehydrogenase from *Microcystis aeruginosa* PCC7806," *Molecular Biology Reports*, vol. 40, no. 4, pp. 2995–3002, 2013.

[22] T. Hurtado de Mendoza, C. G. Perez-Garcia, T. T. Kroll, N. H. Hoong, D. D. M. O'Leary, and I. M. Verma, "Antiapoptotic protein lifeguard is required for survival and maintenance of Purkinje and granular cells," *Proceedings of the National Academy of Sciences of the United States of America*, vol. 108, no. 41, pp. 17189–17194, 2011.

[23] J. Miro, A. M. Laaref, V. Rofidal et al., "FUBP1: a new protagonist in splicing regulation of the *DMD* gene," *Nucleic Acids Research*, vol. 43, no. 4, pp. 2378–2389, 2015.

[24] B. Chen, D. Zhong, and A. Monteiro, "Comparative genomics and evolution of the HSP90 family of genes across all kingdoms of organisms," *BMC Genomics*, vol. 7, no. 1, p. 156, 2006.

[25] N. Katagiri, T. Kuroda, H. Kishimoto, Y. Hayashi, T. Kumazawa, and K. Kimura, "The nucleolar protein nucleophosmin is essential for autophagy induced by inhibiting Pol I transcription," *Scientific Reports*, vol. 5, no. 1, p. 8903, 2015.

[26] X. Q. Zhang, Y. Pan, C. H. Yu et al., "PDIA3 knockdown exacerbates free fatty acid-induced hepatocyte steatosis and apoptosis," *PLoS One*, vol. 10, no. 7, article e0133882, 2015.

[27] E. Popugaeva, E. Pchitskaya, and I. Bezprozvanny, "Dysregulation of neuronal calcium homeostasis in Alzheimer's disease – a therapeutic opportunity?," *Biochemical and Biophysical Research Communications*, vol. 483, no. 4, pp. 998–1004, 2017.

[28] X. G. Zong and M. X. Jiang, "Effects of dauricine on slow action potentials in myocardium," *Zhongguo Yao Li Xue Bao*, vol. 11, no. 3, pp. 241–245, 1990.

[29] S. N. Li and K. Y. Zhang, "Effects of dauricine on action potentials and slow inward currents of guinea pig ventricular papillary muscles," *Zhongguo Yao Li Xue Bao*, vol. 13, no. 6, pp. 535–537, 1992.

[30] S. Wang and R. J. Kaufman, "The impact of the unfolded protein response on human disease," *The Journal of Cell Biology*, vol. 197, no. 7, pp. 857–867, 2012.

[31] J. Q. Qian, "Cardiovascular pharmacological effects of bisbenzylisoquinoline alkaloid derivatives," *Acta Pharmacologica Sinica*, vol. 23, no. 12, pp. 1086–1092, 2002.

[32] I. Bezprozvanny and M. P. Mattson, "Neuronal calcium mishandling and the pathogenesis of Alzheimer's disease," *Trends in Neurosciences*, vol. 31, no. 9, pp. 454–463, 2008.

[33] F. G. De Felice, P. T. Velasco, M. P. Lambert et al., "Aβ-oligomers induce neuronal oxidative stress through an N-methyl-D-aspartate receptor-dependent mechanism that is blocked by the Alzheimer drug memantine," *Journal of Biological Chemistry*, vol. 282, no. 15, pp. 11590–11601, 2007.

[34] L. He, L. Li, J. Wu et al., "Experimental studies on the antioxidation effect of dauricine (Dau)," *Chinese Traditional and Herbal Drugs*, vol. 28, no. 8, pp. 479–481, 1997.

[35] A. Grimm, K. Friedland, and A. Eckert, "Mitochondrial dysfunction: the missing link between aging and sporadic Alzheimer's disease," *Biogerontology*, vol. 17, no. 2, pp. 281–296, 2016.

[36] L. I. Yan-Hong and P. L. Gong, "The protective effect of dauricine on cerebral ischemia in mice," *Chinese Pharmacological Bulletin*, vol. 20, no. 5, pp. 564–567, 2004.

[37] W. Scheper and J. J. M. Hoozemans, "The unfolded protein response in neurodegenerative diseases: a neuropathological perspective," *Acta Neuropathologica*, vol. 130, no. 3, pp. 315–331, 2015.

[38] L. Hedskog, C. M. Pinho, R. Filadi et al., "Modulation of the endoplasmic reticulum-mitochondria interface in Alzheimer's disease and related models," *Proceedings of the National Academy of Sciences of the United States of America*, vol. 110, no. 19, pp. 7916–7921, 2013.

[39] J. Grosskreutz, L. Van Den Bosch, and B. U. Keller, "Calcium dysregulation in amyotrophic lateral sclerosis," *Cell Calcium*, vol. 47, no. 2, pp. 165–174, 2010.

[40] S. S. Cao and R. J. Kaufman, "Endoplasmic reticulum stress and oxidative stress in cell fate decision and human disease," *Antioxidants & Redox Signaling*, vol. 21, no. 3, pp. 396–413, 2014.

[41] A. Higa and E. Chevet, "Redox signaling loops in the unfolded protein response," *Cellular Signalling*, vol. 24, no. 8, pp. 1548–1555, 2012.

[42] S. S. Cao and R. J. Kaufman, "Unfolded protein response," *Current Biology*, vol. 22, no. 16, pp. R622–R626, 2012.

[43] N. Sovolyova, S. Healy, A. Samali, and S. E. Logue, "Stressed to death - mechanisms of ER stress-induced cell death," *Biological Chemistry*, vol. 395, no. 1, pp. 1–13, 2014.

[44] Y. Chen and F. Brandizzi, "IRE1: ER stress sensor and cell fate executor," *Trends in Cell Biology*, vol. 23, no. 11, pp. 547–555, 2013.

[45] V. Rhein, X. Song, A. Wiesner et al., "Amyloid-beta and tau synergistically impair the oxidative phosphorylation system in triple transgenic Alzheimer's disease mice," *Proceedings of the National Academy of Sciences of the United States of America*, vol. 106, no. 47, pp. 20057–20062, 2009.

[46] A. Eckert, R. Nisbet, A. Grimm, and J. Gotz, "March separate, strike together–role of phosphorylated TAU in mitochondrial dysfunction in Alzheimer's disease," *Biochimica et Biophysica Acta*, vol. 1842, no. 8, pp. 1258–1266, 2014.

[47] Y. Wang, D. Zhong, X. Chen, and J. Zheng, "Identification of quinone methide metabolites of dauricine in human liver microsomes and in rat bile," *Chemical Research in Toxicology*, vol. 22, no. 5, pp. 824–834, 2009.

[48] H. Jin, S. Shen, X. Chen, D. Zhong, and J. Zheng, "CYP3A-mediated apoptosis of dauricine in cultured human bronchial epithelial cells and in lungs of CD-1 mice," *Toxicology and Applied Pharmacology*, vol. 261, no. 3, pp. 248–254, 2012.

[49] K. S. P. McNaught, P.-A. Carrupt, C. Altomare et al., "Isoquinoline derivatives as endogenous neurotoxins in the aetiology of Parkinson's disease," *Biochemical Pharmacology*, vol. 56, no. 8, pp. 921–933, 1998.

Hindawi
Oxidative Medicine and Cellular Longevity
Volume 2018, Article ID 4528184, 10 pages
https://doi.org/10.1155/2018/4528184

Research Article

Cytoprotective Roles of a Novel Compound, MHY-1684, against Hyperglycemia-Induced Oxidative Stress and Mitochondrial Dysfunction in Human Cardiac Progenitor Cells

Woong Bi Jang,[1] **Ji Hye Park**,[1] **Seung Taek Ji**,[1] **Na Kyung Lee**,[1] **Da Yeon Kim**,[1] **Yeon Ju Kim**,[1] **Seok Yun Jung**,[1,2] **Songhwa Kang**,[1] **Shreekrishna Lamichane**,[1,3] **Babita Dahal Lamichane**,[1] **Jongseong Ha**,[1] **Jisoo Yun**,[1] **Hyung Ryong Moon**,[4] **Sang Hong Baek**,[5] **Hae Young Chung**,[3] and **Sang-Mo Kwon**[1,2,6]

[1]*Laboratory for Vascular Medicine and Stem Cell Biology, Medical Research Institute, Department of Physiology, School of Medicine, Pusan National University, Yangsan 50612, Republic of Korea*
[2]*Convergence Stem Cell Research Center, Pusan National University, Yangsan, Republic of Korea*
[3]*Molecular Inflammation Research Center for Aging Intervention, College of Pharmacy, Pusan National University, Busan, Republic of Korea*
[4]*Laboratory of Medicinal Chemistry, College of Pharmacy, Pusan National University, Busan, Republic of Korea*
[5]*Laboratory of Cardiovascular Disease, Division of Cardiology, School of Medicine, The Catholic University of Korea, Seoul, Republic of Korea*
[6]*Research Institute of Convergence Biomedical Science and Technology, Pusan National University Yangsan Hospital, Yangsan, Republic of Korea*

Correspondence should be addressed to Hyung Ryong Moon; mhr108@pusan.ac.kr, Sang Hong Baek; whitesh@catholic.ac.kr, Hae Young Chung; hyjung@pusan.ac.kr, and Sang-Mo Kwon; smkwon323@hotmail.com

Received 10 January 2018; Accepted 1 April 2018; Published 30 May 2018

Academic Editor: Lisbell Estrada

Diabetic cardiomyopathy (DCM) is tightly linked to heart disorders and dysfunction or death of the cardiomyocytes including resident cardiac progenitor cells (CPCs) in diabetic patients. In order to restore loss of function of resident or transplanted CPCs, much research has focused on novel therapeutic strategies including the discovery of novel function-modulating factors such as reactive oxygen species (ROS) scavengers. Here, we developed and defined a novel antioxidant, MHY-1684, for enhancing the angiogenic potential of CPCs against ROS-related DCM. Short-term treatment with MHY-1684 restored ROS-induced CPC cell death. Importantly, MHY-1684 decreased hyperglycemia-induced mitochondrial ROS generation and attenuated hyperglycemia-induced mitochondrial fragmentation. We observed that the activation process of both Drp1 (phosphorylation at the site of Ser616) and Fis-1 is drastically attenuated when exposed to high concentrations of D-glucose with MHY-1684. Interestingly, phosphorylation of Drp1 at the site of Ser637, which is an inhibitory signal for mitochondrial fusion, is restored by MHY-1684 treatment, suggesting that this antioxidant may affect the activation and inhibition of mitochondrial dynamics-related signaling and mitochondrial function in response to ROS stress. In conclusion, our finding of the novel compound, MHY-1684, as an ROS scavenger, might provide an effective therapeutic strategy for CPC-based therapy against diabetic cardiomyopathy.

1. Introduction

Diabetes mellitus (DM), commonly called as diabetes, is a common public health problem worldwide. The most severe problems associated with diabetes are the various DM-related complications such as cardiovascular diseases, renal diseases, neuropathy, and diabetic nephropathy. In general, the primary cause of diabetes is a dysregulation of the blood

glucose level due to a malfunction in insulin secretion [1]. This malfunction is caused by the destruction of pancreatic beta cells in type I diabetes and insulin resistance in type II diabetes. Regardless of the type, diabetes is categorized as a disease where blood glucose is elevated, and this eventually leads to hyperglycemia, which is a major cause of cardiovascular disease. In clinical settings, it has been reported that the death ratio of diabetes patients with cardiovascular disease is much higher than normal patients with cardiovascular disease [2, 3]. Furthermore, hyperglycemia causes additional complications such as neuropathy, stroke, diabetic ketoacidosis, and a hyperosmolar hyperglycemic state [4, 5].

Diabetic cardiomyopathy (DCM) leads to heart disorders and dysfunction or death of the resident cardiomyocytes in diabetic patients. DCM is characterized by an altered lipid composition and mitochondrial dysfunction in diabetic hearts [6], which develop from various causative factors such as oxidative stress, mitochondrial dysfunction, endothelial cell loss, inflammation, autophagy, and mitophagy [7, 8]. In order to reduce the risk of heart failure, DCM needs to be controlled via reducing hyperglycemia and improving the cellular function of cardiomyocytes or resident cardiac progenitor cells (CPCs). In a clinical setting, hyperglycemia by induced DCM affects CPC viability and the angiogenic potential of resident CPCs or transplanted CPCs [9]. Therefore, identifying novel factors that have cytoprotective effects against hyperglycemia is a prerequisite for cell-based therapies in the treatment of DCM.

It is generally well known that the overproduction of reactive oxygen species (ROS) has a critical impact on the development of diabetic complications [10]. Excess ROS in tissues gives rise to mitochondrial dysfunction, which eventually causes cell senescence and cell death, as well as the reduced bioactivity of pancreatic cells including tissue stem cells [11, 12]. Several studies have focused on the cytoprotective effect of natural or synthetic compounds as ROS scavengers [13–15]. Recently, we showed that oleuropein-primed endothelial progenitor cells (EPCs) modulate the potential of vascular repair against activating the ROS-induced extracellular signal-regulated kinase 1/2-peroxiredoxin (ERK1/2-Prdx) pathway [15]. Moreover, pretreatment with lycopene attenuates ROS-induced apoptosis in human mesenchymal stem cell (hMSC) through the protein kinase B-manganese superoxide dismutase (AKT-MnSOD) pathway [14].

Accumulating evidence has suggested that mitochondrial dynamics including mitochondrial fission and fusion maintain mitochondrial homeostasis [16]. For example, several research groups have clearly demonstrated the specific disruption of mitochondrial dynamics by fission-related inhibitors including specific targeting of dynamin-related protein 1 (Drp-1), which eventually induces cell death and promotes heart disease [17–19]. Multiple therapeutic strategies have been attempted, including the specific targeting of ROS-induced mitochondrial fragmentation [20], hyperglycemia-related cardiac stem cell homing [21], and hyperglycemia-induced angiogenic capacity of CPCs [9]. Recently, we also reported that hyperglycemia in CPCs alters mitochondrial dynamics and increases the expression of fission-related proteins, including mitochondrial fission 1 protein (Fis1) and Drp1. Moreover, we showed that the specific blockage of glucose transporter 1 (GLUT1) improved cell viability, tube formation, and regulation of mitochondrial dynamics in CPCs [17]. Nevertheless, there are still few reports that identify novel compounds for enhancing CPC bioactivities against DCM.

Thus, the aim of this study is to develop a novel antioxidant compound against hyperglycemia-induced cardiomyopathy and evaluate the potential roles of our compound in oxidative stress, cell death, and mitochondrial dynamics in CPCs.

2. Material and Methods

2.1. Isolation of Human c-Kit-Positive Cardiac Progenitor Cells ($hCPCs^{c\text{-}kit+}$). $hCPCs^{c\text{-}kit+}$ were isolated from human infant-derived heart tissues after surgical procedures, as described in a previously modified protocol [22]. The Ethical Review Board of the Pusan National University Yangsan Hospital, Gyeongsangnam-do, Republic of Korea, approved the protocols. To perform this isolation, the biopsied heart specimens were minced and incubated in 0.2% collagenase type II (Worthington, NJ, USA) at 37°C for 30 min to obtain single cardiac cells. Single cardiac cells were incubated in Ham's F12 media (HyClone, UT) containing 10% fetal bovine serum (FBS, Gibco, CA, USA), 1x penicillin/streptomycin (P/S, Welgene, Daegu, Republic of Korea), 2.5 U human erythropoietin (hEPO, R&D Systems, Minneapolis, MN, USA), 5 μg basic human recombinant fibroblast growth factor (bFGF, PeproTech, Rocky Hill, NJ, USA), and 0.2 mM glutathione (Sigma-Aldrich, St. Louis, CA, USA). When single cardiac cells were grown to a high enough confluence for sorting, single cardiac cells were conjugated to the c-kit primary antibody (Santa Cruz Biotechnology, Santa Cruz, CA, USA) and sorted by magnetic activated cell sorting (MACS).

2.2. Measurement of Peroxynitrite ($ONOO^-$) Scavenging Activity. $ONOO^-$ (Eugene, Oregon, USA) scavenging was measured using monitoring the oxidation of dihydrorhodamine 123 (DHR 123, Eugene, Oregon, USA) by modifying the method [23]. $ONOO^-$ scavenging by the oxidation of DHR 123 was measured on a microplate fluorescence spectrophotometer FL 500 (BioTek Instruments, USA) with excitation and emission wavelengths of 485 nm and 530 nm, respectively, at room temperature. The background and final fluorescent intensities were measured at 5 min after treatment with or without SIN-1 (final concentration, 10 mM) or authentic $ONOO^-$ (final concentration, 10 mM) in 0.3 N sodium hydroxide. Oxidation of DHR 123 by decomposition of SIN-1 (Sigma-Aldrich, St. Louis, CA, USA) gradually increased, whereas authentic $ONOO^-$ rapidly oxidized DHR 123 with its final fluorescent intensity being stable over time.

2.3. $hCPC^{c\text{-}kit+}$ Cultures and MHY-1684. $hCPCs^{c\text{-}kit+}$ were maintained in HAM's F12 culture media at 37°C in

humidified 5% CO_2. D-(+) glucose (Sigma-Aldrich, St. Louis, CA, USA) was added to the normal culture media. MHY-1684 was dissolved in DMSO (100 mM) and further diluted for different concentrations. Same concentration of DMSO was added to the control group of all experiments. MHY-1684 was used as an antioxidant. hCPCs were treated with D-(+) glucose and MHY-1684 at various concentrations.

2.4. Cell Viability Assay. Cell viability was measured using the WST Kit (Ez-Cytox, Dail Lab, Seoul, Republic of Korea). $hCPCs^{c\text{-}kit+}$ were seeded on 96-well plates with D-(+) glucose and MHY-1684 at various concentrations. Culture plates were incubated for 24, 48, and 72 h. After incubation, the culture medium with D-(+) glucose and MHY-1684 at various concentrations was changed to the WST solution. The plates were then incubated for 1 h, and the absorbance was measured at 450 nm using a spectrophotometer (Tecan, Grodig, Austria).

2.5. Western Blot Analysis. Whole cells were lysed with RIPA lysis and extraction buffer (Thermo Fisher Scientific, Waltham, MA, USA) with a protease inhibitor cocktail (Sigma-Aldrich, St. Louis, CA, USA) on ice, and the total protein concentration was quantified using a Bicinchoninic Acid Kit (Thermo Scientific, Rockford, IL, USA). In general, 10–25 μg of total protein was separated by 8–15% sodium dodecyl sulfate polyacrylamide gel electrophoresis, and the proteins were transferred to polyvinylidene fluoride (PVDF, Millipore, Billerica, MA, USA) membranes. The membranes were blocked with 5% skim milk for 1 h at room temperature and incubated with primary antibodies overnight at 4°C. Subsequently, these membranes were incubated with horseradish peroxidase- (HRP-) conjugated secondary antibodies for 1 h at room temperature (Millipore), and protein bands were visualized using the enhanced chemiluminescence reagents (Thermo Fisher Scientific). The following primary antibodies were used: phosphorylated extracellular signal-regulated kinase (p-ERK, Cell Signaling Technology, Danvers, MA, USA), extracellular signal-regulated kinase (ERK, Cell Signaling Technology), phosphorylated protein kinase-B (p-AKT, Cell Signaling Technology), protein kinase-B (AKT, Cell Signaling Technology), AMP-activated protein kinase (AMPK, Cell Signaling Technology), glyceraldehyde-3-phosphate dehydrogenase (GAPDH, Santa Cruz Biotechnology, Santa Cruz, CA, USA), β-actin (Santa Cruz), $p\text{-Drp1ser}^{616}$ (Cell Signaling Technology), $p\text{-DRP1ser}^{637}$ (Cell Signaling Technology), Drp1 (Cell Signaling Technology), Fis1 (Abcam, Cambridge, MA, USA), mitofusin-1 (Mfn-1, Santa Cruz), and optic atrophy 1 (OPA1, Abcam). The following secondary antibodies were used: goat anti-rabbit IgG and goat anti-mouse IgG (Enzo Life Sciences, Farmingdale, USA).

2.6. Tube Formation Assay. 96-Well plates were coated with 70 μL of Matrigel (BD Biosciences, Franklin Lakes, NJ) and incubated at 37°C for 30 min. hCPCs were seeded in 96-well plates with Matrigel and then incubated for 6 h. After the incubation, total tube length was measured by counting the number of tubes visualized in one microscopic field per well (40x magnification) at least 3 independent replicates using the ImageJ software (free software from National Institutes of Health).

2.7. Measurement of Mitochondrial ROS. Mitochondrial ROS was determined using the fluorescent MitoSOX probe (Invitrogen, Carlsbad, CA, USA). hCPCs were incubated in HAM's F12 culture media with 2 μM MitoSOX Red for 30 min at 37°C in a 5% CO_2 atmosphere. After the incubation, the cells were washed with phosphate-buffered saline (PBS), and the fluorescence was assessed by fluorescence-activated cell sorting (FACS; BD Accuri C6, San Jose, CA, USA). Mitochondrial ROS were analyzed using BD FACS-Diva software (BD Biosciences, Bedford, MA).

2.8. Cell Death Analysis. To measure apoptotic cell death, hCPCs were detected by FACS (BD Accuri C6) with annexin V/propidium iodide (PI) Apoptosis Detection Kit (BD Biosciences, San Diego, CA, USA). Gently, hCPCs were harvested after the addition of culture media that contained D-(+) glucose and MHY-1684. The cells were then treated with annexin V/PI for at least 15 min in the dark according to the manufacturer's instructions.

2.9. Immunofluorescence. Mitochondrial morphology was measured in hCPCs stained with 200 nM MitoTracker Red CMXRos (Molecular Probes, Eugene, OR, USA) with a confocal microscope (Olympus, FV1000, Tokyo, Japan). To determine any alteration in mitochondrial morphology, we measured mitochondrial total length using the ImageJ software.

2.10. Statistical Analysis. All experimental results are presented as the mean ± standard deviation (SD) using ANOVA. Comparisons between the two groups were performed using the unpaired Student's t-test. A value of $p < 0.05$ was considered statistically significant.

3. Results

3.1. Development of a Novel Compound, MHY-1684, for Enhancing the Bioactivity of hCPCs. In order to develop a novel compound, we designed a MHY-1684 as an antioxidant compound, which is synthesized based on the kojic acid (Figure 1(a)). Previously, antioxidant effect of kojic acid has been reported [24, 25]. It confirmed the antioxidant effect of MHY-1684 (Supplementary Table 1, Supplementary Materials). To evaluate the cytotoxicity of MHY-1684 on hCPCs, we treated the cells with 0.1, 1, 10, 100 μM, and 1 mM MHY-1684 for 24 h. Cell viability decreased significantly when cells were exposed to more than 10 μM MHY-1684. Therefore, we optimized all experiments using less than 10 μM MHY-1684 (Figure 1(b)). To evaluate the impact of MHY-1684 on hCPC bioactivity, we next investigated the effect of MHY-1684 on hCPC tube-forming ability and cell proliferation, including an investigation into the ERK1/2 and AKT pathway. Treatment of hCPC with MHY-1684 for 24 h significantly increased the expression of p-ERK and p-AKT (Figures 1(c) and 1(d)), as well as enhanced hCPC tube-forming

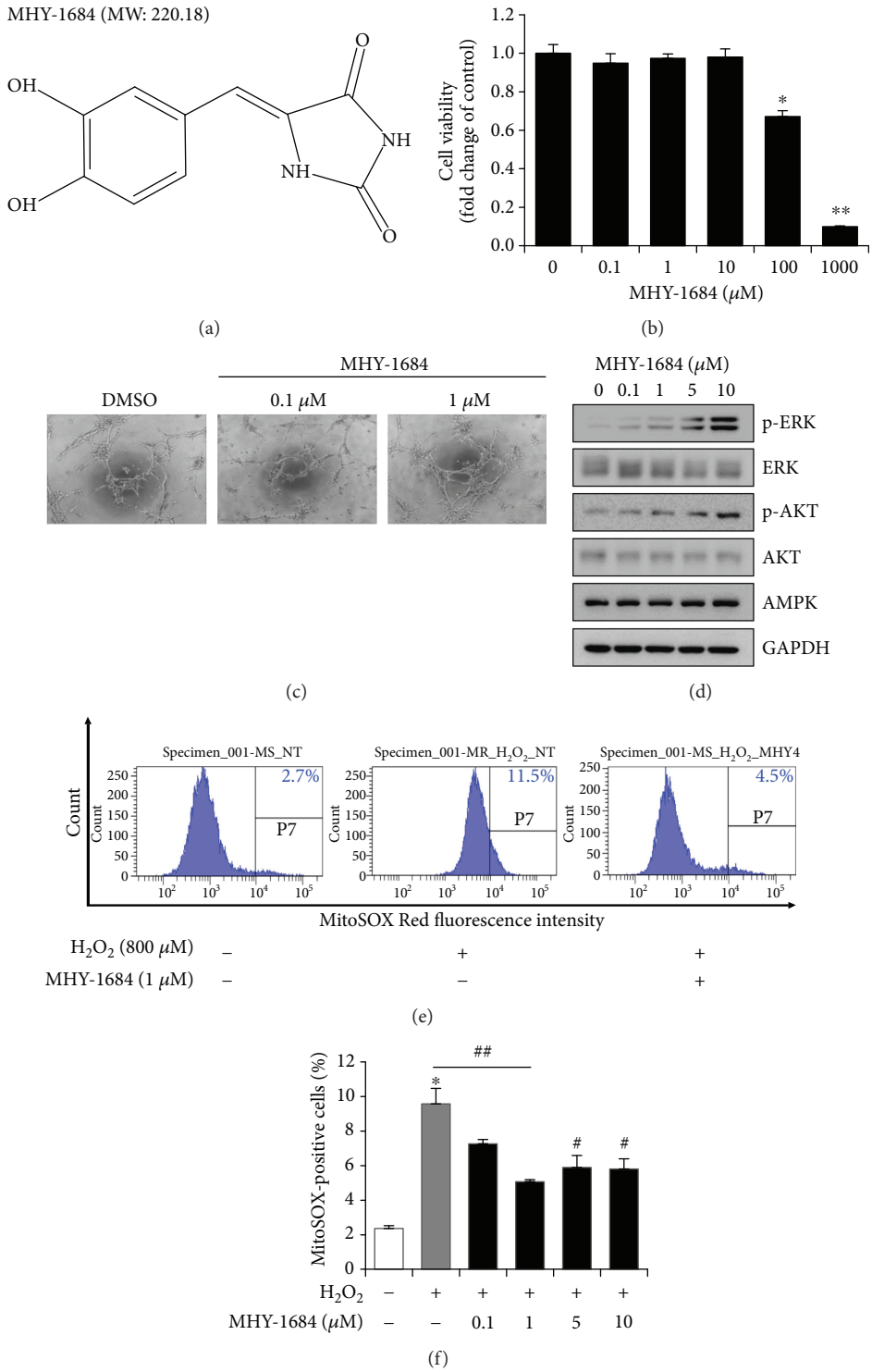

Figure 1: The role of MHY-1684 as an ROS scavenger in hCPCs. (a) The chemical structure of MHY-1684. (b) hCPCs were seeded in 96-well plates and cultured with the indicated concentrations of MHY-1684 for 24 h. Cell viability was assessed using the WST assay. Values are the mean ± S.E.M. $^{*}p < 0.05$ and $^{**}p < 0.01$ as compared with the control group. (c) The tube-forming ability of hCPCs was examined when cells were exposed to MHY-1684 for 24 h. The tubular-like network was evaluated using a Matrigel tube formation assay. (d) After treatment with MHY-1684 for 24 h, the prosurvival-related proteins (ERK-1, AKT-1) were analyzed by Western blotting. (e) hCPCs were pretreated with the indicated concentrations of MHY-1684 for 24 h prior to hydrogen peroxide (H_2O_2, 800 μM) treatment. Mitochondrial ROS levels in hCPCs were measured by flow cytometry with MitoSOX Red. (f) Histogram indicates median value ± S.E.M. of MitoSOX-positive cells when exposed to H_2O_2. MitoSOX-positive cells increased when exposed to H_2O_2; however, when cotreated with MHY-1684, the MitoSOX-positive cells decreased significantly. Values are the mean ± S.E.M. $^{*}p < 0.05$ and $^{**}p < 0.01$ as compared with the control group; $^{\#}p < 0.05$ and $^{\#\#}p < 0.01$ as compared with the group treated with 25 mM D-(+) glucose for 72 h.

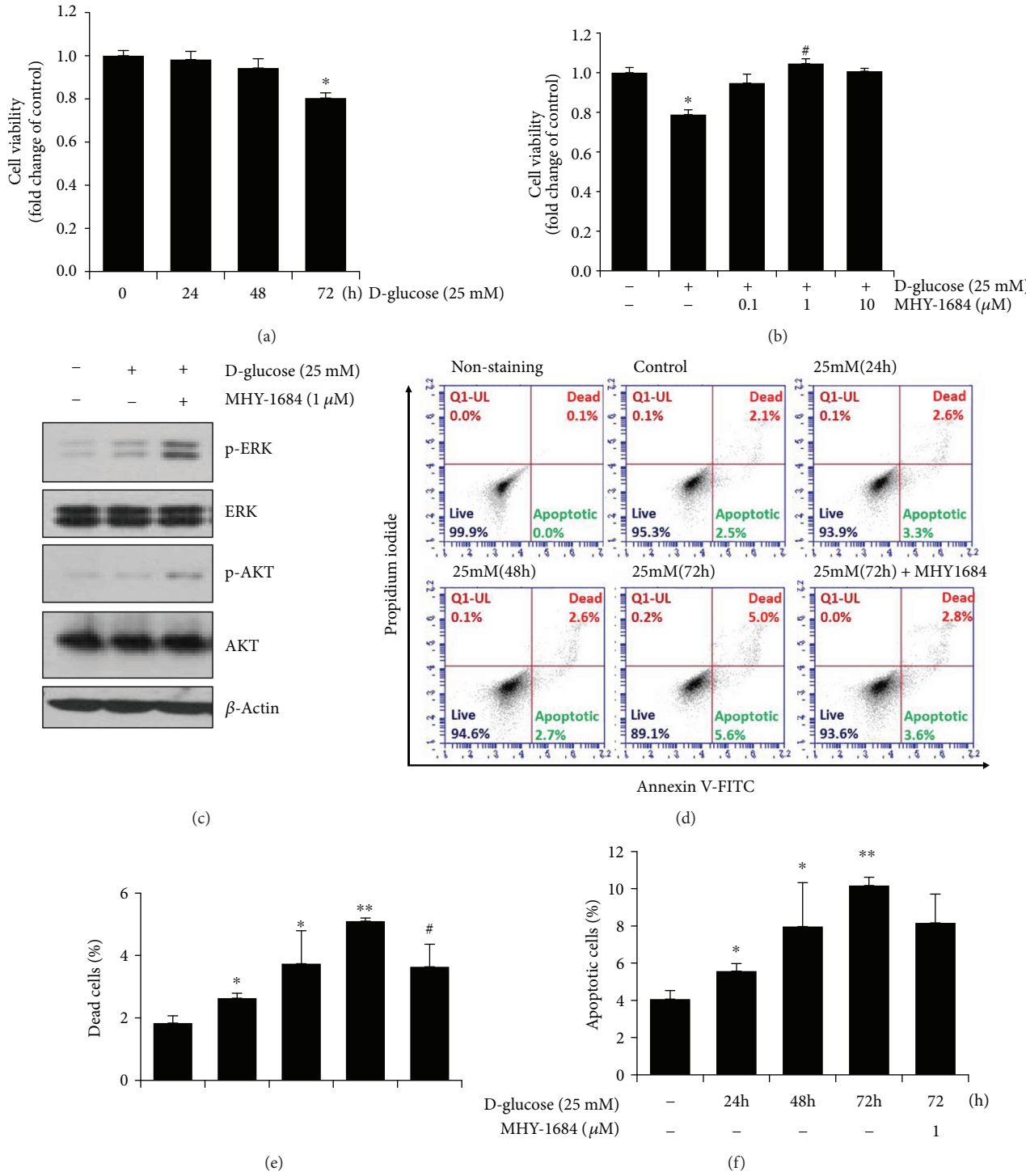

Figure 2: Effect of MHY-1684 on hyperglycemia-induced cell death of hCPCs. (a) hCPCs were treated with 25 mM D-(+) glucose for 0–72 h, and cell viability was subsequently assessed. (b) Following the cotreatment of hCPCs with MHY-1684 (0.1, 1, and 10 μM) and 25 mM D-glucose for 72 h, cell viability was assessed. Values are the mean ± S.E.M. $^{*}p < 0.05$ as compared with the control group; $^{\#}p < 0.05$ as compared with the 25 mM D-(+) glucose-treated group. (c) After treatment with MHY-1684 for 24 h in 25 mM D-(+) glucose, the prosurvival-related proteins (ERK-1, AKT-1) were analyzed by Western blotting. (d) hCPCs were incubated with 25 mM D-(+) glucose for 0–72 h with or without 1 μM MHY-1684 for 72 h. hCPCs were stained with annexin V/PI, and then, hCPCs were measured by flow cytometry. hCPCs were classified as viable cells (annexin V-/PI-), apoptotic cells (annexin V+/PI-, annexin V+, PI+), and dead cells (annexin V+/PI+). (e) Dead cell population is expressed as a percent of the total cell population. (f) Apoptotic cell population is expressed as a percent of the total cell population. Values are the mean ± S.E.M. $^{*}p < 0.05$ and $^{**}p < 0.01$ as compared with the control group; $^{\#}p < 0.05$ as compared with the group treated with 25 mM D-(+) glucose for 72 h.

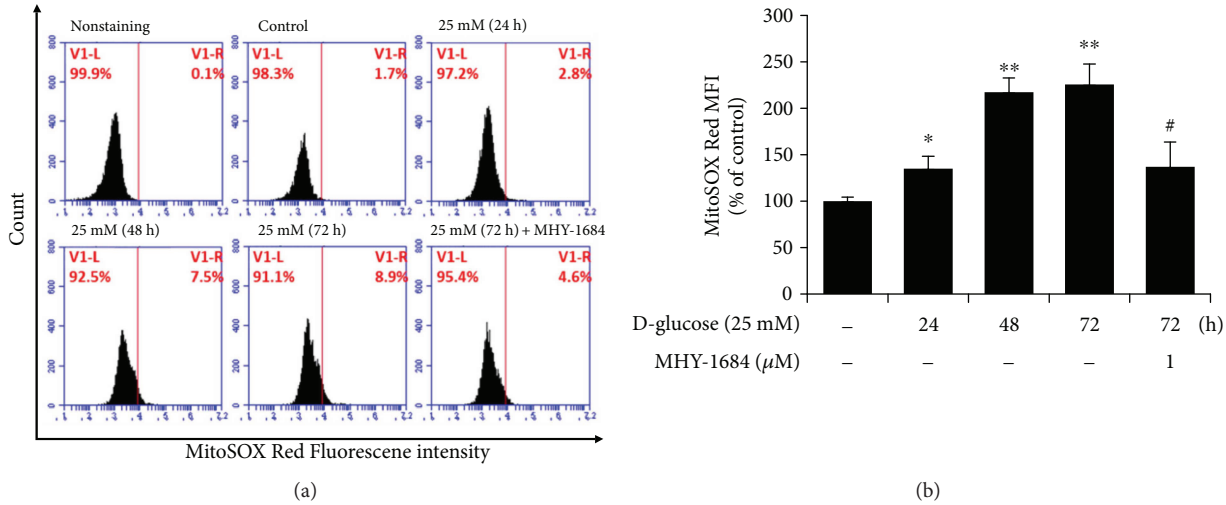

(a) (b)

Figure 3: MHY-1684 attenuates mitochondrial ROS generation. (a) hCPCs were treated with 25 mM D-(+) glucose for 0–72 h and 1 μM MHY-1684 for 72 h. Mitochondrial ROS were labeled with MitoSOX Red, and hCPCs were analyzed by flow cytometry. (b) Histogram indicates median value ± S.E.M. of MitoSOX mean fluorescence intensity (MFI) when exposed to D-(+) glucose. MitoSOX-positive cells increased in a time-dependent manner when exposed to D-(+) glucose; however, when cotreated with MHY-1684, the MitoSOX-positive cells decreased significantly. Values are the mean ± S.E.M $^{*}p < 0.05$, $^{**}p < 0.01$ as compared with the control group, $^{\#}p < 0.05$ as compared with the group treated with 25 mM D-(+) glucose for 72 h.

capacity, suggesting that MHY-1684 affects hCPC angiogenic potential and cell proliferation.

3.2. Antioxidant Effect of MHY-1684 on H_2O_2-Induced ROS in hCPCs. To determine the potential role of MHY-1684 as an antioxidant, we examined mitochondrial ROS generation in response to oxidative stress. Specifically, when hCPCs were exposed to 800 μM of H_2O_2, a significant amount of mitochondrial ROS was produced. In contrast, hCPCs pretreated with MHY-1684 displayed a dramatic decrease in the level of mitochondrial ROS, suggesting that MHY-1684 has an inhibitory effect on mitochondrial ROS generation (Figures 1(e) and 1(f)).

3.3. Cytoprotective Effect of MHY-1684 on Hyperglycemia-Induced Cell Death in hCPCs. To investigate whether hyperglycemia induced cell death in hCPCs, we treated hCPCs with 25 mM D-(+) glucose in a time-dependent manner. As a result, we found that this concentration of glucose induced a significant amount of hCPC cell death in 72 h (Figure 2(a)). Importantly, hCPCs cotreated with D-(+) glucose and MHY-1684 significantly attenuated hyperglycemia-induced cell death (Figure 2(b)). Furthermore, we also observed an increase in the expression of proliferation-related markers including p-ERK and p-AKT (Figure 2(c)), suggesting that MHY-1684 might promote cell proliferation.

3.4. Cytoprotective Effect of MHY-1684 on Hyperglycemia-Induced Apoptosis in hCPCs. To investigate whether hyperglycemia-induced cell death was caused by hyperglycemia-induced apoptosis, we evaluated hCPC cell death via annexin V/PI staining. As shown in Figure 2(d), the high glucose condition significantly increased the percentage of dead cells in the hCPC population. In contrast, pretreatment of hCPCs with MHY-1684 and high glucose for 72 h significantly attenuated the hyperglycemia-induced hCPC cell death (Figures 2(d)–2(f)).

3.5. MHY-1684 Attenuates Mitochondrial ROS Generation. Based on a previous report that hyperglycemia-induced apoptosis is caused by mitochondrial ROS [17], we investigated the effect of MHY-1684 on hyperglycemia-induced mitochondrial ROS generation. As shown in Figure 3(a), when exposed to hyperglycemia, hCPCs produced more mitochondrial ROS. Importantly, cotreatment of hCPCs with MHY-1684 and D-(+) glucose significantly decreased mitochondrial ROS (Figures 3(a) and 3(b)), indicating that MHY-1684 might protect hCPCs from apoptotic cell death by blocking mitochondrial ROS generation.

3.6. MHY-1684 Attenuates Mitochondrial Fission via Regulating Fission/Fusion-Related Proteins. To examine the effect of MHY-1684 on hyperglycemia-induced mitochondrial fragmentation [20], we observed mitochondria morphological changes following hCPC treatment with glucose and MHY-1684. As shown in Figure 4(a), total mitochondrial length decreased significantly when cells were exposed to 25 mM D-(+) glucose. In contrast, cotreatment of hCPCs with 1 μM MHY-1684 and 25 mM D-(+) glucose for 72 h significantly attenuated mitochondrial fragmentation (Figures 4(a) and 4(b)). To investigate the molecular mechanism by which this attenuation occurs, we next examined the expression of mitochondrial dynamics-related proteins including both the fission-associated Drp1 and Fis-1 and the fusion-associated Mfn-1 and Opa-1 by Western blotting. Notably, the activation of both Drp1 (phosphorylation at the site of Ser616) and Fis-1 is drastically attenuated when exposed to high concentrations of D-(+) glucose. Interestingly, the phosphorylation of Drp1 at Ser637, which is an inhibitory signal for mitochondrial

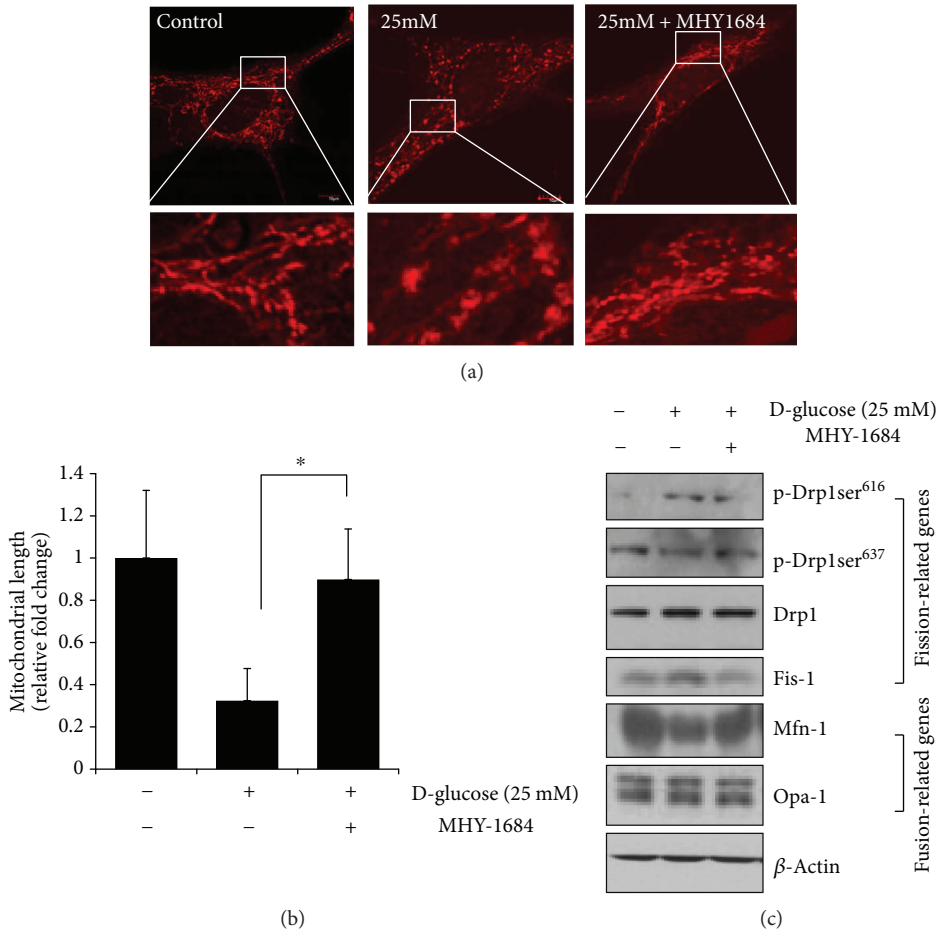

Figure 4: MHY-1684 attenuates mitochondrial fission via regulating fission/fusion-related proteins. (a) Confocal image of hCPCs stained with MitoTracker Red CMXRos after cotreatment with 1 μM MHY-1684 and 25 mM D-(+) glucose for 72 h. (b) Mitochondrial length was analyzed when hCPCs were incubated with 1 μM MHY-1684 after being exposed to 25 mM D-(+) glucose. Results are presented as means ± SD. $^{*}p < 0.05$ versus 25 mM D-(+) glucose. (c) Expression of the mitochondrial fragmentation-related marker Fis1, Drp1, OPA1, and Mfn1 when incubated with 1 μM MHY-1684 after being exposed to 25 mM D-(+) glucose.

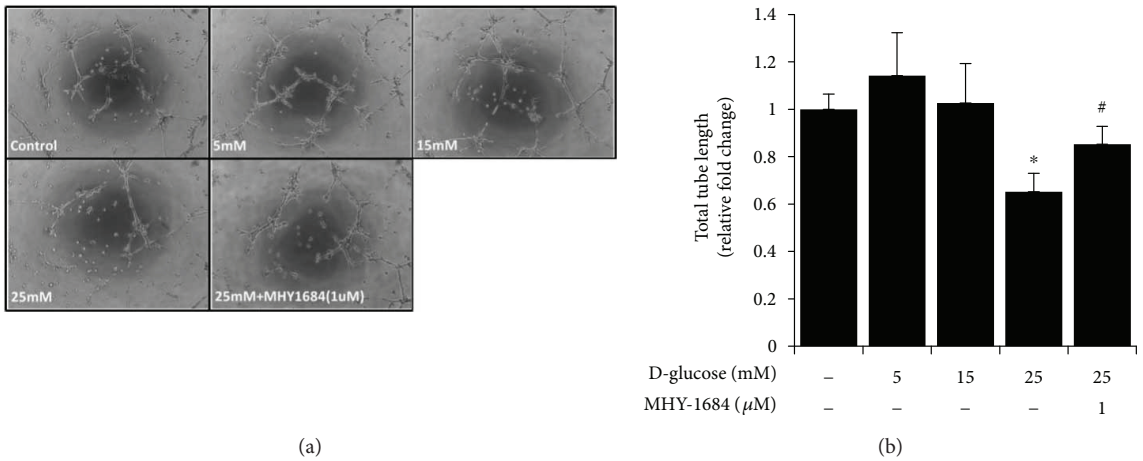

Figure 5: MHY-1684 rescues the tube-forming capacity of hCPCs during hyperglycemia. (a) The tube formation ability of hCPCs treated with 1 μM MHY-1684 and 25 mM D-(+) glucose for 72 h. The ability for hCPCs to form capillary-like structures in vitro was evaluated using a Matrigel tube formation assay. (b) Quantification of the total length of tube-like structures. $^{*}p < 0.05$ as compared with the control group, $^{\#}p < 0.05$ as compared with the group treated with 25 mM D-(+) glucose for 72 h.

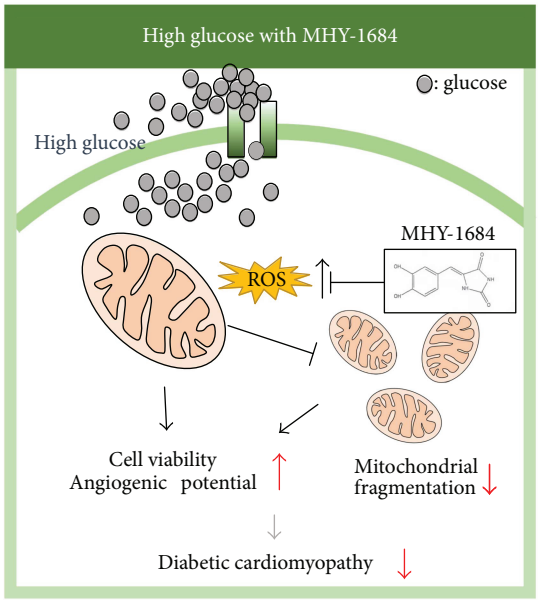

Figure 6: Proposed working model. MHY-1684 plays a critical role in ROS generation, restores the angiogenic potential, and reduces cell death of hCPCs via regulating mitochondrial dynamics.

fusion, is restored following hCPC treatment with MHY-1684. In contrast, when hCPCs are treated with MHY-1684, the expression of Mfn-1 is significantly restored, suggesting that treatment with MHY-1684 might affect the activation and inhibition of mitochondrial dynamics-related signaling and mitochondrial function in response to ROS stress (Figure 4(c)).

3.7. Cytoprotective Effect of MHY-1684 on hCPC Tube-Forming Capacity during Hyperglycemia. To determine whether pretreatment with MHY-1684 enhances the angiogenic bioactivity of hCPCs in response to hyperglycemia, we examined the tube-forming potential of MHY-1684-treated hCPCs. The tube-forming capacity decreased significantly in the presence of 25 mM D-(+) glucose. However, the hyperglycemia-reduced tube-forming capacity of hCPCs was rescued significantly when cotreated with MHY-1684 (Figures 5(a) and 5(b)), suggesting that MHY-1684 improves the angiogenic function of hCPCs during hyperglycemia.

4. Discussion

Although the clinical impact of CPC-based therapies is emerging [26] and the therapeutic effect of CPCs in ischemic cardiovascular disease models seems to be clearly demonstrated, there is a limitation based on the quality and quantity of resident CPCs that can be used for therapeutic applications in a clinical setting. The medical community is limited because patient-derived CPCs possess reduced therapeutic bioactivities due to multiple risk factors including age, smoking, diabetics, and hyperglycemia. In order to achieve a significant therapeutic effect from transplanted CPCs, there has been an increased focus on the discovery of novel function-modulating factors including ROS scavengers [13–15]. In this report, we identified a novel antioxidant, MHY-1684, which enhanced hCPC bioactivity against ROS-related diabetic cardiomyopathy. Interestingly, short-term treatment with MHY-1684 in ex vivo-expanded CPCs attenuated hyperglycemia-induced mitochondrial fragmentation and cell death. This suggests that MHY-1684 might be a novel priming agent for CPC-based therapies for diabetic cardiomyopathy via reducing mitochondrial ROS production and regulating mitochondrial dynamics.

Mitochondria are energy-producing organelles that are mobile and harbor dynamic network structures. Maintaining mitochondrial dynamics is an important part of tissue homeostasis in that disordered mitochondrial dynamics is associated with various diseases [27]. Existing evidence also suggests that mitochondrial fragmentation occurs during hyperglycemia and thereby causes hCPC dysfunction [17]. Our results support the importance of the proper modulation of hyperglycemia-related mitochondrial dynamics. Pretreatment of hCPCs with MHY-1684 dramatically reduced hyperglycemia-related mitochondria fission via attenuating the activation of Drp-1 and Fis-1. This was demonstrated by Western blotting using both p-Drp-1^{616} and Fis-1 antibodies (Figures 4(a) and 4(b)). In contrast, both p-Drp-1^{637} and the fusion-related protein, Mfn-1, became reversely activated during hyperglycemia. These results suggest that the disordered mitochondrial dynamics is partially restored by MHY-1684 (Figure 4(c)).

Mitochondrial ROS are formed naturally as a metabolic by-product in cells, and they play crucial roles in cell signaling, proliferation, homeostasis, and cell death [28]. In the clinical setting, hyperglycemia causes the overproduction of ROS, which disrupts cell structures and causes cell death [29], leading to cardiomyopathy. To reduce the effects of hyperglycemia such as the development of diabetic cardiomyopathy, mitochondrial ROS needs to be controlled. Therefore, our novel ROS scavenger, which enhances cellular function including tube formation and hCPC cell survival, might be therapeutic in a CPC-based therapy against diabetic cardiomyopathy. Specific modulation of ROS-related hyperglycemia is also an important issue because hyperglycemia inhibits the angiogenic capacity of transplanted cells and resident stem/progenitor cells and suppresses cell homing by regulating the ERK1/2 pathway [9, 21]. In our current study, we demonstrated that the attenuation of ROS by MHY-1684 activates the ERK1/2 and AKT signaling pathways. Multiple studies support the fact that ROS overproduction suppresses ERK1/2 and AKT signaling and eventually leads to cell death [30, 31], suggesting that augmented ERK1/2 and AKT signaling partially affects the rescue process mediated by MHY-1684 in hyperglycemia-induced diabetic cardiomyopathy.

5. Conclusion

Our results demonstrated that MHY-1684 enhances hCPC cellular function against ROS and hyperglycemia. Importantly, MHY-1684 attenuated mitochondrial ROS generation during hyperglycemia and significantly reduced

mitochondrial fragmentation via regulating Drp-1 and Fis-1. MHY-1684 also decreased ROS-induced cell death (Figure 6). In conclusion, the novel compound, MHY-1684, is an ROS scavenger that might be an effective therapeutic agent for the CPC-based therapy against diabetic cardiomyopathy.

Data Availability

The data used to support the findings of this study are available from the corresponding author upon request.

Conflicts of Interest

The authors declare that there are no conflicts of interest regarding the publication of this article.

Acknowledgments

This work was supported by a grant from the National Research Foundation (NRF-2015M3A9B4051053) and Korean Health Technology R&D Project, Ministry of Health and Welfare (HI17C1662) funded by the Korean government. The authors thank Aging Tissue Bank at Busan National University for providing materials and research information.

Supplementary Materials

Supplementary Table 1: $ONOO^-$ (10 μM) scavenging activities of chemicals (40 μM). The potency of scavenging activity following the addition of authentic $ONOO^-$ or SIN-1 was in the following order: MHY-1684 > penicillamine > resveratrol. MHY-1684 showed the strongest effect for scavenging $ONOO^-$ of chemicals. *(Supplementary Materials)*

References

[1] Authors/Task Force Members, L. Rydén, P. J. Grant et al., "ESC guidelines on diabetes, pre-diabetes, and cardiovascular diseases developed in collaboration with the EASD: the task force on diabetes, pre-diabetes, and cardiovascular diseases of the European Society of Cardiology (ESC) and developed in collaboration with the European Association for the Study of Diabetes (EASD)," *European Heart Journal*, vol. 34, no. 39, pp. 3035–3087, 2013.

[2] D. S. H. Bell, "Heart failure: the frequent, forgotten, and often fatal complication of diabetes," *Diabetes Care*, vol. 26, no. 8, pp. 2433–2441, 2003.

[3] T. P. Di Lorenzo, M. Peakman, and B. O. Roep, "Translational mini-review series on type 1 diabetes: systematic analysis of T cell epitopes in autoimmune diabetes," *Clinical & Experimental Immunology*, vol. 148, no. 1, pp. 1–16, 2007.

[4] S. Hagg, L. M. Thorn, J. Putaala et al., "Incidence of stroke according to presence of diabetic nephropathy and severe diabetic retinopathy in patients with type 1 diabetes," *Diabetes Care*, vol. 36, no. 12, pp. 4140–4146, 2013.

[5] A. E. Kitabchi, G. E. Umpierrez, J. M. Miles, and J. N. Fisher, "Hyperglycemic crises in adult patients with diabetes," *Diabetes Care*, vol. 32, no. 7, pp. 1335–1343, 2009.

[6] X. Han, D. R. Abendschein, J. G. Kelley, and R. W. Gross, "Diabetes-induced changes in specific lipid molecular species in rat myocardium," *Biochemical Journal*, vol. 352, no. 1, pp. 79–89, 2000.

[7] D. A. Chistiakov, A. N. Orekhov, and Y. V. Bobryshev, "The impact of FOXO-1 to cardiac pathology in diabetes mellitus and diabetes-related metabolic abnormalities," *International Journal of Cardiology*, vol. 245, pp. 236–244, 2017.

[8] S. Kobayashi and Q. Liang, "Autophagy and mitophagy in diabetic cardiomyopathy," *Biochimica et Biophysica Acta (BBA) - Molecular Basis of Disease*, vol. 1852, no. 2, pp. 252–261, 2015.

[9] A. S. D. Molgat, E. L. Tilokee, G. Rafatian et al., "Hyperglycemia inhibits cardiac stem cell-mediated cardiac repair and angiogenic capacity," *Circulation*, vol. 130, no. 11, Supplemet 1, pp. S70–S76, 2014.

[10] P. Rosen, P. P. Nawroth, G. King, W. Moller, H. J. Tritschler, and L. Packer, "The role of oxidative stress in the onset and progression of diabetes and its complications: a summary of a Congress Series sponsored by UNESCO-MCBN, the American Diabetes Association and the German Diabetes Society," *Diabetes/Metabolism Research and Reviews*, vol. 17, no. 3, pp. 189–212, 2001.

[11] H. Azumi, N. Inoue, Y. Ohashi et al., "Superoxide generation in directional coronary atherectomy specimens of patients with angina pectoris: important role of NAD(P)H oxidase," *Arteriosclerosis, Thrombosis, and Vascular Biology*, vol. 22, no. 11, pp. 1838–1844, 2002.

[12] E. Takimoto and D. A. Kass, "Role of oxidative stress in cardiac hypertrophy and remodeling," *Hypertension*, vol. 49, no. 2, pp. 241–248, 2007.

[13] J. G. Cho, J. H. Lee, S. H. Hong et al., "Tauroursodeoxycholic acid, a bile acid, promotes blood vessel repair by recruiting vasculogenic progenitor cells," *Stem Cells*, vol. 33, no. 3, pp. 792–805, 2015.

[14] J. Y. Kim, J. S. Lee, Y. S. Han et al., "Pretreatment with lycopene attenuates oxidative stress-induced apoptosis in human mesenchymal stem cells," *Biomolecules & Therapeutics*, vol. 23, no. 6, pp. 517–524, 2015.

[15] S. H. Choi, H. B. Joo, S. J. Lee et al., "Oleuropein prevents angiotensin II-mediated: human vascular progenitor cell depletion," *International Journal of Cardiology*, vol. 181, pp. 160–165, 2015.

[16] J. Piquereau, F. Caffin, M. Novotova et al., "Mitochondrial dynamics in the adult cardiomyocytes: which roles for a highly specialized cell?," *Frontiers in Physiology*, vol. 4, p. 102, 2013.

[17] H. Y. Choi, J. H. Park, W. B. Jang et al., "High glucose causes human cardiac progenitor cell dysfunction by promoting mitochondrial fission: role of a GLUT1 blocker," *Biomolecules & Therapeutics*, vol. 24, no. 4, pp. 363–370, 2016.

[18] K. N. Papanicolaou, R. Kikuchi, G. A. Ngoh et al., "Mitofusins 1 and 2 are essential for postnatal metabolic remodeling in heart," *Circulation Research*, vol. 111, no. 8, pp. 1012–1026, 2012.

[19] Y. Chen, Y. Liu, and G. W. Dorn, "Mitochondrial fusion is essential for organelle function and cardiac homeostasis," *Circulation Research*, vol. 109, no. 12, pp. 1327–1331, 2011.

[20] S. Wu, F. Zhou, Z. Zhang, and D. Xing, "Mitochondrial oxidative stress causes mitochondrial fragmentation via differential modulation of mitochondrial fission–fusion proteins," *The FEBS Journal*, vol. 278, no. 6, pp. 941–954, 2011.

[21] T. She, X. Wang, Y. Gan et al., "Hyperglycemia suppresses cardiac stem cell homing to peri-infarcted myocardium via regulation of ERK1/2 and p38 MAPK activities," *International Journal of Molecular Medicine*, vol. 30, no. 6, pp. 1313–1320, 2012.

[22] S. H. Choi, S. Y. Jung, S. M. Yoo et al., "Amine-enriched surface modification facilitates expansion, attachment, and maintenance of human cardiac-derived c-kit positive progenitor cells," *International Journal of Cardiology*, vol. 168, no. 1, pp. 100–107, 2013.

[23] H. R. Choi, J. S. Choi, Y. N. Han, S. J. Bae, and H. Y. Chung, "Peroxynitrite scavenging activity of herb extracts," *Phytotherapy Research*, vol. 16, no. 4, pp. 364–367, 2002.

[24] A. J. Gomes, C. N. Lunardi, S. Gonzalez, and A. C. Tedesco, "The antioxidant action of *Polypodium leucotomos* extract and kojic acid: reactions with reactive oxygen species," *Brazilian Journal of Medical and Biological Research*, vol. 34, no. 11, pp. 1487–1494, 2001.

[25] M. L. Gonçalez, D. G. Marcussi, G. M. F. Calixto, M. A. Corrêa, and M. Chorilli, "Structural characterization and in vitro antioxidant activity of kojic dipalmitate loaded W/O/W multiple emulsions intended for skin disorders," *BioMed Research International*, vol. 2015, Article ID 304591, 8 pages, 2015.

[26] R. Bolli, A. R. Chugh, D. D'Amario et al., "Cardiac stem cells in patients with ischaemic cardiomyopathy (SCIPIO): initial results of a randomised phase 1 trial," *The Lancet*, vol. 378, no. 9806, pp. 1847–1857, 2011.

[27] S. L. Archer, "Mitochondrial dynamics — mitochondrial fission and fusion in human diseases," *The New England Journal of Medicine*, vol. 369, no. 23, pp. 2236–2251, 2013.

[28] T. P. Devasagayam, J. C. Tilak, K. K. Boloor, K. S. Sane, S. S. Ghaskadbi, and R. D. Lele, "Free radicals and antioxidants in human health: current status and future prospects," *The Journal of the Association of Physicians of India*, vol. 52, pp. 794–804, 2004.

[29] T. V. Fiorentino, A. Prioletta, P. Zuo, and F. Folli, "Hyperglycemia-induced oxidative stress and its role in diabetes mellitus related cardiovascular diseases," *Current Pharmaceutical Design*, vol. 19, no. 32, pp. 5695–5703, 2013.

[30] Y. Poloz and V. Stambolic, "Obesity and cancer, a case for insulin signaling," *Cell Death & Disease*, vol. 6, no. 12, article e2037, 2015.

[31] B. Zhang, Q. Y. Xie, Y. Quan, X. M. Pan, and D. F. Liao, "Reactive oxygen species induce cell death via Akt signaling in rat osteoblast-like cell line ROS 17/2.8," *Toxicology and Industrial Health*, vol. 31, no. 12, pp. 1236–1242, 2015.

Hindawi
Oxidative Medicine and Cellular Longevity
Volume 2018, Article ID 4153574, 8 pages
https://doi.org/10.1155/2018/4153574

Research Article

Serum 8-Oxo-dG as a Predictor of Sensitivity and Outcome of Radiotherapy and Chemotherapy of Upper Gastrointestinal Tumours

Ali Pour Khavari,[1] **Yongping Liu**,[2] **Ellen He**,[3] **Sven Skog**,[3] **and Siamak Haghdoost**[1,4]

[1]*Department of Molecular Biosciences, The Wenner-Gren Institute, Stockholm University, Svante Arrhenius vag 20C, 10691 Stockholm, Sweden*
[2]*Clinical Oncology Laboratory, Department of Oncology, Changzhou Tumour Hospital Affiliated to Suzhou University, Honghe Road No. 68, Xinbei Area, Changzhou 213032, China*
[3]*Sino-Swed Molecular Bio-Medicine Research Institute, Shenzhen, China*
[4]*CIMAP-LARIA, University of Caen Normandy, Campus Jules Horowitz, Bd. Henri Becquerel, 14076 Caen, France*

Correspondence should be addressed to Yongping Liu; liuyongping026@126.com

Received 9 January 2018; Revised 16 March 2018; Accepted 4 April 2018; Published 23 May 2018

Academic Editor: Claudio Cabello-Verrugio

The level of oxidative stress is important in the initiation and progression of various age-related diseases, such as cancer. The level of oxidative stress may also play a significant role in cancer patients' response to treatment. We aimed to investigate whether serum 8-oxo-dG as a marker of oxidative stress is a predictor of tumour response. We used modified ELISA with a two-step filtration to analyse 8-oxo-dG in serum. The relationship between 8-oxo-dG levels, tumour response, and toxicity was studied in 19 oesophageal cancer patients who received radiotherapy and 16 gastric cancer patients who received chemotherapy. In the radiotherapy and the merged radio- and chemotherapy groups, the baseline levels of 8-oxo-dG were significantly lower in responder patients than in nonresponder patients and the increments after treatment were greater. In comparison with patients whose serum 8-oxo-dG levels decrease after treatment, patients with increasing levels had a longer median "progression-free survival." Our results, although preliminary, suggest that serum levels of 8-oxo-dG may potentially be used to predict the sensitivity and outcome of radiotherapy and chemotherapy of upper gastrointestinal tumours. Patients with 8-oxo-dG levels that are low prior to treatment and subsequently increase after treatment may be more likely to benefit from the therapy.

1. Introduction

Oesophageal and gastric cancers are significant causes of morbidity and mortality. In 2012, gastric cancer was estimated to be the fifth most common cancer worldwide and the third leading cause of cancer death. While oesophageal cancer is less common than gastric cancer, its high mortality rate places it as the sixth leading cause of cancer-related deaths worldwide. Risk factors such as heavy smoking, genetic background, heavy alcohol consumption, certain food types, and hot beverages increase the risk of oesophageal and gastric cancer. In general, both oesophageal and gastric cancers are associated with poor prognosis despite improvements to their treatments by including advanced diagnostic and therapeutic methods [1, 2]. Prognostic biomarkers may play a significant role in choosing efficient treatments, reducing side effects, and improving quality of life. Currently, the main treatments for oesophageal and gastric cancers are surgery, radiotherapy, and chemotherapy, separately or in combination. The cytotoxic effects of radiotherapy and chemotherapy are mediated partly by the induction of reactive oxygen species (ROS), which leads to oxidative stress. Due to their unpaired electrons, ROS are unstable and react with other molecules, for example, lipids, proteins, RNA, DNA, dNTP, and NTP, modifying their structures and functions. Consequently, the functions of the cell become compromised. One of the

frequently studied oxidative DNA base damages is 8-hydroxy-2′-deoxyguanosine (8-oxo-dG). 8-Oxo-dG is produced when ROS, for example, hydroxyl radicals, react with guanine in DNA or deoxyguanosine triphosphate (dGTP) in the cytoplasm. We have previously shown that the origin of extracellular 8-oxo-dG is the cytoplasmic content of dGTP which can be converted into 8-oxo-dGTP by free radical attack [3–5]. 8-Oxo-dG is excreted into extracellular environments such as urine, blood, and saliva. Elevated oxidative stress can partly explain the characteristics of cancer cells, for example, genomic instability, elevated proliferation rate, chemotherapy resistance, and metastasis [6].

Several publications show that levels of oxidative stress, measured with 8-oxo-dG in urine or blood serum, can be a useful biomarker for the response to radiation therapy and chemotherapy in cancer patients [7–9]. Additionally, several research groups have shown that the levels of 8-oxo-dG and MTH1 protein, an 8-oxo-dGTPase, play important prognostic roles in oesophageal as well as in gastric cancers [10–12]. However, the commercial ELISA kits available for detection of extracellular 8-oxo-dG are not specific [13], and other chromatographic-based methods, for example, high-pressure liquid chromatography (HPLC) with electrochemical detection or liquid chromatography with mass spectrometry detection (LC-MS/MS), are expensive, require sophisticated equipment and highly skilled personnel, and cannot be routinely used in the oncological clinics. Therefore, we have set up a sensitive and specific method where we first filter the serum sample on a Bond Elut column to isolate a fraction containing 8-oxo-dG and then use this fraction to determine 8-oxo-dG by a modified ELISA [3, 14].

We have previously reported that the levels of radiation-induced urinary and serum 8-oxo-dG could be used as a marker for determining individual radiation sensitivity in breast as well as in head and neck cancer patients [15–17]. In the present study, we investigated the relationship between serum levels of 8-oxo-dG and the therapy outcome of oesophageal and gastric cancers as well as therapy-related side effects. Blood samples from patients were collected at two time points: (1) before the start of oncological treatment and (2) two weeks after completed treatment. The levels of 8-oxo-dG in their blood serum were measured using our modified ELISA method.

2. Materials and Methods

2.1. Patients. Thirty-five patients with malignant tumours (stages III to IV) were recruited during March 2015 to July 2015 and underwent radiotherapy or chemotherapy at Changzhou Tumour Hospital. Patients with two different diagnoses were studied: 19 with oesophageal and 16 with gastric cancer. All patients had measurable lesions. The total group of patients is composed of 29 males and 6 females, ranging in age from 34 to 79 years, with a median age of 66 years. None of them had received previous radiotherapy or chemotherapy. The tumours were histologically and/or cytologically confirmed. The clinical stage of the tumours was confirmed based on the results of examination by X-ray, computed tomography (CT), magnetic resonance imaging (MRI), and other imaging examinations. All patients had an Eastern Cooperative Oncology Group (ECOG) performance status of ≤2, adequate bone marrow reserve, normal liver function, normal heart function, and normal kidney function. Furthermore, the patients had no history of prior malignancy. The study was performed in accordance with the ethical standards and approved by the Chinese Ethical Committee at Changzhou Tumour Hospital (Dnr 2015SY-001-01).

2.2. Treatments. Among the patients, 19 patients with local advanced oesophageal cancer received radiotherapy with 6 MeV photons. The planning target volume (PTV) encompassed the primary tumour site and a margin of approximately 1.5 cm. The prescription doses of PTV were 60 Gy in 30 fractions over a period of six weeks. 16 gastric cancer patients were treated with standard chemotherapy drug combination: folinic acid, fluorouracil, and oxaliplatin (FOLFOX4) 4 times during 2 weeks.

2.3. Response Evaluation. Tumour response was assessed according to the response evaluation criteria in solid tumours (RECIST) [18]: a complete response (CR) was defined as a complete disappearance of all objective evidence of disease, a partial response (PR) was defined as at least a 30% decrease in the sum of the longest diameters (LD) of tumour taking the baseline sum diameters as the reference, progressive disease (PD) was defined as a 20% increase in the sum of the LD of tumours or the appearance of one or more new lesions, and stable disease (SD) was defined as neither sufficient shrinkage to qualify for PR nor sufficient increase to qualify for PD. In this study, patients who achieved a CR or PR were classified as responders and all remaining patients were considered nonresponders.

2.4. Follow-Up. Physical examinations, measurement of carcinoembryonic antigen CA199 and thymidine kinase 1 (marker of proliferation) levels, and whole-body computed tomography were carried out every 3 months in the first year and every 6 months thereafter to evaluate therapy response. Progression-free survival (PFS) was the time from study entry until disease progression, death, or the day of the last follow-up visit, whichever came first. The Radiation Therapy Oncology Group (RTOG) scoring schema [19] was used to evaluate the acute radiation-related toxicity to the chest wall skin and oesophageal mucosa. In order to facilitate statistical analysis, we classified patients displaying side effects of RTOG grades 2, 3, and 4 as the moderate or severe group. The toxicity of chemotherapy was graded according to NCI-CTC, version 4.0 (available at http://www.oncology.tv/SymptomManagement).

2.5. ELISA Measurement of Serum 8-Oxo-dG. 3 ml of blood samples was collected in tubes without anticoagulant. After about two hours, the blood serum was isolated by centrifuging the tubes at 250 ×g for 20 minutes. 8-Oxo-dG was measured using a modified competitive ELISA as described previously [3, 4, 16]. All samples were coded and analysed blindly. The ELISA kit was provided by Health Biomarkers Sweden AB. Briefly, 800 μl blood serum was filtered using a C18 solid phase extraction

Bond Elut column (Varian, CA) as described previously [14]. The filtration step is necessary to remove products other than 8-oxo-dG that could cross-react with the monoclonal antibody. The purified samples were lyophilised and reconstituted to 1 ml by adding PBS. The filtration step was repeated once more. 90 μl of the purified samples was processed further for the detection of 8-oxo-dG according to the protocol provided by the company. The absorbance of the samples was read at 450 nm using an automatic ELISA plate reader. Each sample was analysed in triplicate, and the samples belonging to one individual patient were analysed using the same 96-well ELISA plate. A standard curve for 8-oxo-dG (0.05–10 ng/ml) was established for each plate covering the range of 8-oxo-dG in the samples. Validation of the modified ELISA method was performed by HPLC-EC during the previous study [4]. Comparisons between the modified ELISA and the HPLC-EC methods showed a linear correlation at the concentration range found in human blood serum ($r^2 = 0.87$, $p < 0.05$). There was no correlation between ELISA and HPLC-EC results when unfiltered samples were used.

2.6. Measurement of Serum TK1. The concentration of serum TK1 (STK1p) was measured using a commercial kit based on an improved chemiluminescent (ECL) dot blot assay as described by the manufacturer (SSTK Ltd., Shenzhen, China). 3 μl samples of serum was directly applied to a nitrocellulose membrane in duplicate. The serum samples were probed with an anti-TK1 chicken IgY antibody raised against a peptide (residue 195-225, GQPAG PDNKE NCPVP GKPGE AVAAR KLFAPQ). The TK1 peptide was dotted at different concentrations (2.2, 6.6, and 20 pM) as a quality control standard. The intensities of the spots on the membrane were determined by the CIS-l Imaging System (SSTK Ltd., Shenzhen, China). From the intensities of the TK1 quality control standards of known concentrations, the concentration of STK1p was calculated and expressed as pM. For a detailed description of the STK1p assay, see Chen et al. [20]. Within this study, 2.0 pM of STK1p was used as a risk threshold value.

2.7. Measurement of Serum CA199. Serum CA199 levels were measured using the ADVIA Centaur® XP automated Immunoassay System (Siemens Healthcare Diagnostics, Erlangen, Germany) according to the manufacturer's protocol. Levels of serum CA199 ≥ 37 U/ml were considered abnormal.

2.8. Statistical Methods. For the statistical analysis, the paired sample *t*-test and the independent sample *t*-test were used. The chi-square test was used to determine correlations between the changes of 8-oxo-dG concentration and the responses of tumour to treatments or acute side effects. Kaplan-Meier survival curves and the log-rank test were used to analyse univariate distributions for progression-free survival. A *p* value lower than 0.05 was considered to indicate a significant difference.

3. Results

3.1. Associations between Serum 8-Oxo-dG and Clinicopathological Features. In the merged group of patients, the baseline 8-oxo-dG concentrations were significantly associated with the degree of tumour differentiation. Patients with highly differentiated tumours had higher 8-oxo-dG in the serum (0.48 ± 0.30 ng/ml) in comparison to patients with poorly or undifferentiated tumours (0.25 ± 0.17 ng/ml) (Table 1). Serum 8-oxo-dG was significantly related to the tumour marker CA199 and to gender, but not to TK1 (Table 1).

3.2. Associations between Changes of Serum 8-Oxo-dG Level and Tumour Response. To investigate if changes of serum 8-oxo-dG level are associated with tumour response, we divided the patients into 2 groups: those who showed objective response (CR + PR) and individuals with no response (PD + SD), respectively. Additionally, the association between tumour response and 8-oxo-dG was investigated in the patients treated with radiotherapy (oesophageal cancer) or chemotherapy (gastric cancer) as separate groups and as one merged group. The changes of 8-oxo-dG concentrations are summarised in Table 2. We found that the changes of serum 8-oxo-dG were associated with the tumour response. In Table 3, the levels of 8-oxo-dG in the serum are presented for each therapy group based on their response before and 2 weeks after treatment. As shown in Table 3, the levels of 8-oxo-dG increased in the merged group, CR + PR, from 0.21 to 0.38 ng/ml ($p < 0.05$). The increases for radiotherapy patients were from 0.25 to 0.43 ng/ml ($p < 0.05$) and for chemotherapy patients from 0.17 to 0.27 ng/ml (nonsignificant). For SD + PD groups, a decrease or no change of 8-oxo-dG was found when the levels of 8-oxo-dG after treatment were compared to the baseline levels. To explore whether baseline serum 8-oxo-dG level could predict the outcome of radiotherapy and chemotherapy, we analysed the relationship between baseline serum 8-oxo-dG and tumour response in different treatment groups. The overall results presented in Table 3 indicate that the CR + PR groups have lower baseline 8-oxo-dG in comparison to the SD + PD groups. These observations suggest that patients with low baseline levels of serum 8-oxo-dG that then increase markedly after treatment are more sensitive to treatment.

3.3. Associations between Changes of Serum 8-Oxo-dG Level and Side Effects of Radiotherapy or Chemotherapy. To investigate if changes of serum 8-oxo-dG level are associated with acute side effects, we compared the serum 8-oxo-dG concentrations before and after treatment in patients with severe side effects to the concentrations in the patients that displayed almost no side effects. In the radiotherapy group, we found that an increase in serum 8-oxo-dG level was closely related to acute skin reactions and acute oesophageal mucosa reactions ($p = 0.047$ and 0.018, resp.). In the chemotherapy group, patients with an increase in serum 8-oxo-dG appeared to be more prone to suffer from 3 or 4 degrees of bone marrow suppression and 3 or 4 degrees of gastrointestinal reactions when compared to patients with declining concentrations, although the difference between the groups did not reach statistical significance ($p = 0.09$ and $p = 0.21$, resp.) (Table 4).

Table 1: Associations between serum 8-oxo-dG level and characteristics of the study cohorts.

Type	Mean (ng/ml)	±SD	n	p value
Age (median age: 66 years)				
≥66	0.28	0.19	21	
<66	0.33	0.29	14	0.511
Gender				
Male	0.26	0.18	29	
Female	0.48	0.36	6	0.049
CA199				
≥37 U/ml	0.44	0.35	9	
<37 U/ml	0.24	0.15	26	0.027
TK1				
≥2 pmol/ml	0.30	0.20	22	
<2 pmol/ml	0.29	0.25	13	0.954
Differentiation				
Highly or moderately differentiated	0.48	0.30	8	
Poorly differentiated or undifferentiated	0.25	0.17	27	0.011

Table 2: Associations between changes of serum 8-oxo-dG and tumour response.

Changes of serum 8-oxo-dG	Tumour response CR + PR	SD + PD	χ^2	p value
All patients ($n = 35$)				
Increase	11	3		
Decline	6	15	8.41	0.006
The radiotherapy group ($n = 19$)				
Increase	7	1		
Decline	4	7	4.96	0.026
The chemotherapy group ($n = 16$)				
Increase	4	2		
Decline	2	8	3.48	0.062

3.4. Associations between Serum 8-Oxo-dG Levels and Progression-Free Survival. The median PFS was 9 months (range, 2–17 months). Figure 1(a) shows the Kaplan-Meier survival curves for all patients with serum 8-oxo-dG level decline or increase. The changes in the serum concentration of 8-oxo-dG were calculated by subtracting the baseline concentration before treatment from the concentration of serum 8-oxo-dG two weeks after the radiotherapy or chemotherapy. Compared to the patients whose serum 8-oxo-dG declined, the patients with increasing serum 8-oxo-dG concentration had a significantly longer median PFS (median PFS, no defined versus 8 months). Figures 1(b) and 1(c) show the Kaplan-Meier survival curves for patients who received radiotherapy and chemotherapy, respectively. When compared to patients whose serum 8-oxo-dG declined, chemotherapy-treated patients with increasing serum 8-oxo-dG concentrations had significantly longer median PFS, while the difference did not reach statistical significance for the radiotherapy group (median PFS, no defined versus 7 months in the radiotherapy group and no defined versus no defined in the chemotherapy group, $p < 0.086$ and 0.001, resp.).

The median time of follow-up was 9 months. Some of the patients underwent follow-up at 17 months. During the study period, 4 of the 35 patients (11.4%) deceased. As a result of the low death rate, a meaningful determination of association between serum 8-oxo-dG level and death was not possible to perform.

4. Discussion

Within the present investigation, we used a modified ELISA method for the detection of 8-oxo-dG in blood serum of the patients. Extracellular 8-oxo-dG originates from 8-oxo-dGTP in the nucleotide pool when free radicals react with dGTP. MTH1 hydrolyses 8-oxo-dGTP to 8-oxo-dGMP. 8-Oxo-dGMP is further dephosphorylated, and 8-oxo-dG is released from the intra- to the extracellular milieu where it can be detected and used as a marker for oxidative stress [3, 4]. We found that the baseline levels of 8-oxo-dG in the serum of responder patients (chemo- and radiotherapy—CR + PR) were significantly lower compared to the levels in nonresponder patients (SD + PD) (0.21 ± 0.15 ng/ml and 0.52 ± 0.34 ng/ml, resp.). When breaking down the results into radiotherapy and chemotherapy groups, we still observe a significantly lower level of 8-oxo-dG in the CR + PR group as compared to the SD + PD group for radiotherapy patients (0.25 ± 0.14 and 0.46 ± 0.25 ng/ml, $p = 0.048$), while for the chemotherapy group, the level of 8-oxo-dG was only nonsignificantly lower in the CR + PR than in the SD + PD group (0.17 ± 0.16 and 0.37 ± 0.32 ng/ml, resp.). The data indicates that patients with lower 8-oxo-dG in the serum before the start of oncological treatment have better prognosis than patients with higher 8-oxo-dG levels suggesting that baseline levels of 8-oxo-dG in the serum of oesophageal and gastric cancer patients may have a prognostic value.

These results are also in accord with previously published data on ovarian, renal, and hepatocellular carcinoma as well

Table 3: Concentrations of serum 8-oxo-dG before and after the treatment.

Types	All patients (ng/ml)		Radiotherapy group (ng/ml)		Chemotherapy group (ng/ml)	
	CR + PR	SD + PD	CR + PR	SD + PD	CR + PR	SD + PD
Before treatment	0.21 ± 0.15	$0.52 \pm 0.34^{\star}$	0.25 ± 0.14	$0.46 \pm 0.25^{\star\star}$	0.17 ± 0.16	0.37 ± 0.32
After treatment	$0.38 \pm 0.32^{*}$	0.35 ± 0.23	$0.43 \pm 0.33^{**}$	0.33 ± 0.17	0.27 ± 0.24	0.39 ± 0.36

$^{*}p = 0.04$ and $^{**}p = 0.05$ compared with the values before treatment; $^{\star}p = 0.013$ and $^{\star\star}p = 0.048$ compared with the values in the CR + PR groups.

Table 4: Associations between changes of serum 8-oxo-dG and acute side effects.

Acute side effects	Changes of serum 8-oxo-dG		χ^2	p value
	Increase	Decline		
Radiotherapy group ($n = 19$)				
Moderate or severe skin reaction				
Yes	3	0		
No	6	10	3.96	0.047
Moderate or severe oesophageal mucosa reaction				
Yes	4	0		
No	5	10	5.63	0.018
Chemotherapy group ($n = 16$)				
3 or 4 degrees of bone marrow suppression				
Yes	3	2		
No	2	9	2.79	0.09
3 or 4 degrees of gastrointestinal reaction				
Yes	3	3		
No	2	8	1.57	0.21

as lung cancer [8, 14, 21, 22]. It was shown that there is an association between 8-oxo-dG levels, tumour size, and clinical stage in renal cell carcinoma.

Another interesting finding is the observation of the changes in the levels of 8-oxo-dG after the treatments (Table 3). The results show that the levels of 8-oxo-dG increase significantly in the CR + PR groups, almost 2-fold, after the treatment compared to the baseline levels. On the contrary, the levels of 8-oxo-dG in the SD + PD groups (all patients and radiotherapy and chemotherapy groups) did not increase after the treatments and may have decreased. It should be noted that the baseline level of 8-oxo-dG is higher in the SD + PD group, indicating that the SD + PD patients are already at a state of stress and their cells cannot cope with additional ROS induced by the treatments. The high baseline levels of oxidative stress in the SD + PD groups may have various causes including higher metabolic activity due to large tumour burden, tumour aggressiveness, and type of tumours. In this case, exposed cells may die and not produce additional 8-oxo-dG. In contrast, patients in the CR + PR groups have lower oxidative stress; therefore, they can cope with and excrete elevated 8-oxo-dGTP induced by the treatments. A summary of the results and some suggested mechanisms that have been introduced in the discussion are presented in Figure 2.

Individual 8-oxo-dG levels before and after treatment could have a predictive value when considering the side effects of the treatments. The data presented in Table 4 indicates that radiotherapy-treated patients, whose 8-oxo-dG levels are increased after therapy, are at increased risk of severe skin reactions and severe mucosa reactions, while in comparison with the chemotherapy groups, no correlations between 8-oxo-dG levels and acute side effects were observed.

The results presented here indicate that it might be possible to distinguish the CR + PR group from the SD + PD group considering the baseline 8-oxo-dG as well as changes of 8-oxo-dG levels after the treatment. However, there is an overlap between these groups indicating that 8-oxo-dG analysis alone cannot predict sensitivity to treatment. We plan to study other factors, for example, expression of oxidative stress proteins to investigate whether combinations of protein expression with excretion of 8-oxo-dG would better predict treatment response.

CA199 is a tumour-related biomarker mainly used for monitoring the efficiency of tumour treatment, but not for diagnosis of malignant diseases. TK1 is a proliferation biomarker useful for the prognosis of recurrence and survival of malignant patients and also for early discovery of premalignancy and malignancy in health screening [23, 24]. While CA199 and 8-oxo-dG correlated with one another, TK1 did not correlate with 8-oxo-dG, indicating that 8-oxo-dG in serum may not correlate with tumour proliferation rate, but instead with the presence of tumour in the body. In this respect, CA199 behaves like 8-oxo-dG and did not correlate with serum TK1. This is in agreement with previous studies of tumour patients [23]. Thus, it should be remembered that different tumour-related biomarkers reflect different properties of a tumour and should be used in combination.

The aim of cancer treatment is to optimise the probability of tumour control while minimising the unwanted acute or late side effects. However, since there is no test for individual prediction of radio- and chemosensitivity available for clinical use, the maximal dose delivered is adapted to those few sensitive patients who show severe side effects. Therefore, developing predictive tests would allow for the majority of the cancer patients to be treated with higher doses, hopefully leading to improved tumour control and reduced side effects.

Our previous research indicates that extracellular 8-oxo-dG could be used as a biomarker to predict the sensitivity of cancer patients to radiotherapy when considering the side effects [15–17]. We established the dose-response relationship for radiation-induced oxidative stress using 8-oxo-dG in blood serum after irradiation of whole blood samples. The blood samples were collected from breast cancer as well as head and neck cancer patients, all with varying degrees of posttreatment side effects. The patients were grouped into radiosensitive and normo-sensitive groups based on their acute or late

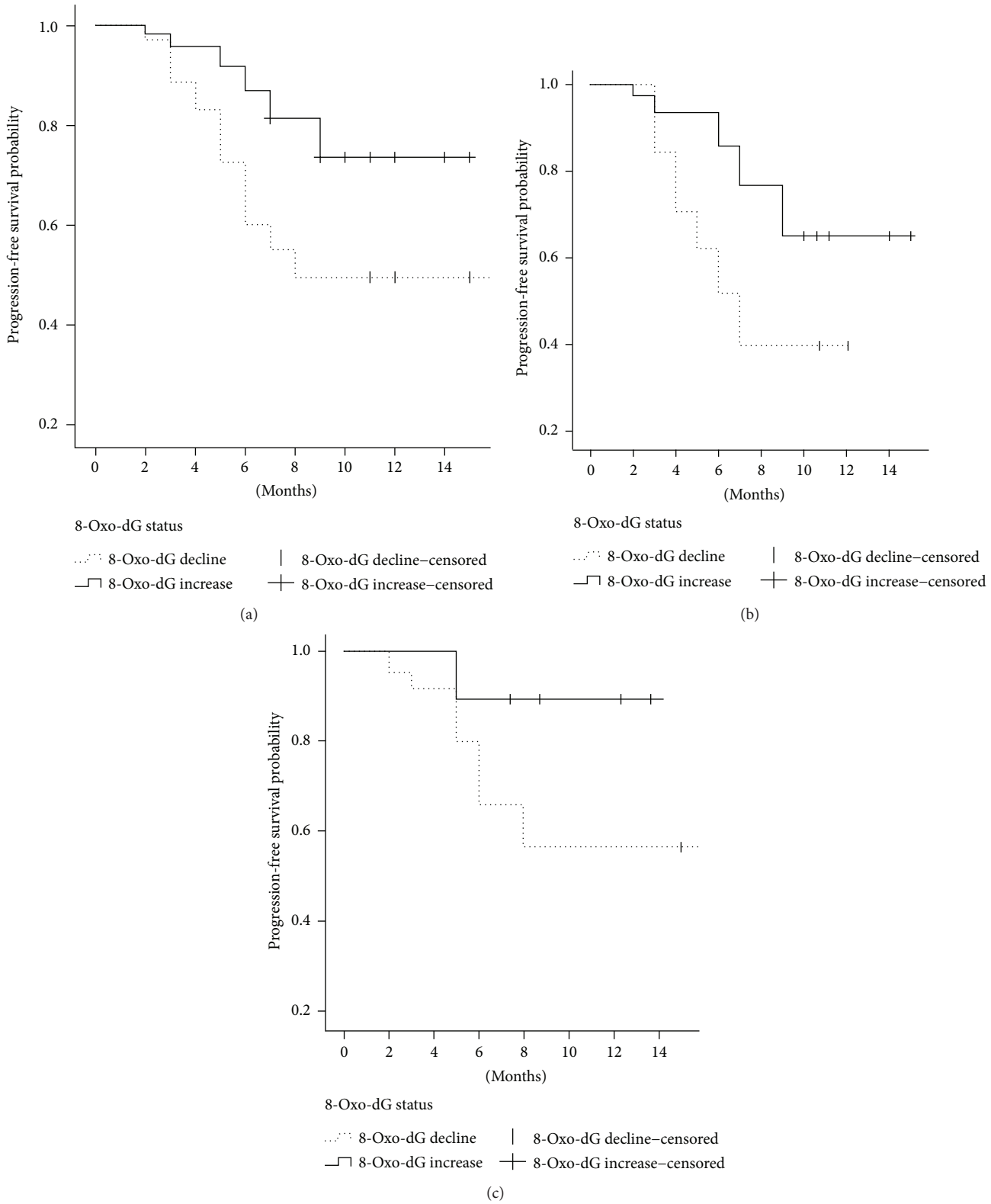

Figure 1: Kaplan-Meier survival curves for all patients (a), radiotherapy treatment (b) and chemotherapy treatment (c) with serum 8-oxo-dG level decline or increase. Censored values indicate patients who died and patients without disease progression.

radiotherapy-induced side effects, for example, acute skin reaction in breast cancer and osteoradionecrosis in head and neck cancer patients. We found that the dose response for radiation-induced 8-oxo-dG in serum differs between radiosensitive and normo-sensitive patients. In the normo-sensitive groups, the baseline levels of 8-oxo-dG were lower in comparison to those in the radiosensitive groups, and furthermore, the increments after treatment were larger.

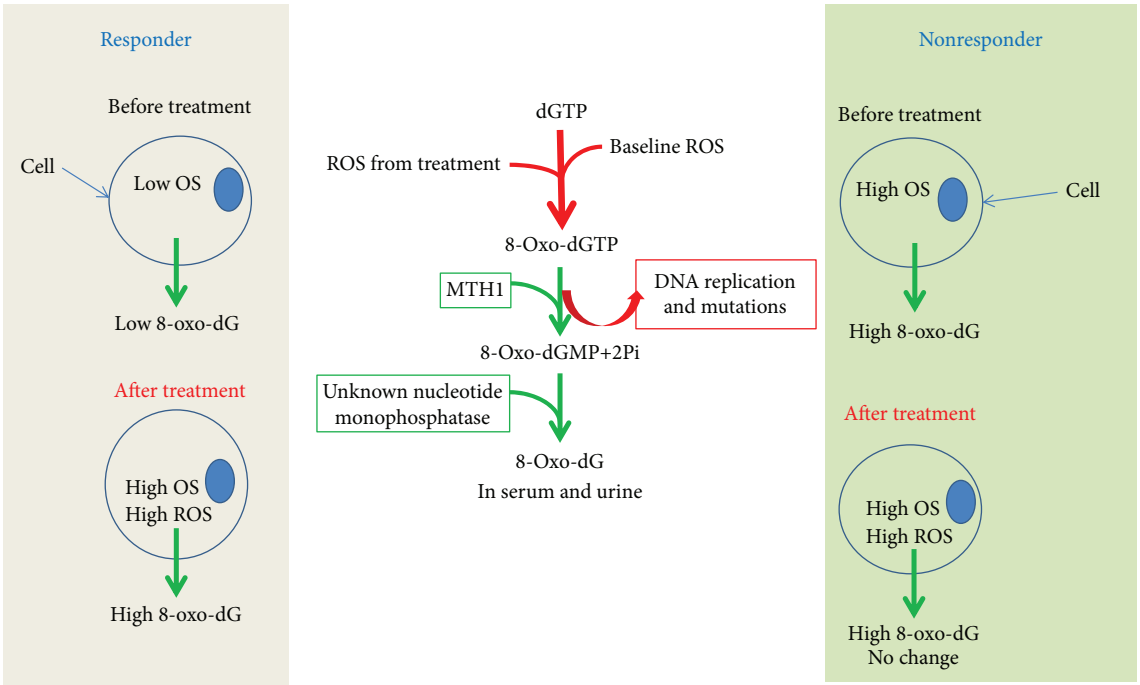

Figure 2: Schematic picture of the obtained results and possible mechanisms comparing a cell from a responder with that from a nonresponder. OS: oxidative stress.

However, 2-3 weeks after start of radiotherapy the level of 8-oxo-dG in urine of the sensitive patients increased and reached a level similar to that in normo-patients. This data may indicate that the radiosensitive patiients excrete 8-oxo-dG in a slower manner. Using a proteomic approach, we could show that several antioxidant proteins, for example, SOD1, PRDX2, and PARK7, were downregulated in the normo-sensitive patients and some antioxidant proteins, for example, BLVRB and PRDX2, were upregulated in the radiosensitive breast cancer patients [16, 25]. These results indicated that the expression of antioxidant proteins as well as oxidative stress levels play important roles in the sensitivity of breast cancer and "head and neck" cancer patients to radiotherapy. For the prediction of the effect of chemotherapy, further investigations are required. Consistent with previous studies [9], we found a significant prognostic value for 8-oxo-dG in serum for oesophageal and gastric cancers. Patients whose baseline 8-oxo-dG levels are low and increase after treatment may be more likely to benefit from radiotherapy or chemotherapy. Our findings are new but should be considered preliminary due to the low number of patients involved within this study.

Data Availability

The data used to support the findings of this study are available from the corresponding author upon request.

Conflicts of Interest

There is no conflict of interest.

Authors' Contributions

Ali Pour Khavari and Yongping Liu contributed equally to this work.

Acknowledgments

The present study was supported by the Swedish Radiation Safety Authority, the Sven and Lilly Lawskis Foundation, the Science and Technology Planning Project of Changzhou, Jiangsu Province (Grant no. CE20165052), the Changzhou Health Bureau Project (Grant no. ZD201616), the Jiangsu Province Health Department (Grant no. Z201616), the "333 Talents Training Project" of Jiangsu Province (Grant nos. 2016 III-0727 and BRA2017114), and the "Talents Training Project" for the Key Medical Innovation of Changzhou (Grant no. 2016CZLJ021). The authors would like to thank Associate Professor Siv Osterman Golkar for the valuable comments and discussions.

References

[1] Z. Song, Y. Wu, J. Yang, D. Yang, and X. Fang, "Progress in the treatment of advanced gastric cancer," *Tumor Biology*, vol. 39, no. 7, 2017.

[2] K. Fujitani, "Overview of adjuvant and neoadjuvant therapy for resectable gastric cancer in the East," *Digestive Surgery*, vol. 30, no. 2, pp. 119–129, 2013.

[3] S. Haghdoost, S. Czene, I. Näslund, S. Skog, and M. Harms-Ringdahl, "Extracellular 8-oxo-dG as a sensitive parameter for oxidative stress *in vivo* and *in vitro*," *Free Radical Research*, vol. 39, no. 2, pp. 153–162, 2005.

[4] S. Haghdoost, L. Sjolander, S. Czene, and M. Harms-Ringdahl, "The nucleotide pool is a significant target for oxidative stress," *Free Radical Biology and Medicine*, vol. 41, no. 4, pp. 620–626, 2006.

[5] S. Shakeri Manesh, T. Sangsuwan, A. Pour Khavari, A. Fotouhi, S. N. Emami, and S. Haghdoost, "MTH1, an 8-oxo-2′-deoxyguanosine triphosphatase, and MYH, a DNA glycosylase, cooperate to inhibit mutations induced by chronic exposure to oxidative stress of ionising radiation," *Mutagenesis*, vol. 32, no. 3, pp. 389–396, 2017.

[6] S. Toyokuni, K. Okamoto, J. Yodoi, and H. Hiai, "Persistent oxidative stress in cancer," *FEBS Letters*, vol. 358, no. 1, pp. 1–3, 1995.

[7] S. Borrego, A. Vazquez, F. Dasí et al., "Oxidative stress and DNA damage in human gastric carcinoma: 8-oxo-7′8-dihydro-2′-deoxyguanosine (8-oxo-dG) as a possible tumor marker," *International Journal of Molecular Sciences*, vol. 14, no. 2, pp. 3467–3486, 2013.

[8] M. Pylvas-Eerola, P. Karihtala, and U. Puistola, "Preoperative serum 8-hydroxydeoxyguanosine is associated with chemoresistance and is a powerful prognostic factor in endometrioid-type epithelial ovarian cancer," *BMC Cancer*, vol. 15, no. 1, p. 493, 2015.

[9] M. Erhola, S. Toyokuni, K. Okada et al., "Biomarker evidence of DNA oxidation in lung cancer patients: association of urinary 8-hydroxy-2′-deoxyguanosine excretion with radiotherapy, chemotherapy, and response to treatment," *FEBS Letters*, vol. 409, no. 2, pp. 287–291, 1997.

[10] W. J. Song, P. Jiang, J. P. Cai, and Z. Q. Zheng, "Expression of cytoplasmic 8-oxo-Gsn and MTH1 correlates with pathological grading in human gastric cancer," *Asian Pacific Journal of Cancer Prevention*, vol. 16, no. 15, pp. 6335–6338, 2015.

[11] J. Duan, H. Zhang, S. Li et al., "The role of miR-485-5p/NUDT1 axis in gastric cancer," *Cancer Cell International*, vol. 17, no. 1, p. 92, 2017.

[12] H. He, Y. Zhao, N. Wang, L. Zhang, and C. Wang, "8-Hydroxy-2′-deoxyguanosine expression predicts outcome of esophageal cancer," *Annals of Diagnostic Pathology*, vol. 18, no. 6, pp. 326–328, 2014.

[13] L. Barregard, P. Møller, T. Henriksen et al., "Human and methodological sources of variability in the measurement of urinary 8-oxo-7,8-dihydro-2′-deoxyguanosine," *Antioxidants & Redox Signaling*, vol. 18, no. 18, pp. 2377–2391, 2013.

[14] S. Haghdoost, Y. Maruyama, R. Pecoits-Filho et al., "Elevated serum 8-oxo-dG in hemodialysis patients: a marker of systemic inflammation?," *Antioxidants & Redox Signaling*, vol. 8, no. 11-12, pp. 2169–2173, 2006.

[15] S. Haghdoost, P. Svoboda, I. Naslund, M. Harms-Ringdahl, A. Tilikides, and S. Skog, "Can 8-oxo-dG be used as a predictor for individual radiosensitivity?," *International Journal of Radiation Oncology, Biology, Physics*, vol. 50, no. 2, pp. 405–410, 2001.

[16] S. Skiöld, I. Naslund, K. Brehwens et al., "Radiation-induced stress response in peripheral blood of breast cancer patients differs between patients with severe acute skin reactions and patients with no side effects to radiotherapy," *Mutation Research/Genetic Toxicology and Environmental Mutagenesis*, vol. 756, no. 1-2, pp. 152–157, 2013.

[17] D. Danielsson, K. Brehwens, M. Halle et al., "Influence of genetic background and oxidative stress response on risk of mandibular osteoradionecrosis after radiotherapy of head and neck cancer," *Head & Neck*, vol. 38, no. 3, pp. 387–393, 2016.

[18] E. A. Eisenhauer, P. Therasse, J. Bogaerts et al., "New response evaluation criteria in solid tumours: revised RECIST guideline (version 1.1)," *European Journal of Cancer*, vol. 45, no. 2, pp. 228–247, 2009.

[19] J. D. Cox, J. Stetz, and T. F. Pajak, "Toxicity criteria of the Radiation Therapy Oncology Group (RTOG) and the European Organization for Research and Treatment of Cancer (EORTC)," *International Journal of Radiation Oncology, Biology, Physics*, vol. 31, no. 5, pp. 1341–1346, 1995.

[20] Z. Chen, H. Zhou, S. Li et al., "Serological thymidine kinase 1 (STK1) indicates an elevated risk for the development of malignant tumours," *Anticancer Research*, vol. 28, no. 6B, pp. 3897–3907, 2008.

[21] H. Miyake, I. Hara, S. Kamidono, and H. Eto, "Prognostic significance of oxidative DNA damage evaluated by 8-hydroxy-2′-deoxyguanosine in patients undergoing radical nephrectomy for renal cell carcinoma," *Urology*, vol. 64, no. 5, pp. 1057–1061, 2004.

[22] S. Tabur, S. N. Aksoy, H. Korkmaz, M. Ozkaya, N. Aksoy, and E. Akarsu, "Investigation of the role of 8-OHdG and oxidative stress in papillary thyroid carcinoma," *Tumor Biology*, vol. 36, no. 4, pp. 2667–2674, 2015.

[23] J. Zhou, E. He, and S. Skog, "The proliferation marker thymidine kinase 1 in clinical use," *Molecular and Clinical Oncology*, vol. 1, no. 1, pp. 18–28, 2013.

[24] Z. H. Chen, S. Q. Huang, Y. Wang et al., "Serological thymidine kinase 1 is a biomarker for early detection of tumours—a health screening study on 35,365 people, using a sensitive chemiluminescent dot blot assay," *Sensors*, vol. 11, no. 12, pp. 11064–11080, 2011.

[25] S. Skiold, O. Azimzadeh, J. Merl-Pham et al., "Unique proteomic signature for radiation sensitive patients; a comparative study between normo-sensitive and radiation sensitive breast cancer patients," *Mutation Research/Fundamental and Molecular Mechanisms of Mutagenesis*, vol. 776, pp. 128–135, 2015.

Hindawi
Oxidative Medicine and Cellular Longevity
Volume 2018, Article ID 6296802, 14 pages
https://doi.org/10.1155/2018/6296802

Research Article

The Role of TLR4 on PGC-1α-Mediated Oxidative Stress in Tubular Cell in Diabetic Kidney Disease

Shuguang Yuan,[1] Xuemei Liu,[1] Xuejing Zhu,[1] Zhong Qu,[2] Zailiang Gong,[1] Jun Li,[1] Li Xiao,[1] Yuan Yang,[1] Hong Liu,[1] Lin Sun,[1] and Fuyou Liu[1]

[1]*Department of Nephrology, The Second Xiangya Hospital, Central South University, Changsha, Hunan, China*
[2]*Changsha Central Hospital, Changsha, Hunan, China*

Correspondence should be addressed to Xuejing Zhu; zhuxuejing5225209@csu.edu.cn

Received 4 January 2018; Revised 24 March 2018; Accepted 4 April 2018; Published 16 May 2018

Academic Editor: Raquel Rodrigues-Díez

The role and precise mechanism of TLR4 in mitochondria-related oxidative damage and apoptosis of renal tubules in diabetic kidney disease (DKD) remain unclear. We examined the expression of TLR4 in renal biopsy tissues. Db/db diabetic mice and HK-2 cells cultured under high glucose (HG) were used as in vivo and vitro models. Real-time RT-PCR, Western blot, and immunohistochemistry were performed to examine the mRNA and protein levels of TLR4, NF-κB, PGC-1α, cytochrome C, and cleaved caspase-3. ATP level, activity of electron transport chain complex III, and antioxidant enzymes were investigated for mitochondrial function. Electron microscopy (EM) and MitoTracker Red CMXRos were used for mitochondrial morphology alteration. DHE staining and TUNEL assay were detected for ROS accumulation and apoptosis. PGC-1α plasmids were used for the overexpression of PGC-1α in HK-2. TAK242 and parthenolide were used as TLR4 and NF-κB blockers, respectively. Results showed that TLR4 was extensively expressed in the renal tubules of DKD patients and db/db diabetic mice, which was positively related to the tubular interstitial damage score and urinary β-NAG levels. In diabetic mice, inhibition of TLR4 could reverse the decreased expression of PGC-1α, increased expression of cytochrome C and cleaved caspase-3, mitochondrial dysfunction and deformation, increased accumulation of ROS, and activation of tubular cell apoptosis. In vitro, inhibition of TLR4 or NF-κB showed consistent results. PGC-1α overexpression could reverse the mitochondrial dysfunction, increased cleaved caspase-3, and apoptosis in HK-2 cells treated with HG. Data indicated that the TLR4/NF-κB signaling pathway might be the upstream pathway of PGC-1α and promote the tubular damage of DKD by modulating the mitochondria-related oxidative damage and apoptosis.

1. Introduction

Toll-like receptors (TLRs) are pattern recognition receptors and play a fundamental role in the activation of innate and adaptive immune responses [1, 2]. Among the 11 human TLRs, TLR4 has been implicated in the pathogenesis of acute and chronic renal disorders such as acute kidney injury (AKI), renal fibrosis, and DKD [3, 4]. Further researches have reported that TLR4 knockout diabetic mice have reduced the expression of MyD88 and TRIF and decreased NF-κB activity and the release of inflammatory cytokines and renal fibrosis [5, 6]. In addition, HG was proved to induce the overexpression of TLR4 through NF-κB-dependent signaling and lead to the accumulation of ROS in podocytes [7], indicating the important role of TLR4 NF-κB signaling in the mechanism of DKD progression. According to our previous study, renal tubular oxidative stress injury and apoptosis play a key role in the progression of DKD in high glucose (HG) conditions [8]. These let us speculate that activation of the TLR4-NF-κB signaling pathway might be involved in mitochondrial dysfunction and mitochondria-related oxidative damage of renal tubular epithelial cell (RTEC) in hyperglycemia, which is gradually to have an extremely important effect in the progression of DKD.

The peroxisome proliferator-activated receptor γ coactivator-1 (PGC-1) including PGC-1α, PGC-1β, and PRC is attributed to the nuclear transcription activating factor and has intimate relationship with substance metabolism [9].

PGC-1α is proved to stimulate mitochondrial biogenesis and respiration through the induction of uncoupling protein 2 (UCP-2) and the regulation of nuclear respiratory factors (NRFs) [10]. In addition, our previous study has also confirmed that, by adjusting transcription factors such as NRFs, PGC-1α could protect mitochondrial respiratory chain function and antioxidant enzymes, so as to maintain the stability of the mitochondrial structure and function [8]. Moreover, in cardiac cells, researchers found that NF-κB p65 represses PGC-1α activity leading to metabolic dysregulation that underlies heart dysfunction and failure [11]. However, the protective effect of PGC-1α on mitochondria and its relationship with TLR4/NF-κB signaling path in DKD are not fully clear and need to be further investigated.

Our aim of this study is to explore the function of the TLR4/NF-κB pathway in mitochondria-related oxidative damage and apoptosis of RTEC in hyperglycemia and to investigate the role of PGC-1α in the TLR4/NF-κB pathway in DKD.

2. Results

2.1. TLR4 Expression Was Upregulated in Renal Biopsy Specimens of DKD Patients. The clinical characteristics of the DKD patients and N-DKD as controls in this study are shown in Table 1. PASM and PAS staining showed morphological changes in both glomerular and tubulointerstitial areas, including mesangial area expansion (Figure 1(a), B, arrow), focal tubular atrophy, and interstitial fibrosis (Figure 1(a), D, arrow) in DKD patients, compared with those in non-DKD patients. Significantly, in the N-DKD group, mitochondria with an elongated cylindrical shape with organized cristae were shown by electron microscopy (Figure 1(a), G). However, diffused fragmented mitochondria were observed in DKD patients (Figure 1(a), H). The mitochondrial changes in EM were quantified (Figure 1(c)): mitochondrial length was measured in tubular cells to determine the percentage of cells that showed filamentous mitochondria less than 1% long (>2 μm). $^*P < 0.05$ compared with the N-DKD group. An observably enhanced TLR4 expression was demonstrated by IHC staining in the renal tubules of DKD patients (Figures 1(a), F, and 1(b)). Correlation analysis showed that TLR4 expression was positively correlated with the interstitial fibrosis and tubular atrophy (IFTA) scores and urinary β-NAG level as a tubular injury marker (Figures 1(d) and 1(e)).

2.2. Inhibition of TLR4 Protects Tubular Cell by Regulating Mitochondria-Related Proteins in Diabetic dbdb Mice. The levels of blood urea nitrogen (BUN), serum creatinine (Cr), urine protein (Upro), and urinary albumin : creatinine ratio (ACR) were significantly increased in the db/db group; $^*P < 0.05$ compared with the db/m group. However, BUN, Cr, and Upro were significantly attenuated following treatment with TAK242 (Table 2), $^{**}P < 0.05$ compared with the db/db mice group. These results suggested that TAK242 administration could preserve the renal function of db/db mice to a certain extent.

Table 1: Clinical characteristics of the patients.

	N-DKD	DKD
Sex (male/female)	4/8	5/7
Age (year)	24.92 ± 3.50	45.42 ± 4.01*
Blood glucose (mmol/L)	4.60 ± 0.25	8.69 ± 1.03*
Urine protein (g/24 h)	1.71 ± 0.99	5.87 ± 1.02*
Serum creatinine (μmol/l)	66.74 ± 9.67	174.48 ± 27.68*
Triglyceride (mmol/L)	1.40 ± 0.38	2.06 ± 0.31

Values are means ± SE; $^*P < 0.05$, compared with N-DKD.

Loss of brush border and early tubular atrophy were observed compared with the control group by HE staining (Figure 2(a), A–C), which were ameliorated by the injection of TLR4 inhibitor TAK242. The urinary excretion of β-NAG, which is a marker of tubular damage, was reflected by a significant increase in diabetic dbdb mice, while it was substantially reduced by intrarenal injection of TAK242 (Figure 2(b), B2).

TLR4 was increased in dbdb mice by Western blot (Figure 2(c)). Immunohistochemistry and Western blot show a notable increase in protein expression of cytochrome C (Figures 2(a), A1, G and H, A3, and 2(d), D1, D4) and cleaved caspase-3 (Figures 2(a), A1, D–F, A2, and 2(d), D1, D3) and a decrease in PGC-1α (Figure 2(d), D1, D2). Their changes were markedly reversed following the injection of TAK242.

2.3. Inhibition of TLR4 Protects Tubular Cell from Mitochondrial-Dependent Apoptosis by Regulating Mitochondrial Structure and Function in Diabetic dbdb Mice. ROS production was stained with red fluorescence by ROS-sensitive vital dye DHE and increased notably in the tubules of diabetic dbdb mice. Under the inhibition of TLR4 expression, ROS generation was significantly reduced (Figure 3(a), A1, A–C, A2). In addition, the inhibition of TLR4 expression dramatically reduced the degree of apoptosis in the tubular cells of diabetic dbdb mice by TUNEL assay (Figure 3(a), A1, D–F, A3). Tubular cells show elongated mitochondria with organized cristae in dbm mice (Figure 3(a), A1, G) (marked by asterisks); however, in the dbdb group, most mitochondria exhibited spherical shapes and had cristolysis (Figure 3(a), A1, H), which was partly attenuated following treatment with TAK242 (Figure 3(a), A1, I, A4).

The level of ATP production (Figure 3(b)), activity of electron transport chain complex III (Figure 3(c)), and activity of antioxidant enzymes: catalase (CAT) and manganese superoxide dismutase (MnSOD) (Figures 3(d) and 3(e)) were significantly decreased in the dbdb mouse group, which could be reversed following the injection of TAK242. These indicated that inhibition of TLR4 could attenuate the depression of mitochondrial functions in diabetic mice.

2.4. HG Increased TLR4 Expression and Activated NF-κB p65 Phosphorylation in HK-2 Cells under HG Ambience. As shown in Figure 4, the protein level of TLR4 increased in a

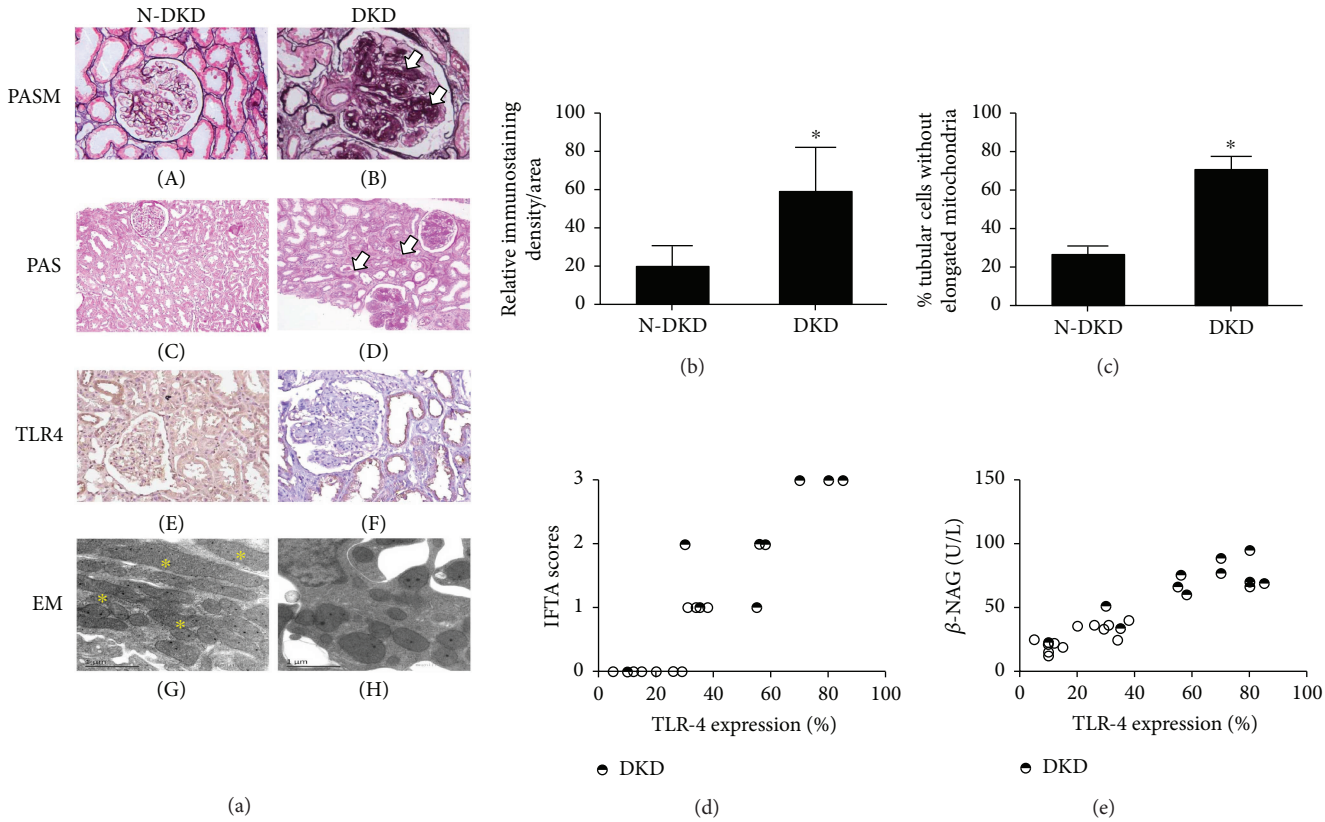

Figure 1: TLR4 expression was upregulated in renal biopsy specimens of DKD patients. (a) PASM (magnification ×200) and PAS (magnification ×100) staining were done to renal biopsy tissues of patients with DKD (A1, B, D) and N-DKD (A, C). IHC studies demonstrated the expression of TLR4 in renal biopsy tissues of patients with DKD versus N-DKD (F versus E). EM detected tubular mitochondria of renal tissue of DKD patients compared with N-DKD (H–I versus G) (scale bars: 1 μm). Asterisks indicate elongated (>2 μm) mitochondria. (b) Renal cortical relative expression of TLR4 in renal biopsies of patients with DKD and N-DKD. (c) Quantification of mitochondrial fragmentation of renal tubular cells. (d) and (e) The correlation between TLR4 expression and tubular atrophy and interstitial fibrosis (IFTA) scores ($r = 0.76$, $P < 0.01$) and urinary β-NAG levels ($r = 0.89$, $P < 0.01$) were observed in the scatter plots. Values are means ± SEM. $^{*}P < 0.05$.

concentration- and time-dependent manner in HK-2 cells, and beta-actin served as a loading control (Figures 4(a) and 4(b)). In addition, the expression of phospho-NF-κB p65 increased significantly in HK-2 cells treated with 30 mM HG for 2 h compared to the control (Figure 4(c)), while TLR4 inhibitor (TAK242, 5 μM) [12] reversed HG-induced NF-κB p65 phosphorylation (Figure 4(e)) for 2 h and for 24 h (Figure 4(f)), which indicates that NF-κB is the downstream signal molecule of TLR4. Consistent with the protein expression, the mRNA level of NF-κB p65 increased in HK-2 cells treated with 30 mM HG for 2 h compared to the control, while TAK242 reversed HG-induced activation of NF-κB p65 phosphorylation (Figure 4(d)), which indicates that HG activated the TLR4/NF-κB signaling pathway.

2.5. Inhibition of TLR4/NF-κB Signaling Reversed the Expression of PGC-1α and Caspase-3 and ROS Production in HK-2 Cells under HG Ambience. RT-PCR (Figure 5(a), A1, A2) and Western blot (Figure 5(b), B1–B3) results showed that mRNA and protein levels of apoptosis-related protein cleaved caspase-3 were increased in the HG group (Figures 5(a), A2, and 5(b), B3), while mRNA and protein expression of mitochondria-related protein PGC-1α decreased in the HG group (Figures 5(a), A1, and 5(b), B2). This trend was overturned by TAK242 and NF-κB blocker (parthenolide, 10 μM).

For measurements of ROS, MitoSOX Red reagent (red color) was used. The cells have very low MitoSOX fluorescence in the cytoplasm of cells in the 5.5 Glu group (Figure 5(c), C1, A). HG significantly triggers an increase in mitochondrial superoxide formation (Figure 5(c), C1, B, C2). TLR4 and NF-κB blocker could prevent HG-induced ROS production ($^{**}P < 0.01$).

These data suggested that the TLR4/NF-κB pathway might be involved in HG-induced mitochondria-related ROS accumulation and apoptosis. In addition, the expression of PGC-1α increased in TLR4/NF-κB blocked groups suggesting that PGC-1α might be a downstream protein of the TLR4/NF-KB signaling pathway in HG-induced changes in HK-2 cells.

2.6. Inhibition of TLR4/NF-κB Signaling Reversed Mitochondrial Cytochrome C Release, Mitochondrial Morphology, Function, and Early Apoptosis in HK-2 Cells under HG Ambience. At a

Table 2: Physical and metabolic parameters in mice.

	db/m	db/db	db/db + TAK242
Body weight (g)	35.9 ± 0.52	64.00 ± 5.02*	58.42 ± 1.54*
Blood urea nitrogen (mmol/L)	5.59 ± 0.36	11.42 ± 0.88*	7.04 ± 0.38**
Serum creatinine (μmol/L)	3.76 ± 0.19	16.77 ± 0.92*	8.91 ± 0.35**
Urine protein (mg/24 h)	7.53 ± 0.35	26.30 ± 1.15*	15.31 ± 0.66**
ACR (μg/mg Cr)	0.23 ± 0.01	2.89 ± 0.07*	2.76 ± 0.08*

Values are means ± SE; *$P < 0.05$, compared with the db/m group; **$P < 0.05$, compared with the db/db group; urinary albumin : creatinine ratio (ACR).

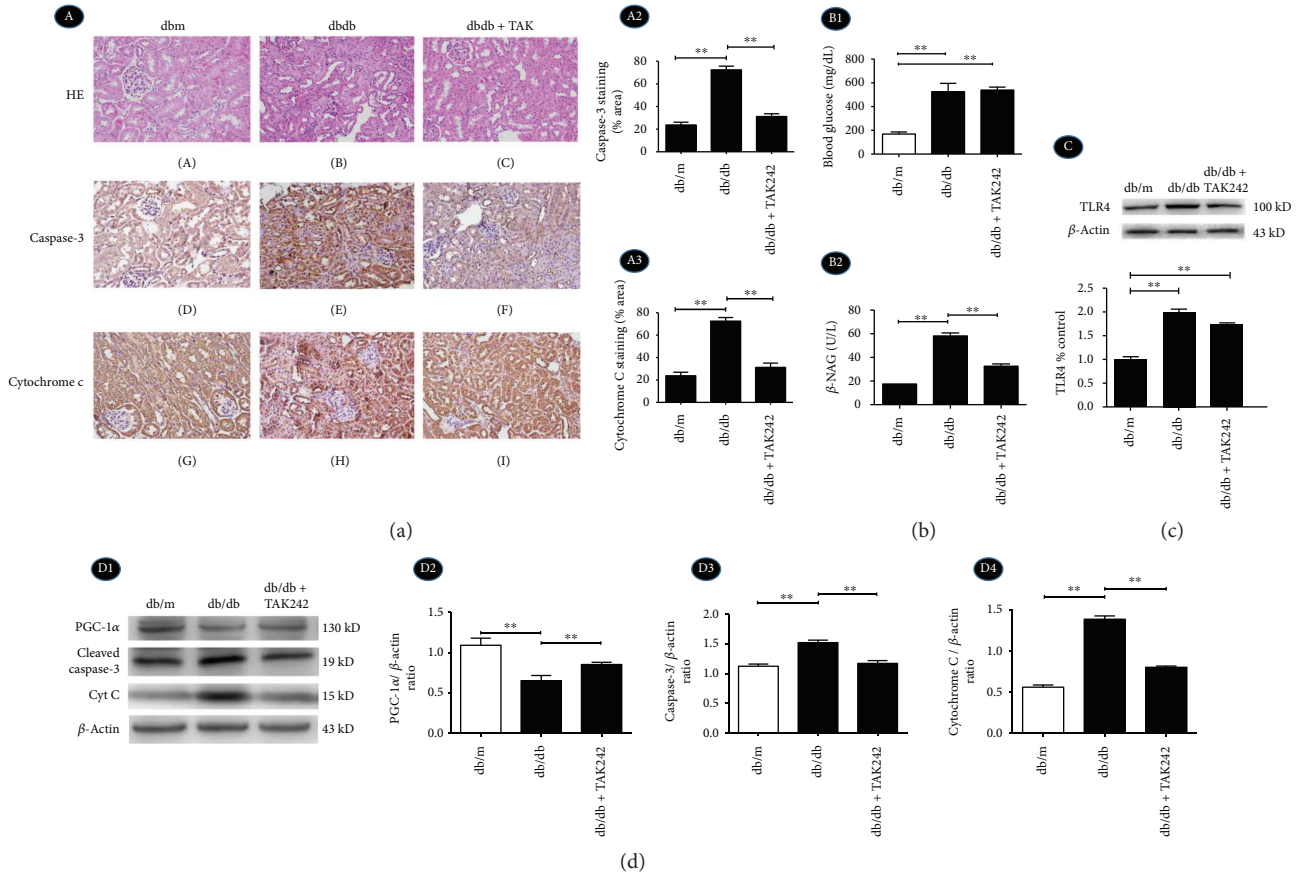

Figure 2: Inhibition of TLR4 protects tubular cell injury by regulating mitochondria-related proteins in diabetic dbdb mice. Dbdb mice received an intraperitoneal injection with the vehicle alone (dbdb group) or TLR4 inhibitor TAK242 (dbdb + TAK group). dbm mice were served as a control. (a) A1, A–C: HE staining was done to renal biopsy tissues of the mice (magnification ×200); A1, D–F: IHC for caspase-3 in tubular cells; A1, G–I: IHC for cytochrome C (magnification ×200); A2 and A3: semiquantification of IHC staining of caspase-3 and cytochrome C. (b) B1: Serum blood glucose level; B2: urinary excretion β-NAG levels in different groups. (c) Western blot for the protein expression of TLR4. (d) D1–D4: Western blot for the protein expressions of PGC-1α, caspase-3, and cytochrome C. Data were expressed as means ± SEM; **$P < 0.01$.

30 mM concentration of D-glucose, release of cytochrome C from mitochondria to cytoplasm was increased in HK-2 cells by Western blot (Figure 6(a), A1–A3), suggesting a remarkable HG-induced mitochondrial malfunction. With the intervention of the TLR4 inhibitor (TAK242) and NF-κB blocker (parthenolide), the translocation of cytochrome C was ameliorated (Figure 6(a), A1–A3). The level of ATP production (Figure 6(b)), activity of electron transport chain complex III (Figure 6(c)), and activity of CAT and MnSOD (Figures 6(d) and 6(e)) were significantly decreased in the HG group, which could be reversed in the TAK242 + 30 Glu group and parthenolide + 30 Glu group. These indicated that HG activated TLR4/NF-κB signaling to influence mitochondrial function.

As shown in Figure 6(f), mitochondria, which were stained by MitoTracker with red fluorescence, were filamentous with a thread-like appearance and were often interconnected to form a network in the control group (Figure 6(f), F1, A, F). The mitochondria were fragmented into spheres during HG treatment (Figure 6(f), F1, B, G),

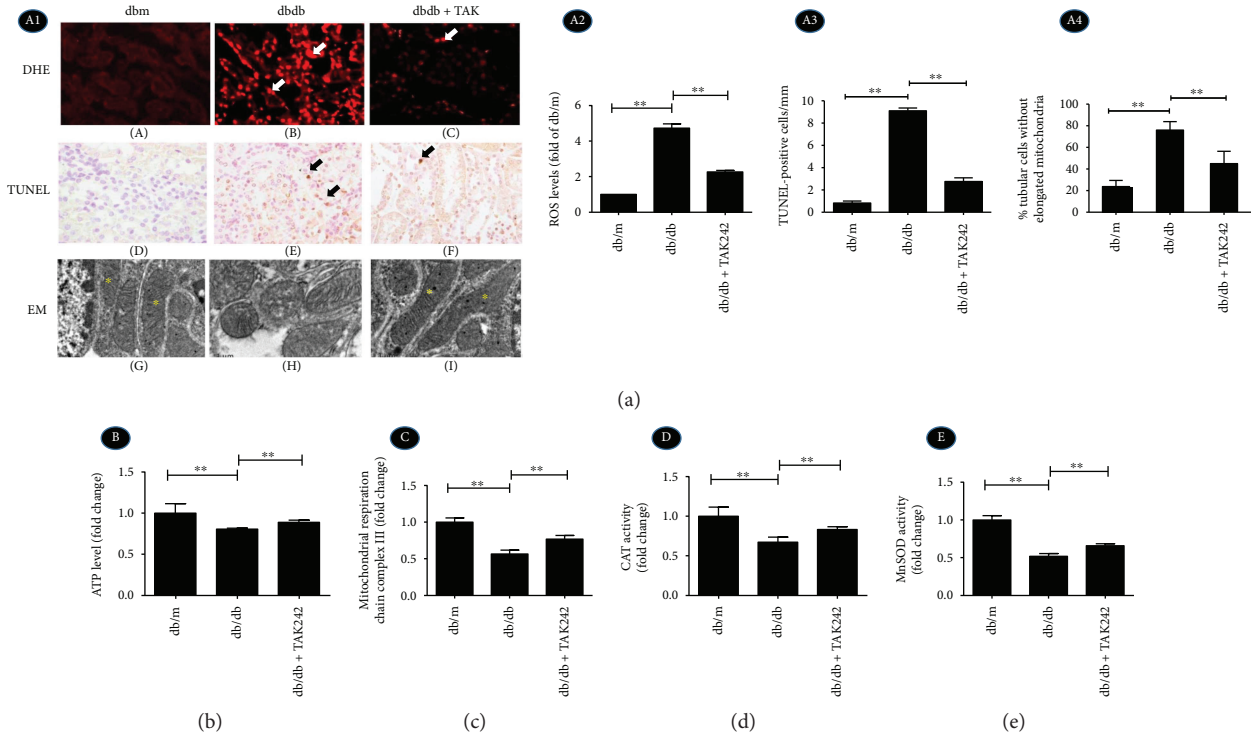

Figure 3: Inhibition of TLR4 protects tubular cells from mitochondrial-dependent apoptosis by regulating mitochondrial structure and function in diabetic dbdb mice. (a) A1, A–C: DHE with red fluorescence for ROS accumulation; A1, D–F: IHC of TUNEL assay for apoptosis (arrow show) (magnification ×400); A1, G–I: EM shows tubular mitochondria of renal tubular cells of dbdb mice (magnification ×20000). A2: Quantification of DHE staining expressed as fold of dbm mice. A3: Quantification of TUNEL-positive cells. A4: Relative percentage of renal tubular cells without elongated mitochondria. (b) The level of ATP production. (c) The activity of mitochondrial respiratory chain complex III. (d) Activity of CAT. (e) Activity of MnSOD. $^{**}P < 0.01$. The values in (b–e) were displayed as fold change compared to the control.

while TAK242 and parthenolide treatment reversed this trend (Figure 6, F1, D, E, H, I, F2).

In addition, Hoechst 33258 staining shows that HG (30 mM) increased karyorrhexis, which was a hint of early apoptosis, while TAK242 and parthenolide treatment reversed this trend (Figure 6(g), arrow shown). These data demonstrated that HG induced mitochondrial malfunction and aggravated nuclear fragmentation of early apoptotic cells by activating the TLR4/NF-κB signaling pathway.

2.7. Overexpression of PGC-1α Diminished HG-Induced Caspase-3 Expression in HK-2 Cells under the Inhibition of the TLR4/NF-κB Signaling Pathway. HK-2 cells were divided into six groups with different treatments: (1) control group with 5.5 mM glucose (5.5 Glu), (2) high glucose group with 30 mM glucose (30 Glu), (3) PGC-1α plasmid group with 30 mM glucose (PGC-1α + 30 Glu), (4) PGC-1α empty plasmid group with 30 mM glucose (empty vector + 30 Glu), (5) PGC-1α plasmid with 30 mM glucose and TAK242 (PGC-1α + TAK242 + 30 Glu), and (6) PGC-1α plasmid with 30 mM glucose and parthenolide (PGC-1α + parthenolide + 30 Glu). HG increased the expression of cleaved caspase-3, but PGC-1α overexpression reduced the level of cleaved caspase-3 in mRNA (Figure 7(a), A2) and protein levels (Figure 7(b), B1–B3), supporting the notion that PGC-1α overexpression is involved in HG-induced cell apoptosis. Furthermore, the results also demonstrated that phospho-NF-κB p65 increased in HK-2 cells with 30 mM HG for 2 h (Figure 7(c)) and 24 h (Figure 7(d)), while it did not decrease in PGC-1α-overexpressed cells, which further proved that PGC-1α might be the downstream protein of the TLR4/NF-κB signaling pathway in HG-induced changes in HK-2 cells.

2.8. Overexpression of PGC-1α Restored HG-Induced Mitochondrial Membrane Potential ($\triangle\Psi_m$) Alteration and Apoptosis in HK-2 Cells under the Inhibition of the TLR4/NF-κB Signaling Pathway. By flow cytometry analysis, a loss of mitochondrial $\triangle\Psi_m$ detected by TMRM staining was observed under 30 mM HG ambience in cells undergoing early apoptosis, which was recovered to baseline with the overexpression of PGC-1α (Figures 8(a), A). In addition, the apoptotic rate was only 11.92% with 5 mM D-glucose in HK-2 cells, but peaked at 68.1% in the 30 Glu group (Figures 8(b), B), which was agreed with the reported literature that high glucose led to increased cell apoptosis. However, the apoptotic rate was, respectively, 52.27% in the "PGC-1α + 30 Glu group," 59.86% in the "PGC-1α + TAK242 + 30 Glu group," and 47.12% in the "PGC-1α + parthenolide + 30 Glu group," which were significantly decreased when compared with that of the 30 Glu group. Statistics indicated that PGC-1α overexpression inhibited HG-induced loss of mitochondrial $\triangle\Psi_m$ and apoptosis in HK-2 cells.

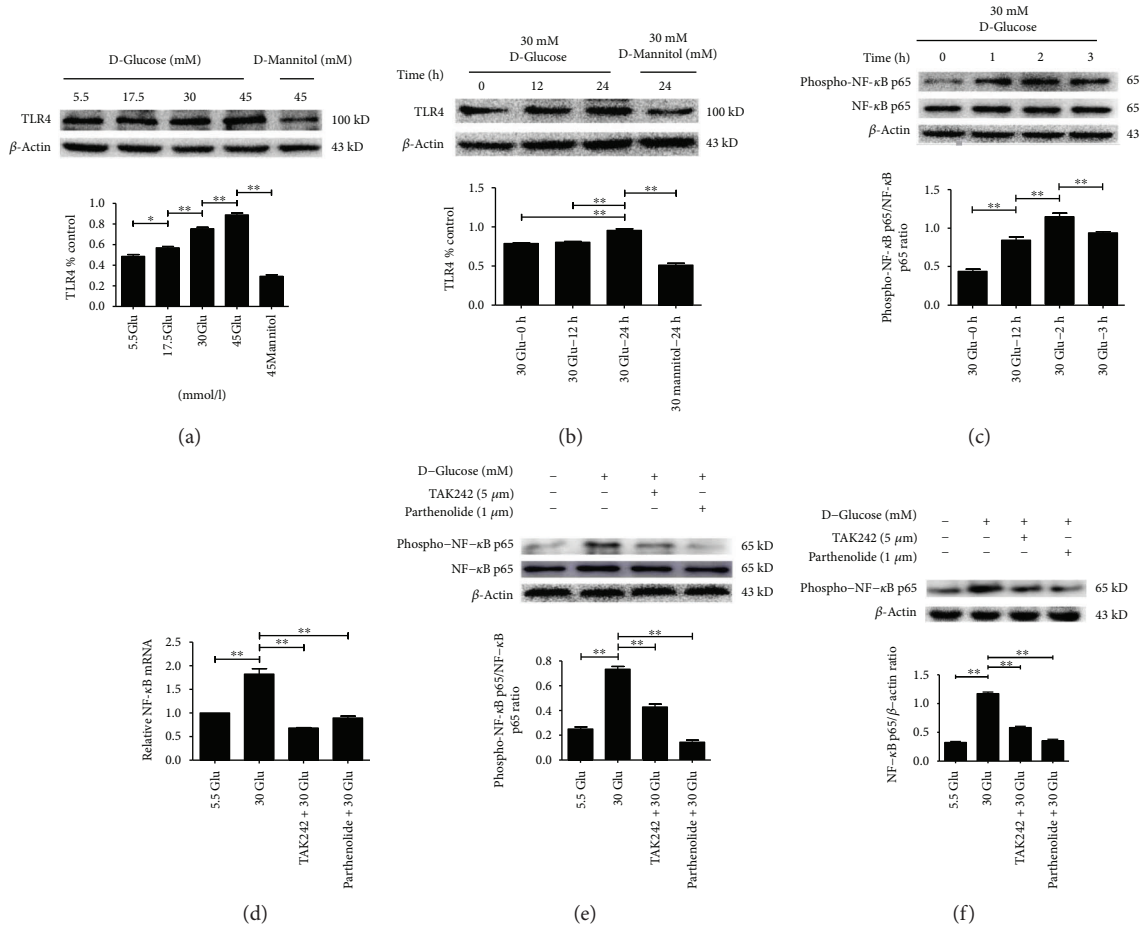

Figure 4: HG increased TLR4 expression and activated NF-κB p65 phosphorylation in HK-2 cells. a–b: Protein levels of TLR4 in HK-2 cells following exposure to D-glucose (5.5 mM, 17.5 mM, 30 mM, and 45 mM) for 24 h (a) or D-glucose (30 mmol/L) for various times (0 h, 12 h, and 24 h) (b), and expression of NF-κB p65 and phospho-NF-κB p65 of cells exposed to 30 mM HG for indicated time points (0 h, 1 h, 2 h, and 3 h) (c) were determined by Western blot analysis. d–f: HK-2 cells were treated with TLR4 inhibitor (TAK242, 5 μM) for 2 h prior to HG (30 mM) treatment for 2 h (e) or 24 h (f) and with NF-κB blocker (parthenolide, 10 μM) and HG (30 mM) for 2 h (e) or 24 h (f), and the samples were collected for RT-PCR (d) and Western blot analysis (e–f). Each assay was representative of three independent experiments. Data were expressed as means ± SEM; $^{*}P < 0.05$ and $^{**}P < 0.01$.

3. Discussion

Recently, researches have demonstrated that mitochondria-related oxidative damage and apoptosis play a key role among the multifactorial pathogenesis of DKD patients [13, 14]. In addition, TLR4 has been previously described involving in hyperglycemia-induced inflammatory state of renal tubulus in vitro and vivo [15, 16], but its role in oxidative damage and apoptosis in renal tubular cells in DKD remains unclear. This study describes a cascade event that links TLR4/NF-κB activation to mitochondria-related oxidative damage and apoptosis through downregulation of PGC-1α in renal tubular cells under HG condition.

There are increasing evidences showing the significance of the TLR4 pathway in the development of DKD [17]. However, most of them were focusing on its effect related to the tubulointerstitial inflammatory response [4, 12]. In this study, we found that TLR4 was extensively expressed in tubular cells in the kidney of patients with DKD and was coexistent with fragmented mitochondria. Further analysis revealed a positive correlation between TLR4 expression and tubular injury. These results indicated that TLR4 might play an important role in mitochondria-related tubular oxidative damage in DKD, besides its activation effect of inflammatory response. This speculation was further identified by a diabetic dbdb mouse model in our study.

Many studies have reported TLR4 to be critical for the activation of NF-κB and subsequent production of proinflammatory cytokines implicated in diseases [18, 19]. Molecular silencing of TLR4 in tubular cells with siRNA attenuated HG-induced IκB/NF-κB activation, indicating that the TLR4-NF-κB signal pathway plays an important role in diabetic nephropathy [20, 21]. In this study, we have also proved that the TLR4 inhibitor could effectively decrease the expression of phospho-NF-κB p65 increased in HK-2 cells under HG conditions, indicating that NF-κB is the downstream signal molecule of TLR4 in tubular cells.

Mitochondrial dysfunction has proved to be a contributing factor in the pathogenesis of DKD [22]. Mitochondria-related

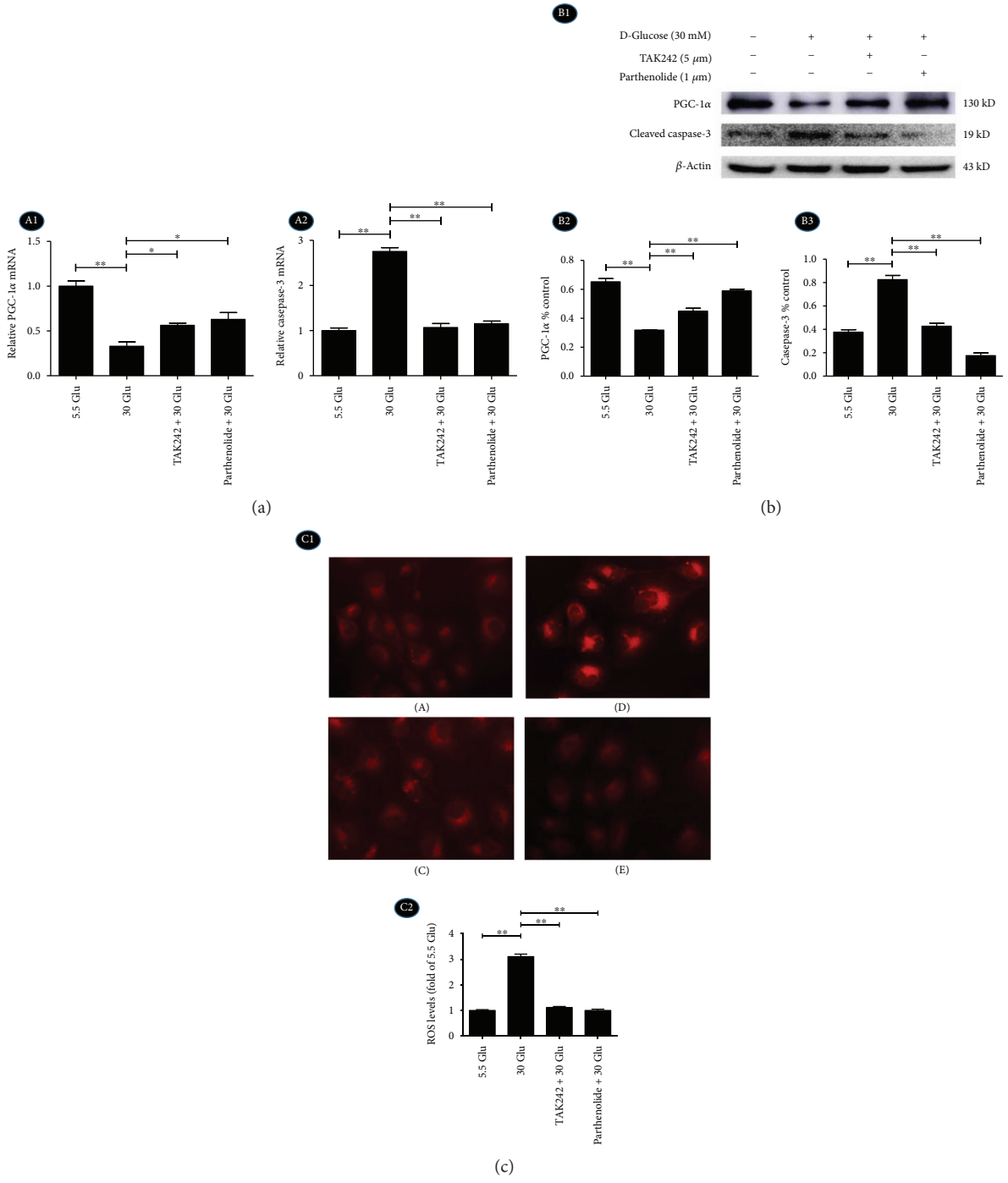

Figure 5: Inhibition of TLR4/NF-κB signaling reversed the expression of PGC-1α and caspase-3 and accumulation of ROS in HK-2 cells in HG ambience. HK-2 cells were treated with TAK242 for 2 h prior to HG (30 mM) treatment for 24 h and with parthenolide and HG (30 mM) for 24 h, and samples were collected for RT-PCR (a) and Western blot analysis (b). (c) C1: MitoSOX Red staining for ROS production (magnification ×200). A: 5.5 Glu group, B: 30 Glu group, C: TAK242 + 30 Glu group, and D: parthenolide + 30 Glu group. C2: Quantification of MitoSOX Red staining. The values were expressed as fold change compared to control. Data were expressed as means ± SEM; $^{*}P < 0.05$ and $^{**}P < 0.01$.

oxidative damage could result in the release of mitochondrial cytochrome c and activation of caspase-3, leading ultimately to apoptosis [23]. In order to investigate the mechanism for the effect of TLR4/NF-κB on the mitochondria-related tubular oxidative damage in hyperglycemia, we inhibited the expression of TLR4 or NF-κB in vivo and in vitro. We observed a partial rescue of HG-induced deformation of mitochondria, inhibition of ATP production, depressed mitochondrial respiration and activity of antioxidant enzymes, and increased caspase-3 and cytoplasm cytochrome c, which indicated that inhibition of the TLR4/NF-κB signaling pathway could protect mitochondrial

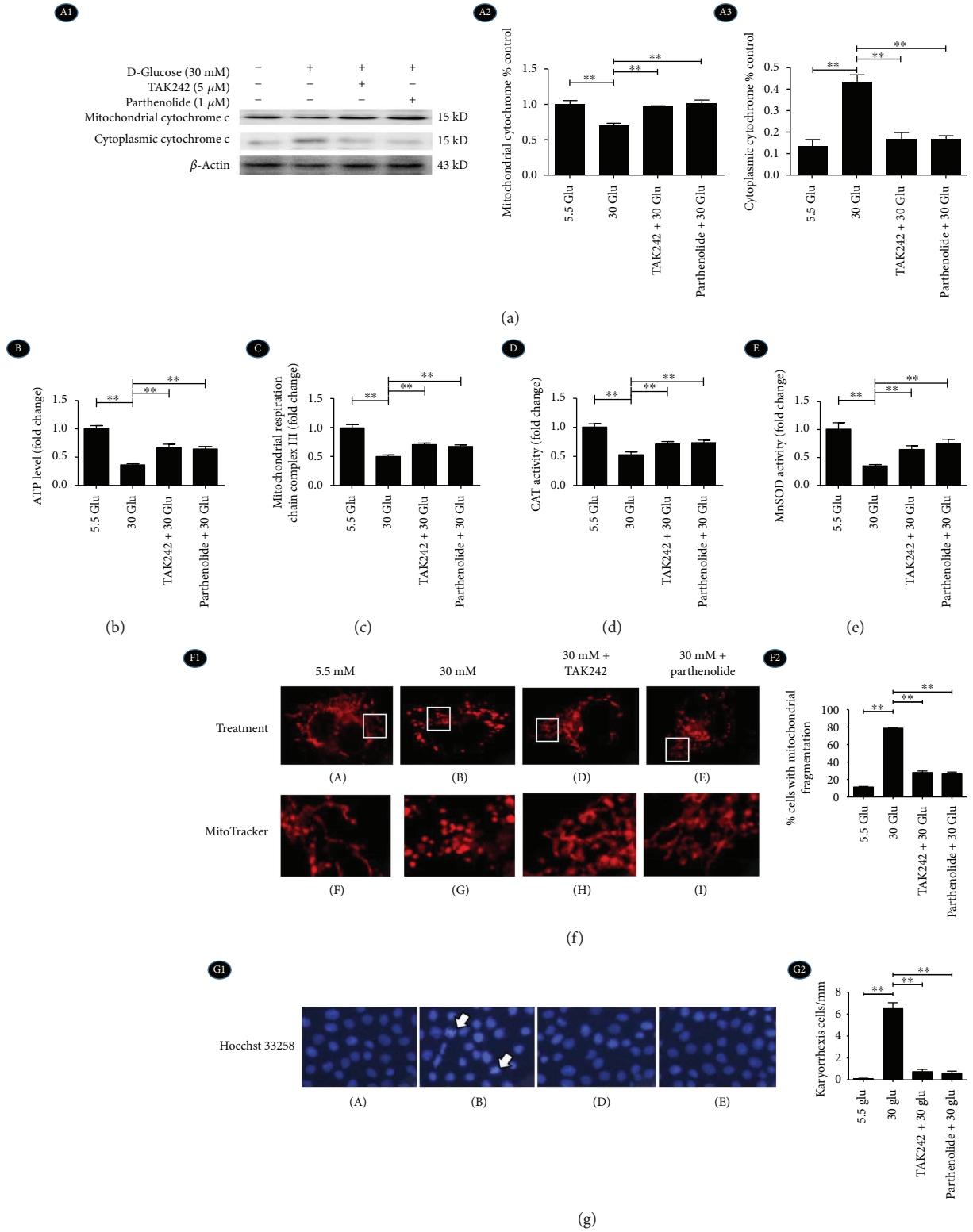

Figure 6: Inhibition of TLR4/NF-κB signaling reversed mitochondrial cytochrome C release, mitochondrial morphology, function, and early apoptosis in HK-2 cells under HG ambience. HK-2 cells were treated with TAK242 for 2 h prior to HG (30 mM) treatment for 24 h and with parthenolide and HG (30 mM) for 24 h. (a) A1–A3: Western blot shows protein expressions of mitochondrial cytochrome C and cytoplasmic cytochrome C. (b) The level of ATP production. (c) The activity of mitochondrial respiratory chain complex III. (d) Activity of CAT. (e) Activity of MnSOD. $^{**}P < 0.01$. The values in b–e were displayed as fold change compared to the control. (f) Fluorescence microscopy shows mitochondria stained with MitoTracker Red CMXRos (red) (F1) and was evaluated to determine the percentage of cells that fragmented mitochondria (F2). (g) Hoechst 33258 staining shows early apoptosis of tubular cell nuclei (blue).

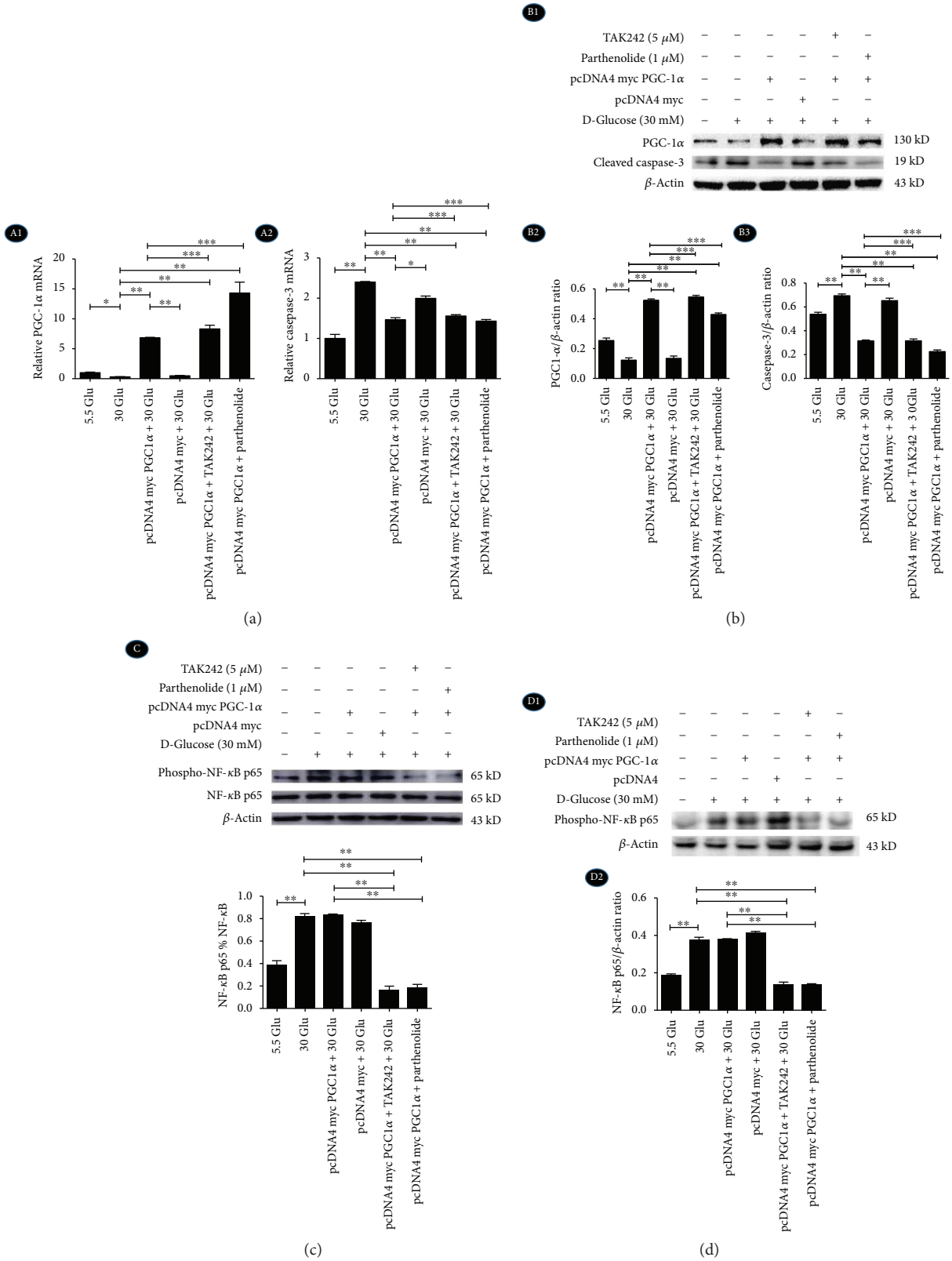

Figure 7: Overexpression of PGC-1α diminished HG-induced caspase-3 expression in HK-2 cells. HK-2 cells were transfected with pcDNA4 myc PGC-1α or pcDNA4 myc (empty vector) for 24 h. (a) A1: The mRNA level of PGC-1α. A2: The mRNA level of cleaved caspase-3. (b) B1-B2: The protein expression of PGC-1α and cleaved caspase-3 were examined by Western blotting. (c) The protein expression of NF-κB p65 and phospho-NF-κB p65 with HG for 2 h. (d) D1-D2: The protein expression of phospho-NF-κB p65 with HG for 24 h. Each assay was representative of three independent experiments. Data were expressed as means ± SEM; $^{*}P < 0.05$, $^{**}P < 0.01$, and $^{***}P > 0.05$.

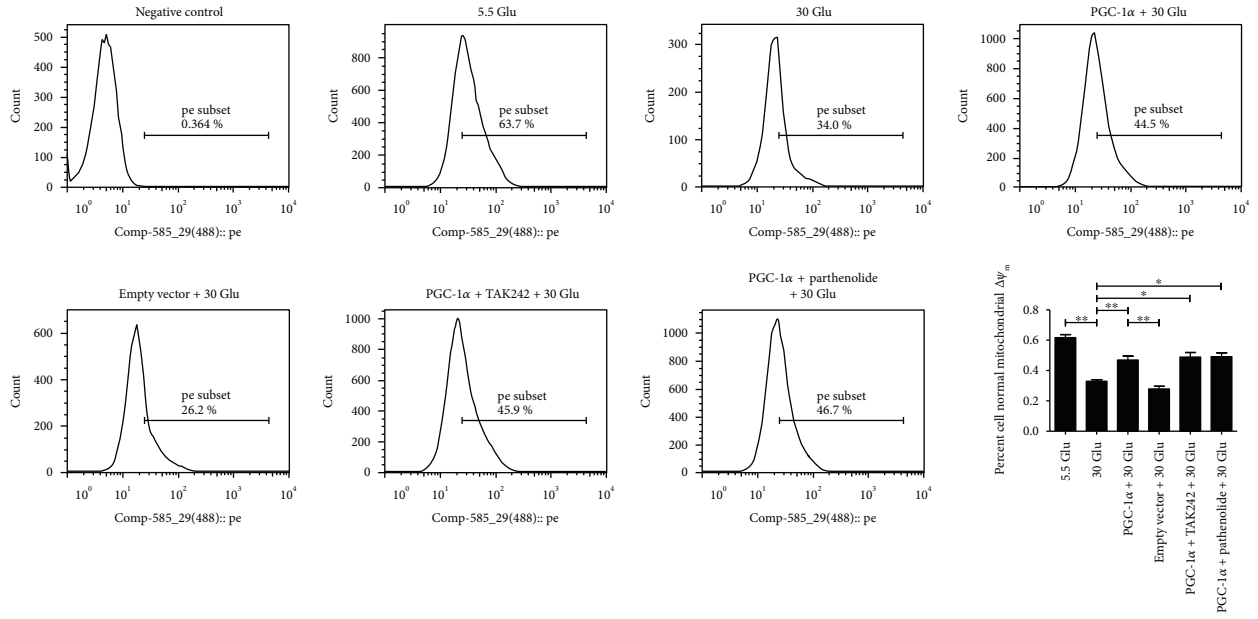

(a)

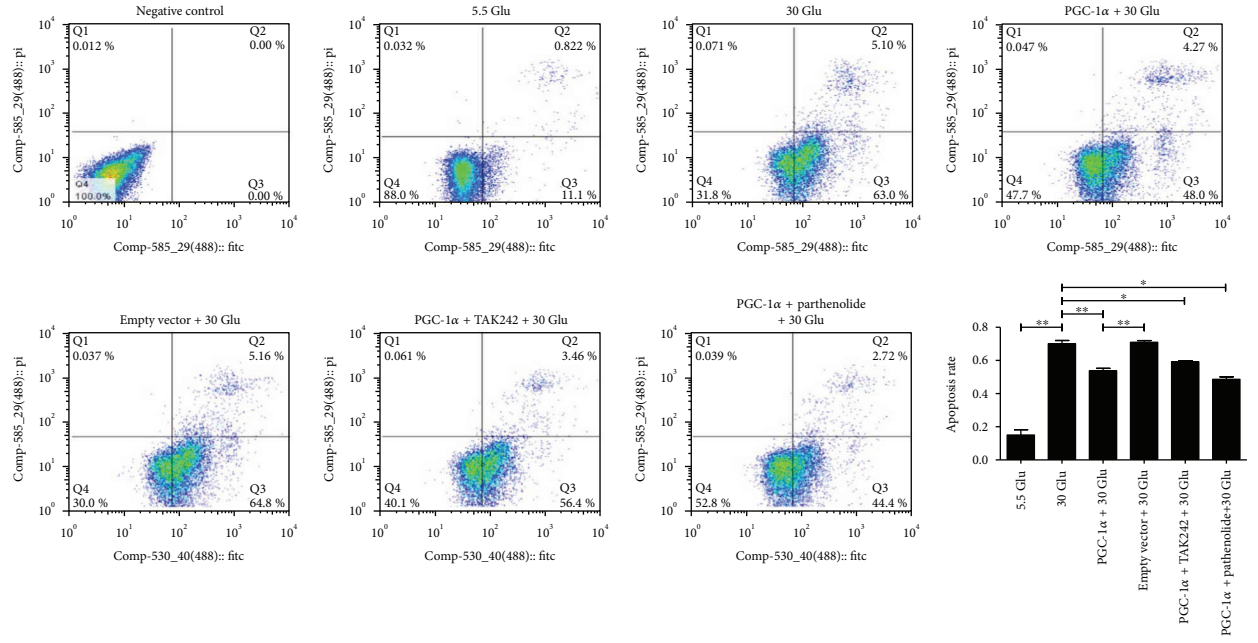

(b)

Figure 8: Overexpression of PGC-1α restored HG-induced mitochondrial $\triangle\Psi_m$ alteration and apoptosis. HK-2 cells were transfected with pcDNA4 myc PGC-1α for 24 h; the PGC-1α-overexpressed cells were treated with TAK242 for 2 h prior to HG (30 mM) treatment, with parthenolide and HG (30 mM) or with HG (30 mM) for 24 h. Mitochondrial $\triangle\Psi_m$ (a) and apoptosis (b) of HK-2 cells were analyzed by flow cytometry analysis. Each assay was representative of three independent experiments. Data were expressed as means ± SEM; $^*P < 0.05$ and $^{**}P < 0.01$.

dysfunction in the tubular cells of diabetic rats and in cultured tubular cells induced by HG. These beneficial effects on tubular cells reverse ROS generation and apoptosis and protect tubular cells from oxidative injury by HG in vivo and in vitro.

Researches have identified mitochondrial fragmentation as a novel mechanism contributing to mitochondrial damage and apoptosis in vivo in mouse models of disease [24]. In tubular cells, a significant portion of mitochondria line up perpendicular to the basement membrane, making an excellent model for studying mitochondrial fragmentation in vivo. Cross sections of tubules normally show 10%–20% longitudinally sectioned long mitochondria, while they appear as short rods or spherical fragments in pathological apoptosis in

disease models. Fragmented mitochondria were found to refuse if the injurious stress is removed before permanent injury happens to trigger apoptosis [25]. In this study, we observed that most of the mitochondria within the injured tubules in renal biopsy tissues and diabetic mice were fragmented and had a randomly disorganized cellular distribution, which could be reversed by inhibition of the TLR4/NF-κB inhibitor, indicating that the TLR4/NF-κB signaling pathway induced mitochondrial fragmentation, which contributes to subsequent tubular cell apoptosis.

As a main regulator of mitochondrial function, PGC-1α exerts a rescuing effect in substance metabolism and oxidative metabolism by regulating mitochondrial biogenesis and ROS scavenging enzymes [26]. An increased PGC-1α expression may protect cells from oxidative stress and oxidative stress-mediated cell apoptosis [27, 28]. In cardiac myocytes, Schilling et al. showed that TLR4 activation could lead to the phosphorylation and nuclear translocation of NF-κB, triggering cardiac energy metabolic reprogramming by repressing genes encoding PGC-1α, and the absence of TLR4 abolished LPS-induced downregulation of PGC-1α, indicating that the suppression of PGC-1α was shown to occur through a TLR4- and NF-κB-dependent mechanism [29]. In this study, we observed that PGC-1α was decreased in a diabetic mouse model and was reversed after the inhibition of TLR4 *in vivo*. In HK-2 cells, overexpression of PGC-1α inhibited a series of HG-induced changes including downregulation of mitochondrial membrane potential, upregulation of apoptosis-related protein cleaved caspase-3, and cell apoptosis directly, verifying the protective function of PGC-1α to mitochondrial function and cell survival in HG condition. Moreover, PGC-1α overexpression did not decrease HG-induced TLR4 activation and NF-κB p65 phosphorylation, further confirming that PGC-1α is a downstream protein of TLR4/NF-κB, which protected renal tubular cells from HG-induced mitochondria-related oxidation and apoptosis.

In conclusion, TLR4 plays a significant role in HG-induced mitochondrial dysfunction, mitochondria-related oxidation, and apoptosis by regulating downstream protein PGC-1α in RTEC, hoping to provide a better understanding and a more effective therapeutic approach for the prevention and treatment of DKD.

4. Materials and Methods

4.1. Main Reagents and Materials. Human kidney proximal tubular epithelial cells (HK-2) were a cell line purchased from the American Type Culture Collection (ATCC, USA). Antibodies were from the following sources: polyclonal anti-TLR4 from Abcam (USA). Monoclonal anti-PGC-1α, monoclonal anti-caspase-3, and NF-κB p65 were from Cell Signaling Technology (Boston, USA). Polyclonal phospho-NF-κB p65 (ser536) antibody was from Bioworld (USA), and polyclonal anti-cytochrome C was from Proteintech (Wuhan, China). Beta-actin and all secondary antibodies for Western blot and immunofluorescence were from Proteintech (Wuhan, China). TAK242 was from MedChem Express (USA), and parthenolide was from Sigma (USA). Plasmids containing pcDNA4 myc PGC-1α (pcDNA4/PGC-1α) was bought from Addgene (USA). Lipofectamine 2000, MitoTracker Red CMXRos, MitoSOX, and TRIzol were purchased from Invitrogen (USA). PrimeScript™ RT reagent Kit with gDNA Eraser and SYBR® Premix Ex Taq™ (Tli RNase H Plus) were from TaKaRa (Japan). Annexin V-FITC Apoptosis Detection Kit was from Beyotime (Shanghai, China). TMRM Detection Kit was from Genmed Scientifics Inc. (USA). Other reagents, including DMEM/F12 medium, bovine serum albumin (FBS), and trypsin, were obtained from Gibco (USA).

4.2. Morphological Analysis of Kidney. 12 patients with DKD and 12 non-DKD controls (normal kidney tissue) were recruited for this study. Human renal biopsy tissues from the 24 cases were studied by staining of PAS and PASM. A semiquantitative scoring system was used to evaluate the tubulointerstitial lesion index, and tubular damage was also scored [30, 31]. All procedures were carried out in accordance with the approved guidelines. All patients did not use adrenal cortical hormones or immunosuppression. The institutional review board and the administrators of the Department of Nephrology in The Second Xiangya Hospital approved the protocol for this study. An informed consent was obtained from all the participants.

The kidney tissue of mice was routinely processed, embedded in paraffin, and sectioned at 2–3 mm thickness, deparaffinized, and rehydrated using standard techniques. Mouse sections were stained with hematoxylin-eosin stain (HE).

4.3. Examination of Mitochondrial Fragmentation in Renal Tissue and HK-2 Cells. The alterations of mitochondria in renal tubules were gauged by electron microscopy (EM). Mitochondria having a length $< 1\ \mu$m and spherical configuration were identified as fragmented. We determined the percentage of cells that had less than 1% long filamentous mitochondria to indicate the degree of mitochondrial fragmentation in patients and mice [24].

MitoTracker Red CMXRos was used for the evaluation of mitochondrial morphology in HK-2 cells. The mitochondria within a cell were often either filamentous or fragmented. In cases of mixed mitochondrial morphology, we classified the cells based on the majority (>70%) of mitochondria, according to earlier studies. For each sample, several random fields of cells (≥100 cells per dish) were evaluated [32, 33].

4.4. Animal Experimental Design. A total of 10 male dbm mice and 20 adult male dbdb mice at 16 weeks of age (body weight 32–40 g) were divided into three groups of 10 animals each. The first group was male dbm mice, which served as a control. The second group of dbdb mice received an intraperitoneal injection with vehicle alone (dbdb group). The third group included dbdb mice which received an intraperitoneal injection of TLR4 inhibitor TAK242 (3 mg/kg for 7 days). All animals were killed at 17 weeks following administration. The Institutional Animal Experimentation Ethics Committee as described above approved the animal experimental protocols.

4.5. Cell Culture. Human kidney proximal tubular epithelial cells (HK-2), an immortalized cell line from the American Type Culture Collection (ATCC, USA), were used in this study. HK-2 cells were cultured in DMEM/F12 medium supplemented with 10% FBS, penicillin 1×10 5 U/L, and streptomycin 100 mg/L. Until being seeded at 80–90% confluence, the cells were exposed to different concentrations of D-glucose and TLR4/NF-κB blockers, and concrete interventions and groupings were as follows: A: 5.5 mM D-glucose (control/5.5 Glu group), B: 30 mM D-glucose (30 Glu group), C: TLR4 inhibitor (TAK242) and 30 mM D-glucose (TAK242 + 30 Glu group), and D: NF-κB blocker (parthenolide) and 30 mM D-glucose (parthenolide + 30 Glu group).

4.6. Immunohistochemistry (IHC). Renal tissue sections from human and mice for immunostaining were deparaffinized and rehydrated. Immunohistochemistry was performed using anti-TLR4 antibody (1 : 100, Abcam, USA), caspase-3 (1 : 100, CST, Boston, USA), and cytochrome c (1 : 100, CST, Boston, USA) antibody as a primary antibody followed by a secondary antibody. Then, slides were visualized by using a DAB detection kit according to the manufacturer's instructions, and the tissue specimens were examined by light microscopy.

For human and mouse tissue sections, the average intensity from at least 20 randomly selected fields was measured using ImageJ software (National Institutes of Health, Bethesda, MD).

4.7. ATP Assay. ATP levels were determined in cell lysates obtained from mouse renal tissue and HK-2 cells using an ATP Assay Kit (Genmed, Shanghai, China). The assays were run according to the manufacturer's instructions. The values were expressed as fold change compared to the control.

4.8. Respiratory Chain Complex III Activity. Mitochondrial respiratory chain complex III activity was measured by using a spectrophotometer (Genmed, Shanghai, China) according to the manufacturer's instruction. The values were expressed as fold change compared to vehicle control.

4.9. Mitochondrial Enzyme Activities. The Superoxide Dismutase Activity Assay Kit (Alexis Biochemicals) and Catalase Activity Colorimetric/Fluorometric Assay Kit (BioVision Inc.) were used for the detection of Mn-SOD and catalase activity, following the manufacturer's guidelines. Enzyme activities were displayed as fold change compared to the control.

4.10. Measurements of Superoxide Generation and Apoptosis. DHE was used for the detection of mitochondrial superoxide generation in vivo. A specific mitochondrial superoxide indicator MitoSOX red (Molecular Probes) was used for the detection of ROS production in HK-2 cells in vitro. 20 randomly selected fields were photographed for tissue sections, and the mean fluorescence intensity was calculated by using NIH ImageJ software and was expressed relative to the control (set as 1).

The TUNEL procedure and Hoechst 33258 staining were used to detect apoptosis following the manufacturer's instructions. 10 random fields of cells (approximately 100 cells per group) were counted to determine the percentage of cells undergoing apoptosis.

4.11. PGC-1α Overexpression. To enforce PGC-1α expression in HK-2 cells, pcDNA4 myc PGC-1α was bought from Addgene (USA). Then, pcDNA4 myc PGC-1α was purified using Plasmid Kit (Qiagen, USA). HK-2 cells were seeded at 70% confluence, and 2.5 μg of pcDNA4 myc PGC-1α or pcDNA4 myc was introduced into HK-2 cells using Lipofectamine 2000 (Invitrogen, USA) on 6-well culture dishes according to the manufacturer's instructions. After 24 h cultivation, the cells were exposed to different concentrations of D-glucose and TLR4/NF-κB blockers, and concrete interventions and groupings were as follows: a: 5.5 mM D-glucose (control/5.5 Glu group); b: 30 mM D-glucose (30 Glu group); c: pcDNA4 myc PGC-1α and 30 mM D-glucose (PGC-1α + 30 Glu group); d: pcDNA4 myc and 30 mM D-glucose (empty vector + 30 Glu group); e: pcDNA4 myc PGC-1α, TAK242, and 30 mM D-glucose (PGC-1α + TAK242 + 30 Glu group); and f: pcDNA4 myc PGC-1α, parthenolide, and 30 mM D-glucose (PGC-1α + parthenolide + 30 Glu group).

4.12. Real-Time Reverse Transcription Polymerase Chain Reaction (Real-Time RT-PCR). Total RNA was isolated with TRIzol (Invitrogen, USA), and 1 μg RNA was used for reverse transcription to generate template cDNA. The relative mRNA levels were determined via fluorogenic quantitative PCR, and β-actin served as an internal reference gene. Specific primers for the use of SYBR Green are as follows: TLR4: 5′-ACCTGTCCCTGAACCCTATG-3′ (forward) and 5′-TCTAAACCAGCCAGACCTTGA-3′ (reverse); NF-κB: 5′-AGCACAGATACCACCAAGACC-3′ (forward) and 5′-CGGCAGTCCTTTCCTACAAG-3′ (reverse); PGC-1α: 5′-TGAGTCTGTATGGAGTGACATCG-3′ (forward) and 5′-ACTTGAGTCCACCCAGAAAGC-3′ (reverse); and caspase-3: 5′-TGCATACTCCACAGCACCTG-3′ (forward) and 5′-TTCTGTTGCCACCTTTCGGT-3′ (reverse). The primer sequences were designed using Primer 5.0 and were searched for specificity. Real-time quantitation was performed on the Applied Biosystems® 7300 system (ABI 7300, USA). The PCR parameters were as follows: 95°C for 30 s followed by 40 cycles of denaturation at 95°C for 5 s and annealing at 60°C for 31 s. The quantitative PCR results were calculated using the $2^{-\Delta\Delta Ct}$ methods.

4.13. Western Blotting (WB). The frozen kidney tissues of mice were lysed with RIPA lysis buffer (Beyotime, Shanghai, China) followed by centrifugation at 12000 rpm at 4°C to obtain cellular proteins in the supernatant. Cell lysate of HK-2 was obtained using RIPA buffer (Beyotime, Shanghai, China) and cocktail (Roche Diagnostics, Mannheim, Germany). The extractions of cell cytoplasmic and mitochondrial fractions were obtained by Mitochondria/Cytosol Fractionation Kit (Abcam, USA) according to the manufacturer's

protocol. The protein concentration was quantified using the BCA method (Beyotime, Shanghai, China). Then, the samples were separated in 10% SDS-polyacrylamide gels, transferred onto polyvinylidene difluoride membranes (Millipore, MA, USA), and incubated overnight at 4°C with primary antibodies. After overnight incubation, membranes were washed 3 times after which they were incubated with secondary antibodies (anti-mouse IgG, Proteintech, Wuhan, China; anti-rabbit IgG, Proteintech, Wuhan, China) for 1 h at room temperature and again washed 3 times. The blots were then detected using ECL (Millipore, MA, USA). Primary antibodies used in this experiment were anti-TLR4 antibody (1 : 1000, Abcam, USA), NF-κB p65 antibody (1 : 1000, CST, Boston, USA), phospho-NF-κB p65 (ser536) antibody (1 : 1000, Bioworld, USA), cytochrome C (1 : 1000, CST, Boston, USA), monoclonal anti-PGC-1α (1 : 1000, CST, Boston, USA), and anti-caspase-3 (1 : 1000, CST, Boston, USA). The intensity of each band was estimated using NIH image software and was normalized to β-actin.

4.14. Assessment of Mitochondrial Membrane Potential ($\triangle \Psi_m$). Mitochondrial $\triangle\Psi_m$ of cells was assessed by TMRM Detection Kit (Genmed Scientifics Inc., USA). HK-2 cells plated on 24-well culture dishes were harvested after trypsinization when they were seeded at 70% confluence, and then the cells were stained with TMRM dyeing liquid according to the manufacturer's instruction. For 20 min incubation in the dark at 37°C, mitochondrial $\triangle\Psi_m$ of cells was examined by a FACSCalibur flow cytometer (BD Biosciences, San Jose, USA). The fluorescence intensity of TMRM was monitored at 575 nm.

4.15. Flow Cytometry Analysis of Apoptosis. Cell apoptosis was measured with Annexin V-FITC Apoptosis Detection Kit (Beyotime, Shanghai, China). According to the manufacturer's instructions, cells were incubated with 195 μL binding buffer containing 5 μL Annexin V-FITC and 10 μL propidium iodide in the dark for 20 min at room temperature. Cell apoptosis was analyzed on a FACSCalibur flow cytometer (BD Biosciences, San Jose, USA).

4.16. Data Analysis. Statistical analysis was carried out using the SPSS 20 software. Results were expressed as mean value s ± standard error of the mean (SEM). Statistical differences among groups were analyzed by one-way ANOVA, and two-tailed P values are reported. P values less than 0.05 were considered statistically significant.

Disclosure

The authors alone are responsible for the content and writing of the article.

Conflicts of Interest

The authors declare no competing financial interests.

Acknowledgments

This work was supported by grants from National Natural Science Foundation of China (81300600, 81470947, 81370832, 81470960, and 81770714), Natural Science Foundation of Hunan Province (2018JJ3728), Free Explore Plan of Central South University (2012QNZT146), and Hunan Province ZuoLi Cup Elite project (0442016001).

References

[1] H. An, C. Qian, and X. Cao, "Regulation of toll-like receptor signaling in the innate immunity," *Science China Life Sciences*, vol. 53, no. 1, pp. 34–43, 2010.

[2] H. J. Anders, B. Banas, and D. Schlondorff, "Signaling danger: toll-like receptors and their potential roles in kidney disease," *Journal of the American Society of Nephrology*, vol. 15, no. 4, pp. 854–867, 2004.

[3] J. Chen, R. John, J. A. Richardson et al., "Toll-like receptor 4 regulates early endothelial activation during ischemic acute kidney injury," *Kidney International*, vol. 79, no. 3, pp. 288–299, 2011.

[4] M. Lin, W. H. Yiu, H. J. Wu et al., "Toll-like receptor 4 promotes tubular inflammation in diabetic nephropathy," *Journal of the American Society of Nephrology*, vol. 23, no. 1, pp. 86–102, 2012.

[5] S. Devaraj, P. Tobias, and I. Jialal, "Knockout of toll-like receptor-4 attenuates the pro-inflammatory state of diabetes," *Cytokine*, vol. 55, no. 3, pp. 441–445, 2011.

[6] I. Jialal, A. M. Major, and S. Devaraj, "Global toll-like receptor 4 knockout results in decreased renal inflammation, fibrosis and podocytopathy," *Journal of Diabetes and its Complications*, vol. 28, no. 6, pp. 755–761, 2014.

[7] M. Wei, Z. Li, L. Xiao, and Z. Yang, "Effects of ROS-relative NF-κB signaling on high glucose-induced TLR4 and MCP-1 expression in podocyte injury," *Molecular Immunology*, vol. 68, no. 2, Part A, pp. 261–271, 2015.

[8] L. Xiao, X. Zhu, S. Yang et al., "Rap1 ameliorates renal tubular injury in diabetic nephropathy," *Diabetes*, vol. 63, no. 4, pp. 1366–1380, 2014.

[9] O. J. Martin, L. Lai, M. M. Soundarapandian et al., "A role for peroxisome proliferator-activated receptor γ coactivator-1 in the control of mitochondrial dynamics during postnatal cardiac growth," *Circulation Research*, vol. 114, no. 4, pp. 626–636, 2014.

[10] N. Gleyzer, K. Vercauteren, and R. C. Scarpulla, "Control of mitochondrial transcription specificity factors (TFB1M and TFB2M) by nuclear respiratory factors (NRF-1 and NRF-2) and PGC-1 family coactivators," *Molecular and Cellular Biology*, vol. 25, no. 4, pp. 1354–1366, 2005.

[11] D. Álvarez-Guardia, X. Palomer, T. Coll et al., "The p65 subunit of NF-κB binds to PGC-1α, linking inflammation and metabolic disturbances in cardiac cells," *Cardiovascular Research*, vol. 87, no. 3, pp. 449–458, 2010.

[12] H. Mudaliar, C. Pollock, M. G. Komala, S. Chadban, H. Wu, and U. Panchapakesan, "The role of toll-like receptor proteins (TLR) 2 and 4 in mediating inflammation in proximal tubules," *American Journal of Physiology Renal Physiology*, vol. 305, no. 2, pp. F143–F154, 2013.

[13] L. Sun, L. Xiao, J. Nie et al., "p66Shc mediates high-glucose and angiotensin II-induced oxidative stress renal tubular injury via

mitochondrial-dependent apoptotic pathway," *American Journal of Physiology Renal Physiology*, vol. 299, no. 5, pp. F1014–F1025, 2010.

[14] J. Peng, X. Li, D. Zhang et al., "Hyperglycemia, p53, and mitochondrial pathway of apoptosis are involved in the susceptibility of diabetic models to ischemic acute kidney injury," *Kidney International*, vol. 87, no. 1, pp. 137–150, 2015.

[15] M. Lin and S. C. W. Tang, "Toll-like receptors: sensing and reacting to diabetic injury in the kidney," *Nephrology Dialysis Transplantation*, vol. 29, no. 4, pp. 746–754, 2014.

[16] M. Lin, W. H. Yiu, R. X. Li et al., "The TLR4 antagonist CRX-526 protects against advanced diabetic nephropathy," *Kidney International*, vol. 83, no. 5, pp. 887–900, 2013.

[17] R. Yu, H. Bo, V. Villani, P. J. Spencer, and P. Fu, "The inhibitory effect of rapamycin on toll like receptor 4 and interleukin 17 in the early stage of rat diabetic nephropathy," *Kidney & Blood Pressure Research*, vol. 41, no. 1, pp. 55–69, 2016.

[18] S. Akira and K. Takeda, "Toll-like receptor signalling," *Nature Reviews Immunology*, vol. 4, no. 7, pp. 499–511, 2004.

[19] L. A. O'Neill, "Therapeutic targeting of toll-like receptors for inflammatory and infectious diseases," *Current Opinion in Pharmacology*, vol. 3, no. 4, pp. 396–403, 2003.

[20] T. Kawai and S. Akira, "TLR signaling," *Seminars in Immunology*, vol. 19, no. 1, pp. 24–32, 2007.

[21] T. Kuwabara, K. Mori, M. Mukoyama, M. Kasahara, H. Yokoi, and K. Nakao, "Macrophage-mediated glucolipotoxicity via myeloid-related protein 8/toll-like receptor 4 signaling in diabetic nephropathy," *Clinical and Experimental Nephrology*, vol. 18, no. 4, pp. 584–592, 2014.

[22] J. M. Forbes and D. R. Thorburn, "Mitochondrial dysfunction in diabetic kidney disease," *Nature Reviews Nephrology*, vol. 14, no. 5, pp. 291–312, 2018.

[23] Y. L. Zou, W. B. Luo, L. Xie, X. B. Mao, C. Wu, and Z. P. You, "Targeting human 8-oxoguanine DNA glycosylase to mitochondria protects cells from high glucose-induced apoptosis," *Endocrine*, pp. 1–13, 2018.

[24] C. Brooks, Q. Wei, S. G. Cho, and Z. Dong, "Regulation of mitochondrial dynamics in acute kidney injury in cell culture and rodent models," *The Journal of Clinical Investigation*, vol. 119, no. 5, pp. 1275–1285, 2009.

[25] D. F. Suen, K. L. Norris, and R. J. Youle, "Mitochondrial dynamics and apoptosis," *Genes & Development*, vol. 22, no. 12, pp. 1577–1590, 2008.

[26] S. D. Chen, D. I. Yang, T. K. Lin, F. Z. Shaw, C. W. Liou, and Y. C. Chuang, "Roles of oxidative stress, apoptosis, PGC-1α and mitochondrial biogenesis in cerebral ischemia," *International Journal of Molecular Sciences*, vol. 12, no. 10, pp. 7199–7215, 2011.

[27] J. St-Pierre, S. Drori, M. Uldry et al., "Suppression of reactive oxygen species and neurodegeneration by the PGC-1 transcriptional coactivators," *Cell*, vol. 127, no. 2, pp. 397–408, 2006.

[28] Y. X. Han, Y. T. Lin, J. J. Xu et al., "Status epilepticus stimulates peroxisome proliferator-activated receptor γ coactivator 1-α/mitochondrial antioxidant system pathway by a nitric oxide-dependent mechanism," *Neuroscience*, vol. 186, pp. 128–134, 2011.

[29] J. Schilling, L. Lai, N. Sambandam, C. E. Dey, T. C. Leone, and D. P. Kelly, "Toll-like receptor-mediated inflammatory signaling reprograms cardiac energy metabolism by repressing peroxisome proliferator-activated receptor γ coactivator-1 signaling," *Circulation: Heart Failure*, vol. 4, no. 4, pp. 474–482, 2011.

[30] X. Zhu, X. Xiong, S. Yuan et al., "Validation of the interstitial fibrosis and tubular atrophy on the new pathological classification in patients with diabetic nephropathy: a single-center study in China," *Journal of Diabetes and Its Complications*, vol. 30, no. 3, pp. 537–541, 2016.

[31] T. W. C. Tervaert, A. L. Mooyaart, K. Amann et al., "Pathologic classification of diabetic nephropathy," *Journal of the American Society of Nephrology*, vol. 21, no. 4, pp. 556–563, 2010.

[32] R. J. Youle and M. Karbowski, "Mitochondrial fission in apoptosis," *Nature Reviews Molecular Cell Biology*, vol. 6, no. 8, pp. 657–663, 2005.

[33] Y. J. Lee, S. Y. Jeong, M. Karbowski, C. L. Smith, and R. J. Youle, "Roles of the mammalian mitochondrial fission and fusion mediators Fis1, Drp1, and Opa1 in apoptosis," *Molecular Biology of the Cell*, vol. 15, no. 11, pp. 5001–5011, 2004.

Hindawi
Oxidative Medicine and Cellular Longevity
Volume 2018, Article ID 1324820, 8 pages
https://doi.org/10.1155/2018/1324820

Research Article

Oxidative and Antioxidative Status of Children with Celiac Disease Treated with a Gluten Free-Diet

Grażyna Rowicka,[1] **Grażyna Czaja-Bulsa**,[2] **Magdalena Chełchowska**,[3] **Agnieszka Riahi**,[1] **Małgorzata Strucińska**,[1] **Halina Weker**,[1] **and Jadwiga Ambroszkiewicz**[3]

[1]*Nutrition Department, Institute of Mother and Child, Warsaw, Poland*
[2]*Clinic of Pediatrics, Gastrology and Children's Rheumatology, Pomeranian Medical University, Szczecin, Poland*
[3]*Department of Screening and Metabolic Diagnostics, Institute of Mother and Child, Warsaw, Poland*

Correspondence should be addressed to Grażyna Rowicka; grazyna.rowicka@imid.med.pl

Received 11 January 2018; Accepted 11 March 2018; Published 2 May 2018

Academic Editor: Claudio Cabello-Verrugio

Aims. Oxidative stress is a factor involved in the pathogenesis of celiac disease (CD), possibly affecting the course of the disease and celiac-related complications. We assessed the intensity of oxidative processes and the efficiency of antioxidant defense in children with celiac disease. *Methods*. Group I ($n = 32$) consisted of children with CD treated with a gluten-free diet, and group II ($n = 24$) consisted of healthy children on a traditional diet. Antioxidative and oxidative status was assessed by measurement of serum total antioxidant capacity (TAC), total oxidant capacity (TOC), and oxidized low-density lipoprotein (ox-LDL) and on the basis of oxidative stress index (OSI). *Results*. There were no significant differences in serum TAC, TOC, ox-LDL, and OSI between children with CD and healthy children. Cluster analysis showed that the group of children with CD is not homogeneous in terms of serum TAC and TOC levels. About 50% of these children had TAC levels < 1.3 mmol/L and TOC levels > 0.35 mmol/L. *Conclusions*. Strict adherence to a gluten-free diet by children with CD seems to be important for maintaining oxidative-antioxidant balance. However, further research is needed to identify factors potentially responsible for increased oxidative stress in some children with celiac disease despite adherence to a gluten-free diet.

1. Introduction

Celiac disease (CD) is an autoimmune, gluten-sensitive inflammatory disorder of the small intestine, which occurs in people with a genetic predisposition. It is one of the more common genetic diseases, with a prevalence of from 1 : 100 up to 1 : 200 in European and American populations [1]. Although there is no precise data on the prevalence of this disease in the Polish population, it seems that only a small percentage of all cases are detected. Celiac disease is characterized by a complex interaction between genetic and environmental factors. The disease is caused by a persistent intolerance of gluten, which is a storage protein found in grains. Gluten is actually made up of two main groups of proteins: gliadins, also known as prolamins, and glutenins. Celiac disease-related gluten intolerance involves certain fractions of prolamins, gliadin found in wheat, secalin found in rye, and hordein found in barley [2]. Our understanding of biochemical and immunological aspects and the mechanisms involved in the toxicity of these prolamins (there are also many prolamins in cereals, including rice and corn, that do not have toxic properties) is growing. Nevertheless, research is underway to better understand the pathogenesis of the disease. The mucosal damage in celiac patients is considered to be induced by the interplay between innate and adaptive immune responses to ingested gluten. The studies have shown that the gliadin sequence contains regions that play an important role in CD pathogenesis by exerting cytotoxic or immunomodulatory activity. The other regions are responsible for triggering oxidative stress and inducing the release of proinflammatory cytokines [3–9].

Oxidative stress is caused by increased production of reactive oxygen species (ROS), exceeding the capacity of physiological antioxidant systems [10, 11]. Inflammation and oxidative stress due to an increase in reactive oxygen species and a decrease of antioxidant defenses seem to be

involved in the molecular mechanisms of celiac disease. It cannot be excluded that they predispose patients with CD to other autoimmune diseases [6, 12–14]. This seems to be particularly true of undiagnosed or diagnosed but untreated/inappropriately treated disease [15, 16].

Efficient antioxidant mechanisms, both enzymatic and nonenzymatic, defend the body against free radical damage. Antioxidant enzymes include, for example, superoxide dismutase (SOD), catalase (CAT), glutathione peroxidase (GPx), glutathione reductase (GR), glutathione S-transferase (GST), and glucose-6-phosphate dehydrogenase (G6PDH). Nonenzymatic mechanisms include, among others, glutathione (GSH), vitamin C (ascorbic acid), vitamin E (α-tocopherol), β-carotene, vitamin A (retinol), flavonoids, and binding proteins—transferrin, ceruloplasmin, and albumin [16]. Some nonenzymatic antioxidants are essential diet components and are found in many food products.

Total antioxidant capacity (TAC) is an expression of a complete ability to neutralize free oxygen radicals that initiate oxidative damage. TAC includes, among others, such factors as uric acid (32–65%), thiol groups of proteins (10–50%), ascorbic acid (6–24%), vitamins A and E (5–10%), and albumin-bound bilirubin (7%). Although uric acid and thiols represent the greatest percentage contribution to TAC, their antioxidant capacity is lower compared with vitamins, which are considered highly efficient nonenzymatic antioxidants. Markers that determine the intensity of the oxidation processes include, inter alia, TOC (total oxidant capacity), measuring the total oxidant capacity in the serum, and ox-LDL (oxidized low-density lipoprotein), indicating the intensity of lipid peroxidation [17].

From a clinical point of view, CD is characterized by a clinical heterogeneity that ranges from asymptomatic to severely symptomatic and by increased morbidity and mortality. Strict lifetime adherence to a gluten-free diet is currently the only available, effective, and safe therapy for celiac disease [18, 19].

The question arises whether the use of a strict gluten-free diet in children with CD is sufficient for maintaining a serum oxidative/antioxidant balance in these children.

The aim of the study was to assess the intensity of oxidative processes and the efficiency of antioxidant defense mechanisms in children with celiac disease treated with a gluten-free diet.

2. Materials and Methods

The study was carried out according to the principles of the Declaration of Helsinki and approved by the Ethics Committee of the Institute of Mother and Child in Warsaw, Poland. Informed consent was obtained from the parents of the study participants and from children aged over 16 years old. The study was conducted as part of statutory task IMiD number OPK 510-25-48.

2.1. Subjects. The study covered 56 children, including 27 girls (48%) and 29 boys (52%) aged between 7 and 18 years, attending the Gastroenterology Outpatient Clinic of the Institute of Mother and Child in Warsaw and the Gastroenterology Outpatient Clinic of Children's Hospital "Zdroje" in Szczecin (SPS ZOZ "Zdroje"). Children with celiac disease diagnosed in accordance with the European Society for Pediatric Gastroenterology Hepatology and Nutrition (ESPGHAN) were included in group I ($n = 32$). These were children on a strict gluten-free diet, as evidenced by the absence of serum IgA and IgG anti-transglutaminase (tTG) antibodies in at least the last year [18]. The control group II included 24 healthy children, whose serological screening detected to be negative and who had no history of any chronic disease.

Exclusion criteria were acute and chronic inflammation, consumption of dietary supplements containing substances with antioxidant activity, and chronic comorbidities that could increase oxidative stress in children with celiac disease.

2.2. Anthropometric Measurements. The children's nutritional status was assessed on the basis of weight and height. Weight (kg) and height (m) were used to calculate body mass index (BMI) as body weight (kg) divided by height squared (m^2). BMI values were compared with BMI norms for age and sex according to OLAF criteria, thus obtaining a BMI z-score, which is a normalized relative weight indicator independent of age and sex [20].

2.3. Blood Sampling and Biochemical Analysis. For biochemical measurements, venous blood (3.0 mL) was taken in the morning hours from fasting patients. Blood was collected in the usual manner, but the full blood count sample was collected into anticoagulated tubes with sodium heparin. In order to obtain plasma, the blood was centrifuged at 2500 ×g at 4°C for 10 minutes. Plasma and serum samples were frozen (−70°C) until measurements of IgA and IgG anti-human tTG antibodies (IgA tTG ab, IgG tTG ab) and concentrations of biochemical parameters (TOC, TAC—max 4 weeks, ox-LDL, vitamin E, ferritin, and uric acid—max 6 months) were performed. The tTG antibody serum levels were assessed using a commercial FluoroEnzymeImmuno Assay kit (Phadia, Sweden), and a value below 7 U/mL was considered negative [21]. Serum total oxidative capacity (TOC) and total antioxidative capacity (TAC) were evaluated by colorimetric/photometric assay using commercially available kits (LDN Labor Diagnostika Nord GmbH & Co. KG, Germany). Determinations of TOC and TAC are based on the reaction of peroxides with peroxidase followed by a color reaction of the chromogenic substrate tetramethylbenzidine. The analytical sensitivity of TOC was 0.06 mmol/L, and the intra- and interassay coefficients of variation (CV) were 4.90% and 7.33%, respectively. The sensitivity of TAC was 0.08 mmol/L, and the intra- and interassay CV were 5.00% and 6.92%, respectively [22].

According to the manufacturer's reference data (manual of LDN Labor Diagnostika Nord GmbH & Co. KG, Germany), the expected value of TOC was <0.35 mmol/L, while TAC indicating sufficient antioxidative capacity was >1.3 mmol/L and indicating borderline antioxidant capacity was between 1.0 and 1.3 mmol/L. Also, in the study of Drabko and Kowalczyk [23], healthy children had a mean value of total antioxidant status at the level of 1.3 mmol/L.

Table 1: Characteristics of the studied children.

Variables	Children with CD ($n = 32$)	Healthy controls ($n = 24$)	p value
Age (years)$^{+}$	13.8 (10.4–16.5)	12.4 (8.4–14.4)	0.089
Treatment with gluten-free diet (years)$^{++}$	7.6 (3.3)	—	—
Weight (kg)$^{+}$	43.2 (28.3–52.5)	42.2 (36.9–59.8)	0.144
Height (cm)$^{++}$	153.8 (19.1)	153.5 (17.2)	0.952
BMI (kg/m^2)$^{++}$	17.3 (3.4)	19.6 (2.4)	0.006*
BMI z-score^{+}	−0.7 (−1.0 to −0.3)	0.4 (−0.4–1.0)	0.0001*

$^{+}$Data are presented as median value and interquartile ranges (1Q–3Q). $^{++}$Data are presented as mean value and standard deviation (SD). *Statistically significant differences ($p < 0.05$). BMI: body mass index; BMI z-score: a normalized relative weight indicator independent of age and sex.

Oxidative stress index (OSI) was defined as the percentage ratio of TOC levels to TAC levels.

Oxidized-LDL (ox-LDL) levels were determined by enzyme-linked immunosorbent assay (ELISA) (Immundiagnostik AG, Bensheim, Germany). The intra- and interassay coefficients of variability were found to be less than 5.7% and 9.0%, respectively. The detection limit was 4.13 ng/mL.

Plasma concentrations of vitamins A (retinol) and E (α-tocopherol) were measured by high-performance liquid chromatography (HPLC, KNAUER, Germany) using a methodology based on the procedure of Zaman et al. [24].

Serum levels of C-reactive protein (CRP), ferritin, and uric acid as well as total cholesterol (TC), HDL cholesterol (HDL-C), LDL cholesterol (LDL-C), and triglyceride (TG) concentrations were determined using standard methods on the Integra Cobas 400 plus analyzer (Roche Diagnostics, Switzerland).

2.4. Statistical Analysis. The appropriate difference significance tests, such as Student's t-test for variables with normal distribution and homogeneity of variance as well as the Mann–Whitney U test for variables with nonnormal distribution, were used to assess the differences between children with CD and the controls in terms of the analyzed anthropometric and biochemical variables.

Data are presented as mean values and standard deviations for variables with normal distribution or medians and interquartile ranges for variables with nonnormal distribution. The Shapiro-Wilk test was used to test the normality of variable distributions.

Pearson's correlation coefficients (Pearson's r) were calculated for oxidative and antioxidant status indicators and other biochemical parameters as well as selected anthropometric and clinical variables. Cluster analysis (CA) was performed with the k-means method to identify groups of children differing in their oxidative and antioxidant status. Two quantitative variables, TOC and TAC, as well as a qualitative variable for group membership (CD/healthy children) were used for CA. $p < 0.05$ was considered statistically significant. Statistica 12 PL was used for statistical analysis.

3. Results

The characteristics of the studied children are presented in Table 1.

The percentage of girls and boys was similar in both groups of children, with 50%/50% in group I and 45.8%/44.2% in group II. Children with celiac disease were on a gluten-free diet for an average of 7 years.

Children in both groups did not differ significantly in terms of age, body weight, or height. Although BMI and BMI z-score were significantly lower in children with CD, the value of BMI z-score pointed to an appropriate nutritional status of children from both groups (BMI z-score <−1;+1>).

As shown in Table 2, there were no significant differences in serum TAC, TOC, ox-LDL, and OSI between patients with CD and healthy children. Vitamin A and ferritin levels were significantly higher in patients with CD compared with healthy children ($p < 0.05$). There were no significant differences in mean serum vitamin E and uric acid levels between the two groups.

Correlations between serum concentrations of oxidative-antioxidative status markers and clinical/biochemical parameters in children with CD are presented in Table 3.

A positive correlation was found between ferritin and TOC levels ($p < 0.05$) as well as HDL cholesterol and ox-LDL levels ($p < 0.01$) in the group of children with celiac disease. Additionally, a negative correlation between vitamin A and ox-LDL levels ($p < 0.01$) as well as HDL and OSI ($p < 0.05$) was shown in this group.

Based on cluster analysis performed with the k-means method, three groups (clusters) of children with varying TOC and TAC levels including two groups of children with celiac disease were identified: CD1 ($n = 17/56$) with mean TAC levels of 1.80 mmol/L and mean TOC levels of 0.167 mmol/L; CD2 ($n = 15/56$) with TAC/TOC levels of 0.89 mmol/L and 0.41 mmol/L, respectively; and the third group consists of healthy children ($n = 24/56$) with mean TAC levels of 1.34 mmol/L and mean TOC levels of 0.29 mmol/L (Figure 1).

Cluster analysis showed that the group of children with celiac disease is not homogeneous in terms of serum TAC and TOC levels, with about 50% of these patients (CD2 cluster, $n = 15/32$) with TAC levels considered insufficient for proper antioxidant defense (<1.3 mmol/L) and TOC levels indicating increased oxidative processes (TOC > 0.35 mmol/L) (Figure 1).

Differences in CRP level between CD1 and CD2 children are presented in Figure 2.

Children with celiac disease (CD1) with TOC and TAC levels within the range of expected values had lower CRP

Table 2: Biochemical parameters in children with CD and healthy controls.

Variables	Children with CD ($n = 32$)	Healthy controls ($n = 24$)	p value
TOC (mmol/L)$^{+}$	0.23 (0.13–0.35)	0.27 (0.16–0.36)	0.608
TAC (mmol/L)$^{++}$	1.38 (0.60)	1.35 (0.42)	0.815
Ox-LDL (ng/mL)$^{+}$	125.4 (68.6–242.0)	147.4 (56.5–446.8)	0.796
OSI^{+}	0.16 (0.07–0.36)	0.20 (0.14–0.27)	0.535
CRP (mg/L)$^{+}$	0.29 (0.15–0.50)	0.40 (0.14–0.90)	0.355
Ferritin (ng/mL)$^{+}$	81.0 (33.1–120.0)	43.4 (26.3–60.1)	0.027*
Uric acid (mg/dL)$^{+}$	4.4 (4.0–5.4)	4.4 (4.1–4.9)	0.868
Vitamin E (μmol/L)$^{+}$	17.8 (15.3–19.7)	18.7 (14.7–20.9)	0.952
Vitamin A (μmol/L)$^{++}$	2.0 (0.42)	1.6 (0.56)	0.026*
Cholesterol total (mg/dL)$^{++}$	167.7 (24.6)	166.9 (24.5)	0.903
Cholesterol HDL (mg/dL)$^{++}$	56.7 (21.8)	59.8 (15.1)	0.567
Cholesterol LDL (mg/dL)$^{+}$	97.0 (83.0–126.0)	95.5 (81.5–117.0)	0.601
Triglycerides (mg/dL)$^{+}$	68.5 (48.0–104.0)	61.0 (48.0–100.0)	0.781

$^{+}$Data are presented as median value and interquartile ranges (1Q–3Q). $^{++}$Data are presented as mean value and standard deviation (SD). *Statistically significant differences ($p < 0.05$). TOC: total oxidant capacity; TAC: total antioxidant capacity; ox-LDL: oxidized low-density lipoprotein; OSI: oxidative stress index; CRP: C-reactive protein.

Table 3: Correlations between serum concentrations of oxidative-antioxidative status markers and clinical/biochemical parameters in children with CD ($n = 32$).

Variables	TOC		TAC		OSI		ox-LDL	
	r	p	r	p	r	p	r	p
Age	−0.14	0.448	0.11	0.549	−0.07	0.711	−0.05	0.813
Treatment with gluten-free diet	0.38	0.055	−0.18	0.387	0.21	0.313	0.33	0.096
BMI z-score	−0.02	0.928	−0.11	0.546	−0.08	0.664	−0.05	0.810
CRP	−0.20	0.293	−0.20	0.294	−0.06	0.751	0.02	0.928
Ferritin	0.43	0.014*	0.10	0.573	0.15	0.422	0.17	0.386
Uric acid	−0.17	0.415	0.05	0.825	−0.09	0.667	−0.13	0.551
Vitamin E	−0.27	0.190	0.33	0.097	−0.35	0.080	−0.07	0.749
Vitamin A	0.06	0.775	−0.14	0.492	0.15	0.461	−0.55	0.003*
Cholesterol total	0.26	0.169	0.17	0.380	0.15	0.421	0.12	0.567
Cholesterol HDL	−0.30	0.109	0.18	0.350	−0.38	0.038*	0.49	0.009*
Cholesterol LDL	0.32	0.089	0.02	0.920	0.31	0.100	−0.18	0.364
Triglycerides	−0.03	0.872	−0.04	0.846	−0.02	0.904	−0.22	0.266

r: Pearson's correlation coefficient, *$p < 0.05$; TOC: total oxidant capacity; TAC: total antioxidant capacity; ox-LDL: oxidized low-density lipoprotein; OSI: oxidative stress index; CRP: C-reactive protein; BMI z-score: normalized relative weight indicator independent of age and sex.

levels (median 0.23; interquartile range 0.12–0.34) compared with children with celiac disease (CD2) with serum TOC and TAC levels not corresponding to the expected values (median 0.41; interquartile range 0.26–0.65) (Figure 2).

4. Discussion

Consumption of gluten by patients with celiac disease induces the overproduction of reactive oxygen species, triggering a cascade of reactions that cause oxidative stress both at the small intestinal mucosa and the whole-body level. Oxidative stress is responsible for free radical damage of important cellular structures, thus adversely modifying their functions [25–28]. A number of studies have been conducted to assess selected markers of antioxidant and oxidative processes in children with celiac disease [6, 15, 29–31]. Our study was conducted as a part of the discussion on whether a gluten-free diet is sufficient for maintaining a serum oxidative/antioxidant balance in children with celiac disease. This may seem doubtful considering the fact that despite strict adherence to the diet (for over 12 months), some celiac patients still experience persistent or recurrent symptoms of refractory celiac disease (RCD) [32]. In the available literature, there are few studies using markers such as TAC, TOC, ox-LDL, and OSI to assess oxidative/antioxidant imbalance in children with celiac disease. Our study

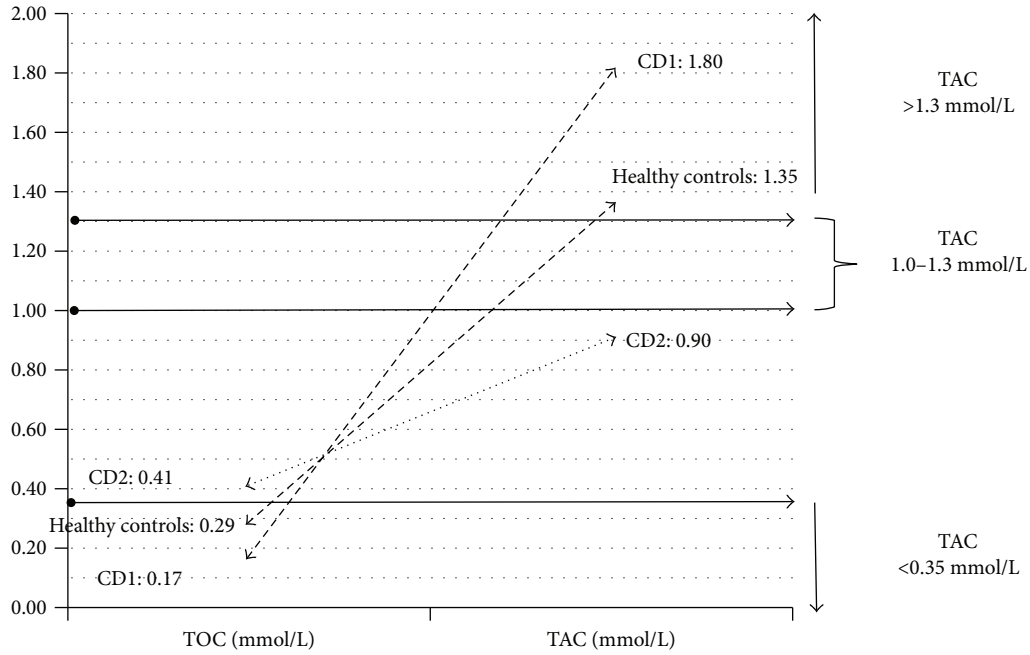

Figure 1: Clusters of children differing in terms of TAC and TOC levels. CD1: children with celiac disease with concentrations of TAC > 1.3 mmol/L and TOC < 0.35 mmol/L. CD2: children with celiac disease with concentrations of TAC < 1.3 mmol/L and TOC > 0.35 mmol/L. Healthy controls with concentrations of TAC > 1.3 mmol/L and TOC < 0.35 mmol/L.

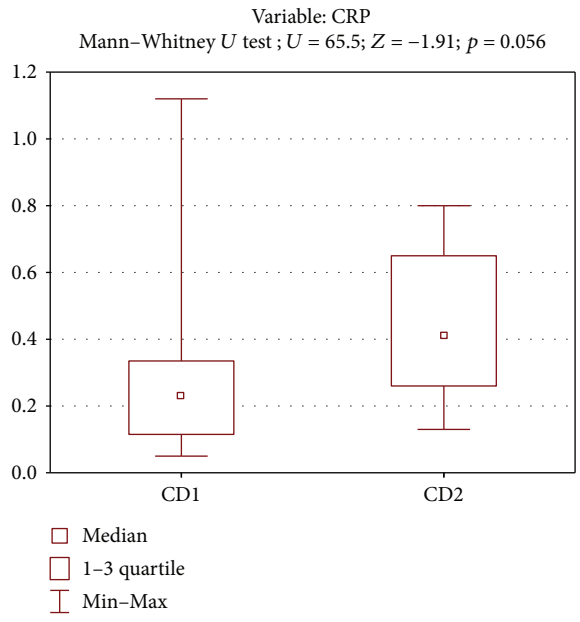

Figure 2: Differences in CRP level between CD1 and CD2 children.

demonstrated no differences in the intensity of oxidative/antioxidant processes assessed based on the above parameters between children with celiac disease treated with a gluten-free diet and healthy children, although the levels of parameters such as ferritin and vitamin A included in TAC were significantly higher in the celiac group. This could suggest that a gluten-free diet is sufficient for maintaining oxidative/antioxidant balance. Nevertheless, a subgroup of children experiencing oxidative stress, despite strict diet adherence, was identified among patients with CD.

The literature data indicates that the antioxidant potential assessed based on various markers both in intestinal mucosa and bodily fluids (blood, urine) is significantly lower in newly diagnosed celiac patients compared with healthy individuals, while the intensity of oxidation processes is higher [6, 15, 29–31]. The results suggest that gliadin disturbs the pro−/antioxidant balance through the overproduction of ROS not only in the small intestinal mucosa of affected persons [33]. An interesting observation was presented by Stojiljković et al. [15], who demonstrated that the severity of the mucosal lesion in celiac patients significantly correlated with the evaluated markers of radical damage. Thus, a positive correlation was found between the severity of histological lesions in the intestinal mucosa and SOD activity as well as LOOH (lipid peroxides) levels, and the activities of CAT, GPx, and GR and the concentration of GSH inversely correlated with the degree of the mucosal lesion. It seems that the lower antioxidant potential in individuals with untreated celiac disease may be due to, among others, an increased demand for antioxidants necessary to compensate for the elevated production of ROS, and thus prevent their adverse effects. Intestinal mucosal damage caused by reactive oxygen species, leading to secondarily impaired absorption of antioxidant nutrients, may also play an important role [30].

A gluten-free diet is usually associated with clinical improvement, the disappearance of serological markers specific for the disease, and regeneration of the small intestinal mucosa in patients with celiac disease. This should be accompanied by significant improvement in the oxidative/antioxidant balance. The beneficial effects of a gluten-free diet on

antioxidant status were demonstrated by Ferretti et al. [34]. The authors showed that although serum TAC levels were indeed lower in patients with celiac disease who used a gluten-free diet compared with the controls, these levels were still significantly higher compared with newly diagnosed patients who were not on a gluten-free diet. In contrast to Ferretti et al., our study showed no significant differences in mean TAC levels between celiac patients on a gluten-free diet and healthy children. It cannot be excluded that in addition to a gluten-free diet, diet duration is also important for maintaining oxidative/antioxidant balance; however, our study showed no significant correlation in this regard. A diet consisting of natural antioxidants also seems to play an important role. It was documented that several dietary components exert anti-inflammatory and antioxidant roles and have a protective effect on the intestinal epithelium [35–37]. In our study, serum vitamin A levels in children with celiac disease were significantly higher compared with those of the controls, while α-tocopherol levels did not differ between the groups. Szaflarska-Poplawska et al. [13] showed no significant differences in serum vitamin A and E levels between children with celiac disease treated with a gluten-free diet and healthy children; however, the levels of these antioxidants were significantly lower in untreated versus treated patients with CD. Vitamin E, as a scavenger of free oxygen radicals, protects polyunsaturated fatty acids (PUFA), a major structural component of the cellular membranes, from peroxidation [38]. Synergistic interactions between vitamin E and vitamin A against lipid peroxidation were documented [39]. In our study, dietary intake of these vitamins in children with celiac disease could have affected the lack of significant differences not only in TAC and TOC levels and OSI values but also in ox-LDL levels between children with celiac disease and healthy children. This may be indicated by the inverse correlation between vitamin A and ox-LDL levels found in the group of children with celiac disease. Furthermore, we also observed a reverse correlation between HDL cholesterol, demonstrating anti-inflammatory and antioxidative activities, with OSI in this patient population. At the same time however, a positive correlation was found between HDL cholesterol and ox-LDL, which would suggest HDL's effect on oxidative stress contrary to the expected one. Nevertheless, OSI seems to better define oxidative stress severity.

Sayar et al. [29] demonstrated that IMA (ischemia-modified albumin stress marker), TOS (total oxidant status), and AOPP (advanced oxidation protein products) levels were significantly lower after just 30 months of a gluten-free diet, while TAC and SH sulfhydryl levels were significantly higher. Similarly in the study by Ertekin et al. [40], serum nitric oxide levels were found to be higher in children with CD than in the control group, and these levels were found to regress after implementing a gluten-free diet. These findings indicated that oxidative stress regressed after the introduction of a gluten-free diet in celiac patients. However, we showed in our study that despite strict adherence to the diet, about 50% of children with celiac disease (CD2) had relatively low TAC levels and high TOC levels, which would indicate oxidative stress. In the same group of children, CRP levels were higher compared with children with celiac disease (CD1) with relatively high TAC and low TOC levels, yet still within the range of reference standards. These results seem to confirm the findings of other authors. Stojiljković et al. [15] point to the fact that oxidative stress may also occur in children with CD who are on a gluten-free diet, as evidenced by differences in the activity of antioxidant enzymes and glutathione (GSH) observed in this group. Szaflarska-Poplawska et al. [13] also observed significant differences in the levels of markers for free radical DNA damage (8-oxodG in DNA isolated from leukocytes and in urine samples) in children with celiac disease compared with healthy children; however, they found no such differences between these parameters in children with treated and untreated celiac disease. Similarly, the study by Odetti et al. [30] indicates that a redox imbalance persists in celiac disease even when asymptomatic. The authors found an increase of markers of oxidative damage of lipids (thiobarbituric acid-reactive substances and lipid hydroperoxides) and proteins (carbonyl groups) in the blood serum of patients with celiac disease compared with healthy individuals. According to the authors, the redox imbalance is probably caused by an absorption deficiency, even if slight. Thus, they suggest that dietary supplementation with antioxidant molecules may offer some benefits. These results suggest that a gluten-free diet is able to only partially improve the functionality of the intestinal mucosa, which leads to the necessity to conduct further studies on this topic.

Our study has some limitations. Firstly, the study included relatively small groups of children, although comparable to those investigated by other authors. Additionally, the group of children with celiac disease was homogeneous, as all children strictly adhered to a gluten-free diet as evidenced by the absence of serum antibodies against tissue transglutaminase. Secondly, data on the content of antioxidants, such as vitamins A, C, and E, or LC-PUFA (long-chain polyunsaturated fatty acid) in the children's diets were missing. However, considering the increased vitamin A levels among children with celiac disease and similar levels of vitamin E in both groups, it can be assumed that the diets of these children were balanced in this regard.

To conclude, strict adherence to a gluten-free diet by children with celiac disease seems to be an important condition for maintaining oxidative-antioxidant balance, as evidenced by a lack of differences in TAC, TOC, ox-LDL, and OSI levels between children treated due to celiac disease and the controls. However, further research is needed to identify factors potentially responsible for increased oxidative stress in some children with celiac disease despite adherence to a gluten-free diet.

Conflicts of Interest

The authors have declared that no competing interests exist.

Authors' Contributions

All authors are aware of and agree to the content of the manuscript, approved the final submitted version, and agreed to be listed as an author of the manuscript. All authors

of this manuscript have directly participated in the execution and analysis of the study.

References

[1] L. Book, J. J. Zone, and S. L. Neuhausen, "Prevalence of celiac disease among relatives of sib pairs with celiac disease in U.S. families," *The American Journal of Gastroenterology*, vol. 98, no. 2, pp. 377–381, 2003.

[2] L. Rodrigo, "Celiac disease," *World Journal of Gastroenterology*, vol. 12, no. 41, pp. 6585–6593, 2006.

[3] R. Ciccocioppo, A. Di Sabatino, and G. R. Corazza, "The immune recognition of gluten in coeliac disease," *Clinical & Experimental Immunology*, vol. 140, no. 3, pp. 408–416, 2005.

[4] L. Shan, Ø. Molberg, I. Parrot et al., "Structural basis for gluten intolerance in celiac sprue," *Science*, vol. 297, no. 5590, pp. 2275–2279, 2002.

[5] G. Mamone, G. Picariello, F. Addeo, and P. Ferranti, "Proteomic analysis in allergy and intolerance to wheat products," *Expert Review of Proteomics*, vol. 8, no. 1, pp. 95–115, 2011.

[6] L. Högberg, C. Webb, K. Fälth-Magnusson et al., "Children with screening-detected coeliac disease show increased levels of nitric oxide products in urine," *Acta Paediatrica*, vol. 100, no. 7, pp. 1023–1027, 2011.

[7] P. H. R. Green and B. Jabri, "Celiac disease," *Annual Review of Medicine*, vol. 57, no. 1, pp. 207–221, 2006.

[8] D. Dewar, S. P. Pereira, and P. J. Ciclitira, "The pathogenesis of coeliac disease," *The International Journal of Biochemistry & Cell Biology*, vol. 36, no. 1, pp. 17–24, 2004.

[9] L. Elli, E. Dolfini, and M. T. Bardella, "Gliadin cytotoxicity and in vitro cell cultures," *Toxicology Letters*, vol. 146, no. 1, pp. 1–8, 2003.

[10] E. Granot and R. Kohen, "Oxidative stress in childhood—in health and disease states," *Clinical Nutrition*, vol. 23, no. 1, pp. 3–11, 2004.

[11] C. Cabello-Verrugio, M. Ruiz-Ortega, M. Mosqueira, and F. Simon, "Oxidative stress in disease and aging: mechanisms and therapies," *Oxidative Medicine and Cellular Longevity*, vol. 2016, Article ID 8786564, 2 pages, 2016.

[12] G. Ferretti, T. Bacchetti, S. Masciangelo, and L. Saturni, "Celiac disease, inflammation and oxidative damage: a nutrigenetic approach," *Nutrients*, vol. 4, no. 4, pp. 243–257, 2012.

[13] A. Szaflarska-Poplawska, A. Siomek, M. Czerwionka-Szaflarska et al., "Oxidatively damaged DNA/oxidative stress in children with celiac disease," *Cancer Epidemiology Biomarkers & Prevention*, vol. 19, no. 8, pp. 1960–1965, 2010.

[14] J. Postępski, V. Opoka-Winiarska, and E. Tuszkiewicz-Misztal, "Znaczenie reakcji wolnorodnikowych w patogenezie wybranych schorzeń u dzieci," *Pediatria Polska*, vol. 75, no. 10, pp. 767–776, 2000.

[15] V. Stojiljković, A. Todorović, N. Radlović et al., "Antioxidant enzymes, glutathione and lipid peroxidation in peripheral blood of children affected by coeliac disease," *Annals of Clinical Biochemistry: International Journal of Laboratory Medicine*, vol. 44, no. 6, Part 6, pp. 537–543, 2007.

[16] V. Stojiljković, A. Todorović, S. Pejić et al., "Antioxidant status and lipid peroxidation in small intestinal mucosa of children with celiac disease," *Clinical Biochemistry*, vol. 42, no. 13-14, pp. 1431–1437, 2009.

[17] G. Spiteller, "The important role of lipid peroxidation processes in aging and age dependent diseases," *Molecular Biotechnology*, vol. 37, no. 1, pp. 5–12, 2007.

[18] S. Husby, S. Koletzko, I. R. Korponay-Szabó et al., "European Society for Pediatric Gastroenterology, Hepatology, and Nutrition guidelines for the diagnosis of coeliac disease," *Journal of Pediatric Gastroenterology and Nutrition*, vol. 54, no. 1, pp. 136–160, 2012.

[19] P. H. R. Green, K. Rostami, and M. N. Marsh, "Diagnosis of coeliac disease," *Best Practice & Research Clinical Gastroenterology*, vol. 19, no. 3, pp. 389–400, 2005.

[20] Z. Kułaga, A. Różdżyńska, I. Palczewska et al., "Percentile charts of height, body mass and body mass index in children and adolescents in Poland – results of the OLAF study," *Standardy Medyczne*, vol. 7, pp. 690–700, 2010.

[21] A. Bürgin-Wolff, I. Dahlbom, F. Hadziselimovic, and C. J. Petersson, "Antibodies against human tissue transglutaminase and endomysium in diagnosing and monitoring coeliac disease," *Scandinavian Journal of Gastroenterology*, vol. 37, no. 6, pp. 685–691, 2002.

[22] O. Erel, "A new automated colorimetric method for measuring total oxidant status," *Clinical Biochemistry*, vol. 38, no. 12, pp. 1103–1111, 2005.

[23] K. Drabko and J. R. Kowalczyk, "Zaburzenia równowagi oksydacyjno-antyoksydacyjnej u dzieci z chorobą nowotworową," *Medycyna Wieku Rozwojowego*, vol. 8, 2, Part 1, pp. 217–223, 2004.

[24] Z. Zaman, P. Fielden, and P. G. Frost, "Simultaneous determination of vitamins A and E and carotenoids in plasma by reversed-phase HPLC in elderly and younger subjects," *Clinical Chemistry*, vol. 39, no. 11, pp. 2229–2234, 1993.

[25] M. Boda, I. Németh, and D. Boda, "The caffeine metabolic ratio as an index of xanthine oxidase activity in clinically active and silent celiac patients," *Journal of Pediatric Gastroenterology and Nutrition*, vol. 29, no. 5, pp. 546–550, 1999.

[26] P. Bergamo, M. Gogliettino, G. Palmieri et al., "Conjugated linoleic acid protects against gliadin-induced depletion of intestinal defenses," *Molecular Nutrition & Food Research*, vol. 55, no. S2, pp. S248–S256, 2011.

[27] E. Dolfini, L. Elli, T. Dasdia et al., "In vitro cytotoxic effect of bread wheat gliadin on the LoVo human adenocarcinoma cell line," *Toxicology in Vitro*, vol. 16, no. 4, pp. 331–337, 2002.

[28] M. C. Maiuri, D. de Stefano, G. Mele et al., "Gliadin increases iNOS gene expression in interferon-γ-stimulated RAW 264.7 cells through a mechanism involving NF-κB," *Naunyn-Schmiedeberg's Archives of Pharmacology*, vol. 368, no. 1, pp. 63–71, 2003.

[29] E. Sayar, S. Özdem, G. Uzun, A. İşlek, A. Yılmaz, and R. Artan, "Total oxidant status, total antioxidant capacity and ischemia modified albumin levels in children with celiac disease," *The Turkish Journal of Pediatrics*, vol. 57, no. 5, pp. 498–503, 2015.

[30] P. Odetti, S. Valentini, I. Aragno et al., "Oxidative stress in subjects affected by celiac disease," *Free Radical Research*, vol. 29, no. 1, pp. 17–24, 1998.

[31] A. Lavy, A. Ben-Amotz, and M. Aviram, "Increased susceptibility to undergo lipid peroxidation of chylomicrons and low-density lipoprotein in celiac disease," *Annals of Nutrition & Metabolism*, vol. 37, no. 2, pp. 68–74, 1993.

[32] J. F. Ludvigsson, J. C. Bai, F. Biagi et al., "Diagnosis and management of adult coeliac disease: guidelines from the British

Society of Gastroenterology," *Gut*, vol. 63, no. 8, pp. 1210–1228, 2014.

[33] B. Dugas, N. Dugas, M. Conti et al., "Wheat gliadin promotes the interleukin-4-induced IgE production by normal human peripheral mononuclear cells through a redox-dependent mechanism," *Cytokine*, vol. 21, no. 6, pp. 270–280, 2003.

[34] G. Ferretti, T. Bacchetti, L. Saturni et al., "Lipid peroxidation and paraoxonase-1 activity in celiac disease," *Journal of Lipids*, vol. 2012, Article ID 587479, 7 pages, 2012.

[35] P. C. Calder, R. Albers, J. M. Antoine et al., "Inflammatory disease processes and interactions with nutrition," *British Journal of Nutrition*, vol. 101, Supplement 1, pp. S1–S45, 2009.

[36] D. Bernardo, B. Martínez-Abad, S. Vallejo-Diez et al., "Ascorbate-dependent decrease of the mucosal immune inflammatory response to gliadin in coeliac disease patients," *Allergologia et Immunopathologia*, vol. 40, no. 1, pp. 3–8, 2012.

[37] O. Vincentini, M. G. Quaranta, M. Viora, C. Agostoni, and M. Silano, "Docosahexaenoic acid modulates in vitro the inflammation of celiac disease in intestinal epithelial cells via the inhibition of $cPLA_2$," *Clinical Nutrition*, vol. 30, no. 4, pp. 541–546, 2011.

[38] K. L. Retsky, M. W. Freeman, and B. Frei, "Ascorbic acid oxidation product(s) protect human low density lipoprotein against atherogenic modification. Anti-rather than prooxidant activity of vitamin C in the presence of transition metal ions," *Journal of Biological Chemistry*, vol. 268, no. 2, pp. 1304–1309, 1993.

[39] L. Tesoriere, A. Bongiorno, A. M. Pintaudi, R. D'Anna, D. D'Arpa, and M. A. Livrea, "Synergistic interactions between vitamin A and vitamin E against lipid peroxidation in phosphatidylcholine liposomes," *Archives of Biochemistry and Biophysics*, vol. 326, no. 1, pp. 57–63, 1996.

[40] V. Ertekin, M. A. Selimoğlu, Y. Türkan, and F. Akçay, "Serum nitric oxide levels in children with celiac disease," *Journal of Clinical Gastroenterology*, vol. 39, no. 9, pp. 782–785, 2005.

Hindawi
Oxidative Medicine and Cellular Longevity
Volume 2018, Article ID 8249693, 12 pages
https://doi.org/10.1155/2018/8249693

Research Article

Gefitinib Inhibits Bleomycin-Induced Pulmonary Fibrosis via Alleviating the Oxidative Damage in Mice

Li Li,[1] Lin Cai,[2] Linxin Zheng,[1] Yujie Hu,[3] Weifeng Yuan,[1] Zhenhui Guo,[4] and Weifeng Li[1]

[1]*Department of Respiratory Medicine, General Hospital of Guangzhou Military Command of PLA, Guangzhou, Guangdong, China*
[2]*Guangdong Food and Drug Vocational College, Guangzhou, Guangdong, China*
[3]*Department of Respiratory Medicine, 458 Hospital of PLA, Guangzhou, Guangdong, China*
[4]*MICU, Guangdong Provincial Key Laboratory of Geriatric Infection and Organ Function Support, General Hospital of Guangzhou Military Command of PLA, Guangzhou, Guangdong, China*

Correspondence should be addressed to Zhenhui Guo; micugzh@126.com and Weifeng Li; gzdoctorlwf@163.com

Received 18 August 2017; Revised 24 October 2017; Accepted 26 November 2017; Published 12 April 2018

Academic Editor: Claudio Cabello-Verrugio

Pulmonary fibrosis (PF) is a life-threatening interstitial lung disease. In this study, we tried to reveal the model of action between high-mobility group box 1 (HMGB1) and α-smooth muscle actin (α-SMA) and the protective role of gefitinib in pulmonary fibrosis induced by the administration of bleomycin aerosol in mice. For the mechanism study, lung tissues were harvested two weeks after modeling to detect the coexpression of HMGB1 and α-SMA by immunohistochemistry and immunofluorescence staining. Protein-DNA interactions were analyzed using a pulldown assay to study the relationship between HMGB1 and α-SMA. For the gefitinib treatment study, the mice were divided into three groups: phosphate-buffered saline (PBS) control group, PBS-treated PF group, and gefitinib-treated PF group. Gavage of gefitinib or PBS (20 mg/kg/day) was performed after bleomycin treatment for two weeks until the mice were sacrificed. Lung and blood samples were collected to assess the histological changes, oxidative stress, and expression of NOXs, HMGB1, EGFR, MAPKs, AP-1, and NF-κB to determine the curative effect and related molecular mechanisms. The results revealed the high coexpression of α-SMA and HMGB1 in some interstitial cells in the fibrotic lung. The DNA-protein pulldown analysis proved that HMGB34367 acted as a novel transcriptional factor for the α-SMA promoter and participated in the eventual development of pulmonary fibrosis. Second, gefitinib could significantly decrease lung fibrotic changes and the level of MDA and recover the T-AOC level. Meanwhile, gefitinib could also reduce the NOX1/2/4, HMGB1, p-EGFR, p-ERK, p-JNK, p-P38, p-NF-κB, p-c-Jun, and p-c-Fos expression levels in fibrotic lungs. The present study suggested that gefitinib could alleviate lung fibrosis through the HMGB1/NOXs-ROS/EGFR-MAPKs-AP-1/NF-κB signal in bleomycin-induced pulmonary fibrosis.

1. Introduction

Idiopathic pulmonary fibrosis (IPF) is a chronic interstitial lung disease with high lethality, a fatal prognosis, and a lack of effective medical therapies [1, 2]. The pathological characteristics of IPF mainly include the disruption of the pulmonary parenchymal matrix and replacement with fibrotic tissues [3, 4]. The development of IPF results in declining lung function and eventual respiratory failure, with a median survival of only 2-3 years following diagnosis [5]. Traditional drugs only have marginal effects against this disease [6]. Details of the mechanisms involved in IPF are also not well established, and there is an extreme lack of effective therapies for IPF.

One possible mechanism involved in IPF is the activation of α-smooth muscle actin (α-SMA). Higher expression of α-SMA is accompanied by more collagen deposition, indicating more severe pulmonary fibrosis (PF) [7]. Understanding the mechanism responsible for α-SMA activation is a potential way to determine the fibrotic pathogenesis. High-mobility group box 1 (HMGB1) is a highly conserved DNA-shepherding protein, which could translocate to the cytoplasm as well as the extracellular space during cell activation,

injury, or death [8]. It has been demonstrated that HMGB1 could promote the expression of α-SMA in fibrotic diseases [9]. The detailed mode of action between HMGB1 and α-SMA in pulmonary fibrosis, however, has not yet been fully interpreted. Another mechanism involved in pulmonary fibrosis is the activation of the epidermal growth factor receptor (EGFR). EGFR has been found to be upregulated in the lung tissues of patients and rodents with pulmonary fibrosis [10–12]. Gefitinib, an EGFR-tyrosine kinase inhibitor (EGFR-TKI), has the ability to inhibit fibroblast proliferation, therefore lessening the collagen and extracellular matrix (ECM) deposition in pulmonary fibrosis [13, 14]. However, the concrete mechanism behind this inhibition has not yet been clearly determined. Oxidative stress is another key pathological process in the development of pulmonary fibrosis [15]. Previous studies have shown that bleomycin administration could increase oxidative stress by increasing the production of nitric-oxide synthase and NADPH oxidase (NOX) through the downstream phosphorylation expression of mitogen-activated protein kinases (MAPKs) [16]. Inhibition of oxidative stress and enhancement of antioxidative ability could alleviate pulmonary fibrosis [17].

Since the potential influence and mechanism of gefitinib on pulmonary fibrosis have not been fully studied, the aim of the present research was (1) to detect the model of action between HMGB1 and α-SMA in pulmonary fibrosis and (2) to study the mechanism and resulting effect of gefitinib in the treatment of pulmonary fibrosis.

2. Materials and Methods

2.1. Drug Sources. Bleomycin hydrochloride (BLM) was purchased from Zhejiang Haizheng Pharmaceutical Co. Ltd. and gefitinib was purchased from AstraZeneca (United States). Other chemicals and reagents were obtained from standard commercial sources.

2.2. Model of Bleomycin-Induced Pulmonary Fibrosis in Mice. SPF female KM mice (20–25 g) were purchased from the animal center of Southern Medical University (Guangzhou, China). Pulmonary fibrosis was induced by intratracheal aerosol inhalation of 3 U/kg of bleomycin dissolved in 0.10 mL of saline using MicroSprayer atomization devices. Phosphate-buffered saline (PBS) control mice ($n = 6$, PBS group) received the same volume of intratracheal aerosol inhalation of PBS. The gefitinib-treated mice ($n = 6$, BLM + Ge group) were treated with gefitinib by gavage at a dose of 20 mg/kg/day dissolved in 0.20 mL saline after bleomycin administration. The PBS-treated mice ($n = 6$, BLM group) received the same volume of PBS by gavage after bleomycin administration. All mice in the three groups were sacrificed two weeks after treatment, and lung and blood samples were processed separately for histological and biochemical studies. The animal experiment was approved by the institutional committee of animal care. The detailed experimental procedure was presented in Figure 1.

2.3. Histological Studies

2.3.1. Hematoxylin and Eosin and Masson's Trichrome Staining. For histological examination, the lungs were fixed in 10% buffered formalin and stained with hematoxylin and eosin (H&E) and Masson's trichrome. Histologic grading was performed by three experienced pathologists using a blinded semiquantitative scoring system. The severity of pulmonary inflammation and fibrosis was scored according to the methods described by Mikawa et al. [18] and Ashcroft et al. [19], respectively.

2.3.2. Immunohistochemistry (IHC). Immunohistochemistry staining was performed to identify the expression and location of α-SMA and HMGB1 in the fibrotic lungs. Antibodies used in the study were anti-α-SMA (1 : 100) and anti-HMGB1 (1 : 200) antibodies (Santa Cruz Biotechnology Inc., CA) diluted in PBS. Slides were deparaffinized and treated with 3% H_2O_2 in H_2O to quench endogenous peroxidase activity. α-SMA and HMGB1 staining was performed at 4°C overnight, followed by exposure to anti-mouse secondary antibody for 60 min. Diaminobenzidine (DAB) (Maxim-Bio, Fuzhou, China) was used as the chromogen. Microscopic observation was performed using a Leica DM LB2 microscope equipped with a digital camera.

2.3.3. Immunofluorescence Staining. For immunofluorescence staining of α-SMA and HMGB1, the sections were pretreated with proteinase K and then blocked with 10% normal donkey serum diluted in PBS containing 0.1% Triton. Sections were then incubated with the polyclonal rabbit anti-α-SMA (1 : 200) and anti-HMGB1 (1 : 300) antibodies (Santa Cruz Biotechnology Inc., CA) diluted in PBS. Tissue sections were washed and subsequently incubated with Alexa fluorophore 488 nm donkey anti-rabbit antibody at 1 : 500 in PBS for 90 min at room temperature and counterstained with 4′,6-diamidino-2-phenylindole (DAPI). Images were acquired using an inverted Leica CTR 6000 fluorescence microscope and were merged using a Leica Application Suite Advanced Fluorescence software (Leica Microsystems (UK) Ltd., Milton Keynes, UK).

2.4. DNA-Protein Pulldown Analysis. A total of 3.8 kb of double-stranded DNA fragments corresponding to the mouse α-SMA promoter fragment −1070 to +2582, including the first exon and part of the first intron (GenBank: U63129 and M57409), was amplified from the VSMP8 plasmid by PCR. The plasmid was a generous gift from Professor Art Strauch (Dorothy M. Davis Heart and Lung Research Institute, Columbus, US). The forward primer 5′-AGCCGT GGGAGCGTGAGT-3′ was linked with a biotin molecule at the N terminal; the reverse primer was 5′-AGACAGCGA GCGAGAAGC-3′. Next, 50 μg of biotinylated DNA fragments were ligated on the surface of 50 μL of streptavidin-coated magnetic beads from a kilobaseBINDER kit (Dynal, Finland) to form DNA-bead complexes according to the manufacturer's protocol [20]. Pulmonary nuclear extracts from BLM- or PBS-treated lung tissues were dialyzed in PBS and diluted to 3μg/μL. Next, 30 μg of proteins were added to 250 μL of a DNA-protein binding buffer (20 mM Hepes, 1 mM EDTA, 10 mM $(NH_4)SO_4$, 1 mM DTT, 0.2% Tween20, 30 mM KCl, 50 ng/μL poly(d(IC)), 5 ng/μL poly L-lysine, and Ph 7.6) mixed with DNA affinity beads and

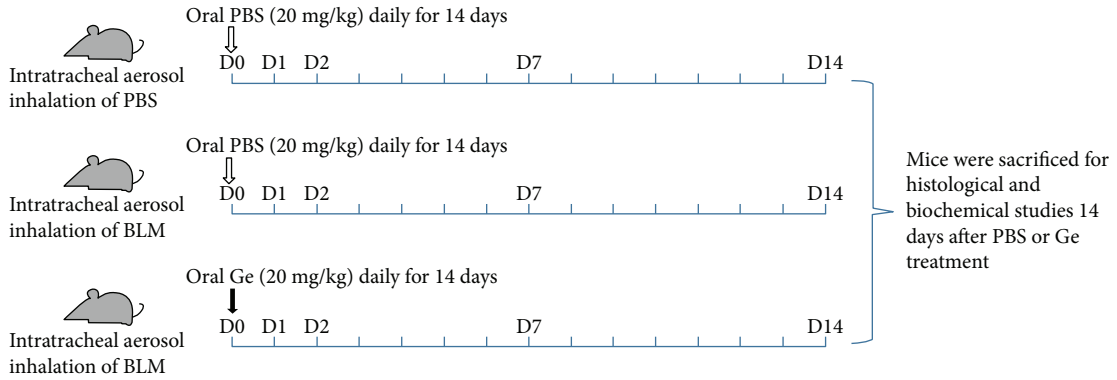

Figure 1: The experimental procedure of the present study.

incubated in a roller at room temperature for 30 min. After being subjected to magnetic separation, the supernatant was discarded, and the beads were washed three times by resuspension in 500 μL binding buffer. Proteins binding with DNA affinity beads were eluted with 20 μL of 0.25 M KCl solution. All the operations mentioned above were in accordance with the protocol of the DNA-binding protein purification kit (Roche, Germany), and samples from the PBS and BLM mice were studied simultaneously. The eluted proteins were then subjected to SDS-PAGE electrophoresis and EMBL silver staining to show the lung nuclear proteins binding with the α-SMA promoter *in vitro*. The differentially displayed protein bands were determined by comparison with protein grams from BLM- and PBS-treated samples and were cut out from the gel with a sterile knife for further liquid chromatography-mass spectrometry (LC-MS/MS) analysis by the Beijing Huada Jierui Biotechnology Co. Ltd. (Beijing, China).

2.5. RNA Preparation and Reverse Transcriptase Polymerase Chain Reaction (RT-PCR). RNA was extracted from the left lung lobes of mice from all three groups using the TRIzol Reagent (Invitrogen, US) according to the manufacturer's recommendations. The lung tissues including HMGB34367, α-SMA, NOX1/2/4, and β-actin mRNA transcripts were measured by RT-PCR. PCR products were size fractionated in 1.5% agarose gels and visualized by ethidium bromide staining. Cycling conditions were (1) 94°C for 5 minutes; (2) 30 cycles at 94°C for 40 seconds, 55°C for 40 seconds, and 72°C for 40 seconds; and (3) a final extension step at 72°C for 10 minutes. The PCR primers were presented as follows: α-SMA, forward primer 5′-ACCCAGATTATGTTTGAGACC-3′ and reverse primer 5′-CCGTCAGGCAGTTCGTAG-3′; HMGB34367, forward primer 5′-ATGGGCAAAGGAGATCCTA-3′ and reverse primer 5′-CCTCATCATCTTCCTCTTC-3′; NOX1, forward primer 5′-TGGCATCCCTTCACTCTGA-3′ and reverse primer 5′-GGCACGCTGGAATTTGTAC-3′; NOX2, forward primer 5′-CCCTCCTATGACTTGGAAATG-3′ and reverse primer 5′-TCCGTCCAGTCTCCCACAATA-3′; NOX4, forward primer 5′-AGACAAATGTAGACACTCACC-3′ and reverse primer 5′-CACAATAAAGGCACAAAGGT-3′; and β-actin, forward primer 5′-AGGGAAATCGTGCGTGACATCAAA-3′ and reverse primer 5′-ACTCATCGTACTCCTGCTTGCTGA-3′.

2.6. Dihydroethidium (DHE) Fluorescence Measurement. The ROS levels in the lungs were assessed by DHE fluorescence. The lung tissues were stored in ethanol-dry ice at −80°C. Serial lung sections (5 μm thickness) were performed and incubated in DHE (10 mmol/L, 30 min, 37°C). The lung tissue fluorescence (adopt excitation at 490 nm, emission at 610 nm) was observed by using a fluorescence microscope.

2.7. Measurement of MDA and T-AOC. The malonaldehyde (MDA) and total antioxidant capacity (T-AOC) levels in the serum and lung tissues were detected by using commercial activity assay kits purchased from the Nanjing Jiancheng Bioengineering Institute.

2.8. Immunoprecipitation and Tyrosine Phosphorylation Assay. Lung proteins were extracted using a RIPA lysate. Equal amounts of proteins were subjected to 8% SDS-PAGE and separated proteins were electrophoretically transferred to polyvinylidene difluoride membranes. The blot was blocked with 5% nonfat dried milk, incubated overnight with anti-NOX1/2/4, anti-HMGB1, anti-EGFR, anti-ERK/JNK/P38, anti-NF-κB/c-Jun/c-Fos, anti-phosphor-EGFR, anti-phosphor-ERK/JNK/P38, anti-phosphor-NF-κB/c-Jun/c-Fos, and anti-β-actin antibody (Santa Cruz Biotechnology Inc., CA), and treated with rabbit anti-mice IgG conjugated with alkaline phosphatase. The protein blot was detected with ECL and the gray scale was analyzed using a Gel-Pro Analyzer system.

2.9. Statistical Analysis. GraphPad Prism 5.0 software (version 5.0, GraphPad Software Inc., La Jolla, CA, USA) was used for statistical analysis. All the data were expressed as the mean ± standard deviation (mean ± SD). Student's *t*-test (2 groups) and (or) one-way ANOVA (multiple groups) was used to detect differences. *P* values less than 0.05 were considered significant.

3. Results

3.1. Expression and Location of α-SMA and HMGB1 in Bleomycin-Induced Pulmonary Fibrosis. H&E and Masson's trichrome staining were adopted to examine the accuracy

and efficiency of the pulmonary fibrosis model. H&E results demonstrated that BLM administration induced focal fibrotic lesions mainly in the subpleural regions with thickened or thickening interalveolar septa (Figures 2(a) and 2(e)). A similar result was observed by Masson's trichrome staining (Figures 2(b) and 2(f)). IHC results revealed that α-SMA and HMGB1 were highly expressed in the BLM-treated lung tissues. The interstitial cells surrounding the bronchioles of the BLM-treated lungs were positively stained by α-SMA (Figures 2(c) and 2(g)) and HMGB1 (Figures 2(d) and 2(h)), especially in the cells surrounding the terminal bronchioles. The immunofluorescence staining revealed the same colocalization of α-SMA and HMGB1 in some interstitial cells, which was in accordance with the IHC results (Figure 3).

3.2. HMGB34367 Increased Its Assembly with α-SMA in Pulmonary Fibrosis Conditions. To discriminate protein members composing the transcriptional complex in the activation of the α-SMA promoter, we developed a system to purify these binding proteins. The results showed that there was a characteristic increase in a 20 kDa protein in the BLM group of mice when compared with the PBS group (Figure 4(a). HMGB34367 was most likely to increase its assembly with α-SMA in pulmonary fibrosis conditions compared with physiological conditions. Next, we examined the mRNA expression of HMGB34367 and α-SMA in the BLM-treated lungs. RT-PCR analysis showed that the transcriptional levels of α-SMA and HMGB34367 were remarkably increased after BLM treatment (Figure 4(b)).

3.3. Gefitinib Decreased Pulmonary Fibrosis Induced by Bleomycin. Lung tissues from the BLM group of mice showed prominent peribronchiolar and interstitial infiltration with inflammatory cells. Extensive cellular thickening of interalveolar septa, interstitial edema, increasing of interstitial cells with a fibroblastic appearance, and interstitial collagen deposition could be detected by the Masson's trichrome staining. Although multifocal parenchymal lesions were still present in lung tissues from the BLM + Ge group mice, the local consolidation was smaller than those in the BLM group. Less edema and collagen deposition, less septal widening, and fewer clusters of inflammatory cells were observed in the lungs from the BLM + Ge group (Figure 5(a)). The lung hydroxyproline (a marker of collagen deposition) levels were increased approximately 3-fold in the BLM group of mice compared with the PBS group (696.34 ± 87.21 μg/g tissue versus 234.52 ± 21.67 μg/g tissue, $P < 0.001$). Treatment with gefitinib significantly reduced the hydroxyproline level (351.28 ± 32.93 μg/g tissue versus 696.34 ± 87.21 μg/g tissue, $P < 0.001$) (Figure 5(b). Meanwhile, semiquantitative scoring of the inflammation (Figure 5(c)) and fibrosis (Figure 5(d)) showed reduced levels in the BLM + Ge group when compared with the BLM group.

3.4. Serum MDA and T-AOC Levels. The imbalance in the oxidation-antioxidant activity is an important pathogenesis in pulmonary fibrosis. Previous reports have shown that excessive oxidative stress plays an important role in the pathogenesis of pulmonary fibrosis [15]. DHE fluorescence was conducted to measure ROS levels in lung tissues. A significant attenuation of fluorescence intensity was noted in the BLM + Ge group when compared with the BLM group (Figures 6(a) and 6(b)). MDA is the metabolite of lipid peroxidation, which could represent the degree of oxidative damage to histiocytes. T-AOC reflects the level of antioxidative capacity in mice. Bleomycin produces a significant increase in serum MDA level compared with the PBS group (66.70 ± 4.46 nmol/mL versus 26.92 ± 10.86 nmol/mL, $P < 0.01$), while treatment with gefitinib significantly reduced the MDA level (39.16 ± 14.15 nmol/mL versus 66.70 ± 4.46 nmol/mL, $P < 0.05$) (Figure 6(c)). The level of serum T-AOC had an inverse tendency compared with the level of MDA, and gefitinib treatment significantly inhibited the reduction of T-AOC after bleomycin administration (9.78 ± 2.94 U/mL versus 2.47 ± 0.44 U/mL, $P < 0.01$) (Figure 6(d)). The levels of MDA (Figure 6(e)) and T-AOC (Figure 6(f)) in the lung tissues also showed the same tendency. These results suggested that gefitinib could alleviate the excessive oxidative stress and enhance the antioxidative ability in the fibrotic lung.

3.5. Gefitinib Decreased the Gene and Protein Levels of NOX1/2/4 Induced by Bleomycin. Activation of NOX enzymes was the major source of ROS production in cells, and NOX1/2/4 were considered to play an essential role in the development of pulmonary fibrosis [21, 22]. In the present study, the lung tissue NOX1/2/4 gene and protein levels in mice exposed to bleomycin were all increased compared with the PBS group. Mice receiving gefitinib treatment after bleomycin administration showed a significant reduction in NOX1/2/4 gene (Figures 7(a) and 7(b)) and protein (Figures 7(c) and 7(d)) levels. These findings confirmed that NOX1/2/4 played an important role in the excessive ROS production in pulmonary fibrosis, and the high expressions could be blocked by gefitinib treatment.

3.6. Gefitinib Significantly Inhibited the HMGB1 Expression and Phosphorylation of EGFR-MAPK Signal Transduction. We measured the HMGB1, total, and phosphorylation expressions of EGFR and MAPKs in the fibrotic lung by Western blot. The results showed that gefitinib significantly inhibited HMGB1 expression, the phosphorylation of EGFR, and subsequently, the phosphorylation of ERK, P38, and JNK (Figure 8).

3.7. Gefitinib Decreased the Activations of AP-1 and NF-κB. Previous studies showed that AP-1 and NF-κB could be activated by the phosphorylation of ERK, JNK, and P38 [23]. Activation of AP-1 and NF-κB could promote the production of proinflammatory factors and profibrotic factors in pulmonary fibrosis [24, 25]. The present study showed that administration of gefitinib did not influence the expressions of NF-κB, c-Jun, and c-Fos in BLM-induced lung tissues. However, the phosphorylation of NF-κB, c-Jun, and c-Fos were all significantly inhibited in accordance with the increased expression of MAPKs after gefitinib treatment (Figure 9).

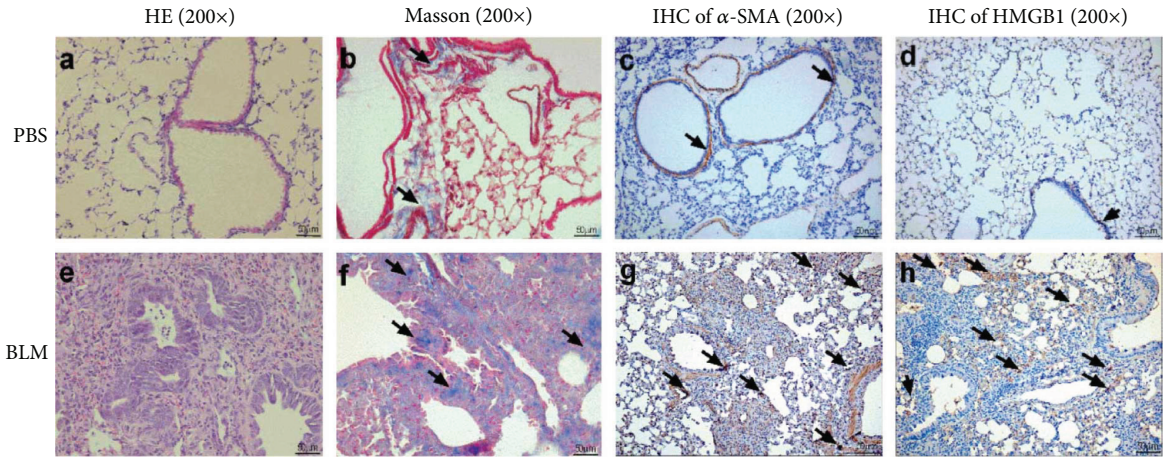

Figure 2: α-SMA and HMGB1 were highly expressed in the lung tissues affected by pulmonary fibrosis. Lung sections from mice were collected on day 14 after intratracheal bleomycin (BLM) or PBS administration and were stained with H&E, Masson's trichrome, and immunohistochemical stains (magnification 200x).

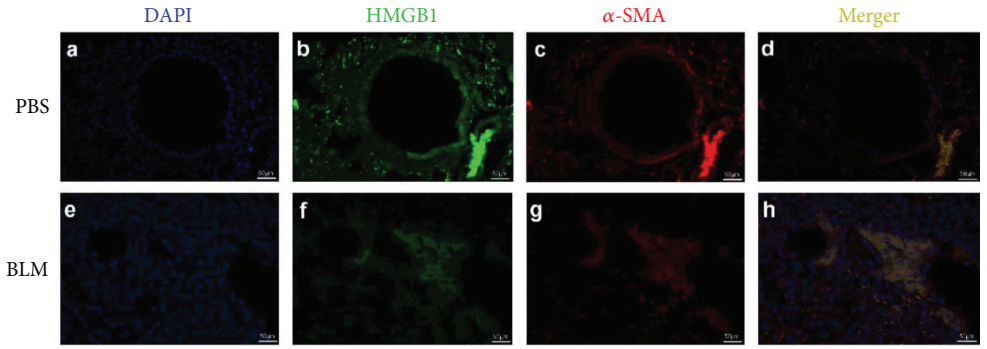

Figure 3: HMGB1 and α-SMA were coexpressed in some interstitial cells. Immunofluorescence staining for high-mobility group box 1 protein (HMGB1) (green) and α-smooth muscle actin (α-SMA) (red) and nuclei staining with DAPI (blue) were performed in fibrotic lung tissues. Yellow fluorescence staining (merged) indicated that some interstitial cells positively costained with HMGB1 and α-SMA (magnification 400x).

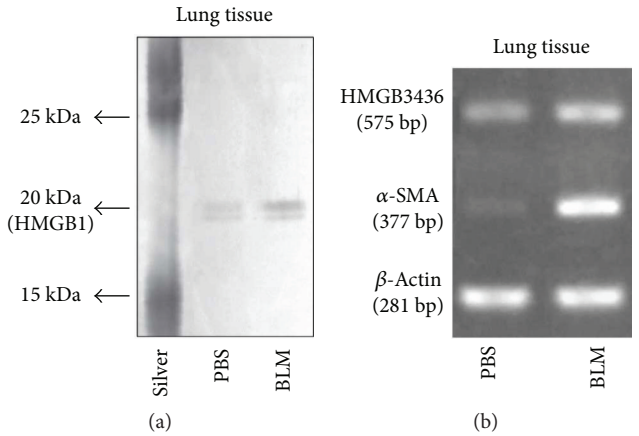

Figure 4: HMGB34367 was involved in direct regulation of α-SMA expression and was highly expressed in the lung tissues affected by pulmonary fibrosis. Lung tissues were collected 2 weeks after bleomycin (BLM) administration. Pulmonary nuclei were extracted from BLM- or PBS-treated lung tissue. (a) A DNA-nuclear protein pulldown method was used to detect the binding of nuclear proteins to the α-smooth muscle actin (α-SMA) promoter. A 20 kDa protein (HMGB34367) enlarged its binding amount with an α-SMA promoter under BLM conditions. (b) The mRNA expressions of α-SMA and HMGB34367 were increased in lung homogenates after BLM exposure.

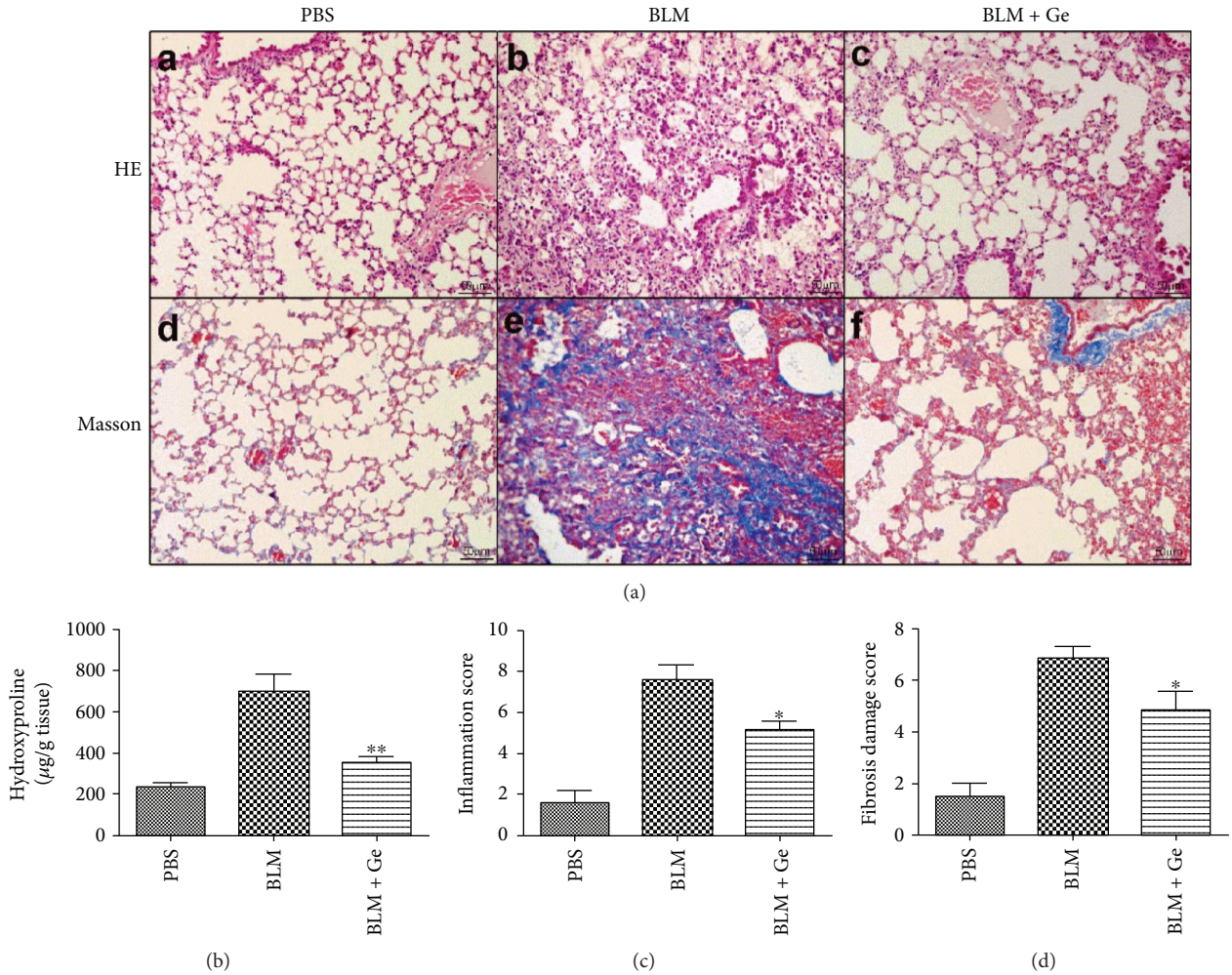

Figure 5: Gefitinib treatment decreased the severity of pulmonary fibrosis. Lung tissues from gefitinib- (Ge-) treated and PBS-treated pulmonary fibrosis mice were collected two weeks after bleomycin (BLM) administration. (a) Pathologic findings of lung tissues stained by H&E and Masson's trichrome (magnification 200x). (b) Lung hydroxyproline levels were significantly decreased by gefitinib treatment. Semiquantitative scoring of the severities and extents of inflammation (b) and fibrosis (c) were reduced in the BLM + Ge group compared with the BLM group. All data were expressed as the mean ± SD, $n = 6$. $^{*}P < 0.05$ versus BLM group, $^{**}P < 0.01$ versus BLM group.

4. Discussion

In the present study, we demonstrated the relationship between HMGB1 and α-SMA and the therapeutic effect of gefitinib in bleomycin-induced pulmonary fibrosis in mice. First, we proved that a member of the HMGB1 protein family (HMGB34367) could act as a novel transcriptional factor for the α-SMA promoter and participate in the process of pulmonary fibrosis. Second, we found that gefitinib was effective in reducing pulmonary fibrosis in mice, which might be associated with the HMGB1/NOXs-ROS/EGFR-MAPKs-AP-1/NF-κB signal (Figure 10).

First, we concentrated on the role of HMGB1 in the development of pulmonary fibrosis. HMGB1 was highly expressed in the fibrotic lung tissues, and inhibition of HMGB1 could significantly alleviate lung injury in mice. Scientists mainly attributed the phenomenon to its role as an important inflammatory factor, and inflammation was a key pathological process in pulmonary fibrosis [26]. However, the detailed molecular mechanism of HMGB1 remained unknown. Immunohistochemistry and immunofluorescence results showed that HMGB1 was located in some interstitial cells in which α-SMA staining was also positive. RT-PCR analysis also showed that the mRNA expression of α-SMA was increased in parallel with the enhanced mRNA expression of HMGB34367 after BLM treatment. Moreover, we found that HMGB34367 was involved in the regulation of α-SMA expression by using a DNA-nuclear protein pulldown method. HMGB34367 was a 20 kDa protein belonging to a specific protein group, most of which had the same structure with HMGB1. The full-length sequence of HMGB34367 was identical to the 1 to 178 amino acid region of HMGB1 protein, which included two DNA binding domains, box A and box B, but lacked the 179–215 acidic C terminal tail region of HMGB1. HMGB1, a highly conserved nuclear protein, could stabilize nucleosomes and allow bending of DNA to facilitate some gene transcription [27]. Taken together, our results suggested that HMGB1 probably participated in the pulmonary fibrosis mainly by (i) digesting into different forms and facilitating α-SMA gene

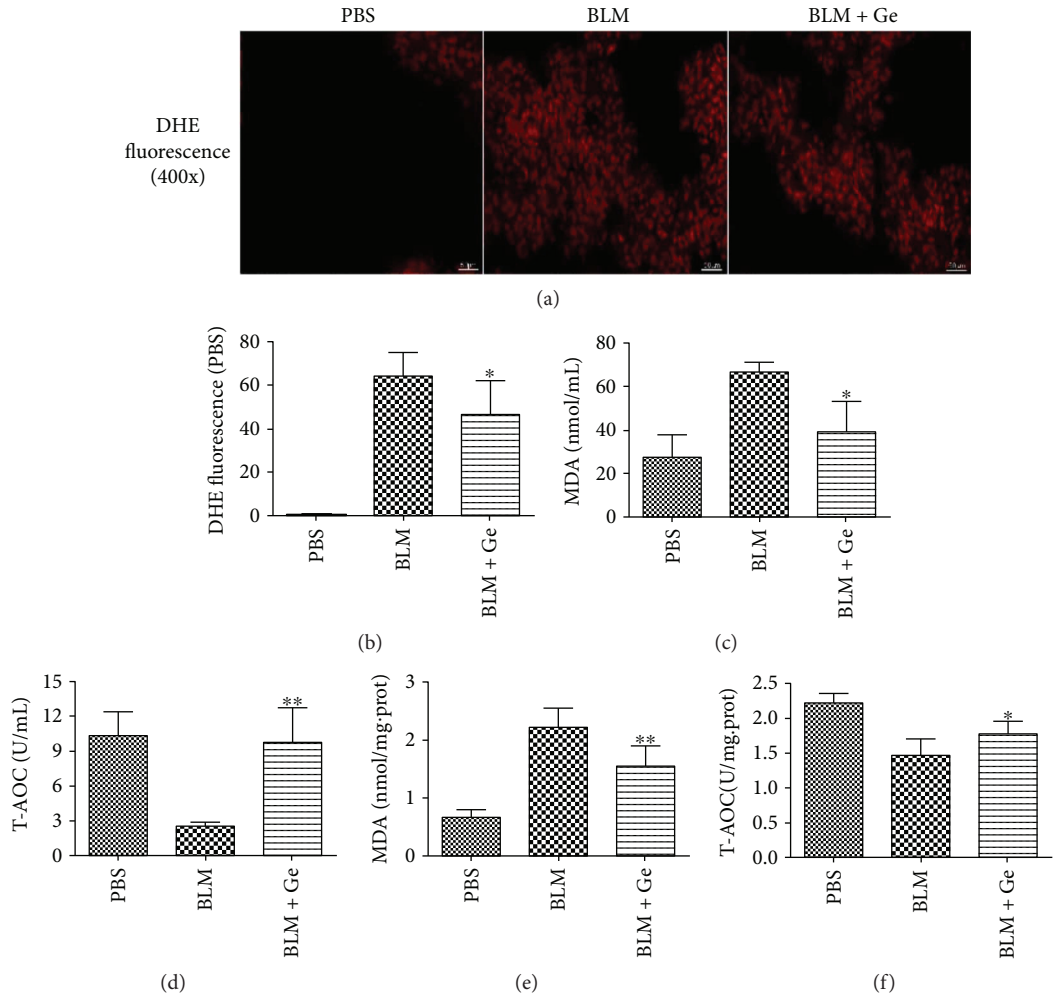

Figure 6: Gefitinib treatment alleviated the oxidative stress of pulmonary fibrosis. Lung tissues from gefitinib- (Ge-) treated and PBS-treated pulmonary fibrosis mice were collected two weeks after bleomycin (BLM) administration. (a) DHE fluorescence was used to detect ROS in the lung tissue (magnification 400x). (b) DHE fluorescence intensity was calculated. Gefitinib treatment significantly decreased serum (c) MDA and increased serum (d) T-AOC in mice. The levels of (e) MDA and (f) T-AOC in the lung tissues from the three groups showed the same results. All data were expressed as the mean ± SD, $n = 6$. $^{*}P < 0.05$ versus BLM group, $^{**}P < 0.01$ versus BLM group.

activation as a transcriptional activator and (ii) being secreted by activated monocytes and macrophages and behaving as an inflammatory cytokine.

Next, we studied the effect of gefitinib on pulmonary fibrosis. In fact, the potential of gefitinib to attenuate pulmonary fibrosis remained controversial. Hardie et al. demonstrated that gefitinib could apparently alleviate the pulmonary fibrosis in mice by decreasing EGFR expression and reversing the formative fibrosis in mice [14]. Subsequently, Ishii et al. found that all different oral doses (20 mg/kg, 90 mg/kg, and 200 mg/kg) of gefitinib could inhibit pulmonary fibrosis in mice, and large doses of gefitinib would not induce or aggravate pulmonary fibrosis [13]. However, Suzuki et al. and Li et al. showed that gefitinib treatment could markedly aggravate lung fibrosis in mice and rats [28, 29]. Moreover, severe lung interstitial disease associated with gefitinib treatment had been reported in some Japanese patients, implying that gefitinib might induce or aggravate this disease [30, 31]. In fact, there were several possible explanations for the different results. First, it might be related to the different breeds of mice or rats that had different responses to gefitinib because of their genetic characteristics. Second, the different doses of gefitinib were important factors causing the contradictory results. Higher doses of gefitinib could result in toxicity more than therapy. Third, the expression and activation of EGFR in different breeds of rodents and their responses to different doses of gefitinib had direct effects on the MAPK signals which could promote or inhibit pulmonary fibrosis. Fourth, the time of administration as well as the method of administration of gefitinib during the experiment also affected the results. Moreover, recent phase II gefitinib clinical trials in Japan announced that there were no differences in the incidence of pulmonary fibrosis between patients who used gefitinib and other chemotherapeutics, suggesting that gefitinib might not be the cause of pulmonary fibrosis [32]. In our previous series of studies, we found that gefitinib apparently inhibited lung collagen deposition and α-SMA expression induced by bleomycin in fibrotic mice [33, 34].

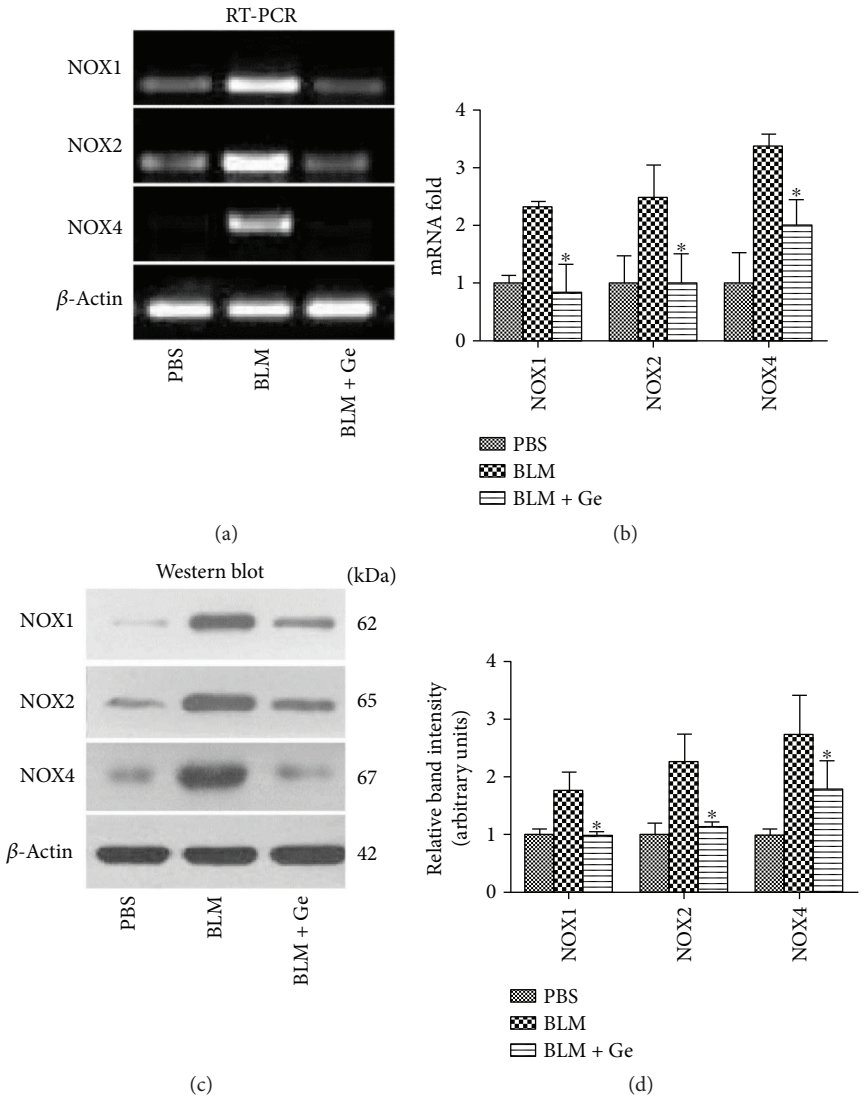

Figure 7: Gefitinib treatment decreased gene and protein expressions of NOX1/2/4 in the lung tissues affected by pulmonary fibrosis. Lung tissues from gefitinib- (Ge-) treated and PBS-treated pulmonary fibrosis mice were collected two weeks after bleomycin (BLM) administration. (a) The NOX1/2/4 gene expressions were identified by reverse transcriptase polymerase chain reaction (RT-PCR). (b) The relative mRNA folds were calculated. (c) The NOX1/2/4 protein expressions were identified by Western blot. (d) The relative band densities were calculated. The NOX1/2/4 gene and protein expressions in the lung tissues were significantly increased after BLM administration. However, gefitinib treatment significantly inhibited NOX1/2/4 expressions. All data were expressed as the mean ± SD, $n = 6$. $^*P < 0.05$ versus BLM group.

To elucidate the antifibrosis mechanism of gefitinib, we investigated oxidative and antioxidant levels in pulmonary fibrosis. Gefitinib completely inhibited the high concentration of MDA induced by bleomycin and recovered the T-AOC ability in pulmonary fibrotic mice. It was certainly well established that NOXs were the primary sources of ROS production that mediated various pulmonary diseases, including IPF and pulmonary hypertension [35, 36]. There were seven members of the NOX family found in mammals: NOX1, NOX2, NOX3, NOX4, NOX5, Duox1, and Duox2. Among them, NOX1, NOX2, and NOX4 had been shown to contribute to tissue fibrosis [37, 38]. NOX4 mRNA and protein expressions were upregulated in pulmonary fibroblasts from patients with IPF and correlated with α-SMA and procollagen I (α1) mRNAs [39]. NOX4-deficient mice were protected from bleomycin-induced pulmonary fibrosis through modulation of epithelial cell death *in vivo* and decreased TGF-β1-mediated ROS production and protection from apoptosis [40]. NOX1 and NOX2 were also reported to contribute to tissue fibrosis in nonpulmonary organ systems. HMGB1 was a proinflammatory factor that was also linked to oxidative stress [8]. The present study showed that gefitinib could also inhibit HMGB1 expression. However, how could this happen, and could gefitinib inhibit the HMGB1 and EFGR synchronously? In fact, HMGB1 could directly signal MAPKs to activate the NF-κB pathway [41]; moreover, HMGB1 could also indirectly signal the MAPK pathway by EGFR activation [42]. Extensive evidence indicated that the MAPK pathway was the downstream

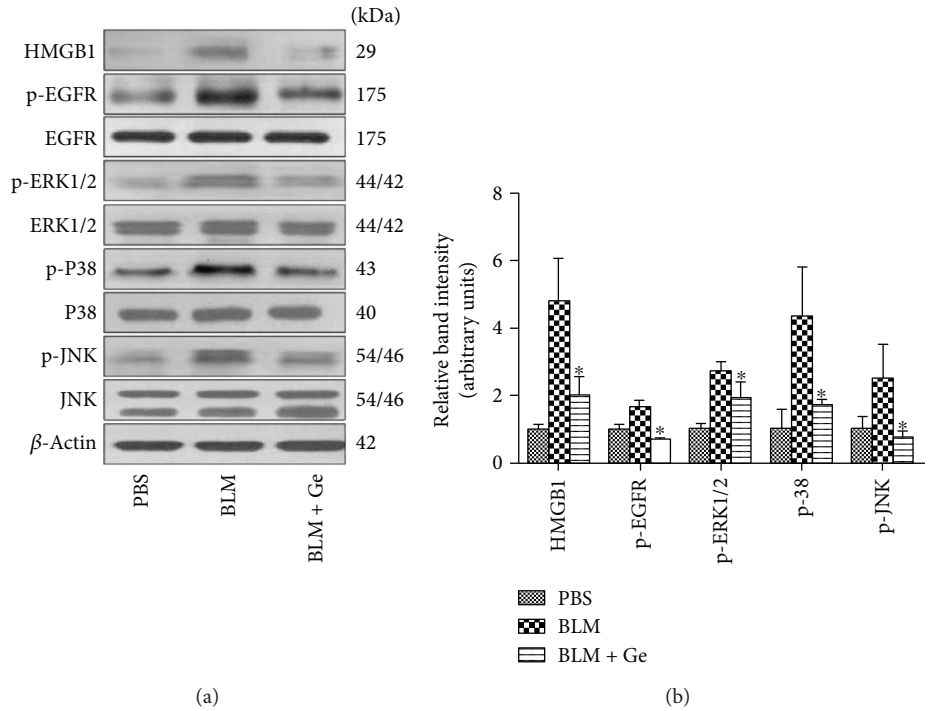

Figure 8: Gefitinib treatment decreased HMGB1 expression and phosphorylation expressions of EGFR and MAPKs in the lung tissues affected by pulmonary fibrosis. Lung tissues from gefitinib- (Ge-) treated and PBS-treated pulmonary fibrosis mice were collected two weeks after bleomycin (BLM) administration. (a) The expression of HMGB1, total, and phosphorylation of EGFR/ERK/P38/JNK in the lung tissues were detected by Western blot. (b) The relative band densities were calculated. Gefitinib treatment significantly inhibited the protein activation of HMGB1 and the phosphorylation of EGFR and MAPKs induced by BLM administration in mice. All data were expressed as the mean ± SD, $n = 6$. $^*P < 0.05$ versus BLM group.

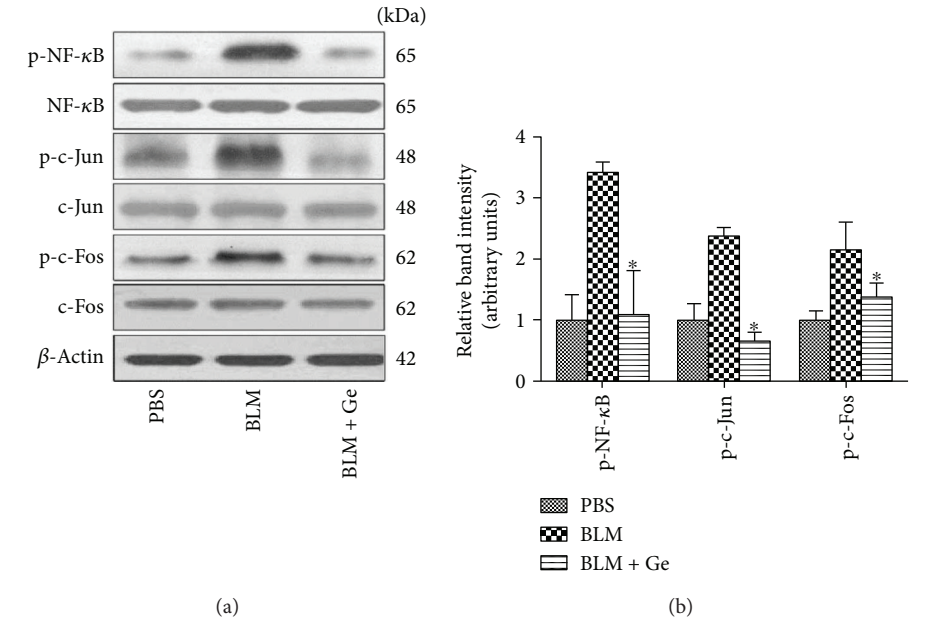

Figure 9: Gefitinib treatment decreased phosphorylation of NF-κB, c-Jun, and c-Fos in the lung tissues affected by pulmonary fibrosis. Lung tissues from gefitinib- (Ge-) treated and PBS-treated pulmonary fibrosis mice were collected two weeks after bleomycin (BLM) administration. (a) The total phosphorylation of NF-κB, c-Jun, and c-Fos in the lung tissues were detected by Western blot. (b) The relative band densities were calculated. Gefitinib treatment significantly inhibited the phosphorylation of NF-κB, c-Jun, and c-Fos induced by BLM administration in mice. All data were expressed as the mean ± SD, $n = 6$. $^*P < 0.05$ versus BLM group.

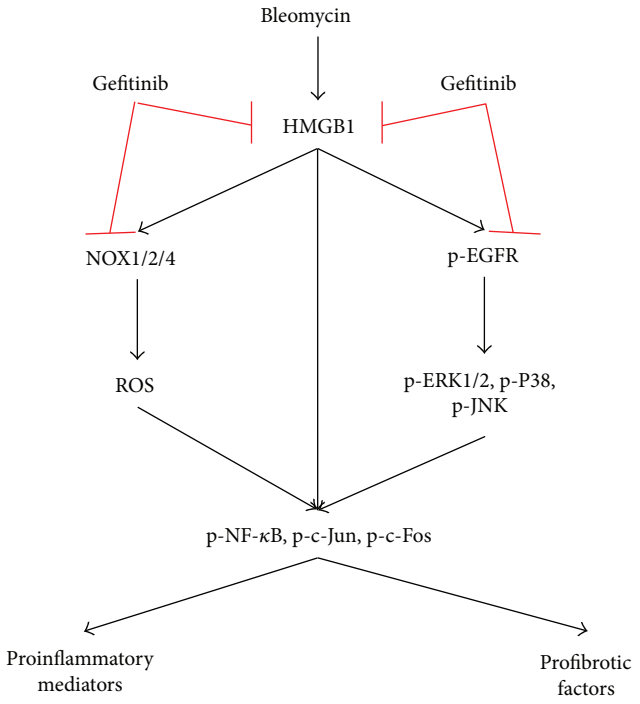

Figure 10: Schematic of gefitinib treatment in pulmonary fibrosis induced by bleomycin administration.

signaling cascade of EGFR, which participated in the development of pulmonary fibrosis [43]. A previous study showed that gefitinib inhibited the expressions of collagen I and III mRNAs by blocking the transactivation of EGFR and the subsequent activation of ERK1/2 in kidney fibrosis [44]. In vascular smooth muscle cells, EGFR increased production of nitric-oxide synthase and NOX enzymes through the downstream phosphorylation expression of ERK and AKT [45]. Our present data implied that gefitinib inhibited pulmonary fibrosis *in vivo* through HMGB1/NOXs-ROS/EGFR-ERK/JNK/P38 pathways.

NF-κB and AP-1 were the important transcription factors that were downstream of ROS and MAPKs [46]. The NF-κB signal transduction pathway was an important pathway involved in inflammation, immunity, cell proliferation, and apoptosis [47]. Previous studies have indicated that in acute lung injury activation of NF-κB could induce the production of proinflammatory mediators; contrarily, inhibiting the NF-κB activation significantly alleviated lung injury [24, 48]. AP-1, as a redox-regulated transcription complex (composed of c-Fos and c-Jun), was activated by MAPK family members via enhancing their downstream transcription factors including Elk-1, c-Jun, ATF2, and CREB, which in turn regulated the expressions of c-Fos and c-Jun. AP-1 and MAPKs proteins could be activated and augmented cyclically [49]. AP-1 and NF-κB could promote the production of proinflammatory mediators and profibrotic factors in pulmonary fibrosis. In the present study, AP-1 and NF-κB participated in the development of pulmonary fibrosis, and this progress was regulated by the phosphorylation and expression of ROS, HMGB1, and MAPKs.

Although many experiments were performed to reveal the effect and mechanism of gefitinib on the development of pulmonary fibrosis, shortcomings also existed. First, it was an animal study, and more evidence from clinical trials and *in vitro* researches are urgently needed. Second, we did not perform knockout, knockdown, or overexpression studies, which were limited by our experimental conditions. We only used RT-PCR, histological examinations, and Western blot to study the detailed molecular mechanisms. In the future, *in vivo* studies utilizing related knockout or knockdown mice as well as *in vitro* studies using primary lung cells and fibroblasts should be launched to verify the mechanism.

5. Conclusions

In summary, we comprehensively investigated the role of the molecule HMGB1, the involvement of oxidation-antioxidant unbalance, and the related molecule transduction mechanism downstream of gefitinib treatment in bleomycin-induced pulmonary fibrosis. These results indicated that HMGB1 contributed to the pulmonary fibrosis and gefitinib attenuated bleomycin-induced collagen deposition and excessive oxidative stress, mainly by suppressing the HMGB1/NOXs-ROS/EGFR-MAPKs-AP-1/NF-κB signal. The present findings have the potential to fundamentally advance our understanding of the molecular mechanism of pulmonary fibrosis and could have important implications in the design of novel and innovative therapeutic approaches targeting pulmonary fibrosis.

Conflicts of Interest

The authors declare no conflict of interest.

Authors' Contributions

Li Li and Lin Cai participated in the conduct of the experiments and in writing the paper; they contributed equally to the work. Linxin Zheng participated in the conduct of immunohistochemistry, Weifeng Yuan participated in the conduct of Western blotting, and Yujie Hu participated in the data analysis. Zhenhui Guo and Weifeng Li provided substantial advice in designing the study and assisted in the division of labor and in revising the paper.

Funding

This study was supported by funding from "Guangzhou Science and Technology Program projects" (Grant no. 201607010310) and the "Natural Science Foundation of Guangdong Province" (Grant no. 2014A030313596).

Acknowledgments

The authors are indebted to all individuals who participated in or helped with this research project.

References

[1] K. C. Meyer, "Pulmonary fibrosis, part I: epidemiology, pathogenesis, and diagnosis," *Expert Review of Respiratory Medicine*, vol. 11, no. 5, pp. 343–359, 2017.

[2] C. Daccord and T. M. Maher, "Recent advances in understanding idiopathic pulmonary fibrosis," *F1000Research*, vol. 5, 2016.

[3] E. A. Kogan, F. V. Tyong, and S. A. Demura, "The mechanism of lung tissue remodeling in the progression of idiopathic pulmonary fibrosis," *Arkhiv Patologii*, vol. 72, no. 4, pp. 30–36, 2010.

[4] N. W. Todd, S. P. Atamas, I. G. Luzina, and J. R. Galvin, "Permanent alveolar collapse is the predominant mechanism in idiopathic pulmonary fibrosis," *Expert Review of Respiratory Medicine*, vol. 9, no. 4, pp. 411–418, 2015.

[5] B. Ley, H. R. Collard, and T. E. King Jr, "Clinical course and prediction of survival in idiopathic pulmonary fibrosis," *American Journal of Respiratory and Critical Care Medicine*, vol. 183, no. 4, pp. 431–440, 2011.

[6] W. J. Canestaro, S. H. Forrester, G. Raghu, L. Ho, and B. E. Devine, "Drug treatment of idiopathic pulmonary fibrosis: systematic review and network meta-analysis," *Chest*, vol. 149, no. 3, pp. 756–766, 2016.

[7] B. C. Willis, J. M. Liebler, K. Luby-Phelps et al., "Induction of epithelial-mesenchymal transition in alveolar epithelial cells by transforming growth factor-β1: potential role in idiopathic pulmonary fibrosis," *The American Journal of Pathology*, vol. 166, no. 5, pp. 1321–1332, 2005.

[8] D. Tang, R. Kang, H. J. Zeh III, and M. T. Lotze, "High-mobility group box 1, oxidative stress, and disease," *Antioxidants & Redox Signaling*, vol. 14, no. 7, pp. 1315–1335, 2011.

[9] L. C. Li, J. Gao, and J. Li, "Emerging role of HMGB1 in fibrotic diseases," *Journal of Cellular and Molecular Medicine*, vol. 18, no. 12, pp. 2331–2339, 2014.

[10] A. Tzouvelekis, P. Ntolios, A. Karameris et al., "Increased expression of epidermal growth factor receptor (EGF-R) in patients with different forms of lung fibrosis," *BioMed Research International*, vol. 2013, Article ID 654354, 11 pages, 2013.

[11] Y. Zhou, J. Y. Lee, C. M. Lee et al., "Amphiregulin, an epidermal growth factor receptor ligand, plays an essential role in the pathogenesis of transforming growth factor-β-induced pulmonary fibrosis," *The Journal of Biological Chemistry*, vol. 287, no. 50, pp. 41991–42000, 2012.

[12] M. Martinelli, A. M. G. Pacilli, S. Rivetti et al., "A role for epidermal growth factor receptor in idiopathic pulmonary fibrosis onset," *Molecular Biology Reports*, vol. 38, no. 7, pp. 4613–4617, 2011.

[13] Y. Ishii, S. Fujimoto, and T. Fukuda, "Gefitinib prevents bleomycin-induced lung fibrosis in mice," *American Journal of Respiratory and Critical Care Medicine*, vol. 174, no. 5, pp. 550–556, 2006.

[14] W. D. Hardie, C. Davidson, M. Ikegami et al., "EGF receptor tyrosine kinase inhibitors diminish transforming growth factor-α-induced pulmonary fibrosis," *American Journal of Physiology-Lung Cellular and Molecular Physiology*, vol. 294, no. 6, pp. L1217–L1225, 2008.

[15] P. Cheresh, S. J. Kim, S. Tulasiram, and D. W. Kamp, "Oxidative stress and pulmonary fibrosis," *Biochimica et Biophysica Acta (BBA) - Molecular Basis of Disease*, vol. 1832, no. 7, pp. 1028–1040, 2013.

[16] C. Y. Fan, M. Katsuyama, and C. Yabe-Nishimura, "PKCδ mediates up-regulation of NOX1, a catalytic subunit of NADPH oxidase, via transactivation of the EGF receptor: possible involvement of PKCδ in vascular hypertrophy," *Biochemical Journal*, vol. 390, no. 3, pp. 761–767, 2005.

[17] H. Chu, Y. Shi, S. Jiang et al., "Treatment effects of the traditional Chinese medicine Shenks in bleomycin-induced lung fibrosis through regulation of TGF-beta/Smad3 signaling and oxidative stress," *Scientific Reports*, vol. 7, no. 1, p. 2252, 2017.

[18] K. Mikawa, K. Nishina, Y. Takao, and H. Obara, "ONO-1714, a nitric oxide synthase inhibitor, attenuates endotoxin-induced acute lung injury in rabbits," *Anesthesia & Analgesia*, vol. 97, no. 6, pp. 1751–1755, 2003.

[19] T. Ashcroft, J. M. Simpson, and V. Timbrell, "Simple method of estimating severity of pulmonary fibrosis on a numerical scale," *Journal of Clinical Pathology*, vol. 41, no. 4, pp. 467–470, 1988.

[20] M. C. Edwards, A. V. Tutter, C. Cvetic, C. H. Gilbert, T. A. Prokhorova, and J. C. Walter, "MCM2–7 complexes bind chromatin in a distributed pattern surrounding the origin recognition complex in *Xenopus* egg extracts," *The Journal of Biological Chemistry*, vol. 277, no. 36, pp. 33049–33057, 2002.

[21] C. Guichard, E. Pedruzzi, M. Fay et al., "The Nox/Duox family of ROS-generating NADPH oxidases," *Medecine Sciences*, vol. 22, no. 11, pp. 953–960, 2006.

[22] L. Hecker, J. Cheng, and V. J. Thannickal, "Targeting NOX enzymes in pulmonary fibrosis," *Cellular and Molecular Life Sciences*, vol. 69, no. 14, pp. 2365–2371, 2012.

[23] K. F. Jiang, G. Zhao, G. Z. Deng et al., "Polydatin ameliorates *Staphylococcus aureus*-induced mastitis in mice via inhibiting TLR2-mediated activation of the p38 MAPK/NF-κB pathway," *Acta Pharmacologica Sinica*, vol. 38, no. 2, pp. 211–222, 2017.

[24] L. Li, W. Wu, W. Huang, G. Hu, W. Yuan, and W. Li, "NF-κB RNAi decreases the Bax/Bcl-2 ratio and inhibits TNF-α-induced apoptosis in human alveolar epithelial cells," *Inflammation Research*, vol. 62, no. 4, pp. 387–397, 2013.

[25] B. Peng, H. Zhu, L. Ma, Y. Wang, C. Klausen, and P. C. K. Leung, "AP-1 transcription factors c-FOS and c-JUN mediate GnRH-induced cadherin-11 expression and trophoblast cell invasion," *Endocrinology*, vol. 156, no. 6, pp. 2269–2277, 2015.

[26] N. Hamada, T. Maeyama, T. Kawaguchi et al., "The role of high mobility group box1 in pulmonary fibrosis," *American Journal of Respiratory Cell and Molecular Biology*, vol. 39, no. 4, pp. 440–447, 2008.

[27] J. Ding, X. Cui, and Q. Liu, "Emerging role of HMGB1 in lung diseases: friend or foe," *Journal of Cellular and Molecular Medicine*, vol. 21, no. 6, pp. 1046–1057, 2017.

[28] H. Suzuki, K. Aoshiba, N. Yokohori, and A. Nagai, "Epidermal growth factor receptor tyrosine kinase inhibition augments a murine model of pulmonary fibrosis," *Cancer Research*, vol. 63, no. 16, pp. 5054–5059, 2003.

[29] L. Li, W. Huang, K. Li et al., "Metformin attenuates gefitinib-induced exacerbation of pulmonary fibrosis by inhibition of TGF-β signaling pathway," *Oncotarget*, vol. 6, no. 41, pp. 43605–43619, 2015.

[30] A. Inoue, Y. Saijo, M. Maemondo et al., "Severe acute interstitial pneumonia and gefitinib," *The Lancet*, vol. 361, no. 9352, pp. 137–139, 2003.

[31] P. Camus, S. Kudoh, and M. Ebina, "Interstitial lung disease associated with drug therapy," *British Journal of Cancer*, vol. 91, Supplement 2, pp. S18–S23, 2004.

[32] H. Kawasaki, K. Nagai, T. Yokose et al., "Clinicopathological characteristics of surgically resected lung cancer associated with idiopathic pulmonary fibrosis," *Journal of Surgical Oncology*, vol. 76, no. 1, pp. 53–57, 2001.

[33] L. Li, W. F. Li, L. Cai, W. F. Yuan, and W. J. Huang, "Gefitinib inhibits α-smooth muscle actin expression in mice with bleomycin-induced lung fibrosis," *Nan Fang Yi Ke Da Xue Xue Bao*, vol. 30, no. 12, pp. 2675–2678, 2010.

[34] W. F. Li, L. Li, W. F. Yuan, and W. J. Huang, "Gefitinib prevents bleomycin-induced lung fibrosis in mice," *Chinese Journal of Pathophysiology*, vol. 26, no. 8, pp. 1565–1569, 2010.

[35] C. H. Yang, W. L. Zhuang, Y. J. Shen, C. J. Lai, and Y. R. Kou, "NADPH oxidase-derived ROS induced by chronic intermittent hypoxia mediates hypersensitivity of lung vagal C fibers in rats," *Frontiers in Physiology*, vol. 7, p. 166, 2016.

[36] B. Sun, X. Wang, Z. Ji et al., "NADPH oxidase-dependent NLRP3 inflammasome activation and its important role in lung fibrosis by multiwalled carbon nanotubes," *Small*, vol. 11, no. 17, pp. 2087–2097, 2015.

[37] S. H. Choi, M. Kim, H. J. Lee, E. H. Kim, C. H. Kim, and Y. J. Lee, "Effects of NOX1 on fibroblastic changes of endothelial cells in radiation-induced pulmonary fibrosis," *Molecular Medicine Reports*, vol. 13, no. 5, pp. 4135–4142, 2016.

[38] N. Sato, N. Takasaka, M. Yoshida et al., "Metformin attenuates lung fibrosis development via NOX4 suppression," *Respiratory Research*, vol. 17, no. 1, p. 107, 2016.

[39] N. Amara, D. Goven, F. Prost, R. Muloway, B. Crestani, and J. Boczkowski, "NOX4/NADPH oxidase expression is increased in pulmonary fibroblasts from patients with idiopathic pulmonary fibrosis and mediates TGFβ1-induced fibroblast differentiation into myofibroblasts," *Thorax*, vol. 65, no. 8, pp. 733–738, 2010.

[40] S. Carnesecchi, C. Deffert, Y. Donati et al., "A key role for NOX4 in epithelial cell death during development of lung fibrosis," *Antioxidants & Redox Signaling*, vol. 15, no. 3, pp. 607–619, 2011.

[41] L. Liu, F. Gao, Y. Ye et al., "Influence of HMGB1/MAPK/mTOR signaling pathway on cell autophagy and chemotherapy resistance in K562 cells," *Zhong Nan Da Xue Bao Yi Xue Ban*, vol. 41, no. 10, pp. 1016–1023, 2016.

[42] L. Feng, D. Xue, E. Chen et al., "HMGB1 promotes the secretion of multiple cytokines and potentiates the osteogenic differentiation of mesenchymal stem cells through the Ras/MAPK signaling pathway," *Experimental and Therapeutic Medicine*, vol. 12, no. 6, pp. 3941–3947, 2016.

[43] Y. Meng, C. H. Yu, W. Li et al., "Angiotensin-converting enzyme 2/angiotensin-(1-7)/Mas axis protects against lung fibrosis by inhibiting the MAPK/NF-κB pathway," *American Journal of Respiratory Cell and Molecular Biology*, vol. 50, no. 4, pp. 723–736, 2014.

[44] S. C. Chen, J. Y. Guh, T. D. Lin et al., "Gefitinib attenuates transforming growth factor-β1-activated mitogen-activated protein kinases and mitogenesis in NRK-49F cells," *Translational Research*, vol. 158, no. 4, pp. 214–224, 2011.

[45] R. R. Rodrigues-Diez, A. B. Garcia-Redondo, M. Orejudo et al., "The C-terminal module IV of connective tissue growth factor, through EGFR/Nox1 signaling, activates the NF-κB pathway and proinflammatory factors in vascular smooth muscle cells," *Antioxidants & Redox Signaling*, vol. 22, no. 1, pp. 29–47, 2015.

[46] G. S. Youn, K. W. Lee, S. Y. Choi, and J. Park, "Overexpression of HDAC6 induces pro-inflammatory responses by regulating ROS-MAPK-NF-κB/AP-1 signaling pathways in macrophages," *Free Radical Biology & Medicine*, vol. 97, pp. 14–23, 2016.

[47] S. Basak and A. Hoffmann, "Crosstalk via the NF-κB signaling system," *Cytokine & Growth Factor Reviews*, vol. 19, no. 3-4, pp. 187–197, 2008.

[48] S. Carnesecchi, C. Deffert, A. Pagano et al., "NADPH oxidase-1 plays a crucial role in hyperoxia-induced acute lung injury in mice," *American Journal of Respiratory and Critical Care Medicine*, vol. 180, no. 10, pp. 972–981, 2009.

[49] M. A. Burmeister, C. N. Young, V. A. Braga, S. D. Butler, R. V. Sharma, and R. L. Davisson, "*In vivo* bioluminescence imaging reveals redox-regulated activator protein-1 activation in paraventricular nucleus of mice with renovascular hypertension," *Hypertension*, vol. 57, no. 2, pp. 289–297, 2011.

Hindawi
Oxidative Medicine and Cellular Longevity
Volume 2018, Article ID 3183794, 12 pages
https://doi.org/10.1155/2018/3183794

Research Article

Young and Especially Senescent Endothelial Microvesicles Produce NADPH: The Fuel for Their Antioxidant Machinery

Guillermo Bodega,[1] **Matilde Alique**,[2] **Lourdes Bohórquez**,[2] **Miriam Morán**,[2] **Luis Magro**,[2] **Lilian Puebla**,[2] **Sergio Ciordia**,[3] **María C. Mena**,[3] **Elvira Arza**,[4] **and Manuel R. Ramírez**[2]

[1]*Departamento de Biomedicina y Biotecnología, Universidad de Alcalá, Alcalá de Henares, 28805 Madrid, Spain*
[2]*Departamento de Biología de Sistemas, Universidad de Alcalá, Alcalá de Henares, 28805 Madrid, Spain*
[3]*Proteomics Facility, Centro Nacional de Biotecnología, CSIC, Campus de Cantoblanco, 28049 Madrid, Spain*
[4]*Unidad Técnica de Microscopía, CNIC, C/ Melchor Fernández Almagro 3, 28029 Madrid, Spain*

Correspondence should be addressed to Guillermo Bodega; guillermo.bodega@uah.es

Received 13 December 2017; Revised 14 February 2018; Accepted 25 February 2018; Published 5 April 2018

Academic Editor: Claudio Cabello-Verrugio

In a previous study, we demonstrated that endothelial microvesicles (eMVs) have a well-developed enzymatic team involved in reactive oxygen species detoxification. In the present paper, we demonstrate that eMVs can synthesize the reducing power (NAD(P)H) that nourishes this enzymatic team, especially those eMVs derived from senescent human umbilical vein endothelial cells. Moreover, we have demonstrated that the molecules that nourish the enzymatic machinery involved in NAD(P)H synthesis are blood plasma metabolites: lactate, pyruvate, glucose, glycerol, and branched-chain amino acids. Drastic biochemical changes are observed in senescent eMVs to optimize the synthesis of reducing power. Mitochondrial activity is diminished and the glycolytic pathway is modified to increase the activity of the pentose phosphate pathway. Different dehydrogenases involved in NADPH synthesis are also increased. Functional experiments have demonstrated that eMVs can synthesize NADPH. In addition, the existence of NADPH in eMVs was confirmed by mass spectrometry. Multiphoton confocal microscopy images corroborate the synthesis of reducing power in eMVs. In conclusion, our present and previous results demonstrate that eMVs can act as autonomous reactive oxygen species scavengers: they use blood metabolites to synthesize the NADPH that fuels their antioxidant machinery. Moreover, senescent eMVs have a stronger reactive oxygen species scavenging capacity than young eMVs.

1. Introduction

Extracellular vesicles are subcellular structures produced by many different cells and located in the extracellular compartment. There are diverse types of extracellular vesicles depending on their biogenesis, content, function, and/or biophysical properties [1, 2]. The most common classification includes three types: microvesicles (MVs) (also termed microparticles or ectosomes), exosomes, and apoptotic bodies [3]. MVs are released from the cell by the budding of the plasma membrane and represent not only a heterogeneous structural population, since their size usually ranges from 0.15 to 1 μm or more, but also a heterogeneous functional group. They are present in all the body fluids: urine, saliva, bile, amniotic liquid, synovial, cerebrospinal, and seminal fluids as well as blood. Plasma MVs are of diverse cellular origin; they can arise from endothelial cells, erythrocytes, platelets, and leucocytes [4]. Blood MVs have been involved in the regular maintenance of endothelial cells [5] and other physiological functions such as coagulation, reticulocyte maturation, and angiogenesis [3] as well as mediators of endothelial dysfunction [6]. They have also been used as therapeutic tools in cardiovascular disease [7].

Reactive oxygen species (ROS) are produced as a consequence of cell metabolism, although the cells contain different mechanisms to eliminate them. In fact, the oxidative stress

caused by an increase of ROS can be considered as an imbalance between ROS production and elimination. Although ROS have physiological roles in the regulation of vascular cell function [8], vascular formation, and development [9], this imbalance has been associated with aging and senescence [10–14] as well as other pathological conditions of the cardiovascular system [15–17], more specifically, with endothelial cell dysfunction [18–24].

NADPH is, obviously, closely related to NADH, another molecule with a reducing activity. Both may act as common mediators in different biological processes. Hence, it is common to find the term NAD(P)H, indicating that both molecules may be involved. Nevertheless, NAD^+ is mainly involved in catabolic reactions and mitochondrial functions, whereas $NADP^+$ is involved in cellular antioxidant systems and anabolic reactions [25]. In fact, NADPH is considered the sole source of reducing power of antioxidant systems [26]. This is the reason why NADPH is considered the "fuel" of the antioxidant machinery. We have recently demonstrated that endothelium-derived MVs (eMVs) have a well-developed and functional enzymatic team to eliminate ROS which, moreover, increases in senescence [27]. Apparently, if eMVs can eliminate ROS, they should (a) contain large amounts of NADPH, (b) obtain it from the plasma, or (c) be able to synthesize it. Thus, the aim of this work was to elucidate these questions. In addition, given the differences observed in our previous study, where senescent eMVs showed a higher capacity of ROS elimination than young eMVs, we have also analyzed the capacity of eMVs obtained from both young and senescent endothelial cells to produce NADPH.

2. Material and Methods

2.1. HUVEC Culture. Cryopreserved human umbilical vein endothelial cells (HUVECs) (ATCC Cat number PCS-100-010) were cultured in endothelial growth medium (Lonza) supplemented with 10% heat-inactivated foetal bovine serum (Sigma-Aldrich). Cultures were maintained at 37°C in a 5% CO_2 atmosphere at 95% humidity. The HUVECs were serially passaged (the replicative senescence model). Cells passaged < 8 times (population doubling (PD) < 20; with PD calculated as [ln{number of cells harvested} − ln{number of cells seeded}/ln2]) were regarded as young endothelial cells, while those passaged 27–35 times (PD > 96) were regarded as senescent [28]. The proliferation rate of the latter cells is remarkably reduced, and more than 70% are positive for senescence-associated β-galactosidase. Prior to use, HUVEC extracts from cells passaged 4–8 (young pool) and from cells passaged 27–35 (senescent pool) were mixed (performed in quadruplicate).

2.2. Isolation and Characterization of Young and Senescent eMV. Young and senescent HUVEC-derived MVs were isolated from their culture medium. Briefly, samples were centrifuged using serial centrifugations (15 min at 3000 rpm, 30 min at 14,000 rpm), and pellets were frozen and stored at −20°C until use. Prior to use, MVs from cells passaged 4–8 (young pool) and from cells passaged 27–35 (senescent pool) were mixed (performed in quadruplicate).

MVs from a medium containing young and senescent HUVEC cells were characterized in terms of size using a Beckman Coulter Cytomics FC 500 flow cytometer running CXP software. MVs were considered to be those events gated with a size between 0.5–1.5 μm; this gate was established from the side scatter versus forward scatter dot plot produced in a standardization experiment using the SPHERO™ Flow Cytometry Nano Fluorescent Size Standard Kit (Spherotech). The latter has size-calibrated fluorescent beads ranging from 0.1–1.9 μm in diameter. Events below 0.2 μm were excluded in order to adequately distinguish true events from the background; events > 1.9 μm were excluded to prevent possible confusion with apoptotic bodies. The absolute number of MVs (events) per μL was determined using Flow Count calibrator beads (Beckman Coulter) according to the manufacturer's recommendations and employing CXP software: (MVs counted × standard beads/L)/(standard beads counted). Data were recorded as the mean of three independent measurements of the same sample. The same number of senescent and young MVs was used in comparative analyses.

2.3. Western Blotting. The total protein content of extracts from young and senescent eMVs (performed using CytoBuster Protein Extraction Reagent lysis buffer (Millipore)), which contains a protease and a phosphatase inhibitor cocktail (Roche), was quantified using a BCA Protein Assay Kit (Pierce), employing BSA as the standard. Briefly, equal amounts of protein (25 μg protein/lane) were diluted with a reducing sample buffer and separated by 4–20% Mini-PROTEAN® TGX™ Precast Protein Gels under reducing conditions. These proteins were then transferred onto nitrocellulose membranes (BioRad), blocked with TBS containing 0.1% Tween 20 and 5% dry nonfat milk for 1 h at room temperature, and incubated in the same buffer with different primary antibodies (anti-6PGL, Santa Cruz, sc-398833, dilution 1 : 500, 28 kDa; anti-GK, Santa Cruz, sc-393555, dilution 1/250, 61 kDa; anti-PSPH, Santa Cruz, sc-271421, dilution 1/250, 25 kDa). After washing with TBST, the membranes were incubated with Novex horseradish peroxidase-conjugated secondary antibodies followed by 2 additional washing steps with TBST. Bands were visualized with Luminata Crescendo Western HRP substrate (Millipore). Ponceau red (Sigma) staining was used as a loading control. Bands were quantified using Image J software (NIH) and normalized to Ponceau red.

2.4. Mass Spectrometry for NADPH Analysis. The presence of $NADP^+$ and NADPH in eMVs was analyzed using a HPLC system Agilent 1100 coupled in-line to a TSQ Quantum triple quadrupole mass spectrometer (Thermo Scientific) equipped with an ESI source. Samples were prepared according to the "hot water/buffer extraction" protocol from Ortmayr [29]. Briefly, eMVs (50×10^6) were added to 250 μL of 5 mM ammonium acetate buffer at pH 8.0. The supernatant was collected after sample incubation for 3 min at 85°C, cooling on dry ice, and centrifugation for 10 min at $4000 \times g$. Equipment settings were also obtained from Ortmayr [29] (see Table 1). Mass spectra were recorded in negative mode for $NADP^+$ and NADPH. The column used was ACE Excel

Table 1: Compound optimization table in MS/MS mode.

	$NADP^+$	NADPH
Molecular formula in MS	$C_{21}H_{27}N_7O_{17}P_3$	$C_{21}H_{29}N_7O_{17}P_3$
Parent mass	742 *m*/*z*	744 *m*/*z*
Product ion (*m*/*z*)/collision energy	619.96 *m*/*z*/17 v	426.16 *m*/*z*/35 v
	407.89 *m*/*z*/34 v	407.96 *m*/*z*/36 v
	272.82 *m*/*z*/38 v	396.96 *m*/*z*/32 v

3 C18 -PFP 150 mm × 3.0 mm + 3 μm. Mass spectra of the column eluates were recorded in MS/MS mode using methanol and H_2O, adding 5 mM ammonium acetate. Nitrogen was used as the ion source gas. The sheath gas pressure was set at 40 (arbitrary units), the auxiliary gas pressure was set at 2 (arbitrary units), and the spray voltage was set at 3000 V. The capillary temperature was set at 350°C. Argon was used as the collision gas for collision-induced dissociation at a pressure of 1.5 mTorr (Q2). Data were acquired using Xcalibur Control Software.

2.5. Proteomic Analysis. Proteomic analysis involved in-gel protein digestion followed by HPLC and mass spectrometry (MS). In order to obtain sufficiently large samples, the four HUVEC "young pool" extracts (see Section 2.2) were mixed, as were the four HUVEC "senescent pool" extracts, and the corresponding pools for the MVs. These four samples were dissolved in lysis buffer (8 M urea, 2 M thiourea, 5% CHAPS, 2 mM TCEP-HCl, and protease inhibitors). MVs were lysed by ultrasonication (10 strokes, low amplitude) on ice. The lysates were then centrifuged at 20,000 ×g for 10 min at 4°C, and the supernatant containing the solubilized proteins was used for LC-MS/MS experiments. Total protein concentration was determined using the Pierce 660 nm protein assay (Thermo). An aliquot of each sample was diluted with loading sample buffer and then loaded onto 1.2 cm wide wells of a conventional SDS-PAGE gel (1 mm thick, 4% stacking gel, and 12% resolving gel). The run was stopped as soon as the front entered 1 cm into the resolving gel, so that the whole proteome became concentrated at the stacking/resolving gel interface. The separated protein bands were visualized by Coomassie staining, excised, cut into cubes (cross section 1 mm^2), deposited in 96-well plates, and processed automatically in a Proteineer DP (Bruker Daltonics). The digestion protocol used was based on Shevchenko et al. [30] with minor variations: gel plugs were washed firstly with 50 mM ammonium bicarbonate and secondly with acetonitrile prior to reduction with 10 mM dithiothreitol in 25 mM ammonium bicarbonate solution; alkylation was performed with 55 mM indoleacetic acid in 50 mM ammonium bicarbonate solution. The gel pieces were then rinsed, firstly with 50 mM ammonium bicarbonate and secondly with acetonitrile, and subsequently dried under a stream of nitrogen. Proteomics grade trypsin (Sigma-Aldrich) at a final concentration of 16 ng/μL in 25% acetonitrile/50 mM ammonium bicarbonate solution was added and digestion allowed to proceed at 37°C for 4 h. The reaction was stopped by adding 50% acetonitrile/0.5% trifluoroacetic acid for peptide extraction. The tryptic-eluted peptides were dried by speed-vacuum centrifugation and then desalted on StageTip C18 Pipette tips (Thermo Scientific) until analysis by mass spectrometry.

A 1 μg aliquot of each sample was subjected to 1D-nano LC ESI-MSMS analysis using an Eksigent Technologies nanoLC Ultra 1D plus nanoliquid chromatography system coupled to a high-speed Triple TOF 5600 mass spectrometer (SCIEX) with a Nanospray III source. The analytical column used was a silica-based reversed phase Acquity UPLC M-Class Peptide BEH C18 Column (75 μm × 150 mm, 1.7 μm particle size, and 130 Å pore size) (Waters). The trap column was a C18 Acclaim PepMap™ 100 (Thermo Scientific) (100 μm × 2 cm, 5 μm particle diameter, and 100 Å pore size), switched on-line with the analytical column. The loading pump delivered a solution of 0.1% formic acid in water at 2 μL/min. The nanopump provided a flow-rate of 250 nL/min and was operated under gradient elution conditions. Peptides were separated using a 2–90% mobile phase B gradient (mobile phase A: 2% acetonitrile, 0.1% formic acid; mobile phase B: 100% acetonitrile, 0.1% formic acid) for 250 min. The injection volume was 5 μL.

Data acquisition was performed with a Triple TOF 5600 System (SCIEX) (ionspray voltage floating 2300 V, curtain gas 35 psi, interface heater temperature 150°C, ion source gas 1 25 psi, and declustering potential 100 V). All data were acquired using information-dependent acquisition (IDA) mode with Analyst® TF 1.7 software (SCIEX). The following IDA parameters were chosen: a 0.25 s MS survey scan in the mass range 350–1250 Da, followed by 35 MS/MS scans of 100 ms in the mass range 100–1800 (total cycle time: 4 s). Switching criteria were set to ions greater than a mass to charge ratio (*m*/*z*) of 350 and smaller than 1250, with a charge state of 2–5 and an abundance threshold of more than 90 counts/s (cps). Former target ions were excluded for 15 s. The IDA rolling collision energy (CE) parameters script was used for automatically controlling the CE.

MS and MS/MS data obtained from individual samples were processed using Analyst TF 1.7 software. Raw data file conversion tools were used to generate mgf files which were then compared (using Mascot Server v.2.5.1 software; Matrix Science) to those in the UniProt *Homo sapiens* protein database. The latter contains 40,530 coding genes and their corresponding reversed entries. The search parameters were set as follows: carbamidomethyl (C) as the fixed modification and acetyl (protein N-term) and oxidation (M) as the variable modifications. Peptide mass tolerance was set to 25 ppm and 0.05 Da for fragment mass. Two missed cleavages were allowed. False discovery rates (≤1% at the spectral level) for peptide identification were calculated manually.

2.6. Functional Experiments. Two functional experiments were carried out in order to (1) test the ability of MVs to use blood metabolites to feed the NAD(P)H synthesis machinery, and (2) visually demonstrate that these metabolites induce NAD(P)H formation.

In the first experiment, five different blood metabolites were tested separately on young and senescent eMVs: lactate, pyruvate, glucose, branched-chain amino acids (BCAA; Val, Leu, Ileu), and glycerol. The concentration used was higher

than the plasma value found in the bibliography (included in Figure 1): 7 mM, 0.5 mM, 15 mM, 0.3 mM, and 0.3 mM, respectively. In each tube, the test sample was formed by adding: 2 μL of blood metabolite, 5 μL of lysate including 10^6 eMVs, and 5 μL of 3 mM NADPH (Santa Cruz Biotechnology, reference number 202725A). No metabolites were included in the control samples. NADPH was used as the internal control; in fact, this experimental design allowed us to analyze the metabolite-induced changes in the $NAD(P)^+$/NAD(P)H ratio. For example, for a certain metabolite, a lower ratio indicates that this metabolite increases the reduced form. After a 10 min incubation, 1 μL of the sample was analyzed in a microvolume spectrophotometer (DeNovis DS-11 spectrophotometer), and the $NAD(P)^+$/NAD(P)H ratio was determined by absorbance measurement at 260 nm/340 nm, respectively. The experiment was repeated three times using duplicated samples; twelve measures were performed in each case.

To visualize NAD(P)H synthesis, the eMVs (young and senescent) were incubated for 10 min with the blood metabolites previously described. Subsequently, 10 μL of each sample including 40,000 eMVs was dropped into the center of a small water-repellent circle made on a slide with a PAP pen. The drop and the circle were wrapped up with a coverslip and observed in a Zeiss LSM 780 multiphoton confocal microscope with a Mai-Tai DS (690–1040 nm tunable) laser. The excitation wavelength was 735 nm, more than twice that of NAD(P)H (340 nm), and the laser intensity was set at 5.5%. The detection range was 396–502 nm.

2.7. Statistical Analysis. Data were analyzed using R software. The two-tailed Student *t*-test was used to analyze differences in Western blotting results. Data of our first functional experiment (ability of MVs to use blood metabolites to feed the NAD(P)H synthesis machinery) were analyzed as follows. Kruskal-Wallis test (with post hoc Dunn's test) was performed for the comparison of the effect of metabolites in young eMVs and senescent eMVs. Mann–Whitney–Wilcoxon rank-sum test was used to compare the effect of every molecule between young and senescent: glucose in young versus glucose in senescent and so on. Significance was set at $p < 0.05$.

3. Results

This section has been organized in three parts: (1) proteomic analysis, where we describe the biochemical pathways in eMVs which are directed at synthetizing NADPH; (2) the presence of $NADP^+$ in eMVs; and (3) functional analysis, to demonstrate whether or not eMVs can synthesize NAD(P)H after activation of the pathways previously described. In the text that follows, the enzymes are named using the acronyms included in Table 2, the generic name (GN), and the metabolites with the acronyms included in Figure 1.

3.1. Proteomic Analysis. The pentose phosphate pathway (PPP) is the main biochemical route to synthesize NADPH. Hence, our first objective was to search for the presence of enzymes that participate in this pathway using mass spectrometry (MS) analysis of young and senescent eMVs. The majority of PPP enzymes were detected in this MS analysis, as shown in Table 2, except for 6PGL, GK, and PSPH, which were detected by Western blot (WB) analysis (Figure 2).

We next carried out a more detailed analysis of the enzymes detected in our MS results in order to connect the PPP with other biochemical routes. Table 2 includes the enzymes of the PPP and those of related metabolic routes proposed according to our proteomic analysis. To clarify these routes, a diagram of all the metabolic pathways proposed is included in Figure 1.

The organization of the different enzymes found in our proteomic analysis led us not only to establish the hypothetical biochemical routes that may be operative in the eMVs but also to point out the metabolites that feed these biochemical routes (Figure 1). All in all, it seems that both young and especially senescent eMVs have a very well-developed enzymatic organization designed to optimize NADPH production, and this is mainly due to the bidirectionality of most of these enzymatic activities. Besides the glycolytic pathways, which use glucose, lactate, and pyruvate, it is very important to point out the possibility that BCAA and glycerol can also be used to direct metabolites to the PPP. Mitochondria are also involved in this strategic metabolic organization: they can act as an NADPH biosynthetic organelle (note the high content of GLUD1 (number 22)) and supply AKG to the serine and 3PHP pathway. Enzymes involved in serine and glycerate metabolism are also included in these biochemical pathways using 3PHP and 3PG as metabolic intermediates.

One of the most interesting results was the higher content of most of these enzymes in senescent eMVs when compared with young eMVs; in fact, their enzymatic machinery seems to be designed to direct metabolites to the PPP or to obtain NADPH from new routes not included in young eMVs. The bold numbers in Table 2 indicate an increase > 25% when young and senescent eMVs were compared. A route specially used in senescent eMVs is the serine and PHP pathway, as suggested by the high content of the enzymes involved (numbers from 23 to 27) in senescent eMVs. The use of glutamine to form F6P using GFPT2 (number 28) is also especially elevated in senescent eMVs. Moreover, at the bottom of Table 2, we have included five enzymes that synthesize NADPH but are not included in Figure 1. Note that IDH1 and IDH2 are decreased in senescent eMVs, whereas the last three enzymes are increased.

3.2. Functional Analysis. We carried out two types of functional analysis; one to test the capacity of the proposed blood metabolites to feed the enzymatic machinery involved in reducing power synthesis and the other one to visualize this reducing power in eMVs. Unfortunately, NADH and NADPH are closely related molecules whose absorption and emission spectra are almost equal and, thereby, it has been impossible for us to separate NADH from NADPH in these functional analyses.

In order to study the effect of blood metabolites on NAD(P)H synthesis, eMVs were incubated 30 min with

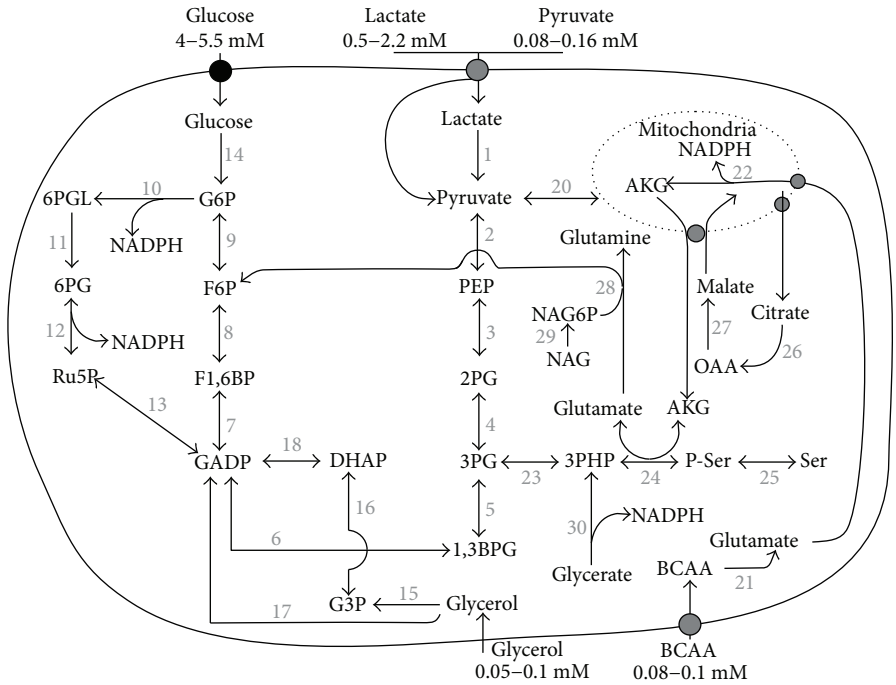

Figure 1: Schematic diagram of an eMV including the proposed metabolic pathways according to the proteomic results. The blood plasma metabolites that can feed these routes and their plasma concentrations under control conditions are also included. 1,3BPG: 1,3-bisphosphoglycerate; 2PG: 2-phosphoglycerate; 3PG: 3-phosphoglycerate; 3PHP: 3-phosphohydroxypyruvate; 6PG: 6-phosphogluconate; 6PGL: 6-phosphoglucono-1,5-lactone; AKG: alpha-ketoglutarate; BCAA: branched-chain amino acids; DHAP: dihydroxyacetone 3-phosphate; F1,6BP: fructose 1,6-biphosphate; F6P: fructose 6-phosphate; G3P: glycerol 3-phosphate; G6P: glucose 6-phosphate; GADP: glyceraldehyde 3-phosphate; NAG: N-acetylglucosamine; NAG6P: N-acetylglucosamine-6-phosphate; OAA: oxaloacetate; PEP: phosphoenolpyruvate; P-Ser: phosphoserine; Ru5P: ribulose 5-phosphate.

the proposed metabolites (lactate, pyruvate, glucose, glycerol, and BCCA). These metabolites were incubated separately at a concentration that doubled the maximal value indicated in Figure 1. The absorbance ratio 260 nm/340 nm is a measure of the relative proportion of $NAD(P)^+$/NAD(P)H. In young eMVs, lactate and pyruvate diminished significantly this ratio, which indicates that both metabolites induced the formation of NAD(P)H. However, in senescent eMVs, all the metabolites tested induced a decrease in this ratio, glycerol and pyruvate being statistically significant. Statistically significant differences were also observed for glucose, glycerol, and BCAA when the effect of metabolites was compared in young and senescent eMVs (Figure 3).

An experiment using multiphoton confocal microscopy was performed to visualize the production of NAD(P)H by eMVs after incubation with the previously used metabolites. In order to detect only the reduced forms, eMVs were excited at 340 nm (670 nm in the multiphoton confocal microscope), and emission was detected at 460 nm. Only after incubation with the proposed blood metabolites could eMVs be clearly visualized, demonstrating that eMVs have the capacity to synthesize reducing power (NAD(P)H) (Figure 4), although not all vesicles were able to produce fluorescence. Only lactate and pyruvate induced fluorescence in young eMVs, and senescent eMVs seemed to be more efficient in producing fluorescence.

3.3. $NADP^+$ and NADPH in eMVs. An MS analysis was carried out to accurately detect the presence of $NADP^+$ and NADPH in eMVs. As can be seen in Figure 5, the presence of both cofactors was demonstrated in eMVs, although the content of $NADP^+$ was greater than that of the reduced form. Differences in the $NADP^+$/NADPH ratio were not observed either following incubation with the blood metabolites or between young and senescent eMVs.

4. Discussion

In a recent work, we demonstrated the existence of a functional machinery for ROS detoxification in HUVEC eMVs [27]; now, our present study demonstrates that these HUVEC eMVs, especially those derived from senescent cells, can synthesize NAD(P)H, the fuel that feeds the antioxidant machinery, used as precursors of different blood plasma metabolites. The combination of both results indicates that eMVs are subcellular structures with an autonomous capacity for ROS scavenging, as had been suggested by Soleti et al. [31]; eMV protection against oxidative stress regulating eNOS/Akt signaling has also been recently demonstrated [32]. Figure 6 shows a schematic drawing that represents our past and present results on the role of eMVs as ROS scavengers.

The presence of some antioxidant enzymes in plasma MVs [33–35], in endothelial-derived MVs [36], and in

Table 2: Proteomic analysis of young and senescent eMVs. PS: protein score; PSM: peptide-spectrum match; NP: number of peptides (MS/MS scores are sums for the validated peptides assigned to each protein); **C**: coverage. PS, PSM, and NP are usually considered quantitative variables in the proteomic analysis. Bold numbers in the "senescent columns" indicate a 25% increase in senescent eMVs; italic numbers in "young columns" indicate a 25% reduction in senescent eMVs. The 5 proteins at the bottom of the table are the enzymes that synthesize NADPH. UniProt: UniProt code; GN: generic name.

Enzymes		UniProt	GN	Young eMVs				Senescent eMVs			
				PS	PSM	NP	**C**%	PS	PSM	NP	**C**%
1	L-Lactate dehydrogenase B chain	**P07195**	**LDHB**	644	17	10	32	**837**	**18**	**12**	33.8
	L-Lactate dehydrogenase A chain	**P00338**	**LDHA**	458	14	7	25.6	**1023**	**26**	**15**	**53.6**
	L-Lactate dehydrogenase A-like 6A	**Q6ZMR3**	**LDHAL6A**	104	2	1	6.3	105	2	1	6.3
	L-Lactate dehydrogenase A-like 6B	**Q9BYZ2**	**LDHAL6B**					**38**	**1**	**1**	**4.5**
2	Pyruvate kinase	**P14618**	**PKM**	1425	40	24	56.9	**1675**	**44**	24	60.8
3	Alpha-enolase	**P06733**	**ENO1**	810	14	10	49.8	**1376**	**31**	**18**	**60.4**
	Gamma-enolase	**P09104**	**ENO2**	288	6	3	13.8	**542**	**10**	**7**	**38.5**
	Beta-enolase	**P13929**	**ENO3**	319	6	3	13.6	**425**	**9**	**5**	**18.7**
4	Phosphoglycerate mutase 1	**P18669**	**PGAM1**	197	6	3	33.5	**352**	**11**	**6**	**44.5**
5	Phosphoglycerate kinase 1	**P00558**	**PGK1**	524	12	7	46.5	519	12	8	45.6
6	Glyceraldehyde-3-phosphate dehydrogenase	**P04406**	**GAPDH**	1645	50	23	75.5	**1939**	**65**	**27**	72.2
7	Fructose-bisphosphate aldolase A	**P04075**	**ALDOA**	565	12	9	44.2	**1202**	**29**	**19**	**59.9**
	Fructose-bisphosphate aldolase C	**P09972**	**ALDOC**	310	5	4	25.5	**474**	**9**	**7**	25.3
8	Fructose-2,6-bisphosphatase	**Q9NQ88**	**TIGAR**					**46**	**1**	**1**	**6.7**
9	Glucose-6-phosphate isomerase	**P06744**	**GPI**					**272**	**6**	**5**	**20.6**
10	Glucose-6-phosphate 1-dehydrogenase	**P11413**	**G6PD**					**45**	**1**	**1**	**11.8**
11	6-Phosphogluconolactonase	**O95336**	**6PGL**				Western blot				
12	6-Phosphogluconate dehydrogenase, decarboxylating	**P52209**	**PGD**	162	3	3	22.2	160	3	3	24.2
13	Transketolase	**P29401**	**TKT**	**238**	7	4	**14.4**	185	6	4	19.3
14	Hexokinase-1	**P19367**	**HK1**	265	5	5	16.4	262	7	5	9.6
15	Glycerol kinase	**P32189**	**GK**				Western blot				
16	Glycerol-3-phosphate dehydrogenase, mitochondrial	**P43304**	**GPD2**	52	1	1	39				
17	Alcohol dehydrogenase [NADP(+)]	**P14550**	**AKR1A1**					**44**	**1**	**1**	**7.1**
18	Triosephosphate isomerase	**P60174**	**TPI1**	434	8	7	52.4	**523**	**12**	8	54.9
19	Glutamine-fructose-6-phosphate aminotransferase	**O94808**	**GFPT2**	43	1	1	4.3	**84**	**4**	**2**	4.4
	Glutamine-fructose-6-phosphate aminotransferase	**Q06210**	**GFPT1**					**241**	**4**	**4**	8.9
20	Pyruvate dehydrogenase E1 component subunit alpha	**P08559**	**PDHA1**	**5**	**3**	**13.8**	**80**	2	1	5.4	
	Pyruvate dehydrogenase E1 component subunit beta	**P11177**	**PDHB**	**114**	**2**	**2**	**17.3**	38	1	1	9.7
21	Branched-chain amino acid aminotransferase, mitochondria	**O15382**	**BCAT2**					**94**	**1**	**1**	**6.4**
22	Glutamate dehydrogenase 1, mitochondrial	**P00367**	**GLUD1**	329.0	11.0	5.0	24.0	**637.0**	**17.0**	**11.0**	**35.5**
23	D-3-Phosphoglycerate dehydrogenase	**O43175**	**PHGDH**	80	2	1	5.1	**391**	**8**	**6**	**23.3**
24	Phosphoserine aminotransferase	**Q9Y617**	**PSAT1**					**47**	**1**	**1**	**5.4**
25	Phosphoserine phosphatase	**PSPH**	**P78330**				Western blot				
26	ATP-citrate synthase	**P53396**	**ACLY**	286	6	5	16.7	**358**	**8**	**6**	**13.4**
27	Malate dehydrogenase, cytoplasmic	**P40925**	**MDH1**	99	3	1	10.8	**176**	**5**	**3**	**17.7**
28	Glutamine-fructose-6-phosphate aminotransferase	**O94808**	**GFPT2**	43	1	1	4.3	**84**	**4**	**2**	**4.4**
29	N-Acetyl-D-glucosamine kinase	**Q9UJ70**	**NAGK**					**193**	**3**	**3**	**22.1**
30	Glyoxylate reductase/hydroxypyruvate reductase	**Q9UBQ7**	**GRHPR**					**38**	**1**	**1**	**3**
Other NAD(P)H-related enzymes											
	Isocitrate dehydrogenase (NADP) cytoplasmic	**O75874**	**IDH1**	**41**	**1**	**1**	**2.7**				
	Isocitrate dehydrogenase (NADP), mitochondrial	**P48735**	**IDH2**	**254.0**	**6.0**	**5.0**	**38.7**	133.0	3.0	3.0	30.8
	Flavin reductase (NADPH) Alpha-aminoadipic semialdehyde	**P30043**	**BLVRB**					**37**	**1**	**1**	**12.1**
	Alpha-aminoadipic semialdehyde dehydrogenase	**P49419**	**ALDH7A1**	111	2	2	11.9	**207**	**5**	**4**	**16.5**
	NAD(P)H dehydrogenase (quinone)	**P15559**	**NQO1**					**39**	**1**	**1**	**6.6**

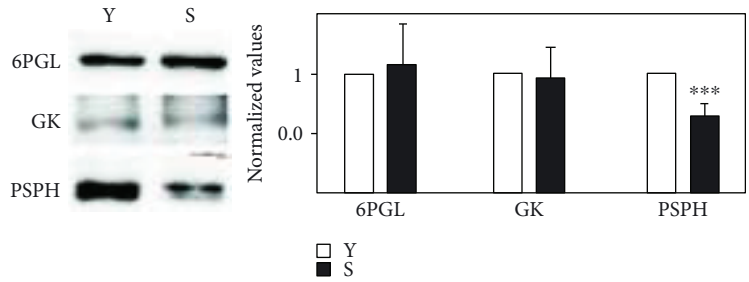

Figure 2: Western blot analysis of 6PGL, GK, and PSPH and the corresponding normalized analysis. A representative pool is included in the figure: young (Y) and senescent (S). THP-1 cells were used as a positive control (not shown). Bands were located at the expected molecular weight of 6PGL (28 kDa), GK (61 kDa), and PSPH (25 kDa). Protein data for the eMVs was normalized against the intensity of Ponceau red staining. Bars represent mean ± SD ($n = 4$ pools). $^{***}p < 0.001$.

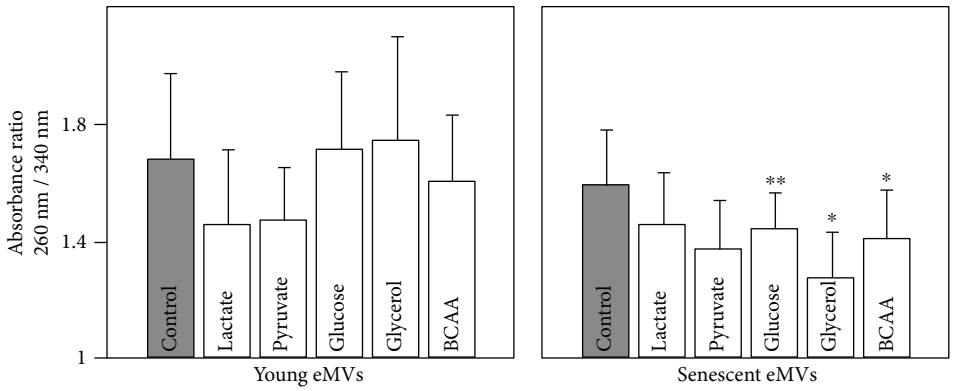

Figure 3: Effect of incubating eMVs with different blood plasma metabolites on the ratio of absorbance at 260 nm and 340 nm, absorption peaks of NAD(P) and NAD(P)H, respectively. No blood metabolites were added to control eMVs. Error bars represent SD; $n = 3$. To clarify the plot, only statistical significance of the Mann–Whitney–Wilcoxon rank-sum test is included. $^{*}p < 0.05$, $^{**}p < 0.01$. In the Kruskall-Wallis test for young eMVs, significant differences were observed in control versus lactate and pyruvate ($p < 0.05$) and between glucose versus lactate ($p < 0.01$). Significant differences were also observed for senescent eMVs in control versus glycerol and pyruvate ($p < 0.05$) and between glycerol versus glucose and lactate ($p < 0.01$).

HUVEC-derived MVs [31] had been already demonstrated. However, in our previous work [27], we demonstrated that HUVECs had a complete antioxidant machinery and that their MVs included a specific group of functional enzymes mainly involved in O_2^- and H_2O_2 detoxification. Moreover, to date, the possibility of NADPH synthesis in MVs has not been considered in the literature. As far as we know, this is the first time that the capacity of NADPH synthesis is ascribed to eMVs, although the existence of some PPP enzymes has been demonstrated in exosomes [37], and some enzymes included in Table 2 have also been found in different proteomic studies: numbers 1, 5, 6, 7, and 18 and IDH2 [36]; numbers 5, 6, and 7 [33]; numbers 6 and 7 and ALDH [35]; and numbers 10, 20, and 27 and ALDH [34]. The synthesis of NADPH in eMVs seems logical; it makes no sense to contain an antioxidant machinery without the capacity of synthesizing the molecule that feeds it.

NADPH is considered the essential reductant for antioxidant systems. Unfortunately, its absorption and emission spectra are very similar to that of NADH. The appearance of FLIM [38, 39] and MS [29] methods, however, has made it possible to study these metabolites separately. FLIM permits the monitoring of MVs, but the use of MS is ideal for quantitative comparative studies of oxidized ($NADP^+$) and reduced (NADPH) forms. eMVs have an important handicap: it is difficult and very expensive to obtain large amounts of eMVs using HUVEC. This handicap has made our attempts to determine the $NADP^+$/NADPH ratio using the standard commercial kits for NADPH analysis impossible. This problem can be resolved using FLIM, but this technique is very expensive and not usually available in most laboratories. While it is true that MS does not require big amounts of sample, even so, it is complicated to obtain enough eMVs for MS, and this problem gets worse in endothelial senescent cells because it is not easy to reach PD > 96. Note that the volume of 50×10^6 eMVs can be, more or less, 0.025 mm^3 of sample. Moreover, NADPH is not very stable [40]; heat specially induces its oxidation to $NADP^+$, and MS samples have to be intensely heated up. This might explain not only the low signal of NADPH but also the lack of differences observed in our MS analysis after incubation with blood metabolites or between young and senescent eMVs. In addition, NADPH has a lower—one order of magnitude—response factor than $NADP^+$. The filtering and

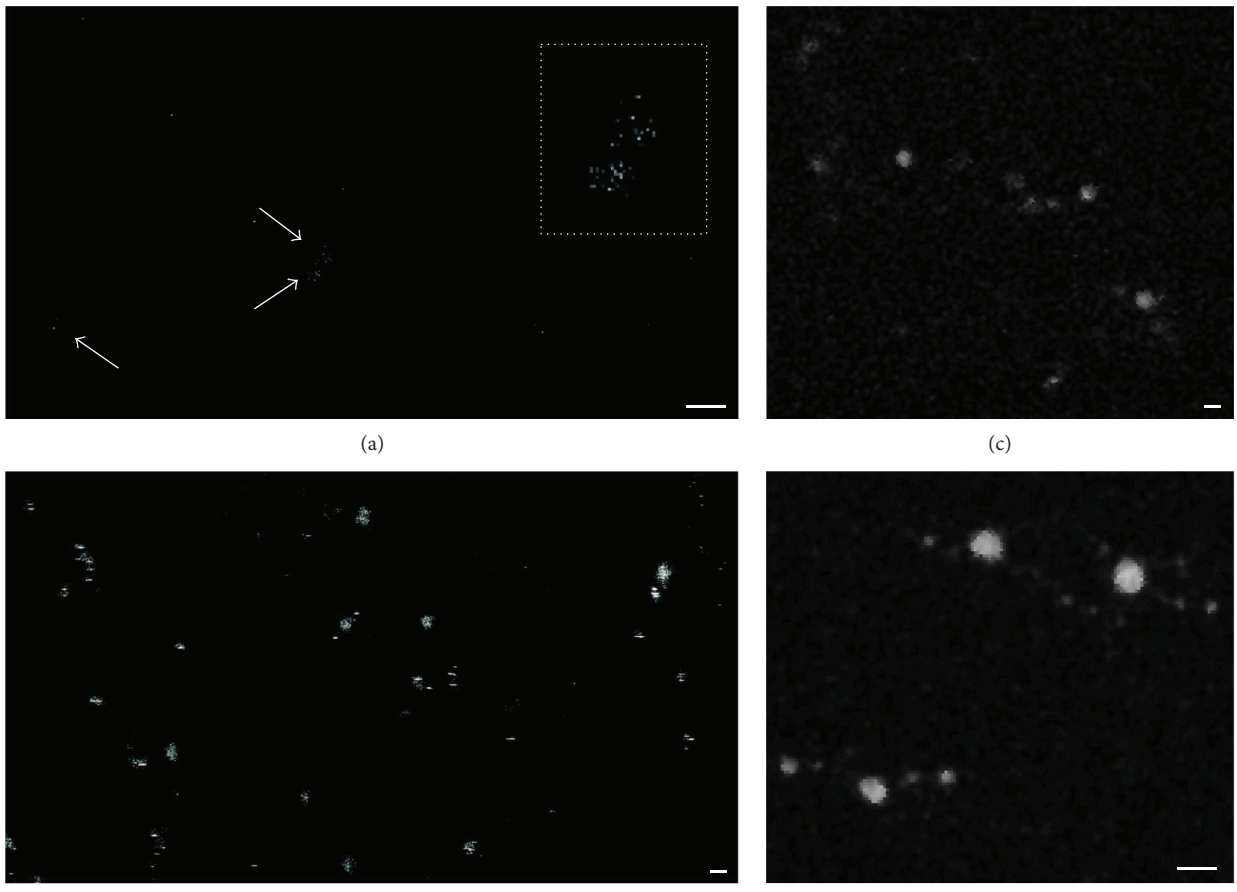

Figure 4: eMVs observed with a multiphoton confocal microscope. (a) Young eMVs under control conditions; arrows indicate eMVs. The square delimited by a dotted line is a magnification of the two eMVs indicated by the two arrows. (b) Senescent eMVs after glycerol incubation. (c) Young eMVs after lactate incubation. (d) Senescent eMVs after pyruvate incubation. The different size of the eMVs in the image is due to the fact that the eMVs were floating in the buffer in different positions in the z-axis. eMVs were obtained after mixing four pools. Scale bar, 1 μm.

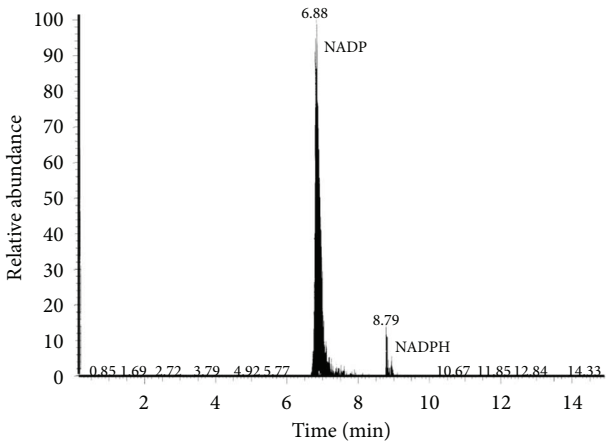

Figure 5: MS analysis of $NADP^+$ (6.88 elution time) and NADPH (8.79 elution time) content in senescent eMVs. eMVs were obtained after mixing four pools. $NADP^+$ MW: 742 D, NADPH MW: 744 D.

dilution of the samples, as well as the existence of carbohydrates in the molecule (the ribose rings), that makes MS analysis difficult, must also be considered.

In this work, we propose a model of organization of the metabolic routes in eMVs in accordance with our proteomic analysis (MS and WB) (see Figure 1). Although both young and senescent eMVs can synthesize reducing power, the latter have a stronger synthetic machinery. In fact, it seems that senescent eMVs redesign their metabolic machinery to optimize NADPH synthesis. This new metabolic reorganization has some interesting hallmarks. Mitochondrial activity is deeply affected in order to diminish its activity: (1) ADP/ATP translocases diminish or disappear: translocase 1 from 362 (young eMVs) to 0 (senescent eMVs) (protein score values), translocase 2 from 580 to 102, and translocase 3 from 549 to 0; (2) mitochondrial aminotransferases also diminish or disappear: ornithine aminotransferase from 55 to 0, aspartate aminotransferase from 520 to 251, and serine hydroxymethyltransferase from 339 to 122; (3) pyruvate dehydrogenase which contributes to transforming pyruvate into acetyl-CoA, a metabolite used in the tricarboxylic acid

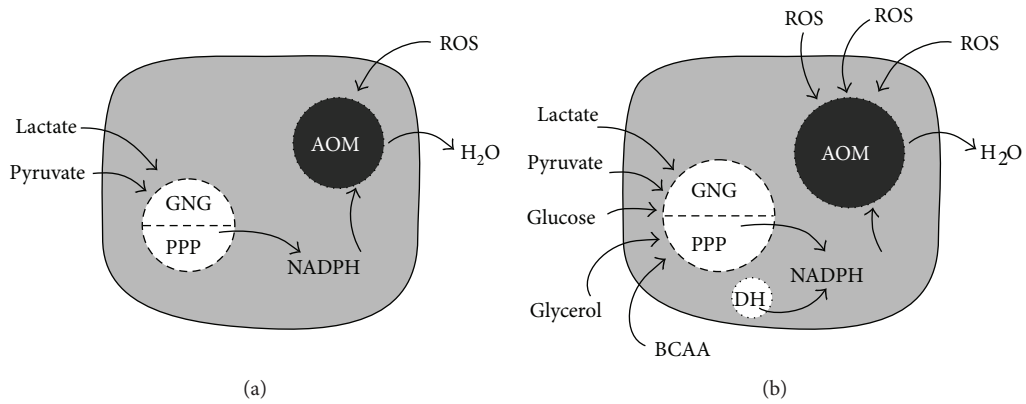

Figure 6: A young (a) and a senescent (b) eMV. AOM: antioxidant machinery; PPP: pentose phosphate pathway; GNG: gluconeogenesis; ROS: reactive oxygen species; DH: dehydrogenases; BCAA: branched-chain amino acids. Note that the senescent eMV has larger enzymatic machineries, uses more metabolites to feed them, and also has a higher capacity for ROS scavenging.

(TCA) cycle, is diminished in senescent eMVs (see enzyme number 20 in Table 2); and (4) the TCA enzymes are unbalanced; for example, succinic dehydrogenase is not present in senescent eMVs, whereas isocitrate dehydrogenase and aconitase are diminished. The incorporation of pyruvate to the glycolytic pathway (note that PK (number 2) is augmented) and the sequestering of AKG in the serine and glutamine pathways in order to synthesize 3PG and F6P are in accordance with this depletion of mitochondrial metabolic activity.

It is well known that the main enzymes involved in NADPH synthesis are PPP dehydrogenases [41], isocitrate dehydrogenases, aldehyde dehydrogenases, malic enzyme, and NAD kinase [42]. PPP dehydrogenases (enzyme numbers 10 and 12) and alcohol (enzyme number 17) and aldehyde dehydrogenases are increased in senescent eMVs, as well as NAD(P)H dehydrogenase and flavin reductase (see the last three enzymes of Table 2). Moreover, two other dehydrogenases, GLUD1 (number 22), involved in mitochondrial NADPH synthesis, and LDH (number 1) (NAD-dependent), are strongly increased. Isocitrate dehydrogenase, however, is diminished (see above paragraph), and malic enzyme and NAD kinase have not been detected. A serine-related folate-dependent NADPH production has been demonstrated in proliferating [43] and in cancer [44] cells; however, the enzymes of this route have not been detected in our study.

Under high oxidative conditions, the PPP consumes more glucose to compensate for the depleted GSH [45]; in fact, a high oxidative stress drives G6P to the PPP, generating NADPH for antioxidant defenses [46], and a mechanistic link between increased G6PD (number 10) activity, elevated NADPH, and improved antioxidant protection has been suggested [47]. An activation of the PPP has also been demonstrated in cancer cells, probably to produce more NADPH to combat oxidative stress [48]; indeed, the existence of PPP enzymes has been demonstrated in exosomes of ovarian cancer cells in proteomic analysis [37]. Human skin cells also activate the PPP in response to oxidative stress [49], and senescent fibroblasts show increased glycolysis and PPP to reduce ROS production, upregulation of pathways involved in redox homeostasis [50], and alterations in nicotinamide metabolism [51]. Moreover, another different metabolic possibility has been suggested for ROS scavenging; the enzyme biliverdin reductase has been involved in a ROS-scavenging mechanism in a subpopulation of epididymal fluid MVs, protecting spermatozoa against ROS released from dying cells [52].

Evidence that MVs are a heterogeneous population is continuously increasing [53]. This heterogeneity can be considered at least from two different points of view: structural (size) and functional (biochemical). In our functional analysis using multiphoton confocal microscopy, not all MVs emitted fluorescence after their stimulation. In fact, we think that only a part of the eMVs could act as ROS scavengers. We have just seen that to accomplish this function, it is necessary to reorganize the metabolic routes of the eMVs, and it is logical to assume that this drastic reorganization may not be useful for other functions supported by MVs; for example, for those MVs capable of ROS synthesis and involved in signaling processes [54–56].

eMVs, or at least a subpopulation of them, produce reducing power, but the enzymatic machinery involved in this process also needs to be fed. In this study, we have demonstrated that lactate, pyruvate, glucose, glycerol, and BCAA fuel this reducing power synthetic machinery. All these metabolites are present in blood plasma and, except glycerol that diffuses freely, need membrane transporters to cross the plasma membrane and get into the MVs. Lactic acid can also diffuse freely; however, in the blood, it is dissociated and present as lactate (ionized) that cannot pass through the plasma membrane. The use of these metabolites is different in young (only use lactate and pyruvate) and senescent eMVs (use all). Obviously, the higher reducing power synthesis capacity of senescent cells is in accordance with their wider metabolite availability. On the other hand, the use of some of these metabolites could represent another metabolic advantage; for example, the use of lactate may serve to regulate lactate concentration and to prevent lactic acidosis and redox regulation in plasma. We have not detected monocarboxylate transporters (lactate and pyruvate transporters), neutral amino acid transporters, or glucose transporters in our proteomic study; however, the fluorescence emission

after incubation of the eMVs with these metabolites implies the existence of a transport system. A low expression of these transporters could explain this result, but the fast (a few minutes) emission of fluorescence in eMVs after incubation with these metabolites suggests the contrary. The possibility that the membrane proteins, due to their hydrophobicity, are harder to detect in MS, indeed requiring thiourea to solubilize them, should be considered.

The contribution of ROS to aging has been widely documented, although the beneficial effects produced by ROS have led to a new interpretation of this traditional view [57–59]. An increase of ROS production has also been related with senescence, an experimental model widely used in aging studies [20, 24, 60] and also demonstrated in our previous work in senescent endothelial cells [27]. In accordance with the stronger capacity of ROS elimination demonstrated by senescent eMVs in our previous work, the present study demonstrates a strong increase of the machinery involved in NADPH synthesis in senescent eMVs. However, the stronger capacity of senescent endothelial cells and their MVs to eliminate ROS and the higher ROS production observed in senescence seems paradoxical. Their increased capacity for ROS scavenging might be an adaptive mechanism to the higher oxidative stress of senescent cells, and it could be considered a strategy used by senescent cells to promote cell survival. Unfortunately, this increased ROS scavenging is unable to compensate the higher levels of oxidative stress associated with senescence. On the other hand, eMVs can not only eliminate ROS but can also be effective in protecting against oxidative stress, suppressing NADPH oxidase and ROS production [32]. Finally, it should be considered that these results are obtained using the *in vitro* replicative senescent model in HUVEC; undoubtedly, this is a starting point that needs to be confirmed in *in vivo* aging models.

5. Conclusions

Our present and previous results demonstrate that eMVs can act as autonomous ROS scavengers: they use blood metabolites to synthesize NADPH that fuels their antioxidant machinery; moreover, senescent eMVs have a stronger ROS-scavenging capacity. Whether alterations in the ability of eMVs to regulate the oxidant/antioxidant balance can act as etiopathogenic mechanisms in diseases associated to a misbalance in oxidative stress is left out of this study but probably merits to be considered in order to use these MVs as diagnostic tools and/or therapeutic targets.

Conflicts of Interest

The authors have no conflicts of interest to declare.

Authors' Contributions

Guillermo Bodega, Matilde Alique, and Manuel R. Ramírez designed the study. Sergio Ciordia and María C. Mena carried out mass spectrometry analysis; Matilde Alique the Western blot analysis; Guillermo Bodega, Lourdes Bohórquez, Miriam Morán, and Luis Magro the functional analysis; and Guillermo Bodega and Elvira Arza the multiphoton confocal microscopy. Guillermo Bodega, Matilde Alique, Lilian Puebla, and Manuel R. Ramírez wrote the manuscript. All authors read and approved the final manuscript.

Acknowledgments

This work was funded by the Plan Nacional Proyectos de Investigación en Salud of Instituto de Salud Carlos III (ISCIII), EU FEDER Grant (PI14/00806). All proteomic analyses were performed at the Proteomics Facility of the Spanish National Center for Biotechnology (CNB-CSIC) (a member of ProteoRed, PRB2-ISCIII, financed via grant PT13/0001). The authors thank José María Arribas (Espectrometría de Masas y Análisis Elemental, Universidad de Alcalá) for NADPH analysis and Dr. Marcos Marvá (Departamento de Física y Matemáticas, Universidad de Alcalá) for statistical analysis.

References

[1] E. van der Pol, A. N. Böing, P. Harrison, A. Sturk, and R. Nieuwland, "Classification, functions, and clinical relevance of extracellular vesicles," *Pharmacological Reviews*, vol. 64, no. 3, pp. 676–705, 2012.

[2] M. Colombo, G. Raposo, and C. Théry, "Biogenesis, secretion, and intercellular interactions of exosomes and other extracellular vesicles," *Annual Review of Cell and Developmental Biology*, vol. 30, no. 1, pp. 255–289, 2014.

[3] M. Yáñez-Mó, P. R. M. Siljander, Z. Andreu et al., "Biological properties of extracellular vesicles and their physiological functions," *Journal of Extracellular Vesicles*, vol. 4, no. 1, article 27066, 2015.

[4] J.-D. Tissot, G. Canellini, O. Rubin et al., "Blood microvesicles: from proteomics to physiology," *Translational Proteomics*, vol. 1, no. 1, pp. 38–52, 2013.

[5] S. M. Craige, S. Kant, and J. F. Keaney Jr., "Reactive oxygen species in endothelial function – from disease to adaptation," *Circulation Journal*, vol. 79, no. 6, pp. 1145–1155, 2015.

[6] M. L. Liu and K. J. Williams, "Microvesicles: potential markers and mediators of endothelial dysfunction," *Current Opinion in Endocrinology, Diabetes and Obesity*, vol. 19, no. 2, pp. 121–127, 2012.

[7] A. Fleury, M. C. Martinez, and S. Le Lay, "Extracellular vesicles as therapeutic tools in cardiovascular diseases," *Frontiers in Immunology*, vol. 5, p. 370, 2014.

[8] D. Vara and G. Pula, "Reactive oxygen species: physiological roles in the regulation of vascular cells," *Current Molecular Medicine*, vol. 14, no. 9, pp. 1103–1125, 2014.

[9] Y. Zhou, H. Yan, M. Guo, J. Zhu, Q. Xiao, and L. Zhang, "Reactive oxygen species in vascular formation and development," *Oxidative Medicine and Cellular Longevity*, vol. 2013, Article ID 374963, 14 pages, 2013.

[10] M. El Assar, J. Angulo, S. Vallejo, C. Peiró, C. F. Sánchez-Ferrer, and L. Rodríguez-Mañas, "Mechanisms involved in the aging-induced vascular dysfunction," *Frontiers in Physiology*, vol. 3, p. 132, 2012.

[11] M. El Assar, J. Angulo, and L. Rodríguez-Mañas, "Oxidative stress and vascular inflammation in aging," *Free Radical Biology & Medicine*, vol. 65, pp. 380–401, 2013.

[12] R. Brandes, I. Fleming, and R. Busse, "Endothelial aging," *Cardiovascular Research*, vol. 66, no. 2, pp. 286–294, 2005.

[13] Y. Mikhed, A. Daiber, and S. Steven, "Mitochondrial oxidative stress, mitochondrial DNA damage and their role in age-related vascular dysfunction," *International Journal of Molecular Sciences*, vol. 16, no. 12, pp. 15918–15953, 2015.

[14] A. A. Puca, A. Carrizzo, F. Villa et al., "Vascular ageing: the role of oxidative stress," *The International Journal of Biochemistry & Cell Biology*, vol. 45, no. 3, pp. 556–559, 2013.

[15] N. S. Dhalla, R. M. Temsah, and T. Netticadan, "Role of oxidative stress in cardiovascular diseases," *Journal of Hypertension*, vol. 18, no. 6, pp. 655–673, 2000.

[16] H. Li, S. Horke, and U. Förstermann, "Oxidative stress in vascular disease and its pharmacological prevention," *Trends in Pharmacological Sciences*, vol. 34, no. 6, pp. 313–319, 2013.

[17] N. R. Madamanchi, A. Vendrov, and M. S. Runge, "Oxidative stress and vascular disease," *Arteriosclerosis, Thrombosis, and Vascular Biology*, vol. 25, pp. 29–38, 2005.

[18] D. J. Kurz, S. Decary, Y. Hong, E. Trivier, A. Akhmedov, and J. D. Erusalimsky, "Chronic oxidative stress compromises telomere integrity and accelerates the onset of senescence in human endothelial cells," *Journal of Cell Science*, vol. 117, no. 11, pp. 2417–2426, 2004.

[19] E. Schulz, E. Anter, and J. F. Keaney Jr., "Oxidative stress, antioxidants, and endothelial function," *Current Medicinal Chemistry*, vol. 11, no. 9, pp. 1093–1104, 2004.

[20] J. D. Erusalimsky and C. Skene, "Mechanisms of endothelial senescence," *Experimental Physiology*, vol. 94, no. 3, pp. 299–304, 2009.

[21] V. Victor, N. Apostolova, R. Herance, A. Hernandez-Mijares, and M. Rocha, "Oxidative stress and mitochondrial dysfunction in atherosclerosis: mitochondria-targeted antioxidants as potential therapy," *Current Medicinal Chemistry*, vol. 16, no. 35, pp. 4654–4667, 2009.

[22] D. R. Seals, K. L. Jablonski, and A. J. Donato, "Aging and vascular endothelial function in humans," *Clinical Science*, vol. 120, no. 9, pp. 357–375, 2011.

[23] A. J. Donato, R. G. Morgan, A. E. Walker, and L. A. Lesniewski, "Cellular and molecular biology of aging endothelial cells," *Journal of Molecular and Cellular Cardiology*, vol. 89, Part B, pp. 122–135, 2015.

[24] R. Liu, H. Liu, Y. Ha, R. G. Tilton, and W. Zhang, "Oxidative stress induces endothelial cell senescence via downregulation of Sirt6," *BioMed Research International*, vol. 2014, Article ID 902842, 13 pages, 2014.

[25] W. Ying, "NAD^+/NADH and $NADP^+$/NADPH in cellular functions and cell death: regulation and biological consequences," *Antioxidants & Redox Signaling*, vol. 10, no. 2, pp. 179–206, 2008.

[26] L. Agledal, M. Niere, and M. Ziegler, "The phosphate makes a difference: cellular functions of NADP," *Redox Report*, vol. 15, no. 1, pp. 2–10, 2010.

[27] G. Bodega, M. Alique, L. Bohórquez, S. Ciordia, M. C. Mena, and M. R. Ramírez, "The antioxidant machinery of young and senescent human umbilical vein endothelial cells and their microvesicles," *Oxidative Medicine and Cellular Longevity*, vol. 2017, Article ID 7094781, 12 pages, 2017.

[28] J. Carracedo, P. Buendía, A. Merino et al., "Cellular senescence determines endothelial cell damage induced by uremia," *Experimental Gerontology*, vol. 48, no. 8, pp. 766–773, 2013.

[29] K. Ortmayr, *Quantitative Analysis of $NADP^+$ and NADPH in Yeast, [M.S. thesis]*, University of Natural Resources and Life Science, Vienna, Austria, 2013.

[30] A. Shevchenko, M. Wilm, O. Vorm, and M. Mann, "Mass spectrometric sequencing of proteins silver-stained polyacrylamide gels," *Analytical Chemistry*, vol. 68, no. 5, pp. 850–858, 1996.

[31] R. Soleti, E. Lauret, R. Andriantsitohaina, and M. Carmen Martínez, "Internalization and induction of antioxidant messages by microvesicles contribute to the antiapoptotic effects on human endothelial cells," *Free Radical Biology & Medicine*, vol. 53, no. 11, pp. 2159–2170, 2012.

[32] A. M. Mahmoud, F. L. Wilkinson, E. M. McCarthy et al., "Endothelial microparticles prevent lipid-induced endothelial damage via Akt/eNOS signaling and reduced oxidative stress," *The FASEB Journal*, vol. 31, no. 10, pp. 4636–4648, 2017.

[33] M. Jin, G. Drwal, T. Bourgeois, J. Saltz, and H. M. Wu, "Distinct proteome features of plasma microparticles," *Proteomics*, vol. 5, no. 7, pp. 1940–1952, 2005.

[34] D. B. Peterson, T. Sander, S. Kaul et al., "Comparative proteomic analysis of PAI-1 and TNF-alpha-derived endothelial microparticles," *Proteomics*, vol. 8, no. 12, pp. 2430–2446, 2008.

[35] D. Povero, A. Eguchi, H. Li et al., "Circulating extracellular vesicles with specific proteome and liver microRNAs are potential biomarkers for liver injury in experimental fatty liver disease," *PLoS One*, vol. 9, no. 12, article e113651, 2014.

[36] K. Little, D. Smalley, N. Harthun, and K. Ley, "The plasma microparticle proteome," *Seminars in Thrombosis and Hemostasis*, vol. 36, no. 8, pp. 845–856, 2010.

[37] H. Yi, X. Zheng, J. Song, R. Shen, Y. Su, and D. Lin, "Exosomes mediated pentose phosphate pathway in ovarian cancer metastasis: a proteomics analysis," *International Journal of Clinical and Experimental Pathology*, vol. 8, no. 12, pp. 15719–15728, 2015.

[38] T. S. Blacker, Z. F. Mann, J. E. Gale et al., "Separating NADH and NADPH fluorescence in live cells and tissues using FLIM," *Nature Communications*, vol. 5, p. 3936, 2014.

[39] T. S. Blacker and M. R. Duchen, "Investigating mitochondrial redox state using NADH and NADPH autofluorescence," *Free Radical Biology & Medicine*, vol. 100, pp. 53–65, 2016.

[40] J. T. Wu, L. H. Wu, and J. A. Knight, "Stability of NADPH: effect of various factors on the kinetics of degradation," *Clinical Chemistry*, vol. 32, no. 2, pp. 314–319, 1986.

[41] A. Stincone, A. Prigione, T. Cramer et al., "The return of metabolism: biochemistry and physiology of the pentose phosphate pathway," *Biological Reviews of the Cambridge Philosophical Society*, vol. 90, no. 3, pp. 927–963, 2015.

[42] N. Pollak, C. Dölle, and M. Ziegler, "The power to reduce: pyridine nucleotides – small molecules with a multitude of functions," *The Biochemical Journal*, vol. 402, no. 2, pp. 205–218, 2007.

[43] J. Fan, J. Ye, J. J. Kamphorst, T. Shlomi, C. B. Thompson, and J. D. Rabinowitz, "Quantitative flux analysis reveals folate-dependent NADPH production," *Nature*, vol. 510, no. 7504, pp. 298–302, 2014.

[44] A. Antonov, M. Agostini, M. Morello, M. Minieri, G. Melino, and I. Amelio, "Bioinformatics analysis of the serine and glycine pathway in cancer cells," *Oncotarget*, vol. 5, no. 22, pp. 11004–11013, 2014.

[45] M. F. McMullin, "The molecular basis of disorders of the red cell membrane," *Journal of Clinical Pathology*, vol. 52, no. 4, pp. 245–248, 1999.

[46] R. B. Hamanaka and N. S. Chandel, "Warburg effect and redox balance," *Science*, vol. 334, no. 6060, pp. 1219-1220, 2011.

[47] S. Nóbrega-Pereira, P. J. Fernández-Marcos, T. Brioche et al., "G6PD protects from oxidative damage and improves healthspan in mice," *Nature Communications*, vol. 7, article 10894, 2016.

[48] K. C. Patra and N. Hay, "The pentose phosphate pathway and cancer," *Trends in Biochemical Sciences*, vol. 39, no. 8, pp. 347–354, 2014.

[49] A. Kuehne, H. Emmert, J. Soehle et al., "Acute activation of oxidative pentose phosphate pathway as first-line response to oxidative stress in human skin cells," *Molecular Cell*, vol. 59, no. 3, pp. 359–371, 2015.

[50] E. L. James, R. D. Michalek, G. N. Pitiyage et al., "Senescent human fibroblasts show increased glycolysis and redox homeostasis with extracellular metabolomes that overlap with those of irreparable DNA damage, aging, and disease," *Journal of Proteome Research*, vol. 14, no. 4, pp. 1854–1871, 2015.

[51] E. L. James, J. A. E. Lane, R. D. Michalek, E. D. Karoly, and E. K. Parkinson, "Replicatively senescent human fibroblasts reveal a distinct intracellular metabolic profile with alterations in NAD+ and nicotinamide metabolism," *Scientific Reports*, vol. 6, no. 1, article 38489, 2016.

[52] R. Sullivan, "Epididymosomes: a heterogeneous population of microvesicles with multiple functions in sperm maturation and storage," *Asian Journal of Andrology*, vol. 17, no. 5, pp. 726–729, 2015.

[53] B. Giebel, "On the function and heterogeneity of extracellular vesicles," *Annals of Translational Medicine*, vol. 5, no. 6, p. 150, 2017.

[54] M. C. Larson, C. A. Hillery, and N. Hogg, "Circulating membrane-derived microvesicles in redox biology," *Free Radical Biology & Medicine*, vol. 73, pp. 214–228, 2014.

[55] D. Burger, M. Turner, M. N. Munkonda, and R. M. Touyz, "Endothelial microparticle-derived reactive oxygen species: role in endothelial signaling and vascular function," *Oxidative Medicine and Cellular Longevity*, vol. 2016, Article ID 5047954, 10 pages, 2016.

[56] Q. Zhang, M. Shang, M. Zhang et al., "Microvesicles derived from hypoxia/reoxygenation-treated human umbilical vein endothelial cells promote apoptosis and oxidative stress in H9c2 cardiomyocytes," *BMC Cell Biology*, vol. 17, no. 1, p. 25, 2016.

[57] S. I. Liochev, "Reactive oxygen species and the free radical theory of aging," *Free Radical Biology & Medicine*, vol. 60, pp. 1–4, 2013.

[58] J. Viña, C. Borras, K. M. Abdelaziz, R. García-Valles, and M. C. Gomez-Cabrera, "The free radical theory of aging revisited: the cell signaling disruption theory of aging," *Antioxidants & Redox Signaling*, vol. 19, no. 8, pp. 779–787, 2013.

[59] A. B. Salmon, A. Richardson, and V. I. Pérez, "Update on the oxidative stress theory of aging: does oxidative stress play a role in aging or healthy aging?," *Free Radical Biology & Medicine*, vol. 48, no. 5, pp. 642–655, 2010.

[60] H. Unterluggauer, B. Hampel, W. Zwerschke, and P. Jansen-Dürr, "Senescence-associated cell death of human endothelial cells: the role of oxidative stress," *Experimental Gerontology*, vol. 38, no. 10, pp. 1149–1160, 2003.

Hindawi
Oxidative Medicine and Cellular Longevity
Volume 2018, Article ID 2063179, 17 pages
https://doi.org/10.1155/2018/2063179

Review Article

Role of Oxidative Stress as Key Regulator of Muscle Wasting during Cachexia

Johanna Ábrigo,[1,2] **Alvaro A. Elorza**,[2,3] **Claudia A. Riedel**,[1,2] **Cristian Vilos**,[4,5] **Felipe Simon**,[1,2] **Daniel Cabrera**,[6,7] **Lisbell Estrada**,[8] **and Claudio Cabello-Verrugio**[1,2]

[1]*Departamento de Ciencias Biológicas, Facultad de Ciencias Biológicas, Universidad Andres Bello, Santiago, Chile*
[2]*Millennium Institute of Immunology and Immunotherapy, Santiago, Chile*
[3]*Centro de Investigaciones Biomédicas, Facultad de Ciencias Biológicas & Facultad de Medicina, Universidad Andres Bello, Santiago, Chile*
[4]*Laboratory of Nanomedicine and Targeted Delivery, Center for Integrative Medicine and Innovative Science, Faculty of Medicine, and Center for Bioinformatics and Integrative Biology, Faculty of Biological Sciences, Universidad Andres Bello, Santiago, Chile*
[5]*Center for the Development of Nanoscience and Nanotechnology (CEDENNA), Universidad de Santiago de Chile, Santiago, Chile*
[6]*Departamento de Gastroenterología, Facultad de Medicina, Pontificia Universidad Católica de Chile, Santiago, Chile*
[7]*Departamento de Ciencias Químicas y Biológicas, Facultad de Salud, Universidad Bernardo O'Higgins, Santiago, Chile*
[8]*Centro Integrativo de Biología y Química Aplicada, Universidad Bernardo O'Higgins, Santiago, Chile*

Correspondence should be addressed to Claudio Cabello-Verrugio; claudio.cabello@unab.cl

Received 11 November 2017; Accepted 7 February 2018; Published 28 March 2018

Academic Editor: Rodrigo Franco

Skeletal muscle atrophy is a pathological condition mainly characterized by a loss of muscular mass and the contractile capacity of the skeletal muscle as a consequence of muscular weakness and decreased force generation. Cachexia is defined as a pathological condition secondary to illness characterized by the progressive loss of muscle mass with or without loss of fat mass and with concomitant diminution of muscle strength. The molecular mechanisms involved in cachexia include oxidative stress, protein synthesis/degradation imbalance, autophagy deregulation, increased myonuclear apoptosis, and mitochondrial dysfunction. Oxidative stress is one of the most common mechanisms of cachexia caused by different factors. It results in increased ROS levels, increased oxidation-dependent protein modification, and decreased antioxidant system functions. In this review, we will describe the importance of oxidative stress in skeletal muscles, its sources, and how it can regulate protein synthesis/degradation imbalance, autophagy deregulation, increased myonuclear apoptosis, and mitochondrial dysfunction involved in cachexia.

1. Introduction

Skeletal muscle atrophy is a pathological condition mainly characterized by a loss of muscular mass and the contractile capacity of skeletal muscle that produces muscular weakness and decreased force generation [1–6]. This pathological condition affects a large number of individuals and can be generated by several causes, including pathologic status and aging. Among the main causes are disuse, a state that can be produced by prolonged rest, immobilization, or hind-limb unloading [7–9]; denervation, which is characterized by alterations in neuromuscular connections produced under clinical conditions, such as trauma, diabetic neuropathy, degenerative disease, and spinal cord injury [10–16]; sepsis, an inflammatory syndrome produced mainly by bacterial infections [17–21]; sarcopenia, a physiological process of aging that decreases mobility and aggravates inflammatory diseases and other age-related diseases [22–28]; and chronic

diseases that cause collateral damage in muscles by producing atrophic conditions termed cachexia [29–38], which will be the focus of this review.

2. Cachexia

Cachexia is defined as a pathological condition that is secondary to illness and characterized by the progressive loss of muscle mass with or without loss of fat mass [39]. Cachexia typically manifests in patients with chronic diseases such as cancer, diabetes, obesity, chronic obstructive pulmonary disease (COPD), chronic heart failure (CHF), chronic liver disease (CLD), and chronic kidney disease (CKD) [40], which affect the quality of life and survival of patients [41]. In addition to chronic illness, cachexia is associated with diseases that cause inflammation such as AIDS and sepsis [42]. The prevalence of cachexia is 1% of the total patient population, and it is severely increased among cancer (50–80%), AIDS (10–35%), CHF (5–15%), CKD (30–60%), and COPD (27–35%) patients [42–44].

Even though different types of diseases can induce cachexia, one important common feature of these conditions is alteration of the plasma levels of several soluble factors (termed "atrophic factors"), such as angiotensin II (Ang-II), transforming growth factor type beta (TGF-β), myostatin, glucocorticoids, tumor necrosis factor alpha (TNF-α), and interleukin 1 and 6 (IL-1 and IL-6) [45–54] (Figure 1). These molecules can modulate the different mechanisms involved in the loss of mass and function of skeletal muscle [3, 46, 48, 49, 53, 55–59].

2.1. Mechanisms Involved in the Generation and Development of Cachexia. One of the main features of cachexia is the diminution of muscle strength. There are several molecular mechanisms and signaling pathways involved in cachexia that can explain this phenomenon: (i) oxidative stress, (ii) protein synthesis/degradation imbalance, (iii) autophagy deregulation, (iv) increased myonuclear apoptosis, and (v) mitochondrial dysfunction (Figure 2).

Oxidative stress is one of the most common mechanisms of different causes of cachexia, and two important characteristics of muscle in cachectic patients are increased ROS levels and oxidation-dependent protein modifications [60–62]. Additionally, oxidative stress can modulate other mechanisms involved in cachexia. In the following sections, we will describe the generation of oxidative stress, how oxidative stress regulates the aforementioned molecular mechanisms, and their roles in cachexia.

3. Oxidative Stress

Skeletal muscle is a tissue that continuously produces oxidant species such as reactive oxygen species (ROS) and reactive nitrogen species (RNS) (for details about RNS, see [63]), which are in balance with antioxidant mechanisms. The production of ROS species is a normal process in all cells (including skeletal muscle cells) in which signaling molecules regulate different pathways essential for cell viability [64, 65]. Skeletal muscle cells produce several types of ROS that differ in terms of origin, localization, stability, and reactivity [66]. The role of ROS in muscle can seem contradictory since they can act as signaling molecules in normal processes such as regeneration and repair [67] and promote mitochondrial biogenesis during exercise [68], but local sustained ROS levels may cause tissue injury due to oxidative damage [69].

The imbalance produced by an increase in oxidant species levels and/or a decrease in antioxidant species generates the loss of normal redox equilibrium in cells, a condition denominated as *oxidative stress*, which corresponds to redox status; can injure several cellular organelles, proteins, lipids, and membranes; and affects muscle function [70] (Figure 1).

The main features of oxidant and antioxidant species will be described in the following sections, and we will principally describe their participation and contribution to the generation of cachexia in patients with chronic diseases.

3.1. Types and Features of ROS. Superoxide anion ($O_2{\cdot}^-$), hydrogen peroxide (H_2O_2), and hydroxyl radical (OH·) are the main ROS found in most tissues [64]. Several studies suggest that the major ROS produced in skeletal muscle fibers is $O_2{\cdot}^-$ [71, 72], which is very labile and undergoes enzymatic or spontaneous dismutation by reduction to more stable species, such as H_2O_2. H_2O_2 is a nonradical weak oxidant with a relatively long half-life that can diffuse across cell membranes and therefore acts as an important intracellular signaling molecule [73, 74]. Additionally, H_2O_2 can generate OH· in the presence of active free iron ions or other transition metals, a process known as the Fenton reaction. OH· reacts immediately with any surrounding biomolecules, resulting in most of the deleterious effects associated with oxidative stress. In this context, considering that skeletal muscle contains 10–15% of total body iron—mainly in myoglobin and mitochondria—it could be especially sensitive to alterations due to oxidative stress. Thus, iron homeostasis can be considered a comodulator of ROS signaling and effects [75].

The main cellular macromolecules can be damaged by ROS. Cellular membranes can be damaged by the changes that produce OH· on lipids by attacking polyunsaturated fatty acid lipid residues and generating peroxyl radical [76]. DNA is affected because purine and pyrimidine bases and deoxyribose are damaged by OH [76]. OH· targets proteins by damaging their amino acid residues, such as lysine, arginine, histidine, proline, and threonine, causing the formation of protein carbonyls. In addition, the sulfhydryl group in amino acids undergoes irreversible oxidation [76].

3.2. Sources of ROS in Skeletal Muscle Cells. ROS in cells can be produced by different sources, such as mitochondria, sarcoplasmic reticulum, and sarcolemma. Additionally, the main enzymes involved in ROS generation under physiopathological conditions are nicotinamide adenine dinucleotide phosphate (NADPH) oxidase and xanthine oxidase (XO) (Figure 2).

The Nox protein family is composed of subunits of the NADPH oxidase enzyme complex that have catalytic and electron-transporting functions [77]. The Nox family consists of seven members, Nox1–5 and two dual oxidases (Duox), Duox1 and Duox2 [78]. Structurally, Nox isoforms

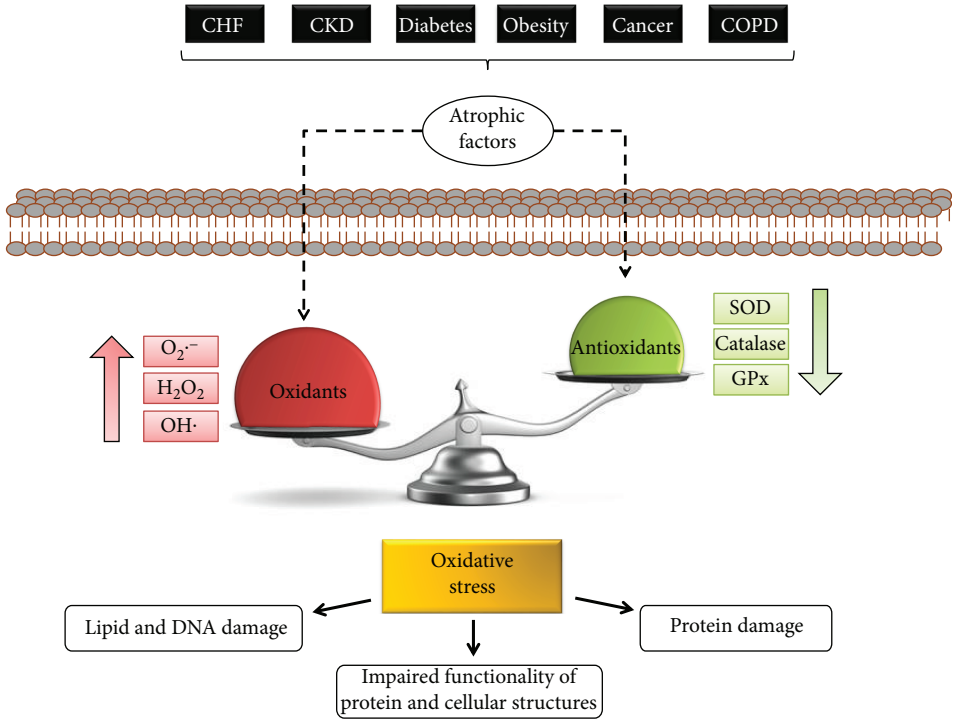

Figure 1: Oxidative stress in muscle is produced by an imbalance between oxidant and antioxidant species. Soluble atrophic factors produced by different diseases induce an imbalance of the oxidative state, increasing oxidant species such as $O_2\cdot^-$, H_2O_2, and OH· and decreasing antioxidant species such as catalase, glutathione peroxidase (GPx), and superoxide dismutase (SOD). This imbalance is denominated as "oxidative stress" and produces oxidative damage in lipids, DNA, and proteins, impairing functionality of proteins and cellular structures.

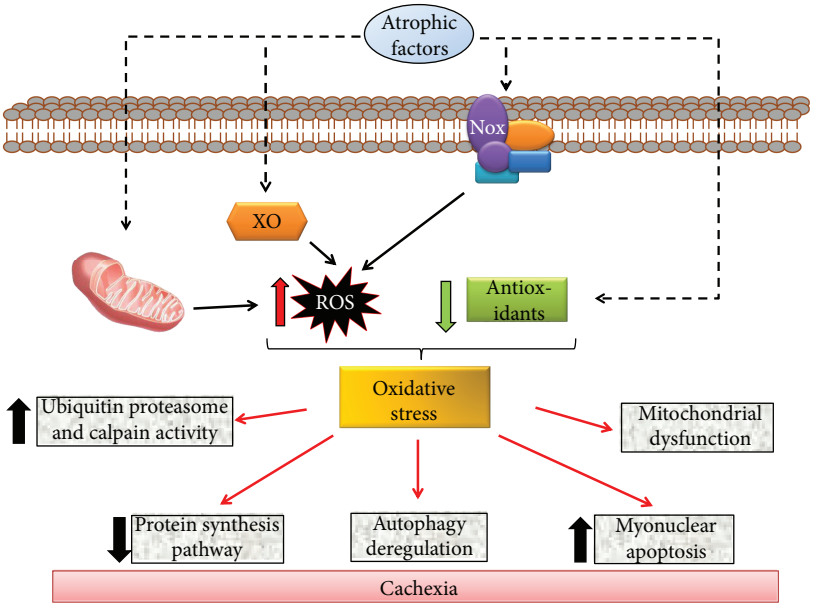

Figure 2: Molecular mechanisms involved in cachexia are modulated by oxidative stress. Atrophic factors can generate oxidative stress in skeletal muscle by the activation of different sources of reactive oxygen species, such as the mitochondria, xanthine oxidase (XO), and NADPH oxidase complex with Nox subunit, in addition to the decrease in antioxidant species. Oxidative stress is able to produce mitochondrial dysfunction, increase ubiquitin proteasome system activity, increase myonuclear apoptosis, decrease the protein synthesis pathway, and deregulate autophagy, all of which are involved in cachexia-skeletal muscle atrophy.

contain FAD and NADPH binding sites, two heme molecules, and six transmembrane alpha helices with cytosolic N- and C-termini [78, 79]. Several proteins can interact with Nox isoforms. For example, Nox1–4 can bind to $p22^{phox}$, while Nox1–2 can bind to small GTPases such as Rac. Nox2 can bind to $p47^{phox}$ and $p67^{phox}$ as well as the cytosolic

protein $p40^{phox}$ [78, 80]. Nox4 has been reported to bind to the polymerase (DNA-directed) delta-interacting protein 2 (PolDip2) [81]. NADPH oxidases are enzymes that serve a primary function in the production of superoxide/ROS. Nox1, Nox2, and Nox5 mainly produce $O_2\cdot^-$, while Nox4 mainly produces H_2O_2 [82, 83]. Nox4 is constitutively active, and modulation of its expression may thus be a major activity regulator, whereas Nox1 can be activated by Nox activator 1 (NOXA1) protein, Nox2 can be activated by $p67^{phox}$, and Nox5 can be activated by calmodulin [78, 79].

In skeletal muscle, the NADPH oxidase complex is reportedly located on transverse tubules (T-tubules), the sarcolemma, and the sarcoplasmic reticulum. In addition, skeletal muscle expresses only the Nox2 and Nox4 isoforms and partner proteins such as $p22^{phox}$, $p67^{phox}$, $p47^{phox}$, and $p40^{phox}$ [84, 85]. Interestingly, $O_2\cdot^-$ generated from Nox has been implicated in progressive skeletal muscle damage [86]. Recent evidence demonstrated that NADPH oxidase overactivity leads to atrophy of glycolytic muscle in a rat model of heart failure (HF) [87]. Interestingly, the mechanism also involved the NF-κB activation and increased p38 phosphorylation and was reduced by aerobic exercise training, suggesting that NADPH oxidase activity can be a good candidate for targeting and treating the muscle wasting [87].

Xanthine dehydrogenase (XDH), the most common form of xanthine oxidoreductase (XOR) in tissue, can be converted to xanthine oxidase (XO) via oxidation of sulfhydryl residues or proteolysis [88]. XO is an enzyme belonging to the molybdenum protein family with a homodimer structure and a molecule mass of 290 kDa. It contains two separate substrate-binding sites [88]. Functionally, XO causes oxidation of hypoxanthine to xanthine and then to uric acid [89, 90]. During reoxidation of XO, O_2 acts as an electron acceptor, producing superoxide radical and hydrogen peroxide [91]. During these reactions, $O_2\cdot^-$ and H_2O_2 are formed [91]. Spontaneously or under the influence of enzyme superoxide dismutase (SOD), $O_2\cdot^-$ are transformed into H_2O_2 and O_2 [88]. The conversion of XDH to XO is assumed to be required for radical generation and tissue injury, although some evidence suggests that XDH directly participates in $O_2\cdot^-$ generation in ischemic tissue [92, 93]. In this context, it has been proposed that ischemia induces conversion of XDH into XO as well as production of hypoxanthine, which reacts with O_2 during reperfusion and generates a high amount of superoxide radical from XO [94]. Early studies have suggested that ROS arising from XO plays an important role in the inflammatory response to physical eccentric contractions or high-intensity or long-lasting exercise as well as in injuries caused by ischemia-reperfusion processes [95, 96]. These studies are in agreement with those reporting the role of XO in muscle injury associated with exhaustive physical exercise [97–99]. In skeletal muscle, XO is localized mainly in the vascular endothelium [100]. The intake of enzyme inhibitors diminishes the release of $O_2\cdot^-$ in the vessels of contracting muscles, which has proven to be effective for reducing muscle fatigue *in vivo* [101, 102]. Another study shows that suppression of XO activity by allopurinol may increase maximum isometric strength in the skeletal muscle of old mice [103]. In addition, administration of allopurinol and subsequent XO inhibition prevent muscular atrophy by inhibiting the p38 MAPK-atrogin-1 pathway and may have beneficial clinical effects, such as resistance against muscular atrophy in patients with permanent immobilization, sarcopenia, or cachexia [104, 105].

A third component that produces ROS in skeletal muscle is mitochondria. Skeletal muscle is a tissue that constantly demands ATP for energy production. ATP is generated via the activity of the mitochondrial electron transport chain (ETC) mainly at two sites: (i) complex I, where it is generated by auto-oxidation of the flavin mononucleotide from the NADH-dehydrogenase, and (ii) complex III, where its generation depends on auto-oxidation of unstable semiquinone, which is an intermediate of the Q-cycle reaction [106]. The ETC is located in the inner mitochondrial membrane. In this membrane, oxygen is consumed, resulting in the liberation of electrons that can quickly react with cellular proteins, resulting in their oxidation, or with molecules such as H_2O or H_2O_2, generating more reactive molecules. Additionally, about 1–3% of the total oxygen utilized by the mitochondria is incompletely reduced and remains as ROS [107]. Compared with other tissues, skeletal muscle has a high number of mitochondria, and therefore, the contribution of this organelle to oxidative stress is very relevant.

3.3. Antioxidant Species in Skeletal Muscle. It is well known that skeletal muscle features high metabolic activity and oxidative capacity. Considering the importance of ROS production in skeletal muscle, the antioxidant system is essential for maintenance of cellular oxidative homeostasis. There are several antioxidant enzymes, including superoxide dismutase (SOD), catalase, and glutathione peroxidase (GPx) [108]. SOD has three isoforms: SOD1, which is located in the intracellular cytoplasmic compartment; SOD2, which is found in mitochondria; and SOD3, which is located in the extracellular matrix. This enzyme is a specific antioxidant for $O_2\cdot^-$ and catalyzes the dismutation of $O_2\cdot^-$ to H_2O_2 [108]. Some studies have indicated that mice lacking SOD1 lose muscle mass, suggesting that it plays a role in the maintenance of muscle fibers [109]. Catalase is present in cytoplasmic compartments and in mitochondria [110]. It catalyzes the conversion of H_2O_2 to H_2O and O_2 [111]. The enzymatic activity of catalase is higher in oxidative myofibers than in fast glycolytic fibers [112]. As an ROS scavenger, GPx has the same function, but with higher affinity for H_2O_2 than for catalase [108].

Five GPx isoforms have been described in mammals with different cellular localizations and substrate specificities. GPx1 is localized predominantly in the cytosol and somewhat in the mitochondrial matrix. GPx3 is present in the extracellular space [113]. GPx4 is a membrane-associated enzyme that is partly localized in the mitochondrial intermembrane space.

Studies have indicated that a decrease in antioxidant levels in response to diseases can lead to an imbalance in the redox state of the cell, causing oxidative damage [66, 114, 115] (Figure 1).

3.4. Oxidative Stress in Cachexia. Patients with chronic heart failure (CHF) or chronic kidney disease (CKD) develop

cachexia associated with their pathologic status [116–118]. One of the main participants in this phenomenon is Ang-II, an endogenous peptide with atrophic activity in skeletal muscle. Patients with CHF and CKD have increased levels of circulating Ang-II [119–121]. Interestingly, Ang-II induces ROS production in skeletal muscle cells through its AT-1 receptor, as demonstrated by a study that found that losartan, an AT-1 receptor blocker, eliminates the oxidative effect of Ang-II [122]. Additionally, the atrophic effects mediated by Ang-II depend on ROS [123, 124]. In this context, Zhao et al. [125] and Cabello-Verrugio et al. [126] demonstrated that rats and mice infused with Ang-II have high ROS levels in skeletal muscle as well as major expression of $gp91^{phox}$, a Nox subunit, suggesting that Nox increases ROS levels. Similar results were obtained in muscle cells incubated with Ang-II (i.e., they exhibited enhanced Nox activity) [124]. Moreover, the use of apocynin, a Nox inhibitor, blocks ROS production, suggesting that Ang-II increases ROS levels in skeletal muscle via a Nox-dependent mechanism [122]. Further, Ang-II promotes membrane mitochondrial depolarization, which increases mitochondrial ROS production, therefore contributing to oxidative stress in skeletal muscle [127]. Together, these results indicate that, in the presence of high levels of Ang-II, ROS is an important factor in the development of muscle atrophy in cachectic patients with chronic disease.

Patients with cancer cachexia have exhibited protein oxidation in skeletal muscle, suggesting the involvement of oxidative stress in cachexia [128]. In particular, patients with cancer present elevated ROS levels and decreased antioxidant levels in serum [66, 129]. They also have increased levels of mitochondrial uncoupling proteins (UCP) such as UCP2 and UCP3, which could lead to uncoupling of ETC and thus to the loss of mitochondrial membrane potential, increasing ROS production in mitochondria [130–133]. Additionally, cancer increases the levels of several proinflammatory cytokines involved in the pathogenesis of cachexia and oxidative damage, such as IL-1, IL-6, and TNF-α [134–137]. TNF-α induces ROS production by mitochondria and Nox activation [106, 138, 139]. Sullivan-Gunn et al. demonstrated that the expression of the Nox enzyme subunits Nox2, $p40^{phox}$, and $p67^{phox}$ was decreased in the muscle of mice with cancer cachexia, in spite of increased superoxide levels. However, these mice also exhibited decreased levels of antioxidant proteins such as SOD1, SOD2, and GPx [140], as reported previously [66, 141]. These results suggest that the development of oxidative stress in association with cancer-induced cachexia can be attributed, at least partially, to increased ROS levels and failure of the antioxidant systems that operate in muscle cells. Other evidence has indicated that inhibition of XO reduces skeletal muscle wasting and improves outcomes in a rat model of cancer cachexia, suggesting that other sources may contribute to oxidative stress [142].

4. Redox Regulation of Molecular Mechanisms of Cachexia

4.1. Imbalance in the Protein Synthesis/Degradation. All types of skeletal muscle atrophy are associated with a decrease in the levels of myofibrillar proteins, mainly myosin heavy chain, myosin light chain, and troponin, which are essential parts of the sarcomere structure [7, 39, 143]. The myosin proteins form a complex with actin and are responsible for muscle contraction [6]. In cachectic conditions, there is an imbalance in the degradation and/or synthesis of myofibrillar proteins, explaining their decreased levels. Under muscle atrophy conditions such as cachexia, the ubiquitin proteasome system (UPS) and calpains are the main mechanisms involved in the degradation of muscle proteins [144].

4.1.1. The Ubiquitin Proteasome System. The UPS acts by the coordinated action of three enzymes: E1 (enzyme activator of ubiquitin), E2 (enzyme conjugator of ubiquitin), and E3 (ubiquitin ligase). All are involved in the labeling of specific proteins with ubiquitin (Ub) molecules. Ubiquitinated proteins are then degraded by proteasome 26S subunits [145]. E3 ubiquitin ligases are a family of enzymes that determine which protein will be ubiquitinated and degraded [1, 145]. In cachectic skeletal muscle, the levels of two E3 ubiquitin ligases are increased: MAFbx/atrogin-1 and MuRF-1. These muscle-specific enzymes target myofibrillar proteins, such as myosin, and factors involved in myogenesis, such as MyoD [145, 146]. Interestingly, our research and that of others have demonstrated that UPS is overactivated by soluble factors such as Ang-II and TGF-β1, which are increased during cachexia [45, 46, 48, 49, 147, 148].

UPS is the principal proteolytic mechanism described in skeletal muscle atrophy associated with chronic diseases. In pathological conditions, this pathway can be overactivated in multiple ways, including oxidative stress. Li et al. studied the effect of H_2O_2 on UPS markers in myotubes, showing that ubiquitin-conjugating activity is stimulated concomitant with an increase in the expression of E2 and E3 enzymes [149]. Additionally, a study by Russell et al. employing a murine model of cancer cachexia indicated that ubiquitin gene expression increases downstream Nox-generated ROS production, suggesting that Nox plays a role in cancer cachexia [124, 150] (Figure 2).

In chronic diseases, systemic increase of ROS can promote oxidative stress and alterations in peripheral tissues such as skeletal muscle, increasing the levels of proinflammatory transcription factors, such as nuclear factor kappa B (NF-κB), that regulate specific UPS genes [60, 124]. In skeletal muscle, NF-κB is activated and translocated to the nucleus to induce MuRF-1 expression [151]. Additionally, NF-κB increases the expression of proinflammatory cytokines such as IL-6 and TNF-α, two important soluble factors involved in the development of skeletal muscle atrophy that increases ROS production and activate UPS, forming a positive feedback mechanism [50, 151–153].

These results indicate that, in skeletal muscle, ROS upregulates the expression of key components of UPS and increases their activity and that Nox participates in this phenomenon.

4.1.2. Calpains. Calpains are Ca^{2+}-activated proteases coded by 15 genes in humans that are involved in the selective cleavage of target proteins [154]. In skeletal muscle, calpain

1 (μ-calpain) and calpain 2 (m-calpain) participate in skeletal muscle atrophy [155]. Specifically, active calpains are able to cleave cytoskeletal proteins such as titin and nebulin, which are responsible for anchoring contractile proteins, as well as several kinases, phosphatases, and oxidized contractile proteins, such as actin and myosin [155, 156]. There is evidence that oxidative stress increases the expression of calpains in murine and human skeletal muscle cells [157, 158].

Studies have found that oxidative stress increases calpain activity in skeletal muscle cells [157, 158]. Specifically, H_2O_2 is able to increase calpain 1 activity in murine skeletal muscle cells and induce activation of calpain 1 and calpain 2 in human skeletal muscle cells [157, 158]. In line with these findings, antioxidant treatment of disused skeletal muscle has been found to prevent both oxidative stress and calpain 1 activation [159]. Together, these investigations confirm that oxidative stress in skeletal muscle can activate calpain.

The main regulators of calpain activity are cytosolic calcium and calpastatin, an endogenous calpain inhibitor [155, 160]. Thus, increased oxidative stress-dependent calpain activity is likely due to an increase in the cytosolic level of free calcium, which also depends on oxidative stress [158, 161, 162].

4.1.3. Anabolic Pathways. Despite the fact that increased catabolism in skeletal muscle is the principal mechanism involved in the imbalance of protein content, reduced anabolism also contributes to this phenomenon. Induction of protein synthesis is determined by the Akt/mTOR (mammalian target of rapamycin) pathway and depends on insulin-like growth factor-1 receptor (IGFR), which can be activated by different factors, such as amino acids, insulin, and IGF-1. After IGFR binds to IGF-1, it is phosphorylated and activated, inducing activation of PI3K, which phosphorylates Akt and, consequently, mTOR, promoting protein synthesis [163]. Additionally, there is evidence that IGF-1 inhibits proteolysis in skeletal muscle by avoiding overactivation of UPS, suggesting regulation of both processes [164–166]. Previous reports have indicated that the circulating level of IGF-1 is reduced in patients with pathological conditions such as sepsis, cancer, and liver diseases [167–169]. Furthermore, soluble factors such as TNF-α and Ang-II act upstream of the IGF-1 pathway, inhibiting PI3K-Akt signaling and the downstream pathway. An example of this regulation involves the Forkhead box O (FoxO), a transcription factor normally phosphorylated by active PI3K-Akt/PKB that is kept inactive in the cytoplasm. When the synthesis pathway for TNF-α and Ang-II is inhibited, FoxO translocates to the nucleus and induces expression of the E3 ubiquitin ligases MAFbx/atrogin 1 and MuRF-1, increasing protein degradation [170].

Several factors, including ROS, are involved in the regulation of the PI3K-Akt pathway. Low ROS levels induce activation of the anabolic pathway, while high ROS levels inhibit it [171, 172] (Figure 2). Previous studies have established that Akt is a redox-sensitive protein that is activated in the presence of excess H_2O_2; however, this effect can be a consequence of indirect mechanisms such as oxidative inactivation of phosphatases or loss of feedback inhibition via MAPKs [173]. Increased ROS levels can induce protein oxidation in specific cysteine residues, inhibiting the activity of phosphorylases such as PKA that induce the activation of Akt [174]. The use of antioxidants such as *N*-acetyl cysteine (NAC) after oxidative stress stimulus prevents ROS increases and avoids inhibition of Akt activity [175], indicating that oxidation plays a role in this phenomenon. Additionally, inhibition of two important ROS sources, Nox and the mitochondrial ETC, activates Akt [175]. In skeletal muscle, ROS can be involved in the activation of metabolic effects by other signaling pathways independent of insulin, stimulating, for example, glucose transport during exercise, specifically during muscle contraction [176, 177].

4.2. Deregulation of Autophagy. The autophagy-lysosomal pathway is a normal mechanism that maintains cell homeostasis by removing old and damaged cellular components. This process eliminates portions of the cytoplasm, organelles, and protein aggregates in double-membrane vesicles, called autophagosomes, which are then fused with lysosomes for degradation [178]. Autophagy is often described as a five-step process: (1) induction, (2) expansion, (3) elongation and completion of autophagosomes, (4) fusion with lysosomes, and (5) degradation of proteins and organelles [63, 179]. Autophagy is induced by the formation of the pre-autophagosome structure, which occurs by activation of the ULK1 complex [179]. One of the main negative regulators of this step is mTORC1, and consequently all factors that prevent mTORC1 activation can promote autophagy [179]. The stage of expansion is characterized by the formation of phagophore, a fractional autophagosome membrane, and the recruitment of several Atg proteins, including the essential Atg6 (also called beclin-1) [179]. The elongation and completion of autophagosomes involve Atg genes (e.g., Atg5, Atg7, Atg8, and Atg12) [179]. During this stage, LC3B protein (Atg8) is posttranslationally modified from its inactive form (LC3I) to its active form (LC3II), which is a component of autophagosomes [180, 181]. Next, the autophagosome is fused with a lysosome, and the autophagosome's contents (i.e., cytosolic proteins and organelles) are transferred to lysosomal proteases (i.e., cathepsins B, D, and L) [179]. The fifth and final step of autophagy involves cathepsin-mediated degradation of proteins and organelles (i.e., the cargo) contained within the autophagosome [179–181].

Under pathological conditions, autophagy increases in association with muscle wasting induced by proatrophic stimuli, fasting, high-fat diet/insulin resistance, hypoxia, and exercise [182]. In addition, impaired autophagy has been reported in several myopathies [183–185]. Interestingly, a bidirectional relation between autophagy and oxidative stress has been reported, with some studies finding an increase in autophagy induced by ROS and other studies finding an increase in ROS induced by autophagy [182].

It has been demonstrated that, in patients with COPD, locomotor muscles feature increased autophagy [186, 187]. Recently, a study employing a murine model of sepsis induced by cecal ligation and perforation showed that limb muscles exhibit higher autophagy than do respiratory muscles [188]. Another recent study using an experimental model of CKD revealed a correlation between skeletal muscle

oxidative stress, muscle catabolism, and autophagy, finding that inhibition of oxidative stress could improve muscle atrophy by enhancing mitophagy [189]. Moreover, a C26 cell-induced cancer model demonstrated that exercise increased autophagy flux, improving muscle homeostasis, probably due to the removal of damaged proteins and mitochondria [190].

Several studies have suggested that autophagy is activated by oxidative stress, but a study of expression of a mutant form of superoxide dismutase 1 (SOD1G93A) in skeletal muscle revealed a causal relation between oxidative stress, activation of autophagy, and muscle atrophy and weakness [191–194]. Although the mechanisms involved in the regulation of autophagy by ROS during skeletal muscle wasting are not yet known, studies have suggested that several signaling pathways participate in this regulation. Thus, it has been suggested that ROS can induce autophagy by regulating the activation of the PI3K/Akt/mTORC1 signaling pathway. A model of muscle atrophy by disuse demonstrated that ROS can inhibit Akt/mTOR signaling and consequently induce autophagy [195]. However, a skeletal muscle model employing dystrophic *mdx* mice revealed that Nox2-derived ROS can activate the Src/PI3K/Akt pathway and, subsequently, mTORC1, leading to autophagy inhibition [183].

Inactivation of PTEN (a phosphatase and tensin homolog deleted on chromosome 10) results in increased cellular PIP3 levels, activation of PI3K/Akt, and subsequent activation of autophagy [182]. One inhibitor of PTEN is oxidative stress [196, 197]. PTEN can also regulate ROS production, resulting in a feedback loop in which it has been suggested that Nox participates in [197]. While ROS has been shown to activate Akt through inhibition of PTEN in C2C12 myotubules, its role in regulating autophagy in skeletal muscle has not been directly assessed [196].

ROS-dependent regulation of autophagy may also occur through p38 MAPK. In skeletal muscle, the participation of p38 MAPK in autophagy was found in a model of muscle atrophy induced by sepsis [17]. The same model was used to demonstrate the involvement of ROS in p38 MAPK regulation of autophagy [198]. In other tissues, the p38 MAPK/p53 pathway has been shown to activate autophagy, but this pathway has not yet been evaluated in skeletal muscle [199, 200].

AMPK, a widely investigated indicator of cellular energy levels and regulator of muscle metabolism during exercise, may be another possible mechanism for redox regulation of autophagy in association with skeletal muscle wasting [201]. Alterations in redox balance have been shown to regulate AMPK activity [202]. Moreover, a study using C2C12 cells showed that, during nutrient deprivation and rapamycin treatment, there is an increase in mitochondria-derived ROS, which promotes skeletal muscle autophagy, and this effect is mediated in part by activation of AMPK and inhibition of Akt [194].

4.3. Myonuclear Apoptosis. Apoptosis is defined as programmed cell death. In skeletal muscle, this process is called myonuclear apoptosis and has distinctive characteristics compared to apoptosis of other tissues because muscle fibers are multinucleated cells. Myonuclear apoptosis involves elimination of the fiber segments that surround the apoptotic nucleus (known as the myonuclear domain), not the complete fiber [203–205].

The mechanisms involved in the generation of apoptotic nuclei have not been clearly elucidated. However, two principal signaling pathways are involved in apoptosis: extrinsic and intrinsic pathways. The extrinsic pathway is mediated by factors of the TNF family or Ang-II, which activate death receptors and induce activation of pro-caspase 8 by proteolytic cleavage. The intrinsic pathway is dependent on mitochondria and triggers an imbalance between antiapoptotic factors such as Bcl-2 (diminished) and apoptotic factors such as Bax (elevated) that might induce cytochrome *c* release and promote the formation of the mitochondrial transitory pore. Then, cytochrome *c* binds to apoptosis protease-activating factor-1 (Apaf-1) and pro-caspase 9 in the cytoplasm to form an apoptosome complex, which induces activation of caspase 9 (initiator caspase) [206]. Both the extrinsic and intrinsic pathways converge in the activation of effectors such as caspase 3. Caspase 3 activates endonuclease G, which triggers DNA fragmentation, degradation of genetic material by proteases, and posterior formation of apoptotic bodies eliminated by phagocytic cells.

Myonuclear apoptosis is increased in pathologies such as COPD, CHF, CKD, and obesity [38, 207–210]. Our group and others have found that cachectic muscle induced by Ang-II develops myonuclear apoptosis and that this is one of the main factors involved in overactivation of myonuclear apoptosis and the consequent increase in muscle weakness [45, 118, 211–213].

In other cell types, oxidative stress has been described as a potent inducer of cell death [214]. In an experimental model of cancer cachexia in which an XO inhibitor was used to reduce caspase-3 activity, Springer et al. showed that ROS production and proteasome activity decrease in skeletal muscle and consequently prevent body weight loss in animals [142]. Additionally, the mitochondrial apoptotic pathway is activated by a direct or indirect effect of ROS because increasing ROS can induce expression and mitochondrial translocation of the proapoptotic factor Bax, in turn inducing formation of the mitochondrial transition pore. Patients with cancer or CHF often present with hyperuricemia (incremented levels of uric acid), a condition in which XO activity is upregulated in the affected tissue and the systemic ROS level is increased [215]. Recently, studies employing a murine model of obesity induced by a high-fat diet (HFD) have shown that muscle weakness and protein degradation are accompanied by increased ROS levels and myonuclear apoptotic markers in muscle fibers [216].

4.4. Mitochondrial Dysfunction. Mitochondria play a key role in muscle physiology and metabolism. As mentioned throughout this review, mitochondria are the main producers of ATP and one of the main sources of ROS. However, other signaling intermediates such as calcium, NAD^+/NADH, acetyl-CoA, and alpha-ketoglutarate are also produced/released to control muscle metabolism and epigenetics [217–219]. Mitochondrial function depends on the success of the

mitochondrial life cycle, which involves mitochondrial biogenesis, remodeling through mitochondrial fusion and fission events called mitochondrial dynamics (MtDy), and degradation through a process called selective mitochondrial autophagy or mitophagy [220–223]. Any disruption of the mitochondrial life cycle will lead to mitochondrial dysfunction, which is characterized by low ATP levels and/or high ROS production [224, 225].

Superoxide ($O_2\cdot^-$) is a byproduct of the ETC that can be converted to H_2O_2 by SOD2. As previously mentioned, O^{2-} and H_2O_2, which are both abundant in mitochondria, generate OH· (hydroxyl radical), which is the most reactive and harmful reactive radical for mitochondrial function. ROS will not only oxidize the respiratory complexes of ETC and mitochondrial DNA, among other macromolecules, but will also increase ROS production by damaged mitochondria, leading to a vicious cycle that ends in cell death due to apoptosis and/or necrosis [226, 227].

In addition to the antioxidant mechanisms previously described in this manuscript, mitochondria have more complex defense systems, including triple A proteases and mitochondrial unfolded protein response (mtUPR), which protect against cytotoxic protein aggregates and misfolded proteins, and the mitochondrial life cycle itself, which acts as a quality control system to eliminate old, dysfunctional, and depolarized mitochondria through mitophagy [225, 228–231].

The mitochondrial life cycle and defense systems are both defective in cachectic conditions, negatively impacting mitochondrial function. As previously reported, mitochondrial biogenesis, mitochondrial dynamics, and mitophagy are defective in skeletal and cardiac muscle cells with altered mitochondrial content and morphology; disruption of mitochondrial fusion and exacerbation of mitochondrial fission; altered mitophagy; reduced ETC activity; increased ROS generation; and proneness to apoptosis and mPTP opening [232, 233]. At the level of mitochondrial content, there is a reduction in the expression of PGC1-alpha, the master regulator of mitochondrial biogenesis; nuclear receptor factor 1 and transcription factor A, both of which control nuclear and mitochondrial gene expression for proper mitochondrial function; and SIRT1, a deacetylase that controls PGC1-alpha activity [232, 233]. At the level of mitochondrial dynamics, expression of the fusion proteins MFN1 and MFN2 reduces, and the level of the FIS1 and DRP1 fission proteins is increased [232, 233]. In addition, mitophagy, defined by expression of the LC3, PARKIN, PINK, and Atg5 markers, increases. However, there are some controversial points about mitophagy, which will be discussed later. Finally, at the level of the ETC, the respiratory complexes cytochrome *c* oxidase (complex IV) and cytochrome bc_1 (complex III) and the mobile component of cytochrome *c* showed reduced expression. A similar result was observed for the enzyme citrate synthase that forms part of Krebs cycle [232, 233].

It has been recently shown that mitochondrial biogenesis, mitochondrial dynamics, and mitophagy are interconnected. This means that there is a perfect balance between the need for mitochondrial dynamics in mitophagy and the need for mitophagy in mitochondrial biogenesis [234–239]. Mitophagy is essential for mitochondrial turnover to maintain a healthy mitochondria population, control the amount of cellular ROS, and eliminate damaged and ROS-producing mitochondria. Thus, mitophagy failure is associated with an accumulation of dysfunctional mitochondria and decreased mitochondrial biogenesis. Several studies performed in cachectic muscle have reported increased mitophagy indicated by the expression of mitophagy markers [232]. However, other studies have reported reduced mitophagy in patients with cancer cachexia [224]. Given these conflicting findings, it is important to consider mitophagy in terms of flux. Diminished mitophagic flux will cause accumulation of mitophagic markers and damaged mitochondria and decreased mitochondrial biogenesis, generating a pool of dysfunctional mitochondria in accordance with the pathology of cachexia.

5. Conclusions

As mentioned in this review, cachexia is a pathological condition that affects skeletal muscle and leads to weakness and loss of strength and muscle mass. This condition is secondary to other pathologies that affect other tissues and is characterized by the participation of secreted soluble factors that produce an atrophic effect in skeletal muscle.

We know that different mechanisms are involved in the development of skeletal muscle atrophy, such as UPS overactivation, protein synthesis pathway diminution, autophagy deregulation, increased myonuclear apoptosis, and oxidative stress, which are activated depending on the stimuli. In this review, we have shown that, even though each mechanism can act independently and play an important role in muscle weakness, the mechanisms are interconnected. In particular, we emphasized oxidative stress as an atrophic mechanism that affects the other mentioned mechanisms. We highlighted the importance of redox state regulation in muscle cells in order to maintain homeostasis and the deleterious effects produced when this balance is lost. In conclusion, although all these mechanisms can generate harmful effects in muscle through different pathways, oxidative stress modulates all of them and can produce a more harmful effect or accelerate muscle damage. Therefore, reduction or prevention of oxidative imbalance in muscle is of vital importance.

Abbreviations

AIDS: Acquired immune deficiency syndrome
AMP: Adenosine monophosphate
AMPK: AMP-activated protein kinase
Ang-II: Angiotensin II
Apaf-1: Apoptotic protease-activating factor-1
AT-1: Angiotensin II receptor type 1
Atg: Autophagy-related gene
ATP: Adenosine triphosphate
CHF: Chronic heart failure
CKD: Chronic kidney disease
CLD: Chronic liver disease
COPD: Chronic obstructive pulmonary disease
DRP1: Dynamin-related protein
Duox: Dual oxidases

E1: Enzyme activator of ubiquitin
E2: Enzyme conjugator of ubiquitin
E3: Ubiquitin ligase
ETC: Electron transport chain
FAD: Flavin adenine dinucleotide
FIS1: Mitochondrial fission 1 protein
FoxO: Forkhead box O
GPx: Glutathione peroxidase
GTPase: Guanosine triphosphatase
HFD: High-fat diet
H_2O_2: Hydrogen peroxide
IL-1: Interleukin 1
IL-6: Interleukin 6
IGF-1: Insulin-like growth factor-1
IGFR: Insulin-like growth factor-1 receptor
MAFbx: Muscle atrophy F-box
MAPK: Mitogen-activated protein kinases
MFN1: Mitofusin 1
mPTP: Mitochondrial permeability transition pore
MtDy: Mitochondrial dynamics
mtUPR: Mitochondrial unfolded protein response
MuRF-1: Muscle RING finger 1
MyoD: Myogenic differentiation factor
NAC: *N*-Acetyl cysteine
NADPH: Nicotinamide adenine dinucleotide phosphate
NF-κB: Nuclear factor kappa B
NFR1: Nuclear receptor factor 1
Nox: NADPH oxidase subunity
NOXA1: Nox activator 1
$O_2\cdot^-$: Superoxide anion
OH·: Hydroxyl radical
PGC1-alpha: Peroxisome proliferator-activated receptor gamma coactivator 1-alpha
PI3K: Phosphoinositide 3-kinase
PINK: PTEN-induced putative kinase
PKA: Protein kinase A
PolDip2: Polymerase (DNA-directed) delta-interacting protein 2
PTEN: Phosphatase and tensin homolog deleted on chromosome 10
RNS: Reactive nitrogen species
ROS: Reactive oxygen species
SIRT1: Sirtuin 1
SOD: Superoxide dismutase
Src: Proto-oncogene tyrosine-protein kinase
TFAM: Transcription factor A, mitochondrial
TGF-β: Transforming growth factor type beta
TNF-α: Tumor necrosis factor-alpha
UPS: Ubiquitin proteasome system
UCP: Uncoupling proteins
ULK1: Unc-51 like autophagy activating kinase
XDH: Xanthine dehydrogenase
XO: Xanthine oxidase
XOR: Xanthine oxidoreductase.

Conflicts of Interest

The authors declare that there is no conflict of interest regarding the publication of this paper.

Acknowledgments

This study was supported by research grants from National Fund for Scientific and Technological Development (FONDECYT 1161646 to Claudio Cabello-Verrugio, 1161288 to Felipe Simon, 1161438 to Cristian Vilos, and 11171001 to Daniel Cabrera), Millennium Institute of Immunology and Immunotherapy (P09-016-F to Claudio Cabello-Verrugio, Felipe Simon, Alvaro A. Elorza, and Claudia A. Riedel), Programa de Cooperación Científica Internacional ECOS-CONICYT (C16S02 to Claudio Cabello-Verrugio), UNAB-DI (741-15/N to Claudio Cabello-Verrugio, Felipe Simon, Alvaro A. Elorza, and Claudia A. Riedel), and BASAL Grant CEDENNA (FB0807 to Cristian Vilos). Johanna Ábrigo thanks CONICYT for providing a PhD scholarship (21161353).

References

[1] R. W. Jackman and S. C. Kandarian, "The molecular basis of skeletal muscle atrophy," *American Journal of Physiology-Cell Physiology*, vol. 287, no. 4, pp. C834–C843, 2004.

[2] P. Bonaldo and M. Sandri, "Cellular and molecular mechanisms of muscle atrophy," *Disease Models & Mechanisms*, vol. 6, no. 1, pp. 25–39, 2013.

[3] A. Fanzani, V. M. Conraads, F. Penna, and W. Martinet, "Molecular and cellular mechanisms of skeletal muscle atrophy: an update," *Journal of Cachexia, Sarcopenia and Muscle*, vol. 3, no. 3, pp. 163–179, 2012.

[4] N. E. Brooks and K. H. Myburgh, "Skeletal muscle wasting with disuse atrophy is multi-dimensional: the response and interaction of myonuclei, satellite cells and signaling pathways," *Frontiers in Physiology*, vol. 5, p. 99, 2014.

[5] D. M. Callahan, M. S. Miller, A. P. Sweeny et al., "Muscle disuse alters skeletal muscle contractile function at the molecular and cellular levels in older adult humans in a sex-specific manner," *The Journal of Physiology*, vol. 592, no. 20no. 20, pp. 4555–4573, 2014.

[6] M. S. Miller, D. M. Callahan, and M. J. Toth, "Skeletal muscle myofilament adaptations to aging, disease, and disuse and their effects on whole muscle performance in older adult humans," *Frontiers in Physiology*, vol. 5, p. 369, 2014.

[7] S. C. Bodine, "Disuse-induced muscle wasting," *The International Journal of Biochemistry & Cell Biology*, vol. 45, no. 10, pp. 2200–2208, 2013.

[8] F. W. Booth and P. D. Gollnick, "Effects of disuse on the structure and function of skeletal muscle," *Medicine & Science in Sports & Exercise*, vol. 15, no. 5, pp. 415–420, 1983.

[9] Y. Ohira, T. Yoshinaga, T. Nomura et al., "Gravitational unloading effects on muscle fiber size, phenotype and myonuclear number," *Advances in Space Research*, vol. 30, no. 4, pp. 777–781, 2002.

[10] M. D. Allen, D. W. Stashuk, K. Kimpinski, T. J. Doherty, M. L. Hourigan, and C. L. Rice, "Increased neuromuscular transmission instability and motor unit remodelling with diabetic neuropathy as assessed using novel near fibre motor unit potential parameters," *Clinical Neurophysiology*, vol. 126, no. 4, pp. 794–802, 2015.

[11] B. M. Carlson, "The biology of long-term denervated skeletal muscle," *European Journal of Translational Myology*, vol. 24, no. 1, pp. 3293–3293, 2014.

[12] M. J. Castro, D. F. Apple Jr, E. A. Hillegass, and G. A. Dudley, "Influence of complete spinal cord injury on skeletal muscle cross-sectional area within the first 6 months of injury," *European Journal of Applied Physiology and Occupational Physiology*, vol. 80, no. 4, pp. 373–378, 1999.

[13] Y. Dionyssiotis, K. Stathopoulos, G. Trovas, N. Papaioannou, G. Skarantavos, and P. Papagelopoulos, "Impact on bone and muscle area after spinal cord injury," *BoneKEy Reports*, vol. 4, p. 633, 2015.

[14] L. Giangregorio and N. McCartney, "Bone loss and muscle atrophy in spinal cord injury: epidemiology, fracture prediction, and rehabilitation strategies," *The Journal of Spinal Cord Medicine*, vol. 29, no. 5, pp. 489–500, 2006.

[15] R. R. Roy, K. M. Baldwin, and V. R. Edgerton, "8 The plasticity of skeletal muscle: effects of neuromuscular activity," *Exercise and Sport Sciences Reviews*, vol. 19, pp. 269–312, 1991.

[16] S. L. Rowan, K. Rygiel, F. M. Purves-Smith, N. M. Solbak, D. M. Turnbull, and R. T. Hepple, "Denervation causes fiber atrophy and myosin heavy chain co-expression in senescent skeletal muscle," *PLoS One*, vol. 7, no. 1, article e29082, 2012.

[17] A. Doyle, G. Zhang, E. A. Abdel Fattah, N. T. Eissa, and Y. P. Li, "Toll-like receptor 4 mediates lipopolysaccharide-induced muscle catabolism via coordinate activation of ubiquitin-proteasome and autophagy-lysosome pathways," *The FASEB Journal*, vol. 25, no. 1, pp. 99–110, 2011.

[18] G. Tiao, S. Hobler, J. J. Wang et al., "Sepsis is associated with increased mRNAs of the ubiquitin-proteasome proteolytic pathway in human skeletal muscle," *The Journal of Clinical Investigation*, vol. 99, no. 2, pp. 163–168, 1997.

[19] G. Tiao, M. Lieberman, J. E. Fischer, and P. O. Hasselgren, "Intracellular regulation of protein degradation during sepsis is different in fast- and slow-twitch muscle," *The American Journal of Physiology-Regulatory, Integrative and Comparative Physiology*, vol. 272, 3 Part 2, pp. R849–R856, 1997.

[20] M. R. Pinsky, "Dysregulation of the immune response in severe sepsis," *The American Journal of the Medical Sciences*, vol. 328, no. 4, pp. 220–229, 2004.

[21] M. J. Dehoux, R. P. van Beneden, L. Fernández-Celemín, P. L. Lause, and J. P. Thissen, "Induction of MafBx and Murf ubiquitin ligase mRNAs in rat skeletal muscle after LPS injection," *FEBS Letters*, vol. 544, no. 1–3, pp. 214–217, 2003.

[22] M. Vinciguerra, A. Musaro, and N. Rosenthal, "Regulation of muscle atrophy in aging and disease," *Advances in Experimental Medicine and Biology*, vol. 694, pp. 211–233, 2010.

[23] W. J. Evans and W. W. Campbell, "Sarcopenia and age-related changes in body composition and functional capacity," *The Journal of Nutrition*, vol. 123, Supplement 2, pp. 465–468, 1993.

[24] R. A. Dennis, B. Przybyla, C. Gurley et al., "Aging alters gene expression of growth and remodeling factors in human skeletal muscle both at rest and in response to acute resistance exercise," *Physiological Genomics*, vol. 32, no. 3, pp. 393–400, 2008.

[25] P. Kortebein, A. Ferrando, J. Lombeida, R. Wolfe, and W. J. Evans, "Effect of 10 days of bed rest on skeletal muscle in healthy older adults," *JAMA*, vol. 297, no. 16, pp. 1769–1774, 2007.

[26] M. Cesari, S. B. Kritchevsky, R. N. Baumgartner et al., "Sarcopenia, obesity, and inflammation—results from the Trial of Angiotensin Converting Enzyme Inhibition and Novel Cardiovascular Risk Factors study," *The American Journal of Clinical Nutrition*, vol. 82, no. 2, pp. 428–434, 2005.

[27] M. Cesari, B. W. Penninx, M. Pahor et al., "Inflammatory markers and physical performance in older persons: the InCHIANTI study," *The Journals of Gerontology Series A: Biological Sciences and Medical Sciences*, vol. 59, no. 3, pp. M242–M248, 2004.

[28] W. R. Frontera, V. A. Hughes, R. A. Fielding, M. A. Fiatarone, W. J. Evans, and R. Roubenoff, "Aging of skeletal muscle: a 12-yr longitudinal study," *Journal of Applied Physiology*, vol. 88, no. 4, pp. 1321–1326, 2000.

[29] V. E. Baracos, L. Martin, M. Korc, D. C. Guttridge, and K. C. H. Fearon, "Cancer-associated cachexia," *Nature Reviews Disease Primers*, vol. 4, article 17105, 2018.

[30] K. A. Kern and J. A. Norton, "Cancer cachexia," *JPEN Journal of Parenteral and Enteral Nutrition*, vol. 12, no. 3, pp. 286–298, 1988.

[31] M. J. Tisdale, "Cachexia in cancer patients," *Nature Reviews Cancer*, vol. 2, no. 11, pp. 862–871, 2002.

[32] Y. J. Akashi, J. Springer, and S. D. Anker, "Cachexia in chronic heart failure: prognostic implications and novel therapeutic approaches," *Current Heart Failure Reports*, vol. 2, no. 4, pp. 198–203, 2005.

[33] M. P. Okoshi, F. G. Romeiro, S. A. Paiva, and K. Okoshi, "Heart failure-induced cachexia," *Arquivos Brasileiros de Cardiologia*, vol. 100, no. 5, pp. 476–482, 2013.

[34] M. Plauth and E. T. Schutz, "Cachexia in liver cirrhosis," *International Journal of Cardiology*, vol. 85, no. 1, pp. 83–87, 2002.

[35] A. Laviano, Z. Krznaric, K. Sanchez-Lara, I. Preziosa, A. Cascino, and F. Rossi Fanelli, "Chronic renal failure, cachexia, and ghrelin," *International Journal of Peptide*, vol. 2010, Article ID 648045, 5 pages, 2010.

[36] R. H. Mak, A. T. Ikizler, C. P. Kovesdy, D. S. Raj, P. Stenvinkel, and K. Kalantar-Zadeh, "Wasting in chronic kidney disease," *Journal of Cachexia, Sarcopenia and Muscle*, vol. 2, no. 1, pp. 9–25, 2011.

[37] B. C. Frier, E. G. Noble, and M. Locke, "Diabetes-induced atrophy is associated with a muscle-specific alteration in NF-κB activation and expression," *Cell Stress and Chaperones*, vol. 13, no. 3, pp. 287–296, 2008.

[38] B. Sishi, B. Loos, B. Ellis, W. Smith, E. F. du Toit, and A. M. Engelbrecht, "Diet-induced obesity alters signalling pathways and induces atrophy and apoptosis in skeletal muscle in a prediabetic rat model," *Experimental Physiology*, vol. 96, no. 2, pp. 179–193, 2011.

[39] W. J. Evans, J. E. Morley, J. Argilés et al., "Cachexia: a new definition," *Clinical Nutrition*, vol. 27, no. 6, pp. 793–799, 2008.

[40] J. E. Morley, D. R. Thomas, and M. M. Wilson, "Cachexia: pathophysiology and clinical relevance," *The American Journal of Clinical Nutrition*, vol. 83, no. 4, pp. 735–743, 2006.

[41] S. D. Anker and R. Sharma, "The syndrome of cardiac cachexia," *International Journal of Cardiology*, vol. 85, no. 1, pp. 51–66, 2002.

[42] S. von Haehling and S. D. Anker, "Prevalence, incidence and clinical impact of cachexia: facts and numbers—update 2014," *Journal of Cachexia, Sarcopenia and Muscle*, vol. 5, no. 4, pp. 261–263, 2014.

[43] L. M. Leitner, R. J. Wilson, Z. Yan, and A. Gödecke, "Reactive oxygen species/nitric oxide mediated inter-organ communication in skeletal muscle wasting diseases,"

Antioxidants & Redox Signaling, vol. 26, no. 13, pp. 700–717, 2017.

[44] J. M. Argilés, S. Busquets, B. Stemmler, and F. J. López-Soriano, "Cancer cachexia: understanding the molecular basis," *Nature Reviews Cancer*, vol. 14, no. 11, pp. 754–762, 2014.

[45] C. Cabello-Verrugio, G. Cordova, and J. D. Salas, "Angiotensin II: role in skeletal muscle atrophy," *Current Protein & Peptide Science*, vol. 13, no. 6, pp. 560–569, 2012.

[46] P. Du Bois, C. Pablo Tortola, D. Lodka et al., "Angiotensin II induces skeletal muscle atrophy by activating TFEB-mediated *MuRF1* expression," *Circulation Research*, vol. 117, no. 5, pp. 424–436, 2015.

[47] S. Sukhanov, T. Yoshida, A. Michael Tabony et al., "Angiotensin II, oxidative stress and skeletal muscle wasting," *The American Journal of the Medical Sciences*, vol. 342, no. 2, pp. 143–147, 2011.

[48] J. Abrigo, J. C. Rivera, F. Simon, D. Cabrera, and C. Cabello-Verrugio, "Transforming growth factor type beta (TGF-β) requires reactive oxygen species to induce skeletal muscle atrophy," *Cellular Signalling*, vol. 28, no. 5, pp. 366–376, 2016.

[49] C. L. Mendias, J. P. Gumucio, M. E. Davis, C. W. Bromley, C. S. Davis, and S. V. Brooks, "Transforming growth factor-beta induces skeletal muscle atrophy and fibrosis through the induction of atrogin-1 and scleraxis," *Muscle & Nerve*, vol. 45, no. 1, pp. 55–59, 2012.

[50] M. B. Reid and Y. P. Li, "Tumor necrosis factor-α and muscle wasting: a cellular perspective," *Respiratory Research*, vol. 2, no. 5, pp. 269–272, 2001.

[51] F. Haddad, F. Zaldivar, D. M. Cooper, and G. R. Adams, "IL-6-induced skeletal muscle atrophy," *Journal of Applied Physiology*, vol. 98, no. 3, pp. 911–917, 2005.

[52] S. P. Janssen, G. Gayan-Ramirez, A. van den Bergh et al., "Interleukin-6 causes myocardial failure and skeletal muscle atrophy in rats," *Circulation*, vol. 111, no. 8, pp. 996–1005, 2005.

[53] O. Zamir, P. O. Hasselgren, T. Higashiguchi, J. A. Frederick, and J. E. Fischer, "Tumour necrosis factor (TNF) and interleukin-1 (IL-1) induce muscle proteolysis through different mechanisms," *Mediators of Inflammation*, vol. 1, no. 4, pp. 247–250, 1992.

[54] B. M. Rezk, T. Yoshida, L. Semprun-Prieto, Y. Higashi, S. Sukhanov, and P. Delafontaine, "Angiotensin II infusion induces marked diaphragmatic skeletal muscle atrophy," *PLoS One*, vol. 7, no. 1, article e30276, 2012.

[55] T. Kadoguchi, S. Kinugawa, S. Takada et al., "Angiotensin II can directly induce mitochondrial dysfunction, decrease oxidative fibre number and induce atrophy in mouse hindlimb skeletal muscle," *Experimental Physiology*, vol. 100, no. 3, pp. 312–322, 2015.

[56] C. W. Keller, C. Fokken, S. G. Turville et al., "TNF-α induces macroautophagy and regulates MHC class II expression in human skeletal muscle cells," *The Journal of Biological Chemistry*, vol. 286, no. 5, pp. 3970–3980, 2011.

[57] J. Y. Lee, N. S. Hopkinson, and P. R. Kemp, "Myostatin induces autophagy in skeletal muscle in vitro," *Biochemical and Biophysical Research Communications*, vol. 415, no. 4, pp. 632–636, 2011.

[58] Y. P. Li, Y. Chen, J. John et al., "TNF-α acts via p38 MAPK to stimulate expression of the ubiquitin ligase atrogin1/MAFbx in skeletal muscle," *The FASEB Journal*, vol. 19, no. 3, pp. 362–370, 2005.

[59] P. M. Sanders, S. T. Russell, and M. J. Tisdale, "Angiotensin II directly induces muscle protein catabolism through the ubiquitin-proteasome proteolytic pathway and may play a role in cancer cachexia," *British Journal of Cancer*, vol. 93, no. 4, pp. 425–434, 2005.

[60] Y. P. Li, R. J. Schwartz, I. D. Waddell, B. R. Holloway, and M. B. Reid, "Skeletal muscle myocytes undergo protein loss and reactive oxygen-mediated NF-κB activation in response to tumor necrosis factor α," *The FASEB Journal*, vol. 12, no. 10, pp. 871–880, 1998.

[61] A. Laviano, M. M. Meguid, I. Preziosa, and F. R. Fanelli, "Oxidative stress and wasting in cancer," *Current Opinion in Clinical Nutrition and Metabolic Care*, vol. 10, no. 4, pp. 449–456, 2007.

[62] M. C. Gomes-Marcondes and M. J. Tisdale, "Induction of protein catabolism and the ubiquitin-proteasome pathway by mild oxidative stress," *Cancer Letters*, vol. 180, no. 1, pp. 69–74, 2002.

[63] S. K. Powers, A. B. Morton, B. Ahn, and A. J. Smuder, "Redox control of skeletal muscle atrophy," *Free Radical Biology and Medicine*, vol. 98, pp. 208–217, 2016.

[64] W. Droge, "Free radicals in the physiological control of cell function," *Physiological Reviews*, vol. 82, no. 1, pp. 47–95, 2002.

[65] S. K. Powers and M. J. Jackson, "Exercise-induced oxidative stress: cellular mechanisms and impact on muscle force production," *Physiological Reviews*, vol. 88, no. 4, pp. 1243–1276, 2008.

[66] E. Barreiro, B. de la Puente, S. Busquets, F. J. López-Soriano, J. Gea, and J. M. Argilés, "Both oxidative and nitrosative stress are associated with muscle wasting in tumour-bearing rats," *FEBS Letters*, vol. 579, no. 7, pp. 1646–1652, 2005.

[67] J. G. Tidball, "Inflammatory processes in muscle injury and repair," *American Journal of Physiology-Regulatory, Integrative and Comparative Physiology*, vol. 288, no. 2, pp. R345–R353, 2005.

[68] P. J. Adhihetty, I. Irrcher, A. M. Joseph, V. Ljubicic, and D. A. Hood, "Plasticity of skeletal muscle mitochondria in response to contractile activity," *Experimental Physiology*, vol. 88, no. 1, pp. 99–107, 2003.

[69] P. A. Kramer, J. Duan, W. J. Qian, and D. J. Marcinek, "The measurement of reversible redox dependent post-translational modifications and their regulation of mitochondrial and skeletal muscle function," *Frontiers in Physiology*, vol. 6, p. 347, 2015.

[70] P. Mecocci, G. Fanó, S. Fulle et al., "Age-dependent increases in oxidative damage to DNA, lipids, and proteins in human skeletal muscle," *Free Radical Biology and Medicine*, vol. 26, no. 3-4, pp. 303–308, 1999.

[71] L. A. Callahan, Z. W. She, and T. M. Nosek, "Superoxide, hydroxyl radical, and hydrogen peroxide effects on single-diaphragm fiber contractile apparatus," *Journal of Applied Physiology*, vol. 90, no. 1, pp. 45–54, 2001.

[72] M. B. Reid and W. J. Durham, "Generation of reactive oxygen and nitrogen species in contracting skeletal muscle: potential impact on aging," *Annals of the New York Academy of Sciences*, vol. 959, no. 1, pp. 108–116, 2002.

[73] J. M. Gutteridge and B. Halliwell, "Free radicals and antioxidants in the year 2000. A historical look to the future," *Annals*

of the New York Academy of Sciences, vol. 899, pp. 136–147, 2000.

[74] E. A. Veal, A. M. Day, and B. A. Morgan, "Hydrogen peroxide sensing and signaling," *Molecular Cell*, vol. 26, no. 1, pp. 1–14, 2007.

[75] M. Altun, E. Edström, E. Spooner et al., "Iron load and redox stress in skeletal muscle of aged rats," *Muscle & Nerve*, vol. 36, no. 2, pp. 223–233, 2007.

[76] D. Trachootham, W. Lu, M. A. Ogasawara, N. R. D. Valle, and P. Huang, "Redox regulation of cell survival," *Antioxidants & Redox Signaling*, vol. 10, no. 8, pp. 1343–1374, 2008.

[77] T. Maraldi, "Natural compounds as modulators of NADPH oxidases," *Oxidative Medicine and Cellular Longevity*, vol. 2013, Article ID 271602, 10 pages, 2013.

[78] K. Bedard and K. H. Krause, "The NOX family of ROS-generating NADPH oxidases: physiology and pathophysiology," *Physiological Reviews*, vol. 87, no. 1, pp. 245–313, 2007.

[79] D. I. Brown and K. K. Griendling, "Nox proteins in signal transduction," *Free Radical Biology and Medicine*, vol. 47, no. 9, pp. 1239–1253, 2009.

[80] T. Ueyama, K. Lekstrom, S. Tsujibe, N. Saito, and T. L. Leto, "Subcellular localization and function of alternatively spliced Noxo1 isoforms," *Free Radical Biology and Medicine*, vol. 42, no. 2, pp. 180–190, 2007.

[81] A. N. Lyle, N. N. Deshpande, Y. Taniyama et al., "Poldip2, a novel regulator of Nox4 and cytoskeletal integrity in vascular smooth muscle cells," *Circulation Research*, vol. 105, no. 3, pp. 249–259, 2009.

[82] S. Coso, I. Harrison, C. B. Harrison et al., "NADPH oxidases as regulators of tumor angiogenesis: current and emerging concepts," *Antioxidants & Redox Signaling*, vol. 16, no. 11, pp. 1229–1247, 2012.

[83] I. Takac, K. Schröder, L. Zhang et al., "The E-loop is involved in hydrogen peroxide formation by the NADPH oxidase Nox4," *Journal of Biological Chemistry*, vol. 286, no. 15, pp. 13304–13313, 2011.

[84] G. Cheng, Z. Cao, X. Xu, E. G. V. Meir, and J. D. Lambeth, "Homologs of gp91*phox*: cloning and tissue expression of Nox3, Nox4, and Nox5," *Gene*, vol. 269, no. 1-2, pp. 131–140, 2001.

[85] D. Javeshghani, S. A. Magder, E. Barreiro, M. T. Quinn, and S. N. Hussain, "Molecular characterization of a superoxide-generating NAD(P)H oxidase in the ventilatory muscles," *American Journal of Respiratory and Critical Care Medicine*, vol. 165, no. 3, pp. 412–418, 2002.

[86] A. Mansouri, F. L. Muller, Y. Liu et al., "Alterations in mitochondrial function, hydrogen peroxide release and oxidative damage in mouse hind-limb skeletal muscle during aging," *Mechanisms of Ageing and Development*, vol. 127, no. 3, pp. 298–306, 2006.

[87] T. F. Cunha, L. R. G. Bechara, A. V. N. Bacurau et al., "Exercise training decreases NADPH oxidase activity and restores skeletal muscle mass in heart failure rats," *Journal of Applied Physiology*, vol. 122, no. 4, pp. 817–827, 2017.

[88] D. A. Kostić, D. S. Dimitrijević, G. S. Stojanović, I. R. Palić, A. S. Đorđević, and J. D. Ickovski, "Xanthine oxidase: isolation, assays of activity, and inhibition," *Journal of Chemistry*, vol. 2015, Article ID 294858, 8 pages, 2015.

[89] P. Cos, L. Ying, M. Calomme et al., "Structure-activity relationship and classification of flavonoids as inhibitors of xanthine oxidase and superoxide scavengers," *Journal of Natural Products*, vol. 61, no. 1, pp. 71–76, 1998.

[90] A. Mittal, A. R. J. Phillips, B. Loveday, and J. A. Windsor, "The potential role for xanthine oxidase inhibition in major intra-abdominal surgery," *World Journal of Surgery*, vol. 32, no. 2, pp. 288–295, 2008.

[91] E. E. Kelley, N. K. H. Khoo, N. J. Hundley, U. Z. Malik, B. A. Freeman, and M. M. Tarpey, "Hydrogen peroxide is the major oxidant product of xanthine oxidase," *Free Radical Biology and Medicine*, vol. 48, no. 4, pp. 493–498, 2010.

[92] W. Doehner and U. Landmesser, "Xanthine oxidase and uric acid in cardiovascular disease: clinical impact and therapeutic options," *Seminars in Nephrology*, vol. 31, no. 5, pp. 433–440, 2011.

[93] M. C. I. Lee, M. Velayutham, T. Komatsu, R. Hille, and J. L. Zweier, "Measurement and characterization of superoxide generation from xanthine dehydrogenase: a redox-regulated pathway of radical generation in ischemic tissues," *Biochemistry*, vol. 53, no. 41, pp. 6615–6623, 2014.

[94] F. Sanchis-Gomar, H. Pareja-Galeano, C. Perez-Quilis et al., "Effects of allopurinol on exercise-induced muscle damage: new therapeutic approaches?," *Cell Stress and Chaperones*, vol. 20, no. 1, pp. 3–13, 2015.

[95] Y. Hellsten, U. Frandsen, N. Orthenblad, B. Sjødin, and E. A. Richter, "Xanthine oxidase in human skeletal muscle following eccentric exercise: a role in inflammation," *The Journal of Physiology*, vol. 498, no. 1, pp. 239–248, 1997.

[96] A. Kadambi and T. C. Skalak, "Role of leukocytes and tissue-derived oxidants in short-term skeletal muscle ischemia-reperfusion injury," *American Journal of Physiology-Heart and Circulatory Physiology*, vol. 278, no. 2, pp. H435–H443, 2000.

[97] M. C. Gomez-Cabrera, A. Martínez, G. Santangelo, F. V. Pallardó, J. Sastre, and J. Viña, "Oxidative stress in marathon runners: interest of antioxidant supplementation," *The British Journal of Nutrition*, vol. 96, no. S1, Supplement 1, pp. S31–S33, 2006.

[98] M. C. Gómez-Cabrera, F. V. Pallardó, J. Sastre, J. Viña, and L. García-del-Moral, "Allopurinol and markers of muscle damage among participants in the Tour de France," *JAMA*, vol. 289, no. 19, pp. 2503-2504, 2003.

[99] J. Viña, M. C. Gomez-Cabrera, A. Lloret et al., "Free radicals in exhaustive physical exercise: mechanism of production, and protection by antioxidants," *IUBMB Life*, vol. 50, no. 4, pp. 271–277, 2000.

[100] N. Linder, J. Rapola, and K. O. Raivio, "Cellular expression of xanthine oxidoreductase protein in normal human tissues," *Laboratory Investigation*, vol. 79, no. 8, pp. 967–974, 1999.

[101] J. K. Barclay and M. Hansel, "Free radicals may contribute to oxidative skeletal muscle fatigue," *Canadian Journal of Physiology and Pharmacology*, vol. 69, no. 2, pp. 279–284, 1991.

[102] D. A. Stofan, L. A. Callahan, A. DiMARCO, D. E. Nethery, and G. S. Supinski, "Modulation of release of reactive oxygen species by the contracting diaphragm," *American Journal of Respiratory and Critical Care Medicine*, vol. 161, 3 Part 1, pp. 891–898, 2000.

[103] M. J. Ryan, J. R. Jackson, Y. Hao, S. S. Leonard, and S. E. Alway, "Inhibition of xanthine oxidase reduces oxidative stress and improves skeletal muscle function in response to electrically stimulated isometric contractions in aged mice,"

Free Radical Biology and Medicine, vol. 51, no. 1, pp. 38–52, 2011.

[104] F. Derbre, B. Ferrando, M. C. Gomez-Cabrera et al., "Inhibition of xanthine oxidase by allopurinol prevents skeletal muscle atrophy: role of p38 MAPKinase and E3 ubiquitin ligases," *PLoS One*, vol. 7, no. 10, p. e46668, 2012.

[105] F. Sanchis-Gomar, H. Pareja-Galeano, J. Cortell-Ballester, and C. Perez-Quilis, "Prevention of acute skeletal muscle wasting in critical illness," *Minerva Anestesiologica*, vol. 80, p. 748, 2014.

[106] K. Schulze-Osthoff, A. C. Bakker, B. Vanhaesebroeck, R. Beyaert, W. A. Jacob, and W. Fiers, "Cytotoxic activity of tumor necrosis factor is mediated by early damage of mitochondrial functions. Evidence for the involvement of mitochondrial radical generation," *The Journal of Biological Chemistry*, vol. 267, no. 8, pp. 5317–5323, 1992.

[107] A. Boveris, "[57] Determination of the production of superoxide radicals and hydrogen peroxide in mitochondria," *Methods in Enzymology*, vol. 105, pp. 429–435, 1984.

[108] I. N. Zelko, T. J. Mariani, and R. J. Folz, "Superoxide dismutase multigene family: a comparison of the CuZn-SOD (SOD1), Mn-SOD (SOD2), and EC-SOD (SOD3) gene structures, evolution, and expression," *Free Radical Biology and Medicine*, vol. 33, no. 3, pp. 337–349, 2002.

[109] F. L. Muller, W. Song, Y. Liu et al., "Absence of CuZn superoxide dismutase leads to elevated oxidative stress and acceleration of age-dependent skeletal muscle atrophy," *Free Radical Biology and Medicine*, vol. 40, no. 11, pp. 1993–2004, 2006.

[110] D. F. Dai, Y. A. Chiao, G. M. Martin et al., "Mitochondrial-targeted catalase: extended longevity and the roles in various disease models," *Progress in Molecular Biology and Translational Science*, vol. 146, pp. 203–241, 2017.

[111] G. K. Sakellariou, A. P. Lightfoot, K. E. Earl, M. Stofanko, and B. McDonagh, "Redox homeostasis and age-related deficits in neuromuscular integrity and function," *Journal of Cachexia, Sarcopenia and Muscle*, vol. 8, no. 6, pp. 881–906, 2017.

[112] B. Pereira, L. F. B. Costa Rosa, D. A. Safi, M. H. G. Medeiros, R. Curi, and E. J. H. Bechara, "Superoxide dismutase, catalase, and glutathione peroxidase activities in muscle and lymphoid organs of sedentary and exercise-trained rats," *Physiology & Behavior*, vol. 56, no. 5, pp. 1095–1099, 1994.

[113] R. Brigelius-Flohe, "Glutathione peroxidases and redox-regulated transcription factors," *Biological Chemistry*, vol. 387, no. 10-11, pp. 1329–1335, 2006.

[114] L. L. Ji, "Antioxidant signaling in skeletal muscle: a brief review," *Experimental Gerontology*, vol. 42, no. 7, pp. 582–593, 2007.

[115] J. M. McCord and M. A. Edeas, "SOD, oxidative stress and human pathologies: a brief history and a future vision," *Biomedicine & Pharmacotherapy*, vol. 59, no. 4, pp. 139–142, 2005.

[116] S. Kinugawa, S. Takada, S. Matsushima, K. Okita, and H. Tsutsui, "Skeletal muscle abnormalities in heart failure," *International Heart Journal*, vol. 56, no. 5, pp. 475–484, 2015.

[117] A. Kaltsatou, G. K. Sakkas, K. P. Poulianiti et al., "Uremic myopathy: is oxidative stress implicated in muscle dysfunction in uremia?," *Frontiers in Physiology*, vol. 6, p. 102, 2015.

[118] P. Delafontaine and M. Akao, "Angiotensin II as candidate of cardiac cachexia," *Current Opinion in Clinical Nutrition and Metabolic Care*, vol. 9, no. 3, pp. 220–224, 2006.

[119] S. D. Anker, W. Steinborn, and S. Strassburg, "Cardiac cachexia," *Annals of Medicine*, vol. 36, no. 7, pp. 518–529, 2004.

[120] A. Q. Adigun and A. A. L. Ajayi, "The effects of enalapril-digoxin-diuretic combination therapy on nutritional and anthropometric indices in chronic congestive heart failure: preliminary findings in cardiac cachexia," *European Journal of Heart Failure*, vol. 3, no. 3, pp. 359–363, 2001.

[121] J. S. Chamberlain, "ACE inhibitor bulks up muscle," *Nature Medicine*, vol. 13, no. 2, pp. 125-126, 2007.

[122] Y. Wei, J. R. Sowers, R. Nistala et al., "Angiotensin II-induced NADPH oxidase activation impairs insulin signaling in skeletal muscle cells," *The Journal of Biological Chemistry*, vol. 281, no. 46, pp. 35137–35146, 2006.

[123] L. C. Semprun-Prieto, S. Sukhanov, T. Yoshida et al., "Angiotensin II induced catabolic effect and muscle atrophy are redox dependent," *Biochemical and Biophysical Research Communications*, vol. 409, no. 2, pp. 217–221, 2011.

[124] S. T. Russell, H. Eley, and M. J. Tisdale, "Role of reactive oxygen species in protein degradation in murine myotubes induced by proteolysis-inducing factor and angiotensin II," *Cellular Signalling*, vol. 19, no. 8, pp. 1797–1806, 2007.

[125] W. Zhao, S. A. Swanson, J. Ye et al., "Reactive oxygen species impair sympathetic vasoregulation in skeletal muscle in angiotensin II–dependent hypertension," *Hypertension*, vol. 48, no. 4, pp. 637–643, 2006.

[126] C. Cabello-Verrugio, M. G. Morales, J. C. Rivera, D. Cabrera, and F. Simon, "Renin-angiotensin system: an old player with novel functions in skeletal muscle," *Medicinal Research Reviews*, vol. 35, no. 3, pp. 437–463, 2015.

[127] A. K. Doughan, D. G. Harrison, and S. I. Dikalov, "Molecular mechanisms of angiotensin II–mediated mitochondrial dysfunction: linking mitochondrial oxidative damage and vascular endothelial dysfunction," *Circulation Research*, vol. 102, no. 4, pp. 488–496, 2008.

[128] H. L. Eley and M. J. Tisdale, "Skeletal muscle atrophy, a link between depression of protein synthesis and increase in degradation," *The Journal of Biological Chemistry*, vol. 282, no. 10, pp. 7087–7097, 2007.

[129] G. Mantovani, A. Macciò, C. Madeddu et al., "Antioxidant agents are effective in inducing lymphocyte progression through cell cycle in advanced cancer patients: assessment of the most important laboratory indexes of cachexia and oxidative stress," *Journal of Molecular Medicine*, vol. 81, no. 10, pp. 664–673, 2003.

[130] D. Sanchis, S. Busquets, B. Alvarez, D. Ricquier, F. J. López-Soriano, and J. M. Argilés, "Skeletal muscle UCP2 and UCP3 gene expression in a rat cancer cachexia model," *FEBS Letters*, vol. 436, no. 3, pp. 415–418, 1998.

[131] C. Bing, M. Brown, P. King, P. Collins, M. J. Tisdale, and G. Williams, "Increased gene expression of brown fat uncoupling protein (UCP)1 and skeletal muscle UCP2 and UCP3 in MAC16-induced cancer cachexia," *Cancer Research*, vol. 60, no. 9, pp. 2405–2410, 2000.

[132] S. Busquets, V. Almendro, E. Barreiro, M. Figueras, J. M. Argilés, and F. J. López-Soriano, "Activation of UCPs gene expression in skeletal muscle can be independent on both circulating fatty acids and food intake. Involvement of ROS in a model of mouse cancer cachexia," *FEBS Letters*, vol. 579, no. 3, pp. 717–722, 2005.

[133] P. Collins, C. Bing, P. McCulloch, and G. Williams, "Muscle UCP-3 mRNA levels are elevated in weight loss associated with gastrointestinal adenocarcinoma in humans," *British Journal of Cancer*, vol. 86, no. 3, pp. 372–375, 2002.

[134] G. Strassmann, M. Fong, J. S. Kenney, and C. O. Jacob, "Evidence for the involvement of interleukin 6 in experimental cancer cachexia," *The Journal of Clinical Investigation*, vol. 89, no. 5, pp. 1681–1684, 1992.

[135] J. Gelin, L. L. Moldawer, C. Lönnroth, B. Sherry, R. Chizzonite, and K. Lundholm, "Role of endogenous tumor necrosis factor alpha and interleukin 1 for experimental tumor growth and the development of cancer cachexia," *Cancer Research*, vol. 51, no. 1, pp. 415–421, 1991.

[136] G. Mantovani, A. Macciò, P. Lai, E. Massa, M. Ghiani, and M. C. Santona, "Cytokine activity in cancer-related anorexia/cachexia: role of megestrol acetate and medroxyprogesterone acetate," *Seminars in Oncology*, vol. 25, no. 2, Supplement 6, pp. 45–52, 1998.

[137] H. J. Smith and M. J. Tisdale, "Signal transduction pathways involved in proteolysis-inducing factor induced proteasome expression in murine myotubes," *British Journal of Cancer*, vol. 89, no. 9, pp. 1783–1788, 2003.

[138] R. C. Langen, A. M. Schols, M. C. Kelders, J. L. Van Der Velden, E. F. Wouters, and Y. M. Janssen-Heininger, "Tumor necrosis factor-α inhibits myogenesis through redox-dependent and -independent pathways," *American Journal of Physiology-Cell Physiology*, vol. 283, no. 3, pp. C714–C721, 2002.

[139] Y. S. Kim, M. J. Morgan, S. Choksi, and Z. G. Liu, "TNF-induced activation of the Nox1 NADPH oxidase and its role in the induction of necrotic cell death," *Molecular Cell*, vol. 26, no. 5, pp. 675–687, 2007.

[140] M. J. Sullivan-Gunn, S. P. Campbell-O'Sullivan, M. J. Tisdale, and P. A. Lewandowski, "Decreased NADPH oxidase expression and antioxidant activity in cachectic skeletal muscle," *Journal of Cachexia, Sarcopenia and Muscle*, vol. 2, no. 3, pp. 181–188, 2011.

[141] G. Mantovani and C. Madeddu, "Cancer cachexia: medical management," *Support Care Cancer*, vol. 18, no. 1, pp. 1–9, 2010.

[142] J. Springer, A. Tschirner, K. Hartman et al., "Inhibition of xanthine oxidase reduces wasting and improves outcome in a rat model of cancer cachexia," *International Journal of Cancer*, vol. 131, no. 9, pp. 2187–2196, 2012.

[143] V. Banduseela, J. Ochala, K. Lamberg, H. Kalimo, and L. Larsson, "Muscle paralysis and myosin loss in a patient with cancer cachexia," *Acta Myologica*, vol. 26, no. 3, pp. 136–144, 2007.

[144] S. H. Lecker, R. T. Jagoe, A. Gilbert et al., "Multiple types of skeletal muscle atrophy involve a common program of changes in gene expression," *The FASEB Journal*, vol. 18, no. 1, pp. 39–51, 2004.

[145] M. Sandri, "Protein breakdown in muscle wasting: role of autophagy-lysosome and ubiquitin-proteasome," *The International Journal of Biochemistry & Cell Biology*, vol. 45, no. 10, pp. 2121–2129, 2013.

[146] J. P. Gumucio and C. L. Mendias, "Atrogin-1, MuRF-1, and sarcopenia," *Endocrine*, vol. 43, no. 1, pp. 12–21, 2013.

[147] D. L. Waning, K. S. Mohammad, S. Reiken et al., "Excess TGF-β mediates muscle weakness associated with bone metastases in mice," *Nature Medicine*, vol. 21, no. 11, pp. 1262–1271, 2015.

[148] C. Cabello-Verrugio, J. C. Rivera, and D. Garcia, "Skeletal muscle wasting: new role of nonclassical renin-angiotensin system," *Current Opinion in Clinical Nutrition and Metabolic Care*, vol. 20, no. 3, pp. 158–163, 2017.

[149] Y. P. Li, Y. Chen, A. S. Li, and M. B. Reid, "Hydrogen peroxide stimulates ubiquitin-conjugating activity and expression of genes for specific E2 and E3 proteins in skeletal muscle myotubes," *American Journal of Physiology-Cell Physiology*, vol. 285, no. 4, pp. C806–C812, 2003.

[150] S. T. Russell, P. M. A. Siren, M. J. Siren, and M. J. Tisdale, "Attenuation of skeletal muscle atrophy in cancer cachexia by D-myo-inositol 1,2,6-triphosphate," *Cancer Chemotherapy and Pharmacology*, vol. 64, no. 3, pp. 517–527, 2009.

[151] Y. P. Li and M. B. Reid, "NF-κB mediates the protein loss induced by TNF-α in differentiated skeletal muscle myotubes," *American Journal of Physiology-Regulatory, Integrative and Comparative Physiology*, vol. 279, no. 4, pp. R1165–R1170, 2000.

[152] M. D. Layne and S. R. Farmer, "Tumor necrosis factor-α and basic fibroblast growth factor differentially inhibit the insulin-like growth factor-I induced expression of myogenin in C2C12 myoblasts," *Experimental Cell Research*, vol. 249, no. 1, pp. 177–187, 1999.

[153] M. Pedersen, H. Bruunsgaard, N. Weis et al., "Circulating levels of TNF-alpha and IL-6-relation to truncal fat mass and muscle mass in healthy elderly individuals and in patients with type-2 diabetes," *Mechanisms of Ageing and Development*, vol. 124, no. 4, pp. 495–502, 2003.

[154] R. L. Campbell and P. L. Davies, "Structure-function relationships in calpains," *The Biochemical Journal*, vol. 447, no. 3, pp. 335–351, 2012.

[155] D. E. Goll, V. F. Thompson, H. Li, W. Wei, and J. Cong, "The calpain system," *Physiological Reviews*, vol. 83, no. 3, pp. 731–801, 2003.

[156] A. J. Smuder, A. N. Kavazis, M. B. Hudson, W. B. Nelson, and S. K. Powers, "Oxidation enhances myofibrillar protein degradation via calpain and caspase-3," *Free Radical Biology and Medicine*, vol. 49, no. 7, pp. 1152–1160, 2010.

[157] J. M. McClung, A. R. Judge, E. E. Talbert, and S. K. Powers, "Calpain-1 is required for hydrogen peroxide-induced myotube atrophy," *American Journal of Physiology-Cell Physiology*, vol. 296, no. 2, pp. C363–C371, 2009.

[158] E. Dargelos, C. Brulé, P. Stuelsatz et al., "Up-regulation of calcium-dependent proteolysis in human myoblasts under acute oxidative stress," *Experimental Cell Research*, vol. 316, no. 1, pp. 115–125, 2010.

[159] M. A. Whidden, A. J. Smuder, M. Wu, M. B. Hudson, W. B. Nelson, and S. K. Powers, "Oxidative stress is required for mechanical ventilation-induced protease activation in the diaphragm," *Journal of Applied Physiology*, vol. 108, no. 5, pp. 1376–1382, 2010.

[160] S. K. Powers, A. N. Kavazis, and J. M. McClung, "Oxidative stress and disuse muscle atrophy," *Journal of Applied Physiology*, vol. 102, no. 6, pp. 2389–2397, 2007.

[161] E. Dargelos, S. Poussard, C. Brulé, L. Daury, and P. Cottin, "Calcium-dependent proteolytic system and muscle dysfunctions: a possible role of calpains in sarcopenia," *Biochimie*, vol. 90, no. 2, pp. 359–368, 2008.

[162] J. I. Kourie, "Interaction of reactive oxygen species with ion transport mechanisms," *The American Journal of Physiology-Cell Physiology*, vol. 275, no. 1, pp. C1–C24, 1998.

[163] J. R. Florini, D. Z. Ewton, and S. A. Coolican, "Growth hormone and the insulin-like growth factor system in myogenesis," *Endocrine Reviews*, vol. 17, no. 5, pp. 481–517, 1996.

[164] D. Chrysis and L. E. Underwood, "Regulation of components of the ubiquitin system by insulin-like growth factor I and growth hormone in skeletal muscle of rats made catabolic with dexamethasone," *Endocrinology*, vol. 140, no. 12, pp. 5635–5641, 1999.

[165] D. Hong and N. E. Forsberg, "Effects of serum and insulin-like growth factor I on protein degradation and protease gene expression in rat L8 myotubes," *Journal of Animal Science*, vol. 72, no. 9, pp. 2279–2288, 1994.

[166] M. A. Lawlor and P. Rotwein, "Insulin-like growth factor-mediated muscle cell survival: central roles for Akt and cyclin-dependent kinase inhibitor p21," *Molecular and Cellular Biology*, vol. 20, no. 23, pp. 8983–8995, 2000.

[167] S. P. Attard-Montalto, C. Camacho-Hübner, A. M. Cotterill et al., "Changes in protein turnover, IGF-I and IGF binding proteins in children with cancer," *Acta Paediatrica*, vol. 87, no. 1, pp. 54–60, 1998.

[168] P. Costelli, M. Muscaritoli, M. Bossola et al., "IGF-1 is downregulated in experimental cancer cachexia," *American Journal of Physiology-Regulatory, Integrative and Comparative Physiology*, vol. 291, no. 3, pp. R674–R683, 2006.

[169] J. Fan, P. E. Molina, M. C. Gelato, and C. H. Lang, "Differential tissue regulation of insulin-like growth factor-I content and binding proteins after endotoxin," *Endocrinology*, vol. 134, no. 4, pp. 1685–1692, 1994.

[170] M. Sandri, C. Sandri, A. Gilbert et al., "Foxo transcription factors induce the atrophy-related ubiquitin ligase atrogin-1 and cause skeletal muscle atrophy," *Cell*, vol. 117, no. 3, pp. 399–412, 2004.

[171] J. Papaconstantinou, "Insulin/IGF-1 and ROS signaling pathway cross-talk in aging and longevity determination," *Molecular and Cellular Endocrinology*, vol. 299, no. 1, pp. 89–100, 2009.

[172] N. Bashan, J. Kovsan, I. Kachko, H. Ovadia, and A. Rudich, "Positive and negative regulation of insulin signaling by reactive oxygen and nitrogen species," *Physiological Reviews*, vol. 89, no. 1, pp. 27–71, 2009.

[173] M. Genestra, "Oxyl radicals, redox-sensitive signalling cascades and antioxidants," *Cellular Signalling*, vol. 19, no. 9, pp. 1807–1819, 2007.

[174] J. V. Cross and D. J. Templeton, "Regulation of signal transduction through protein cysteine oxidation," *Antioxidants & Redox Signaling*, vol. 8, no. 9-10, pp. 1819–1827, 2006.

[175] R. Wani, J. Qian, L. Yin et al., "Isoform-specific regulation of Akt by PDGF-induced reactive oxygen species," *Proceedings of the National Academy of Sciences of the United States of America*, vol. 108, no. 26, pp. 10550–10555, 2011.

[176] L. Coderre, K. V. Kandror, G. Vallega, and P. F. Pilch, "Identification and characterization of an exercise-sensitive pool of glucose transporters in skeletal muscle," *The Journal of Biological Chemistry*, vol. 270, no. 46, pp. 27584–27588, 1995.

[177] S. Lund, G. D. Holman, O. Schmitz, and O. Pedersen, "Contraction stimulates translocation of glucose transporter GLUT4 in skeletal muscle through a mechanism distinct from that of insulin," *Proceedings of the National Academy of Sciences of the United States of America*, vol. 92, no. 13, pp. 5817–5821, 1995.

[178] M. Sandri, "Autophagy in skeletal muscle," *FEBS Letters*, vol. 584, no. 7, pp. 1411–1416, 2010.

[179] J. Navarro-Yepes, M. Burns, A. Anandhan et al., "Oxidative stress, redox signaling, and autophagy: cell death versus survival," *Antioxidants & Redox Signaling*, vol. 21, no. 1, pp. 66–85, 2014.

[180] J. J. Lum, R. J. DeBerardinis, and C. B. Thompson, "Autophagy in metazoans: cell survival in the land of plenty," *Nature Reviews Molecular Cell Biology*, vol. 6, no. 6, pp. 439–448, 2005.

[181] B. Levine and G. Kroemer, "Autophagy in the pathogenesis of disease," *Cell*, vol. 132, no. 1, pp. 27–42, 2008.

[182] G. G. Rodney, R. Pal, and R. Abo-Zahrah, "Redox regulation of autophagy in skeletal muscle," *Free Radical Biology and Medicine*, vol. 98, pp. 103–112, 2016.

[183] R. Pal, M. Palmieri, J. A. Loehr et al., "Src-dependent impairment of autophagy by oxidative stress in a mouse model of Duchenne muscular dystrophy," *Nature Communications*, vol. 5, article 4425, 2014.

[184] M. Chrisam, M. Pirozzi, S. Castagnaro et al., "Reactivation of autophagy by spermidine ameliorates the myopathic defects of collagen VI-null mice," *Autophagy*, vol. 11, no. 12, pp. 2142–2152, 2015.

[185] Y. Xiao, C. Ma, J. Yi et al., "Suppressed autophagy flux in skeletal muscle of an amyotrophic lateral sclerosis mouse model during disease progression," *Physiological Reports*, vol. 3, no. 1, article e12271, 2015.

[186] Y. Guo, H. R. Gosker, A. M. W. J. Schols et al., "Autophagy in locomotor muscles of patients with chronic obstructive pulmonary disease," *American Journal of Respiratory and Critical Care Medicine*, vol. 188, no. 11, pp. 1313–1320, 2013.

[187] J. Gea, S. Pascual, C. Casadevall, M. Orozco-Levi, and E. Barreiro, "Muscle dysfunction in chronic obstructive pulmonary disease: update on causes and biological findings," *Journal of Thoracic Disease*, vol. 7, no. 10, pp. E418–E438, 2015.

[188] F. Stana, M. Vujovic, D. Mayaki et al., "Differential regulation of the autophagy and proteasome pathways in skeletal muscles in sepsis," *Critical Care Medicine*, vol. 45, no. 9, pp. e971–e979, 2017.

[189] G. Gortan Cappellari, A. Semolic, G. Ruozi et al., "Unacylated ghrelin normalizes skeletal muscle oxidative stress and prevents muscle catabolism by enhancing tissue mitophagy in experimental chronic kidney disease," *The FASEB Journal*, vol. 31, no. 12, pp. 5159–5171, 2017.

[190] E. Pigna, E. Berardi, P. Aulino et al., "Aerobic exercise and pharmacological treatments counteract cachexia by modulating autophagy in colon cancer," *Scientific Reports*, vol. 6, no. 1, article 26991, 2016.

[191] G. Dobrowolny, M. Aucello, E. Rizzuto et al., "Skeletal muscle is a primary target of $SOD1^{G93A}$-mediated toxicity," *Cell Metabolism*, vol. 8, no. 5, pp. 425–436, 2008.

[192] Y. Chen, M. B. Azad, and S. B. Gibson, "Superoxide is the major reactive oxygen species regulating autophagy," *Cell Death and Differentiation*, vol. 16, no. 7, pp. 1040–1052, 2009.

[193] R. Scherz-Shouval and Z. Elazar, "Regulation of autophagy by ROS: physiology and pathology," *Trends in Biochemical Sciences*, vol. 36, no. 1, pp. 30–38, 2011.

[194] M. Rahman, M. Mofarrahi, A. S. Kristof, B. Nkengfac, S. Harel, and S. N. A. Hussain, "Reactive oxygen species regulation of autophagy in skeletal muscles," *Antioxidants & Redox Signaling*, vol. 20, no. 3, pp. 443–459, 2014.

[195] E. E. Talbert, A. J. Smuder, K. Min, O. S. Kwon, H. H. Szeto, and S. K. Powers, "Immobilization-induced activation of key proteolytic systems in skeletal muscles is prevented by a mitochondria-targeted antioxidant," *Journal of Applied Physiology*, vol. 115, no. 4, pp. 529–538, 2013.

[196] P. L. Tan, T. Shavlakadze, M. D. Grounds, and P. G. Arthur, "Differential thiol oxidation of the signaling proteins Akt, PTEN or PP2A determines whether Akt phosphorylation is enhanced or inhibited by oxidative stress in C2C12 myotubes derived from skeletal muscle," *The International Journal of Biochemistry & Cell Biology*, vol. 62, pp. 72–79, 2015.

[197] A. Nakanishi, Y. Wada, Y. Kitagishi, and S. Matsuda, "Link between PI3K/AKT/PTEN pathway and NOX proteinin diseases," *Aging and Disease*, vol. 5, no. 3, pp. 203–211, 2014.

[198] J. M. McClung, A. R. Judge, S. K. Powers, and Z. Yan, "p38 MAPK links oxidative stress to autophagy-related gene expression in cachectic muscle wasting," *American Journal of Physiology-Cell Physiology*, vol. 298, no. 3, pp. C542–C549, 2010.

[199] L. Yuan, S. Wei, J. Wang, and X. Liu, "Isoorientin induces apoptosis and autophagy simultaneously by reactive oxygen species (ROS)-related p53, PI3K/Akt, JNK, and p38 signaling pathways in HepG2 cancer cells," *Journal of Agricultural and Food Chemistry*, vol. 62, no. 23, pp. 5390–5400, 2014.

[200] W. J. Duan, Q. S. Li, M. Y. Xia, S. I. Tashiro, S. Onodera, and T. Ikejima, "Silibinin activated p53 and induced autophagic death in human fibrosarcoma HT1080 cells via reactive oxygen species-p38 and c-Jun N-terminal kinase pathways," *Biological and Pharmaceutical Bulletin*, vol. 34, no. 1, pp. 47–53, 2011.

[201] S. B. Jorgensen, E. A. Richter, and J. F. Wojtaszewski, "Role of AMPK in skeletal muscle metabolic regulation and adaptation in relation to exercise," *The Journal of Physiology*, vol. 574, no. 1, pp. 17–31, 2006.

[202] I. Irrcher, V. Ljubicic, and D. A. Hood, "Interactions between ROS and AMP kinase activity in the regulation of PGC-1α transcription in skeletal muscle cells," *The American Journal of Physiology-Cell Physiology*, vol. 296, no. 1, pp. C116–C123, 2009.

[203] D. L. Allen, J. K. Linderman, R. R. Roy et al., "Apoptosis: a mechanism contributing to remodeling of skeletal muscle in response to hindlimb unweighting," *The American Journal of Physiology-Cell Physiology*, vol. 273, no. 2, pp. C579–C587, 1997.

[204] A. B. Borisov and B. M. Carlson, "Cell death in denervated skeletal muscle is distinct from classical apoptosis," *The Anatomical Record*, vol. 258, no. 3, pp. 305–318, 2000.

[205] D. L. Allen, R. R. Roy, and V. R. Edgerton, "Myonuclear domains in muscle adaptation and disease," *Muscle & Nerve*, vol. 22, no. 10, pp. 1350–1360, 1999.

[206] S. Gupta, "Molecular steps of tumor necrosis factor receptor-mediated apoptosis," *Current Molecular Medicine*, vol. 1, no. 3, pp. 317–324, 2001.

[207] A. G. Agusti, J. Sauleda, C. Miralles et al., "Skeletal muscle apoptosis and weight loss in chronic obstructive pulmonary disease," *American Journal of Respiratory and Critical Care Medicine*, vol. 166, no. 4, pp. 485–489, 2002.

[208] D. Verzola, V. Procopio, A. Sofia et al., "Apoptosis and myostatin mRNA are upregulated in the skeletal muscle of patients with chronic kidney disease," *Kidney International*, vol. 79, no. 7, pp. 773–782, 2011.

[209] V. Adams, H. Jiang, J. Yu et al., "Apoptosis in skeletal myocytes of patients with chronic heart failure is associated with exercise intolerance," *Journal of the American College of Cardiology*, vol. 33, no. 4, pp. 959–965, 1999.

[210] G. Vescovo, M. Volterrani, R. Zennaro et al., "Apoptosis in the skeletal muscle of patients with heart failure: investigation of clinical and biochemical changes," *Heart*, vol. 84, no. 4, pp. 431–437, 2000.

[211] M. Brink, S. R. Price, J. Chrast et al., "Angiotensin II induces skeletal muscle wasting through enhanced protein degradation and down-regulates autocrine insulin-like growth factor I," *Endocrinology*, vol. 142, no. 4, pp. 1489–1496, 2001.

[212] M. Brink, J. Wellen, and P. Delafontaine, "Angiotensin II causes weight loss and decreases circulating insulin-like growth factor I in rats through a pressor-independent mechanism," *The Journal of Clinical Investigation*, vol. 97, no. 11, pp. 2509–2516, 1996.

[213] C. Meneses, M. G. Morales, J. Abrigo, F. Simon, E. Brandan, and C. Cabello-Verrugio, "The angiotensin-(1–7)/Mas axis reduces myonuclear apoptosis during recovery from angiotensin II-induced skeletal muscle atrophy in mice," *Pflügers Archiv - European Journal of Physiology*, vol. 467, no. 9, pp. 1975–1984, 2015.

[214] P. M. Siu, Y. Wang, and S. E. Alway, "Apoptotic signaling induced by H_2O_2-mediated oxidative stress in differentiated C2C12 myotubes," *Life Sciences*, vol. 84, no. 13-14, pp. 468–481, 2009.

[215] S. D. Anker, W. Doehner, M. Rauchhaus et al., "Uric acid and survival in chronic heart failure: validation and application in metabolic, functional, and hemodynamic staging," *Circulation*, vol. 107, no. 15, pp. 1991–1997, 2003.

[216] J. Abrigo, J. C. Rivera, J. Aravena et al., "High fat diet-induced skeletal muscle wasting is decreased by mesenchymal stem cells administration: implications on oxidative stress, ubiquitin proteasome pathway activation, and myonuclear apoptosis," *Oxidative Medicine and Cellular Longevity*, vol. 2016, Article ID 9047821, 13 pages, 2016.

[217] E. Barreiro and S. Tajbakhsh, "Epigenetic regulation of muscle development," *Journal of Muscle Research and Cell Motility*, vol. 38, no. 1, pp. 31–35, 2017.

[218] R. M. Carr, E. Enriquez-Hesles, R. L. O. Olson, A. Jatoi, J. Doles, and M. E. Fernandez-Zapico, "Epigenetics of cancer-associated muscle catabolism," *Epigenomics*, vol. 9, no. 10, pp. 1259–1265, 2017.

[219] D. T. Shaughnessy, K. McAllister, L. Worth et al., "Mitochondria, energetics, epigenetics, and cellular responses to stress," *Environmental Health Perspectives*, vol. 122, no. 12, pp. 1271–1278, 2014.

[220] M. Liesa, M. Palacin, and A. Zorzano, "Mitochondrial dynamics in mammalian health and disease," *Physiological Reviews*, vol. 89, no. 3, pp. 799–845, 2009.

[221] I. Novak, "Mitophagy: a complex mechanism of mitochondrial removal," *Antioxidants & Redox Signaling*, vol. 17, no. 5, pp. 794–802, 2012.

[222] B. Westermann, "Mitochondrial fusion and fission in cell life and death," *Nature Reviews. Molecular Cell Biology*, vol. 11, no. 12, pp. 872–884, 2010.

[223] R. J. Youle and D. P. Narendra, "Mechanisms of mitophagy," *Nature Reviews Molecular Cell Biology*, vol. 12, no. 1, pp. 9–14, 2011.

[224] E. Marzetti, M. Lorenzi, F. Landi et al., "Altered mitochondrial quality control signaling in muscle of old gastric cancer patients with cachexia," *Experimental Gerontology*, vol. 87, Part A, pp. 92–99, 2017.

[225] R. F. Roberts, M. Y. Tang, E. A. Fon, and T. M. Durcan, "Defending the mitochondria: the pathways of mitophagy and mitochondrial-derived vesicles," *The International Journal of Biochemistry & Cell Biology*, vol. 79, pp. 427–436, 2016.

[226] P. S. Brookes, Y. Yoon, J. L. Robotham, M. W. Anders, and S. S. Sheu, "Calcium, ATP, and ROS: a mitochondrial love-hate triangle," *American Journal of Physiology-Cell Physiology*, vol. 287, no. 4, pp. C817–C833, 2004.

[227] N. Cheema, A. Herbst, D. McKenzie, and J. M. Aiken, "Apoptosis and necrosis mediate skeletal muscle fiber loss in age-induced mitochondrial enzymatic abnormalities," *Aging Cell*, vol. 14, no. 6, pp. 1085–1093, 2015.

[228] N. M. Held and R. H. Houtkooper, "Mitochondrial quality control pathways as determinants of metabolic health," *BioEssays*, vol. 37, no. 8, pp. 867–876, 2015.

[229] S. G. Rhee, H. A. Woo, I. S. Kil, and S. H. Bae, "Peroxiredoxin functions as a peroxidase and a regulator and sensor of local peroxides," *The Journal of Biological Chemistry*, vol. 287, no. 7, pp. 4403–4410, 2012.

[230] R. Scherz-Shouval and Z. Elazar, "ROS, mitochondria and the regulation of autophagy," *Trends in Cell Biology*, vol. 17, no. 9, pp. 422–427, 2007.

[231] G. Twig, A. Elorza, A. J. A. Molina et al., "Fission and selective fusion govern mitochondrial segregation and elimination by autophagy," *The EMBO Journal*, vol. 27, no. 2, pp. 433–446, 2008.

[232] J. A. Carson, J. P. Hardee, and B. N. VanderVeen, "The emerging role of skeletal muscle oxidative metabolism as a biological target and cellular regulator of cancer-induced muscle wasting," *Seminars in Cell & Developmental Biology*, vol. 54, pp. 53–67, 2016.

[233] K. Boengler, M. Kosiol, M. Mayr, R. Schulz, and S. Rohrbach, "Mitochondria and ageing: role in heart, skeletal muscle and adipose tissue," *Journal of Cachexia, Sarcopenia and Muscle*, vol. 8, no. 3, pp. 349–369, 2017.

[234] M. Chen, Z. Chen, Y. Wang et al., "Mitophagy receptor FUNDC1 regulates mitochondrial dynamics and mitophagy," *Autophagy*, vol. 12, no. 4, pp. 689–702, 2016.

[235] A. Lang, R. Anand, S. Altinoluk-Hambüchen et al., "SIRT4 interacts with OPA1 and regulates mitochondrial quality control and mitophagy," *Aging*, vol. 9, no. 10, pp. 2163–2189, 2017.

[236] K. Palikaras, E. Lionaki, and N. Tavernarakis, "Balancing mitochondrial biogenesis and mitophagy to maintain energy metabolism homeostasis," *Cell Death and Differentiation*, vol. 22, no. 9, pp. 1399–1401, 2015.

[237] K. Palikaras, E. Lionaki, and N. Tavernarakis, "Coordination of mitophagy and mitochondrial biogenesis during ageing in *C. elegans*," *Nature*, vol. 521, no. 7553, pp. 525–528, 2015.

[238] C. Ploumi, I. Daskalaki, and N. Tavernarakis, "Mitochondrial biogenesis and clearance: a balancing act," *The FEBS Journal*, vol. 284, no. 2, pp. 183–195, 2017.

[239] J. Sin, A. M. Andres, D. J. R. Taylor et al., "Mitophagy is required for mitochondrial biogenesis and myogenic differentiation of C2C12 myoblasts," *Autophagy*, vol. 12, no. 2, pp. 369–380, 2016.

Hindawi
Oxidative Medicine and Cellular Longevity
Volume 2018, Article ID 5216383, 11 pages
https://doi.org/10.1155/2018/5216383

Research Article

Edaravone Improves Septic Cardiac Function by Inducing an HIF-1α/HO-1 Pathway

Chao He,[1] Wei Zhang,[2] Suobei Li,[2] Wei Ruan,[2] Junmei Xu,[2] and Feng Xiao[2]

[1]*Department of General Surgery, The Second Xiangya Hospital, Central South University, Changsha, Hunan 410011, China*
[2]*Department of Anesthesiology, The Second Xiangya Hospital, Central South University, Changsha, Hunan 410011, China*

Correspondence should be addressed to Feng Xiao; xiaofengcsu@csu.edu.cn

Received 28 September 2017; Revised 20 December 2017; Accepted 6 February 2018; Published 22 March 2018

Academic Editor: Raquel Rodrigues-Díez

Septic myocardial dysfunction remains prevalent and raises mortality rate in patients with sepsis. During sepsis, tissues undergo tremendous oxidative stress which contributes critically to organ dysfunction. Edaravone, a potent radical scavenger, has been proved beneficial in ischemic injuries involving hypoxia-inducible factor- (HIF-) 1, a key regulator of a prominent antioxidative protein heme oxygenase- (HO-) 1. However, its effect in septic myocardial dysfunction remains unclarified. We hypothesized that edaravone may prevent septic myocardial dysfunction by inducing the HIF-1/HO-1 pathway. Rats were subjected to cecal ligation and puncture (CLP) with or without edaravone infusion at three doses (50, 100, or 200 mg/kg, resp.) before CLP and intraperitoneal injection of the HIF-1α antagonist, ME (15 mg/kg), after CLP. After CLP, rats had cardiac dysfunction, which was associated with deformed myocardium, augmented lipid peroxidation, and increased myocardial apoptosis and inflammation, along with decreased activities of catalase, HIF-1α, and HO-1 in the myocardium. Edaravone pretreatment dose-dependently reversed the changes, of which high dose most effectively improved cardiac function and survival rate of septic rats. However, inhibition of HIF-1α by ME demolished the beneficial effects of edaravone at high dose, reducing the survival rate of the septic rats without treatments. Taken together, edaravone, by inducing the HIF-1α/HO-1 pathway, suppressed oxidative stress and protected the heart against septic myocardial injury and dysfunction.

1. Introduction

Sepsis, a systemic deleterious inflammatory response to infection or injury [1], has long been associated with high mortality rate, which mainly results from multiorgan dysfunction and failure [2]. Of note, cardiac dysfunction is highly prevalent during sepsis, which is a major cause of high mortality rate in septic patients [3–6]. However, therapy for this lethal disease is nonspecific and often not effective as current understanding of its pathophysiology remains elusive [7].

Existing evidence indicates that several mechanisms are often associated with septic myocardial dysfunction, including exaggerated oxidative stress, cardiomyocyte apoptosis, contractile dysfunction of the heart, and persistent inflammation [8, 9]. Among these, oxidative stress has been considered a critical contributor in promoting the progression of sepsis-induced organ failure, including myocardial dysfunction [10–12]. Therefore, therapies that can reduce oxidative stress may effectively attenuate the development and progression of septic myocardial dysfunction. Edaravone (EDA), a potent radical scavenger, is clinically employed in stroke patients; moreover, it has been identified as a potential protective agent for cardiovascular diseases result from inflammation, oxidative stress and/or cytokine-induced apoptosis, such as ischemic or diabetic cardiomyopathy [13, 14]. In sepsis, while the antioxidative effect of EDA has been documented in brain [15], pulmonary [16], liver [17], and renal injuries [18], less is known of its effect in septic cardiac complications.

It has been suggested that EDA exerts cardioprotective effects in ischemia/reperfusion injury by scavenging reactive oxygen species (ROS), which then reduces cardiac lipid peroxidation and cardiomyocyte apoptosis [14]. One of the major pathways regulated by ROS relies on the hypoxia-inducible transcription factor-1 (HIF-1), which regulates a myriad of genes that control cellular processes essential to the cardiovascular system, including metabolism,

angiogenesis, cell survival, and oxygen delivery [19]. Activation of HIF-1α, the major functional subunit of HIF-1, has been found cardioprotective by inducing heme oxygenase (HO)-1 [20]. Indeed, HIF-1 is a key regulator of HO-1 which has been identified as one of the most important cardioprotective proteins in a wide variety of tissues in response to oxidative stress and inflammation [20, 21]. Of note, although evidence associating EDA and HIF-1α in cardiac diseases has not been documented in current literature, EDA has been found to regulate HIF-1α in neurological studies related to stroke [15]. Hence, we postulate that EDA may alleviate septic myocardial dysfunction by regulating the HIF-1/HO-1 pathway.

2. Materials and Methods

2.1. Animals. Sprague–Dawley rats (280–320 g) were obtained from the animal center of the Second Xiangya Hospital of Central South University. Rats were housed in individual cages with alternating 12-hour light/dark cycles in a temperature-controlled specific pathogen-free (SPF) environmental room, in which rats were acclimated for one week before experiment. Animals were fasted for 8 hours but had free access to water before the experiments. All animal care and experimental protocols complied with the Guidelines of Central South University for Animal Experimentation and were approved by the Institutional Animal Care and Use Committee at Central South University. All experimental procedures complied with the Guide for the Care and Use of Laboratory Animals (1996).

2.2. Experimental Protocol. The current experiment was conducted in two parts. In the first part, rats were allocated to five groups ($n = 8$ per group): sham (Sham), cecal ligation and puncture (CLP), and low (CLP + L-EDA), medium (CLP + M-EDA), or high dose (CLP + H-EDA) of the edaravone group. Rats were infused slowly with saline (2 mL) or 50 (low), 100 (medium), 200 (high) mg/kg edaravone [22] 10 minutes before CLP. In the second part, rats were allocated to four groups ($n = 8$ per group): Sham, CLP, CLP + H-EDA, and CLP + H-EDA+ 2-methoxyestradiol (ME). ME was injected intraperitoneally at 15 mg/kg (Sigma Aldrich, St. Louis, MO, USA) immediately after CLP in the treatment group. In the sham group, animals have no CLP but have vehicle treatment.

Cardiac function was evaluated by echocardiography under inhaled anesthesia with 1–3% isoflurane and 40% oxygen at 18 hours after operation. Briefly, a heparin saline-filled catheter (500 U/mL) was inserted from the right carotid artery into the left ventricle. Left ventricular systolic pressure (LVSP), left ventricular end diastolic pressure (LVEDP), maximal rate of the increase of left ventricular pressure ($+dp/dt_{max}$), and maximal rate of the decrease of left ventricular pressure ($-dp/dt_{max}$) were recorded by using a PowerLab (4S, Australia) as described previously [23].

2.3. Evaluation for Survival Rate. A cohort of rats ($n = 16$ per group) receiving the same protocols as in the part two of the experiment were used for survival rate evaluation. Rats in each group had free access to food and water and were kept under pathogen-free conditions. A video recorder was used to monitor the animals, and the survival rate was evaluated for 72 hours.

2.4. Cecal Ligation and Puncture (CLP). CLP was performed as described previously [23]. Rats under general anesthesia underwent an abdominal midline incision after disinfection of the abdomen with 10% povidone iodine. The cecum was exposed and subjected to ligation just below the ileocecal valve to maintain bowel continuity. After puncturing twice with an 18-gauge needle, a small amount of bowel content was expelled from the punctures by manual application of sufficient pressure. Then the cecum was returned to the peritoneal cavity, and the abdominal incision was closed in 2 layers. At the end of surgery, 5 mL/kg of 0.9% NaCl was subcutaneously injected in the back. For the sham-operated animals serving as controls, the cecum was mobilized but no ligation or puncture was performed.

2.5. Histopathology Analysis. Rats were sacrificed at 18 hours after surgery by carbon dioxide inhalation. The left ventricular myocardial tissues were collected. Tissue sections of the myocardium were stained with hematoxylin-eosin (H&E) stain, and histological changes were evaluated by microscopy at 400x magnification.

2.6. Immunohistochemistry Assay. After deparaffination and microwave antigen reparation, sections were pretreated with 3% H_2O_2 for 20 minutes to reduce the endogenous peroxidase activity. Then the sections were ordinally incubated with the blocking buffer (10% normal goat serum) at room temperature for 1 hour, then with primary antibodies of 4-hydroxynonenal (HNE) (1/100 dilution; Abcam, Cambridge, UK) at 4°C overnight, followed with biotinylated secondary antibody (1 : 200, Santa Cruz Biotechnology, Inc., Santa Cruz, CA, USA) and avidine-biotinylated peroxidase complex (Vectostain ABC-Kit, Vector Lab, Burlingame, CA, USA) at room temperature for 1 hour. Coloration of sections was processed with diaminobenzidine (DAB, Vector Laboratories, Burlingame, CA, USA) and finished with distilled water. After counterstaining with hematoxylin for 30 seconds, sections were dehydrated with graded ethanol, cleared with dimethylbenzene, and mounted with neutral gums. Figures were captured with a Ti-S inverted microscope (Nikon, Japan) and analyzed with Image-Pro Plus software (version 6.0, Media Cybernetics, USA).

2.7. TUNEL for DNA Fragmentation. Terminal deoxynucleotidyl transferase dUTP nick-end labeling (TUNEL) staining was performed according to the manufacturer's protocol of DeadEnd™ Fluorometric TUNEL System kit (Promega, Madison, WI, USA). Sections were incubated with proteinase K solution (20 μg/mL in PBS) for 10 minutes after deparaffination. TUNEL labeling was conducted with a mix of a 45 μL equilibration buffer, 5 μL nucleotide mix, and 1 μL recombinant terminal deoxynucleotidyl transferase (rTdT) enzyme in a humidified, lucifugal chamber for 1 hour at 37°C. The slides were protected from direct light from this step to the end of experiment. Hoechst 33258 (H-33258, Sigma-Aldrich; 5 mg/mL in distilled water, 3 minutes) was used to

stain nuclei and terminate the TUNEL reaction. Antifade solution was dropped to the area which was mounted by glass coverslips with clear nail polish sealing the edges. The samples were immediately analyzed under a fluorescence microscope using a standard fluorescein filter set to view the green fluorescence of fluorescein at 520 nm and blue Hoechst at 460 nm, then stored at 4°C in dark if necessary.

2.8. Thiobarbituric Acid Reactive Substance (TBARS) Assay for MDA. The MDA concentration was tested by TBARS Parameter™ Kit for measuring oxidative stress (R&D Systems, Minneapolis, USA). All of the steps were strictly performed according to the manufacturer's instruction. In brief, acid-treated samples and standards were added to the included 96-well microplate followed by the TBA reagent. Then the 96-well microplate was incubated at 45°C for 2 hours. The microplate was read at 532 nm, and the intensity of the color corresponds to the level of lipid peroxidation in the sample.

2.9. ELISA for Catalase, HO-1, and HIF-1α Activity. The activity of catalase, HO-1, and HIF-1α was measured in myocardial tissue lysates using colorimetric sandwich ELISA according to the vendor's instructions. All ELISA kits were purchased from LifeSpan BioSciences, Inc., USA.

2.10. Cytokine Measurement by ELISA. Heart tissues were homogenized and then centrifuged. The levels of IL-1β, IL-6, and TNF-α in heart homogenates were measured using ELISA kits according to the manufacturer's instructions (LifeSpan BioSciences, Inc., USA). The concentrations of the cytokines were quantified by referring to standard curves.

2.11. Western Blot. For nuclear purification, nuclear-cytosol extraction kit (Applygen Technologies, Beijing, China) was used according to the manufacturer's instruction. Briefly, the mixture was added with the cytosol extraction buffer supplemented with protease inhibitor cocktail and incubated on ice for 10 minutes. The mixture was then centrifuged at 1000 g for 5 minutes and the resulted pellet contained crude nuclei. The cytosol fraction was extracted by further centrifuging the supernatant at 12000g for 5 minutes. The crude nuclear pellet was incubated in the nuclear extraction buffer on ice for 30 minutes, with vortexing for 10 seconds every 5 minutes, then centrifuged at 12000g for 5 minutes. The resulting supernatant contained the nuclear fraction.

Samples were homogenized, and protein concentrations were determined using the BCA protein assay (Bio-Rad, Hemel Hempstead, Hertfordshire, UK). Fifty micrograms of each prepared sample was separated by 8 or 12% sodium dodecylsulfate polyacrylamide gel electrophoresis, then transferred to polyvinylidene fluoride membranes (EMD Millipore Corporation, Billerica, MA, USA), and incubated with a blocking solution composed of 5% bull serum albumin (BSA) in Tris-buffered saline with Tween (pH 8.0, 10 mm Tris, 150 mm NaCl, 0.1% Tween, TBST). Membranes were incubated overnight (14–16 hours) at 4°C with the corresponding primary antibodies: anti-HIF-α (1 : 2000), anti-Lamin B2 (1 : 1000), anti-HO-1 (1 : 2000), and anti-GAPDH (1 : 1000). All antibodies were purchased from Cell Signaling Technology, Beverly, MA, USA. After being washed with TBST, samples were incubated with the corresponding secondary antibodies for 1 hour at room temperature. Immunoreactive proteins were visualized using the ECL Western blotting system (Pierce Biotechnology, Rockford, IL, USA) and scanned by an Image Master II scanner (GE Healthcare, Milwaukee, WI, USA). All the images were analyzed using ImageQuant™ TL software v2003.03 (GE Healthcare, Milwaukee, WI, USA).

2.12. Statistical Analysis. Data were presented as mean ± standard deviation (SD) and processed by GraphPad Prism 6.0 software. One-way analysis variance (ANOVA) followed by post hoc analysis (Tukey test) was used for comparison between groups after confirmation of homoscedasticity. P value less than 0.05 ($P < 0.05$) was considered statistically significant.

3. Results

3.1. EDA Prevents Sepsis-Induced Myocardial Injury and Cardiac Dysfunction. To assess whether EDA prevents sepsis-induced cardiac injury, EDA was infused at low, medium, or high doses (50, 100, or 200 mg/kg, resp.) 10 minutes prior to CLP surgery. As demonstrated in the H&E staining of the myocardium (Figure 1(a)), the normal architecture of the myocardium as shown in the sham group was deformed after CLP. Pretreatment with high dose of EDA effectively preserved the normal conformation of the myocardium, while low and medium doses of EDA did not. Functional-wise, CLP-induced sepsis severely compromised cardiac function, evidenced by reduced LVSP, dP/dt_{max}, $-dP/dt_{max}$ (Figures 1(b), 1(d), and 1(e)), and increased LVEDP (Figure 1(c)) (CLP versus Sham, $P < 0.05$). Administration of all three doses of EDA improved cardiac function with effectiveness ascending from low to high doses of EDA. EDA at high dosage was found to be the most effective among the tested dosages in prevention of cardiac dysfunction induced by CLP.

3.2. EDA Reduces Myocardial Oxidative Stress in Septic Rats. Sepsis damages myocardium integrity which is associated with upsurge of oxidative stress [24]. After CLP, increased lipid peroxidation was found in the heart as demonstrated in the 4-HNE staining of the myocardium in Figure 2(a), which was accompanied by a significantly increased MDA level (Figure 2(b)) and decreased catalase, HIF-1α, and HO-1 activities (Figures 2(c)–2(e)) (CLP versus Sham, $P < 0.05$). Pretreatment of EDA minimized these changes in a dose-dependent manner that EDA at high dosage most effectively reduced lipid peroxidation and the MDA level and enhanced activities of catalase, HIF-1α, and HO-1 (CLP + H-EDA versus CLP, $P < 0.05$).

3.3. Inhibition of HIF-1α Represses the Antioxidative Effect of EDA in Septic Rats. EDA has been suggested to modify HIF-1α binding activity in astrocyte [25]; however, whether EDA acts via HIF-1α in cardiac injury remains unknown. In CLP-induced sepsis, we observed a significant decrease in protein expressions of HIF-1α in the nucleus along with HO-1 in the

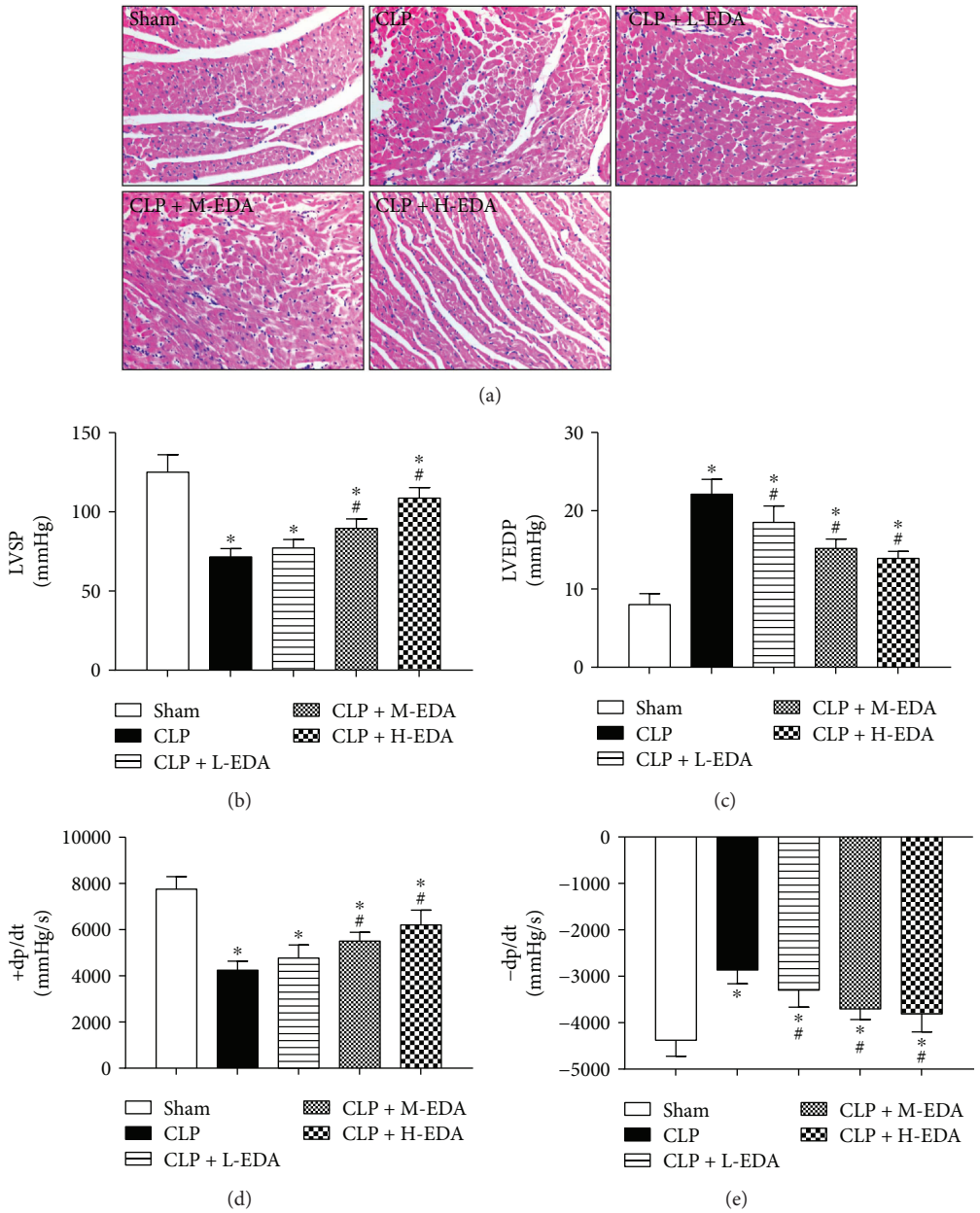

Figure 1: H&E staining of the myocardium and indices of cardiac function in septic rats. Edaravone (EDA) at low (L), medium (M), or high (H) dose was injected intravenously 10 minutes before CLP, respectively. Myocardium architecture was visualized by (a) H&E staining. Cardiac function was demonstrated in terms of (b) left ventricular systolic pressure (LVSP), (c) left ventricular end diastolic pressure (LVEDP), (d) maximal slope of left ventricular systolic pressure increment ($+dP/dt_{max}$), and (e) maximal slope of left ventricular diastolic pressure decrement ($-dP/dt_{max}$). $^{*}P < 0.05$ versus Sham. $^{\#}P < 0.05$ versus CLP. Data are presented as mean ± SEM. $n = 8$ per group.

heart (CLP versus Sham, $P < 0.05$) (Figures 3(a)–3(c)). Pretreatment with H-EDA not only prevented the suppression of HIF-1α and HO-1 but also enhanced their expressions, which reduced the anatomical distortion (H&E stain) and lipid peroxidation (4-HNE stain) in the myocardium after CLP (Figures 3(d) and 3(e)). However, the administration of the HIF-1α inhibitor, ME, abolished these effects of H-EDA in the myocardium (H-EDA + ME versus H-EDA, $P < 0.05$). Deteriorated architecture of the myocardium and increased lipid peroxidation were observed following the inhibition of HIF-1α. Further, besides HO-1, catalase activity and MDA concentration in the heart were significantly lower in the CLP + H-EDA + ME group compared to the CLP + H-EDA group (H-EDA + ME versus H-EDA, $P < 0.05$), suggesting that the antioxidative effect of EDA was reversed by the HIF-1α inhibitor (Figures 3(f) and 3(g)). The presented data implicates that HIF-1α inhibition can reverse the cardioprotective effect of EDA even at high dosage.

3.4. Inhibition of HIF-1α Diminishes the Antiapoptotic Effect of EDA and Aggravated Cardiac Dysfunction in Septic Rats. Cardiomyocyte apoptosis has been closely linked to sepsis-

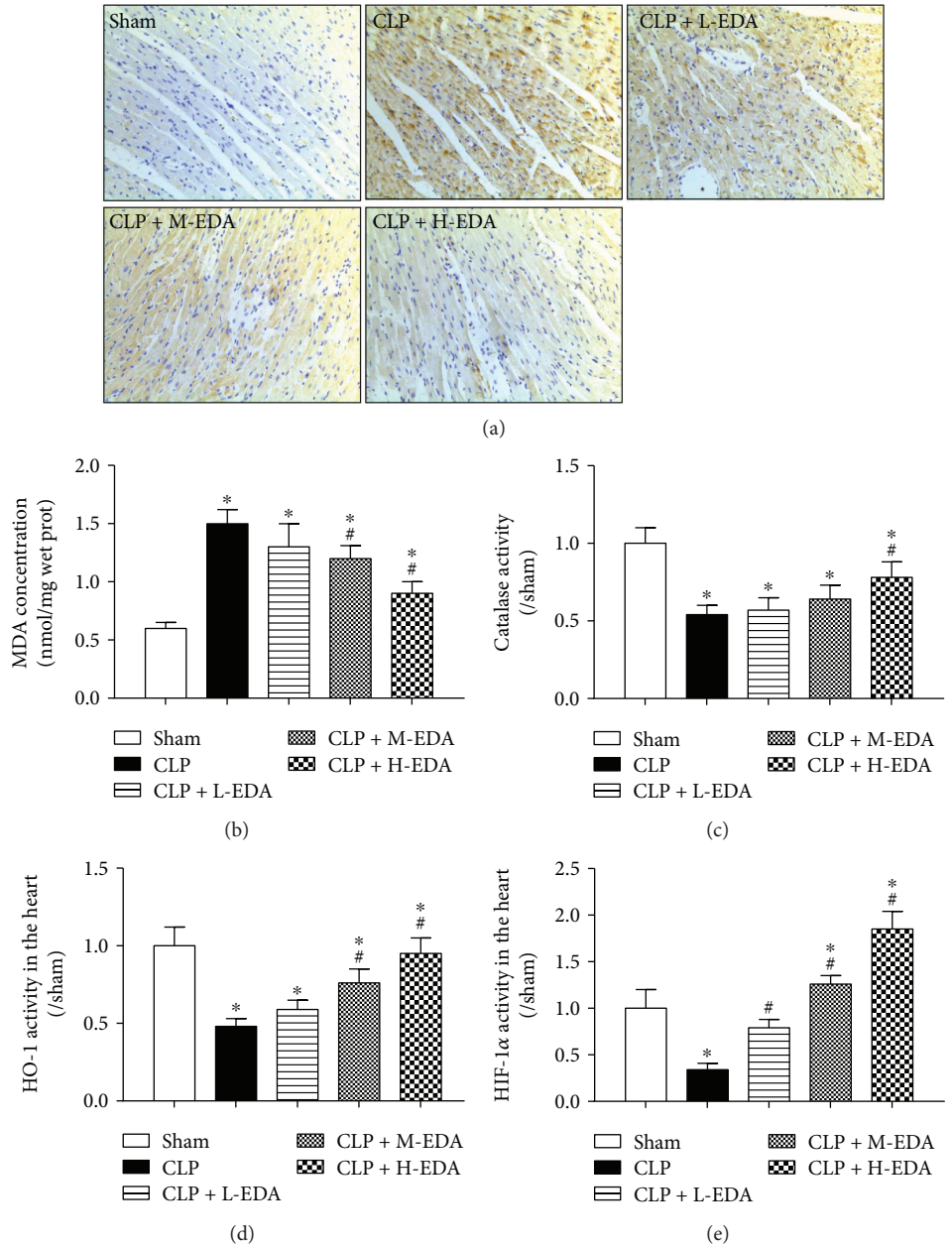

Figure 2: 4-HNE staining of the myocardium and the cardiac level of oxidative stress markers in septic rats. Edaravone (EDA) at low (L), medium (M), or high (H) dose was injected intravenously 10 minutes before CLP, respectively. Lipid peroxidation level in the myocardium was visualized by (a) 4-HNE staining. Cardiac oxidative stress was indicated by levels of (b) MDA concentration, (c) catalase activity, (d) HO-1 activity, and (e) HIF-1α activity in the myocardium. $^{*}P < 0.05$ versus Sham. $^{\#}P < 0.05$ versus CLP. Data are presented as mean ± SEM. $n = 8$ per group.

induced myocardial injury, as well as deleterious inflammatory response in the heart, which leads to heart failure [26]. As demonstrated in the TUNEL assay in the myocardium (Figure 4(a)), TUNEL-positive cells were stained brown (labeled by arrows) as we observed significantly more apoptotic cells in the CLP group compared to the sham group (CLP versus Sham, $P < 0.05$) (Figure 4(b)). Pretreatment of EDA at high dosage markedly reduced the number of apoptotic cardiomyocytes (CLP + H-EDA versus CLP, $P < 0.05$). However, the administration of ME to EDA-pretreated septic rats diminished the antiapoptotic effect of EDA as the number of apoptotic cardiomyocytes was significantly higher in the CLP + H-EDA + ME group than in the CLP + H-EDA group (CLP + H-EDA versus CLP + H-EDA + ME, $P < 0.05$). Additional measurement of the inflammatory markers, IL-6, TNF-α, and IL-1β, in the myocardium revealed upsurge of their expressions after CLP (CLP versus Sham, $P < 0.05$) (Figures 4(c)–4(e)). While H-EDA pretreatment significantly reduced the inflammatory markers (CLP + H-EDA versus CLP, $P < 0.05$), injection of the HIF-1α inhibitor reversed the anti-inflammatory effect of H-EDA (CLP + H-EDA versus CLP + H-EDA + ME, $P < 0.05$).

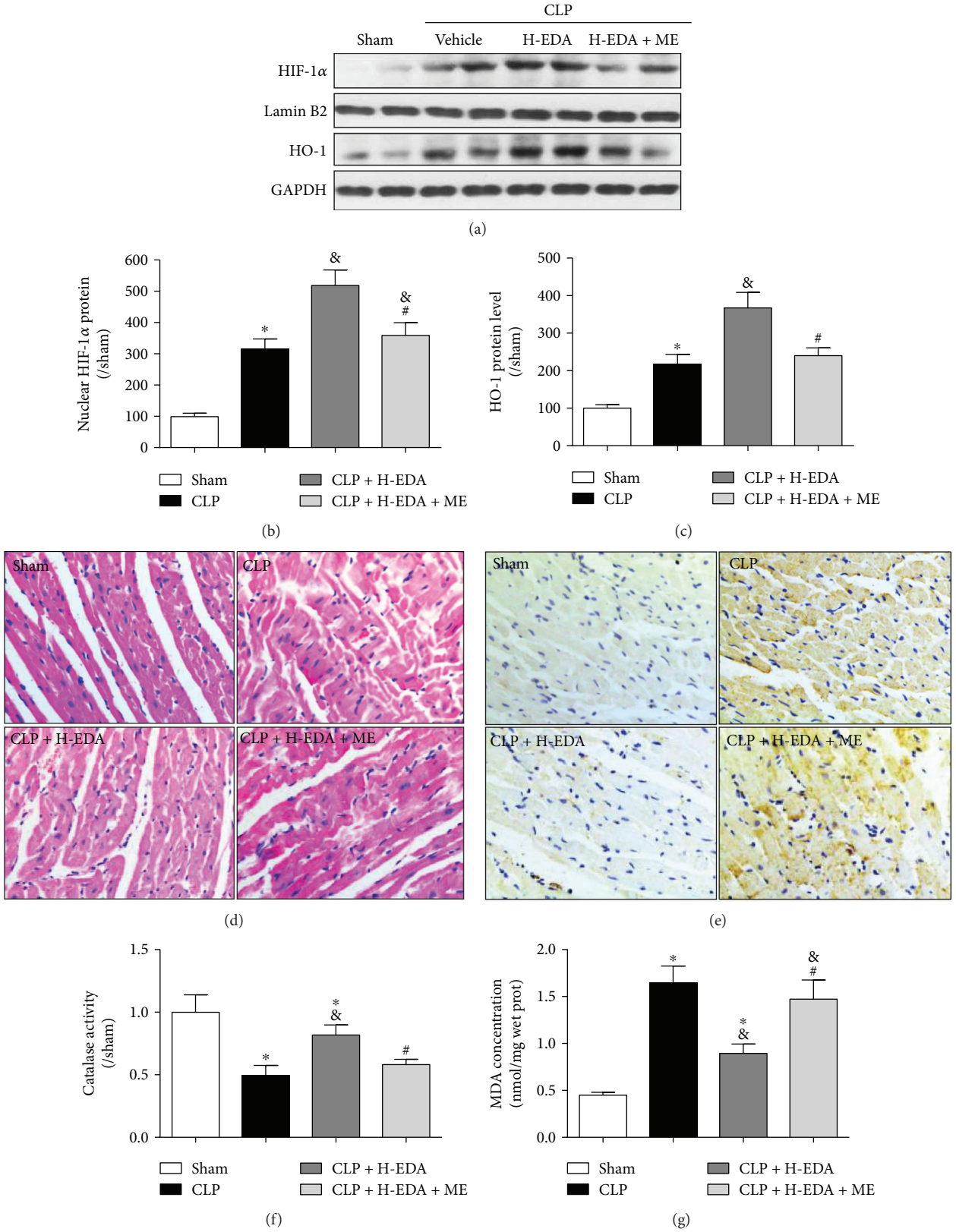

Figure 3: Effect of the HIF-1α antagonist on oxidative stress in edaravone-pretreated septic rats. Edaravone (EDA) at high (H) dose was injected intravenously 10 minutes before CLP, while the HIF-1α antagonist, ME, was injected intraperitoneally after CLP. Protein expressions of (a–c) HIF-1α and HO-1 were assessed in the myocardium. Myocardium architecture and lipid peroxidation level were visualized by (d) H&E staining (×400) and (e) 4-HNE staining (×200), respectively. Levels of (f) MDA concentration and (g) catalase activity were also evaluated in the myocardium. $^{*}P < 0.05$ versus Sham. $^{\&}P < 0.05$ versus CLP. $^{\#}P < 0.05$ versus CLP + H-EDA.

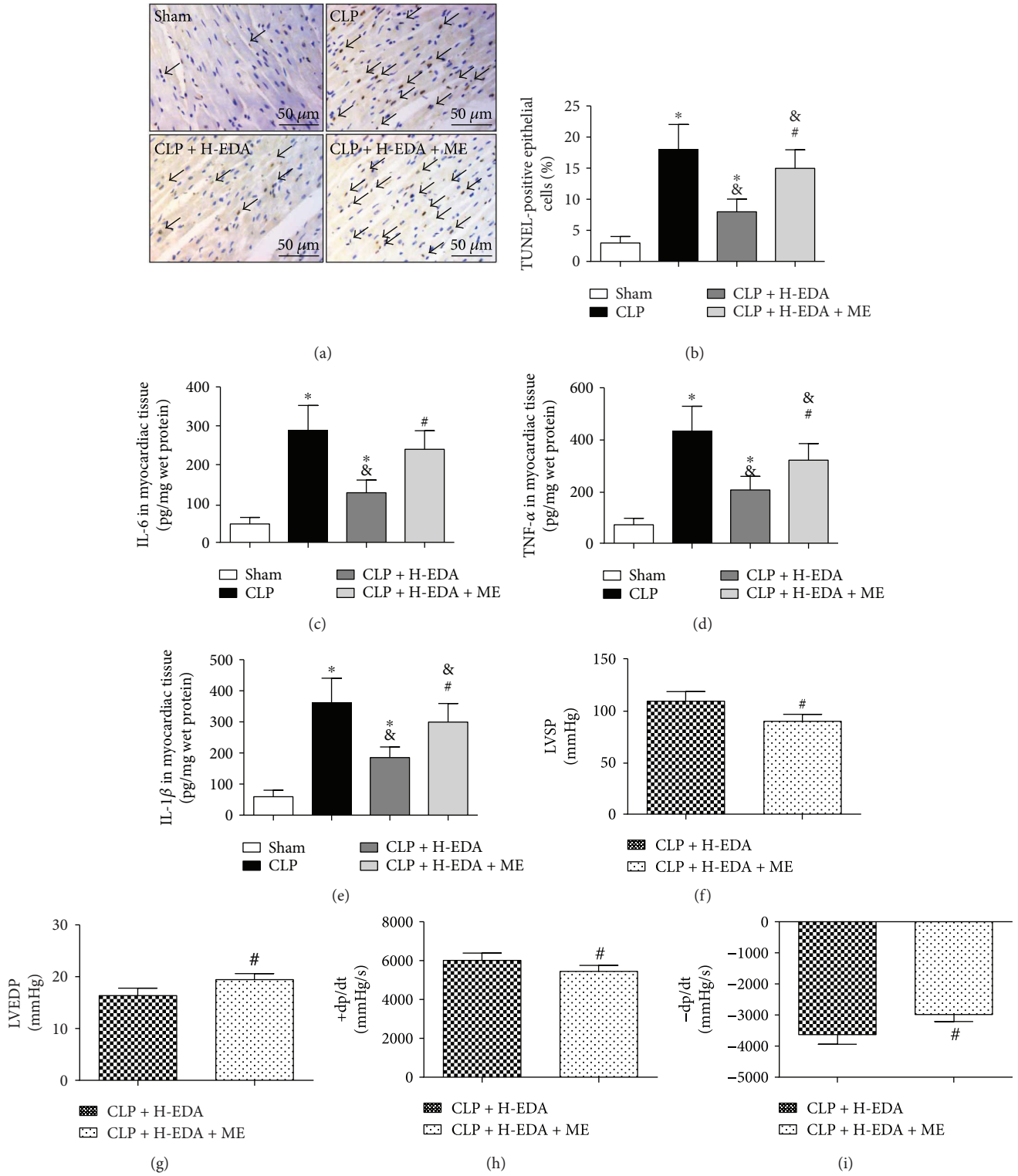

Figure 4: Effect of the HIF-1α antagonist on cardiomyocyte apoptosis and cardiac function in edaravone-pretreated septic rats. Edaravone (EDA) at high (H) dose was injected intravenously 10 minutes before CLP, while the HIF-1α antagonist, ME, was injected intraperitoneally after CLP. Cardiomyocyte apoptosis was assessed by terminal deoxynucleotidyl transferase dUTP nick-end labeling (TUNEL). (a and b) TUNEL-positive cells were stained brown and counted. Black arrows means TUNEL positive cell. Cytokines IL-6 (c), TNF-α (d), and IL-1β (e) were detected by an ELISA method. $^{*}P < 0.05$ versus Sham. $^{\&}P < 0.05$ versus CLP. $^{\#}P < 0.05$ versus CLP + H-EDA. Cardiac function was demonstrated in terms of (f) left ventricular systolic pressure (LVSP), (g) left ventricular end diastolic pressure (LVEDP), (h) maximal slope of left ventricular systolic pressure increment (+dP/dt$_{max}$), and (i) maximal slope of left ventricular diastolic pressure decrement (−dP/dt$_{max}$). $^{\#}P < 0.05$ versus CLP + H-EDA. Data are presented as mean ± SEM. $n = 8$ per group.

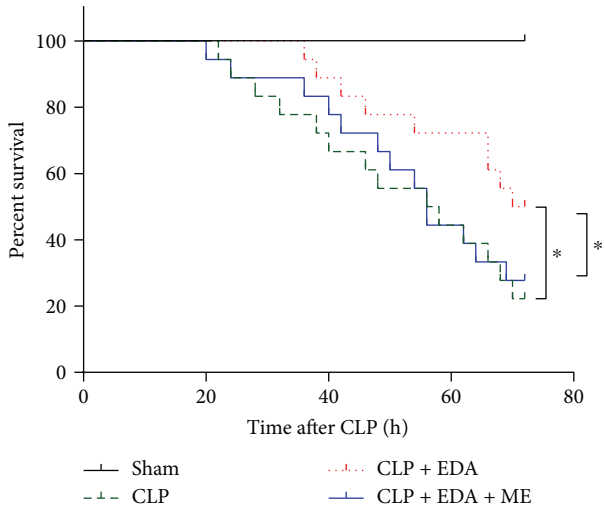

FIGURE 5: Survival rates of rats after CLP. Rats were subjected to CLP with or without pretreatment of high (H) dose of edaravone (EDA) and posttreatment of the HIF-1α antagonist, ME. Survival rate were monitored within 72 hours after CLP. $^*P < 0.05$ versus CLP + H-EDA. Data are presented as mean ± SEM. $n = 16$ per group.

EDA-improved cardiac function was also demoted by the HIF-1α inhibitor. As demonstrated in Figures 4(g)–4(i), the inhibition of HIF-1α by ME in H-EDA-pretreated septic rats significantly reduced LVSP, +dp/dt, and −dp/dt and increased LVEDP with respect to the high-dose EDA-treated group (CLP + H-EDA + ME versus CLP + H-EDA, $P < 0.05$).

3.5. HIF-1α Inhibition Abolished the Survival-Promoting Effect of EDA in Septic Rats. Performance of cardiac function is a key predictor of survival in sepsis [27]. As we have found that EDA provided cardioprotection in septic rats, here we determined whether EDA pretreatment can improve the survival rate of septic rats after CLP. As shown in Figure 5, survival rate of rats dropped to 20% at 72 hours after CLP. Pretreatment of EDA significantly increased survival rate to nearly 50% (CLP + H-EDA versus CLP, $P < 0.05$), whereas the administration of the HIF-1α antagonist reversed the survival rate to as low as in the CLP group (CLP + H-EDA + ME versus CLP + H-EDA, $P < 0.05$).

4. Discussion

In this study, we have shown that EDA can alleviate septic myocardial dysfunction by reducing cardiac oxidative stress through the HIF-1α/HO-1 pathway. In the present CLP model of sepsis in the rat, we observed lethal damage in animal's myocardial morphology and function, manifested by destructed architecture of the myocardium, cardiomyocyte apoptosis, reduced LVSP, dP/dt_{max}, and $-dP/dt_{max}$, and increased LVEDP. These alterations paralleled alterations in oxidative stress that we found significantly augmented lipid peroxidation along with decreased activities of catalase, HIF-1α, and HO-1 in the heart. Intravenous injection of EDA before CLP reversed the alterations in a dose-dependent manner. Moreover, the beneficial effects of EDA, even at high dose, can be demolished by the HIF-1α inhibitor, ME. In particular, the inhibition of HIF-1α reverted the high-dose EDA-induced protein expressions of HIF-1α and HO-1 and the EDA-reduced cardiomyocyte apoptosis. Our findings suggest that EDA, by inducing the HIF-1α/HO-1 pathway in advance of sepsis, can reduce cardiac oxidative stress and prevent septic cardiac dysfunction, which eventually improves animal survival.

Sepsis is a systemic deleterious inflammatory response to infection or injury, in which lung dysfunction is the primary detrimental effect, while dysfunction of other organs such as the heart and kidneys is secondary to lung dysfunction, and also in other situations, cardiac dysfunctions (e.g., heart failure, arrhythmia, and myocardial ischemia) often happen secondary to an abrupt worsening of renal function [28] or lung function [7]. In these regards, exploration of effective means protecting the heart against cardiac dysfunction that can be applied before or after septic cardiac dysfunction is also an important topic and worth of investigation. The current study was aimed at testing the effect of edaravone for pretreatment before septic myocardial dysfunction, which may be more of worth in preventing septic myocardial dysfunction. And our results were consistent with those of the studies of Chen et al. [29] and Chen et al. [30], which showed that trimetazidine and baicalein pretreatment protected the heart from septic myocardial dysfunction.

Our observations extend beyond the current literature on EDA, which has mainly documented its pleiotropic therapeutic effect in ischemia/reperfusion injury in various organs by scavenging ROS [14], among which, a few studies on brain ischemia/reperfusion injury have related EDA to HIF-1α signaling, which suggests that EDA posttreatment represses HIF-1α in the neuron [15, 31]. Here, for the first time, we demonstrated that EDA pretreatment induces HIF-1α in the myocardium and prevents myocardial dysfunction during sepsis. The discrepancy between our finding and the literature may due to differences in cell type and cellular microenvironment, which are thought to be crucial in the regulation of HIF-1α by ROS [32]. During oxidative stress, cellular treatment with ROS scavengers significantly inhibits HIF-1α protein expression and activity in a range of cell types, including myocardial cells [33]. On the other hand, during normoxia, the application of antioxidant either has no effect on HIF-1α or increases HIF-1α expression and activity [34, 35]. Therefore, because previous studies administered EDA to animals after ischemia/reperfusion injury when the microenvironments were under tremendous oxidative stress, HIF-1α was repressed as ROS was by EDA [15, 31].

In contrast, our study treated animals with EDA before CLP injury when the cardiomyocyte was under normoxic condition, thus HIF-1α was induced by EDA. As a matter of fact, earlier studies on the regulation of HIF-1 in response to cellular redox states showed that hydroxyl radicals mediate the inhibition of HIF-1α activity and possibly the degradation of HIF-1α, suggesting that HIF-1 DNA binding requires reducing conditions [35]. Since EDA has been reported to exert antioxidative effects by quenching hydroxyl radicals and hydroxyl radical-dependent lipid peroxidation [14], it is

possible that, in our study, EDA pretreatment induced HIF-1α by scavenging hydroxyl radicals, which also explains the reduced lipid peroxidation in the myocardium of animals treated with EDA.

Indeed, the induction of HIF-1α has been found to be cardioprotective as HIF-1α is a key regulator of HO-1, one of the most important cardioprotective proteins in a panoply of tissues and conditions [20, 36]. HO-1 catalyzes heme oxidation and gives rise to CO, bilirubin, and ferritin, all of which contributes to cellular mechanisms against oxidative damage and death [21] that involve upregulation of catalase [37]. The previous study demonstrated that cardiac-specific overexpression of HO-1 alleviates myocardial ischemia-reperfusion injury [38]. Further, cardiac preconditioning with the HIF-1 activator attenuates postischemic myocardial injury [20]. Therefore, HO-1 is thought to provide both immediate and delayed protections against ischemia-reperfusion injury [36]. In our study, EDA pretreatment dose-dependently induced HIF-1α, HO-1, and catalase activities, which was associated with reduced lipid peroxidation, cardiomyocyte apoptosis, and MDA level in the myocardium together with improved cardiac function at 18 hours after CLP. The delayed protective effect is even prominent in the survival study where we observed about 30% higher survival rate with EDA pretreatment than that without treatment at 72 hours after CLP. These beneficial effects of EDA were attenuated by the HIF-1α inhibitor, suggesting that EDA preconditions the heart against septic cardiac dysfunction via upregulation of HIF-1α which in turn boosts HO-1 expression and exerts cardioprotective effects.

Of note, the mechanisms of the effect of edaravone have been reported to be mediated by enhancement of nitric oxide (NO) [39, 40], which may in turn result in a protective effect in injured cardiac tissues. On the other hand, under normal oxygen tension, the master transcriptional factor HIF-1 activity is usually suppressed due to the rapid, oxygen-dependent degradation of one of its two subunits, HIF-1α. Normoxic HIF-1 activity can be upregulated through NO-mediated S-nitrosylation and stabilization of HIF-1α. So, the EDA may increase NO generation to activate the HIF-1α/HO-1 pathway which takes part in the septic cardioprotective progress. And the *in vitro* study will be performed in the future study to verify our hypothesis. On the other hand, clinically, edaravone as an approved treatment for acute ischemic stroke (AIS) in Japan is recommended by the American Heart Association in the guidelines for the early management of AIS patients [41]. In sepsis, while the preventive/protective effect of edaravone has been demonstrated in the lung, liver, and kidney [16, 17, 42], we sought for its efficacy on cardiac complication, which is a leading cause of death in septic patients. We believe our study has strengthened the support of early application of edaravone in sepsis to reduce the occurrence of cardiac dysfunction. It is of notice that intravenous infusion of edaravone in patients with septic peritonitis for 2 weeks starting from their admission to intensive care unit has been shown to improve inflammatory and oxidative states with better patient outcomes [43]. Thus, it is possible that posttreatment with edaravone is clinically cardioprotective but needs further investigations.

In summary, we have demonstrated for the first time that pretreatment with EDA induces preconditioning-like protection effect in the heart against septic myocardial injury and dysfunction. By inducing the HIF-1α/HO-1 pathway, EDA primed the heart with an active cellular antioxidative mechanism which involves an increased catalase activity and a decreased MDA level in the myocardium. Given that EDA has been used clinically to treat ischemic stroke, the advancing knowledge we have provided here on the cardiac preconditioning effect of EDA via HIF-1α/HO-1 activation in sepsis may support a novel use of EDA as a treatment for septic patients.

Conflicts of Interest

The authors declare that they have no conflict of interest.

Authors' Contributions

Feng Xiao and Chao He designed the experiments, Chao He and Wei Zhang performed the experiments and analyzed the data, Suobei Li and Wei Ruan interpreted the results of the experiments, Wei Ruan and Feng Xiao drafted the manuscript, Junmei Xu edited and revised the manuscript, and Feng Xiao approved the final manuscript.

Acknowledgments

This work was supported by grants from National Natural Science Foundation of China (no. 81600251) and Hunan Provincial Natural Science Foundation of China (nos. 2017JJ3438 and 2017JJ3448).

References

[1] D. Annane, E. Bellissant, and J. M. Cavaillon, "Septic shock," *The Lancet*, vol. 365, no. 9453, pp. 63–78, 2005.

[2] R. C. Bone, R. A. Balk, F. B. Cerra et al., "Definitions for sepsis and organ failure and guidelines for the use of innovative therapies in sepsis. The ACCP/SCCM Consensus Conference Committee. American College of Chest Physicians/Society of Critical Care Medicine," *Chest*, vol. 101, no. 6, pp. 1644–1655, 1992.

[3] D. C. Angus and T. van der Poll, "Severe sepsis and septic shock," *The New England Journal of Medicine*, vol. 369, no. 9, pp. 840–851, 2013.

[4] E. Christaki and S. M. Opal, "Is the mortality rate for septic shock really decreasing?," *Current Opinion in Critical Care*, vol. 14, no. 5, pp. 580–586, 2008.

[5] D. B. Hoover, T. R. Ozment, R. Wondergem, C. Li, and D. L. Williams, "Impaired heart rate regulation and depression of cardiac chronotropic and dromotropic function in polymicrobial sepsis," *Shock*, vol. 43, no. 2, pp. 185–191, 2015.

[6] R. Thangamalai, K. Kandasamy, S. V. Sukumarn et al., "Atorvastatin prevents sepsis-induced downregulation of myocardial β1-adrenoceptors and decreased cAMP response in mice," *Shock*, vol. 41, no. 5, pp. 406–412, 2014.

[7] X. Lv and H. Wang, "Pathophysiology of sepsis-induced myocardial dysfunction," *Military Medical Research*, vol. 3, no. 1, p. 30, 2016.

[8] A. Rudiger and M. Singer, "Mechanisms of sepsis-induced cardiac dysfunction," *Critical Care Medicine*, vol. 35, no. 6, pp. 1599–1608, 2007.

[9] T. Furian, C. Aguiar, K. Prado et al., "Ventricular dysfunction and dilation in severe sepsis and septic shock: relation to endothelial function and mortality," *Journal of Critical Care*, vol. 27, no. 3, pp. 319.e9–319.e15, 2012.

[10] J. P. Sánchez-Villamil, V. D'Annunzio, P. Finocchietto et al., "Cardiac-specific overexpression of thioredoxin 1 attenuates mitochondrial and myocardial dysfunction in septic mice," *The International Journal of Biochemistry & Cell Biology*, vol. 81, Part B, pp. 323–334, 2016.

[11] C. Ritter, M. Andrades, M. L. C. Frota Junior et al., "Oxidative parameters and mortality in sepsis induced by cecal ligation and perforation," *Intensive Care Medicine*, vol. 29, no. 10, pp. 1782–1789, 2003.

[12] D. S. Wheeler, "Oxidative stress in critically ill children with sepsis," *The Open Inflammation Journal*, vol. 4, no. 1, pp. 74–81, 2011.

[13] L. Ji, Y. Liu, Y. Zhang et al., "The antioxidant edaravone prevents cardiac dysfunction by suppressing oxidative stress in type 1 diabetic rats and in high-glucose-induced injured H9c2 cardiomyoblasts," *Canadian Journal of Physiology and Pharmacology*, vol. 94, no. 9, pp. 996–1006, 2016.

[14] K. Kikuchi, S. Tancharoen, N. Takeshige et al., "The efficacy of edaravone (radicut), a free radical scavenger, for cardiovascular disease," *International Journal of Molecular Sciences*, vol. 14, no. 12, pp. 13909–13930, 2013.

[15] P. Zhang, W. Li, L. Li et al., "Treatment with edaravone attenuates ischemic brain injury and inhibits neurogenesis in the subventricular zone of adult rats after focal cerebral ischemia and reperfusion injury," *Neuroscience*, vol. 201, pp. 297–306, 2012.

[16] S. Yamaguchi, M. H. Hussein, G. A.-H. Daoud et al., "Edaravone, a hydroxyl radical scavenger, ameliorates the severity of pulmonary hypertension in a porcine model of neonatal sepsis," *The Tohoku Journal of Experimental Medicine*, vol. 223, no. 4, pp. 235–241, 2011.

[17] H. Kono, M. Asakawa, H. Fujii et al., "Edaravone, a novel free radical scavenger, prevents liver injury and mortality in rats administered endotoxin," *The Journal of Pharmacology and Experimental Therapeutics*, vol. 307, no. 1, pp. 74–82, 2003.

[18] L. Liu, Y. Song, M. Zhao, Z. Yi, and Q. Zeng, "Protective effects of edaravone, a free radical scavenger, on lipopolysaccharide-induced acute kidney injury in a rat model of sepsis," *International Urology and Nephrology*, vol. 47, no. 10, pp. 1745–1752, 2015.

[19] R. V. Shohet and J. A. Garcia, "Keeping the engine primed: HIF factors as key regulators of cardiac metabolism and angiogenesis during ischemia," *Journal of Molecular Medicine*, vol. 85, no. 12, pp. 1309–1315, 2007.

[20] R. Ockaili, R. Natarajan, F. Salloum et al., "HIF-1 activation attenuates postischemic myocardial injury: role for heme oxygenase-1 in modulating microvascular chemokine generation," *American Journal of Physiology-Heart and Circulatory Physiology*, vol. 289, no. 2, pp. H542–H548, 2005.

[21] L. E. Otterbein and A. M. K. Choi, "Heme oxygenase: colors of defense against cellular stress," *American Journal of Physiology-Lung Cellular and Molecular Physiology*, vol. 279, no. 6, pp. L1029–L1037, 2000.

[22] N. Nakajima, S. Watanabe, T. Kiyoi, A. Tanaka, K. Suemaru, and H. Araki, "Evaluation of edaravone against radiation-induced oral mucositis in mice," *Journal of Pharmacological Sciences*, vol. 127, no. 3, pp. 339–343, 2015.

[23] S. Peng, J. Xu, W. Ruan, S. Li, and F. Xiao, "PPAR-γ activation prevents septic cardiac dysfunction via inhibition of apoptosis and necroptosis," *Oxidative Medicine and Cellular Longevity*, vol. 2017, Article ID 8326749, 11 pages, 2017.

[24] J. D. Hunter and M. Doddi, "Sepsis and the heart," *British Journal of Anaesthesia*, vol. 104, no. 1, pp. 3–11, 2010.

[25] A. Ishikawa, H. Yoshida, N. Metoki et al., "Edaravone inhibits the expression of vascular endothelial growth factor in human astrocytes exposed to hypoxia," *Neuroscience Research*, vol. 59, no. 4, pp. 406–412, 2007.

[26] R. S. Hotchkiss and D. W. Nicholson, "Apoptosis and caspases regulate death and inflammation in sepsis," *Nature Reviews Immunology*, vol. 6, no. 11, pp. 813–822, 2006.

[27] B. A. Potz, F. W. Sellke, and M. Ruhul Abid, "Endothelial ROS and impaired myocardial oxygen consumption in sepsis-induced cardiac dysfunction," *Journal of Intensive and Critical Care*, vol. 02, no. 01, 2016.

[28] C. Chelazzi, G. Villa, and A. R. De Gaudio, "Cardiorenal syndromes and sepsis," *International Journal of Nephrology*, vol. 2011, Article ID 652967, 8 pages, 2011.

[29] J. Chen, J. Lai, L. Yang et al., "Trimetazidine prevents macrophage-mediated septic myocardial dysfunction via activation of the histone deacetylase sirtuin 1," *British Journal of Pharmacology*, vol. 173, no. 3, pp. 545–561, 2016.

[30] H. M. Chen, S. F. Liou, J. H. Hsu et al., "Baicalein inhibits HMGB1 release and MMP-2/-9 expression in lipopolysaccharide-induced cardiac hypertrophy," *The American Journal of Chinese Medicine*, vol. 42, no. 4, pp. 785–797, 2014.

[31] S. Lei, P. Zhang, W. Li et al., "Pre- and posttreatment with edaravone protects CA1 hippocampus and enhances neurogenesis in the subgranular zone of dentate gyrus after transient global cerebral ischemia in rats," *ASN Neuro*, vol. 6, no. 6, article 175909141455841, 2014.

[32] S. Bonello, C. Zahringer, R. S. BelAiba et al., "Reactive oxygen species activate the HIF-1α promoter via a functional NFκB site," *Arteriosclerosis, Thrombosis, and Vascular Biology*, vol. 27, no. 4, pp. 755–761, 2007.

[33] J. Pouyssegur and F. Mechta-Grigoriou, "Redox regulation of the hypoxia-inducible factor," *Biological Chemistry*, vol. 387, no. 10-11, pp. 1337–1346, 2006.

[34] A. Sanjuan-Pla, A. M. Cervera, N. Apostolova et al., "A targeted antioxidant reveals the importance of mitochondrial reactive oxygen species in the hypoxic signaling of HIF-1α," *FEBS Letters*, vol. 579, no. 12, pp. 2669–2674, 2005.

[35] A. Gorlach and T. Kietzmann, "Superoxide and derived reactive oxygen species in the regulation of hypoxia-inducible factors," *Methods in Enzymology*, vol. 435, pp. 421–446, 2007.

[36] B. Dawn and R. Bolli, "HO-1 induction by HIF-1: a new mechanism for delayed cardioprotection?," *American Journal of Physiology-Heart and Circulatory Physiology*, vol. 289, no. 2, pp. H522–H524, 2005.

[37] S. Turkseven, A. Kruger, C. J. Mingone et al., "Antioxidant mechanism of heme oxygenase-1 involves an increase in superoxide dismutase and catalase in experimental diabetes," *American Journal of Physiology-Heart and Circulatory Physiology*, vol. 289, no. 2, pp. H701–H707, 2005.

[38] S. F. Yet, R. Tian, M. D. Layne et al., "Cardiac-specific expression of heme oxygenase-1 protects against ischemia and

reperfusion injury in transgenic mice," *Circulation Research*, vol. 89, no. 2, pp. 168–173, 2001.

[39] F. Li, P. Sonveaux, Z. N. Rabbani et al., "Regulation of HIF-1α stability through S-nitrosylation," *Molecular Cell*, vol. 26, no. 1, pp. 63–74, 2007.

[40] E. Pathak and P. R. Mayeux, "*In vitro* model of sepsis-induced renal epithelial reactive nitrogen species generation," *Toxicological Sciences*, vol. 115, no. 2, pp. 475–481, 2010.

[41] K. Kikuchi, S. Tancharoen, T. Ito et al., "Potential of the angiotensin receptor blockers (ARBs) telmisartan, irbesartan, and candesartan for inhibiting the HMGB1/RAGE axis in prevention and acute treatment of stroke," *International Journal of Molecular Sciences*, vol. 14, no. 12, pp. 18899–18924, 2013.

[42] S. Liu, T. Yang, R. Na et al., "The impact of female gender on bladder cancer-specific death risk after radical cystectomy: a meta-analysis of 27,912 patients," *International Urology and Nephrology*, vol. 47, no. 6, pp. 951–958, 2015.

[43] G. F. Elbaradey, N. S. Elshmaa, and H. Hodeib, "Role of edaravone in management of septic peritonitis," *Journal of Anaesthesiology Clinical Pharmacology*, vol. 32, no. 4, pp. 465–469, 2016.